AD NUMBER
AD893612
LIMITATION CHANGES
TO: **Approved for public release; distribution is unlimited.**
FROM: **Distribution authorized to U.S. Gov't. agencies only; Test and Evaluation; DEC 1971. Other requests shall be referred to Air Force Rocket Propulsion Laboratory, Attn: STINFO, Edwards AFB, CA 93523.**
AUTHORITY
AFRPL-RPPR/STINFO, per ltr dtd 31 Jan 1974

AFRPL-TR-72-25

AD893612

FINAL REPORT

Technical Report AFRPL-TR-72-25

Rockwell International
A Division of North American Rockwell Corporation
6633 Canoga Avenue
Canoga Park, California

April 1972

Distribution limited to U.S. Government Agencies only; data based on test and evaluation; 1971. Other requests for this document must be referred to AFRPL (STINFO), Edwards, California 93523.

Air Force Rocket Propulsion Laboratory
Air Force Systems Command
United States Air Force
Edwards, California 93523

When U.S. Government drawings, specifications, or other data are used for any purpose other than a definitely related Government procurement operation, the Government thereby incurs no responsibility nor any obligation whatsoever, and the fact that the Government may have formulated, furnished, or in any way supplied the said drawings, specifications, or other data is not to be regarded by implication or otherwise, as in any manner licensing the holder or any other person or corporation, or conveying any rights or permission to manufacture, use, or sell any patented invention that may in any way be related thereto.

18 19

AFRPL-TR-72-25

6

O_2/H_2 ADVANCED MANEUVERING PROPULSION TECHNOLOGY PROGRAM.

WATER-COOLED SEGMENT TESTING.

9 FINAL REPORT. 1 [illegible]

15 F[illegible]-69-C-[illegible]116

Technical Report AFRPL-TR-72-25

14 R-8[illegible]6

Rocketdyne
A Division of North American Rockwell Corporation
6633 Canoga Avenue
Canoga Park, California

11 Apr [redacted] 72

12 4[illegible] p.

Distribution limited to U.S. Government Agencies only; data based on test and evaluation; December 1971. Other requests for this document must be referred to AFRPL (STINFO), Edwards, California 93523.

Air Force Rocket Propulsion Laboratory
Air Force Systems Command
United States Air Force
Edwards Air Force Base, California 93523

1473

30[illegible]

FOREWORD

This technical report presents the results of the water-cooled segment test evaluations conducted as part of Tasks I and II of the O_2/H_2 Advanced Maneuvering Propulsion Technology (AMPT) program. The work was conducted by the Rocketdyne division of North American Rockwell during the period 1 December 1970 to 3 December 1971 as part of United States Air Force Rocket Propulsion Laboratory Contract F04611-67-C-0116.

The Air Force Program Manager was Mr. W. W. Wells. Mr. H. G. Diem was the Rocketdyne Program Manager, Mr. D. Huang was the Rocketdyne Project Engineer.

This report, Rocketdyne report R-8906, was published 14 April 1972.

This technical report has been reviewed and approved.

W. W. WELLS
AFRPL AMPT Program Manager
LKDS

ABSTRACT

This report describes the analysis, design, fabrication, and test of water-cooled segments to define the most suitable injector configurations and combustion chamber geometries for 25,000-pound-thrust, O_2/H_2, lightweight, aerospike thrust chambers. Two-hundred and seventy-one hot-fire tests with numerous injector and chamber configurations were conducted at chamber pressures between 140 and 988 psi. The injector development was supplemented with cold-flow tests of single injection elements. High measured performance (η_{c*} ~99 percent) was demonstrated in low-volume combustion chambers (3.0-inch length from injector face to the throat). Favorable heat transfer characteristics were established which will enable satisfactory coolant-circuit design for the regeneratively cooled segments which are to be demonstrated in the next phase of the program.

ACKNOWLEDGMENTS

The work reported in this volume represents the concerted effort and expertise of many members of the Rocketdyne organization. Contributions of major significance were made by the following personnel:

G. Allen

W. Blendermann

J. Cordill

V. Jaqua

W. Munyon

J. Shoji

CONTENTS

ILLUSTRATIONS

TABLES

NOMENCLATURE

A	area
A_e	nozzle exit area
A_{inj}	injector face area
annul	annulus
AMPT	Advanced Maneuvering Propulsion Technology
A_t	combustion chamber throat area
ax	axial
BLC	boundary layer coolant
BTU	British Thermal Units
c	contraction
cc	combustion chamber
CRES	corrosion-resistant steel
col. dist.	collection distance
c^*	characteristic velocity
c^*_{vap}	characteristic velocity based upon propellant vaporization
c^*_{mix}	characteristic velocity based upon propellant mixing
deg	degrees
D_f	injector fuel orifice diameter
dia	diameter
D_o	injector oxidizer orifice diameter
$\bar{D}_{30}$	mean drop size
e	exit
ϵ	area expansion ratio
EDM	electrical discharge machining
E_M	mixing uniformity index
eng	engine
f	fuel
F	degrees Fahrenheit
ft	feet
GF_2	gaseous fluorine
GH_2	gaseous hydrogen
GO_2	gaseous oxygen
H_2	hydrogen
Hz	Hertz
h_c	coolant-side heat transfer film coefficient
HF	hot fire

SECTION I

INTRODUCTION

The Advanced Maneuvering Propulsion Technology (AMPT) Program is being conducted to demonstrate the performance and weight potential of a 25,000-pound-thrust, O_2/H_2, aerospike thrust chamber.

Two aerospike engine system designs are being developed on this program (Fig. 1). The first design, called single-panel because only the fuel is used as a regenerative coolant, has an area ratio of 110:1 and a maximum chamber pressure of 750 psia. This design point corresponds exactly to the single-panel thrust chamber demonstrator hardware being fabricated and tested on this program. Some additional performance could be obtained with the single-panel design by enlarging the nozzle area ratio to the maximum possible value of 150:1 at the same chamber pressure. However, the more conservative expansion ratio was selected to provide an additional operating safety margin for the demonstration hardware.

The second aerospike design is called double-panel because both fuel and oxidizer are used as regenerative coolants in the combustion section to provide additional cooling capability. The optimum double-panel has a chamber pressure of 1000 psi and a nozzle expansion ratio of 200:1. This design point defines the maximum possible performance for the aerospike concept at a thrust level of 25,000 pounds. Demonstrator hardware with slightly more conservative operating conditions (950-psi chamber pressure and 190:1 expansion) is being built and tested on this program.

The O_2/H_2 AMPT program contains three tasks as illustrated in Fig. 2. Task I includes all design and analysis on the aerospike thrust chamber demonstration hardware and engine system studies.

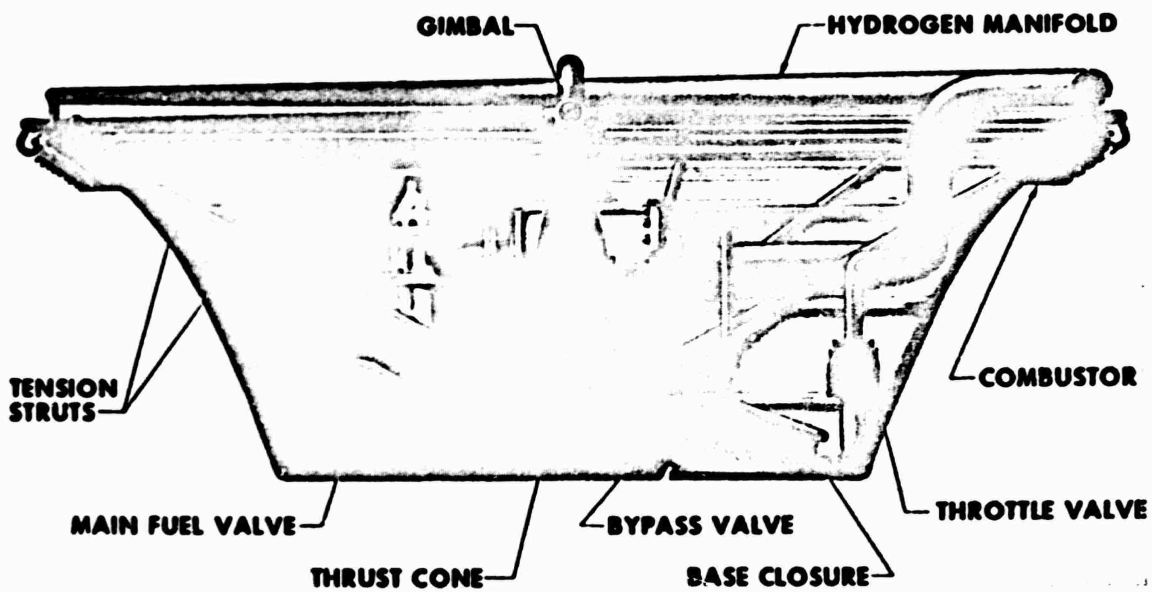

	SINGLE-PANEL DESIGN	DOUBLE-PANEL DESIGN
MAXIMUM CHAMBER PRESSURE, PSIA	750	1000
EXPANSION AREA RATIO	110:1	200:1
NOMINAL ENGINE MIXTURE RATIO	5.5:1	5.5:1
THRUST THROTTLE RATIO	5.0:1	5.0:1
VACUUM SPECIFIC IMPULSE	438	471
DRY ENGINE WEIGHT, POUNDS	260	298
ENGINE L[illegible]GTH, INCHES	24.1	27.0
ENGINE DIAMETER, INCHES	61.6	66.9

Figure 1. 25,000-Pound-Thrust O_2/H_2 Aerospike Engine

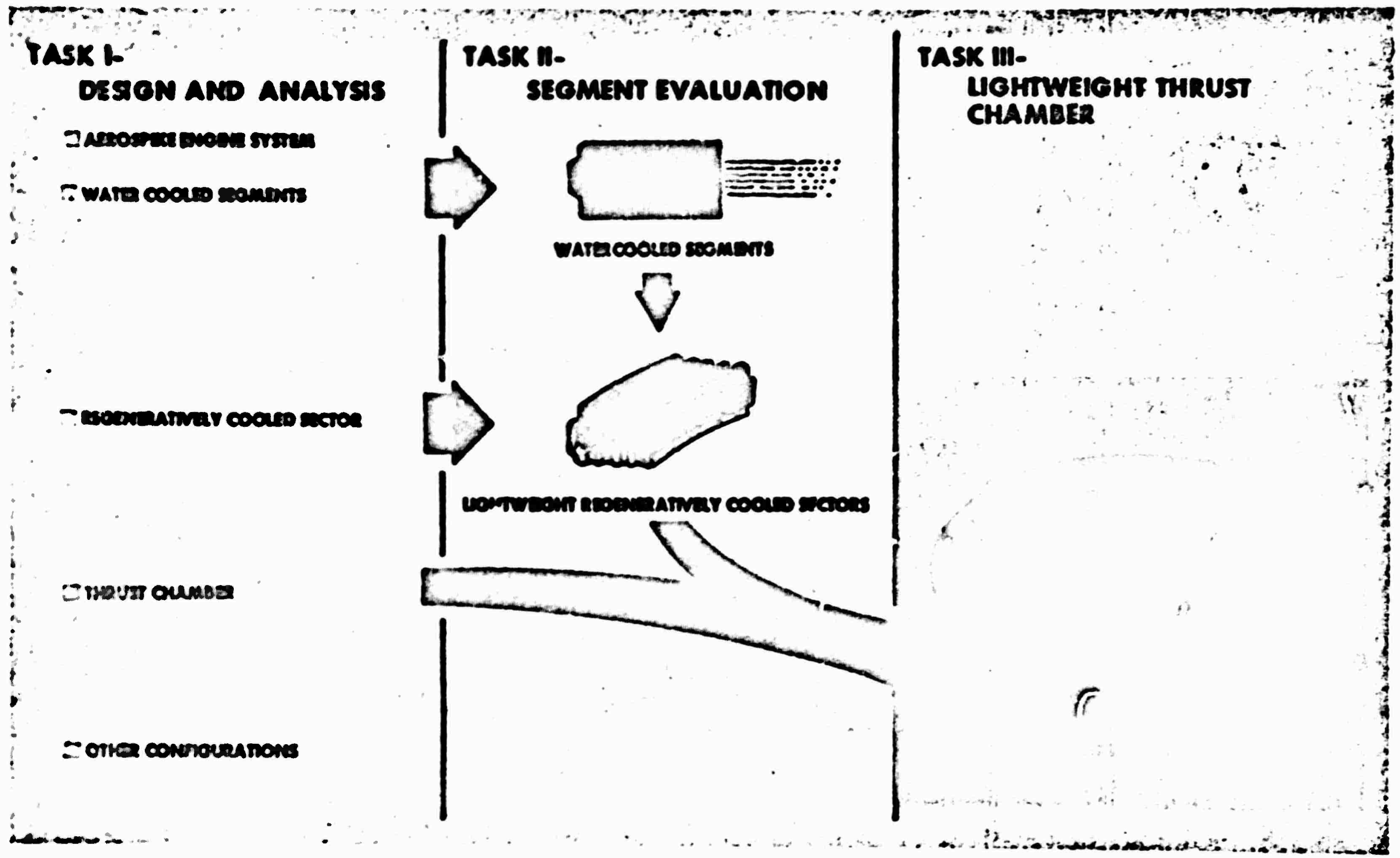

Figure 2. Graphic Program Plan

Task II covers the fabrication and test of water-cooled segments and lightweight regeneratively cooled segments and sectors (a sector is an assembly of three segments). The Task II effort includes both single- and double-panel segment/sector evaluations. Based on the Task II test results, the final design approach will be selected for the complete lightweight demonstrator thrust chamber hardware of Task III. The date of this selection is 1 June 1972.

Based on the results of Task II, two complete lightweight 25,000-pound-thrust aerospike thrust chambers of the selected type will be designed, fabricated, and demonstration tested under simulated altitude conditions at the Air Force Arnold Engineering Development Center. Each of the thrust chambers will be assembled from 24 regeneratively cooled segments of the basic configuration demonstrated during the Task II effort together with a nozzle skirt, base closure, and thrust structure with gimbal.

The water-cooled segment testing of Task II has been completed and is summarized in this report. This test program defined the best injector designs and combustion chamber configurations for the single- and double-panel regeneratively cooled segments of Task II.

SECTION II

SUMMARY

The water-cooled segment evaluation program identified the best injector and combustion chamber designs for both the single-panel and double-panel aerospike configurations. The primary demonstration criteria for the water-cooled segment test program were:

	Single-Panel	Double-Panel
• Chamber Pressure at Full Thrust, psia	750	950
• Throttle Ratio	5:1	5:1
• Minimum η_{c^*} Over the Throttle Range (Percent Theoretical Shifting c*)	97	97

- Combustion Stability: Recovery and Stabilization Within 40 milliseconds after Pulsing at Least 50 Percent Above the Operating Chamber Pressure

One-hundred and seventeen single-panel and 154 double-panel water-cooled segment hot-fire tests were conducted. Triplet, concentric orifice, and coplanar injector types were evaluated for the single-panel using liquid oxidizer and gaseous fuel propellant injection. Triplet, concentric orifice, and trislot injector types were evaluated for the double-panel using gaseous oxidizer and gaseous fuel propellant injection. Variations in combustion chamber geometry were evaluated concurrent with the injector evaluations. The test program results are summarized briefly in Table 1. As shown, the ranges of chamber pressure, mixture ratio, and fuel injection temperature which were tested exceeded the design ranges in each case.

Based on the criteria of high η_{c^*} and acceptable heat transfer, injector/combustion chamber configurations were defined for the single-panel and double-panel designs. The segment combustors for both designs had constant convergent angle chamber walls with a length from injector face to throat of 3.0 inches and an injector end width of 0.5 inch. The throat width (gap) for the single-panel and

TABLE 1. WATER-COOLED SEGMENT TEST SUMMARY

	SINGLE-PANEL	DOUBLE-PANEL
NO. OF FIRING TESTS	117	194
INJECTOR BASIC TYPES	COPLANAR CONCENTRIC TRIPLET (20 DESIGN VARIATIONS)	TRIPLET CONCENTRIC TRISLOT (11 DESIGN VARIATIONS)
CHAMBER COMBUSTION ZONE LENGTH-IN.	3.0 & 4.0 IN.	2.5, 3.0 & 3.5 IN.
CHAMBER INJECTOR END WIDTH - IN.	0.6 & 0.5 IN.	0.5 IN.
CHAMBER WALL CONTOURS	CONTINUOUS CONVERGENT AND STRAIGHT • CONVERGENT	CONTINUOUS CONVERGENT AND STRAIGHT • CONVERGENT
CHAMBER PRESSURE RANGE		
DESIGN	150 TO 750 PSIA	190 TO 950 PSIA
TEST	140 TO 781 PSIA	150 TO 988 PSIA
MIXTURE RATIO RANGE		
DESIGN	5.0 TO 6.0	5.0 TO 6.0
TEST	4.6 TO 6.8	4.3 TO 6.4
FUEL INJECTION TEMPERATURE		
DESIGN	348 TO 700F	537 TO 994F
TEST	55 TO 1000F	54 TO 1064F

double-panel configurations were 0.125 and 0.085 inch, respectively, and corresponded to chamber characteristic lengths (L*) of 7.94 inches and 10.20 inches, respectively.

The selected single-panel injector was a concentric orifice type that utilized liquid oxygen and gaseous hydrogen in a low thrust per element (13 pounds per element at maximum P_c) configuration. The concentric injector element consisted of a recessed, 0.075-inch, oxidizer post with a 0.018-inch fuel annulus surrounding the oxidizer post. The face contained 80 elements arranged in three rows. The injector-combustor assembly met the program η_{c*} requirement of at least 97 percent over the 5:1 (750- to 150-psia chamber pressure) throttle range and was compatible (heat transfer) with the combustor. The injector η_{c*} at the 750-psia chamber pressure design point was 99 percent.

The selected double-panel injector was a triplet, hydrogen-oxygen-hydrogen type that utilized gaseous oxygen and gaseous hydrogen in a low thrust per element

(20.4 pounds per element at maximum P_c) configuration. The injector face had 51 elements arranged in two rows. The fuel and oxidizer orifice diameters were 0.050 and 0.033 inch, respectively, with an included impingement angle between the fuel orifices of 75 degrees. The injector η_{c*} over the 5:1 (950 to 190 psia) throttle range was approximately 99.5 percent.

Following selection of the injector/combustion chamber designs for the single-panel and double-panel segments, a series of stability evaluation tests was conducted with each configuration. Pulse guns were utilized to create steep-fronted overpressures in the combustion chamber. In all tests, the pressure surges damped within 8 milliseconds, thus demonstrating that the stability demonstration criteria (40 milliseconds recovery time) had been met.

The water-cooled segment test results have provided all necessary design criteria for single-panel and double-panel regeneratively-cooled segments and sectors which will be fabricated and demonstration tested in the next part of the program.

SECTION III

THRUST CHAMBER ASSEMBLY DESCRIPTION

The aerospike demonstration thrust chamber consists of an annular combustion chamber with regeneratively cooled inner and outer bodies, assembled from combustor segments, and a regeneratively cooled nozzle extension. The demonstration thrust chamber assembly is shown in Fig. 3. The major components of each thrust chamber assembly type are described below.

COMBUSTION CHAMBER

The combustion chamber utilizes a segmented chamber approach in which 24 combustor segments are stacked within a continuous inner structural ring and a continuous outer structural ring providing a 360-degree circular assembly. At each interface between segment combustors, called the baffle or the side plate region, bolts are installed to connect the inner and outer structural rings.

The design approach, illustrated in Fig. 4 , achieves an aerospike thrust chamber without bonding coolant panels to the pressure and thrust restraining structure, thereby reducing thermally induced strains in the structures, and also avoiding the processing associated with furnace braze joining of the segments and structure. The resulting mechanical assembly allows removal and replacement of individual segments if required. A drawing of the single-panel thrust chamber assembly is shown in Fig. 5.

Single-Panel Regenerative-Cooled Segments. The segments are assembled from a single-piece, NARloy* investment casting to which NARloy closure sheets are brazed to form the complete rectangular coolant passages, as illustrated in Fig. 6 .

The NARloy material was selected because of good castability, brazeability, high thermal conductivity, and required material strength properties at elevated temperatures.

*NARloy is a silver-copper alloy (North American Rockwell trademark).

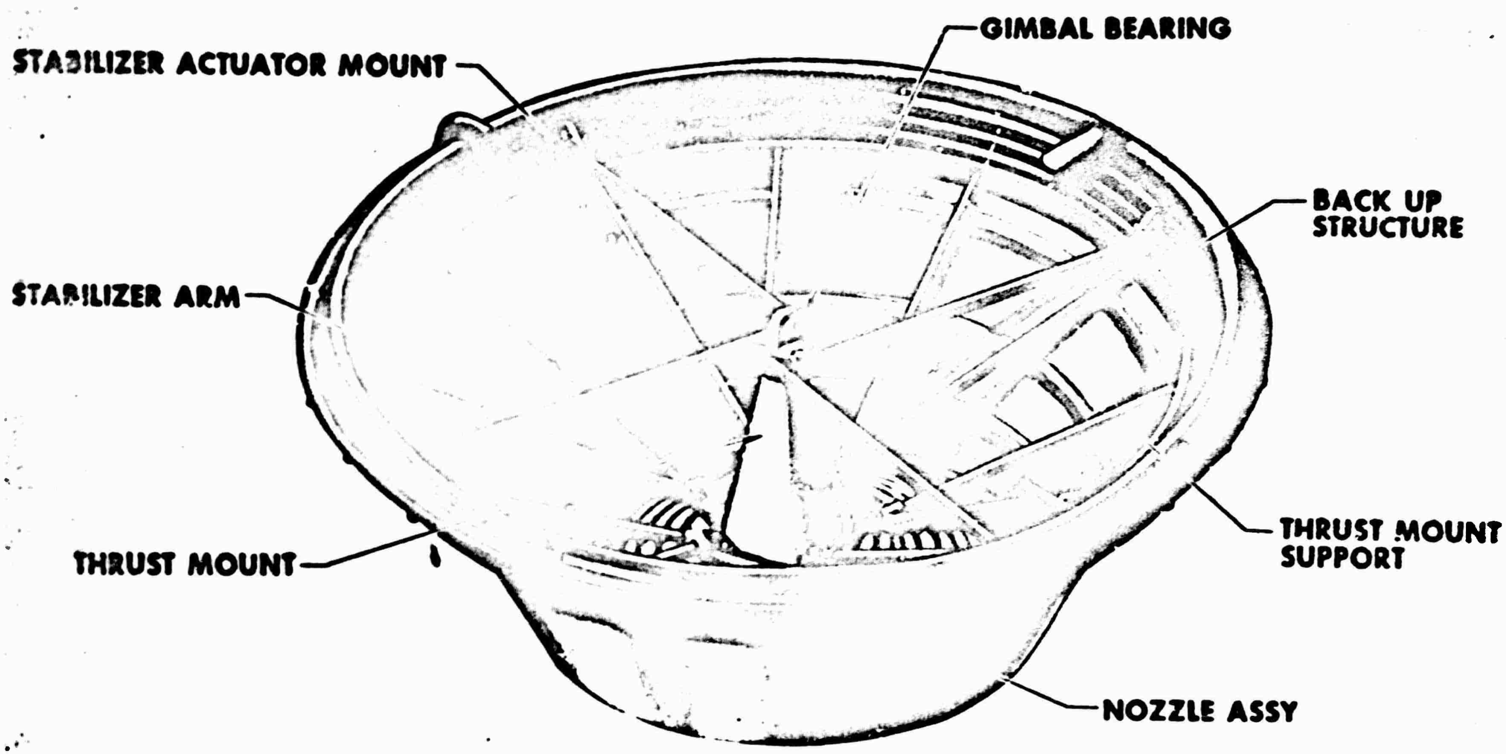

Figure 3. 25,000-Pound-Thrust Demonstration Thrust Chamber Assembly

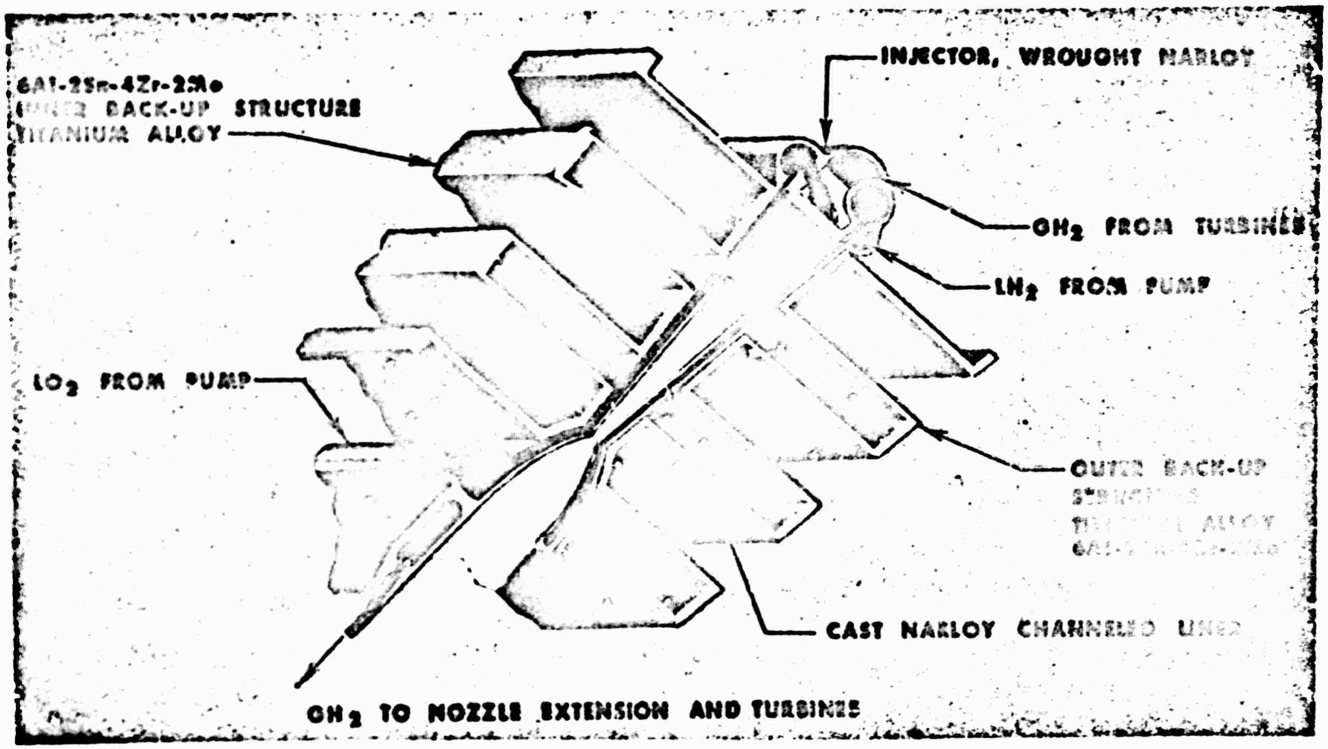

Figure 4. Regeneratively Cooled Double-Panel Lightweight Combustion Chamber Design Approach

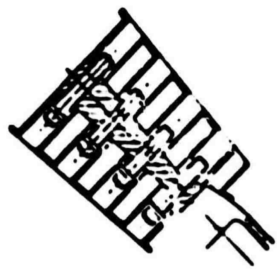

SECTION C-C
TYP 12 PLCS

SECT D-D

SECT
8 PLC

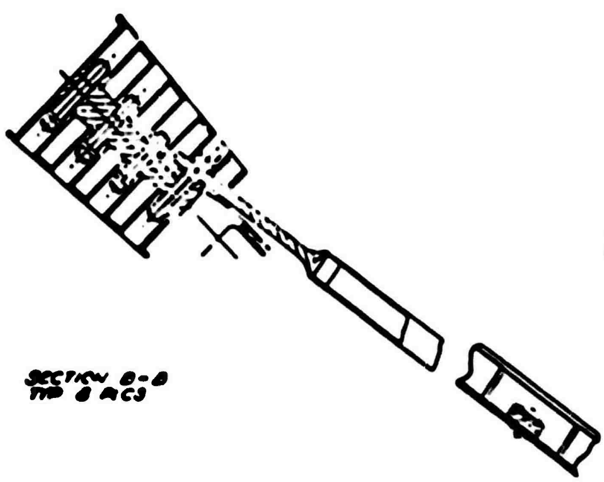

SECTION B-B
TYP 8 PLCS

TYP STRUCTURAL BOLT
TENSIL
SHEAR

11.

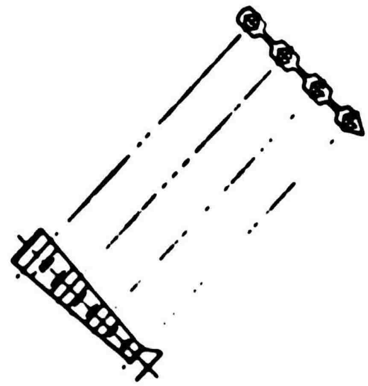

BAFFLE SPLICED DETAIL
TYP ?? PLCS (030037418)
INCONEL 718 (180 KSI @ 70°F)

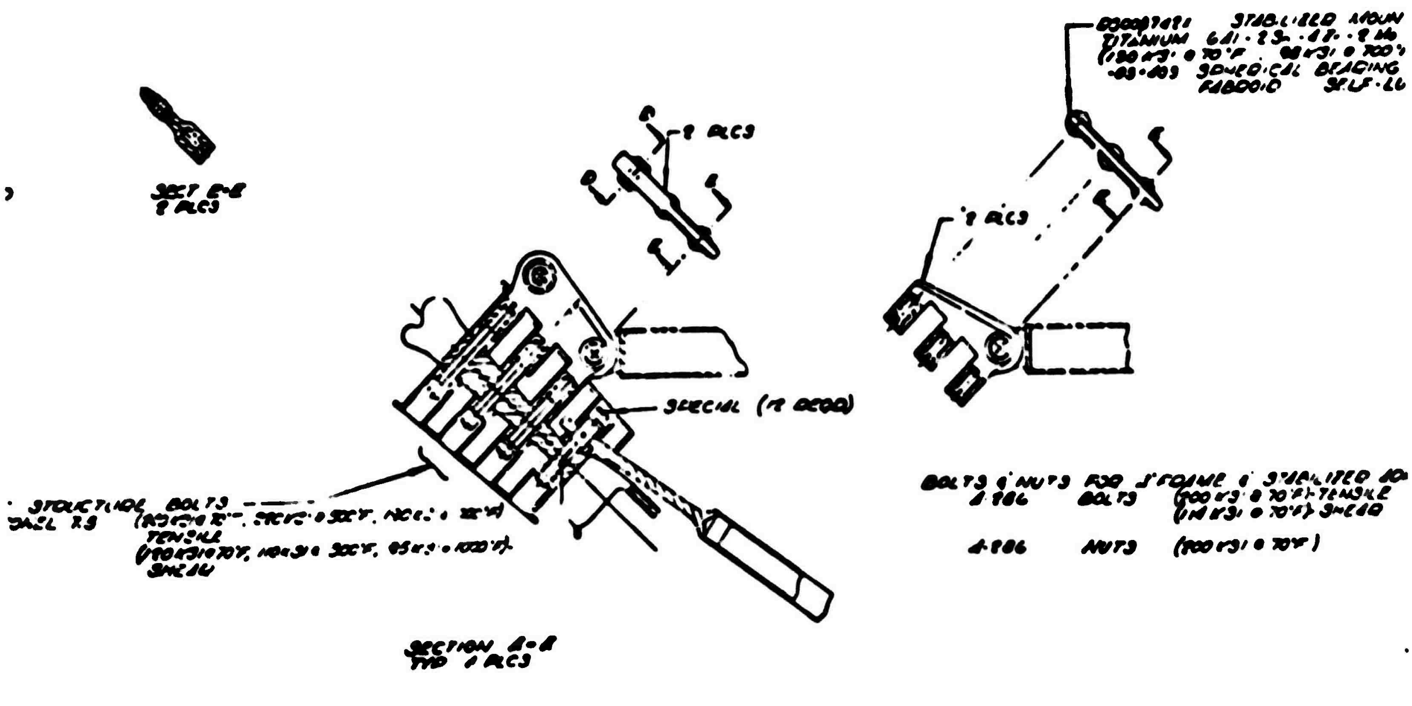

SECTION A-A
TYP 4 PLCS

BOLTS & NUTS FOR S-FRAME & STABILIZED MO[illegible]
A-286 BOLTS (200 KSI @ 70°F) TENSILE
(1?? KSI @ 70°F) SHEAR
A-286 NUTS (200 KSI @ 70°F)

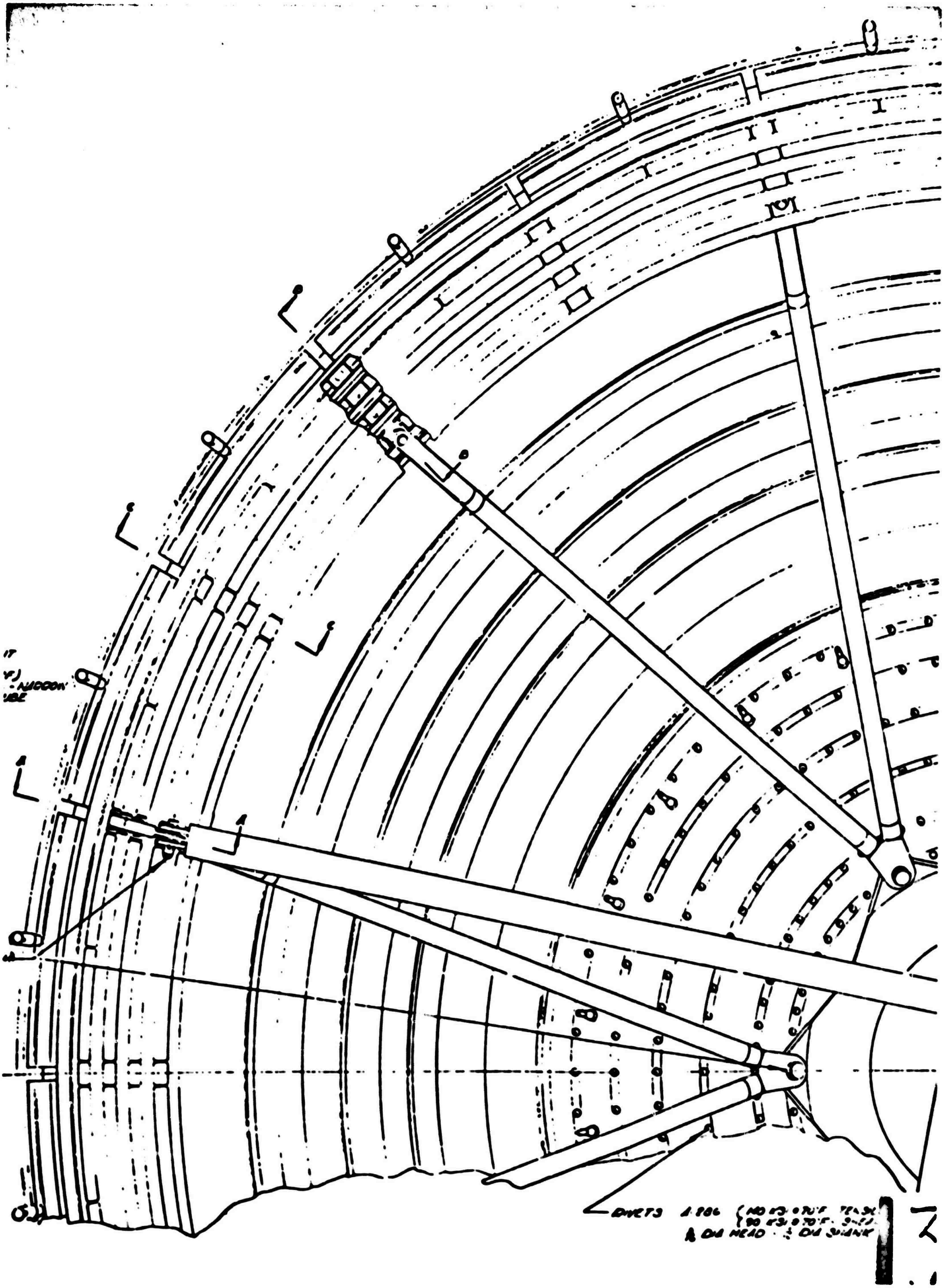
DIA HEAD
DIA SHANK

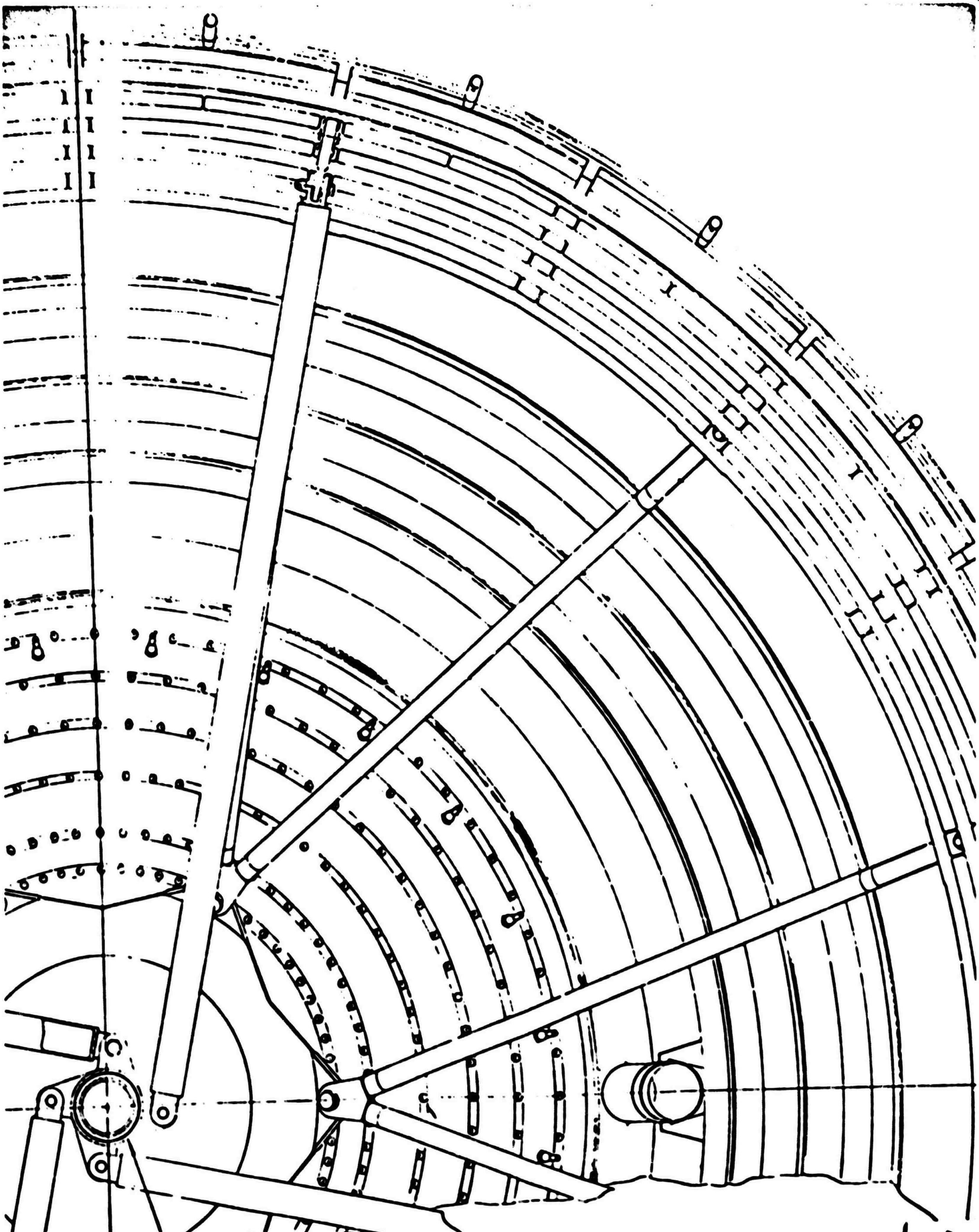
GIMBAL MOUNT REMOVED FOR CLARITY

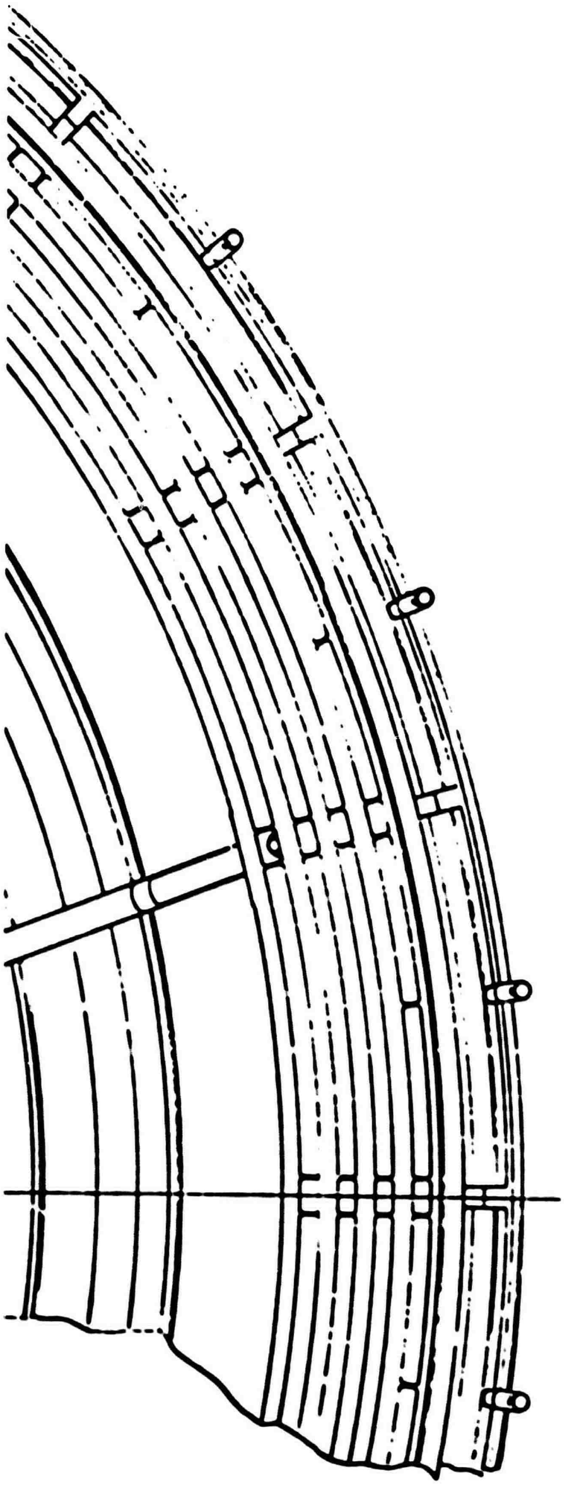
ACTUATOR
STABILIZER

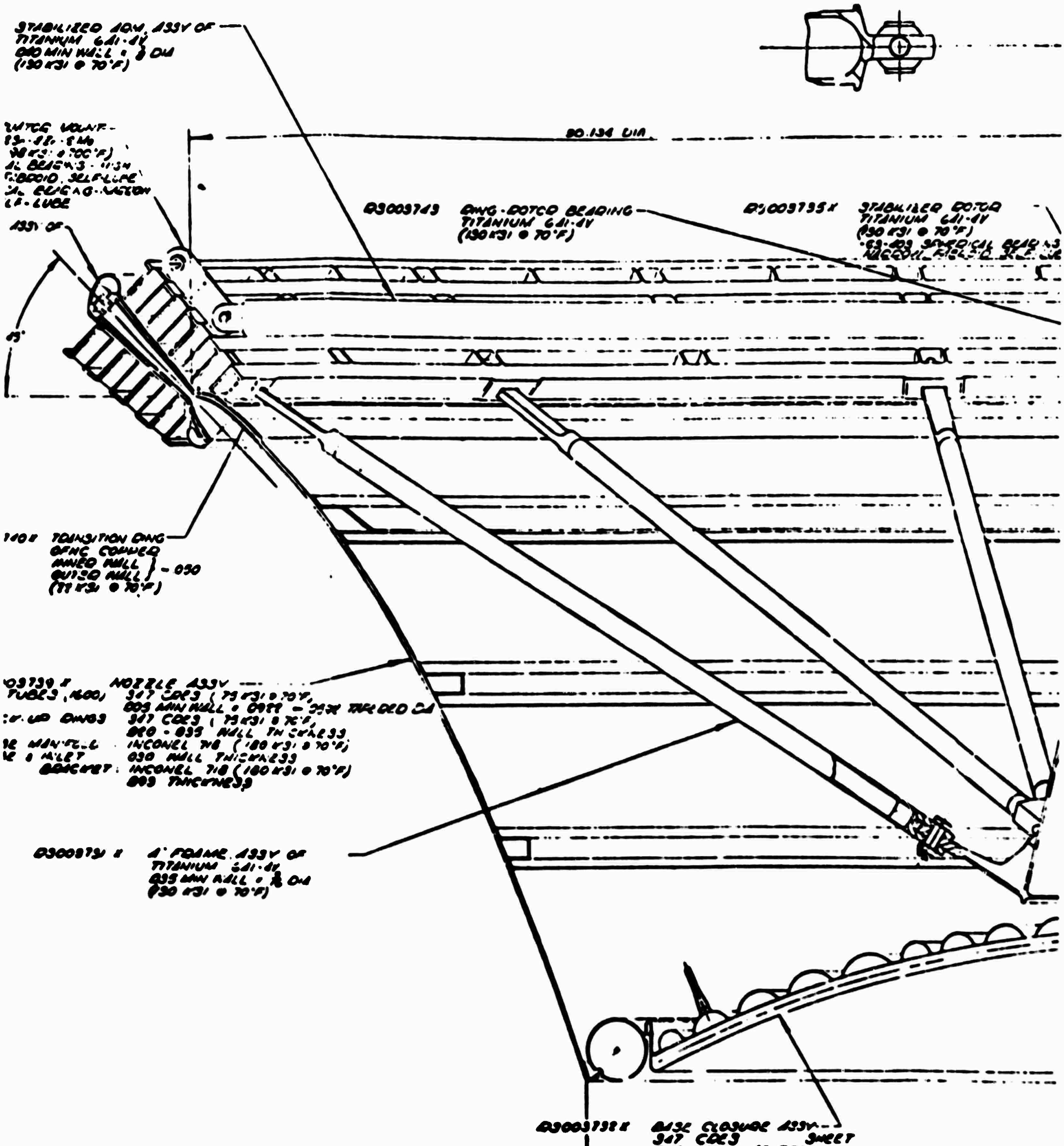

STABILIZED ARM, ASSY OF
TITANIUM 6Al-4V
(130 KSI @ 70°F)
80.134 DIA
ASSY OF
D3003743 RING-ROTOR BEARING
TITANIUM 6Al-4V
(130 KSI @ 70°F)
STABILIZER ROTOR
TITANIUM 6Al-4V
TRANSITION RING
NOZZLE ASSY
347 CRES (75 KSI @ 70°F)
INCONEL 718 (180 KSI @ 70°F)
030 WALL THICKNESS
BRACKET: INCONEL 718 (180 KSI @ 70°F)
4" FRAME ASSY OF
TITANIUM 6Al-4V
(130 KSI @ 70°F)
BASE CLOSURE ASSY
347 CRES SHEET
347 CRES TUBE
(75 KSI @ 70°F)

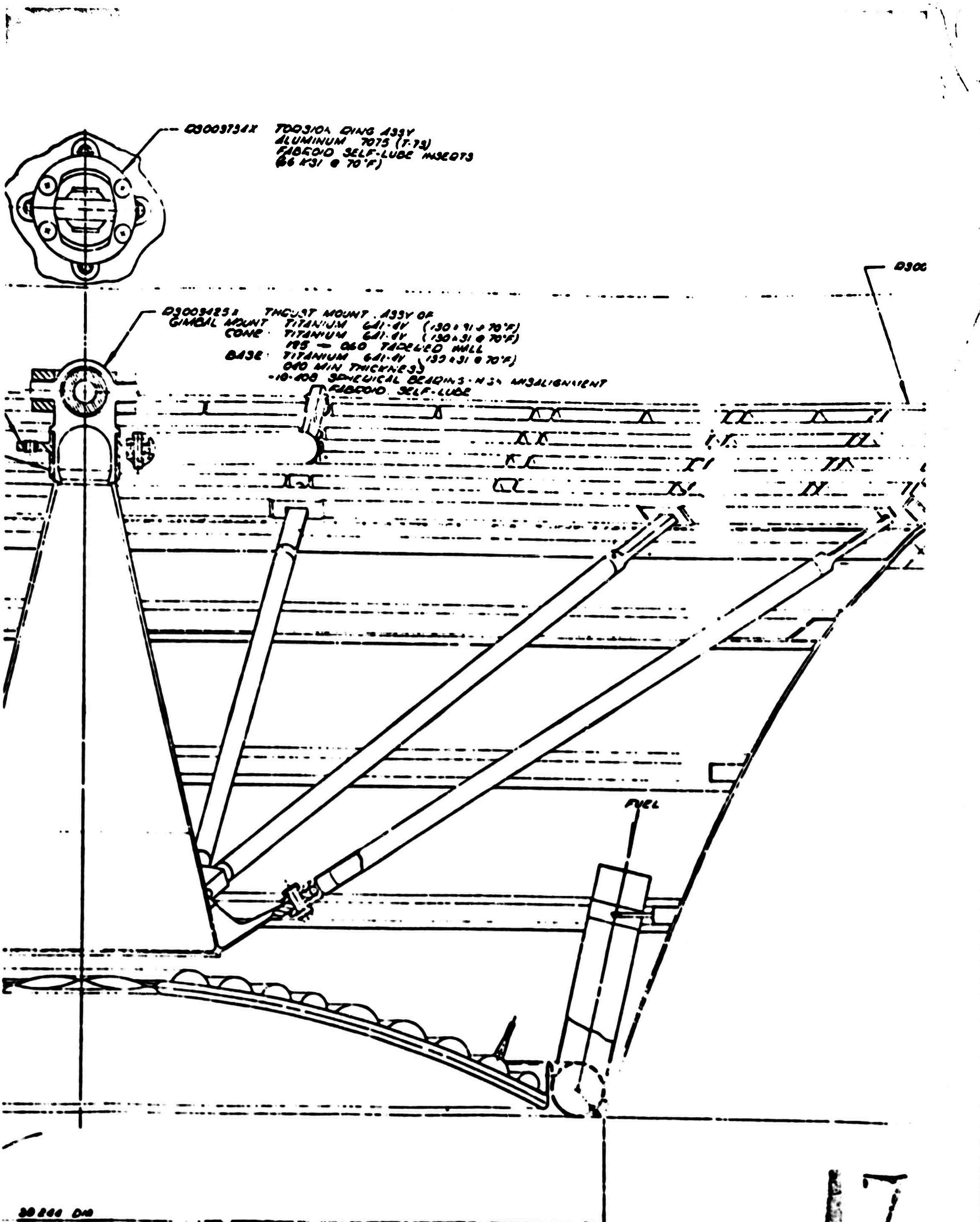
ALUMINUM 7075
SELF-LUBE
THRUST MOUNT
GIMBAL MOUNT TITANIUM
CONE TITANIUM
BASE TITANIUM
MIN THICKNESS
SELF-LUBE
FUEL
DIA

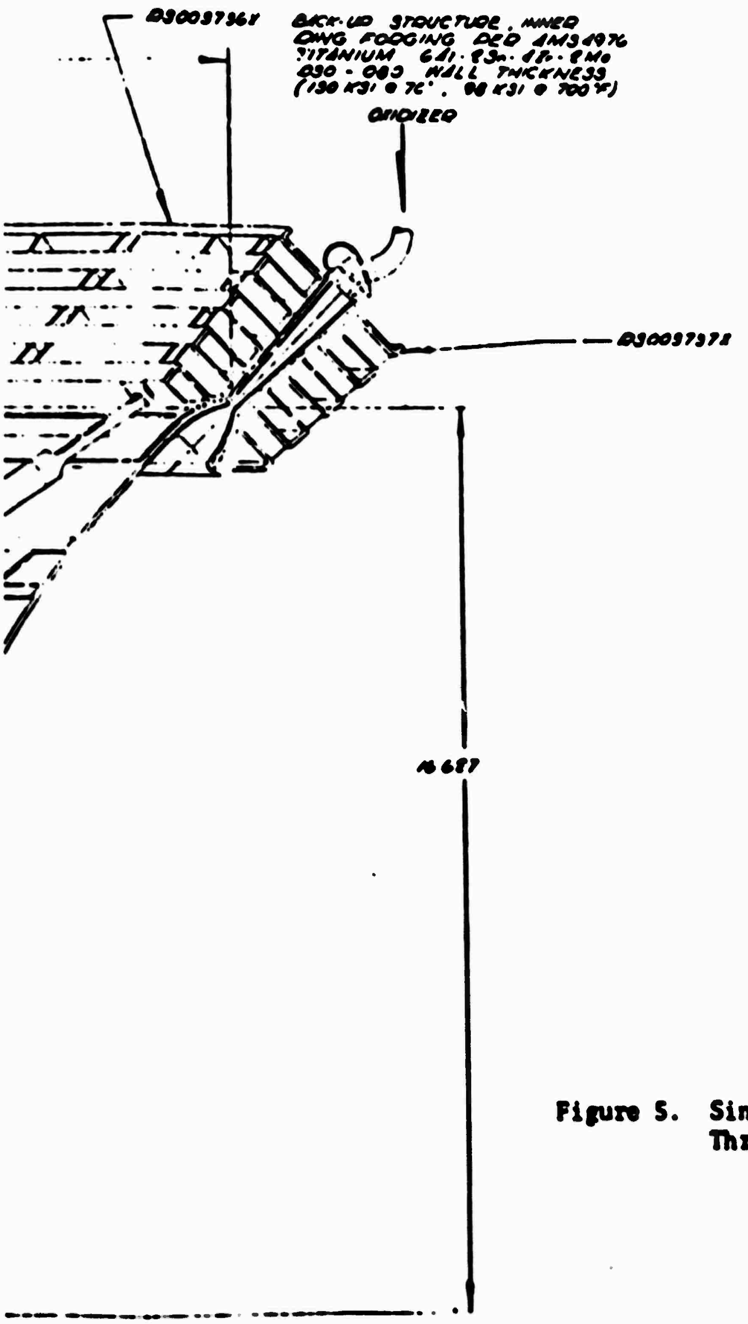

Figure 5. Single-Panel Aerospike Thrust Chamber Assembly

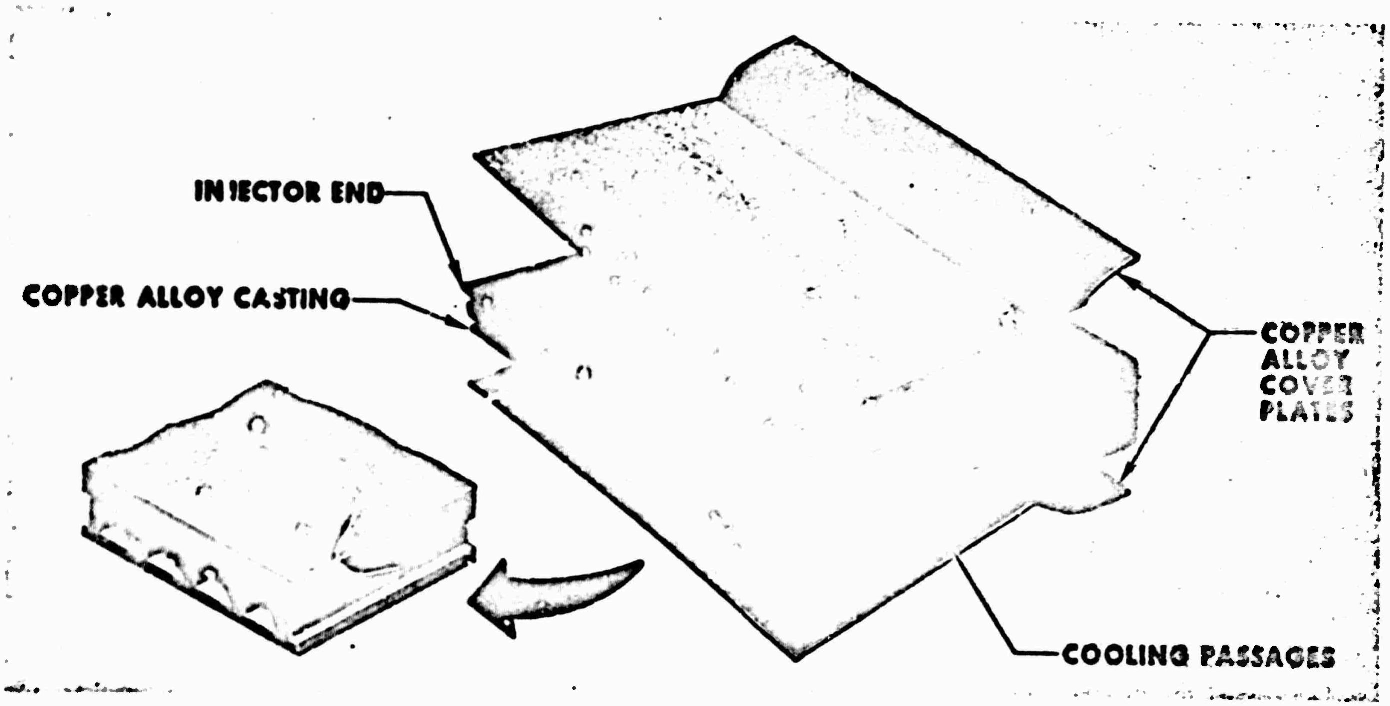

Figure 6. Regeneratively Cooled, Single-Panel Chamber Segment

The primary difference in the design approach between the single-panel or double-panel segments is in the regenerative-cooling design. The single-panel coolant circuit is shown in Fig. 7, and is a single pass in which the nozzle is cooled first and the segment combustor last. With this circuit, the hydrogen enters the tubular nozzle cooling passages at the nozzle exit. After single uppass cooling of the nozzle and the segment combustor inner bodies, the segment combustor side panels are downpass cooled and, finally, the segment combustor outer bodies are uppass cooled to complete the circuit. Downpass designates an injector-to-throat direction, and uppass is the reverse.

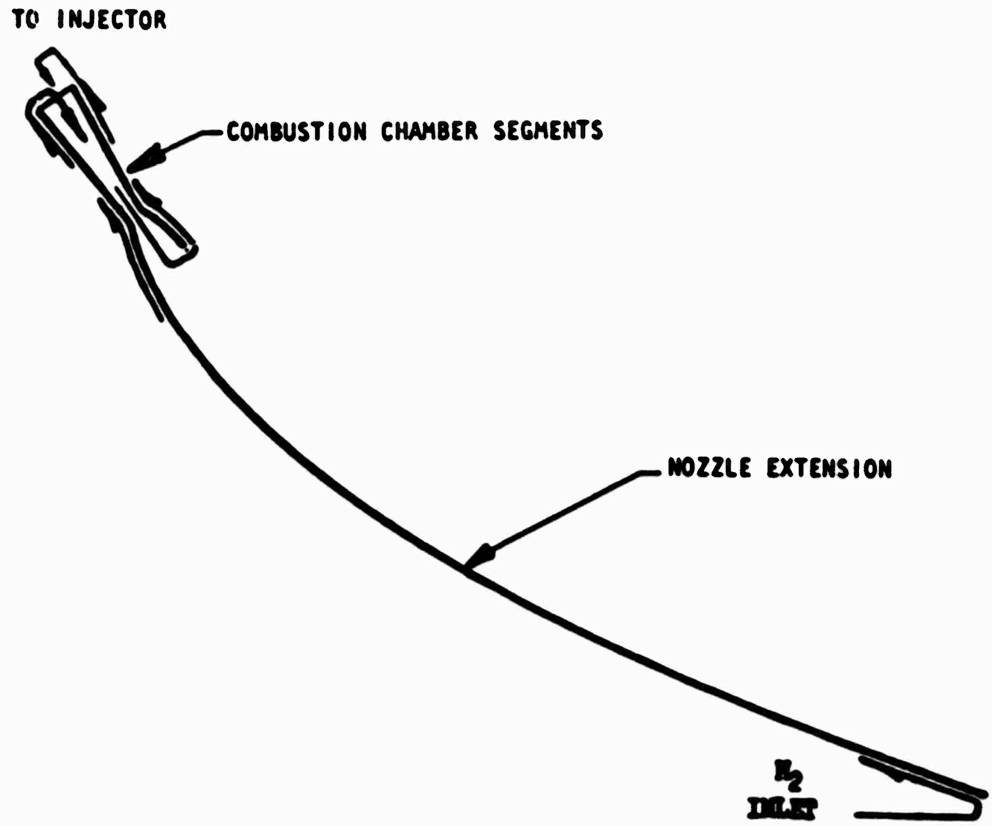

Figure 7. Single-Panel Demonstrator Thrust Chamber Cooling Circuit

Double-Panel Regenerative-Cooled Segment

The segment is assembled from a basic, two-piece (split), NARloy investment casting. The coolant passage closeout procedures are slightly different than those used for the single-panel combustor because of using oxidizer for secondary cooling of the inner wall. The secondary cooling is accomplished as illustrated in Fig. 8, with the oxygen absorbing heat from both the heated coolant hydrogen and from the combustor wall structure.

The outer wall has a brazed-on NARloy closeout sheet toe same as the single-panel chamber, but the inner wall utilizes an individual tube closeout for each coolant passage, as shown in Fig. 9. The tubes are NARloy to obtain consistent mechanical properties and high thermal conductivity.

The complete double-panel thrust chamber regenerative-cooling circuit is shown in Fig. 10, and consists of a double-pass, combustor-first, nozzle-last type circuit. The hydrogen coolant enters the outer wall first and completes an up and down traverse (adjacent coolant passages) followed by a downpass through the side panels, an uppass and downpass through the inner wall, and completes the circuit by flowing single-pass down through the nozzle.

The oxidizer completes a single uppass circuit through the tubes that are attached to the inner combustion chamber wall.

This report covers the development of the specific combustor geometry and injector design criteria for the single-panel and the double-panel regeneratively cooled segments. This development was accomplished by hot-fire testing of water-cooled, calorimetry segment combustors, of various combustor geometries, with nonlightweight, bolt-on injector configurations that permitted modifications.

Following this development, evaluation of regenerative-cooling capability and the lightweight structure reinforcement is to be accomplished by hot-fire testing of regeneratively cooled segment combustors in both single-segment and three-segment (sector) configurations. This development will provide the segment assembly designs for the demonstrator thrust chamber assembly.

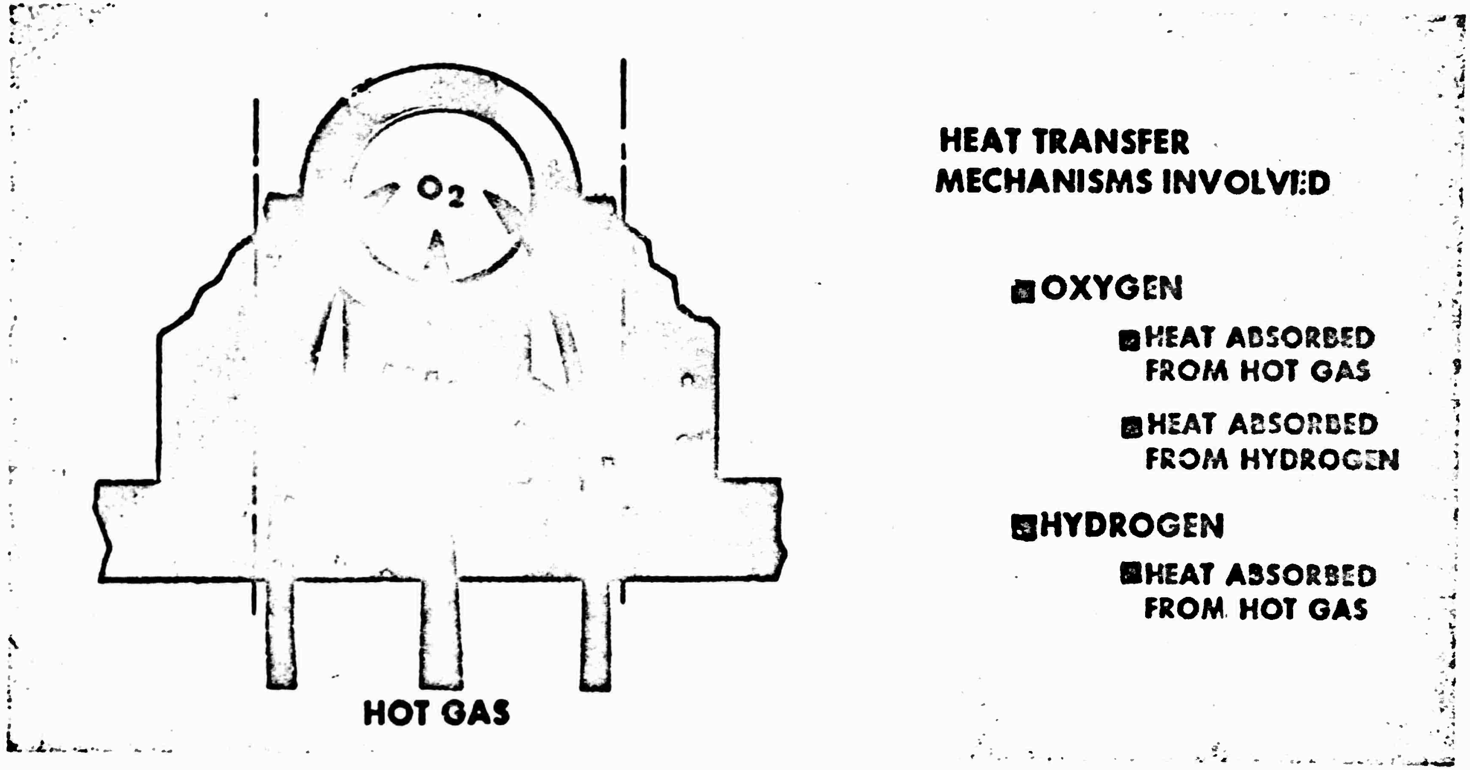

Figure 8. Regeneratively Cooled Chamber Segment, Double-Panel Cooling Concept

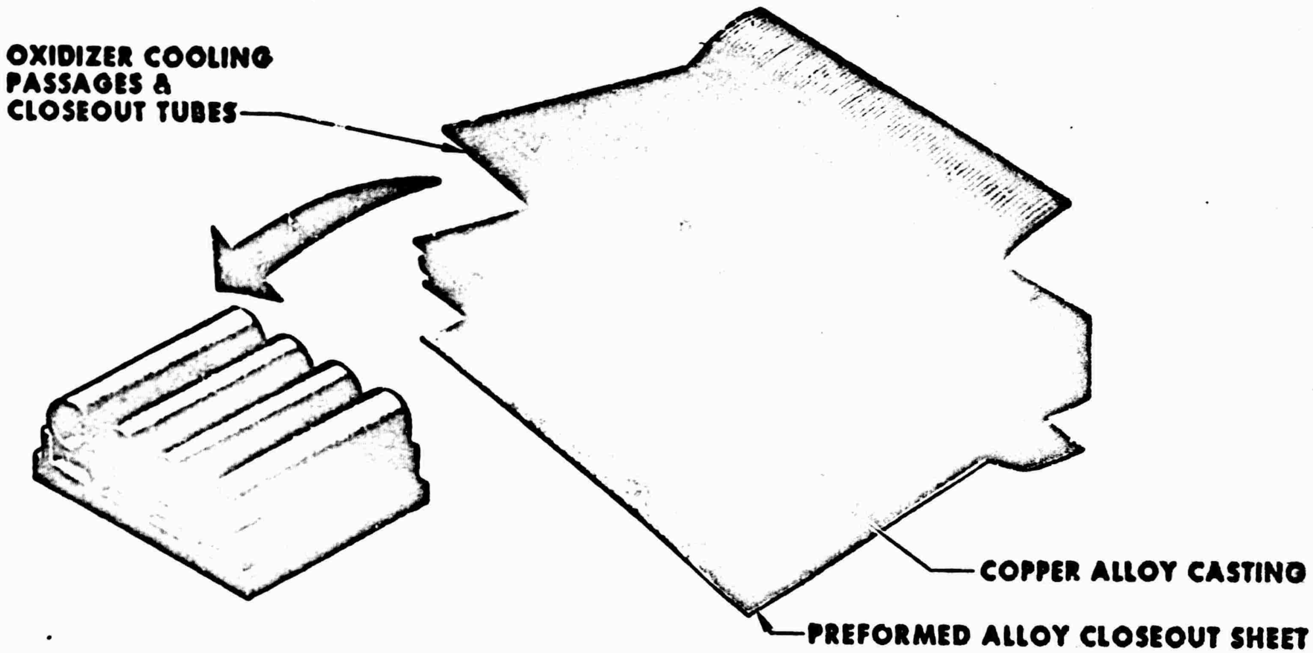

Figure 9. Regeneratively Cooled Double-Panel Chamber Segment

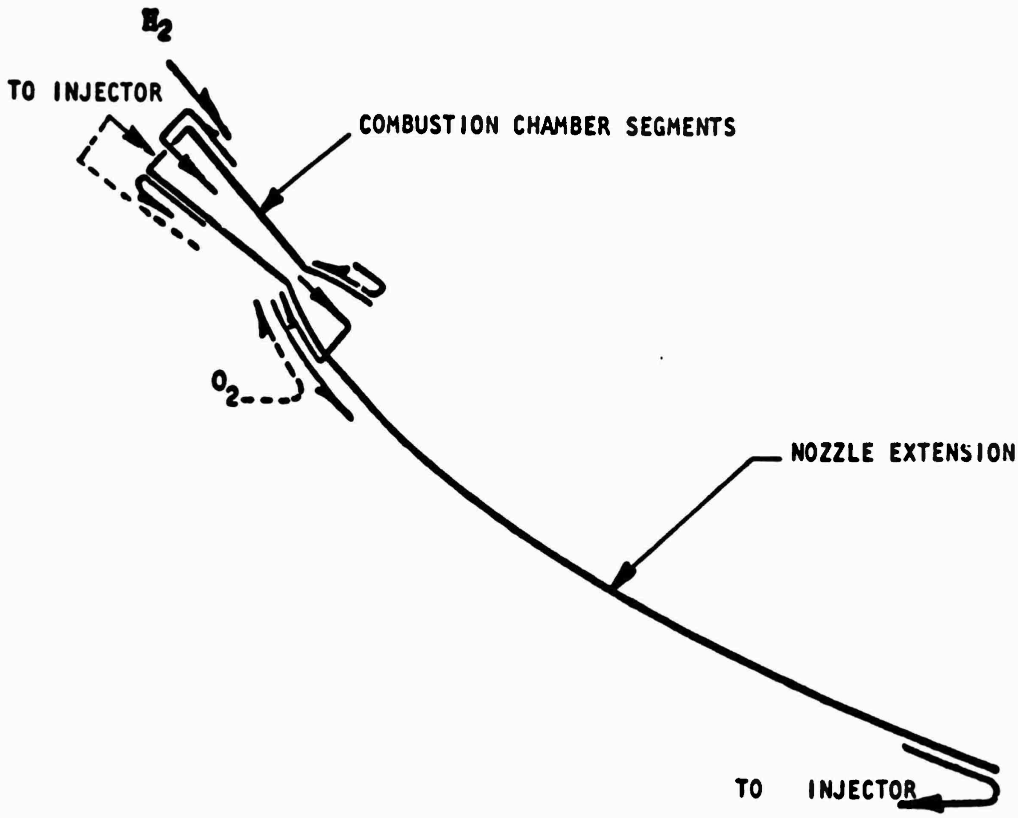

Figure 10. Double-Panel Demonstrator Thrust Chamber Cooling Circuit

SECTION IV

WATER-COOLED SINGLE-PANEL SEGMENT EVALUATION

The determination of the design criteria for the single-panel, regeneratively cooled segment thrust chamber combustor and injector was the primary purpose of the single-panel, water-cooled segment program. Four water-cooled, calorimetry-type, segment thrust chambers and five bolt-on type injectors were designed, fabricated, and hot-fire tested. Variation of chamber combustion zone length and injector element configuration were the primary development parameters. A minimum length chamber was desirable to minimize total thrust chamber weight. Injection element configuration variations of each injector were evaluated, and single-element, cold-flow tests were conducted as part of the program.

The single-panel segment development program is described in the following order: hardware design and fabrication, injector element cold-flow testing, segment hot-fire testing and analysis, and the test evaluation summary.

HARDWARE DESIGN AND FABRICATION

Segment Chambers

Three geometric types of segment chambers were evaluated during the program. The primary differences between types were in the throat area and in the upper combustor zone (injector face area). The general configuration of the chamber types is shown in Fig. 11 .

Unit Numbers 1, 2, and 4. Three segment chambers, designated units 1, 2, and 4, were designed and fabricated (Fig. 11) based on the detailed design criteria presented in Table 2. The following design guidelines were established and followed for the segment combustors:

1. The combustors would be low-volume, minimum L^* so that the regeneratively cooled segments would meet the thrust chamber weight requirements.

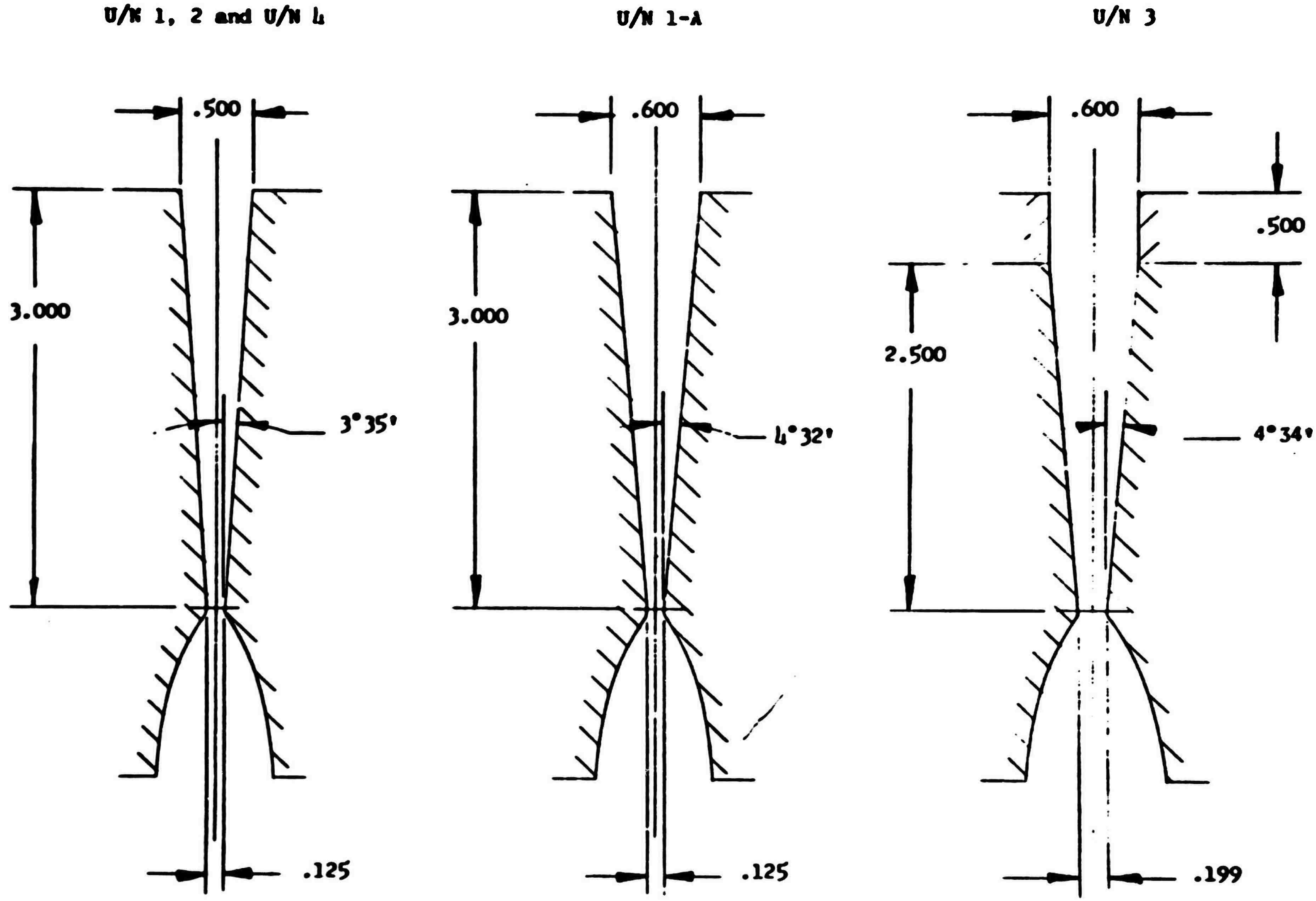

Figure 11. Single-Panel Water-Cooled Segment Chamber Combustor Internal Configuration (Units 1, 1-A, 2, 3, and 4)

TABLE 2. DESIGN CRITERIA FOR SINGLE-PANEL WATER-COOLED SEGMENT CHAMBERS

Design Parameters	Units 1, 2, and 4	Unit 1-A
Chamber Length (side plate-to-side plate at injector end), inches	6.260	6.260
Chamber Length (side plate-to-side plate at throat), inches	5.700	5.700
Width at Injector End, inch	0.500	0.600
Throat Gap, inch	0.125	0.125
Throat Radius, inch	0.125	0.125
Contraction Ratio (A_{inj}/A_t)	4.39	5.28
Expansion Ratio (A_e/A_t)	5.44	5.44
Divergence Nozzle	Curved to match regeneratively cooled segment	Curved to match regeneratively cooled segment
Combustion Zone Wall Configuration		
Side Plates	Straight convergent	Straight convergent
Chamber Walls	Straight convergent	Straight convergent
Combustion Zone Wall Convergence Half-Angle, degrees	3 degrees, 35 minutes	4 degrees, 32 minutes
Combustion Zone Length (L_c), Injector Face to Throat, inches	3.0	3.0
Characteristic Chamber Length (L*), inches	7.94	10.2
Chamber Pressure, psia	750	750

2. Capability would be provided for increasing combustion zone length, L_c, from the basic 3.0 inches to 3.5 and 4.0 inches by use of removable, cooled, 0.5- and 1.0-inch spacers to permit the determination of L_c effect upon performance and heat transfer.

3. The segment chamber would incorporate the capability to obtain local heat flux distribution, total integrated heat rejection rate, and the c* performance of each injector-combustor assembly.

The segment chambers were fabricated of copper and incorporated coolant passages for water cooling. The segment chamber configuration is illustrated in Fig. 12. The design and fabrication techniques were similar to those developed previously under Contract F04611-67-C-0116.

Two-dimensional heat transfer computer analyses were conducted to verify the cooling capability of the water-cooled chamber design. The analyses were conducted at four axial stations: injector end (X = -2.75 inches); slightly below injector end (X = -1.94 inches); immediately above the throat (X = -0.4 inch); and at the throat (X = 0.0 inch). The local heat flux used for analysis corresponded to the analytically predicted local heat flux, 1.18 times the predicted value at the throat region and 2.0 times the predicted value at the injector end. The higher than predicted heat flux values were used to provide for uncertainties and a margin of safety. The results of the analyses are presented in Table 3 . The maximum predicted gas-side wall temperature for 750-psia chamber pressure was 1771 R, at a point located 0.4 inch above the throat. This value is well below the melting point of 2441 R for OFHC copper.

Figure 12. Water-Cooled Segment Chamber

TABLE 3. UNIT 1 SINGLE-PANEL WATER-COOLED SEGMENT, HEAT TRANSFER ANALYSIS RESULTS

Coolant Passage (X=)	Film Coefficient (h_g), Btu/in.^{2}-sec-°F	Local Heat Flux (Q/A), Btu/in.^{2}-sec.	Gas-Wall Temperature (maximum), R	Water Passage Velocity, ft/sec	Water Bulk Temperature, R
0.0	0.00707	33.3	1545	200	600
0.0	0.00834	38.16	1680	200	600
-0.4	0.00582	24.31	1522	200	600
-0.4	0.0078	35.17	1771	200	600
-1.94	0.00413	18.95	1696	100	585
-2.75	0.00263	12.86	1396	100	564

The completed unit 1 segment chamber, which is also typical of units 2 and 4, is shown in Fig. 13. Figure 14 shows the two segment halves prior to and following furnace braze assembly.

The design of unit 4 chamber segment was modified to incorporate a pulse gun for the combustion stability evaluation of the injector-chamber assembly. The pulse gun is shown in Fig. 15. The pulse gun was removable and was in place for stability tests only. The water-cooled plug, shown in Fig. 15, was used during non-pulsing tests to fill the cavity. The other major components (cartridge holder, firing pin assembly, and burst disk retainer) were the same items as used for the previous AMPT program effort (AFRPL-TR-70-127).

The unit 1 chamber was modified during the test program to increase the injector width from 0.500 to 0.600 inch. The chamber was eroded in the upper combustion zone during evaluation of the unit 1 coplanar injector, and the decision was made that an increase in injector width would be evaluated. Evaluation of increased injector element-to-wall spacing, and its effect on performance and heat transfer, was the primary objective. The modification was accomplished by EDM using an electrode machined to provide the desired combustion zone wall convergence angle and injector end width. The modified chamber, unit 1-A, is shown in Fig. 11.

The basic segment chambers had a combustion zone length, L_c, of 3.0 inches. The effect of increased combustion length, i.e., 3.5, 4.0, and 4.5 inches, was one of the items of interest during the development program. The capability to investigate various combustion chamber lengths was provided by use of water-cooled removable spacers. Two water-cooled spacers were provided, 0.500- and 1.00-inch thickness. The spacers incorporated dual O-ring sealing capability and had drilled water-coolant passages.

The spacers were fabricated of OFHC copper and were calorimetry type, so that local heat transfer rates could be obtained. The coolant passages were gun-drilled identical to the segment chamber. A completed spacer is shown in Fig. 16.

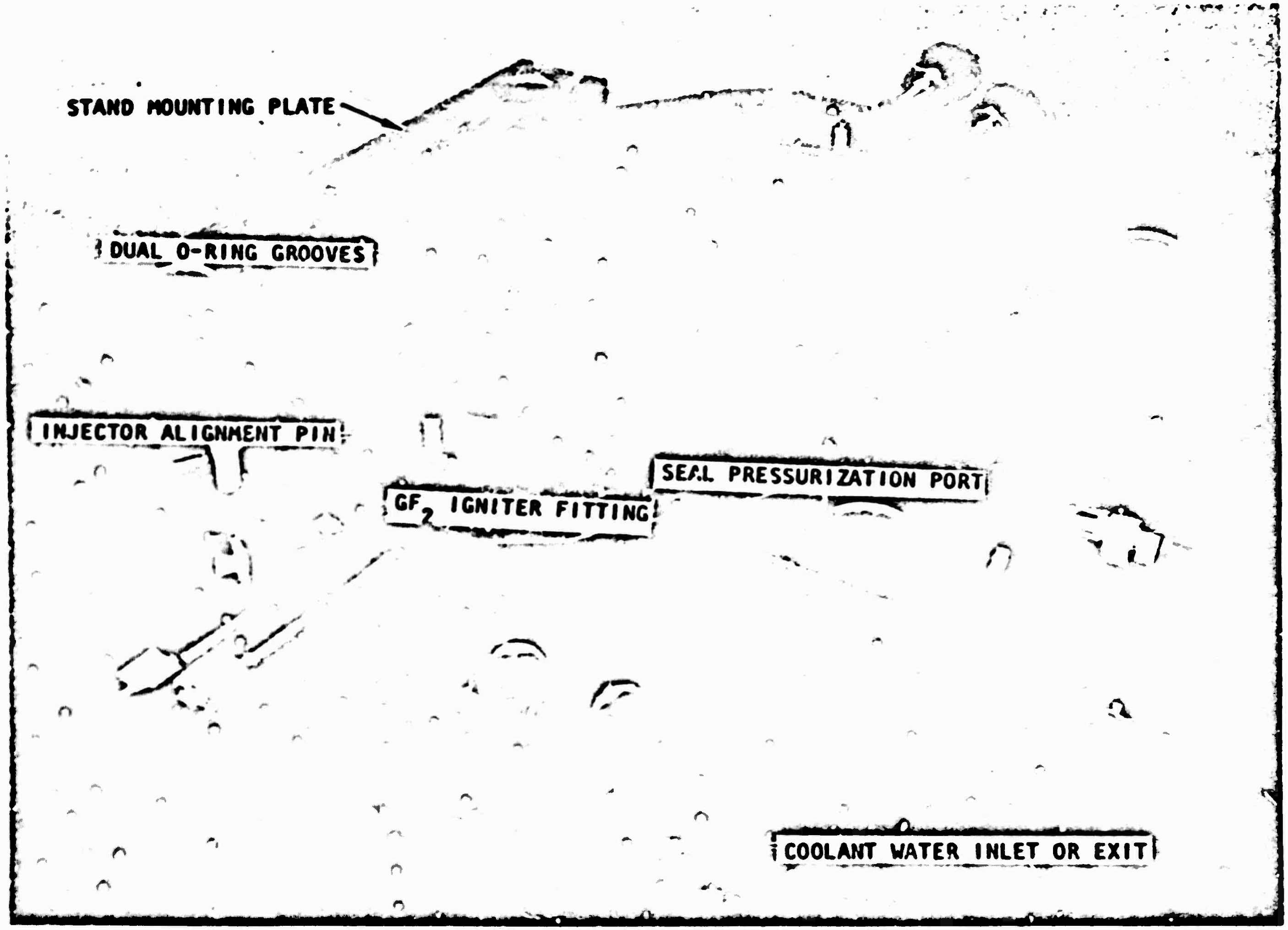

1EH31-1/20/71-C1F

Figure 13. Unit 1 Single-Panel Water-Cooled Segment Chamber, Injector End

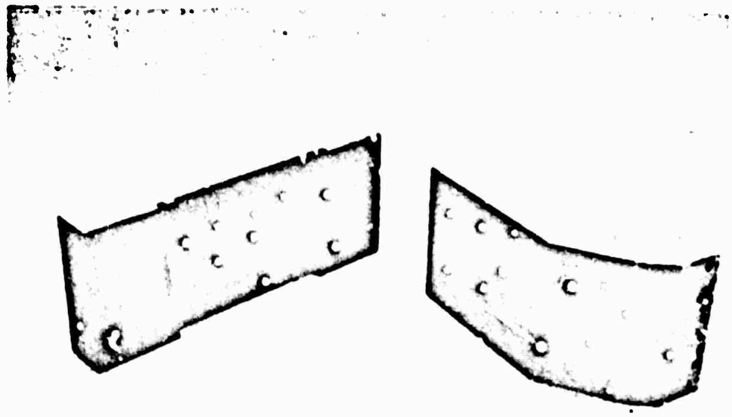

PRE-FURNACE BRAZE ASSEMBLY

POST-FURNACE BRAZE ASSEMBLY

Figure 14. Single-Panel Water-Cooled Segment Chamber

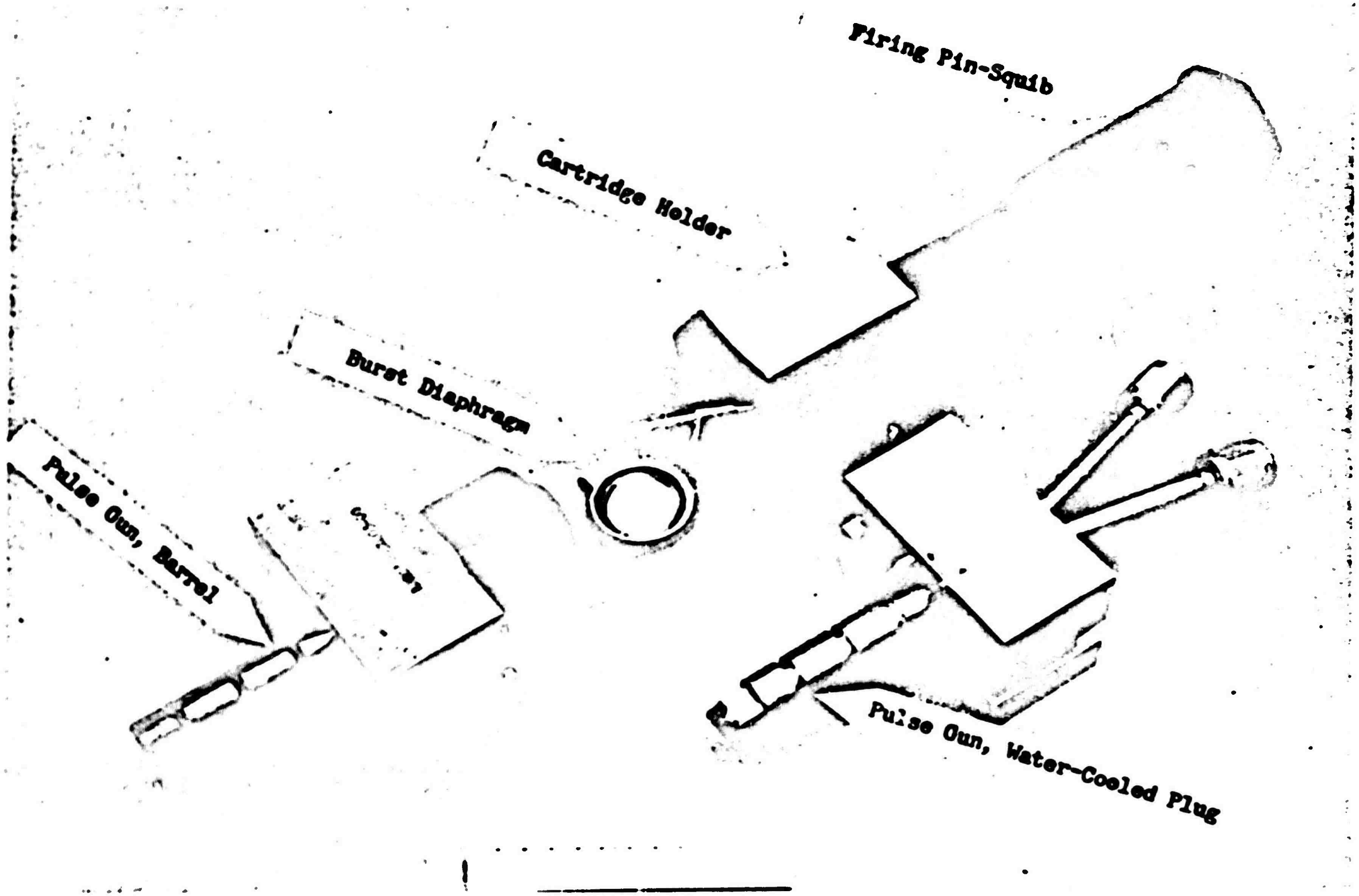

1EH25-12/9/71-1-C2S

Figure 15. Directed Pulse Gun Assembly (Disassembled) and Water-Cooled Pulse Gun Plug

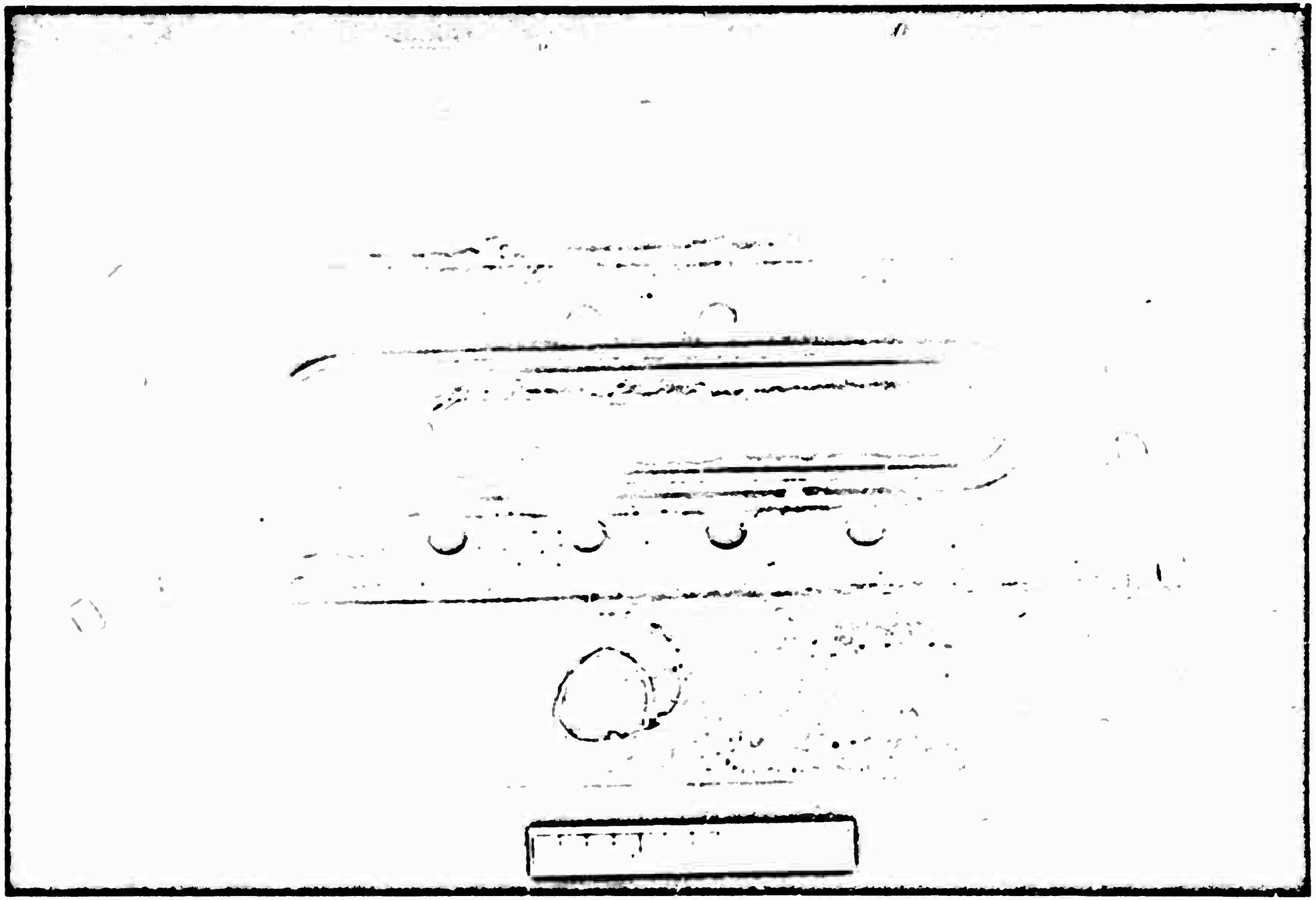

1EH25-12/9/71-1-C3J

Figure 16. Single-Panel Water-Cooled Segment Chamber Spacer for Increased L_c

Following completion of the single-panel segment testing, the spacers were modified and used for the double-panel segment tests. The modifications are described in Section V.

Segment Chamber Unit 3. One additional segment chamber (designated unit 3) was designed and fabricated. The general configuration is presented in Fig. 11 and the detail design criteria in Table 4. The chamber was somewhat different than units 1, 2, and 4. The difference was primarily in throat area and thrust level. Whereas the other chambers (units 1, 2, and 4) were sized for full thrust at 750-psia chamber pressure, unit 3 was sized for full thrust at a chamber pressure of 650 psia. The reason for the lower chamber pressure was that the unit 3 chamber was provided for evaluation of the unit 3 concentric orifice injector which incorporated a different design approach than the initial triplet and coplanar injectors. The Unit 3 injector design was initiated as an IR&D task to provide a fluorine-hydrogen injector with internal heat exchange capability to support the previous AMPT program effort (AFRPL-TR-70-127). Analysis indicated the injector could be used for LO_2-GH_2 and was therefore completed.

The unit 3 chamber design and fabrication were similar to the other water-cooled calorimetry chambers and, though the design chamber pressure was 650 psia, the chamber was tested in excess of 750-psia chamber pressure with no detrimental effects because of the conservative heat transfer design approach.

The chamber segment is shown in Fig. 17. No pulse gun capability was provided in the chamber segment.

Single-Panel-Segment Injectors

Three injector types were selected as having the potential to provide the required c* performance, 97-percent minimum of full shifting c* over the 5:1 throttle range, with satisfactory heat transfer conditions on the combustion chamber. The three types consisted of the coplanar, triplet, and concentric orifice. The single-panel injectors were required to operate with liquid oxygen and gaseous hydrogen.

TABLE 4. DESIGN CRITERIA FOR UNIT 3 WATER-COOLED SEGMENT CHAMBER

DESIGN PARAMETERS	
Chamber Length (side plate-to-side plate at injector end), inch	5.200
Chamber Length (side plate-to-side plate at throat), inch	5.200
Width at Injector End, inch	0.600
Throat gap, inch	0.199
Throat radius, inch	0.870
Contraction Ratio, A_{inj}/A_t	3
Expansion Ratio, Ae/A_t	3.88
Divergent Nozzle Shape	Curved
Combustion Zone Wall Configuration	
Side Plates	Straight, straight
Chamber Walls	Straight, Convergent
Combustion Zone Wall Convergence Half Angle, Degrees	4 degrees 34 min.
Combustion Zone Length, L_c, Injector Face-to-Throat, inch	3.0
Characteristic Chamber Length, L^*, inch	6.05
Chamber Pressure, psia	650

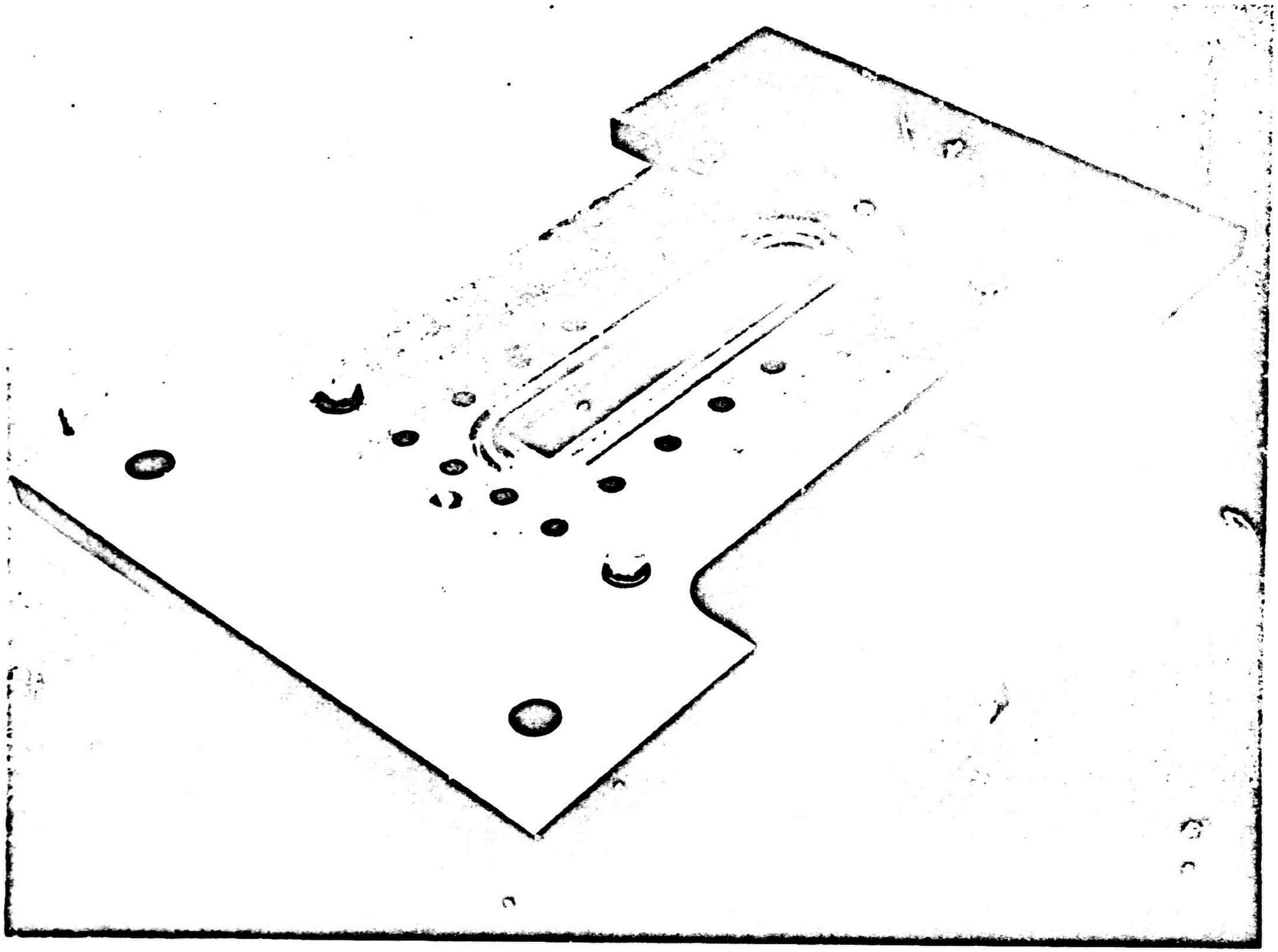

1EH25-12/9/71-C1R

Figure 17. Unit 3 Single-Panel Water-Cooled Segment Chamber

Several modifications were made to each injector during the development program. These modifications and the baseline mechanical design parameters for the injectors are shown in Table 5 and discussed below. Cold-flow testing of the coplanar element was conducted and is discussed in a separate, subsequent section (page 84). Additionally, combustion model analyses, applicable to the coplanar, triplet, and concentric type injectors, were conducted as described later in Appendix I.

Coplanar Injector. Two coplanar injectors, units 1 and 4, were designed and fabricated. The coplanar injector is a superimposed, like-doublet pattern with the oxidizer doublet impinging nearest to the injector face and the fuel doublet impinging further downstream on the same axial line rotated in a plane 90 degrees from the oxidizer orifices. The element is sometimes described as a colinear, biplanar impinging element. The name was shorted to coplanar for convenience.

The element design is illustrated in Fig. 18. The design intent of this injector was to initially atomize the liquid oxygen by direct impingement, and to initiate additional droplet shattering and mixing by entrainment and impingement with the gaseous fuel streams.

Unit 1 Coplanar Injector. The unit 1 coplanar injector incorporated 62 injection elements (as many elements as was practical from a fabrication and feed manifold standpoint) to obtain the minimum thrust per element. The elements were arranged in two staggered rows to provide uniform distribution with minimum overlap of spray patterns. Because the momentum of both propellants was used to promote atomization and mixing, the orifices were sized based on equal pressure drop. Fuel orifices were 0.028-inch diameter and oxidizer orifices were 0.015-inch diameter. All orifices were formed by electrical discharge machining (EDM), and the fuel orifices had a chamfered inlet; however, the oxidizer orifice inlet was inaccessible and was left with a square edge.

The unit 1 coplanar injector was modified to the unit 1-A configuration during the test program (Table 5 and Fig. 18) by increasing all oxidizer orifice diameters to 0.016 inch. This modification was made to determine the effect of decreased oxidizer velocity on performance and heat transfer.

TABLE 5. MECHANICAL DESIGN CHARACTERISTICS OF SINGLE-PANEL INJECTORS

Parameter	Unit 1 Coplanar	Unit 1-A Coplanar	Unit 4 Coplanar	Unit 4-A Coplanar	Unit 4-B Coplanar
Total Orifice Area, in.^{2}					
Fuel	0.0763	0.0763	0.0788	0.1045	0.1208
Oxidizer	0.0219	0.0249	0.0352	0.0352	0.0352
Number of Rows	2 (staggered)	2 (staggered)	2	2	2
Number of Elements	62	62	64	64	62
Injection Density, lb/sec-in.^{2}	0.727/0.145	0.727/0.145	0.727/0.145	0.727/0.145	0.727/0.145
Orifice Diameter, inch					
Fuel	0.028	0.028	0.028	0.028, 0.036	0.028, 0.036, 0.012
Oxidizer	0.015	0.016	0.019	0.019	0.019
Diameter Ratio, D_o/D_f	0.535	0.570	0.680	0.680, 0.528	0.680, 0.528
Number of Orifices					
Fuel	124	124	128	64(0.028),64(0.036)	64(0.028),64(0.036), 116(0.012)
Oxidizer	124	124	128	128	124
Impingement Length-to-Diameter Ratio					
Fuel	6.96	6.96	6.96	6.96	6.96
Oxidizer	4.67	4.39	3.68	3.68	3.68
Included Impingement Angle, degrees					
Fuel	45	45	45	45	45
Oxidizer	60	60	60	60	60
Impingement Distance, inch					
Fuel	0.138	0.138	0.138	0.138	0.138
Oxidizer	0.035	0.035	0.035	0.035	0.035
Fan-to-Wall Angle, degrees	90	90	0	0	0
Element Density, element/sq in.	19.8	19.8	20.4	20.4	19.8
Injection Density, lb/sec per element	0.0367/0.0073	0.0367/0.0073	0.0356/0.0070	0.0356/0.0070	0.0367/0.0073
Element-to-Wall Spacing, inch	0.125	0.125	0.125	0.125	0.125
Thrust per Element, lbf/element	16.13/3.23	16.13/3.23	15.63/3.03	15.63/3.03	16.13/3.23
Combustion Chamber Volume, 3-inch length, cu in.	5.659	5.659	5.659	5.659	5.659

TABLE 5 (Continued)

Parameter	Unit 2 Triplet	Unit 2-A Triplet	Unit 2-B Triplet	Unit 2-C Triplet	Unit 6 Triplet
Total Orifice Area, in.^{2}					
Fuel	0.07897	0.07897	0.0794	0.07897	0.0767
Oxidizer	0.0194	0.02799	0.02799	0.0312	0.02215
Number of Rows	5	5	5	5	6
Number of Elements	110	110	110	110	122
Injection Density, lb/sec-in.^{2}	0.727/0.145	0.727/0.145	0.727/0.145	0.727/0.145	0.727/0.145
Orifice Diameter, inch					
Fuel	0.021	0.021	0.021, 0.012	0.021	0.020
Oxidizer	0.015	0.018	0.018	0.019	0.011, 0.017
Diameter Ratio, D_o/D_f	0.715	0.856	0.856, 1.5	0.905	0.550, 0.850
Number of Orifices					
Fuel	228	228	228(0.021), 44(0.012)	228	244
Oxidizer	110	110	110	110	42(0.011),80(0.017)
Impingement Length-to-Diameter Ratio					
Fuel	6.59	6.59	6.59	6.59	5.20
Oxidizer	8.33	6.95	6.95	6.59	5.40
Included Impingement Angle, degrees					
Fuel	45	45	45	45	60
Oxidizer	0	0	0	0	0
Impingement Distance, inch					
Fuel	0.125	0.125	0.125	0.125	0.104
Oxidizer	0.125	0.125	0.125	0.125	0.09
Fan-to-Wall Angle, degrees	30	30	30	30	0
Element Density, element/sq in.	35.1	35.1	35.1	35.1	39.0
Injection Density, lb/sec/per element	0.0207/0.0041	0.0207/0.0041	0.0207/0.0041	0.0207/0.0041	0.0187/0.0037
Element-to-Wall Spacing, inch	0.120	0.120	0.120	0.120	0.125
Thrust per Element, lbf/element	9.09/1.82	9.09/1.82	9.09/1.82	9.09/1.82	8.20/1.64
Combustion Chamber Volume, 3-inch length, cu in.	5.659	5.659	5.659	5.659	5.659

TABLE 5 (Concluded)

Parameter	Unit 3 Concentric	Unit 7-0.006 Concentric	Unit 7-0.008 Concentric	Unit 7-A Concentric	Unit 7-D Concentric
Total Orifice Area, in.^{2}					
Fuel	0.1402	0.10028	0.1385	0.1152	0.2105
Oxidizer	0.0840	0.08125	0.08125	0.06757	0.11943
Number of Rows	3	3	3	3	3
Number of Elements	96	95	95	79	66
Injection Density, lb/sec-in.^{2}	1.13/0.225	0.727/0.145	0.727/0.145	0.727/0.145	0.727/0.145
Orifice Diameter, inch					
Fuel	0.008 annulus	0.006 annulus	0.008 annulus	0.008 annulus	0.0155 annulus
Oxidizer	0.0334	0.033	0.033	0.033	0.033
Diameter Ratio, D_o/D_f	---	---	---	---	---
Number of Orifices					
Fuel	96	95	95	79	66
Oxidizer	96	95	95	79	66
Impingement Length-to-Diameter Ratio					
Fuel	0	0	0	0	0
Oxidizer	0	0	0	0	0
Included Impingement Angle, degrees					
Fuel	0	0	0	0	0
Oxidizer	0	0	0	0	0
Impingement Distance, inch					
Fuel	0	0	0	0	0
Oxidizer	0	0	0	0	0
Fan-to-Wall Angle, degrees	0	0	0	0	0
Element Density, element/sq in.	30.4	30.3	30.3	25.2	19.1
Injection Density, lb/sec per element	0.0329/0.0066	0.0230/0.0048	0.0239/0.0048	0.0288/0.0058	0.0344/0.0069
Element-to-Wall Spacing, inch	0.100	0.090	0.090	0.090	0.090
Thrust per Element, lbf/element	14.06/2.80	10.5/2.11	10.5/2.11	12.6/2.54	15.1/3.04
Combustion Chamber Volume, 3-inch length, cu in.	12.60	5.659	5.659	5.659	5.659

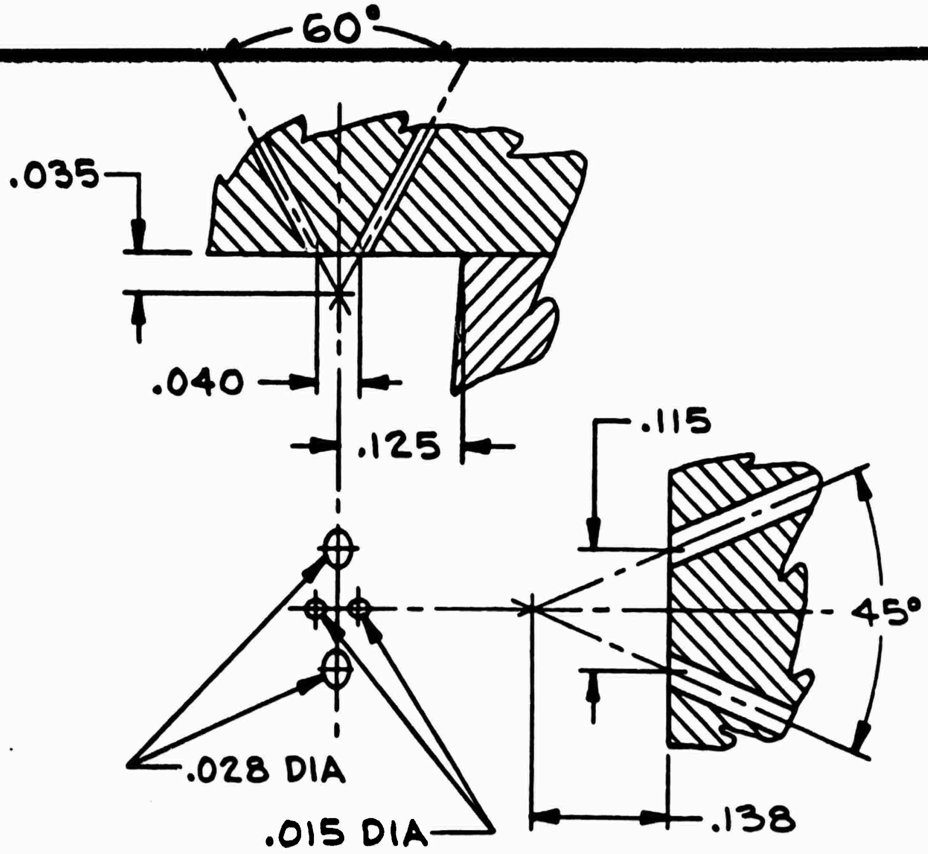

U/N 1

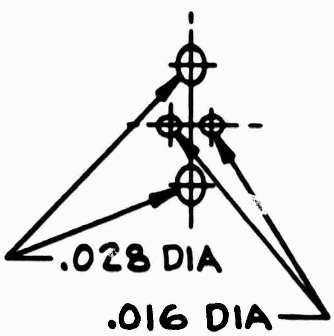

U/N 1A

Figure 18. Unit 1 and 1A Coplanar, Single-Panel Injector, Injection Element Configurations

Unit 4 Coplanar Injector. The unit 4 coplanar injector incorporated 64 injection elements. These elements were arranged in two rows and the elements were identical to the unit 1 elements except for an increased oxidizer orifice diameter (0.019 inch). The elements also were rotated 90 degrees in the injector face plane, so that the oxidizer would not impinge directly on the walls, as was the case with unit 1. The unit 4 coplanar design is shown in Fig. 19 through 21.

The unit 4 coplanar injector was modified to the unit 4A configuration (Table 5 and Fig. 19) by increasing the outboard fuel orifice (closest to combustor wall) diameter to 0.036 inch to provide additional mass flow adjacent to the chamber walls. A final modification, unit 4B configuration, was made to provide fuel fans adjacent to the walls. The modification, shown in Fig. 19, consisted of EDM of two adjacent, 0.012-inch-diameter holes and connecting them by an EDM slot to form a fan. This configuration was not tested.

Coplanar Injector Fabrication. The coplanar injectors were fabricated from single-piece OFHC copper forgings. All manifolding was internal, with EB weld-attached fuel and oxidizer manifold closures. The most critical manufacturing operation was the orifice drilling. Because injector performance was very dependent on the accuracy and quality of the injector orifices, all impinging-type injectors fabricated during the program utilized electrical discharge machining to produce the orifices. A special bushing was used to guide the electrode and ensure accurate location of the orifices and desired impingement angle. Each orifice of an element, e.g., four per coplanar and three per triplet element, were machined with one setup. The bushing was not moved until the element was complete. The results obtained through use of this technique were excellent. No furnace brazing was used during the manufacture of the injectors and, with the exception of the orifice EDM, all machining was conventional. The completed units 1 and 4 coplanar injectors are shown in Fig. 22 and 23.

Following completion of fabrication, the injectors were water-flow tested for calibration of flow pressure drop characteristics and visual evaluation of element flow characteristics. Filtered (40-micron) water was utilized for calibration of both fuel and oxidizer orifices. The flow was discharged to ambient pressure. The fuel orifices also were flow tested with gaseous nitrogen.

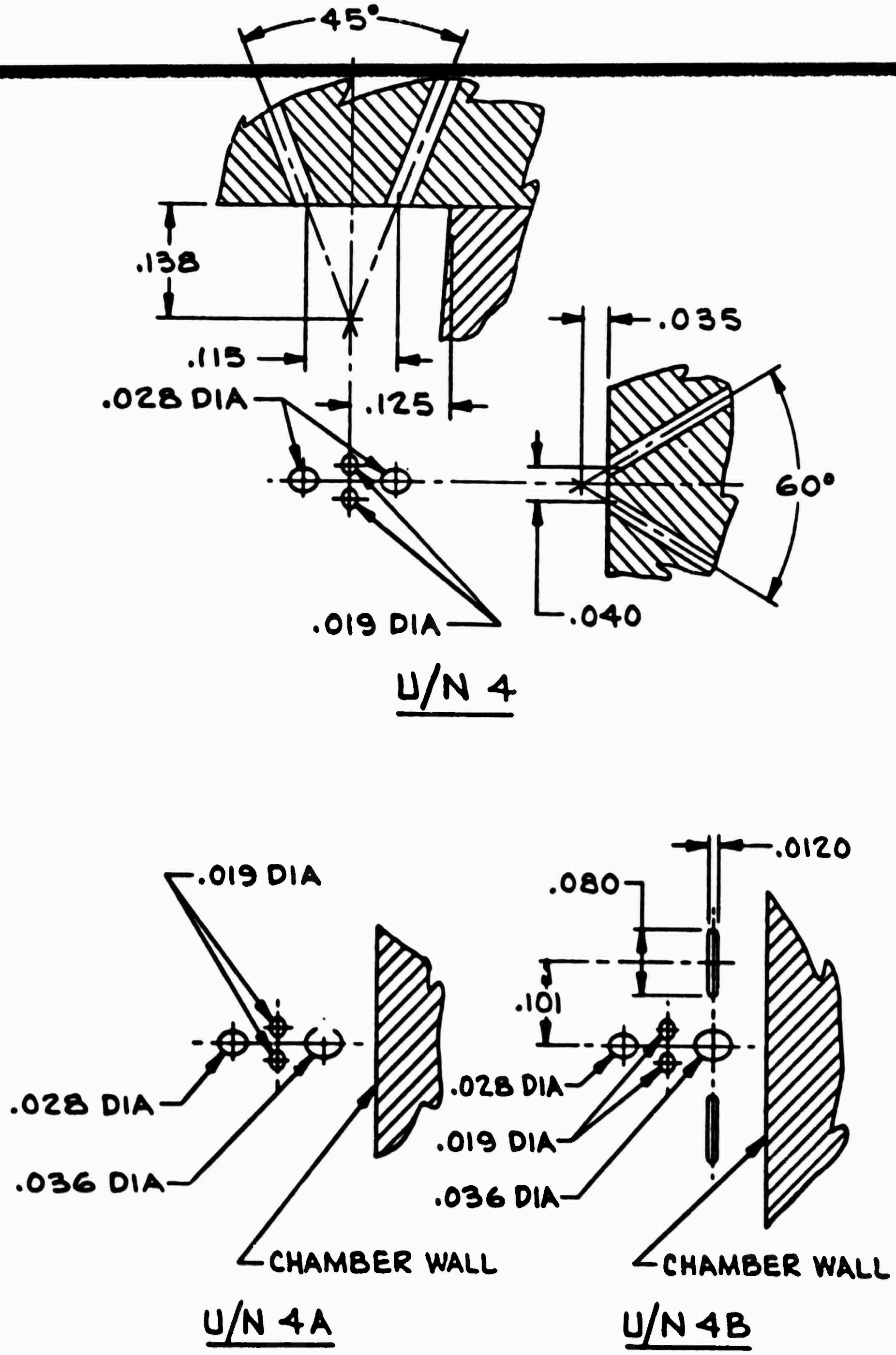

Figure 19. Unit 4 Coplanar, Single-Panel Injector, Injection Element Configurations

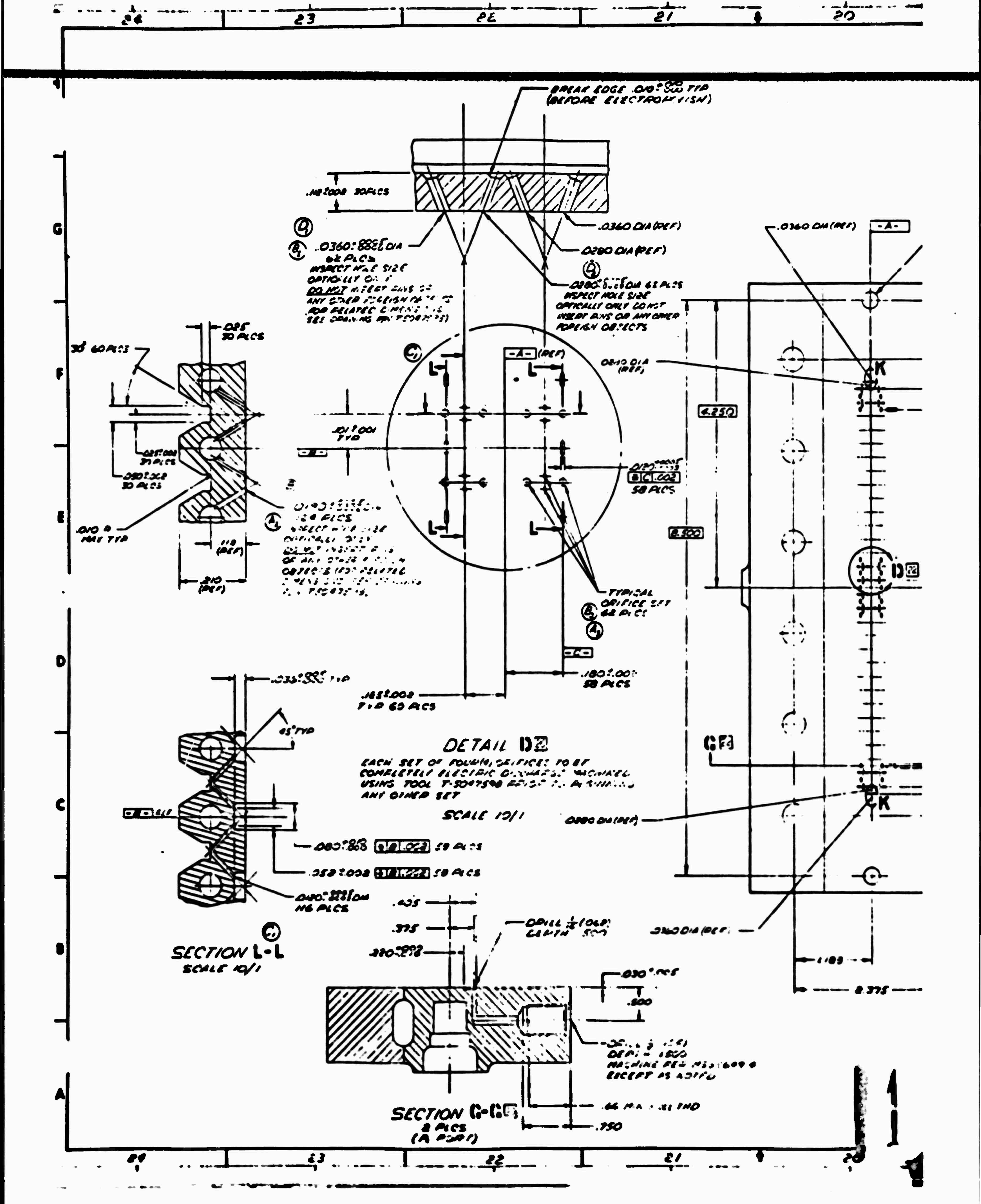

BREAK EDGE .010 TYP (BEFORE ELECTROPOLISH)
.0360 DIA (REF)
.0280 DIA (REF)
62 PLCS
INSPECT HOLE SIZE OPTICALLY ONLY
DO NOT INSERT PINS OR ANY OTHER FOREIGN OBJECTS
TYPICAL ORIFICE SET 62 PLCS
.180±.001 58 PLCS
DETAIL D
EACH SET OF FOUR(4) ORIFICES TO BE COMPLETELY ELECTRIC DISCHARGE MACHINED USING TOOL
ANY OTHER SET
SCALE 10/1
SECTION L-L
SCALE 10/1
SECTION G-G
2 PLCS
(A PORT)
4.250
8.500
1.183
8.375
.750

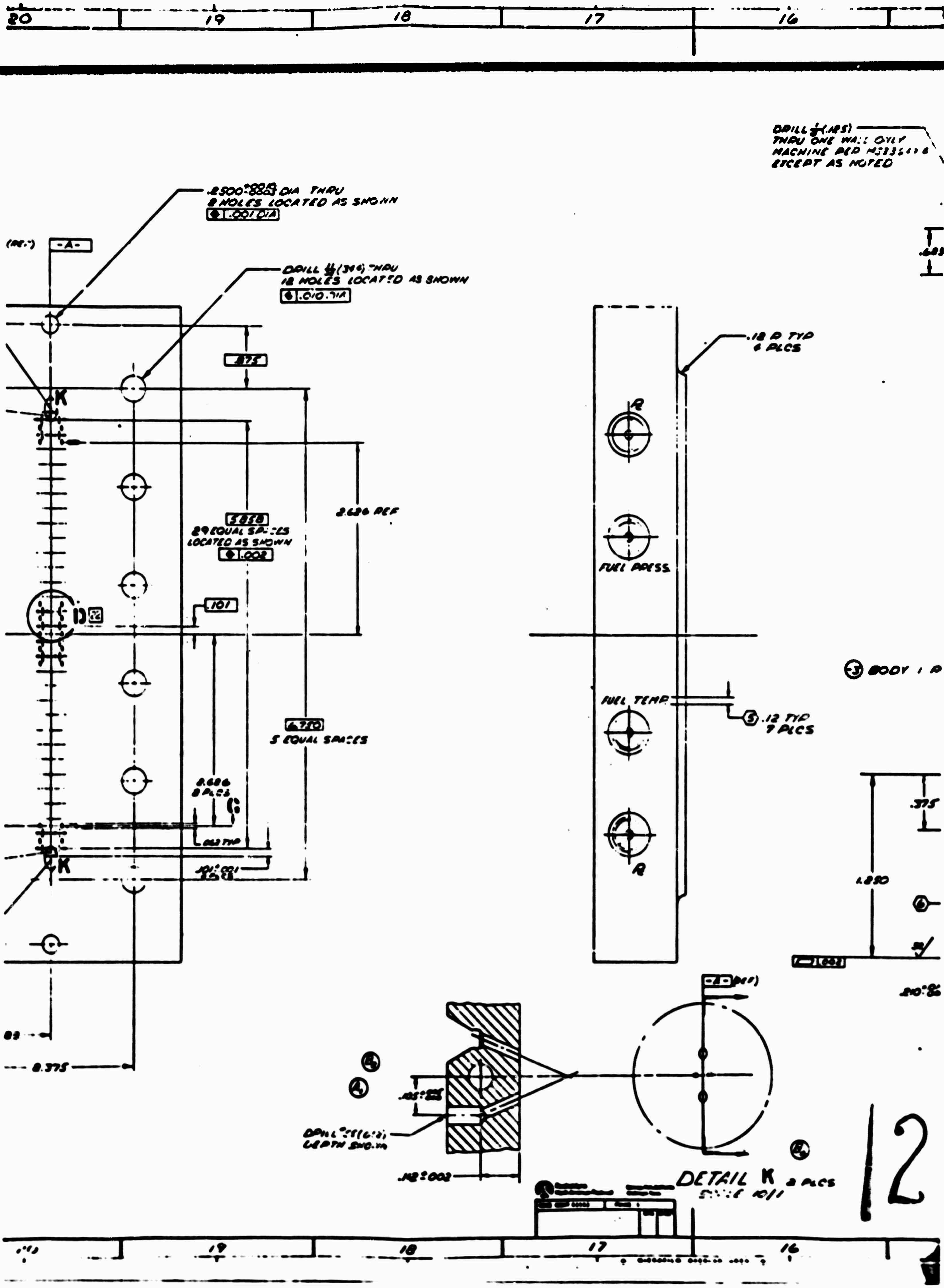
DRILL 1/8 (.125)
THRU ONE WALL ONLY
MACHINE PER
EXCEPT AS NOTED
DIA THRU
2 HOLES LOCATED AS SHOWN
-A-
HOLES LOCATED AS SHOWN
.375
2.626 REF
29 EQUAL SPACES
LOCATED AS SHOWN
.101
5 EQUAL SPACES
8 PLCS
.18 R TYP
4 PLCS
FUEL PRESS
FUEL TEMP
.12 TYP
7 PLCS
BODY
.375
1.890
8.375
DEPTH SHOWN
DETAIL K 2 PLCS
12

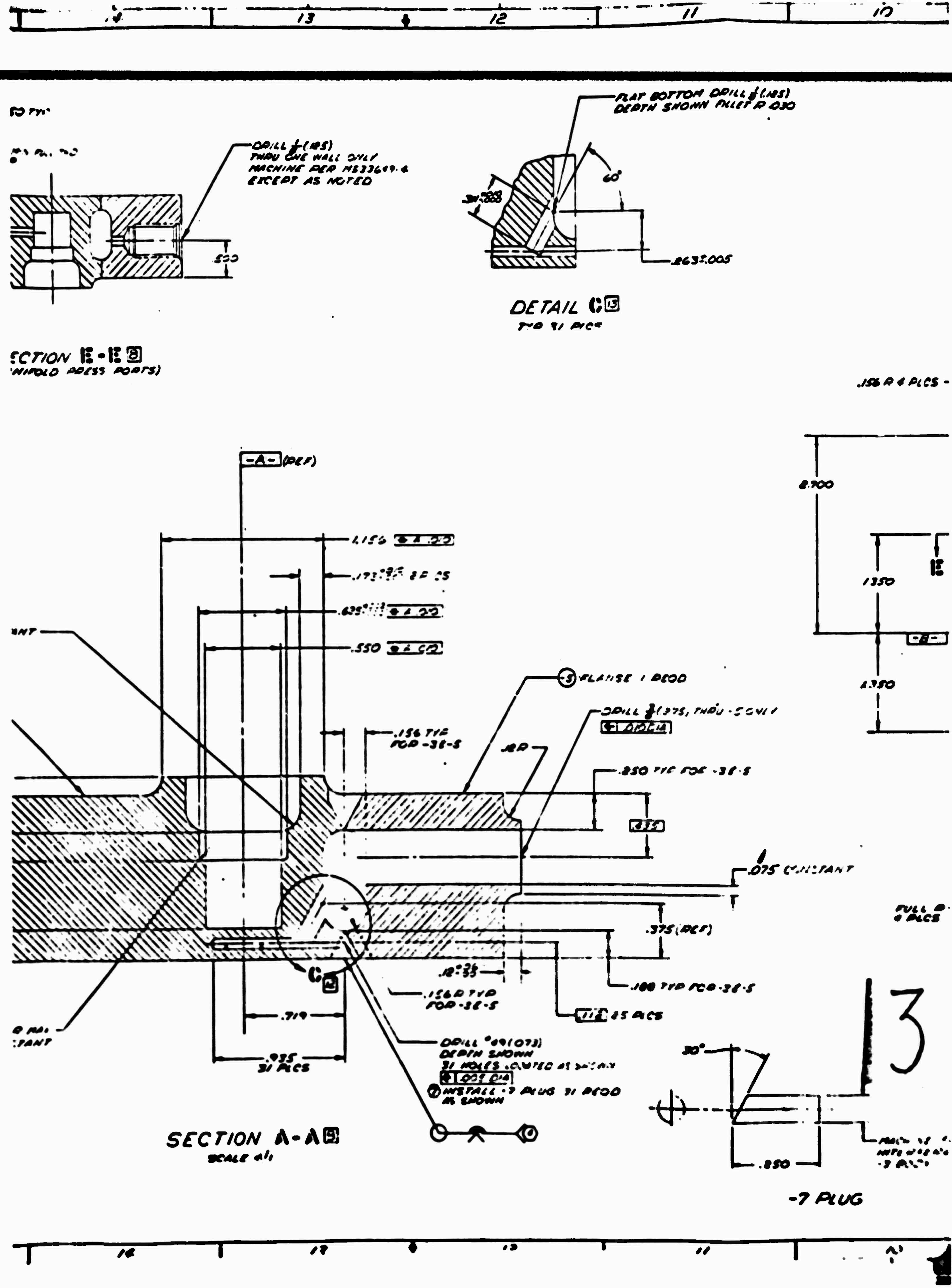
DRILL 1/4(.185) THRU ONE WALL ONLY MACHINE PER MS33649-4 EXCEPT AS NOTED
.500
SECTION E-E
FLAT BOTTOM DRILL (.185) DEPTH SHOWN FILLET R .030
60°
.263±.005
DETAIL C
.156 R 4 PLCS
-A- (REF)
1.156
.550
2.900
1.350
-B-
FLANGE 1 REQD
.156 TYP FOR -38-S
.850 TYP FOR -38-S
.075 CONSTANT
.375 (REF)
.156 R TYP FOR -38-S
.100 TYP FOR -38-S
25 PLCS
.719
.935
31 PLCS
DRILL #49(.073) DEPTH SHOWN
31 HOLES LOCATED AS SHOWN
INSTALL -7 PLUG 31 REQD AS SHOWN
SECTION A-A
SCALE 4/1
30°
.850
-7 PLUG
13

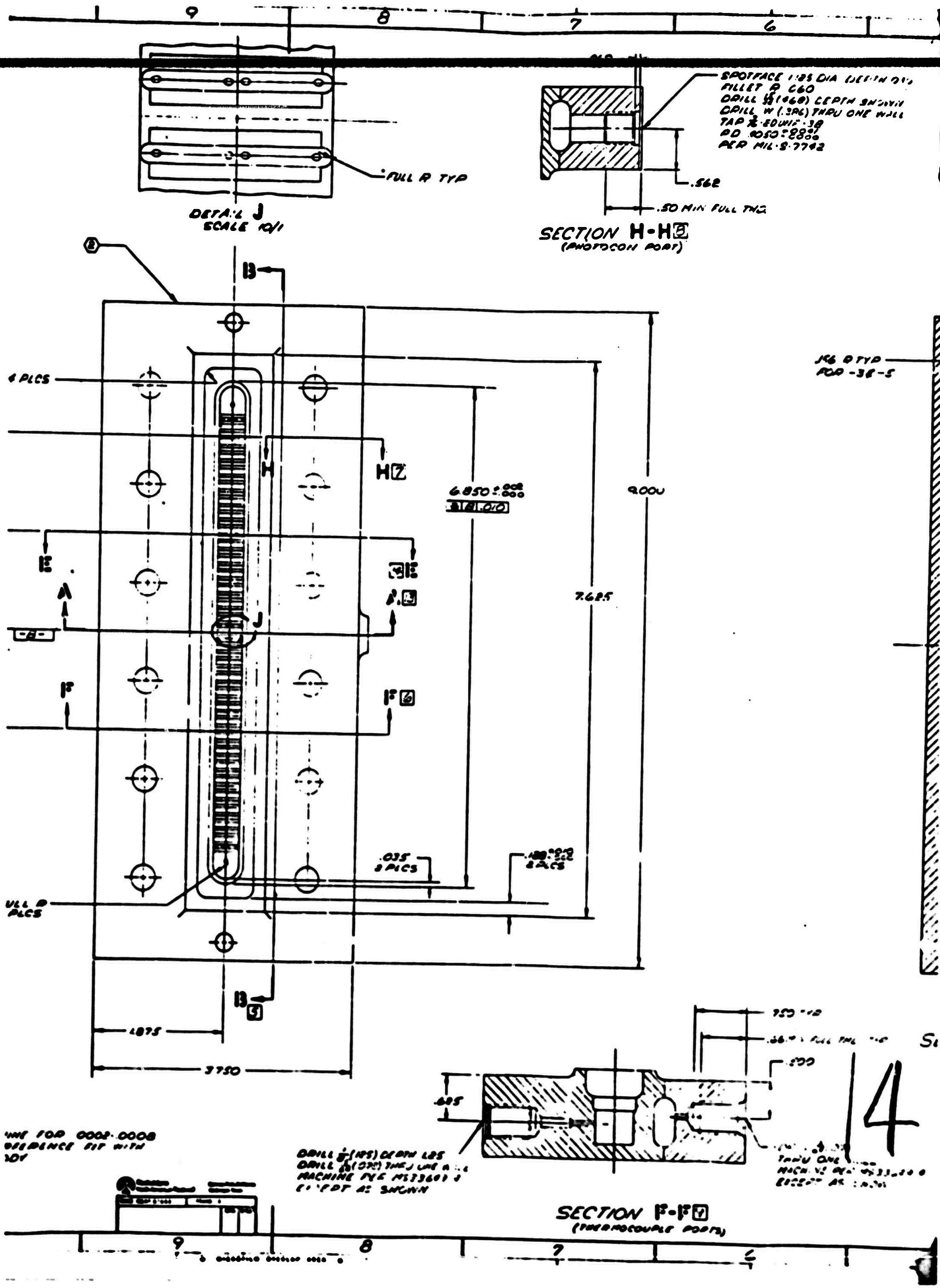

DETAIL J
SCALE 10/1
FULL R TYP
SPOTFACE 1.25 DIA
FILLET R .060
TAP
PER MIL-S-7742
.562
.50 MIN FULL THD
SECTION H-H
(PHOTOCON PORT)
4 PLCS
6.850
9.000
7.625
.035
2 PLCS
FULL R
1.875
3.750
.685
SECTION F-F
(THERMOCOUPLE PORTS)
THRU ONE
14

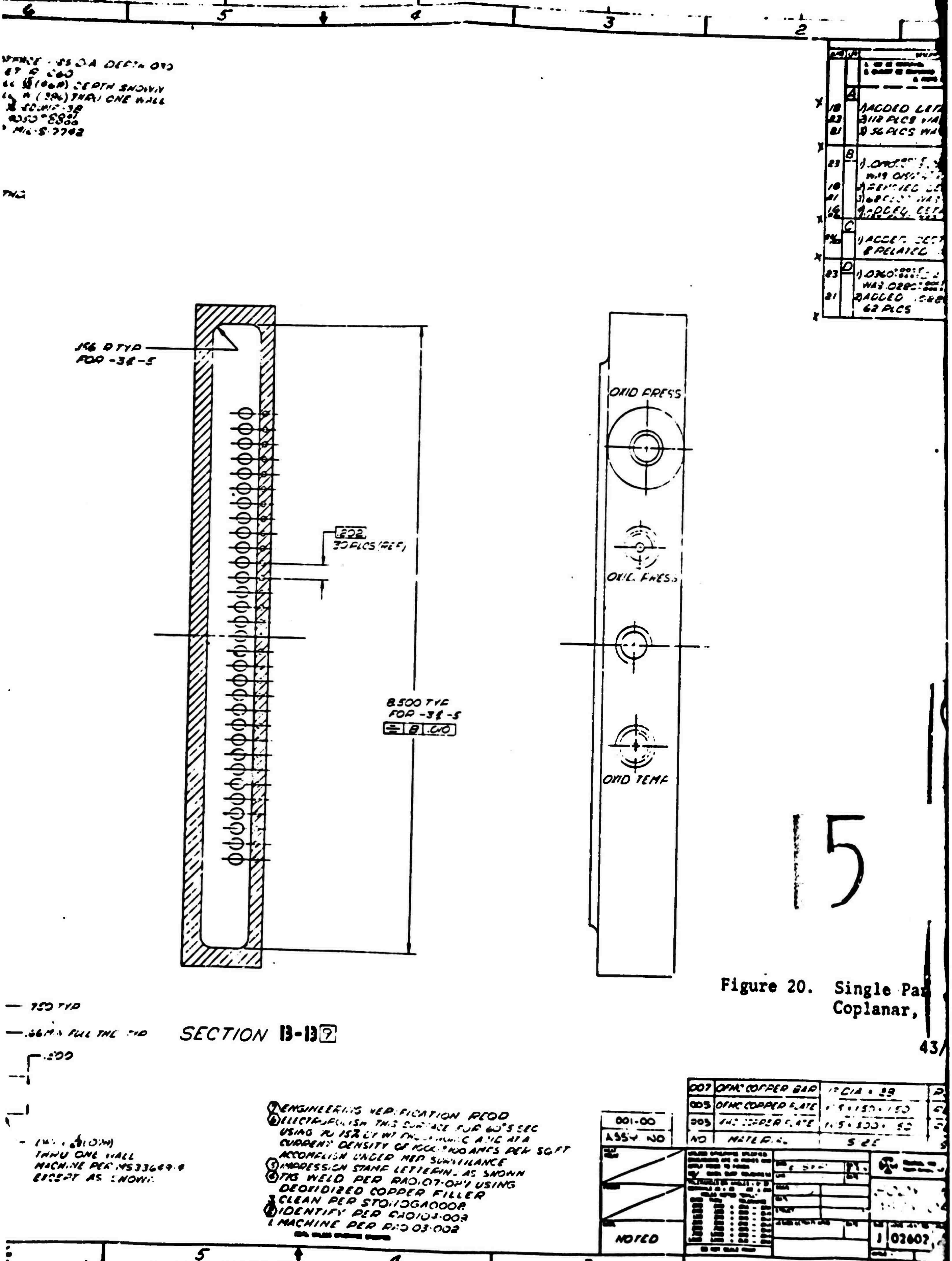

Figure 20. Single Pa
Coplanar,

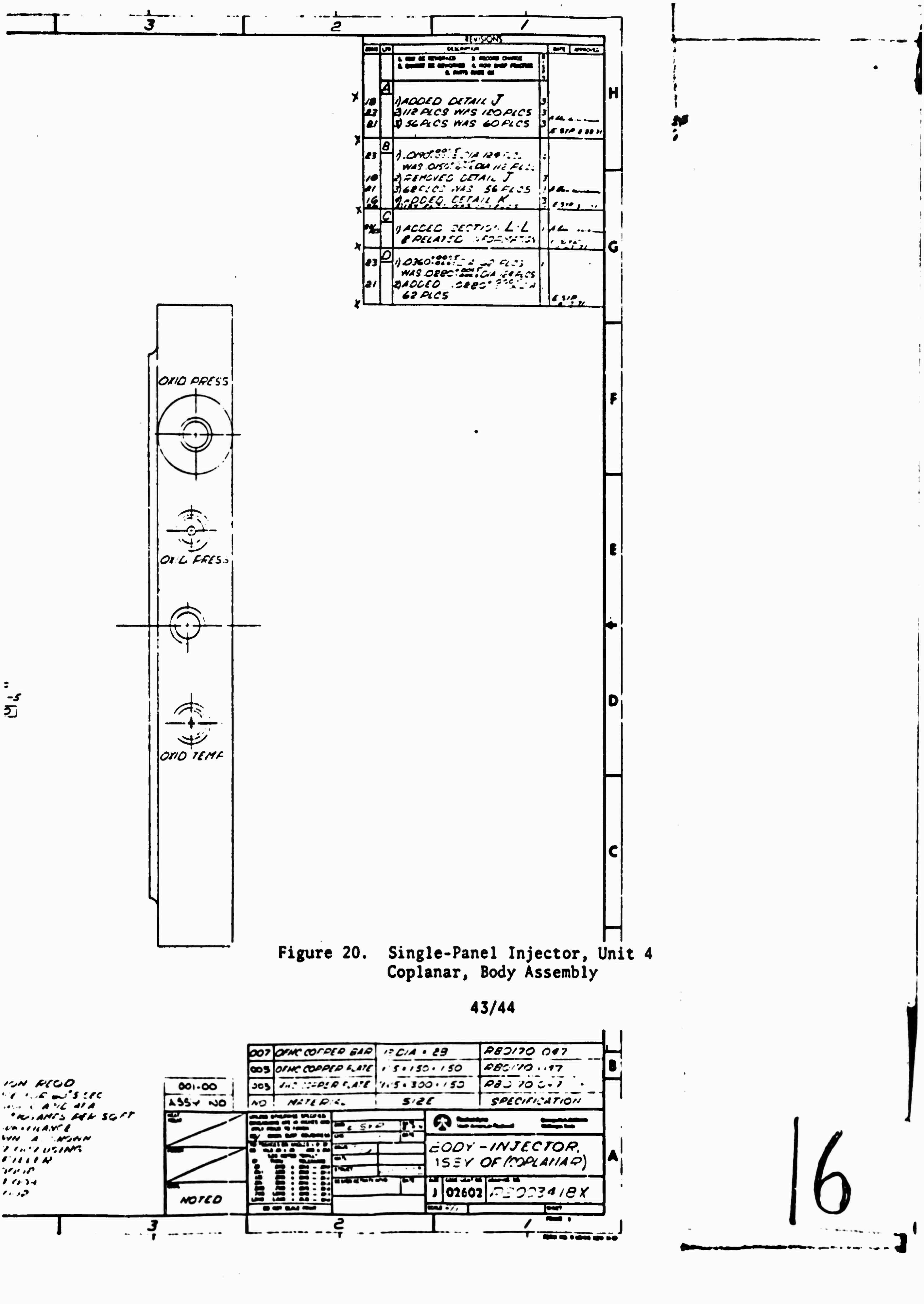

Figure 20. Single-Panel Injector, Unit 4 Coplanar, Body Assembly

H

G

F

E

D

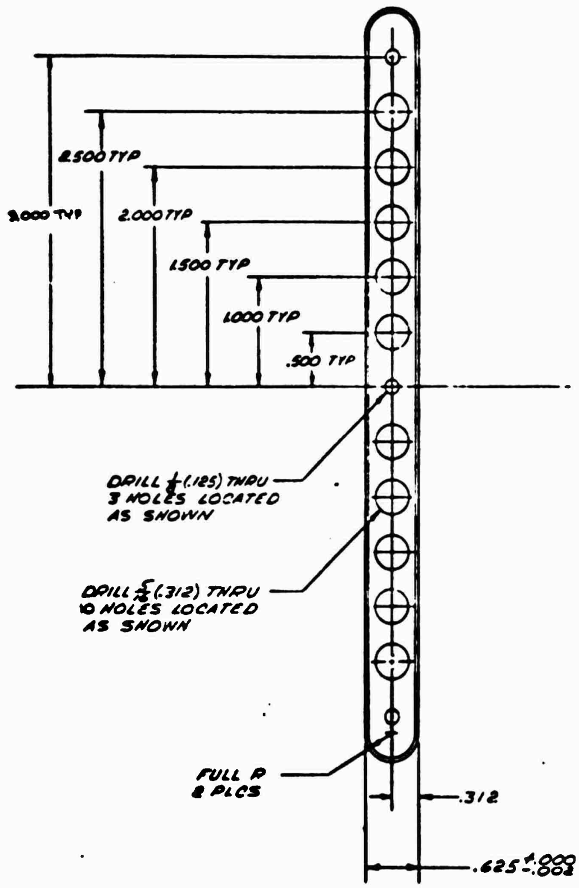

C

—13 D

B

A

24 21 20

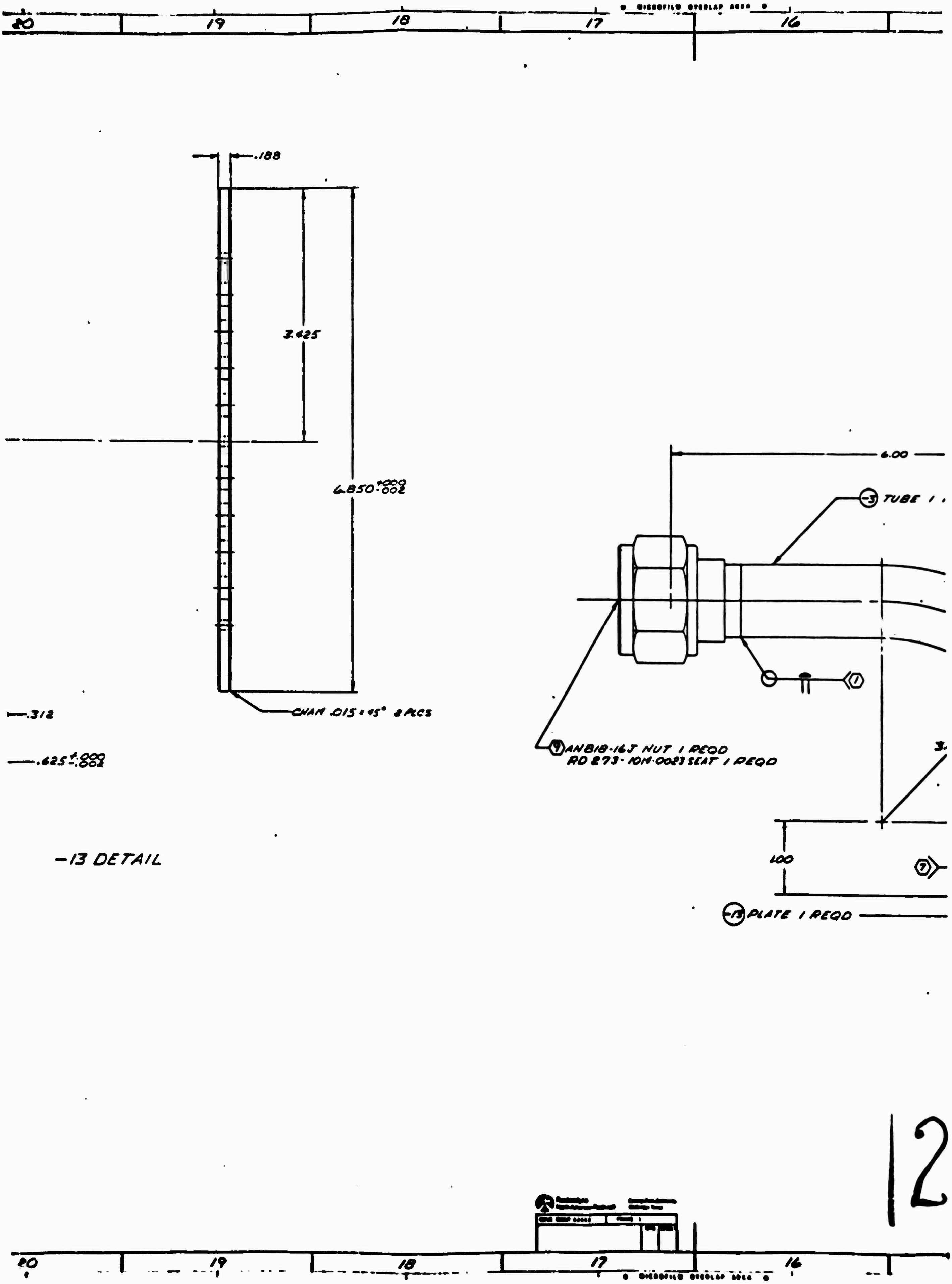
20
19
18
17
16
.188
3.425
6.850 +.000 -.002
CHAM .015 x 45° 2 PLCS
.312
.625 +.000 -.002
-13 DETAIL
6.00
-3 TUBE 1
9 AN818-16J NUT 1 REQD
RD 273-1014-0023 SEAT 1 REQD
1
7
100
-13 PLATE 1 REQD

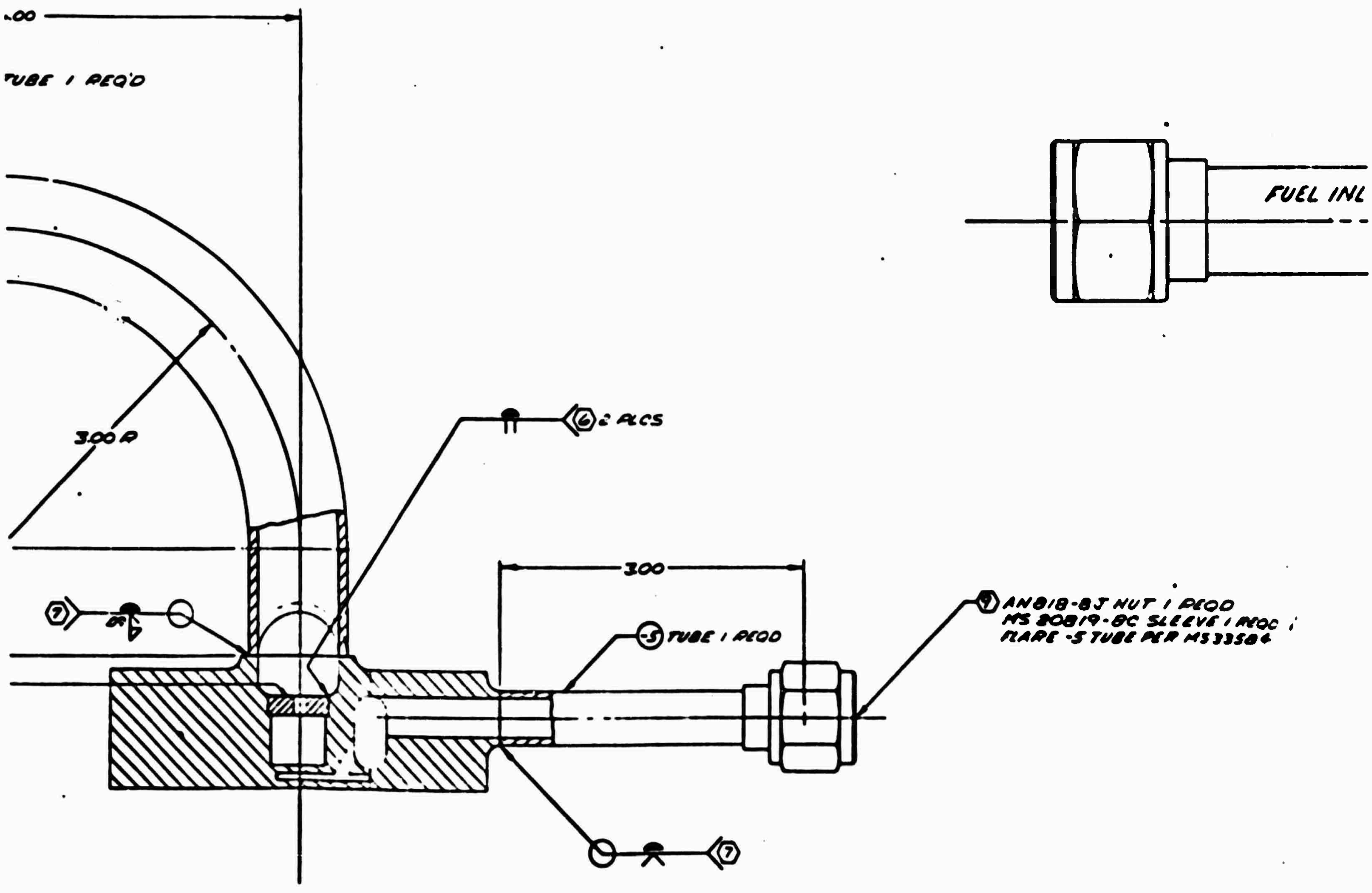
.00
TUBE 1 REQ'D
300 R
6 2 PLCS
7
300
-5 TUBE 1 REQD
9 AN818-8J NUT 1 REQD
MS 20819-8C SLEEVE 1 REQD
FLARE -5 TUBE PER MS33584
FUEL INL
7

SECTION A-A

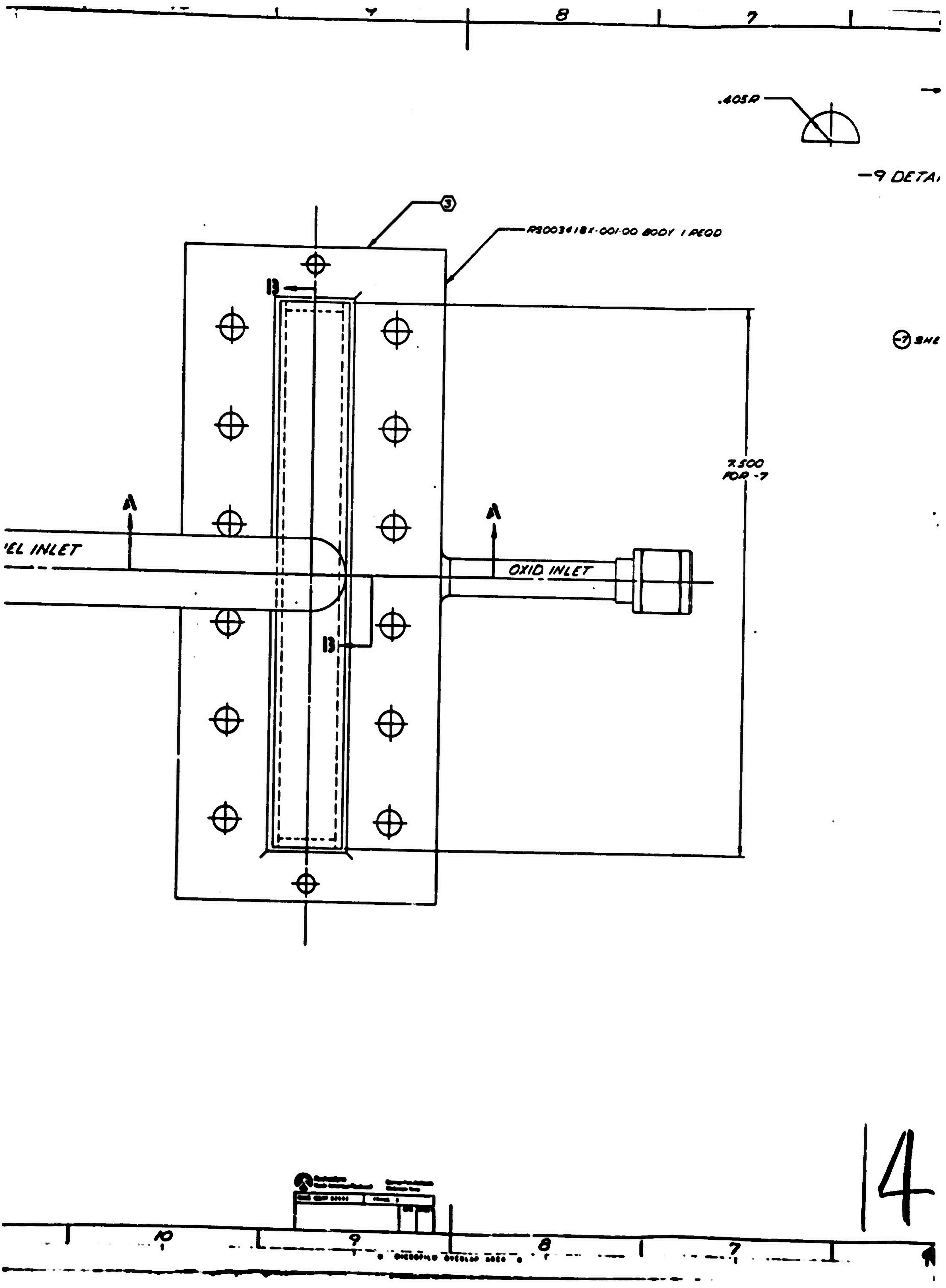
.405R
-9 DETA
BODY 1 REQD
7.500
FOR -7
OXID INLET
A
A
B
B
3

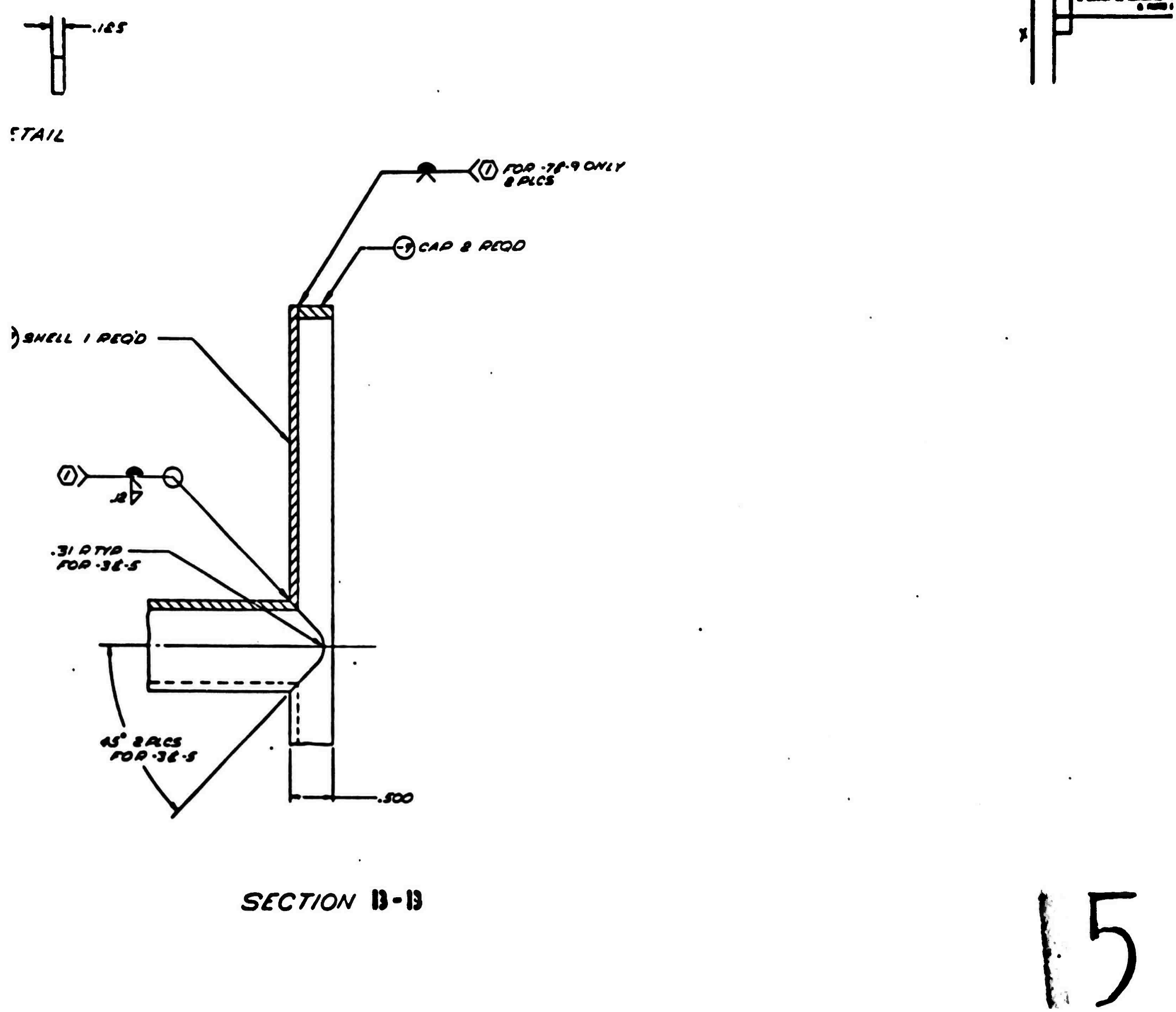

Figure 21. Single-Panel Inj
Coplanar, Assemb

45/46

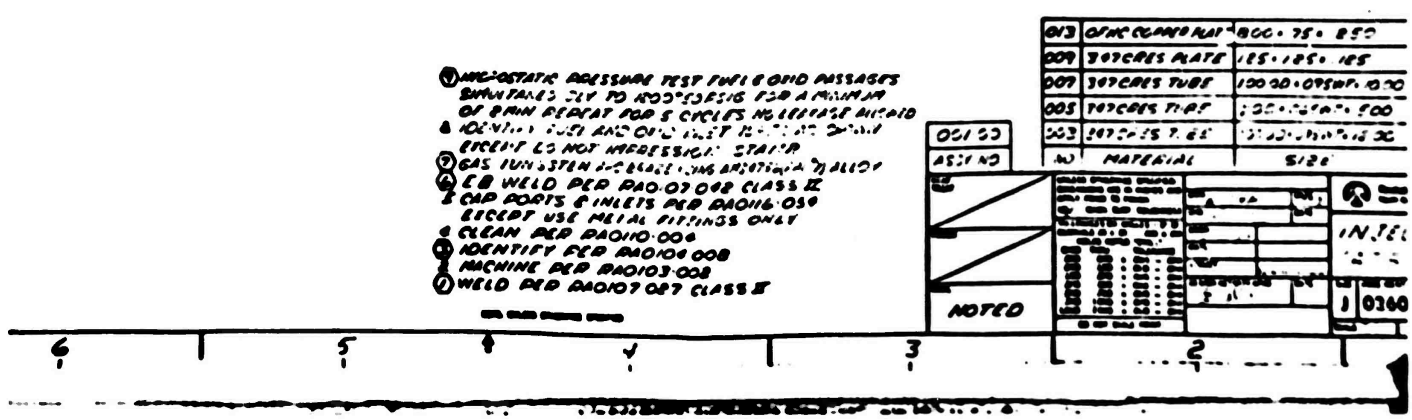

Figure 21. Single-Panel Injector, Unit 4
Co lanar, Assembly

NO	MATERIAL	SIZE	SPECIFICATION
013	OFHC COPPER PLATE	.800 × .75 × .850	RB0170-007
009	307 CRES PLATE	.125 × .125 × .125	[illegible]
007	307 CRES TUBE	.100 OD × .095 WT × 1.000	MIL-T-[illegible]
005	307 CRES TUBE	[illegible] × 5.00	MIL-T-[illegible]
003	307 CRES TUBE	[illegible] × 18.00	MIL-T-[illegible]

ASSY NO

NOTED

INJECTOR COPLANAR
(ASSY OF)

J 02602

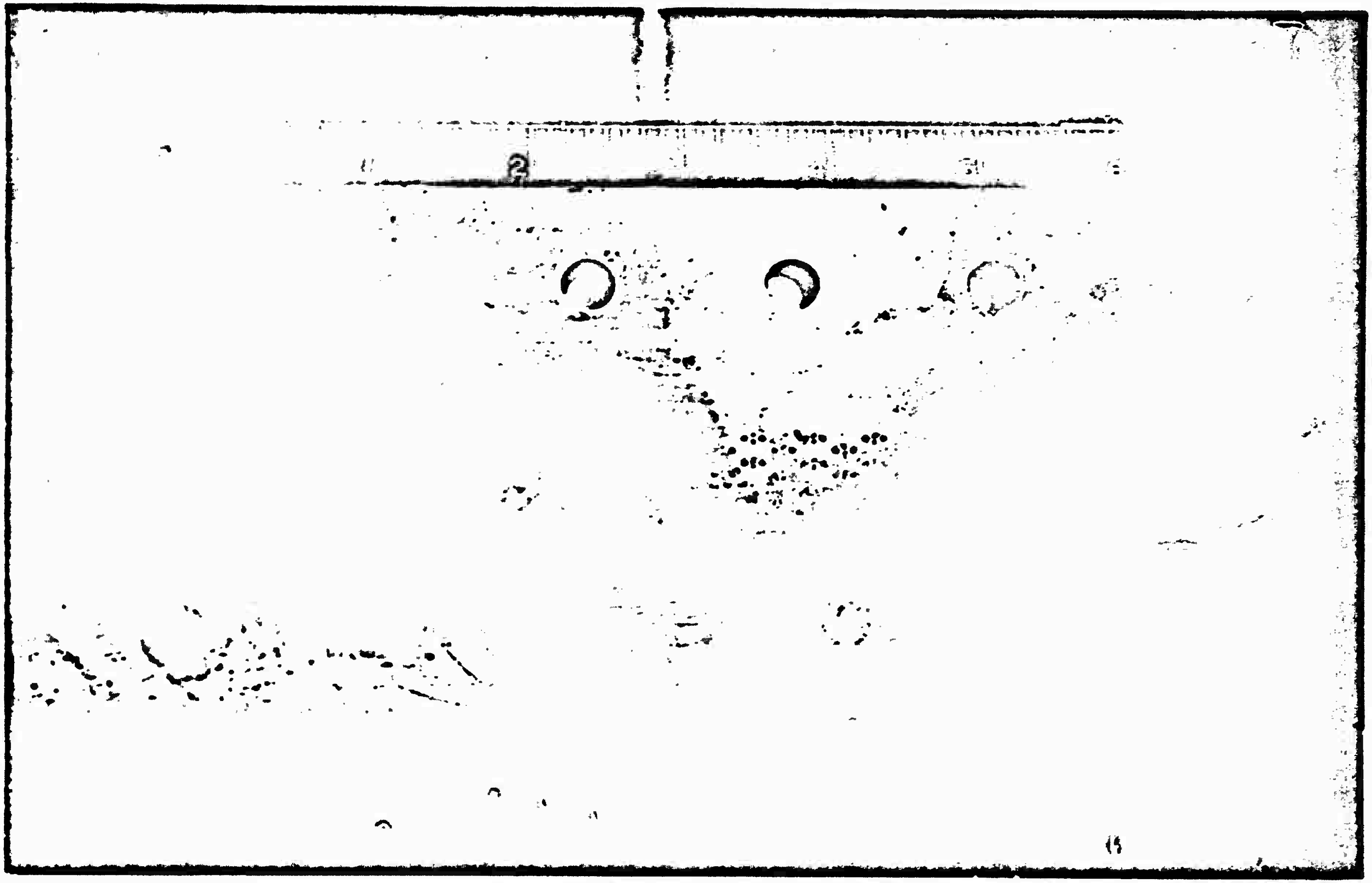

5AA34-2/3/71-S1B

Figure 2? Completed Unit 1 Single-Panel Coplanar Injector

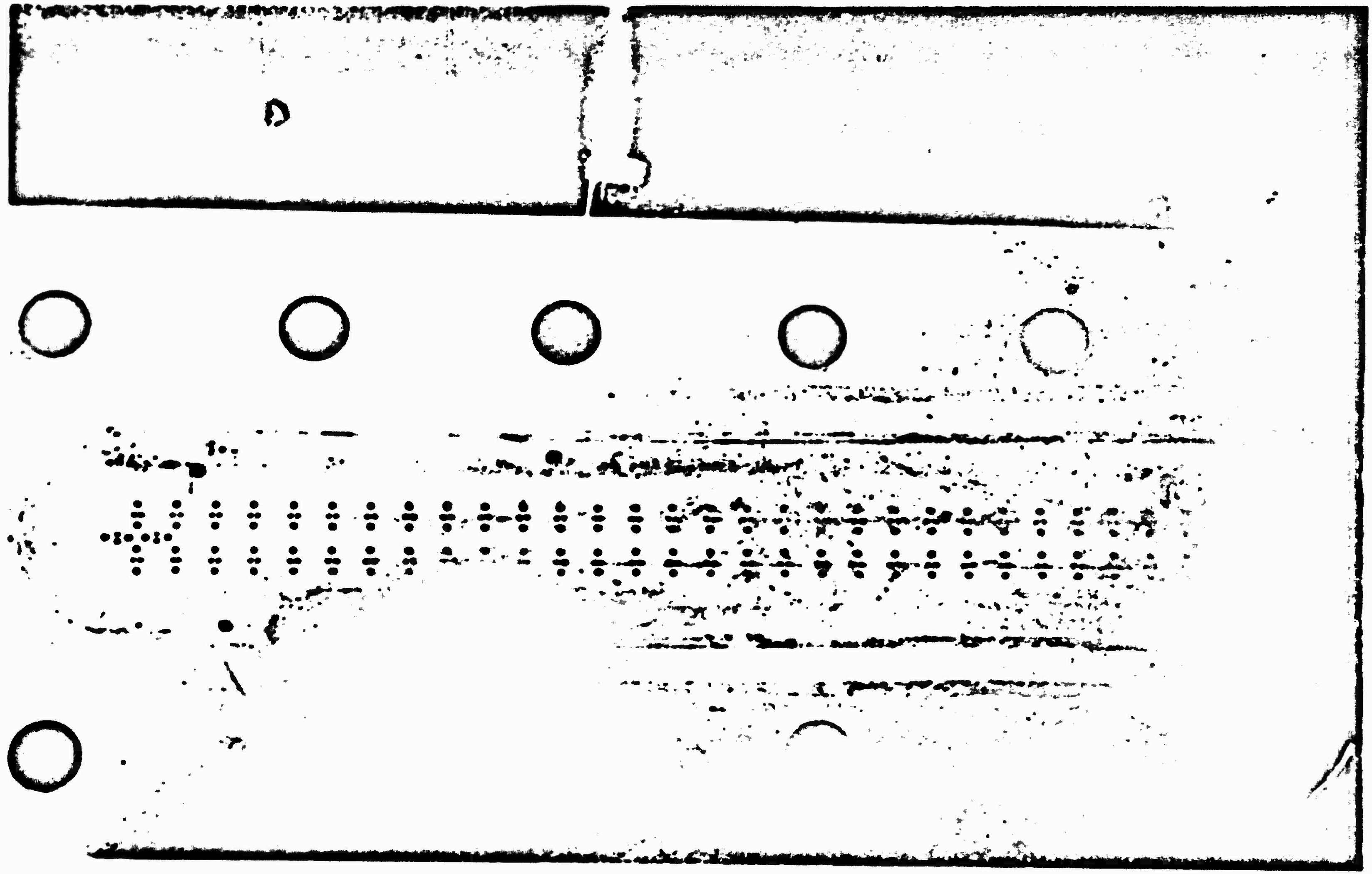

1EH44-3/9/71-C1E

Figure 23. Completed Unit 4 Coplanar Injector

A typical flow test is shown in Fig. 24, with predicted propellant flow pressure loss characteristics based on the water-flow tests (Fig. 25 and 26). Injector hot-fire pressure drop data were predicted using the cold-flow calibration data and a computer flow model program. The output values of pressure drop from the computer models were used for plotting the predicted injector flow characteristics shown in Fig. 25 and 26.

Visually, the stream patterns with the coplanar injector were very good, with well-formed "fans" and well-atomized streams. Impingement points for both oxidizer and fuel doublets were properly located and no significant fan distortion was noted, indicating accurate alignment of streams.

Triplet Injector. The triplet injector was a hydrogen-oxygen-hydrogen configuration, as shown in Fig. 27 through 29. This pattern was selected because the axial oxidizer injection was expected to avoid combustion chamber wall problems with the direct-impinging fuel, promoting mixing and atomization. Elements were arranged 22 per row, in 5 rows, for a total of 110 elements. Two additional, fuel-only elements were located at each end of the combustion chamber to protect the segment chamber side plates. The elements were canted at 30 degrees, in relationship to the chamber walls, to avoid edge impingement between adjacent rows of elements.

The fuel orifices were 0.0205-inch diameter and oxidizer orifices were initially 0.015-inch diameter. The orifices were formed by EDM and the oxidizer orifices had chamfered, step-drilled inlets. The fuel orifice entrances were inaccessible for chamfering. The injector design is shown in Fig. 28 and 29.

One triplet injector (unit 2) was designed and fabricated. Several modifications were made to the unit 2 injector during the test program, and these are shown in Fig. 27. Modification 2A increased the oxidizer orifice size from 0.015 to 0.018 inch for evaluation of decreased oxidizer injection velocity on performance and heat transfer.

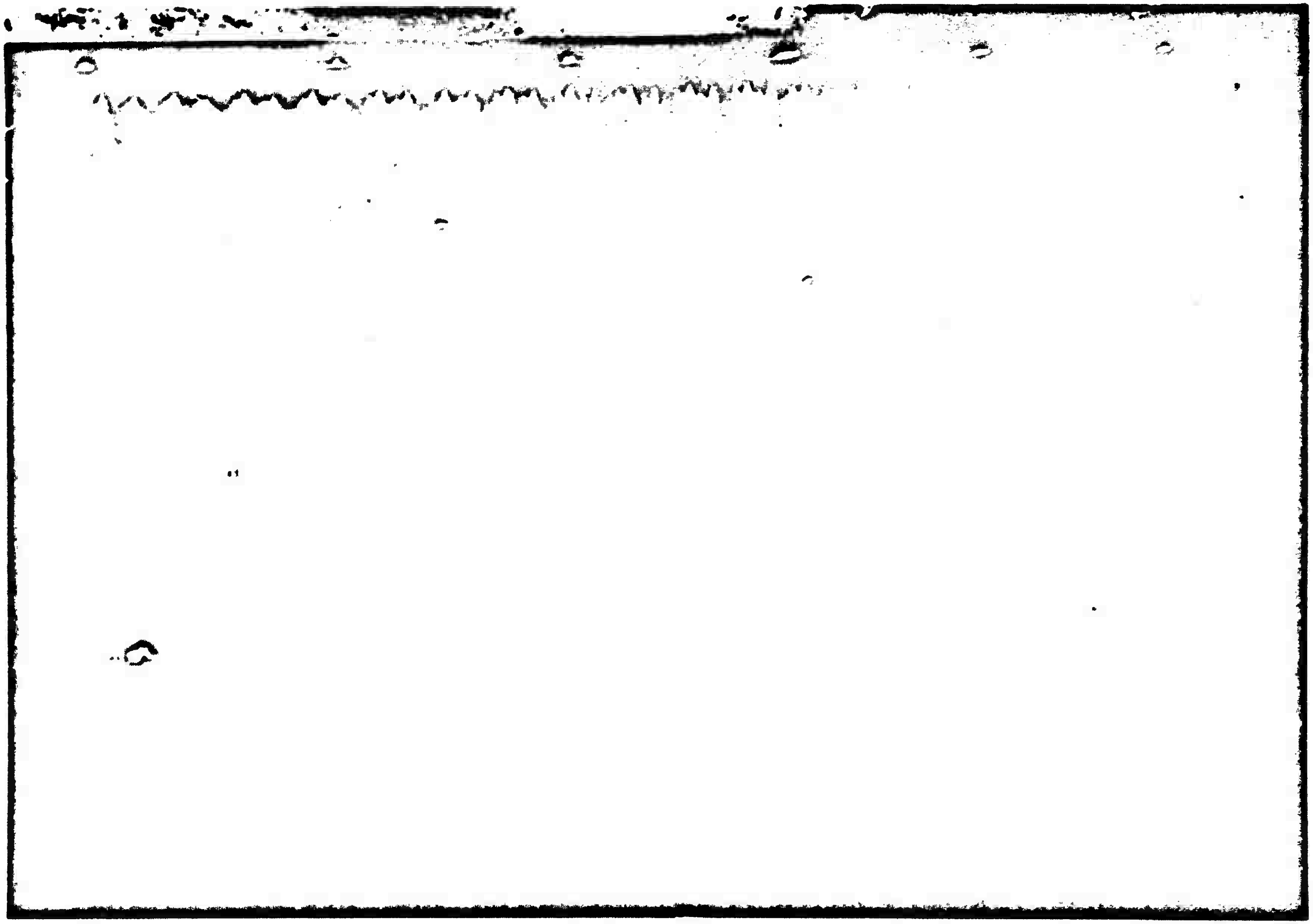

1XX44-1/27/71-C1B

Figure 24. Unit 1 Coplanar Injector Water Flow Test

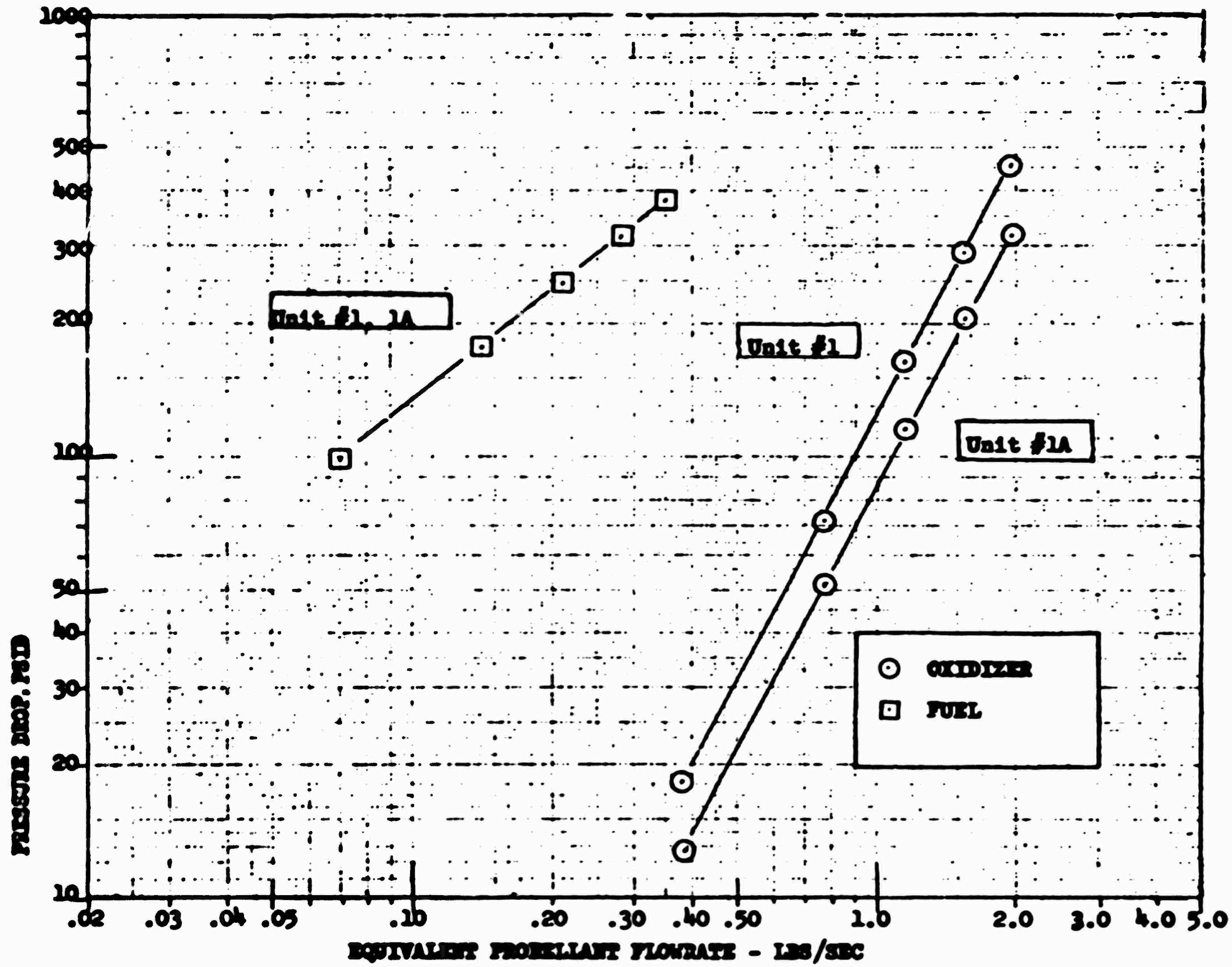

Figure 25. Unit 1 Coplanar Injector Predicted Flow Characteristics (Single Panel)

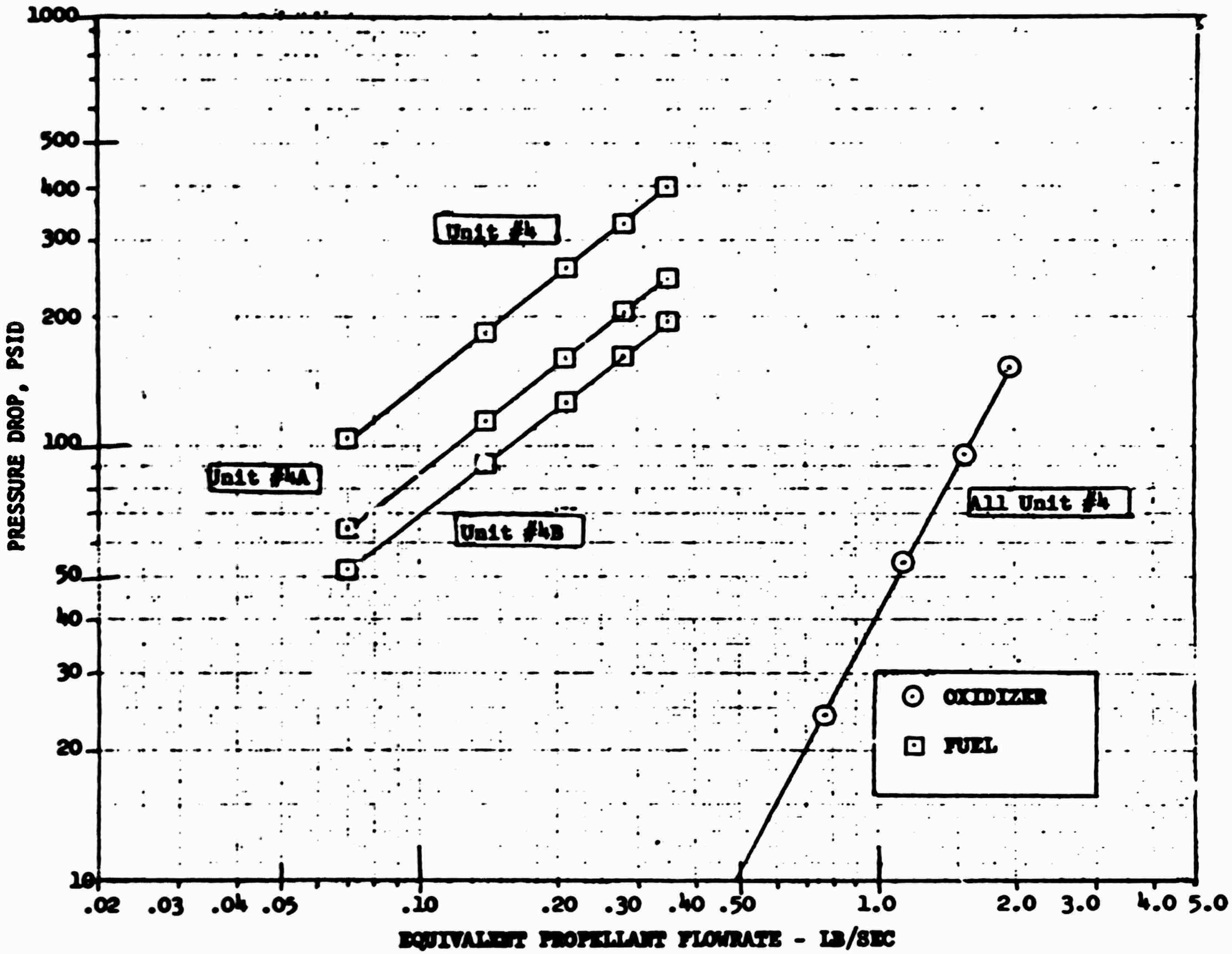

Figure 26. Unit 4 Coplanar Injector Predicted Flow Characteristics (Single Panel)

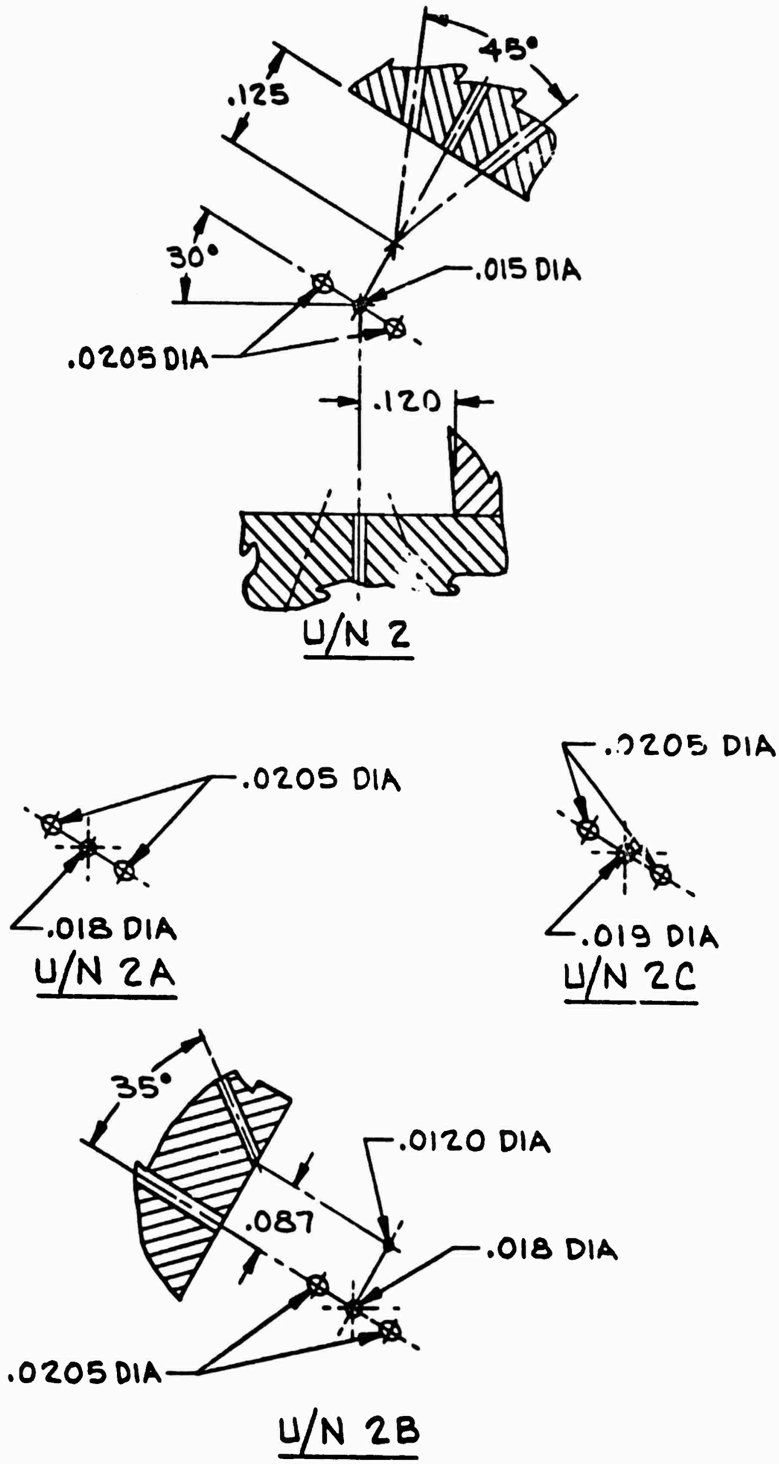

Figure 27. Unit 2 Triplet, Single-Panel Injector, Injection Element Configurations

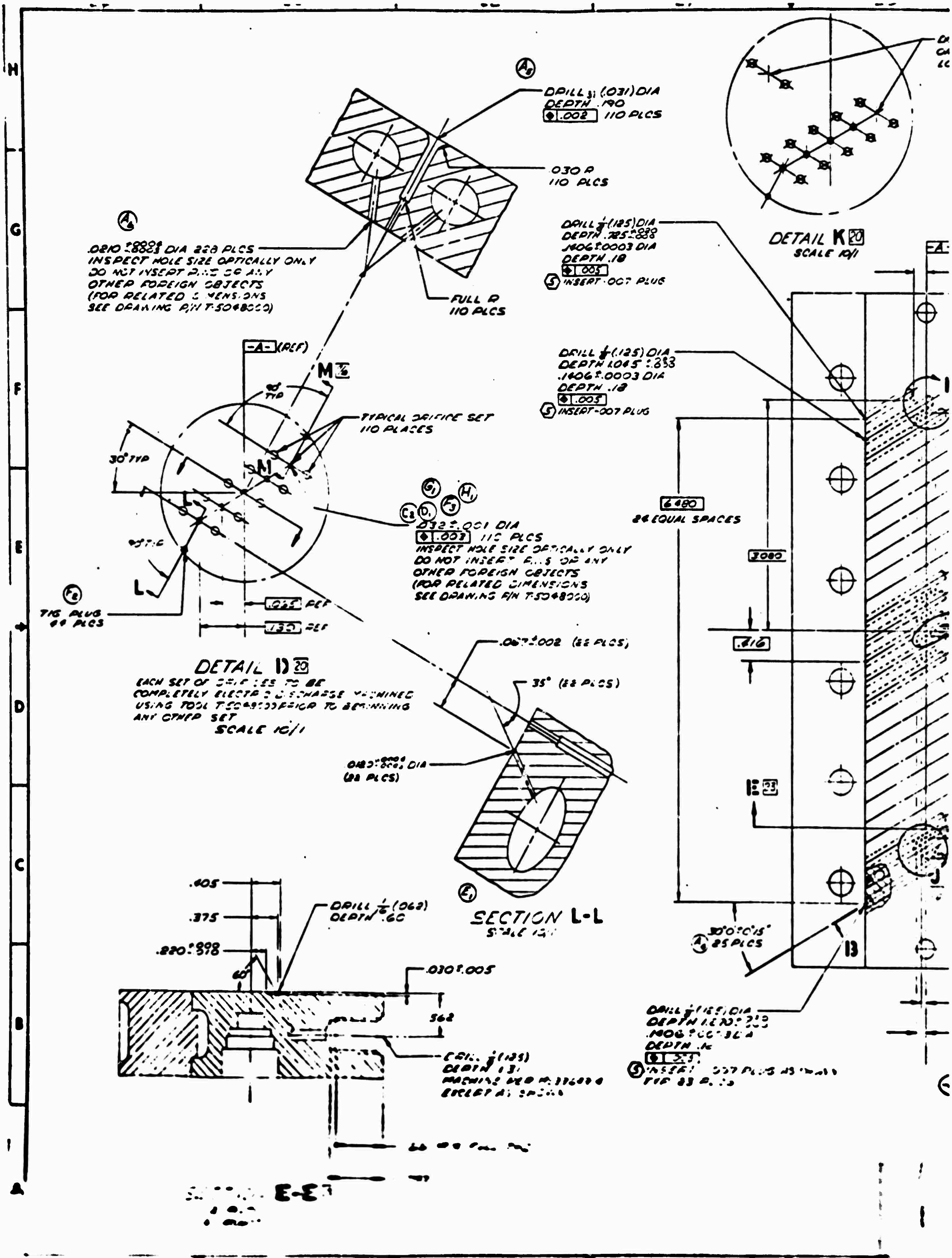
DRILL (.031) DIA
DEPTH .190
.002 110 PLCS
.030 R
110 PLCS
INSPECT HOLE SIZE OPTICALLY ONLY
OTHER FOREIGN OBJECTS
FULL R
110 PLCS
DETAIL K
SCALE 10/1
DRILL (.125) DIA
.1406±.0003 DIA
DEPTH .18
.005
INSERT-007 PLUG
-A- (REF)
90° TYP
TYPICAL ORIFICE SET
110 PLACES
30° TYP
6.480
24 EQUAL SPACES
INSPECT HOLE SIZE OPTICALLY ONLY
DO NOT INSERT
OTHER FOREIGN OBJECTS
(FOR RELATED DIMENSIONS
SEE DRAWING P/N T-5048000)
3.080
TIG PLUG
.416
DETAIL D
SCALE 10/1
35°
(22 PLCS)
.405
.375
SECTION L-L
.030±.005
.562
E-E

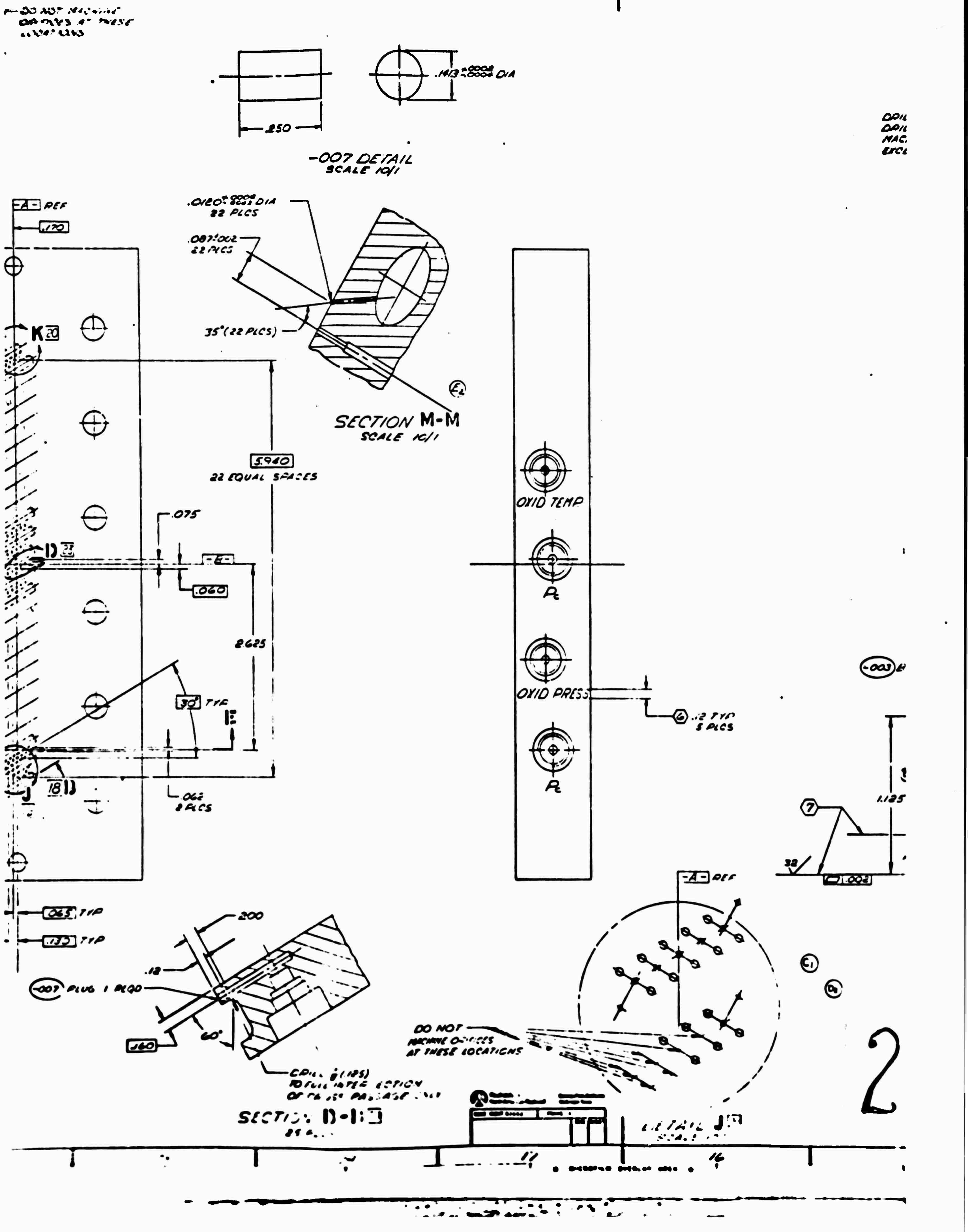

-007 DETAIL
SCALE 10/1
.250
SECTION M-M
SCALE 10/1
22 PLCS
35°(22 PLCS)
5.940
22 EQUAL SPACES
.075
.060
2.625
30° TYP
.062
8 PLCS
.065 TYP
.135 TYP
.200
.12
-007 PLUG 1 REQD
.160
60°
OXID TEMP
OXID PRESS
.12 TYP
5 PLCS
-A- REF
.170
1.125
.002
DO NOT
MACHINE ORIFICES
AT THESE LOCATIONS
-003
2

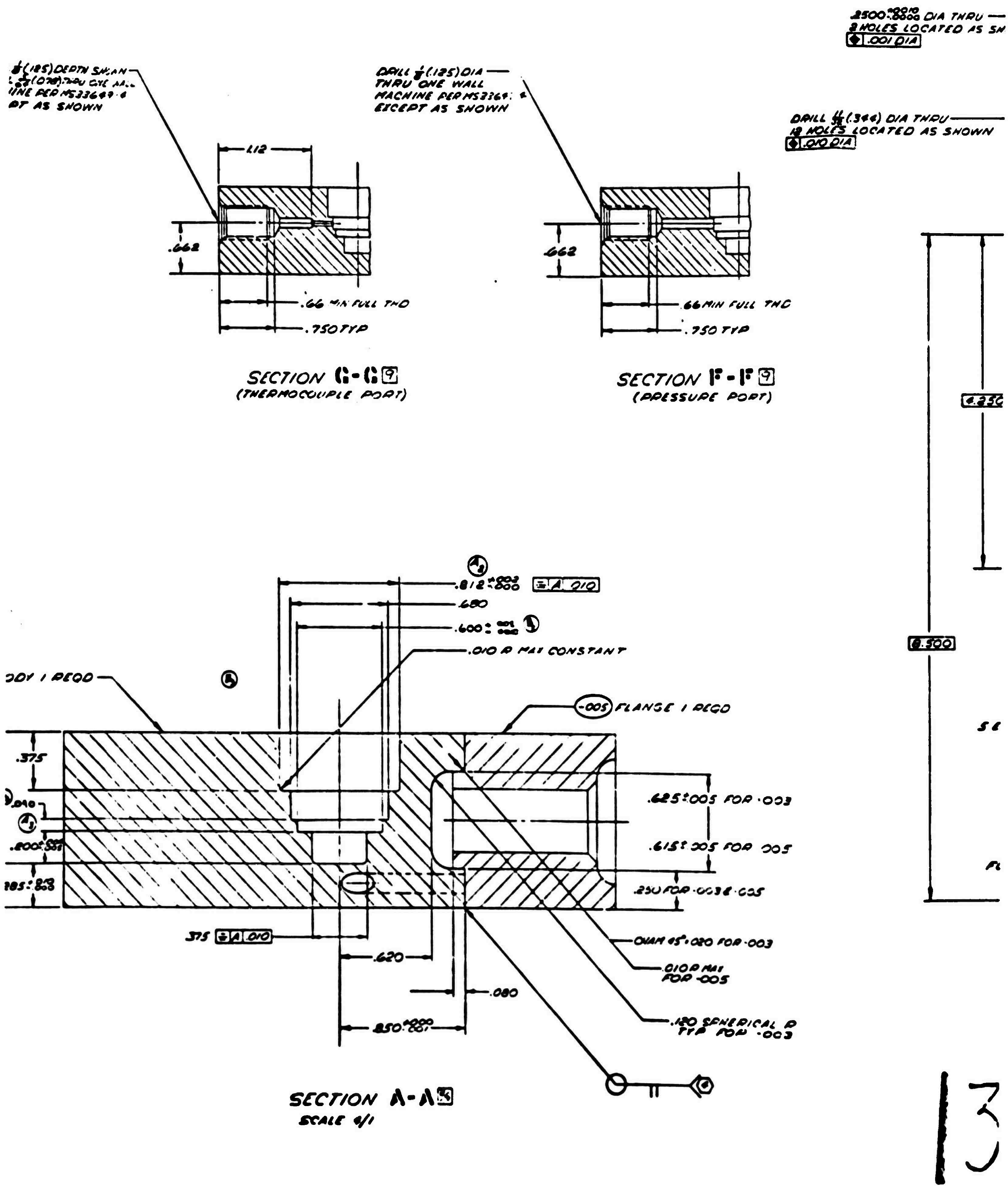

.2500 +.0010 -.0000 DIA THRU
8 HOLES LOCATED AS SH
.001 DIA
DRILL 1/8 (.125) DIA
THRU ONE WALL
MACHINE PER MS3364
EXCEPT AS SHOWN
DRILL 11/32 (.344) DIA THRU
12 HOLES LOCATED AS SHOWN
.010 DIA
1.12
.662
.66 MIN FULL THD
.750 TYP
SECTION G-G
(THERMOCOUPLE PORT)
SECTION F-F
(PRESSURE PORT)
8.500
.812 +.002 -.000
.680
.600
.010 R MAX CONSTANT
FLANGE 1 REQD
.375
.625±.005 FOR -003
.615±.005 FOR -005
.250 FOR -003 & -005
CHAM 45° .020 FOR -003
.010 R MAX FOR -005
.120 SPHERICAL R TYP FOR -003
.620
.080
.850 +.000 -.001
SECTION A-A
SCALE 4/1
14
13
12
11

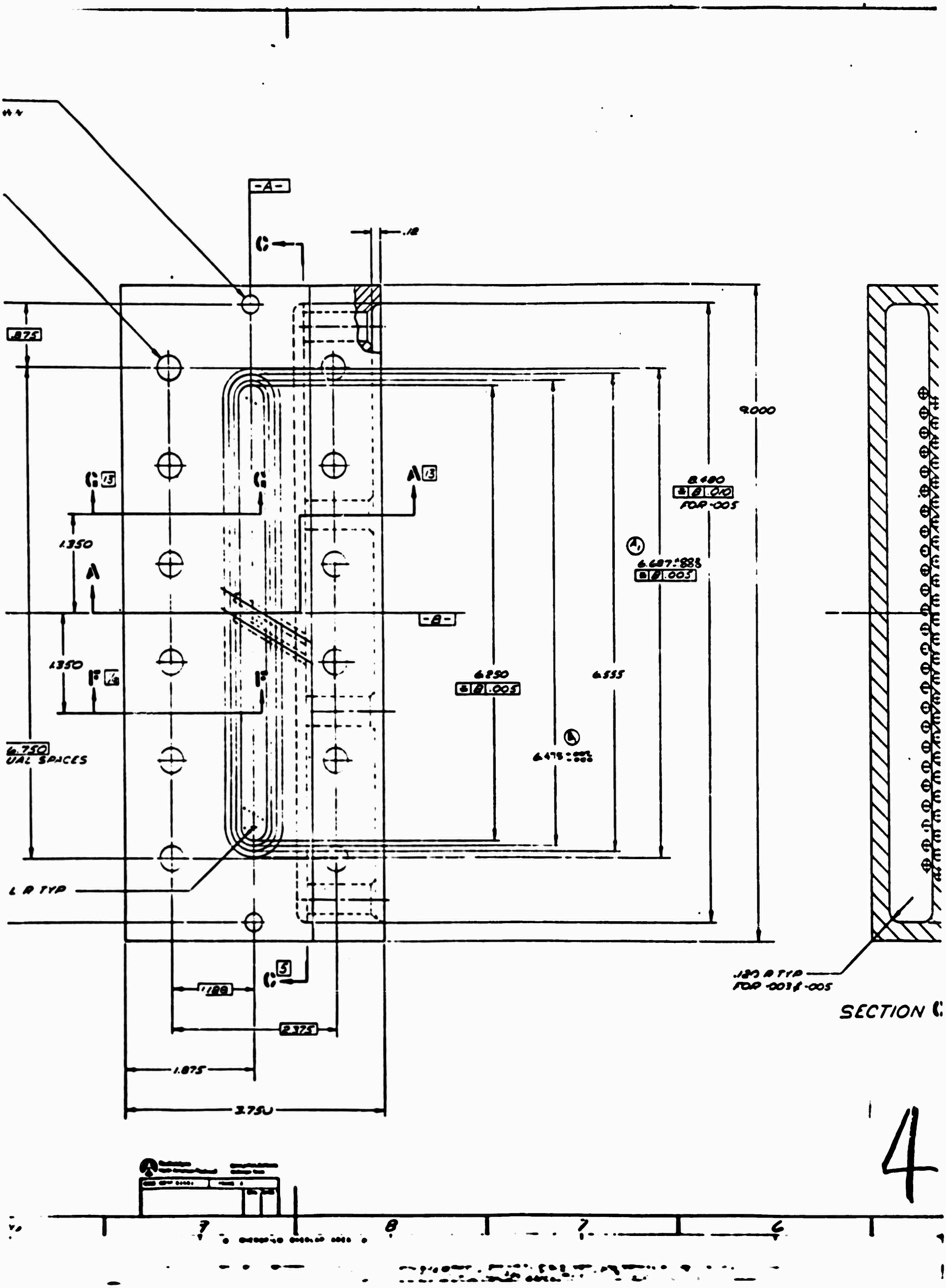

-A-
C
.12
.875
9.000
8.480
FOR .005
6.850
.005
6.555
1.350
A
-B-
1.350
6.750
UAL SPACES
R TYP
.180 R TYP
FOR .003 & .005
SECTION C
.188
2.375
1.875
3.750
4

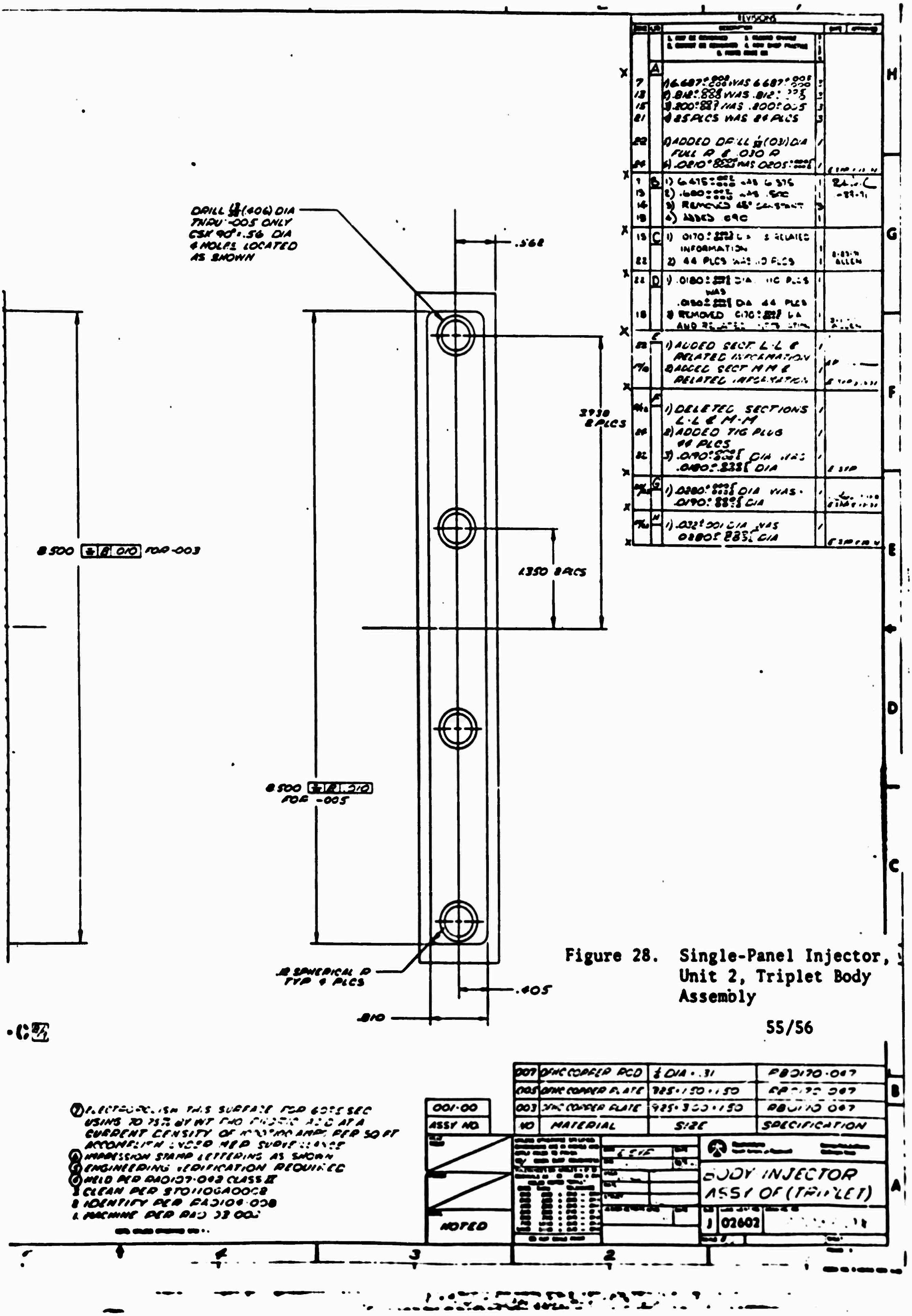

Figure 28. Single-Panel Injector, Unit 2, Triplet Body Assembly

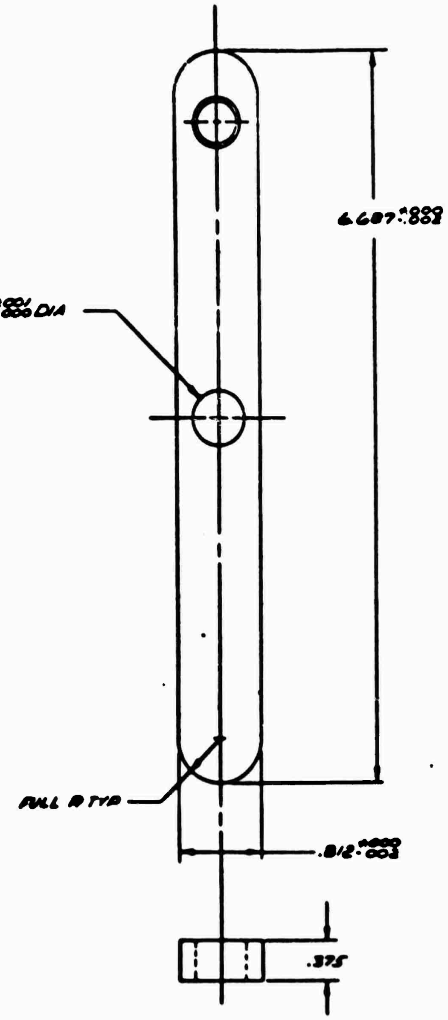

-015 DETAIL

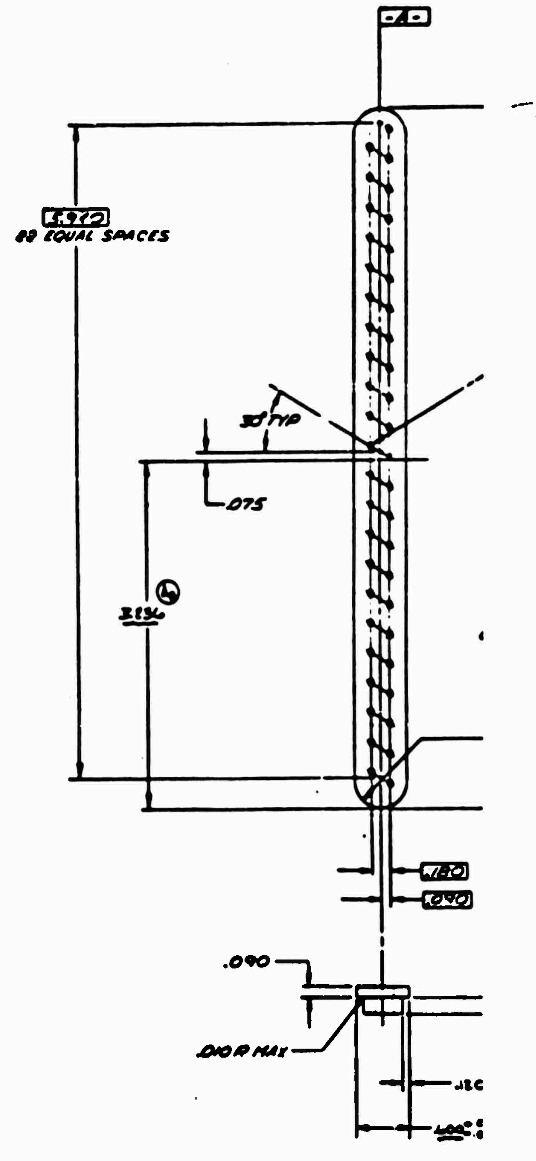

-013 DETAIL

24 23 22 21 20

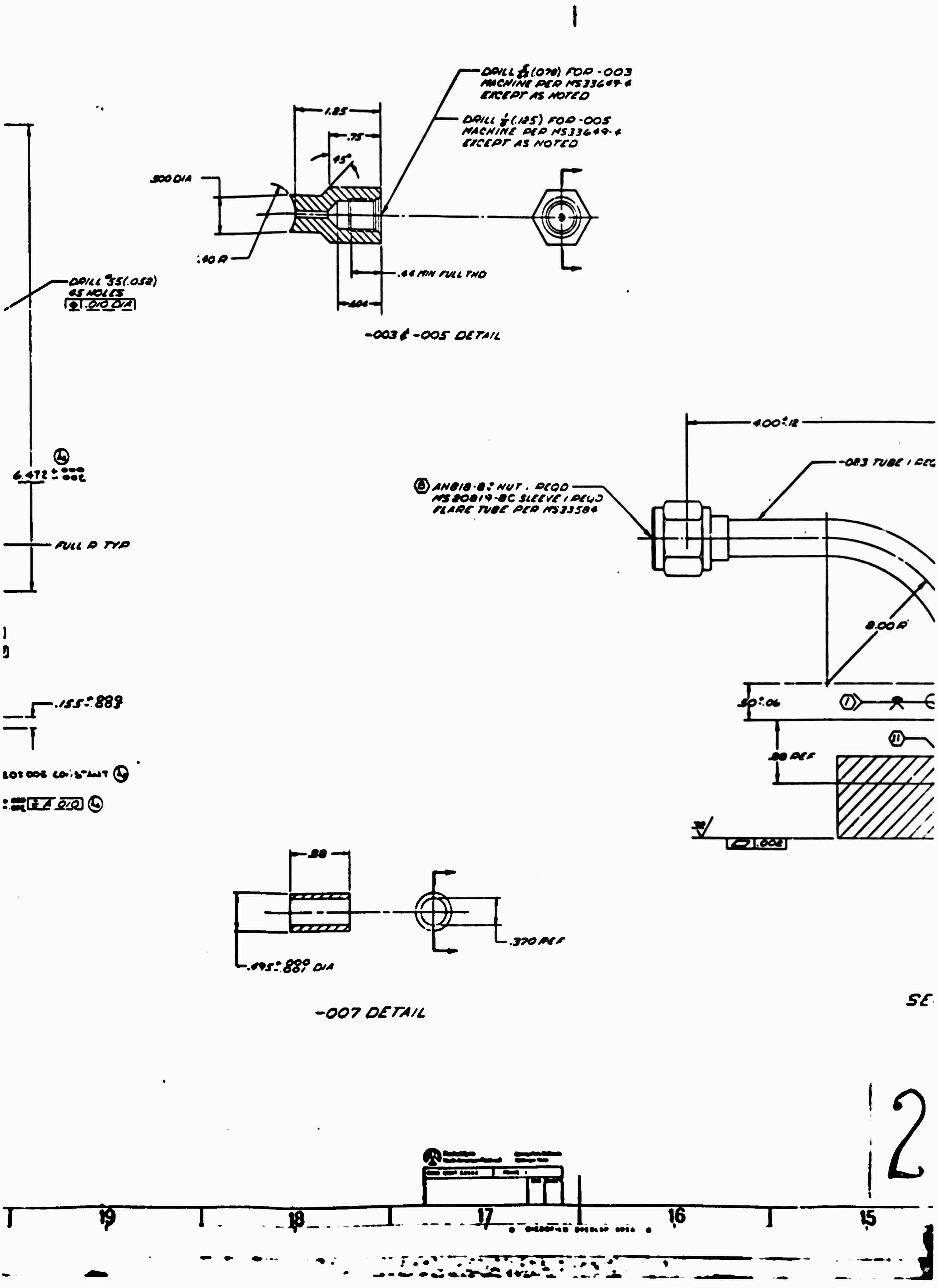

DRILL $\frac{5}{64}$(.078) FOR -003
MACHINE PER MS33649-4
EXCEPT AS NOTED
DRILL $\frac{1}{8}$(.125) FOR -005
MACHINE PER MS33649-4
EXCEPT AS NOTED
1.85
.75
45°
.300 DIA
.10 R
.44 MIN FULL THD
.604
-003 & -005 DETAIL
DRILL #55(.052)
65 HOLES
6.472
FULL R TYP
4.00±.12
-023 TUBE 1 REQ
AN818-8 NUT, 1 REQD
MS20819-8C SLEEVE 1 REQD
FLARE TUBE PER MS33584
8.00 R
.50±.06
.88 REF
.88
.370 REF
-007 DETAIL
SE
2
19
18
17
16
15

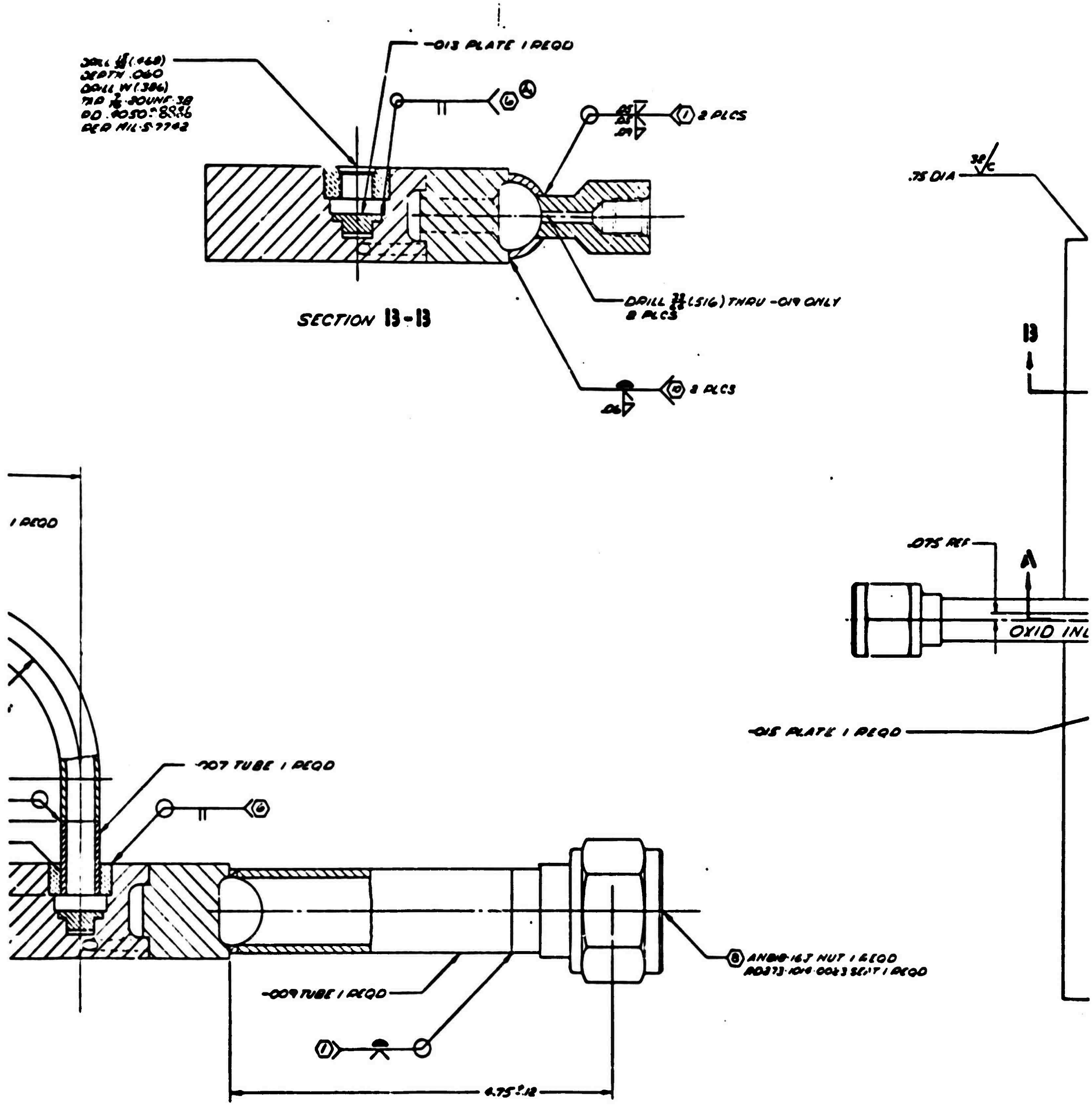

SECTION B-B

SECTION A-A

13

14 13 12 11 10

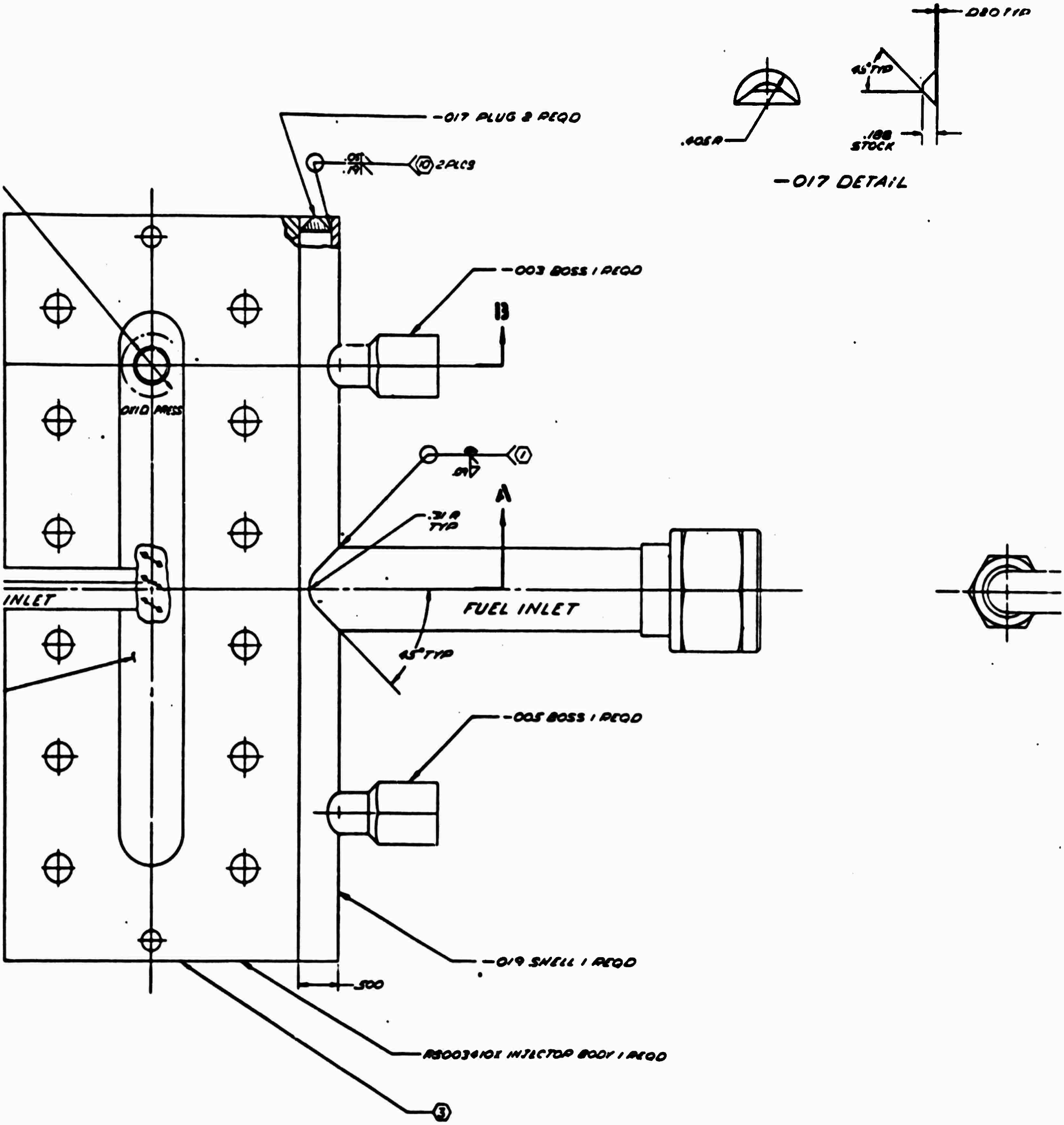

-017 PLUG 2 REQD
2 PLCS
-017 DETAIL
.188 STOCK
45° TYP
-003 BOSS 1 REQD
B
A
.31 R TYP
FUEL INLET
INLET
45° TYP
-005 BOSS 1 REQD
-019 SHELL 1 REQD
.500
INJECTOR BODY 1 REQD

14

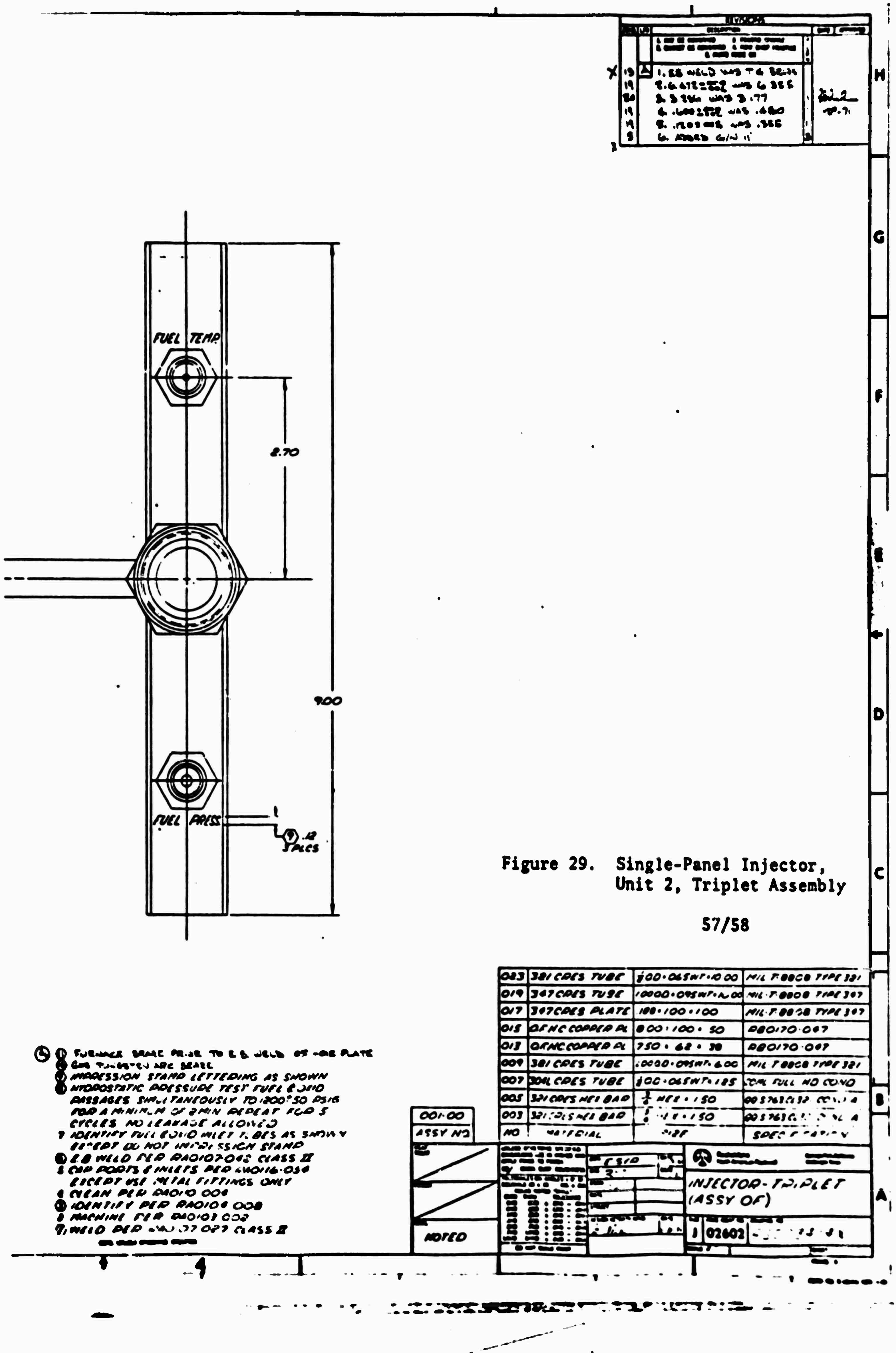

Figure 29. Single-Panel Injector,
Unit 2, Triplet Assembly

Modification 2B added an additional 0.012-inch fuel orifice between the outer elements and the segment wall to evaluate the influence of additional fuel flow near the wall on reducing the heat flux.

Modification 2C plugged the additional 0.012-inch fuel orifices of modification 2B because increased heat flux, rather than reduced heat flux, resulted from the 2B modification during testing. The oxidizer orifice size also was increased to 0.019 inch on the 2C modification for further evaluation of oxidizer injection velocity on performance and heat transfer.

An additional triplet injector (unit 6) was designed but not fabricated when the test results showed that a concentric element-type injector would satisfactorily meet the single-panel program requirements.

The manufacturing of the triplet injector was very similar to the coplanar injectors. The completed injector (unit 2) is shown in Fig. 30.

The injector was water-flow tested following completion of fabrication. A typical flow test is shown in Fig. 31. Visually, the stream patterns were well collimated, and produced well-formed fans. No misimpingement or plugged orifices were noted. The predicted injector pressure loss characteristics are shown in Fig.32 .

There was no cold-flow evaluation of the triplet element.

<u>Concentric Injector</u>. Two concentric injectors, units 3 and 7, were designed and fabricated.

The unit 3 injector effort was initiated prior to the program start on an IR&D task. The injector fabrication was completed and testing accomplished on the AMPS program to complement the single-panel injector development program.

The initial test results were very promising and indicated that a concentric injector designed specifically for the AMPT single-panel combustor was desirable. This injector, designated unit 7, was rescaled and slightly revised from the

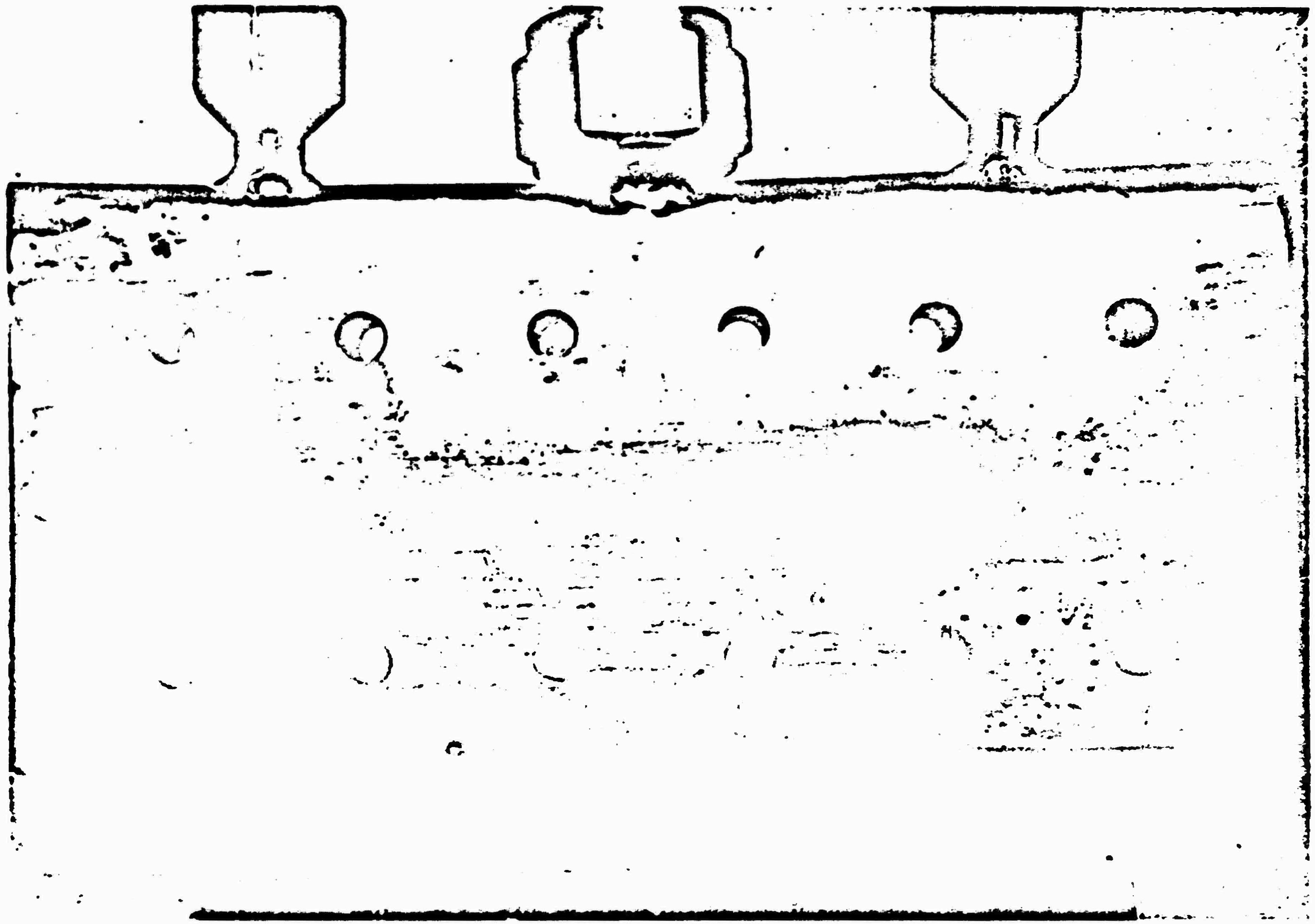

1XE44-2/16/71-C1 1

Figure 30. Completed Unit 2 Triplet Injector

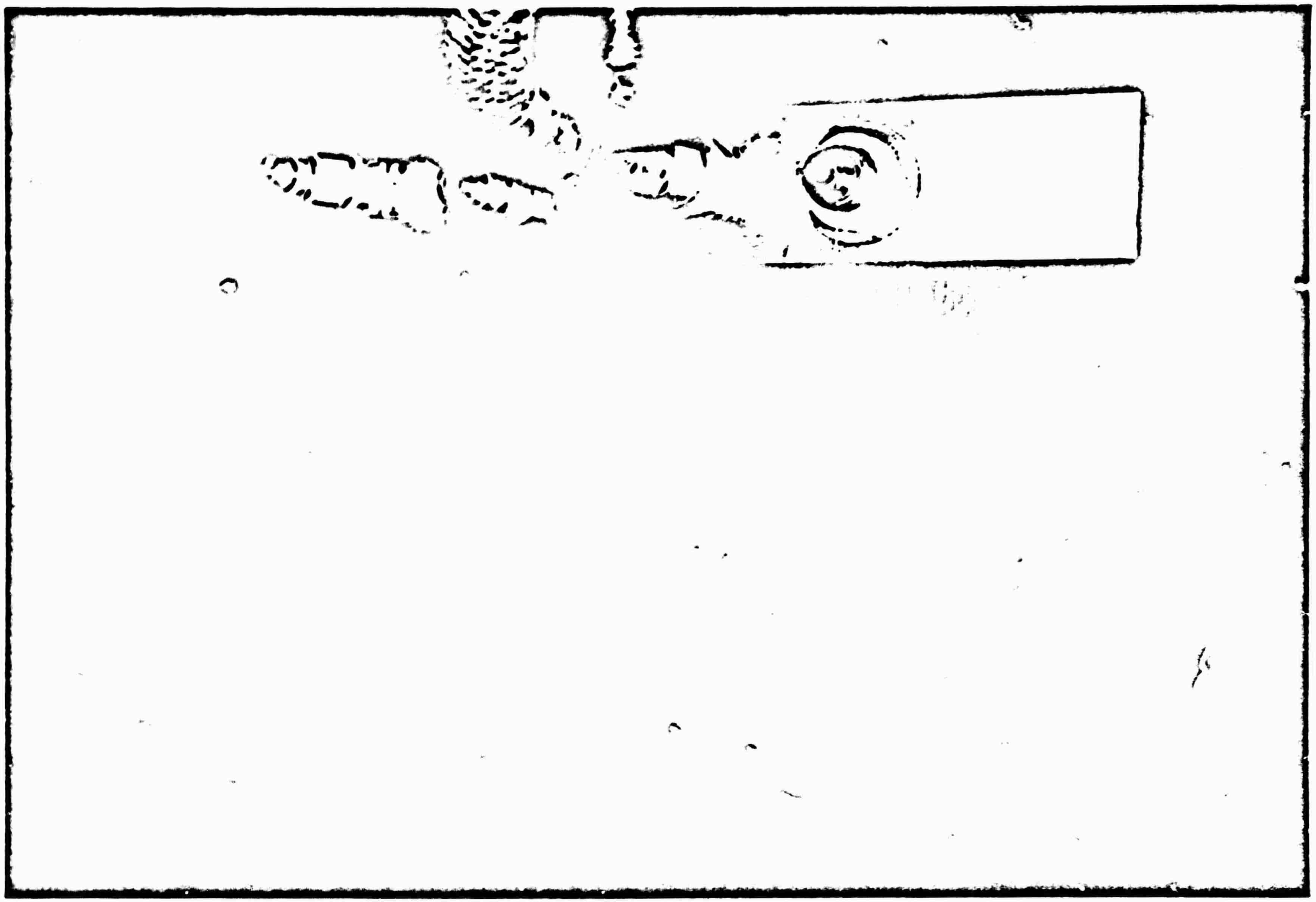

1XE44-2/16/71-C1E

Figure 31. Unit 2 Triplet Injector, Water Flow Oxidizer Side Only (ΔP = 50 psid)

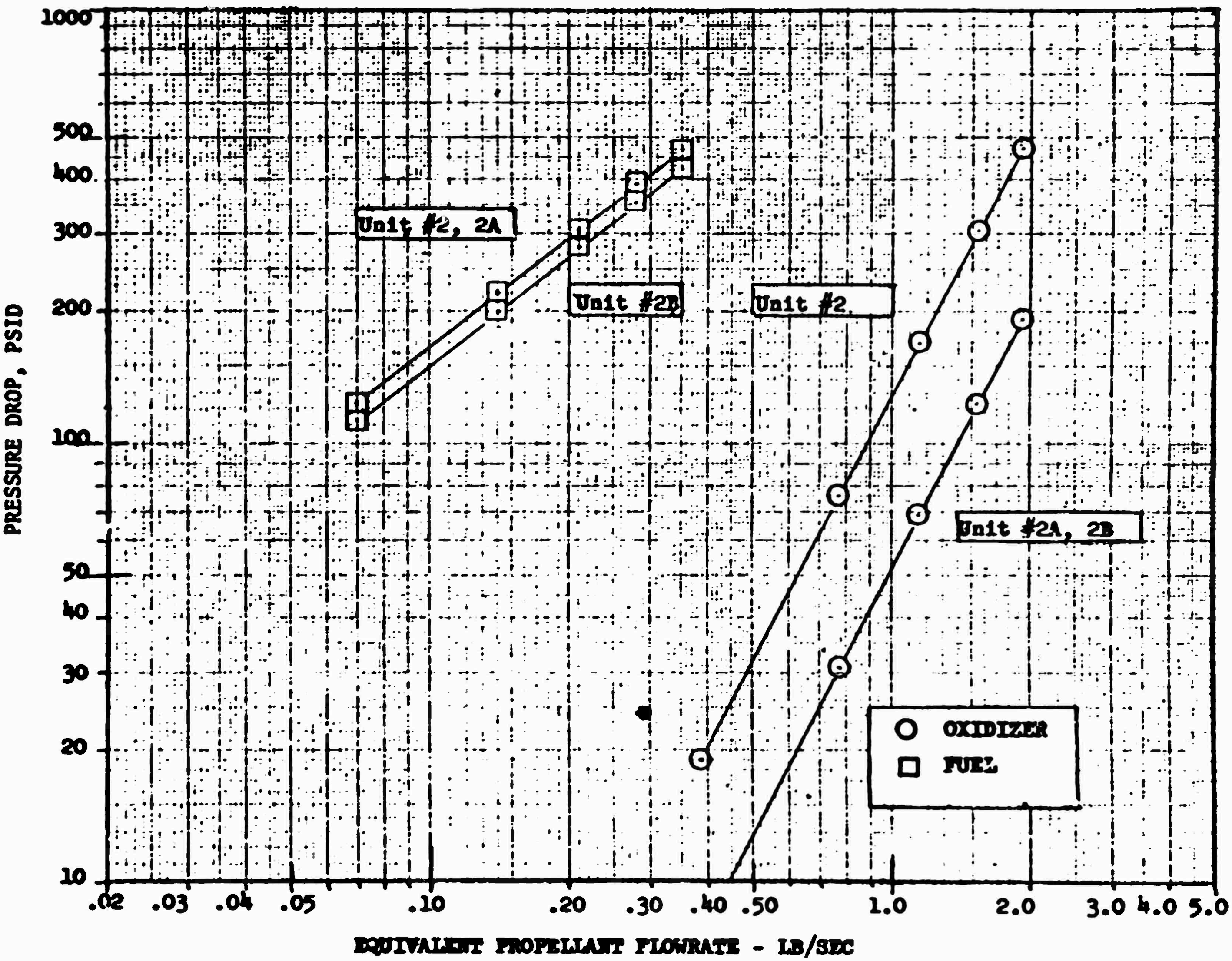

Figure 32. Unit 2 Triplet Injector Predicted Flow Characteristics (Single Panel)

unit 3 injector configuration. This design modification was required because the unit 3 injector had a larger thrust per element than would be necessary for the unit 7 injector (Table 5).

Unit 3 Concentric Injector. Unit 3 injector was a 96-element design with an element configuration as shown in Fig. 33. The mechanical design criteria are noted in Table 5.

The injection element consisted of oxidizer introduced through an oxidizer tube (post) and fuel introduced through an annulus formed by the oxidizer tube OD and an orifice in the face plate. Capability to evaluate several oxidizer post recesses was possible by electrodischarge machining the oxidizer posts to shorten them. This modification was accomplished once during the program to change the recess from 0.050 to 0.075 inch on this injector.

Combustion model studies (described in Appendix I) were conducted for unit 3 injector with varying post recesses (0.050, 0.075, and 0.100 inch) at chamber pressures of 450 and 700 psia. The post recesses for the 0.033-inch-diameter oxidizer orifice corresponded to recess/oxidizer orifice diameter ratios (R/D_0) of 1.5, 2.25, and 3.0. Combustion model predictions of vaporization efficiency, η_{vap}, and cup pressure drop, are shown in Fig. 34 and 35 respectively. Vaporization efficiency was indicated to increase with: (1) increasing chamber pressure at constant R/D_0, and (2) increasing R/D_0 at constant chamber pressure. Cup pressure drop increased in a similar manner.

The fabrication technique used for the unit 3 injector was different than the impinging types. The injector assembly consisted of three major detail parts: face plate, body, and oxidizer tubes. The oxidizer tubes were furnace brazed into a plate which was then electron-beam welded into the body. The injector body and face plate were assembled by electron-beam welding. The completed injector is shown in Fig. 36.

After completion of fabrication, the injector was flow calibrated to establish pressure loss characteristics and verify nonplugging of propellant flow passages; the calibration results are presented in Fig. 37. A typical flow test is shown in Fig. 38.

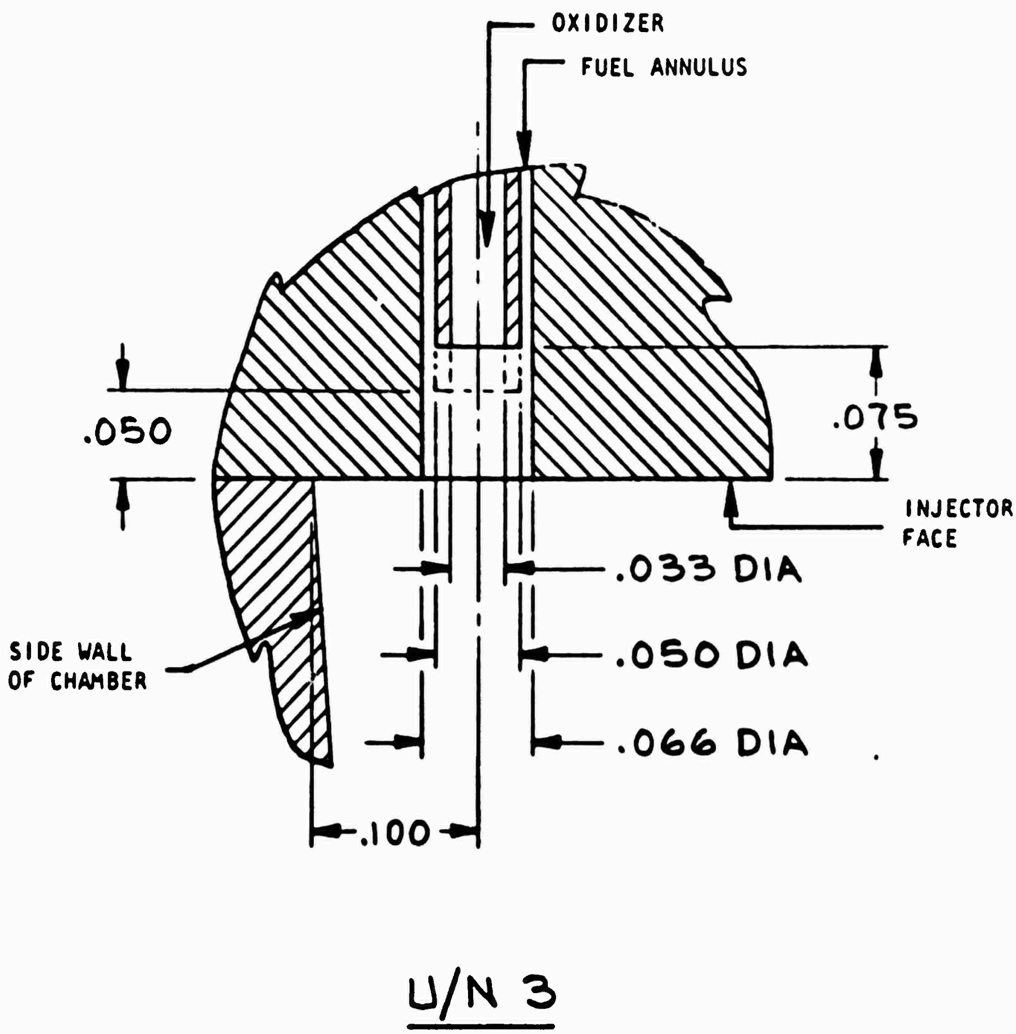

Figure 33. Unit 3 Concentric Orifice, Single-Panel Injector, Injection Element Configuration

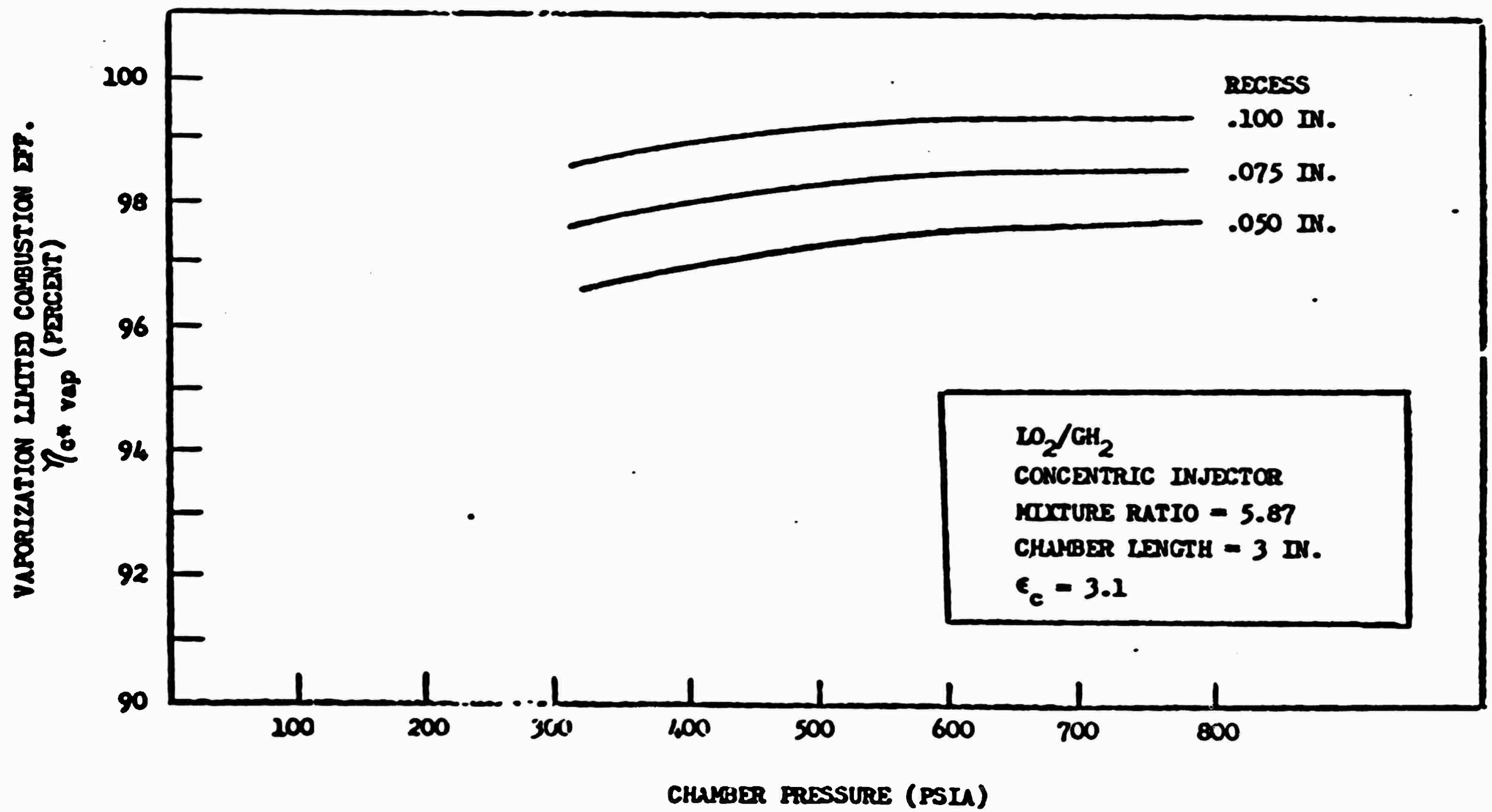

Figure 34. Combustion Model Predicted $\eta_{c^*_{vap}}$ vs P_c for Varying Post Recess for Concentric Injector Unit 2

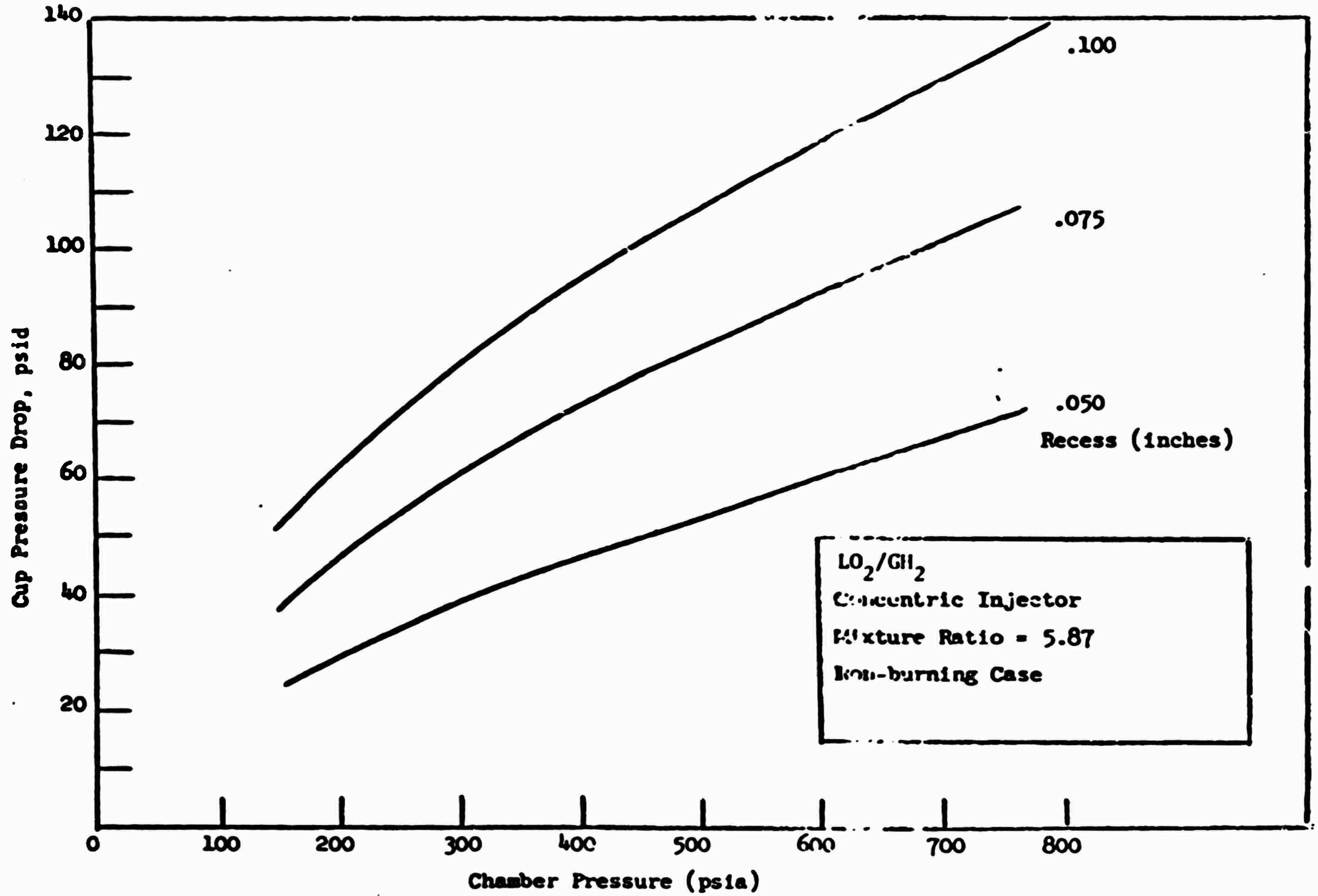

Figure 35. Combustion Model Predicted Cup Pressure Drop vs P_c for Varying Post Recess for Concentric Injector Unit 3

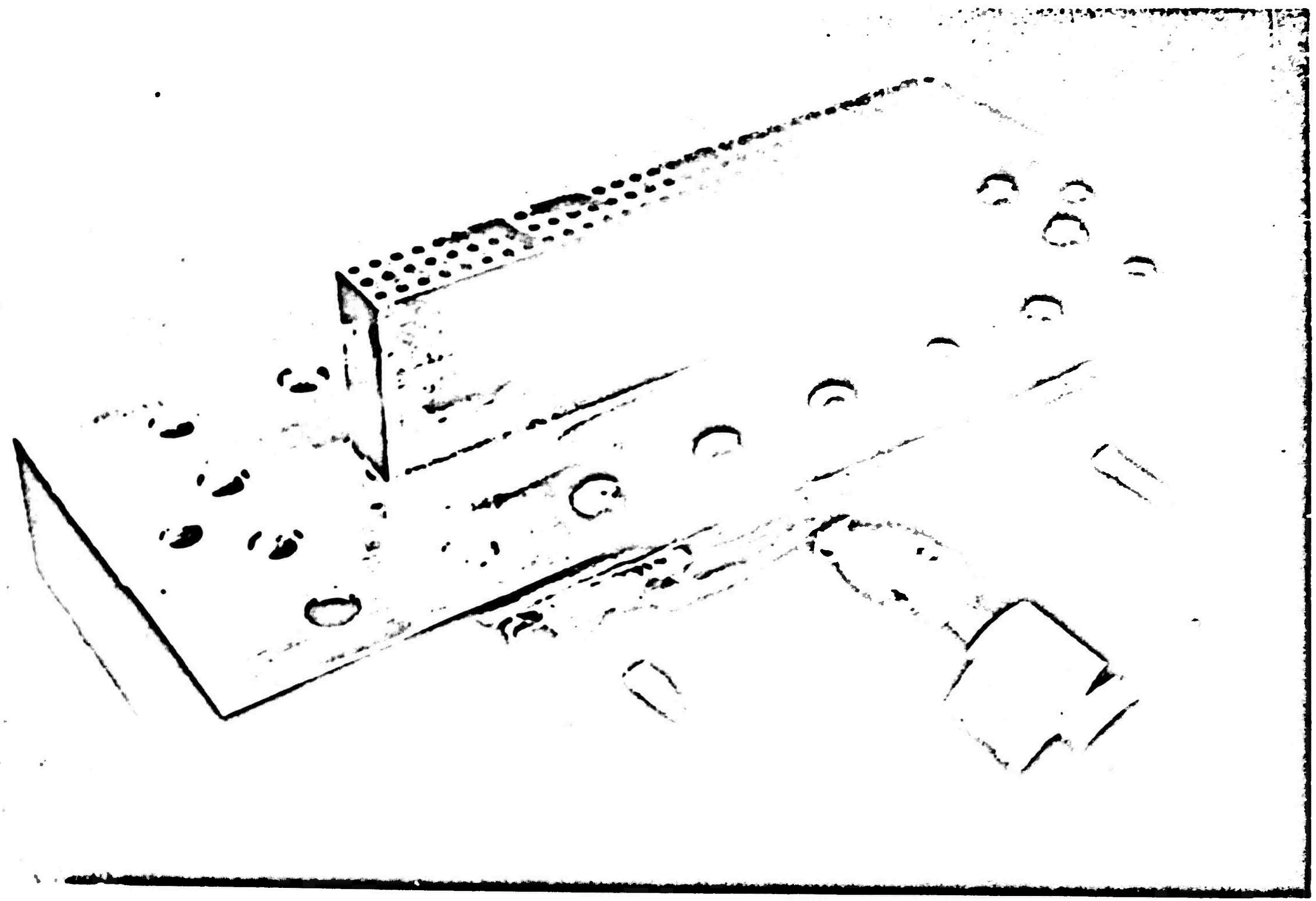

1EH42-3/15/71-C1C

Figure 36. Completed Unit 3 Concentric Orifice Injector

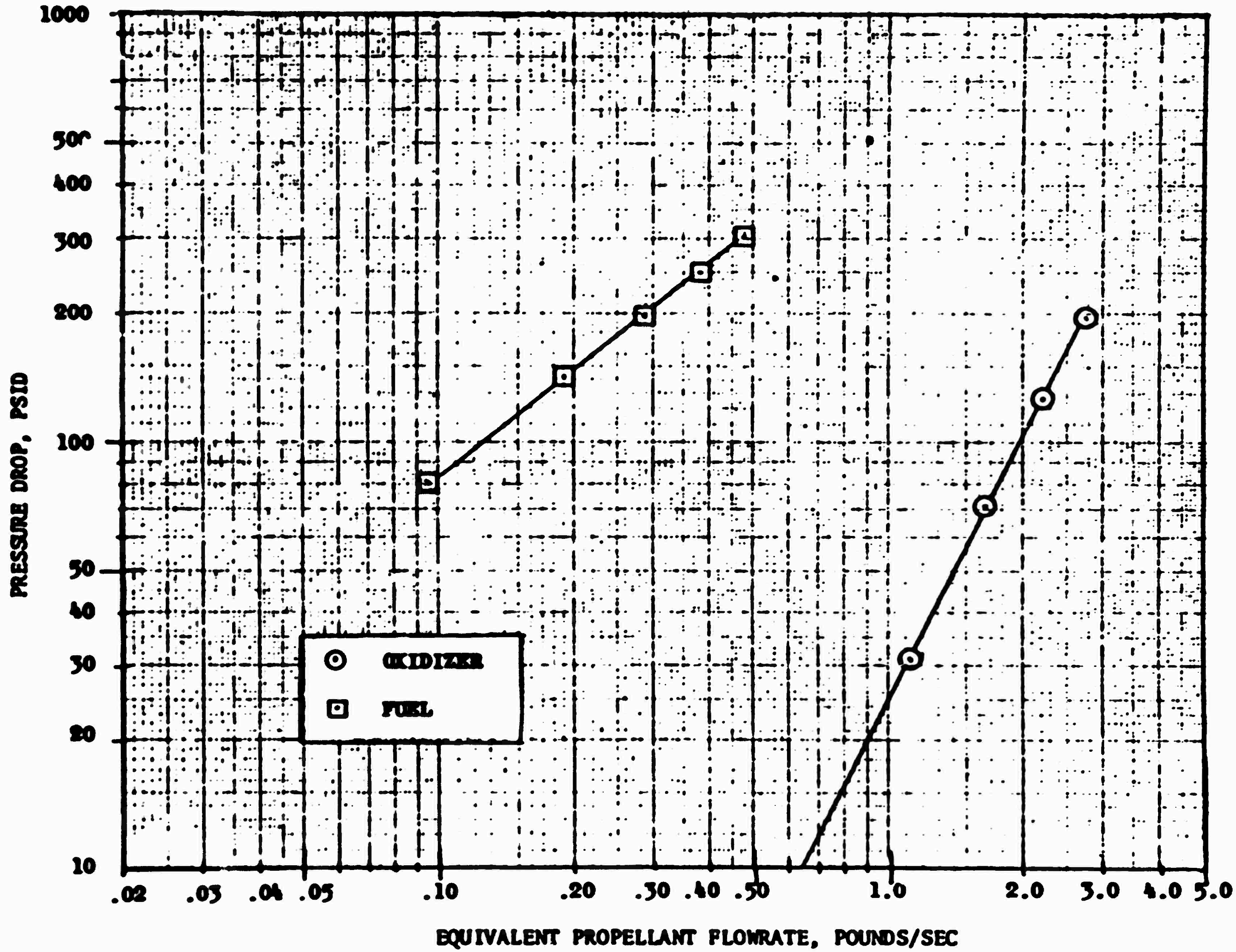

Figure 37. Unit 3 Concentric Injector Predicted Flow Characteristics (Single-Panel Gas-Liquid Case)

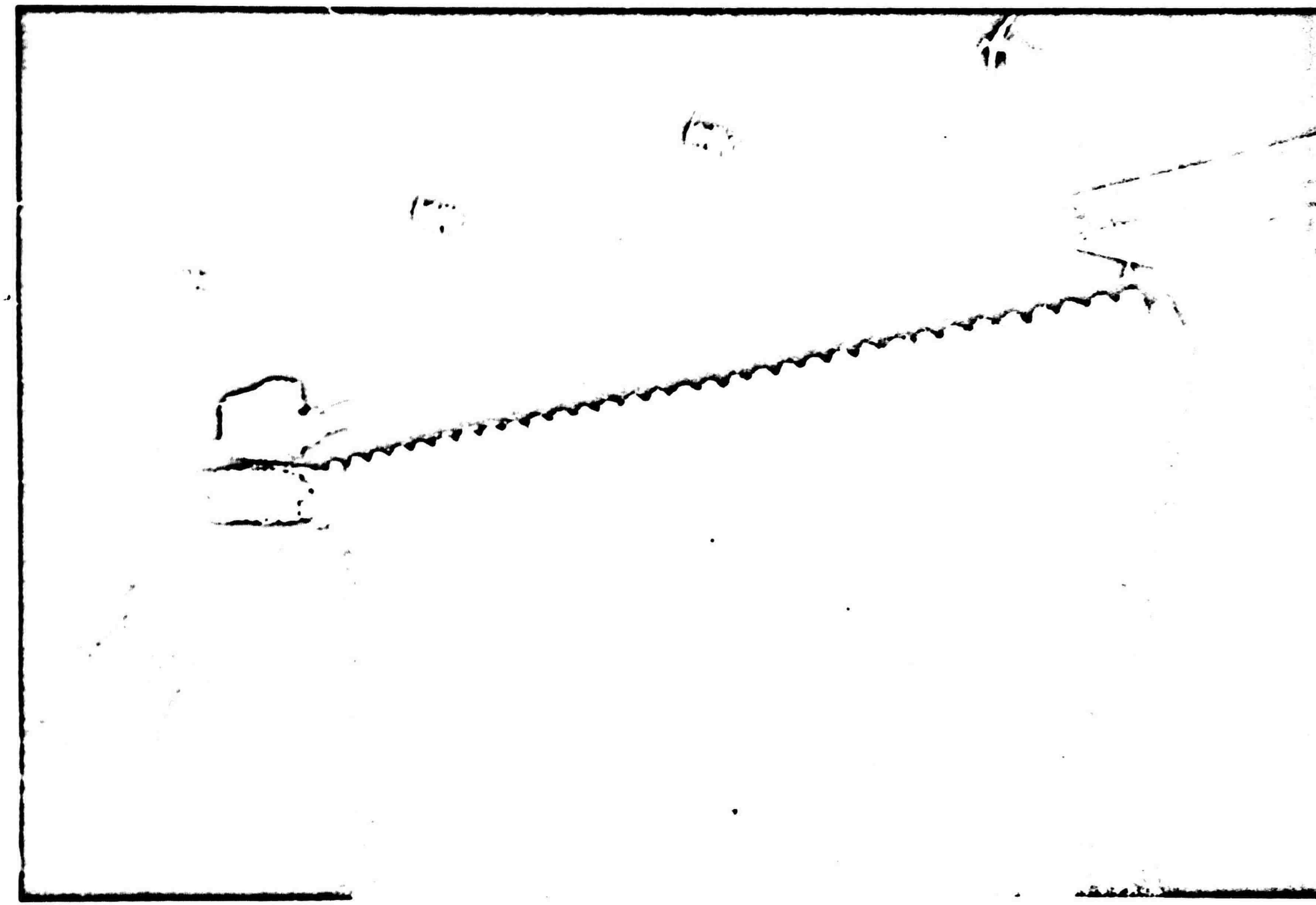

1XZ44-3/4/71-C1B

Figure 38. Unit 3 Concentric Injector, Cold-Flow Test, 4 psid, GN_2-Fuel Side, Water-Oxidizer Side

One modification was made to the injector during the test program which consisted of changing the oxidizer post length from the value that provided a 0.050-inch recess to a shorter length to provide a 0.075-inch recess.

Unit 7 Concentric Injector. Injector unit 7 design is shown in Fig. 39 through 41. The mechanical design parameters are shown in Table 5.

Three candidate element configurations (cases I, II, and III) were subjected to combustion model analysis (described in Appendix I) to aid in selection of the element configuration. The element configurations selected for analysis and the combustion model results are tabulated in Table 6.

Case I represented an element design which: (1) had a fuel injection velocity and total number of elements the same as injector unit 3, and (2) had a fuel gap and oxidizer injection velocity less than injector unit 3. The latter two constraints resulted from the lower thrust requirements of injector unit 7 compared to injector unit 3. Case II represented an element design which: (1) had a fuel gap and total number of elements the same as injector unit 3, and (2) had a fuel and oxidizer injection velocity less than injector unit 3. Case III represented an element design identical to injector unit 3 with a reduction in the number of elements from 96 to 68.

For each of the cases, both increased chamber pressure and increased post recess improved η_{c^*vap}. The vaporization efficiency for cases I and III was similar. For case II, the vaporization efficiency was slightly lower due to the reduced fuel injection velocity. The results in Table 6 apply to vaporization efficiency only and do not account for changes in mixing efficiency, which could occur with the different element designs.

The element corresponding to case I, and shown in Fig. 39, was selected for the initial evaluation based on the following:

1. The mass distribution was much more uniform with the 95-element pattern (one less than unit 3 which had 96) compared to 68 elements.
2. A lower thrust per element was obtained with 95 rather than 68 elements.

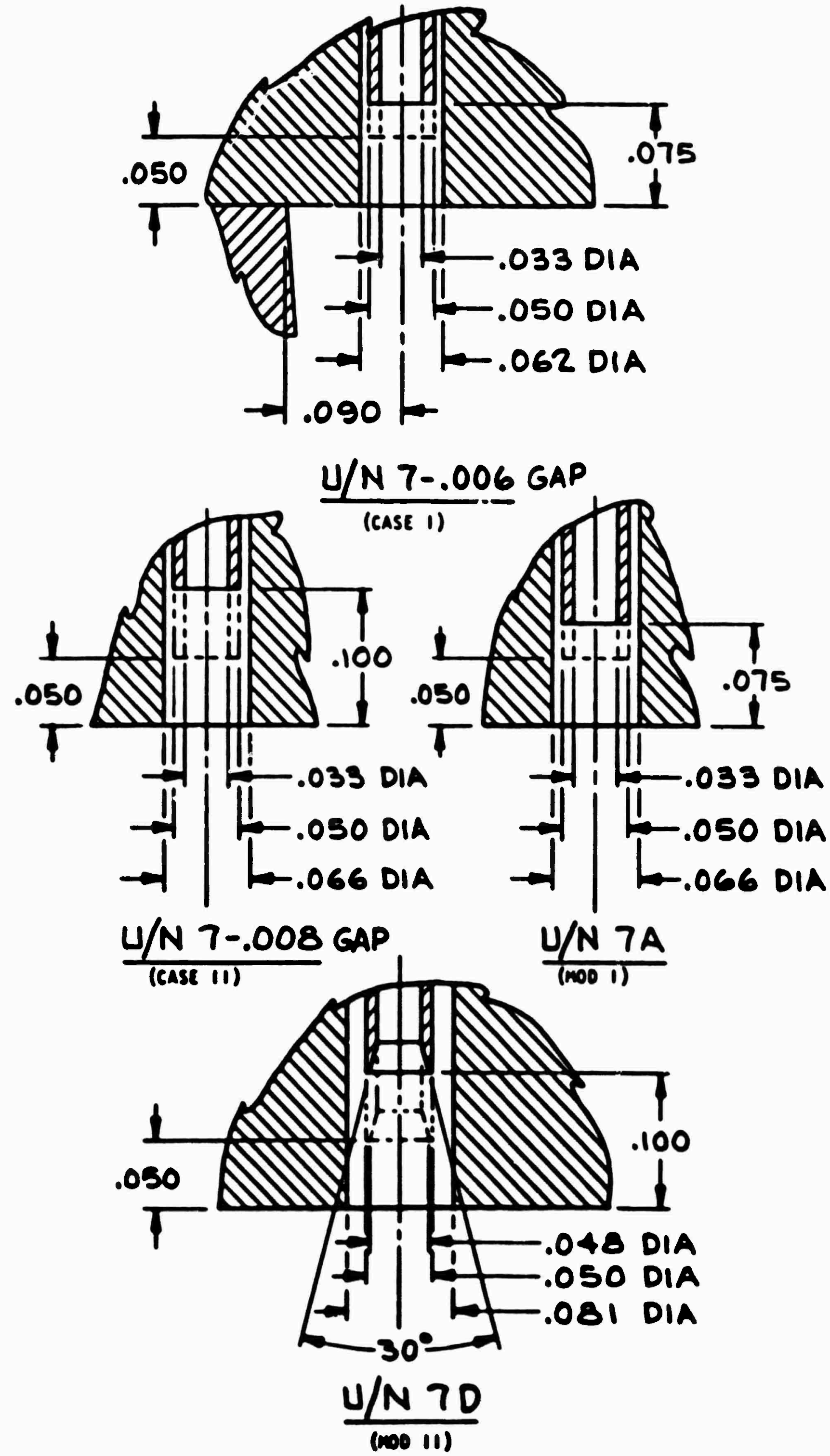

Figure 39. Unit 7 Concentric Orifice Single-Panel Injector, Injection Element Configurations

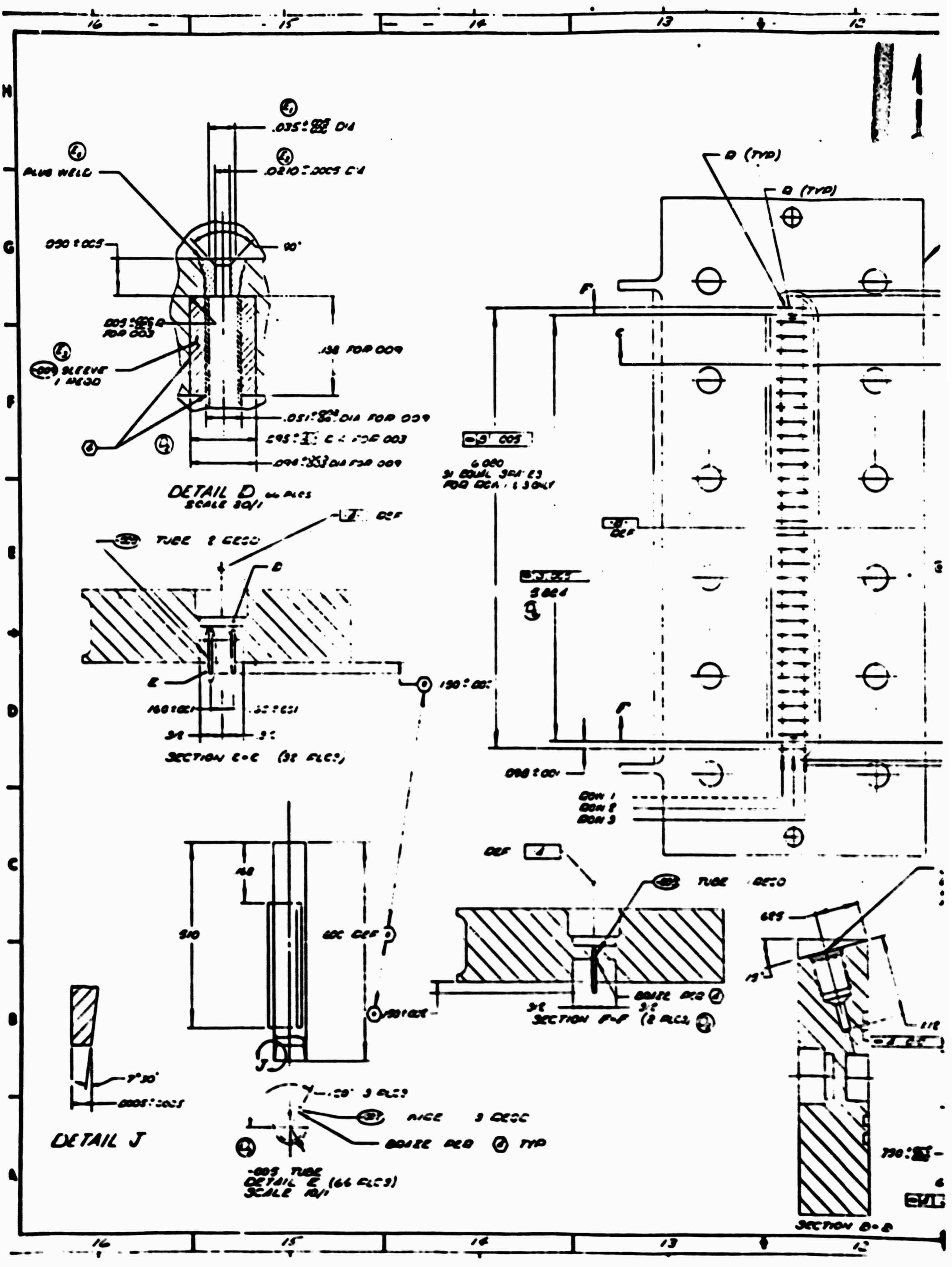

DETAIL D
DETAIL J
SECTION E-E
SECTION F-F
SECTION B-B
DETAIL E
PLUG WELD
SLEEVE
TUBE
BRAZE

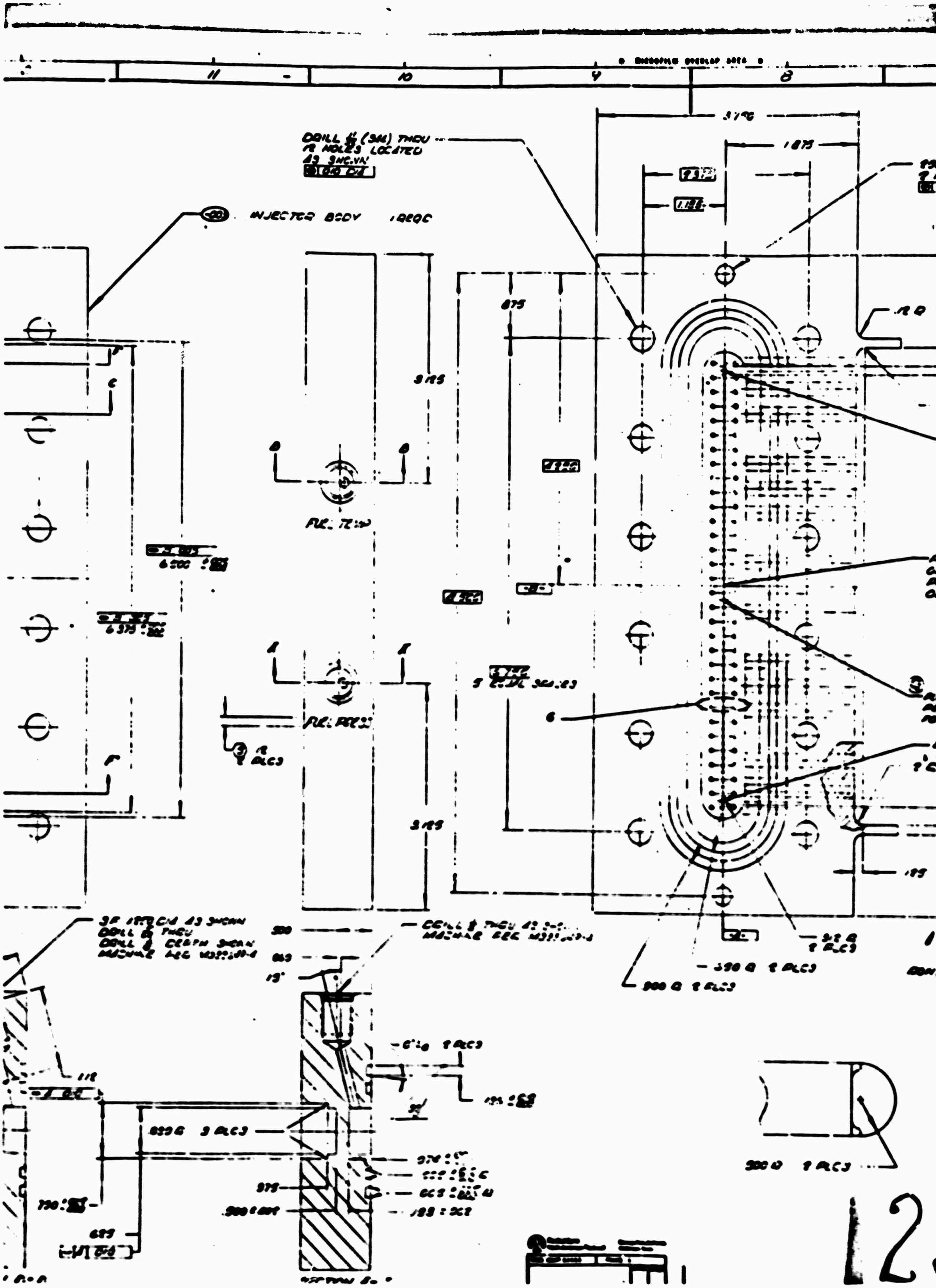

11
10
9
8
DRILL 1/4 (.266) THRU
12 HOLES LOCATED
AS SHOWN
INJECTOR BODY 1 REQD
.875
1.875
3.125
6.200
6.375
.185
.500
.875
12

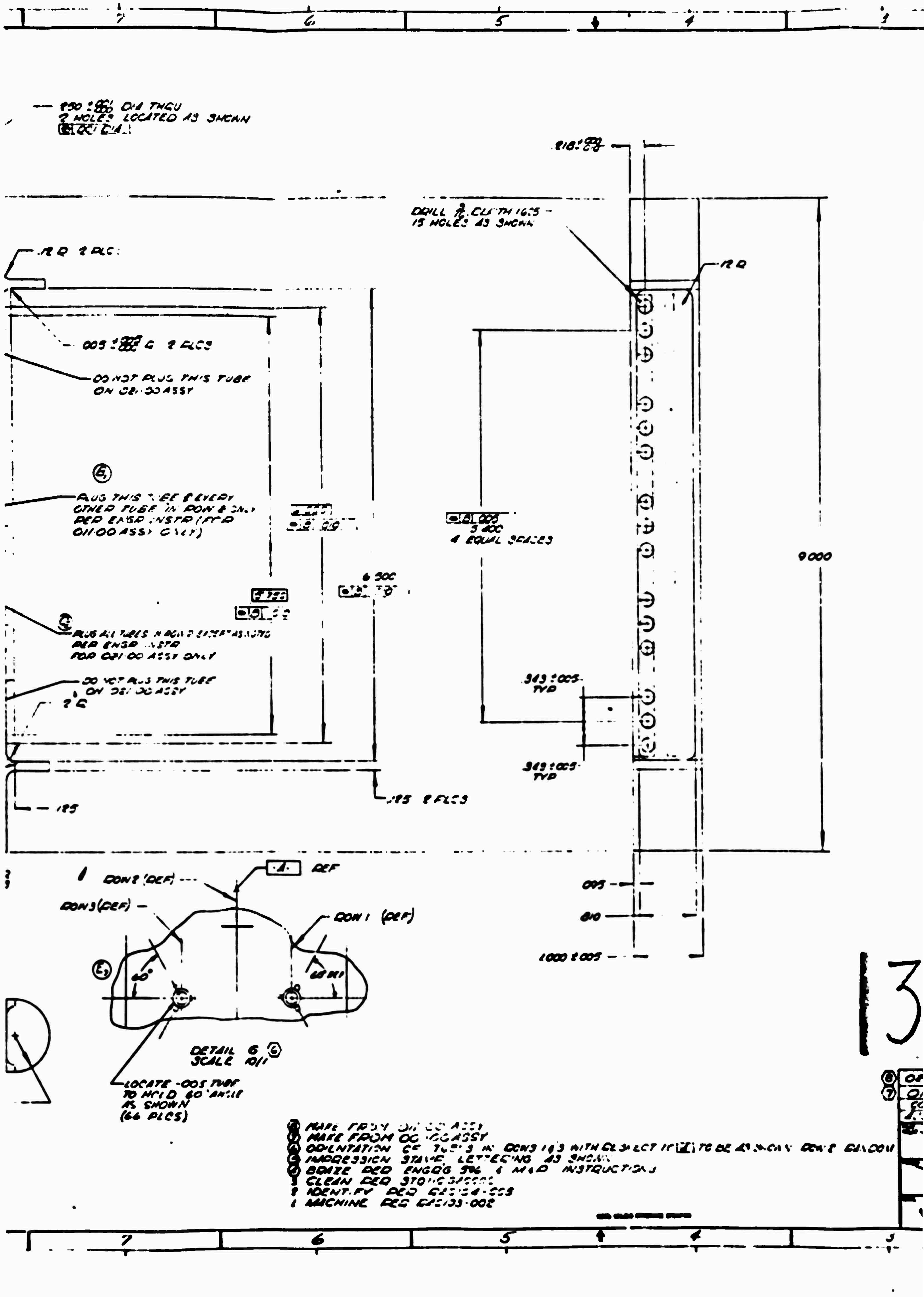

DRILL CL'TH 1625
15 HOLES AS SHOWN
2 HOLES LOCATED AS SHOWN
.12 R 2 PLCS
.12 R
DO NOT PLUG THIS TUBE
ON 021-00 ASSY
PLUG THIS TUBE & EVERY
OTHER TUBE IN ROW & ONLY
PER ENGR INSTR (FOR
011-00 ASSY ONLY)
3.400
4 EQUAL SPACES
9.000
6.500
PLUG ALL TUBES IN ROW
PER ENGR INSTR
FOR 021-00 ASSY ONLY
DO NOT PLUG THIS TUBE
ON 021-00 ASSY
.349 ±.005
TYP
.185 2 PLCS
.185
ROW 2 (REF)
ROW 3 (REF)
ROW 1 (REF)
REF
60°
60 DEG
.095
.810
1.000 ±.005
DETAIL G
SCALE 10/1
LOCATE -005 TUBE
TO HOLD 60° ANGLE
AS SHOWN
(66 PLCS)
IMPRESSION STAMP LETTERING AS SHOWN
BRAZE PER ENGRG 596 & M&P INSTRUCTIONS
CLEAN PER
IDENT.FY PER
1 MACHINE PER
13

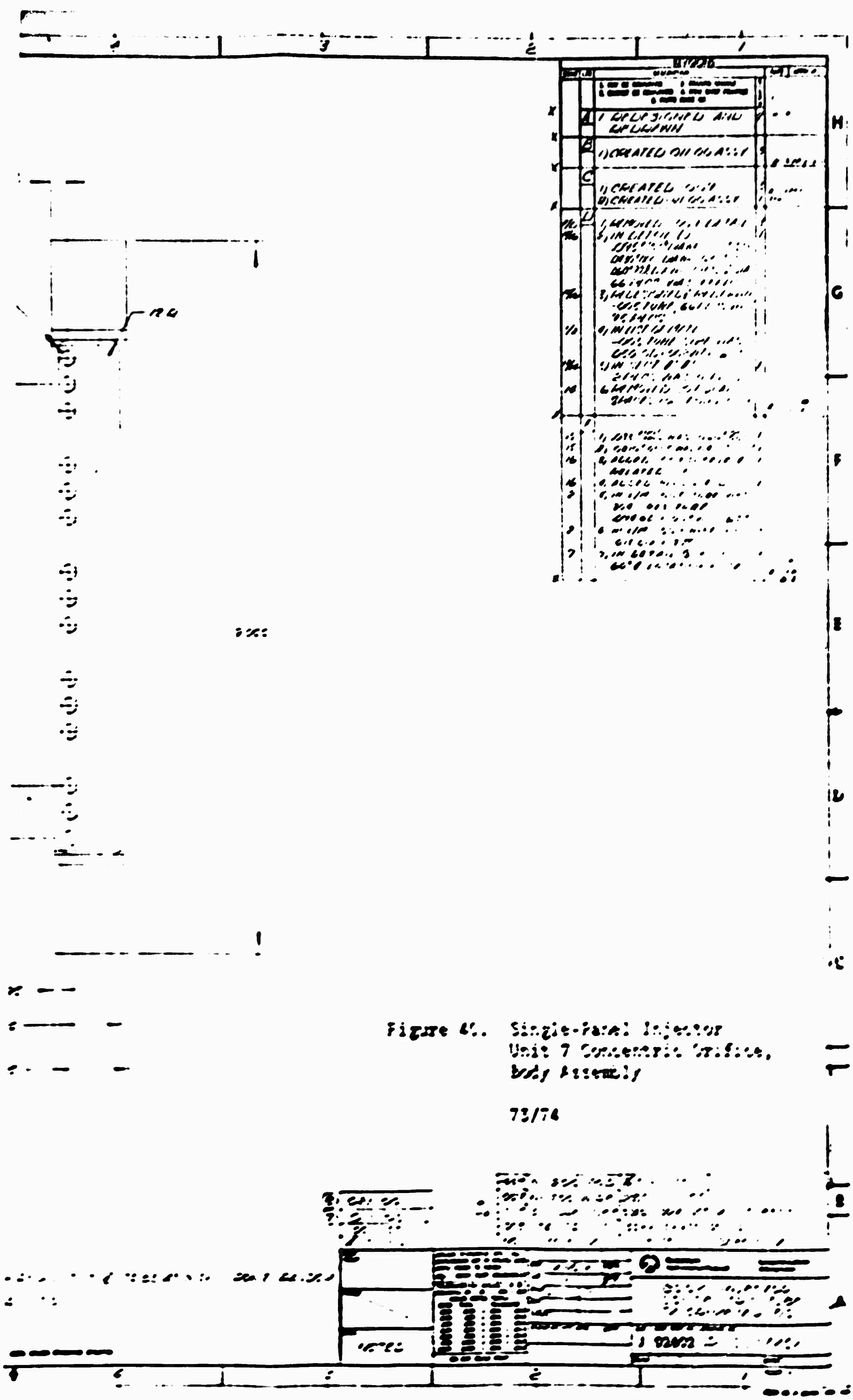

Figure 4[illegible]. Single-Panel Injector Unit 7 Concentric Orifice, Body Assembly

73/74

14

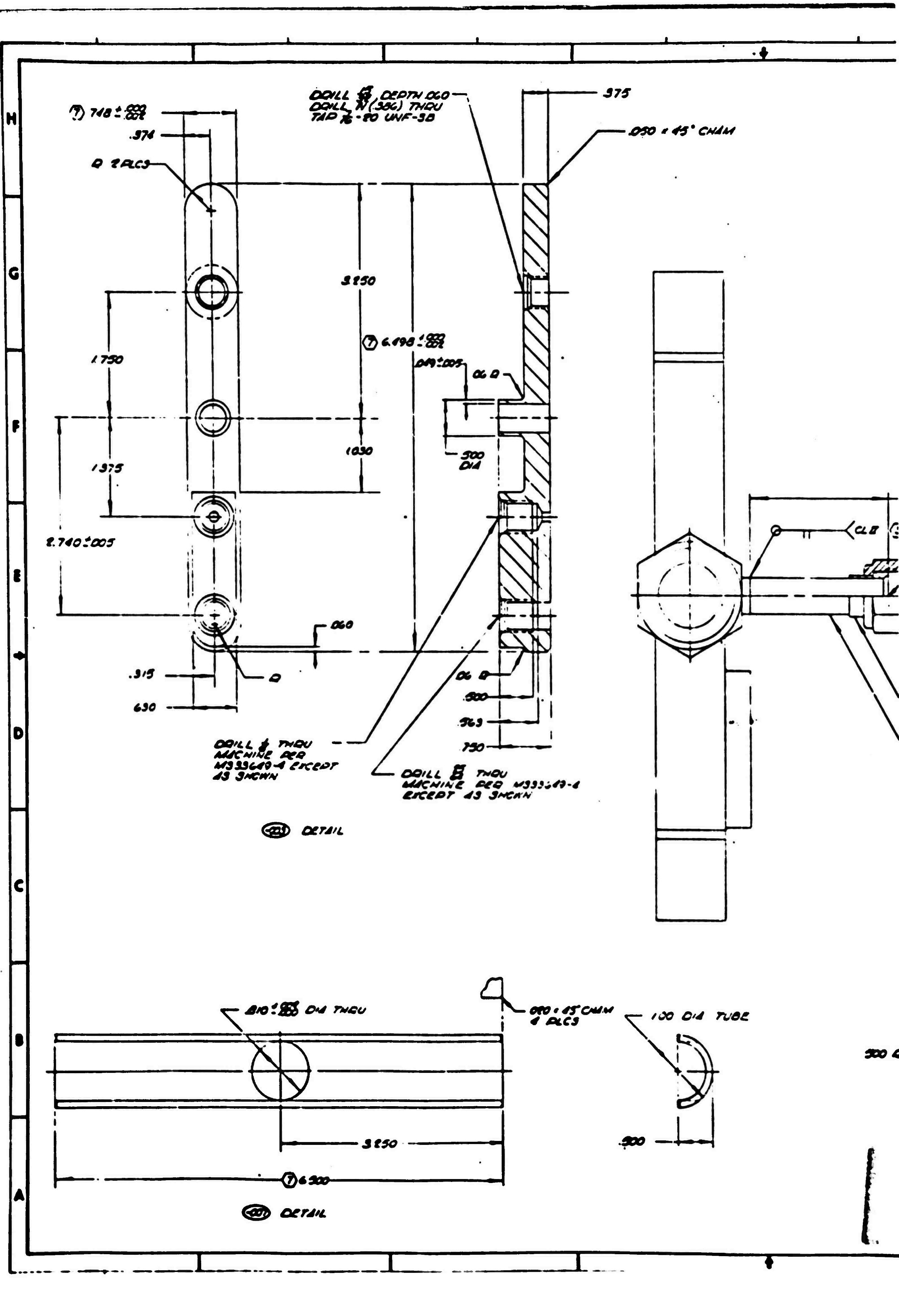
DRILL, DEPTH .060
DRILL (.386) THRU
TAP -20 UNF-3B
.375
.050 x 45° CHAM
.374
Q 2 PLCS
3.250
1.750
1.375
1.030
.500 DIA
2.740±.005
.060
.315
.630
.500
.563
.750
DRILL THRU
MACHINE PER
MS33649-4 EXCEPT
AS SHOWN
DETAIL
.810 DIA THRU
.020 x 45 CHAM
4 PLCS
.100 DIA TUBE
3.250
.300
DETAIL

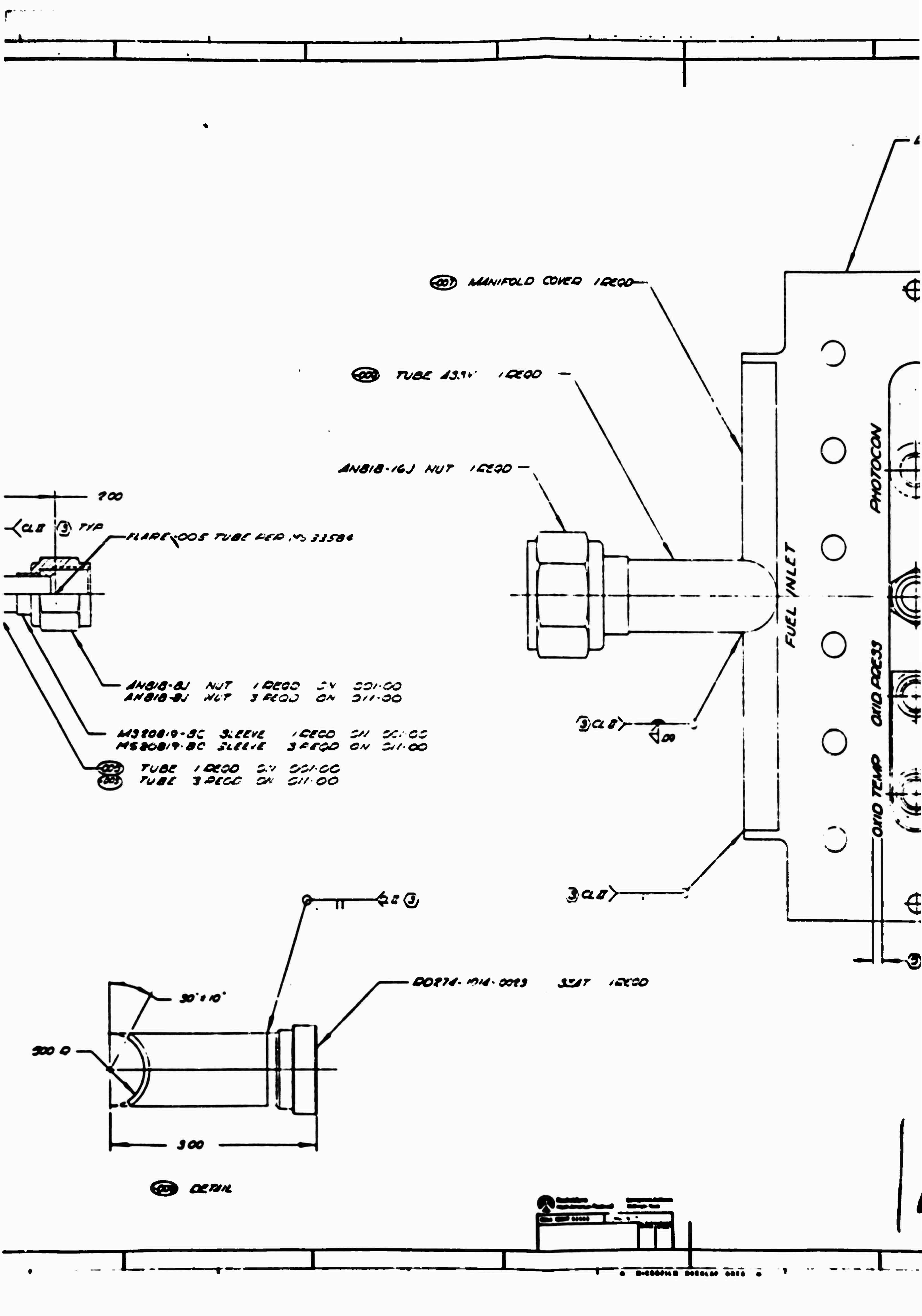

MANIFOLD COVER 1 REQD
TUBE 13.3 1 REQD
AN818-16J NUT 1 REQD
.200
FLARE .005 TUBE PER MS 33584
AN818-8J NUT 1 REQD ON 001-00
AN818-8J NUT 3 REQD ON 011-00
MS20819-8C SLEEVE 1 REQD ON 001-00
MS20819-8C SLEEVE 3 REQD ON 011-00
TUBE 1 REQD ON 001-00
TUBE 3 REQD ON 011-00
PHOTOCON
FUEL INLET
OXID PRESS
OXID TEMP
30° ± 10°
.500
.300
DETAIL

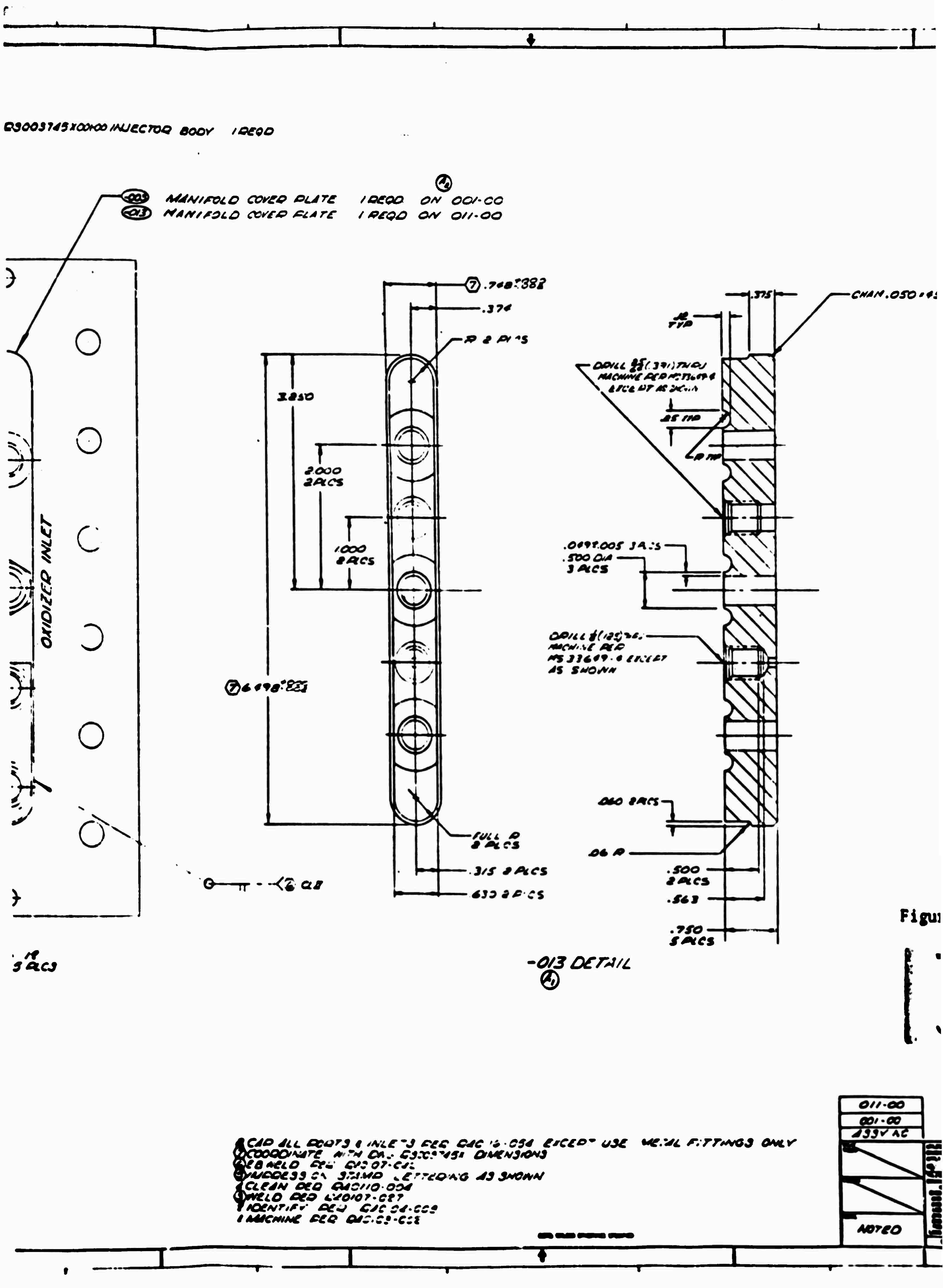

Q3003745X00100 INJECTOR BODY 1REQD
-003 MANIFOLD COVER PLATE 1REQD ON 001-00
-013 MANIFOLD COVER PLATE 1REQD ON 011-00
OXIDIZER INLET
3.850
2.000 2PLCS
1.000 2PLCS
R 2 PLCS
.374
FULL R 2 PLCS
.315 2PLCS
.630 2PLCS
CHAM .050
.375
.500 DIA 3PLCS
.500 2PLCS
.563
.750 5PLCS
.060 2PLCS
.06 R
AS SHOWN
-013 DETAIL
011-00
001-00
NOTED
CAP ALL PORTS & INLETS PER DAC 16-034 EXCEPT USE METAL FITTINGS ONLY
COORDINATE WITH DAC DIMENSIONS
CLEAN PER DAC110-004
MACHINE PER
Figu

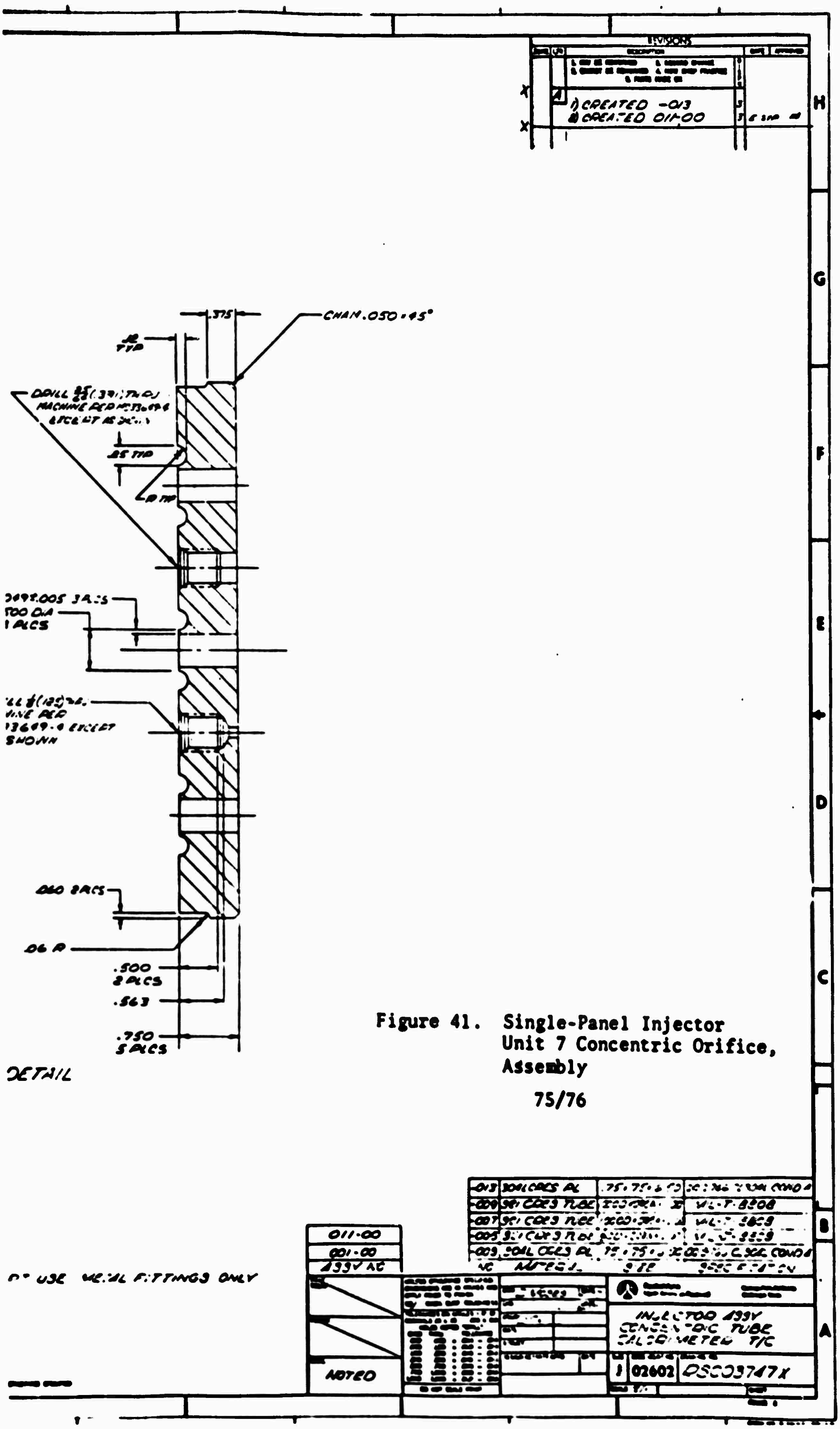

Figure 41. Single-Panel Injector Unit 7 Concentric Orifice, Assembly

14

TABLE 6. COMPUTER COMBUSTION MODEL RESULTS, CONCENTRIC INJECTOR CANDIDATES FOR INJECTOR UNIT 7

	Case 1: 96 Elements 0.006-Inch Fuel Gap			Case 2: 96 Elements 0.008-Inch Fuel Gap			Case 3: 68 Elements 0.008-Inch Fuel Gap		
	η_{vap}	Cup ΔP	Cup Vaporization, percent	η_{vap}	Cup ΔP	Cup Vaporization, percent	η_{vap}	Cup ΔP	Cup Vaporization, percent
700-psia Chamber Pressure									
0.050-Inch Recess	96.38	46.5	19.2	94.59	31.6	16.3	96.9	66	17.2
0.100-Inch Recess	99.05	94.4	40.3	97.65	66	35.5	99.4	135	36.8
450-psia Chamber Pressure									
0.050-Inch Recess	95.91	35.4	21.8	93.79	25	18.8	96.3	51	19.6
0.100-Inch Recess	99.12	74	44.5	97.65	51	39.7	99.3	105	41.0

3. The 95-element pattern would provide roughly the same number of elements per sq in. of injector face as unit 3 injector.

4. The number of elements could be reduced to 68 elements at a later time if desired.

One of the major features of the design was a removable face plate (Fig. 42). This feature provided the capability for rapid rework of injector element parameters such as oxidizer post recess, fuel annulus width, and number of elements. Two face plates were made during the initial fabrication to permit rework of one face while the other was in test. Variation in oxidizer post recess was obtained by conventional machining of the face plate, rather than electrodischarge machining of the oxidizer posts as had been accomplished with unit 3 injector. This feature permitted maintenance of a fixed oxidizer post configuration until an optimum recess-gap configuration was established.

The injector fabrication and assembly technique was different than that used on unit 3 injector. The assembly consisted of a body that contained the manifolding and the brazed-in oxidizer tubes, and a removable face plate. The face plate was copper and the body was corrosion-resistant steel. The completed parts are shown in Fig. 43 and 44.

The injector was flow calibrated following completion of manufacturing. A typical flow test is shown in Fig. 45 and the predicted pressure loss characteristics during test are shown in Fig. 46.

The injector body was modified twice during hot-fire evaluation, in addition to normal recess and annulus variation accomplished by face modification (Fig. 29). The initial modification, units 7 to 7A configuration, removed 16 elements in the center row (every other one) to produce a 79-element injector. The final modification, units 7A to 7D (7B and 7C configuration designed but not released to manufacturing) resulted in a 66-element injector. The pertinent design details are noted in Table 5. Combustion model analyses were conducted for the unit 7D injector modification only, and are described in Appendix I.

DASH NO	S ±	T ±.005	D +.001
-003	.125	.250	.081
-007	.112	.225	.062
-009	.087	.200	.091
-013	.112	.225	.081

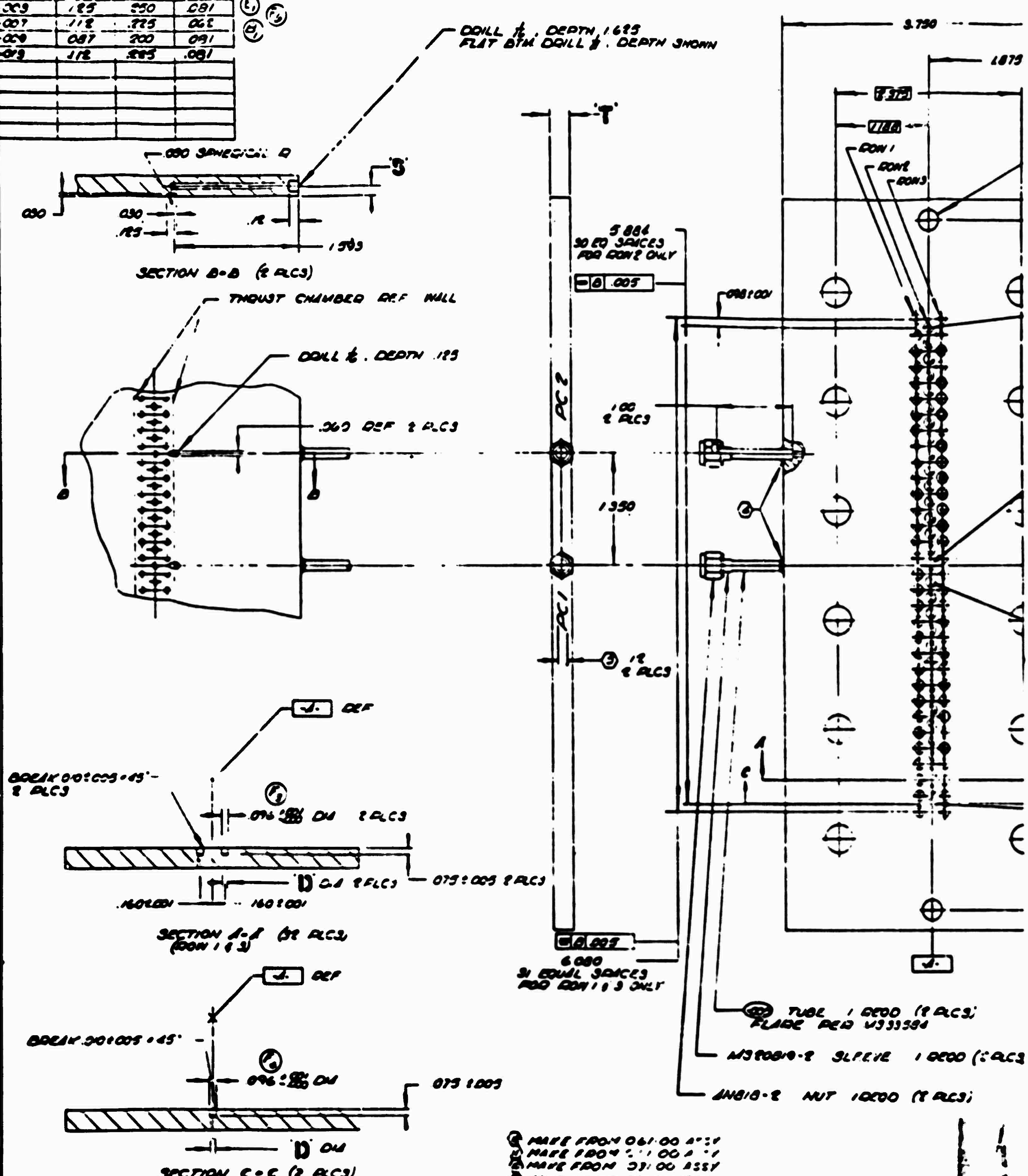

12. MAKE FROM 061-00 ASSY
11. MAKE FROM 051-00 ASSY
10. MAKE FROM 031-00 ASSY
9. MAKE FROM 011-00 ASSY
8. MAKE FROM 021-00 ASSY
7. MAKE FROM 001-00 ASSY
6. MAKE FROM 011-00 ASSY
5. IMPRESSION STAMP LETTERING AS SHOWN BEFORE ORIFICE DR...
4. TIG BRAZE
3. CLEAN PER 3-01-CG-A-00-CE
2. IDENTIFY PER 0A0104-008
1. MACHINE PER 0A0103-008

1

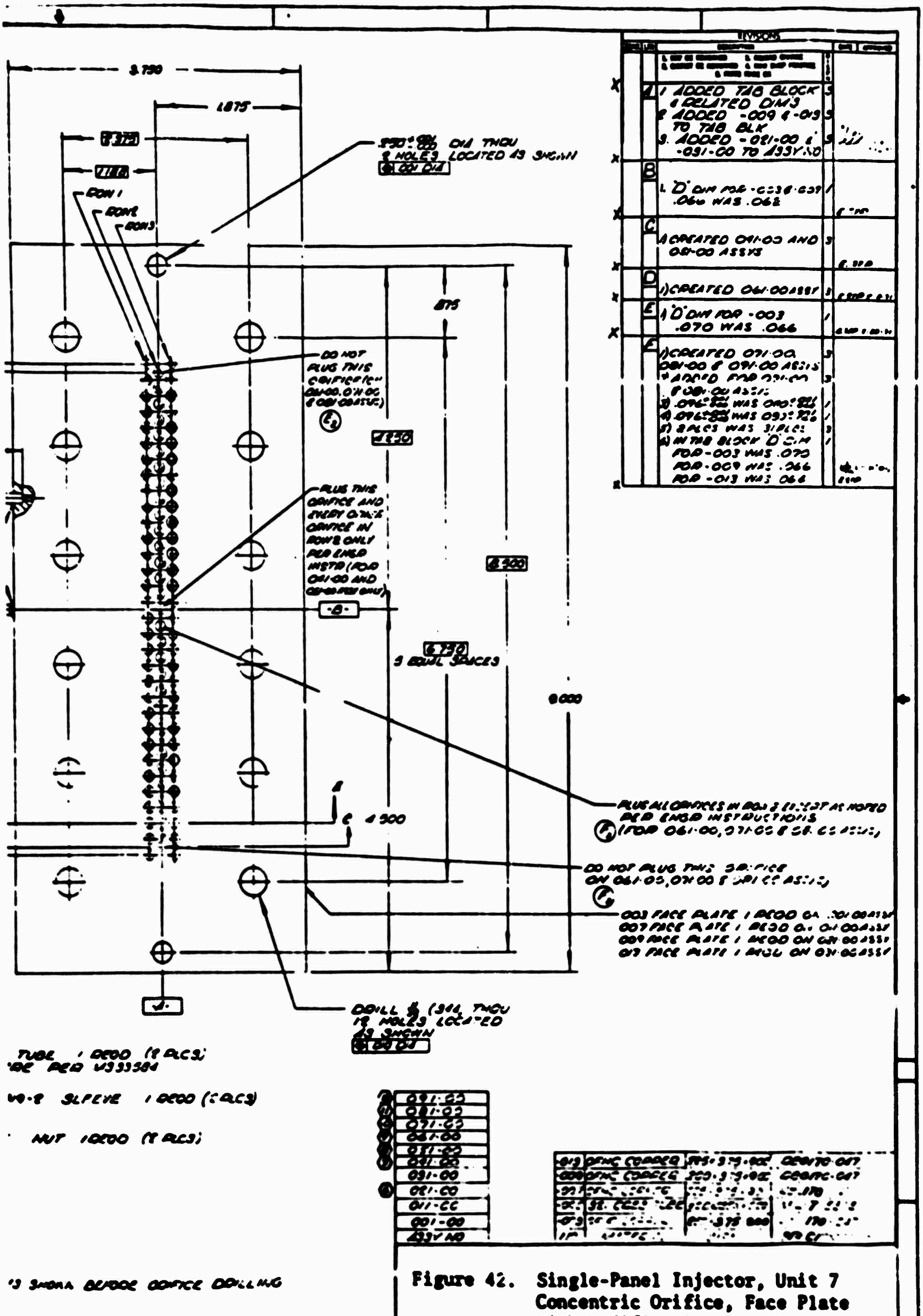

Figure 42. Single-Panel Injector, Unit 7 Concentric Orifice, Face Plate With Modification Details

12

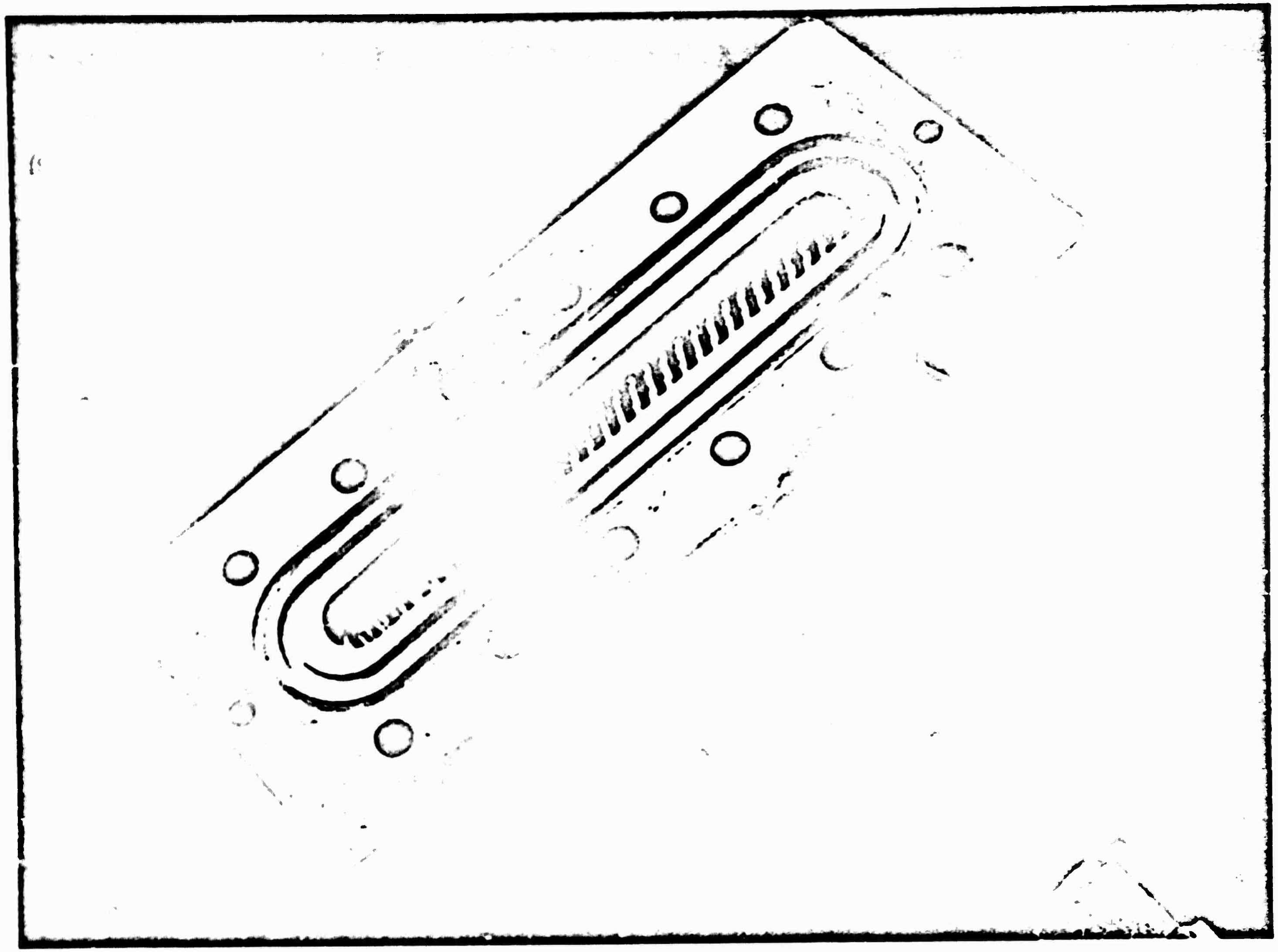

1XX42-4/22/71-C1C

Figure 43. Unit 7 Concentric Orifice Injector Body With Faceplate Removed

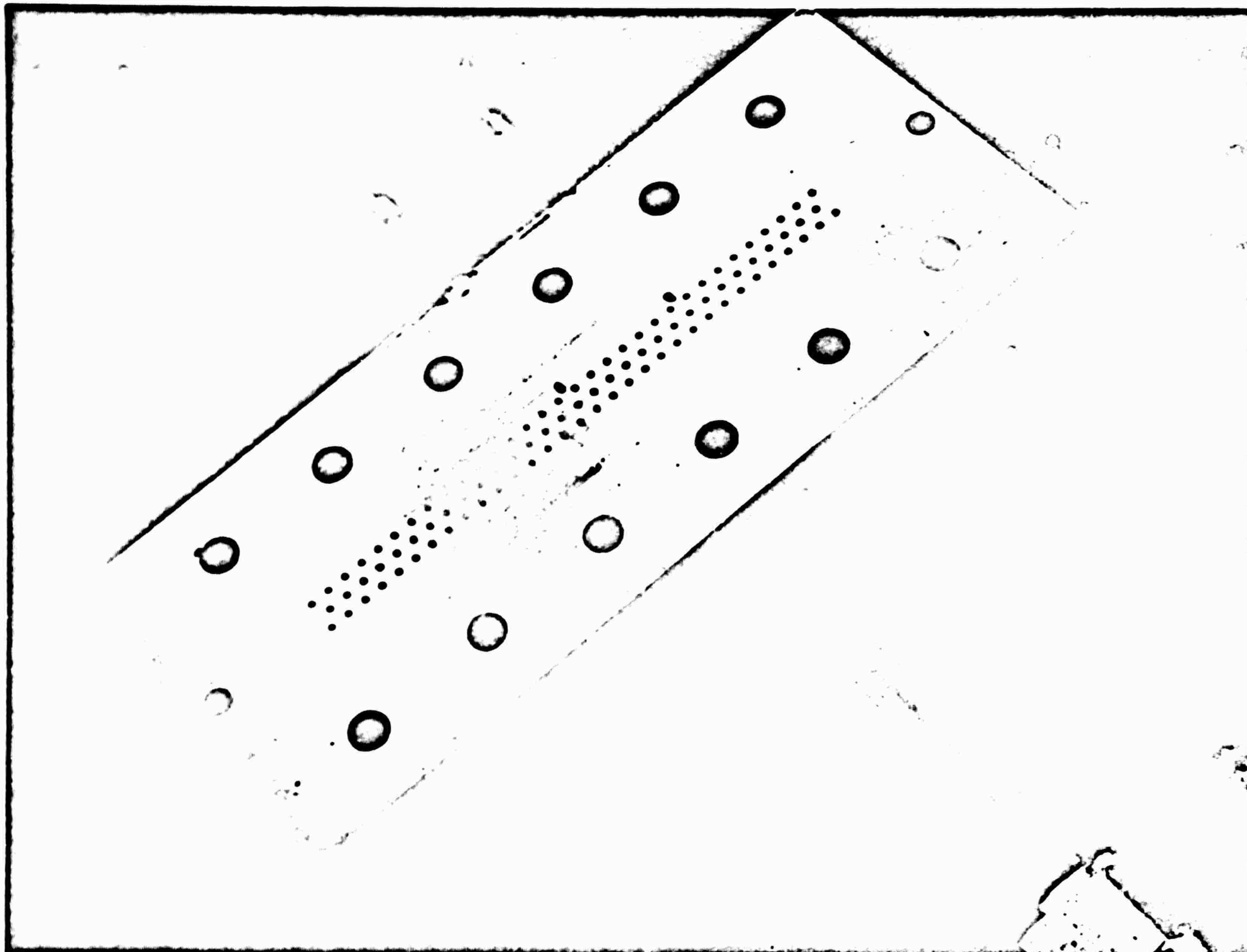

1XX42-4/22/71-C1E

Figure 44. Completed Unit 7 Concentric Orifice Injector With Faceplate Installed

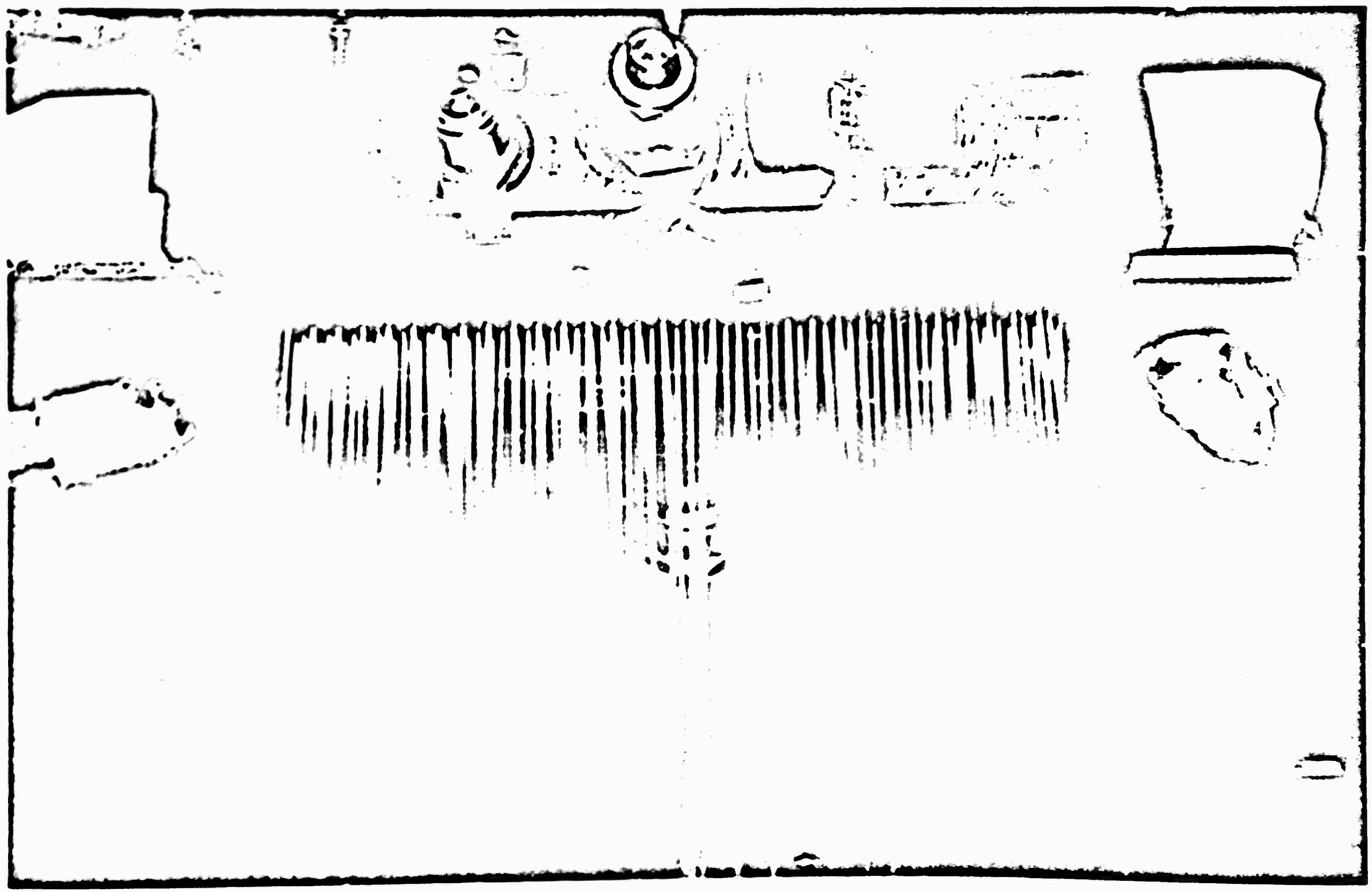

1XX44-4/22/71-C1B

Figure 45. Unit 7 Concentric Orifice Injector Assembly Water Flow, Oxidizer Side Only (100 psid)

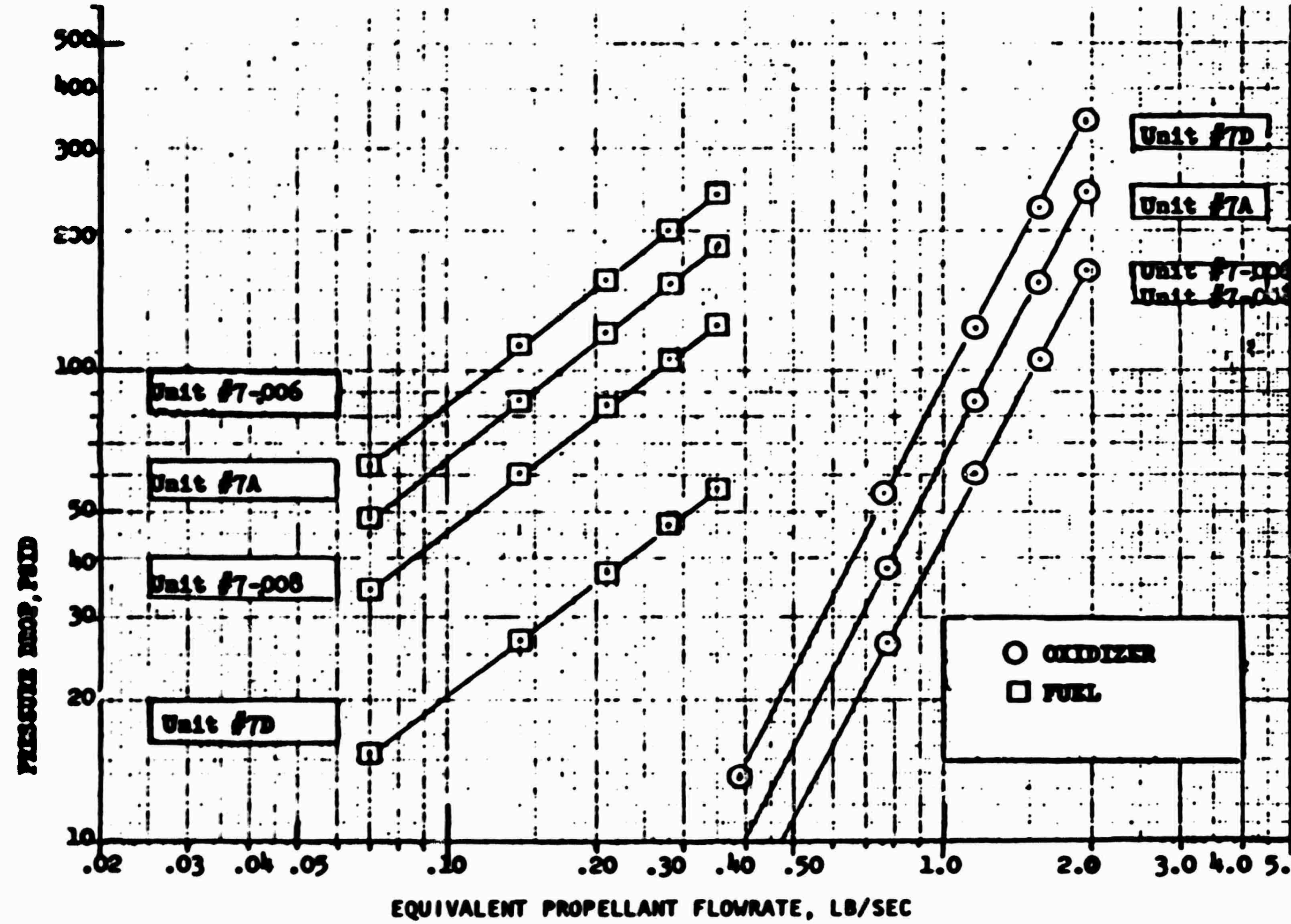

Figure 46. Concentric Injector Predicted Flow Characteristics (Single Panel)

Decrease in the number of elements was accomplished by simply cutting short and welding closed the unwanted oxidizer tubes and welding closed the corresponding orifices in the face plate. Fuel annulus variation was obtained by reaming the face plate orifices to the desired dimension.

INJECTOR SINGLE-ELEMENT COLD-FLOW TESTING

At program start, cold-flow test data were available for gas/liquid elements for both concentric (Ref. 1 and 2) and triplet (Ref. 2) injector; however, for the coplanar injector, no previous cold-flow data were available. Accordingly, single-panel cold-flow effort was conducted, which was limited to evaluation of the performance and chamber compatibility characteristics of the coplanar element.

Basically, the coplanar element consists of a pair of like-impinging stream doublets, one oxidizer and the other fuel. Orifices are located so that the oxidizer fan centers on, and intersects, the fuel fan at right angles. Hot-fire testing, discussed later, showed that this element type had high performance. However, high heat flux and wall erosion were concomitant with high performance. Both the basic coplanar element and modifications of the basic element (oxidizer orifice offset and addition of boundary layer coolant) were evaluated in cold flow. The element modifications were designed to provide a spray mixture ratio bias resulting in low mixture ratio concentrations adjacent to the chamber wall. Reduction of combustion gas mixture ratio and, in turn, flame temperature, in the vicinity of the chamber wall should contribute to a reduction of wall heat flux.

The single-panel injector cold-flow study experimental approach, experimental results, and analysis of results are discussed in subsequent paragraphs.

Experimental Approach

Cold-flow mixing tests were conducted using experimental apparatus and procedures previously developed for gas/liquid distribution experiments (Ref. 1 and 2). Basically, the spray mixing was characterized by: (1) flowing propellant simulants (for the subject effort, oxidizer and fuel were simulated using water and gaseous helium, respectively), and (2) surveying the mass flux distribution of both liquid and gas intercepted at a plane located below the injector face. A probe was used to traverse and measure the mass of liquid and gas intercepted at discrete grid locations in the collection plane. The mass of liquid was assessed from mass collection, and the mass of gas was assessed from analysis of impact pressure measurements.

Single injector elements were employed for all tests. Cold-flow elements were scaled at twice the size (based on area) of hot-fire elements to obtain element feed flows concomitant with instrumentation measurement capabilities. Equivalent impingement angles and scaled impingement distances were used for applicability of cold-flow element geometry modeling to the hot-fire size element.

Cold-flow mixing tests were designed to simulate, as closely as possible, actual hot-firing conditions (i.e., propellant injection momentum, injection velocities, and injection densities) at the 450-psia chamber pressure operating condition (MR = 5.5). Tests were conducted in a pressurized chamber which provided close simulation of hot-fire propellant injection densities. However, gaseous propellant simulant injection velocities were limited to 2800 ft/sec (sonic flow with ambient temperature helium), which were less than the hot-fire injection velocities which approach 4000 ft/sec. Therefore, injection velocity of the oxidizer simulant was reduced accordingly to maintain the same momentum ratio (fuel/oxidizer) characteristic of hot firing. Because mixing is predominantly controlled by momentum exchange, maintenance of the momentum ratio would ensure applicability of the cold-flow results to hot-fire conditions.

Three cold-flow tests were conducted. The first test evaluated the basic coplanar element, as shown in Fig. 47. The second test evaluated the basic coplanar element with incorporation of boundary layer coolant. Boundary layer coolant was incorporated by adding a fuel like-doublet adjacent to the basic coplanar element, as shown in Fig. 47. The third test evaluated a modification of the basic coplanar in which the oxidizer orifices were offset 0.014 inch, as shown in Fig. 47. This offset was intended to shift the oxidizer mass to one side of the spray field, thereby providing lower mixture ratios on the opposing side of the spray field.

(A) Basic Coplanar Element

(B) Basic Coplanar Element with BLC

(C) Modified Coplanar Element with Oxidizer Orifice Offset

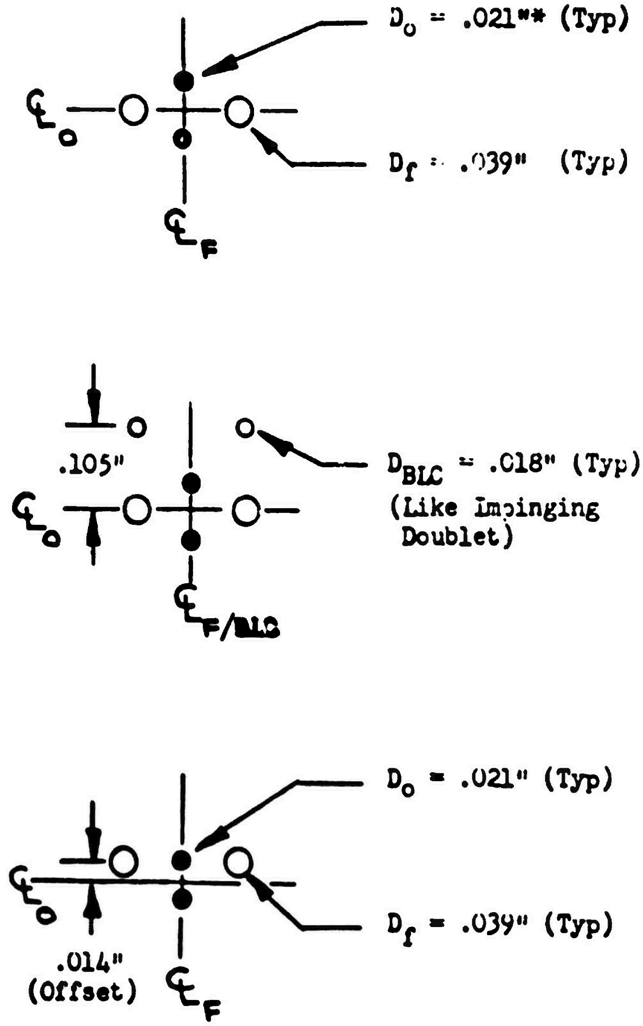

*Cold flow element dimensions $\sqrt{2}$ X hot fire element dimensions (i.e., twice area scale)

Figure 47. Single Injector Element Configurations Evaluated in Cold-Flow Mixing Tests

Experimental Results

Cold-flow data were reduced to provide definition of: (1) the spray mass distribution, (2) the mixing index, E_m, and (3) the mixing efficiency, $\eta_{c^* \, mix}$. A tabulation of E_m and $\eta_{c^* \, mix}$ for each test is listed in Table 7 . Mass flux distribution plots defined the spray distribution for the basic element, basic element with boundary layer coolant, and the modified element.

Element mixing efficiencies are discussed first, followed by presentation of the element spray distribution characteristics.

TABLE 7 . SINGLE-PANEL COPLANAR ELEMENT COLD-FLOW DATA SUMMARY

Element Type	Mixing Index, E_m, percent	Mixing Efficiency, $\eta_{c^* \, mix}$, percent
Basic Coplanar	46	74
Basic Coplanar With Boundary Layer Coolant (BLC)	75	92
Modified Coplanar With Oxidizer Orifice Offset	24	58

Mixing Efficiency. Cold-flow mass collection results can be used for analytic prediction of an injector mixing uniformity index, termed E_m, and combustion efficiency limited by injector mixing, $\eta_{c^* \, mix}$.

The distribution index, E_m, which represented the percentage of total spray that has achieved the intended mixture ratio has been defined by Rupe (Ref. 3). The distribution index is based on a stream tube analysis according to the relationship:

$$E_m = 1 - \left[\sum_i^n M_{f_i} \frac{(R_t - r_i)}{R_t} + \sum_i^{\bar{n}} M_{f_i} \frac{(R_t - r_i)}{R_t - 1} \right] \qquad (1)$$

where

M_{f_i} = mass fraction in i^{th} tube

R_t = total oxidizer/total oxidizer + fuel

r_i = i^{th} tube oxidizer/i^{th} tube oxidizer + fuel

n = number of tubes in which $r_i < R_t$

$\bar{n}$ = number of tubes in which $r_i > R_t$

The distribution index correlation was useful for relative injector comparisons. The distribution index did not explicitly characterize the manner in which spray maldistribution limits combustion efficiency. Propellant mass and mixture ratio distribution characteristics were further related to specific propellant characteristic velocity versus mixture ratio data to determine distribution-limited combustion efficiency, $\eta_{c^* \, mix}$. In general, a higher distribution index corresponds to a higher distribution-limited combustion efficiency.

A prediction of combustion efficiency limited by propellant distribution, $\eta_{c^* \, mix}$, was determined by use of a stream tube analysis, as follows:

$$\eta_{c^* \, mix} = \sum_{i}^{n} \frac{MF_i \; c^*_i}{c^*_{theo}} \qquad (2)$$

where

MF_i = mass fraction in i^{th} tube

c^*_i = theoretical characteristic velocity corresponding to mixture ratio in i^{th} stream tube

c^*_{theo} = theoretical characteristic velocity at the overall injected mixture ratio

n = number of stream tubes

The mixing efficiencies for the different element configurations spanned a wide range. The basic element had a relatively low mixing efficiency ($\eta_{c^* \, mix}$ = 74 percent). Mixing losses associated with the basic element were due to gross spray maldistribution (namely pockets of oxidizer) as were evident in spray distribution plots (shown later). The spray maldistribution was further exemplified with the modified element (oxidizer orifice offset) which yielded a lower mixing efficiency ($\eta_{c^* \, mix}$ = 58 percent). Incorporation of the boundary layer coolant with the basic element yielded a large improvement in mixing efficiency ($\eta_{c^* \, mix}$ = 92 percent). Again, the mode of improvement was evident in spray distribution plots (Fig. 50).

The mixing efficiencies pertained to a single element and, therefore, did not include interelement mixing which occurred with multiple elements on an injector face. In general, interelement mixing,which was related to both element spacing and orientation, tended to raise the overall injector mixing efficiency above that obtained with single elements.

Spray Distribution. The mass flux distribution plots show the spatial location of both fuel and oxidizer flux in the collection plane. The collection plane was subdivided into eight sectors with the element aligned above the center of the collection plane. Data were reduced to show the mass flux profile, of both propellants, through each of the eight sectors. In this manner, the relative concentrations of oxidizer and fuel at discrete locations in the spray field were visually apparent. A normalized mass flux (local mass flux/total injected mass of corresponding propellant) was plotted. In this manner, the overall design mixture ratio was characterized by equal normalized mass flux values of oxidizer and fuel (i.e., where the flux lines intersect). The mass flux ($\dot{W}/A$) values corresponded to larger quantities of mass ($\dot{W}$) at sampling radii further from the center where the area over which the flux applies was greater. The mass flux plots for each test are discussed in the following paragraphs.

The mass flux plot for the basic element is shown in Fig. 48. For further clarification, a schematic sketch of the spray field, as defined by the mass flux plot (Fig. 48), is shown in Fig. 49. The mass flux plot (Fig. 48) shows excess concentrations of oxidizer in the peripherial zones of section 1/8 and 4/5. In the schematic drawing (Fig. 49), the shape of the element spray field is depicted by the elliptical outline, and the concentrations of oxidizer are depicted as shaded zones. Examination of the spray distribution (Fig. 48 and 49) shows that the gaseous fuel momentum: (1) dominates the overall spray field (i.e., the spray field shape corresponds to the gaseous fuel fan), and (2) tends to split the liquid oxidizer spray fan into two discrete pockets, leaving a fuel-rich core zone. This distribution indicates that the oxidizer spray is not penetrating the fuel stream, but rather being directed to two opposing sides of the flow field. Such maldistribution reduces mixing efficiency, $\eta_{c^* \, mix}$.

For the basic elements with BLC (Fig. 50), the fuel BLC fan entrained the excess oxidizer flux in sectors 1/8, located next to the BLC fan, and provided more uniform mixing. Although the BLC fan did not provide a fuel-rich zone at the periphery of sectors 1/8, it substantially reduced the mixture ratio to values near the design mixture ratio of 5.5. The BLC fan did not alter the oxidizer-rich zone in sectors 4/5, located in the spray field opposite the BLC fan.

Modification of the basic element with oxidizer orifice offset changed the spray distribution as intended (Fig. 51). The modification transferred oxidizer flux in the direction of the offset, from sectors 1/8 to sectors 4/5. The increased spray maldistribution was responsible for the reduction in mixing efficiency with this configuration (previously discussed). Further, visual appearance of the element spray indicated that drop size (not measured in this cold-flow study) may have increased with the modified design, as compared to the basic and to the basic with BLC designs.

In summary, the cold-flow results showed that: (1) the element fan shape is controlled by the fuel fan, (2) the single-element mixing efficiency was low (except for elements with BLC), and (3) the mixing efficiency is strongly dependent on the spatial location of oxidizer and fuel sprays (i.e., oxidizer fan offset caused a large loss in mixing efficiency).

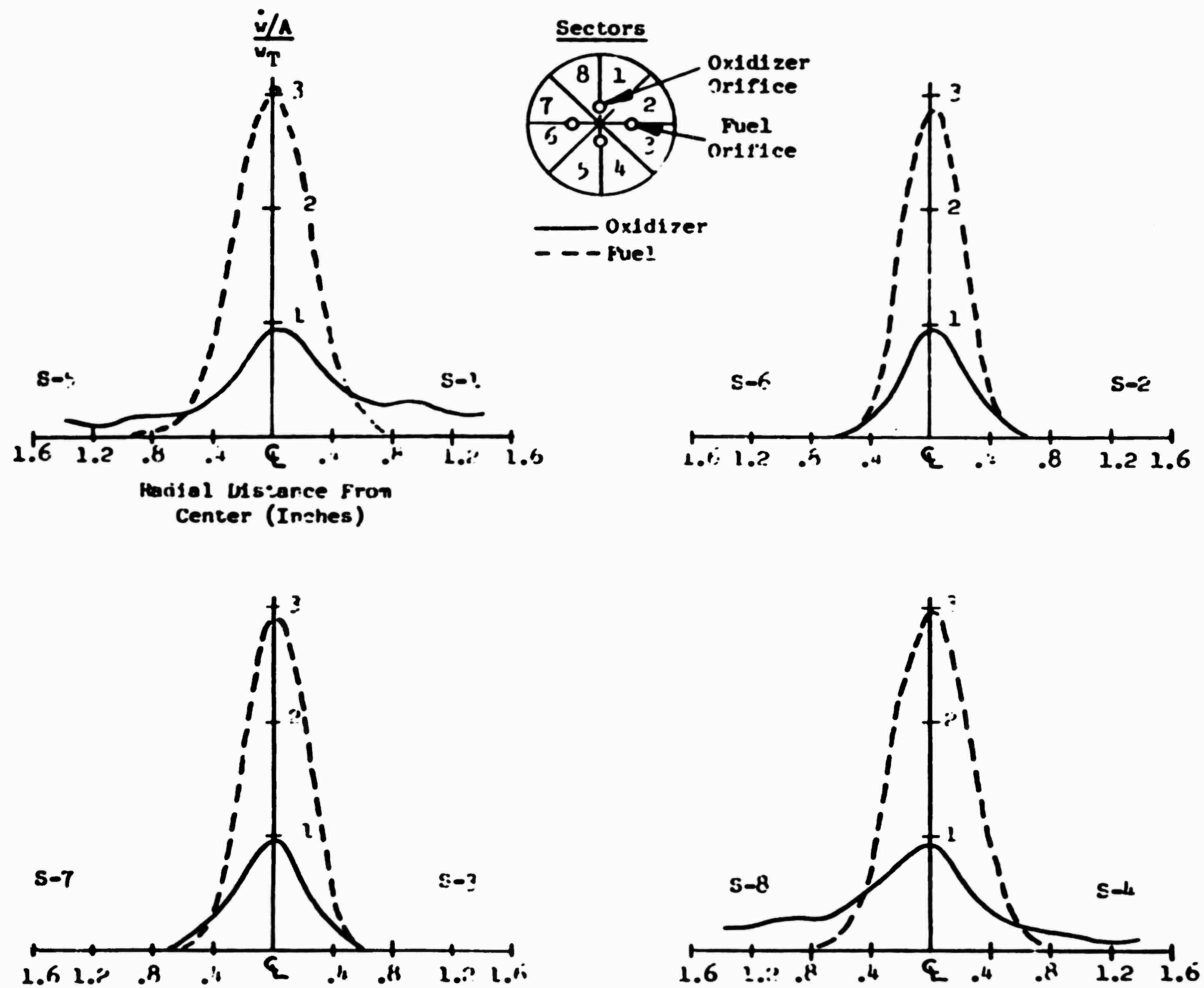

Figure 48. Mass Flux Distribution Plots for Basic Coplanar Element (Test No. 1)

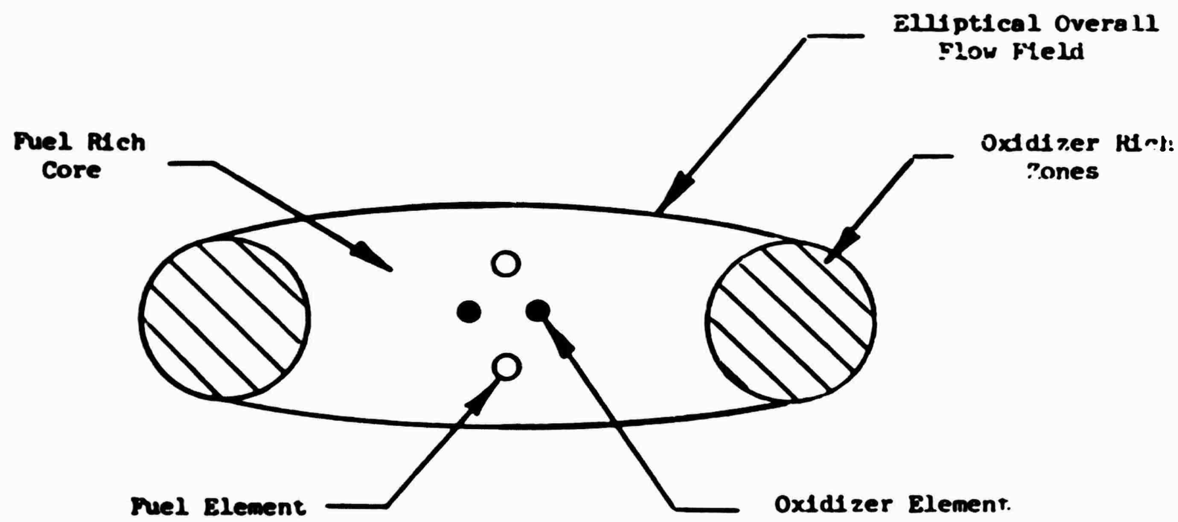

Figure 49. Schematic of Spray Field Mass Flux Distribution for Basic Coplanar Element

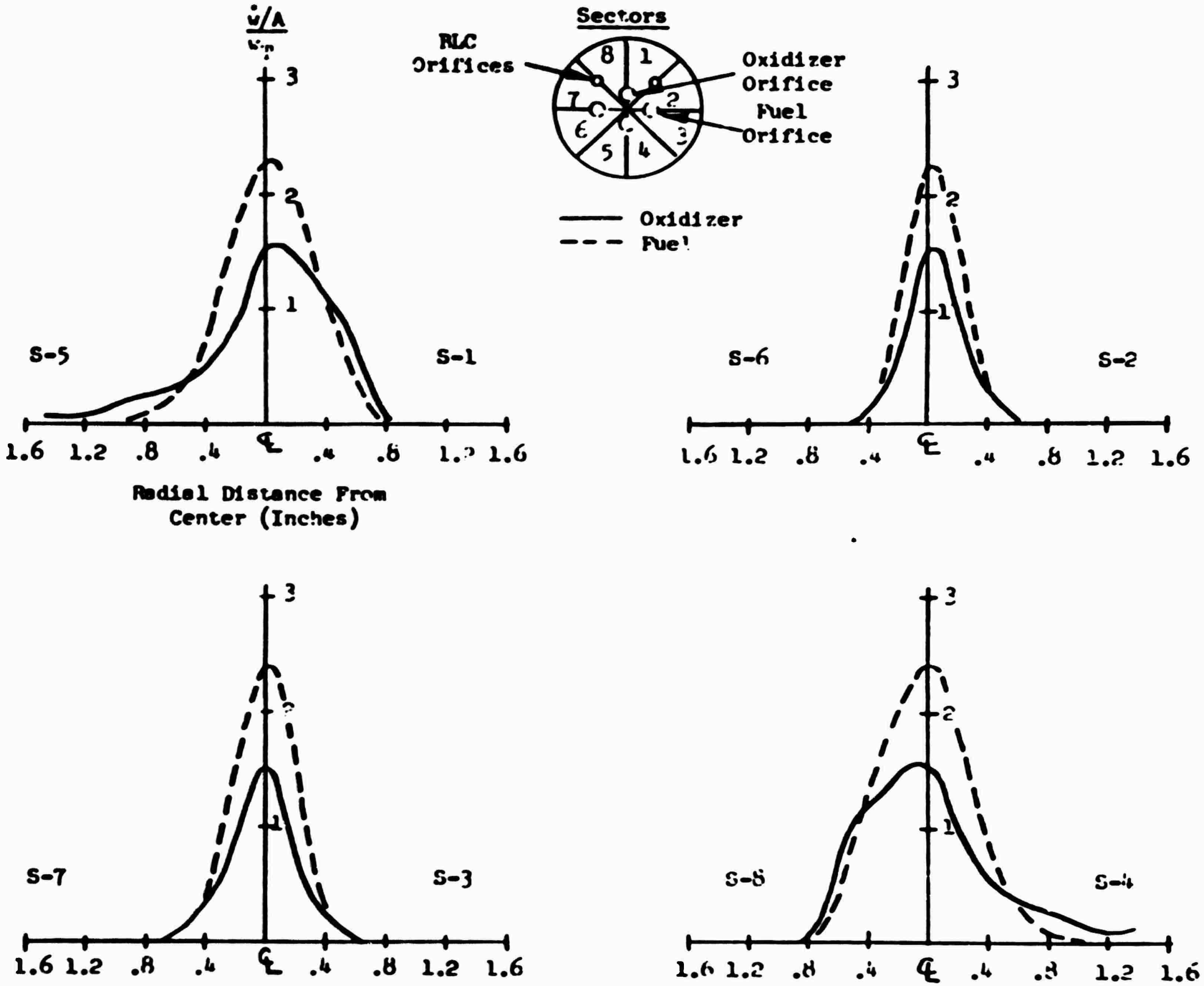

Figure 50. Mass Flux Distribution Plots for Basic Coplanar Element With Boundary Layer Coolant, BLC (Test No. 2)

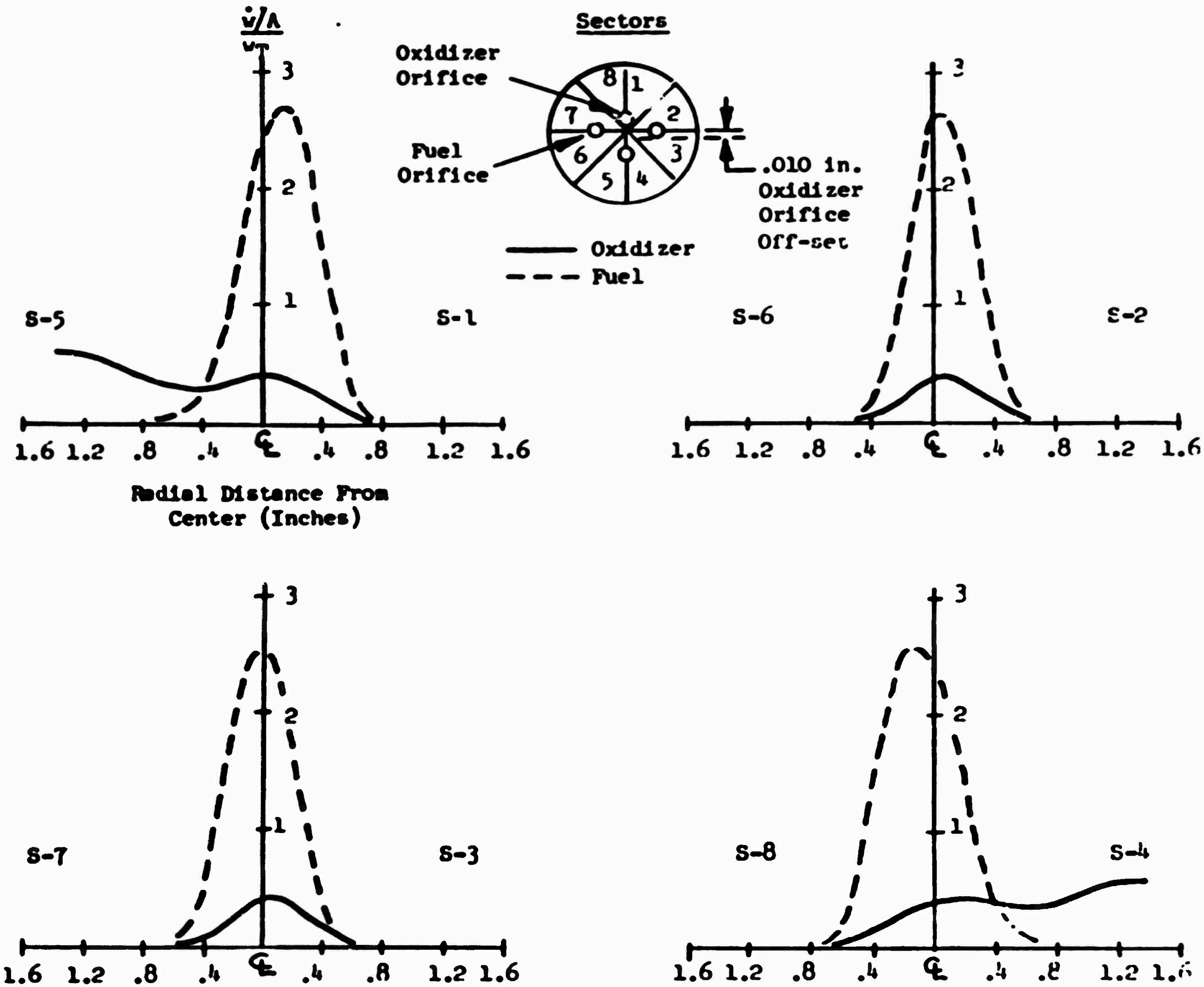

Figure 51. Mass Flux Distribution Plots for Modified Coplanar Element With Oxidizer Orifice Offset (Test No. 3)

SINGLE-PANEL SEGMENT HOT-FIRE TESTING

A total of 117 water-cooled segment tests was made during the single-panel segment evaluation. The total firing time of single-panel segment components was 1342 seconds. All tests were accomplished with LO_2/GH_2 propellants at site altitude conditions (2000 feet above sea level).

Table 8 presents a summary of the tests. All tests were conducted at the Propulsion Research Area, Peter Test Stand. The test facility is described in Section VI. The gaseous hydrogen provided to the injector was preheated, by use of a slug heater, to simulate the fuel injection temperature predicted for the regeneratively cooled segment injector. Table 9 presents the test component configurations that were evaluated, the number of tests, and total test duration applicable to each configuration.

The nominal test conditions for the single-panel water-cooled segments were:

1. Maximum chamber pressure = 750 psia with intermediate pressures of 600, 450, and 300 psia
2. Minimum chamber pressure = 150 psia
3. Injector mixture ratio range = 5.0 to 6.0 (5.5 nominal)
4. Propellant injection temperature: LO_2 ~170 R, GH_2 ~900 R
5. Test durations
   10 seconds at maximum chamber pressure
   20 seconds at minimum chamber pressure
6. Ignition source: gaseous fluorine

Table 8 presents the measured and derived data for each test. The equations and computational techniques used to determine the performance and heat transfer parameters are presented in Appendixes II and III.

The performance and heat transfer data are presented and discussed in this section. The test component hardware operating characteristics and durability also are discussed.

TABLE 8. SINGLE-PANEL WATER-COOLED SEGMENT, TEST DATA AND RESULTS

Test Number	Injector Type	Chamber Type	ε_c	L*, inch	Chamber Pressure (Nozzle), psia	Mixture Ratio	Duration (Steady), seconds	Fuel Injection Temperature, F	Thrust (Sea Level), pounds	Vacuum Thrust, pounds	$\dot{w}_o$, lb/sec	$\dot{w}_f$, lb/sec	Throat Heat Flux, Btu/in²-sec	Injector End Heat Flux, Btu/in²-sec	c*(Pc), ft/sec	c*(F), ft/sec	η_{c^*}(Pc), percent	η_{c^*}(F), percent	Nozzle Flow Separated	Remarks
[illegible]	Coplanar, Unit 1	Unit 1	[illegible]	[illegible]	--	--	--	--	--	--	--	--	--	--	--	--	--	--	-	Ignition only
[illegible]	Coplanar, Unit 1	Unit 1			[illegible]	[illegible]	[illegible]	[illegible]	[illegible]	[illegible]	[illegible]	[illegible]	[illegible]	--	[illegible]	[illegible]	[illegible]	[illegible]	No	Satisfactory test
[illegible]	Coplanar, Unit 1	Unit 1			--	--	[illegible]	--	--	--	--	--	--	--	--	--	--	--	--	Automatic redline cutoff device monitoring liquid oxygen temperature
[illegible]	Coplanar, Unit 1	Unit 1			[illegible]	[illegible]	[illegible]	[illegible]	[illegible]	--	[illegible]	[illegible]	[illegible]	[illegible]	[illegible]	--	[illegible]	--	Yes	Satisfactory test
[illegible]	Coplanar, Unit 1	Unit 1			[illegible]	[illegible]	[illegible]	[illegible]	[illegible]	--	[illegible]	[illegible]	[illegible]	[illegible]	[illegible]	--	[illegible]	--	Yes	Satisfactory test
[illegible]	Coplanar, Unit 1	Unit 1			--	--	[illegible]	--	--	--	--	--	--	--	--	--	--	--	--	Automatic redline cutoff device monitoring liquid oxygen temperature
[illegible]	Coplanar, Unit 1	Unit 1			--	--	[illegible]	--	--	--	--	--	--	--	--	--	--	--	--	Test terminated by exhaust flame discoloration
[illegible]	Coplanar, Unit 1	Unit 1			[illegible]	[illegible]	[illegible]	[illegible]	[illegible]	--	[illegible]	[illegible]	[illegible]	--	[illegible]	--	[illegible]	--	Yes	Satisfactory test
[illegible]	Coplanar, Unit 1	Unit 1			[illegible]	[illegible]	[illegible]	[illegible]	[illegible]	--	[illegible]	[illegible]	[illegible]	[illegible]	[illegible]	--	[illegible]	--	Yes	
[illegible]	Triplet, Unit 2	Unit 1			[illegible]	[illegible]	[illegible]	[illegible]	[illegible]	[illegible]	[illegible]	[illegible]	[illegible]	[illegible]	[illegible]	[illegible]	[illegible]	[illegible]	No	
[illegible]	Triplet, Unit 2	Unit 1			[illegible]	[illegible]	[illegible]	[illegible]	[illegible]	[illegible]	[illegible]	[illegible]	[illegible]	[illegible]	[illegible]	[illegible]	[illegible]	[illegible]	No	
[illegible]	Triplet, Unit 2	Unit 1			[illegible]	[illegible]	[illegible]	[illegible]	[illegible]	[illegible]	[illegible]	[illegible]	[illegible]	[illegible]	[illegible]	[illegible]	[illegible]	[illegible]	No	
[illegible]	Triplet, Unit [illegible]	Unit 1			--	--	[illegible]	--	--	--	--	--	--	--	--	--	--	--	--	Automatic redline cutoff device monitoring liquid oxygen temperature
[illegible]	Triplet, Unit 2	Unit 1			[illegible]	[illegible]	[illegible]	[illegible]	[illegible]	[illegible]	[illegible]	[illegible]	[illegible]	--	[illegible]	[illegible]	[illegible]	[illegible]	No	Satisfactory test
[illegible]	Triplet, Unit 2	Unit 1			[illegible]	[illegible]	[illegible]	[illegible]	[illegible]	[illegible]	[illegible]	[illegible]	[illegible]	[illegible]	[illegible]	[illegible]	[illegible]	[illegible]	No	
[illegible]	Triplet, Unit 2	Unit 1			[illegible]	[illegible]	[illegible]	[illegible]	[illegible]	--	[illegible]	[illegible]	[illegible]	[illegible]	[illegible]	--	[illegible]	--	Yes	
[illegible]	Triplet, Unit 2	Unit 1	[illegible]	[illegible]	[illegible]	[illegible]	[illegible]	[illegible]	[illegible]	--	[illegible]	[illegible]	[illegible]	[illegible]	[illegible]	--	[illegible]	--	Yes	
[illegible]	Triplet, Unit 2	Unit 1			[illegible]	[illegible]	[illegible]	[illegible]	[illegible]	[illegible]	[illegible]	[illegible]	[illegible]	[illegible]	[illegible]	[illegible]	[illegible]	[illegible]	No	
[illegible]	Triplet, Unit 2	Unit 1			[illegible]	[illegible]	[illegible]	[illegible]	[illegible]	[illegible]	[illegible]	[illegible]	[illegible]	[illegible]	[illegible]	[illegible]	[illegible]	[illegible]	No	
[illegible]	Triplet, Unit 2	Unit 1			[illegible]	[illegible]	[illegible]	[illegible]	[illegible]	--	[illegible]	[illegible]	[illegible]	[illegible]	[illegible]	--	[illegible]	--	Yes	
[illegible]	Triplet, Unit 2	Unit 1			[illegible]	[illegible]	[illegible]	[illegible]	[illegible]	--	[illegible]	[illegible]	[illegible]	[illegible]	[illegible]	--	[illegible]	--	Yes	
[illegible]	Triplet, Unit 2	[illegible]	[illegible]	[illegible]	[illegible]	[illegible]	[illegible]	[illegible]	[illegible]	--	[illegible]	[illegible]	[illegible]	[illegible]	[illegible]	--	[illegible]	--	Yes	
[illegible]	Triplet, Unit 2	Unit 1			[illegible]	[illegible]	[illegible]	[illegible]	[illegible]	[illegible]	[illegible]	[illegible]	[illegible]	[illegible]	[illegible]	[illegible]	[illegible]	[illegible]	No	
[illegible]	Coplanar, Unit [illegible]	Unit [illegible]			[illegible]	[illegible]	[illegible]	[illegible]	[illegible]	--	[illegible]	[illegible]	[illegible]	[illegible]	[illegible]	--	[illegible]	--	Yes	
[illegible]	Coplanar, Unit [illegible]	Unit [illegible]			[illegible]	[illegible]	[illegible]	[illegible]	[illegible]	[illegible]	[illegible]	[illegible]	[illegible]	--	[illegible]	[illegible]	[illegible]	[illegible]	No	
[illegible]	Coplanar, Unit [illegible]	Unit [illegible]			[illegible]	[illegible]	[illegible]	[illegible]	[illegible]	[illegible]	[illegible]	[illegible]	[illegible]	[illegible]	[illegible]	[illegible]	[illegible]	[illegible]	No	Test terminated by observer because of exhaust flame discoloration
[illegible]	Coplanar, Unit [illegible]	Unit 2			[illegible]	[illegible]	[illegible]	[illegible]	[illegible]	--	[illegible]	[illegible]	[illegible]	[illegible]	[illegible]	--	[illegible]	--	Yes	Satisfactory test
[illegible]	Coplanar, Unit [illegible]	Unit 2			[illegible]	[illegible]	[illegible]	[illegible]	[illegible]	--	[illegible]	[illegible]	[illegible]	[illegible]	[illegible]	--	[illegible]	--		
[illegible]	Triplet, Unit [illegible]	Unit 2			[illegible]	[illegible]	[illegible]	[illegible]	[illegible]	--	[illegible]	[illegible]	[illegible]	[illegible]	[illegible]	--	[illegible]	--		
[illegible]	Triplet, Unit [illegible]	Unit 2			[illegible]	[illegible]	[illegible]	[illegible]	[illegible]	--	[illegible]	[illegible]	[illegible]	[illegible]	[illegible]	--	[illegible]	--		
[illegible]	Triplet, Unit [illegible]	Unit 2			[illegible]	[illegible]	[illegible]	[illegible]	[illegible]	--	[illegible]	[illegible]	[illegible]	[illegible]	[illegible]	--	[illegible]	--		
[illegible]	Triplet, Unit [illegible]	Unit 2			[illegible]	[illegible]	[illegible]	[illegible]	[illegible]	--	[illegible]	[illegible]	[illegible]	[illegible]	[illegible]	--	[illegible]	--		
[illegible]	Triplet, Unit [illegible]	Unit 2			[illegible]	[illegible]	[illegible]	[illegible]	[illegible]	[illegible]	[illegible]	[illegible]	[illegible]	[illegible]	[illegible]	[illegible]	[illegible]	[illegible]	No	
[illegible]	Coplanar, Unit [illegible]	Unit 2			[illegible]	[illegible]	[illegible]	[illegible]	[illegible]	[illegible]	[illegible]	[illegible]	[illegible]	[illegible]	[illegible]	[illegible]	[illegible]	[illegible]	No	
[illegible]	Coplanar, Unit [illegible]	Unit 2			[illegible]	[illegible]	[illegible]	[illegible]	[illegible]	[illegible]	[illegible]	[illegible]	[illegible]	[illegible]	[illegible]	[illegible]	[illegible]	[illegible]	No	
[illegible]	Coplanar, Unit [illegible]	Unit 2			[illegible]	[illegible]	[illegible]	[illegible]	[illegible]	--	[illegible]	[illegible]	[illegible]	[illegible]	[illegible]	--	[illegible]	--	Yes	
[illegible]	Concentric, Unit 1*	Unit 3			--	--	--	--	--	--	--	--	--	--	--	--	--	--	--	Ignition test
[illegible]	Concentric, Unit 1*	Unit 3			[illegible]	[illegible]	[illegible]	[illegible]	[illegible]	[illegible]	[illegible]	[illegible]	[illegible]	[illegible]	[illegible]	[illegible]	[illegible]	[illegible]	No	Satisfactory test
[illegible]	Concentric, Unit 1*	Unit 3			[illegible]	[illegible]	[illegible]	[illegible]	[illegible]	[illegible]	[illegible]	[illegible]	[illegible]	[illegible]	[illegible]	[illegible]	[illegible]	[illegible]	No	Satisfactory test
[illegible]	Concentric, Unit 1*	Unit 3			--	--	[illegible]	--	--	--	--	--	--	--	--	--	--	--	--	Ignition delay, low F_2 supply pressure
[illegible]	Concentric, Unit 1*	Unit 3			--	--	[illegible]	--	--	--	--	--	--	--	--	--	--	--	--	Ignition delay, low F_2 supply pressure
[illegible]	Concentric, Unit 1*	Unit 3			[illegible]	[illegible]	[illegible]	[illegible]	[illegible]	--	[illegible]	[illegible]	[illegible]	[illegible]	[illegible]	--	[illegible]	--	Yes	Satisfactory test
[illegible]	Concentric, Unit 1*	Unit 3			[illegible]	[illegible]	[illegible]	[illegible]	[illegible]	[illegible]	[illegible]	[illegible]	[illegible]	[illegible]	[illegible]	[illegible]	[illegible]	[illegible]	No	
[illegible]	Concentric, Unit 1*	Unit 3			[illegible]	[illegible]	[illegible]	[illegible]	[illegible]	[illegible]	[illegible]	[illegible]	[illegible]	[illegible]	[illegible]	[illegible]	[illegible]	[illegible]	No	
[illegible]	Concentric, Unit 1*	Unit 3			[illegible]	[illegible]	[illegible]	[illegible]	[illegible]	[illegible]	[illegible]	[illegible]	[illegible]	[illegible]	[illegible]	[illegible]	[illegible]	[illegible]	No	
[illegible]	Concentric, Unit 1**	Unit 3			[illegible]	[illegible]	[illegible]	[illegible]	[illegible]	--	[illegible]	[illegible]	[illegible]	[illegible]	[illegible]	--	[illegible]	--	Yes	
[illegible]	Concentric, Unit 1**	Unit 3			[illegible]	[illegible]	[illegible]	[illegible]	[illegible]	[illegible]	[illegible]	[illegible]	[illegible]	[illegible]	[illegible]	[illegible]	[illegible]	[illegible]	No	
[illegible]	Concentric, Unit 1**	Unit 3			[illegible]	[illegible]	[illegible]	[illegible]	[illegible]	[illegible]	[illegible]	[illegible]	[illegible]	[illegible]	[illegible]	[illegible]	[illegible]	[illegible]	No	
[illegible]	Triplet, Unit [illegible]	Unit 2			[illegible]	[illegible]	[illegible]	[illegible]	[illegible]	--	[illegible]	[illegible]	[illegible]	[illegible]	[illegible]	--	[illegible]	--	Yes	
[illegible]	Triplet, Unit [illegible]	Unit 2			[illegible]	[illegible]	[illegible]	[illegible]	[illegible]	[illegible]	[illegible]	[illegible]	[illegible]	[illegible]	[illegible]	[illegible]	[illegible]	[illegible]	No	
[illegible]	Coplanar, Unit [illegible]	Unit 2			[illegible]	[illegible]	[illegible]	[illegible]	[illegible]	--	[illegible]	[illegible]	[illegible]	[illegible]	[illegible]	--	[illegible]	--	Yes	

*Injector Cool Orifice = [illegible]
**Injector Cool Orifice = [illegible]
NOTE: [illegible]

TABLE 8. (Continued)

Test Number	Injector Type	Chamber Type	ϵ_c	L*, inch	Chamber Pressure (NSC), psia	Mixture Ratio	Duration (Mainstage), seconds	Fuel Injection Temperature, F	Thrust (Sea Level), pounds	Vacuum Thrust, pounds	$\dot{w}_o$, lb/sec	$\dot{w}_f$, lb/sec	Throat Heat Flux, Btu/in.²-sec	Injector End Heat Flux, Btu/in.²-sec	c*(Pc), ft/sec	c*(F), ft/sec	η_{c^*}(Pc), percent	η_{c^*}(F), percent	Nozzle Film Separated	Remarks
[illegible]	[illegible]	[illegible]	5.0	7.0	[illegible]	[illegible]	[illegible]	[illegible]	[illegible]	--	[illegible]	[illegible]	[illegible]	[illegible]	[illegible]	--	[illegible]	--	Yes	Satisfactory test
[illegible]	[illegible]	[illegible]		[illegible]	[illegible]	[illegible]	[illegible]	[illegible]	[illegible]	--	[illegible]	[illegible]	[illegible]	[illegible]	[illegible]	--	[illegible]	--	Yes	
[illegible]	[illegible]	[illegible]		[illegible]	[illegible]	[illegible]	[illegible]	[illegible]	[illegible]	--	[illegible]	[illegible]	[illegible]	[illegible]	[illegible]	--	[illegible]	--	Yes	
[illegible]	[illegible]	[illegible]		7.0	[illegible]	[illegible]	[illegible]	[illegible]	[illegible]	--	[illegible]	[illegible]	[illegible]	[illegible]	[illegible]	--	[illegible]	--	Yes	
[illegible]	[illegible]	[illegible]			--	--	[illegible]	--	--	--	--	--	--	--	--	--	--	--	--	Test terminated by observer because of exhaust flame discoloration
[illegible]	[illegible]	[illegible]			[illegible]	[illegible]	[illegible]	[illegible]	[illegible]	--	[illegible]	[illegible]	[illegible]	[illegible]	[illegible]	--	[illegible]	--	Yes	Satisfactory test
[illegible]	[illegible]	[illegible]			[illegible]	[illegible]	[illegible]	[illegible]	[illegible]	--	[illegible]	[illegible]	[illegible]	[illegible]	[illegible]	--	[illegible]	--	Yes	
[illegible]	[illegible]	[illegible]			[illegible]	[illegible]	[illegible]	[illegible]	[illegible]	--	[illegible]	[illegible]	[illegible]	[illegible]	[illegible]	--	[illegible]	--	Yes	
[illegible]	[illegible]	[illegible]			[illegible]	[illegible]	[illegible]	[illegible]	[illegible]	--	[illegible]	[illegible]	[illegible]	[illegible]	[illegible]	--	[illegible]	--	Yes	
[illegible]	[illegible]	[illegible]			[illegible]	[illegible]	[illegible]	[illegible]	[illegible]	[illegible]	[illegible]	[illegible]	[illegible]	[illegible]	[illegible]	[illegible]	[illegible]	[illegible]	No	
[illegible]	[illegible]	[illegible]			[illegible]	[illegible]	[illegible]	[illegible]	[illegible]	[illegible]	[illegible]	[illegible]	[illegible]	[illegible]	[illegible]	[illegible]	[illegible]	[illegible]	No	
[illegible]	[illegible]	[illegible]			--	--	[illegible]	--	--	--	--	--	--	--	--	--	--	--	--	Test terminated by observer because of exhaust flame discoloration
[illegible]	[illegible]	[illegible]			[illegible]	[illegible]	[illegible]	[illegible]	[illegible]	--	[illegible]	[illegible]	[illegible]	[illegible]	[illegible]	--	[illegible]	--	Yes	Satisfactory test
[illegible]	[illegible]	[illegible]			[illegible]	[illegible]	[illegible]	[illegible]	[illegible]	--	[illegible]	[illegible]	[illegible]	[illegible]	[illegible]	--	[illegible]	--	Yes	
[illegible]	[illegible]	[illegible]			[illegible]	[illegible]	[illegible]	[illegible]	[illegible]	--	[illegible]	[illegible]	[illegible]	[illegible]	[illegible]	--	[illegible]	--	Yes	
[illegible]	[illegible]	[illegible]			--	--	[illegible]	--	--	--	--	--	--	--	--	--	--	--	--	Test terminated by observer because of exhaust flame discoloration
[illegible]	[illegible]	[illegible]			[illegible]	[illegible]	[illegible]	[illegible]	[illegible]	[illegible]	[illegible]	[illegible]	[illegible]	[illegible]	[illegible]	[illegible]	[illegible]	[illegible]	No	Satisfactory test
[illegible]	[illegible]	[illegible]			[illegible]	[illegible]	[illegible]	[illegible]	[illegible]	--	[illegible]	[illegible]	[illegible]	[illegible]	[illegible]	--	[illegible]	--	Yes	
[illegible]	[illegible]	[illegible]			[illegible]	[illegible]	[illegible]	[illegible]	[illegible]	--	[illegible]	[illegible]	[illegible]	[illegible]	[illegible]	--	[illegible]	--	Yes	
[illegible]	[illegible]	[illegible]			[illegible]	[illegible]	[illegible]	[illegible]	[illegible]	--	[illegible]	[illegible]	[illegible]	[illegible]	[illegible]	--	[illegible]	--	Yes	
[illegible]	[illegible]	[illegible]			[illegible]	[illegible]	[illegible]	[illegible]	[illegible]	--	[illegible]	[illegible]	[illegible]	[illegible]	[illegible]	--	[illegible]	--	Yes	
[illegible]	[illegible]	[illegible]			[illegible]	[illegible]	[illegible]	[illegible]	[illegible]	--	[illegible]	[illegible]	[illegible]	[illegible]	[illegible]	--	[illegible]	--	Yes	
[illegible]	[illegible]	[illegible]			[illegible]	[illegible]	[illegible]	[illegible]	[illegible]	[illegible]	[illegible]	[illegible]	[illegible]	[illegible]	[illegible]	[illegible]	[illegible]	[illegible]	No	
[illegible]	[illegible]	[illegible]			[illegible]	[illegible]	[illegible]	[illegible]	[illegible]	--	[illegible]	[illegible]	[illegible]	[illegible]	[illegible]	--	[illegible]	--	Yes	
[illegible]	[illegible]	[illegible]			[illegible]	[illegible]	[illegible]	[illegible]	[illegible]	--	[illegible]	[illegible]	[illegible]	[illegible]	[illegible]	--	[illegible]	--	Yes	
[illegible]	[illegible]	[illegible]			[illegible]	[illegible]	[illegible]	[illegible]	[illegible]	--	[illegible]	[illegible]	[illegible]	[illegible]	[illegible]	--	[illegible]	--	Yes	
[illegible]	[illegible]	[illegible]			[illegible]	[illegible]	[illegible]	[illegible]	[illegible]	--	[illegible]	[illegible]	[illegible]	[illegible]	[illegible]	--	[illegible]	--	Yes	
[illegible]	[illegible]	[illegible]			[illegible]	[illegible]	[illegible]	[illegible]	[illegible]	[illegible]	[illegible]	[illegible]	[illegible]	[illegible]	[illegible]	[illegible]	[illegible]	[illegible]	No	
[illegible]	[illegible]	[illegible]			[illegible]	[illegible]	[illegible]	[illegible]	[illegible]	[illegible]	[illegible]	[illegible]	[illegible]	[illegible]	[illegible]	[illegible]	[illegible]	[illegible]	No	Test terminated by observer because of exhaust flame discoloration
[illegible]	[illegible]	[illegible]			[illegible]	[illegible]	[illegible]	[illegible]	[illegible]	--	[illegible]	[illegible]	[illegible]	[illegible]	[illegible]	--	[illegible]	--	Yes	Satisfactory test
[illegible]	[illegible]	[illegible]			[illegible]	[illegible]	[illegible]	[illegible]	[illegible]	[illegible]	[illegible]	[illegible]	[illegible]	[illegible]	[illegible]	[illegible]	[illegible]	[illegible]	No	
[illegible]	[illegible]	[illegible]			[illegible]	[illegible]	[illegible]	[illegible]	[illegible]	--	[illegible]	[illegible]	[illegible]	[illegible]	[illegible]	--	[illegible]	--	Yes	
[illegible]	[illegible]	[illegible]			[illegible]	[illegible]	[illegible]	[illegible]	[illegible]	[illegible]	[illegible]	[illegible]	[illegible]	[illegible]	[illegible]	[illegible]	[illegible]	[illegible]	No	

*Oxidizer Post Recess = [illegible]
**Oxidizer Post Recess = [illegible]
***Oxidizer Post Recess = [illegible]
****Oxidizer Post Recess = [illegible]

NOTE: Fuel Annulus Gap = [illegible] for Tests [illegible] through [illegible]
Fuel Annulus Gap = [illegible] for Tests [illegible] through [illegible]

TABLE 8. (Concluded)

Number	Injector Type	Chamber Type	L_c	L^*, inch	Chamber Pressure (NSS), psia	Mixture Ratio	Duration (Actual), seconds	Fuel Injection Temperature, F	Thrust (Net Sitel), pounds	Vacuum Thrust, pounds	$\dot{w}_o$, lb_m/sec	$\dot{w}_f$, lb_m/sec	Throat Heat Flux, Btu/in.^{2}-sec	Injector End Heat Flux, Btu/in.^{2}-sec	$c^*(P_c)$, ft/sec	$c^*(F)$, ft/sec	$\eta_{c^*(P_c)}$, percent	$\eta_{c^*(F)}$, percent	Nozzle Flow Separated	Remarks
000-71	Triplet, Unit 2-C	Unit 2	3.0	7.0	464.2	5.50	30.1	460	525.0	--	1.2006	0.2190	25.4	12.0	7916	--	100.9	--	Yes	Satisfactory test
001-71	Triplet, Unit 2-C	Unit 2			134.7	4.93	30.5	726	135.1	--	0.3530	0.0753	6.9	10.0	7642	--	97.0	--	Yes	
002-71	Triplet, Unit 2-C	Unit 2			774.2	5.12	9.0	235	855.6	910.7	1.9470	0.380	30.9	21.5	8130	7562	100.7	99.7	No	
003-71	Concentric, Unit 7A****	Unit 1A		10.2	800.5	5.20	30.2	407	507.1	--	1.1075	0.2266	30.9	22.2	7875	--	100.0	--	Yes	
004-71	Concentric, Unit 7A****	Unit 1A			165.9	5.50	7.1	715	120.1	--	0.4170	0.0736	10.0	12.3	7488	--	85.9	--	Yes	
005-71	Concentric, Unit 7A****	Unit 1A			476.7	5.35	20.2	102	500.0	--	1.2110	0.2263	29.7	10.7	7762	--	97.5	--	Yes	
006-71	Coplanar, Unit 1A	Unit 1A			481.6	5.42	30.2	277	480.0	--	1.2119	0.2215	32.4	17.1	8091	--	100.0	--	Yes	
007-71	Coplanar, Unit 1A	Unit 1A			152.0	5.66	40.0	772	98.2	--	0.4233	0.0740	11.3	11.4	7480	--	85.4	--	Yes	
008-71	Coplanar, Unit 1A	Unit 1A			150.0	5.83	40.0	265	82.2	--	0.4250	0.0720	10.7	5.5	7674	--	101.0	--	Yes	
100-71	Concentric, Unit 7D****	Unit 4		7.0	--	--	0.0	--	-	--	--	--	--	--	--	--	--	--	--	Automatic redline cutoff device monitoring liquid oxygen temperatures
109-71	Concentric, Unit 7D****	Unit 4			463.5	5.50	14.0	446.5	481.7	--	1.1650	0.2087	21.5	15.0	7758	--	97.2	--	--	Satisfactory test
110-71	Concentric, Unit 7D****	Unit 4			161.0	6.76	19.6	630	125.9	--	0.4686	0.0691	9.1	10.6	6965	--	95.7	--	--	
111-71	Concentric, Unit 7D****	Unit 9			453.0	5.60	15.9	70	470.0	--	1.1606	0.2085	21.6	0.0	7765	--	98.5	--	Yes	
112-71	Concentric, Unit 7D****	Unit 8			774.5	5.65	10.4	326	812.2	807.5	1.9059	0.3494	37.1	16.1	7900	7528	98.6	100.2	No	
113-71	Concentric, Unit 7D****	Unit 4			445.2	5.05	15.2	80	476.6	--	1.1649	0.2060	21.9	13.5	7563	--	96.5	--	Yes	
114-71	Concentric, Unit 7D****	Unit 4			--	--	9.0	--	--	--	--	--	--	--	--	--	--	--	--	Automatic redline cutoff device monitoring liquid oxygen temperature
115-71	Concentric, Unit 7D****	Unit 4			--	--	0.0	--	--	--	--	--	--	--	--	--	--	--	--	
116-71	Concentric, Unit 7D****	Unit 4			--	--	3.0	--	--	--	--	--	--	--	--	--	--	--	--	
117-71	Concentric, Unit 7E****	Unit 4			457.2	5.52	7.2	411	476.1	--	1.1655	0.2076	22.4	10.0	8000	--	99.6	--	Yes	Satisfactory test
118-71	Concentric, Unit 7D****	Unit 4			151.5	5.55	11.1	832	117.1	--	0.3020	0.0700	7.7	10.6	7719	--	99.0	--	Yes	
119-71	Concentric, Unit 7D****	Unit 4			277.4	4.50	9.6	437	263.9	--	0.6516	0.1448	15.5	15.1	8325	--	90.5	--	Yes	
120-71	Concentric, Unit 7D****	Unit 4			631.0	5.45	5.0	803	671.4	726.5	1.5644	0.2871	30.4	22.1	8075	7509	99.5	100.5	No	
121-71	Concentric, Unit 7D****	Unit 4			140.7	5.27	0.4	872	113.0	--	0.3727	0.0706	7.4	10.5	7812	--	90.9	--	Yes	Stability test; minor coolant water leakage in combustion zone
122-71	Concentric, Unit 7D****	Unit 4			303.2	5.21	7.9	734	292.2	--	0.7517	0.1444	14.0	16.0	8010	--	98.0	--	Yes	
123-71	Concentric, Unit 7D****	Unit 4			453.2	5.47	6.9	545	460.9	--	1.1530	0.2110	22.4	10.4	7856	--	97.0	--	Yes	
124-71	Concentric, Unit 7D****	Unit 4			603.5	5.37	6.0	413	654.6	700.5	1.5555	0.2899	28.4	21.9	7810	7362	94.7	90.1	No	
125-71	Concentric, Unit 7D****	Unit 4			745.1	5.30	6.9	300	817.4	872.5	1.8937	0.3512	34.2	22.9	7900	7446	96.4	99.9	No	
126-71	Concentric, Unit 7D**	Unit 2			130.5	5.66	10.8	635	107.9	--	0.3059	0.0707	7.1	7.7	7155	--	82.0	--	Yes	Satisfactory test
127-71	Concentric, Unit 7E**	Unit 2			412.9	5.60	15.0	541	462.0	--	1.1620	0.2077	20.9	15.9	7450	--	94.5	--	Yes	
128-71	Coplanar, Unit 1A	Unit 2			141.3	5.65	20.0	747	125.1	--	0.3934	0.0710	6.9	15.0	7529	--	85.9	--	Yes	
129-71	Coplanar, Unit 1A	Unit 2			145.0	5.62	21.2	856	125.5	--	0.4064	0.0725	7.1	13.9	7580	--	85.5	--	Yes	
130-71	Coplanar, Unit 1A	Unit 2			463.7	5.60	20.0	431	520.5	--	1.2346	0.2204	25.0	21.7	7934	--	99.1	--	Yes	
131-71	Coplanar, Unit 1A	Unit 2			460.2	5.54	20.2	430	514.2	--	1.2327	0.2226	21.7	21.0	7882	--	88.9	--	Yes	

**Oxidizer Post Recess = 0.050
****Oxidizer Post Recess = 0.100

NOTE Fuel Annulus Gap = 0.080 for Tests 085-71 through 095-71
Fuel Annulus Gap = 0.0155 for Tests 100-71 through 127-71

TABLE 9. SINGLE-PANEL, WATER-COOLED SEGMENT TEST COMPONENT CONFIGURATIONS

Number of Tests	Total Duration, seconds	Injector	Chamber Length, L_c, inches
9	35.6	Coplanar, unit 1	unit 1, 3.0
6	105.8	Coplanar, unit 1A	unit 2, 3.0
5	124.0	Coplanar, unit 1A	unit 1A, 3.0
5	38.5	Coplanar, unit 4	unit 2, 3.0
3	43.8	Coplanar, unit 4A	
8	65.5	Triplet, unit 2	unit 1, 3.0
6	65.2	Triplet, unit 2	unit 1, 4.0
5	67.7	Triplet, unit 2A	unit 2, 3.0
2	28.2	Triplet, unit 2B	unit 2, 3.0
3	60.1	Triplet, unit 2C	unit 2, 3.0
9	58.5	Concentric, unit 3, 0.050 recess, 0.008 gap	unit 3, 3.0
3	25.7	Concentric, unit 3, 0.075 recess, 0.008 gap	unit 3, 3.0
5	40.8	Concentric, unit 7, 0.050 recess, 0.006 gap	unit 2, 3.0
2	30.4	Concentric, unit 7, 0.060 recess, 0.006 gap	unit 2, 3.0
4	21.0	Concentric, unit 7, 0.075 recess, 0.006 gap	unit 2, 3.0
3	77.0	Concentric, unit 7, 0.050 recess, 0.008 gap	unit 2, 3.0
3	25.4	Concentric, unit 7, 0.075 recess, 0.008 gap	unit 2, 3.0
3	43.5	Concentric, unit 7, 0.100 recess, 0.008 gap	unit 2, 3.0
6	83.0	Concentric, unit 7A 0.075 recess, 0.008 gap	unit 2, 3.0
3	70.5	Concentric, unit 7A, 0.100 recess, 0.008 gap	unit 1A, 3.0
4	56.9	Concentric, unit 7A, 0.100 recess, 0.008 gap	unit 2, 3.0
2	34.8	Concentric, unit 7D, 0.050 recess, 0.0155 gap	unit 2
5	60.0	Concentric, unit 7D, 0.050 recess, 0.0155 gap	unit 4
13	80.0	Concentric, unit 7D, 0.100 recess, 0.0155 gap	unit 4
117	1342	TOTAL	

Coplanar Injector Characteristic Velocity Efficiency

Characteristic velocity (c*) efficiency, as a function of chamber pressure and fuel injection velocity, was evaluated for the coplanar injectors as discussed in the following paragraphs.

Effect of Chamber Pressure. c* efficiency versus chamber pressure for the four coplanar injector configurations tested is shown in Fig. 52. Injector units 1 and 1A exhibited a strong effect of chamber pressure on performance with increasing chamber pressure providing increased performance. The performance level for injector unit 1 was above that for injector unit 1A. This performance differential may be due to the smaller oxidizer orifice size used for injector unit 1, resulting in higher injection velocities, which could aid propellant atomization and enhance performance. Both injector units 1 and 1A exhibited high wall heat flux and wall erosion (page 27) at chamber pressure of 750 psia, negating measurement of steady-state performance data at 750 psia (run time limited).

Injector units 4 and 4A showed slightly decreased performance with increasing chamber pressure. The performance for injector unit 4 was equivalent to, and higher than, the performance of injector unit 1A at chamber pressures of 450 and 150 psia, respectively. Injector unit 4A performance was approximately 4 percent less than that for injector unit 4 over the chamber pressure range tested. Wall heat flux, discussed later, although lower for injector units 4 and 4A, remained sufficiently high to preclude measurement of steady-state performance data at high chamber pressure (P_c = 750 psia).

The heat transfer characteristics of the coplanar element can be explained with knowledge of the coplanar element spray distribution from the cold-flow test discussed previously. Two coplanar injector element face patterns (units 1 and 4), as depicted in Fig. 53, were hot-fire tested. Superimposed on the face patterns (Fig. 53) are the relative location of the overall element flowfield (ellipses) and the excess oxidizer zones (shaded circles) as indicated from cold flow. The unit 1 injector exhibited wall erosion and high local heat flux. The erosion and

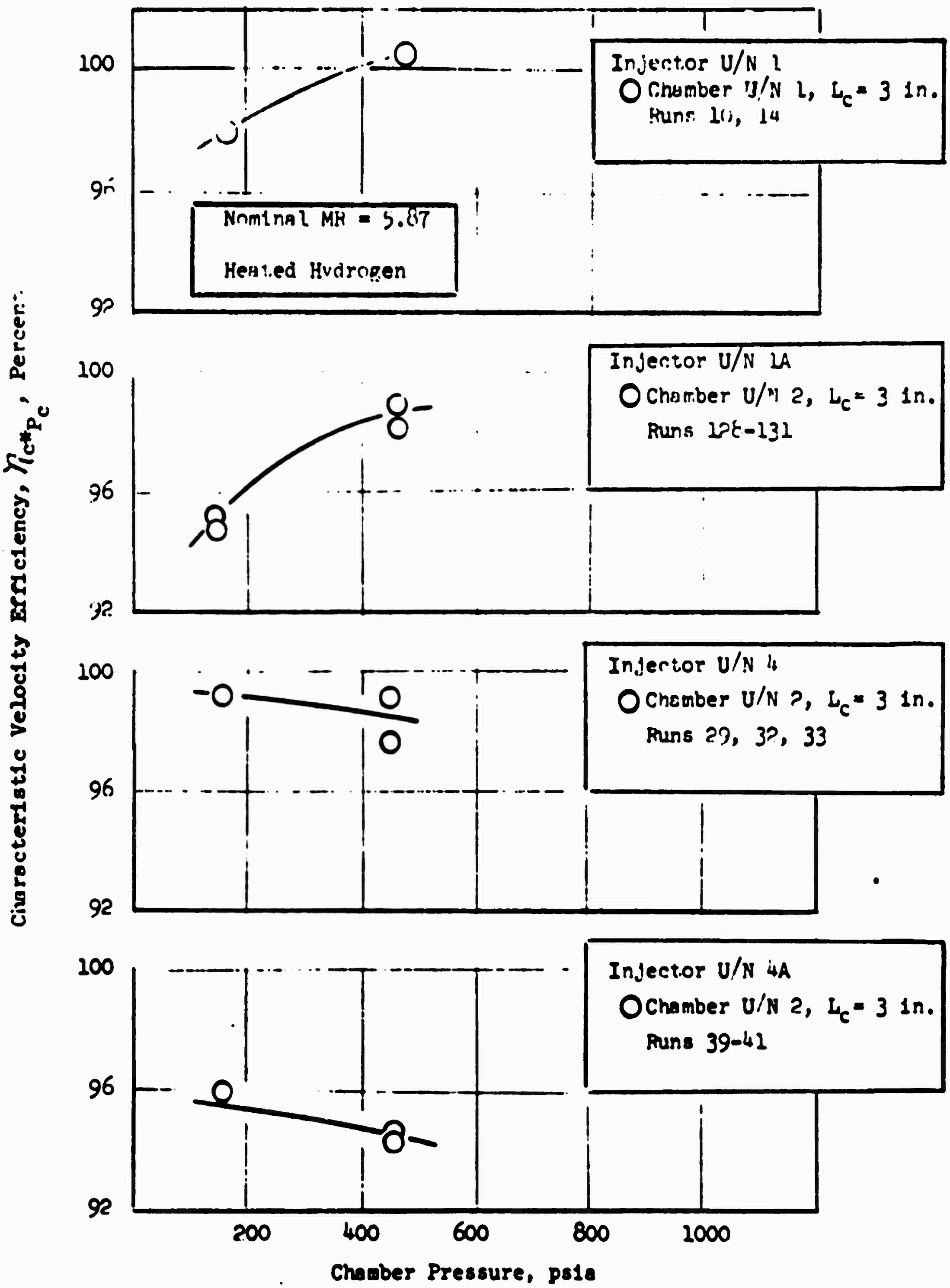

Figure 52. Effect of Chamber Pressure on Characteristic Velocity Efficiency for Single-Panel Coplanar Injectors

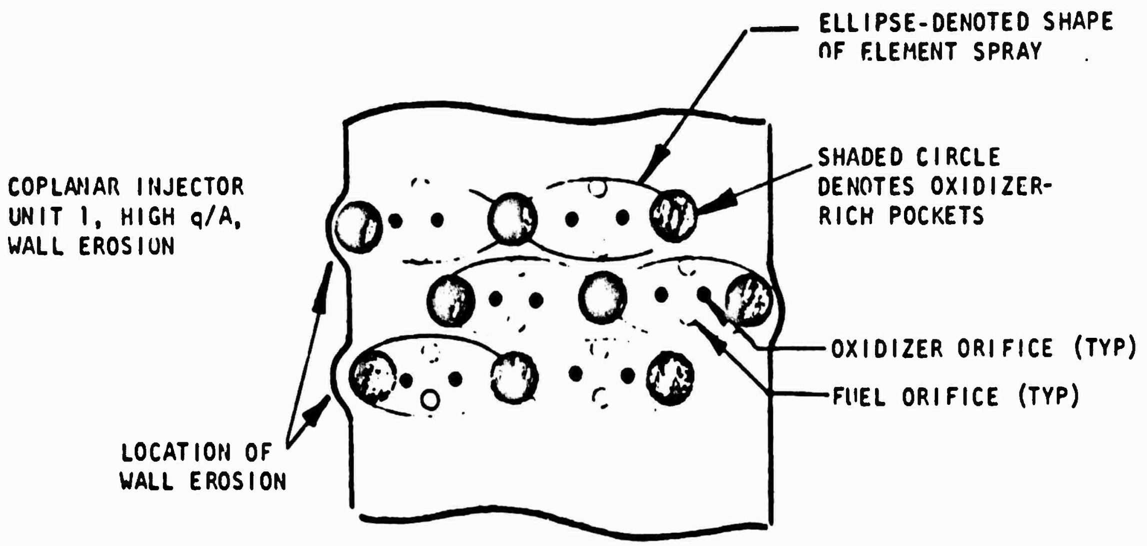

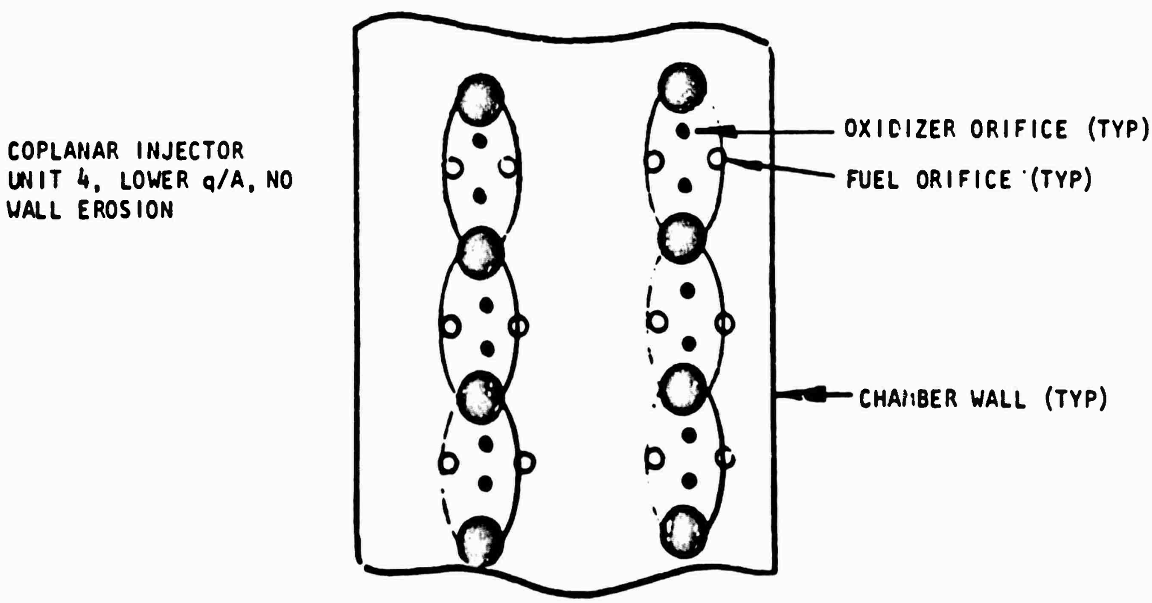

Figure 53. Cold-Flow Implied Spray Distribution for Coplanar Injectors Evaluated in Hot-Fire Test

high heat flux were attributed to oxidizer impingement on the wall. The unit 4 injector showed reduced heat flux without wall erosion. Elimination of wall erosion and reduction of heat flux on the unit 4 injector was accomplished by removal of oxidizer spray from the wall.

The high performance obtained with injector units 1, 1A, and 4 at 450-psia chamber pressure was dependent on extensive interelement mixing. This conclusion results from the fact that cold-flow tests with a single, basic design, coplanar element (representative of that used on injector units 1, 1A, and 4) showed low mixing efficiency. This interelement mixing was achieved by both injector element patterns as shown in Fig. 53. Additionally, the high performance was indicative of good atomization to provide high vaporization efficiency in a 3-inch-long chamber.

The performance differential between injector units 4 and 4A may be due to observations noted in cold-flow testing. Injector unit 4A was modified to increase the diameter of the fuel orifice next to the chamber wall, for purposes of canting the element spray inward. The loss in performance with injector unit 4A could be due to both atomization and mixing losses resulting from spatial displacement of the fuel fan as referenced to the oxidizer fan. Such fan displacement, evaluated in cold-flow testing, can result in gross flow maldistribution (discussed on pages 85 through 94).

Although the BLC configuration evaluated in cold-flow tests provided: (1) improved element mixing and (2) bias control of oxygen concentration, the BLC configuration was not hot-fire tested. Encouraging development effort with other element types precluded further investigation of the coplanar element.

Effect of Fuel Injection Velocity. c* efficiency versus fuel injection velocity for coplanar injector unit 1A is shown in Fig. 54. Data were measured in chamber units 2 and 1A. Both combustion chambers were 3 inches in length. The fuel injection velocity was varied by changing the fuel injection temperature (fuel density change). Combustion performance increased with decreasing fuel injection velocity. This effect may be due to the dominance of the fuel fan in element spray distribution, as described previously in the cold-flow section. As noted in the

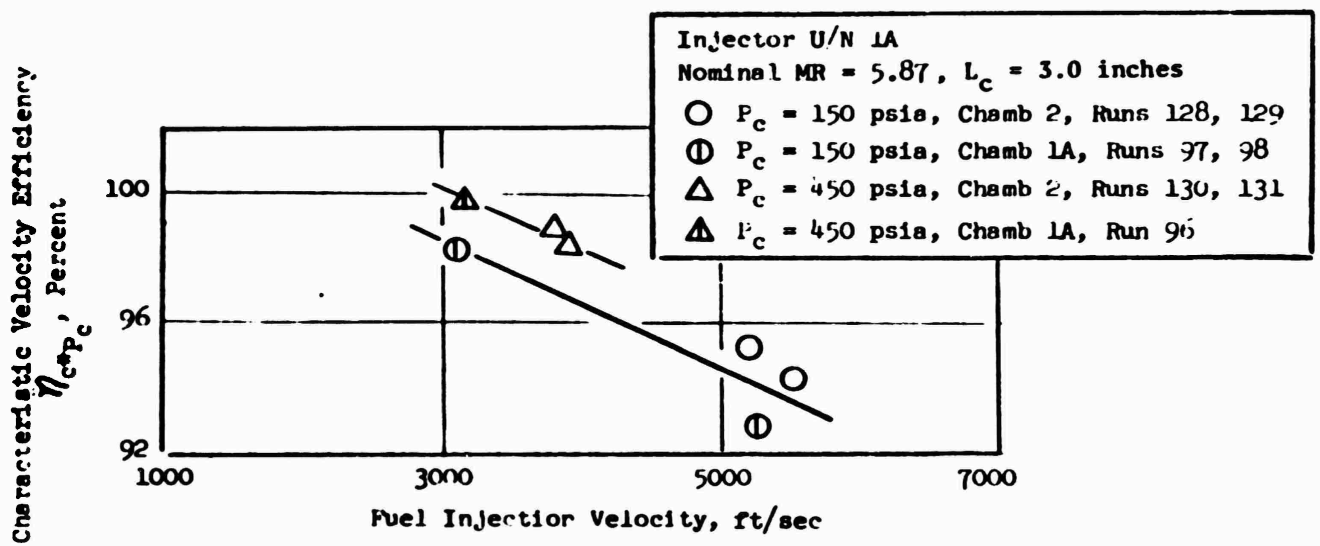

Figure 54. Effect of Fuel Injection Velocity on Characteristic Velocity Efficiency for Single-Panel Coplanar Injectors

cold-flow discussion, the fuel momentum appeared to overwhelm the oxidizer spray fan, splitting the fan into two oxidizer-rich pockets. The increased performance with lower fuel velocity, and lower fuel momentum flux is probably due to a lessening of this oxidizer spray separation effect, resulting in a more uniform distribution of the oxidizer spray.

Triplet Injector Characteristic Velocity Efficiency

c* efficiency was evaluated for the triplet injectors as a function of chamber pressure and mixture ratio. Additionally, a correlation of predicted and measured performance was made.

Effect of Chamber pressure. c* efficiency versus chamber pressure for the four triplet injector configurations tested is shown in Fig. 55. All injectors tested exhibited high performance (99 to 100 percent) over the chamber pressure range (150 to 800 psia). Neither increased oxidizer orifice size (units 2A and 2C) nor inclusion of an additional fuel orifice on elements adjacent to the wall (i.e., three fuel on one oxidizer--unit 2B) appreciably changed performance.

Injector unit 2 was tested in 3- and 4-inch-long combustion chambers. Performance was essentially the same, indicating that complete vaporization occurred in the 3-inch combustion chamber length.

Effect of Mixture Ratio. c* efficiency versus mixture ratio for injector unit 2 is shown in Fig. 56. The c* efficiency increased very slightly with mixture ratio to a maximum value at the design mixture ratio of 5.5.

Performance Correlation. Correlation between measured and predicted vaporization efficiency for triplot injector injector unit 2 was made.

An estimate of measured vaporization efficiency, $\eta_{vap_{meas}}$, was provided by the hot-fire tests. The measured hot-fire performance, $\eta_{c*} \sim 99.5$ percent in 3- and 4-inch-length chambers implied that vaporization was complete (i.e., $\eta_{vap_{meas}} \sim 100$ percent).

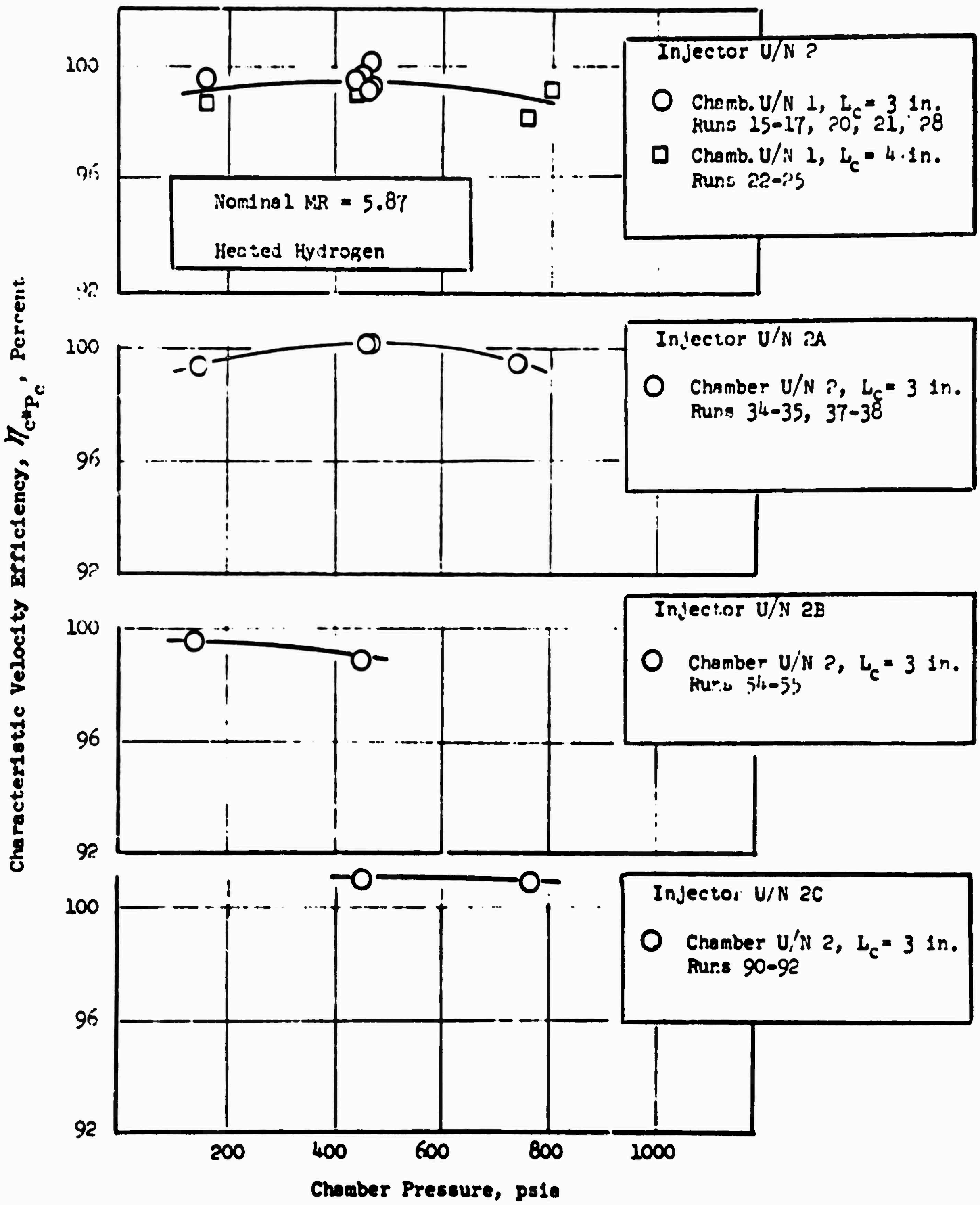

Figure 55. Effect of Chamber Pressure on Characteristic Velocity Efficiency for Single-Panel Triplet Injectors

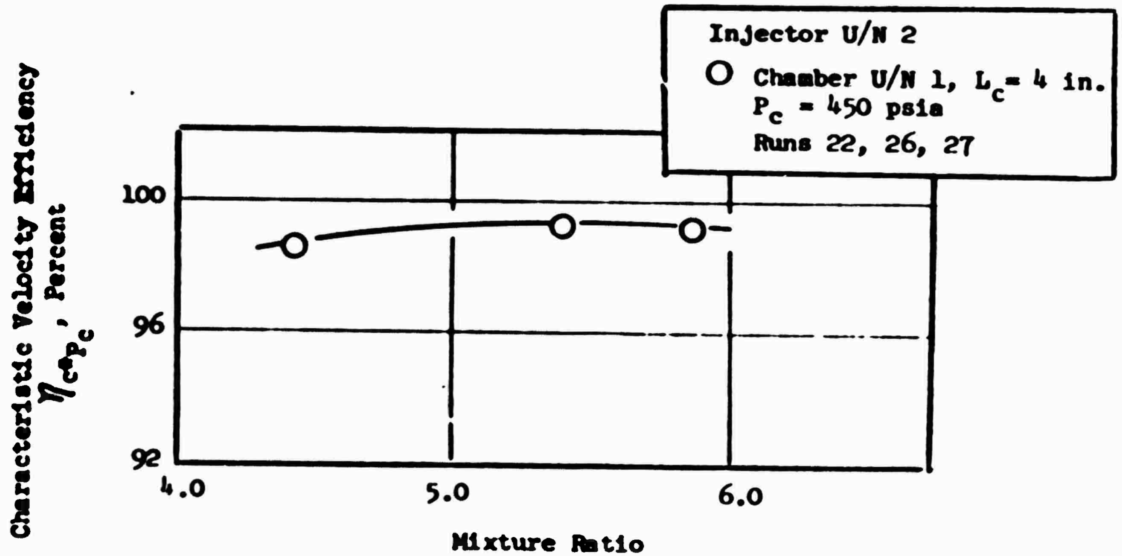

Figure 56. Effect of Mixture Ratio on Characteristic Velocity Efficiency for Single-Panel Triplet Injector

Prediction of vaporization efficiency, $\eta_{vap_{pred}}$ also can be obtained from combustion model analysis using dropsize data from cold-flow atomization tests. Recent cold-flow atomization test (Ref. 4) with conventional triplet elements (O-F-O) provided dropsize data. Under the hypothesis that the dropsize data were applicable to the reversed triplet element (F-O-F), such as used on the AMPT injector, an estimate of AMPT injector dropsize could be made. The dropsize results (Ref. 5) were found to be a function of gas stream dynamic pressure ρV^2. Employing this gas stream dynamic pressure dependence with applicable correction factors for propellant property effects, the predicted dropsize, $\bar{D}_{30}$, for the injector ranged from 20 to 40 microns over the respective chamber pressure range of 750 to 150 psia. Input of these dropsizes to the impinging stream combustion model (see Appendix I, Fig. I-3) resulted in a prediction of complete vaporization (i.e., $\eta_{vap_{pred}}$ = 100 percent).

Therefore, the predicted vaporization efficiency ($\eta_{vap_{pred}}$ = 100 percent) is in agreement with the measured vaporization efficiency ($\eta_{vap_{meas}}$ = 100 percent).

Concentric Injector Characteristic Velocity Efficiency

For the concentric element injectors, c* efficiencies as a function of chamber pressure, oxidizer post recess, and fuel injection velocity were measured. Additionally, correlations were developed for: (1) the variables investigated in hot-fire testing and (2) the performance predicted by the combustion model studies (Appendix I).

Effect of Chamber Pressure. c* efficiency versus chamber pressure for the five injector configurations tested is shown in Fig. 57. Combustion efficiency increased with chamber pressure (at constant oxidizer post recess) for most injector configurations. The performance increase was greater over the chamber pressure range 150 to 450 psia, occurring to a lesser extent at chamber pressures exceeding 450 psia.

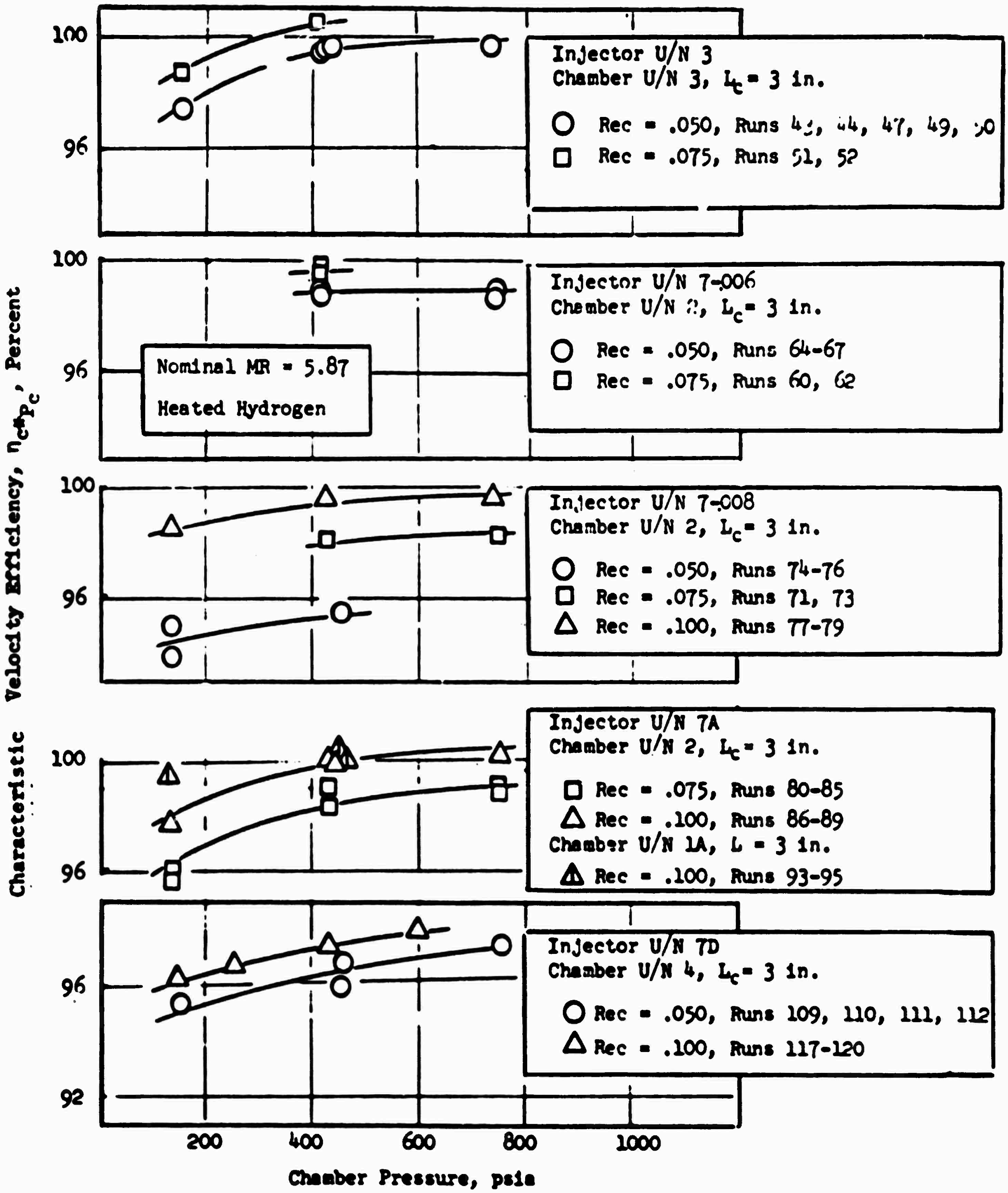

Figure 57. Effect of Chamber Pressure on Characteristic Velocity Efficiency for Single-Panel Concentric Injectors

Chamber unit 2 (0.5-inch injector end width) was used for all tests with injector unit 7 configurations except one series conducted with injector unit 7A which used chamber unit 1A (0.6-inch injector end width). Although the efficiency of injector unit 7A at low chamber pressure (P_c = 150 psia) was higher in chamber unit 1A than in chamber unit 2, the data are considered insufficient to identify an effect of injector face width on performance.

Injector unit 7D, which has the largest fuel gap, delivered performance that was intermediate between (0.050-inch recess) and less than (0.100-inch recess) the performance obtained with injector units 7-.006 and 7-.008. This performance trend with injector unit 7D is in general agreement with that predicted by the combustion model (Appendix I, page I-1).

A series of pulse-gun tests was also conducted with injector unit 7D. Performance results are not shown for those tests because chamber internal water leakage degraded performance on these tests. The stability results are reported in a later section (page 138).

Effect of Oxidizer Post Recess. c* efficiency versus oxidizer post recess at constant chamber pressure is shown in Fig. 58. Combustion efficiency increased with increasing oxidizer post recess for all injector configurations at all chamber pressure levels. The performance increase with recess was less noticeable with injector unit 7D which had the largest fuel gap. Overall, the performance increases measured with increasing post recess from 0.050 to 0.100 inch were in the range of 2 to 4 percent, which agrees very well with the combustion model.

Effect of Fuel Injection Velocity. The fuel injection velocity was varied by: (1) varying the hydrogen gas temperature and (2) varying the hydrogen gas injection area. For the former case, reduction of hydrogen gas temperature increases gas density at constant chamber pressure while the gas velocity is reduced, so that the $(\rho V)_F$ parameter remains essentially constant. For the later case, increase of the hydrogen gas injection area lowers the $(\rho V)_F$ product for a fixed gas density (i.e., fixed chamber pressure).

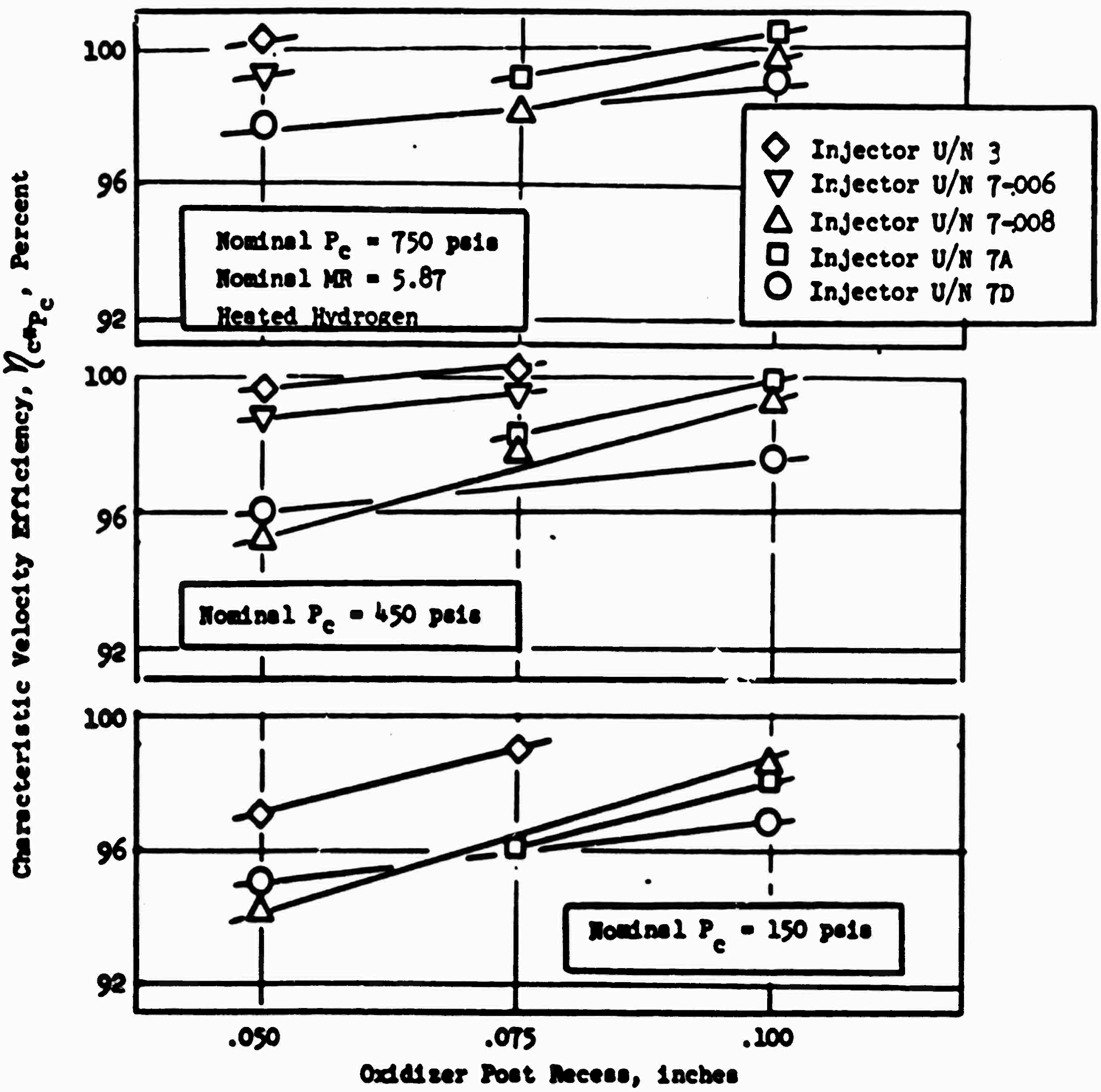

Figure 58. Effect of Oxidizer Post Recess on Characteristic Velocity Efficiency for Single-Panel Concentric Injectors

c* efficiency as a function of $(\rho V)_F$ at constant chamber pressure and post recess for the concentric injectors is plotted in Fig. 59 . The data show an increase in combustion efficiency with increasing $(\rho V)_F$.

Separation of the velocity dependence in the $(\rho V)_F$ effect on performance was obtained by comparison of two injector types with different fuel injection areas. The effect of fuel injection velocity at (1) constant $(\rho V)_F$ and (2) constant $(\rho)_f$ is shown in Fig. 60 . Varying the fuel velocity at constant $(\rho V)_f$ showed essentially no effect on performance. Conversely, reducing the fuel injection velocity at constant $(\rho)_f$ showed a decrease in performance. Therefore, reduced fuel velocity independently lowered performance.

The effect of the $(\rho V)_f$ parameter on c* efficiency is associated with both the mixing and vaporization efficiency. Previous cold-flow studies (Ref. 3) with concentric elements have shown mixing efficiency increases with both increased gas injection velocity and increased gas density. These same cold-flow studies also have shown that atomization improves with increased gas velocity at constant gas density. Similar improvements in atomization with increased gas velocity are predicted by the combustion model studies described in Appendix I.

Performance Correlation With Test Variables. The concentric injector performance was plotted as a function of the product of salient test variables affecting combustion efficiency (i.e., oxidizer post recess and $(\rho V)_f$ at constant chamber pressure, as shown in Fig. 61 . Most test data tend to converge, exhibiting a linear dependence, as shown in Fig. 61.

A similar correlation based on a dimensionless injector geometric parameter (oxidizer post recess/fuel gap x number of elements) also was plotted against injector performance, as shown in Fig. 62 . The data correlation was similar to that previously shown in Fig. 60, as would be expected because (fuel gap x number of elements) is reciprocally proportional to fuel injection velocity.

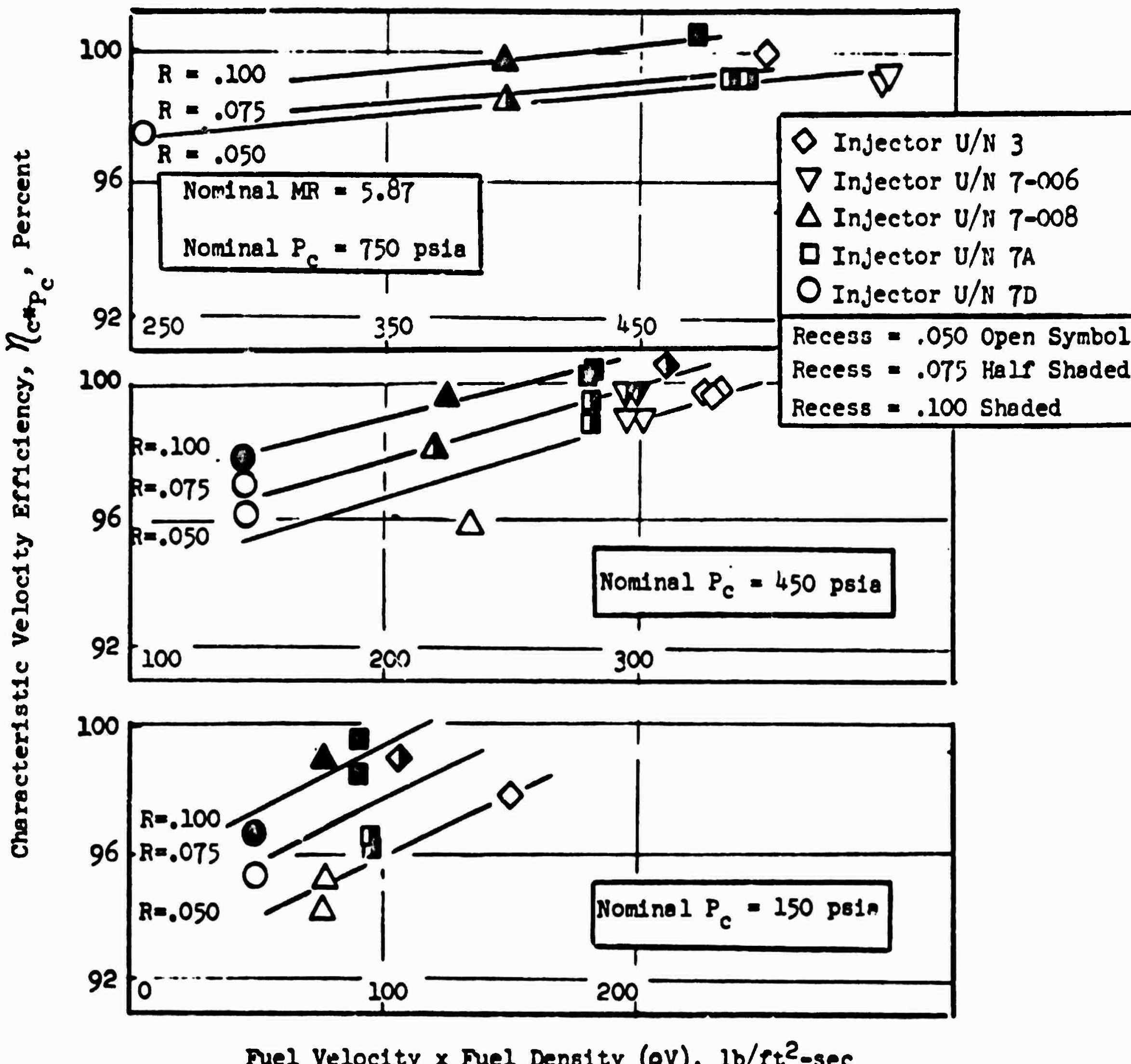

Figure 59. Effect of $(\rho V)_f$ on Characteristic Velocity Efficiency for Single-Panel Concentric Injectors

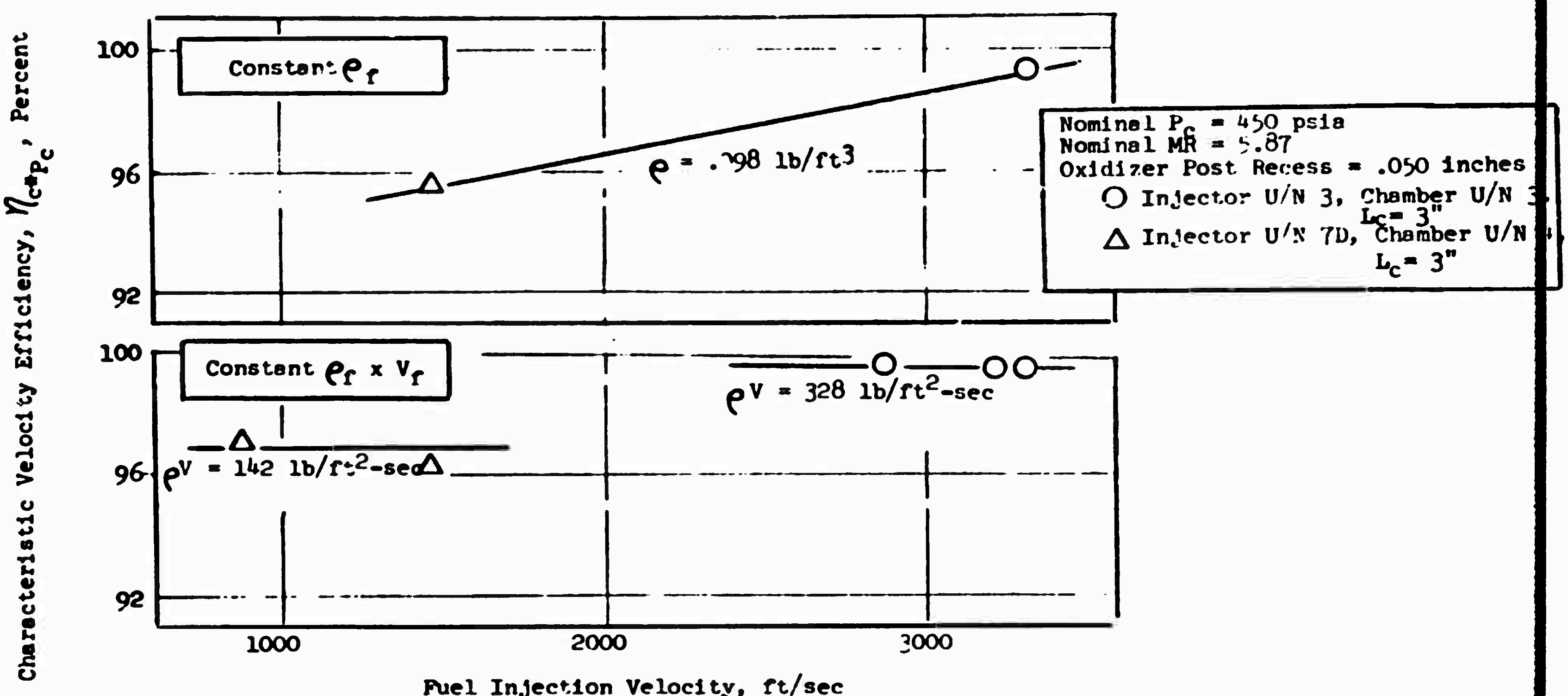

Figure 60. Effect of Fuel Injection Velocity on Characteristic Velocity Efficiency for Single-Panel Concentric Injectors

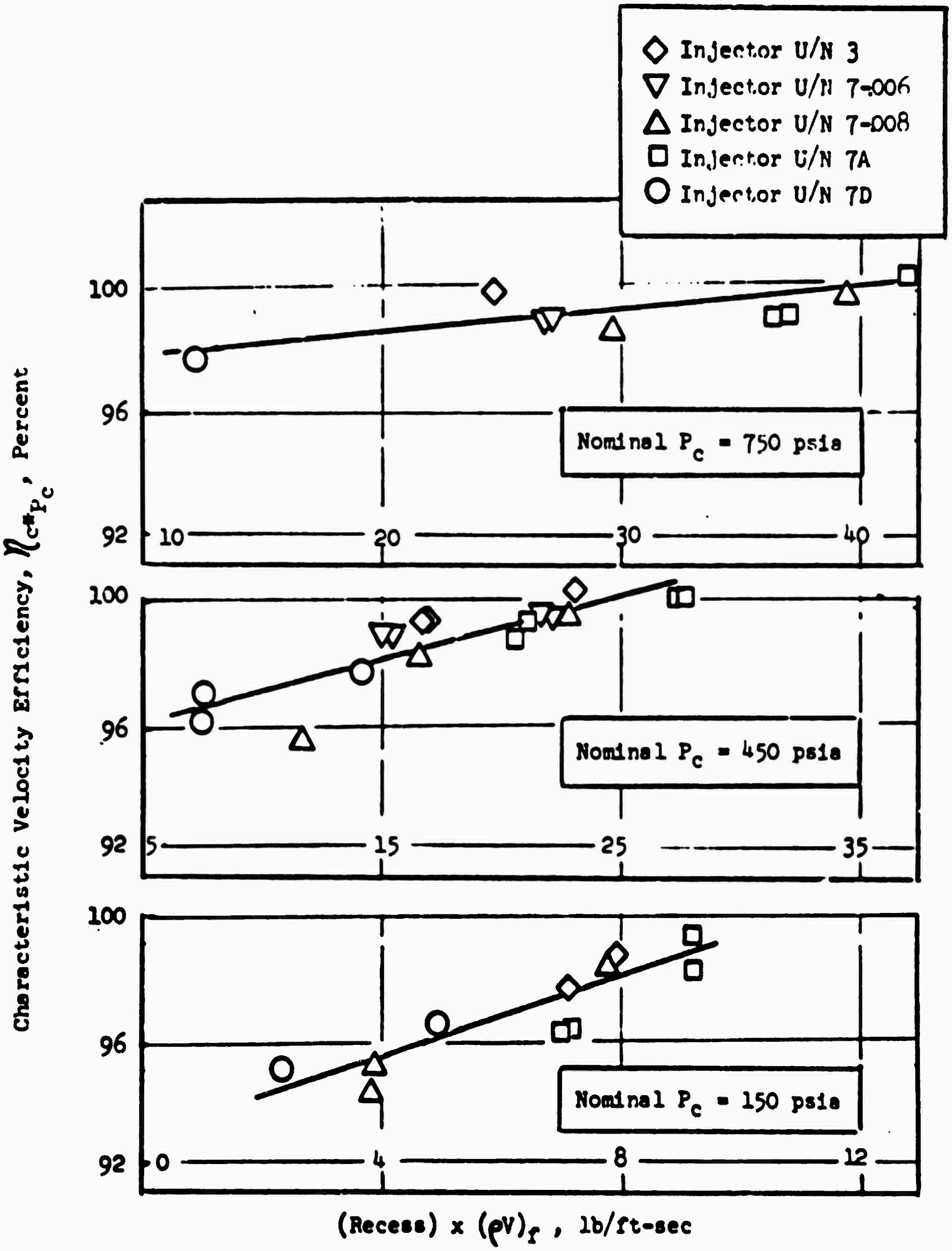

Figure 61 Effect of (Oxidizer Post Recess x $(\rho V)_f$) Product on Characteristic Velocity Efficiency for Single-Panel Concentric Injectors

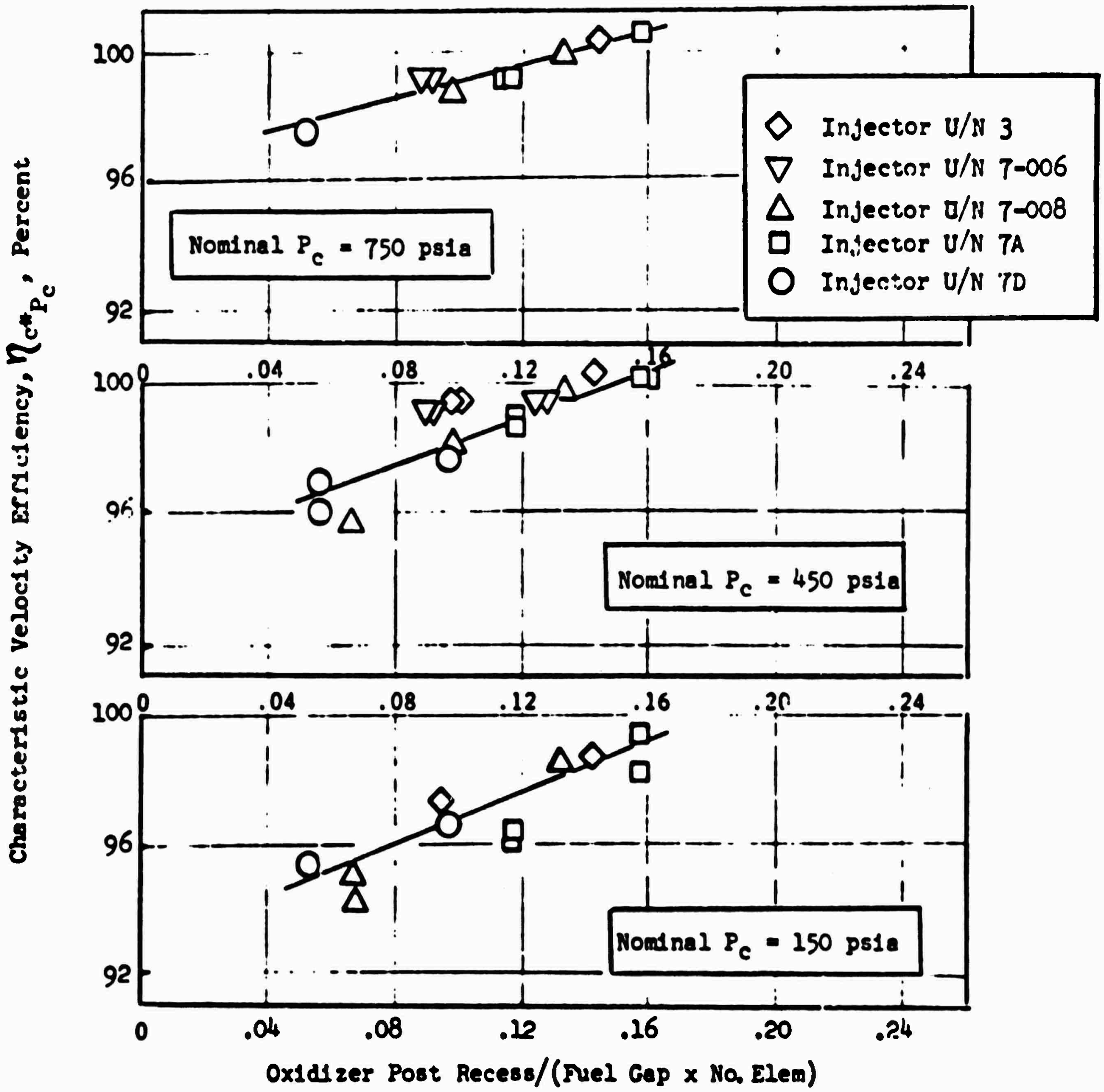

Figure 62. Effect of Nondimensional Correlating Parameter on Characteristic Velocity Efficiency for Single-Panel Concentric Injectors

Performance Correlation With Combustion Model. Measured c* efficiency is plotted versus combustion model predicted vaporization efficiency for the concentric injectors in Fig. 63. Predicted vaporization efficiencies were previously presented in the combustion model studies (see Table 6 and Appendix I). Exact correspondence between measured and predicted values would follow a 45-degree diagonal line passing through the graph origin. The measured performance trend is in agreement with that predicted by vaporization efficiency losses. However, the measured performance level is slightly above the predicted performance level. Based on this correspondence of hot-fire data with vaporization-limited combustion model results, the primary performance loss for concentric injectors is attributed to incomplete vaporization. Accordingly, mixing losses are indicated to be minimal for all the concentric injector designs.

The cup pressure drop afforded another means of correlation with combustion model results. Measured cup pressure drops were assessed by subtracting the known oxidizer orifice hydraulic loss (calibrated in cold-flow tests) from the oxidizer orifice hot-fire pressure drop. The remaining pressure loss represents the contribution of liquid oxygen atomization in the cup, and combustion (if present) in the cup. These measured cup pressure losses as a function of post recess at constant chamber pressures are plotted in Fig. 64 . Included in the figure are the cup pressure losses predicted by the combustion model. The combustion model cup losses account for vaporization but no combustion. The measured cup pressure losses are in agreement with analytic predictions for injector unit 7-.008 (P_c = 450, recess = 0.050 and 0.100 inch) and injector unit 7-.006 (recess = 0.050 inch, P_c = 450 to 750). The remainder of the measured cup pressure losses exceed analytic predictions, indicating the presence of a degree of combustion in the cup.

For combustion to occur in the cup, the fuel injection velocity must be sufficiently low to permit residence time for ignition. Therefore, the ratio of cup ΔP_{meas}/cup ΔP_{pred} (values in excess of 1 indicate an increasing degree of cup burning) was plotted as a function of fuel injection velocity in Fig. 65. The cup ΔP deviation, or cup burning, appears to increase with lower fuel injection velocity and increased chamber pressure and, to a lesser extent, with increased oxidizer post recess.

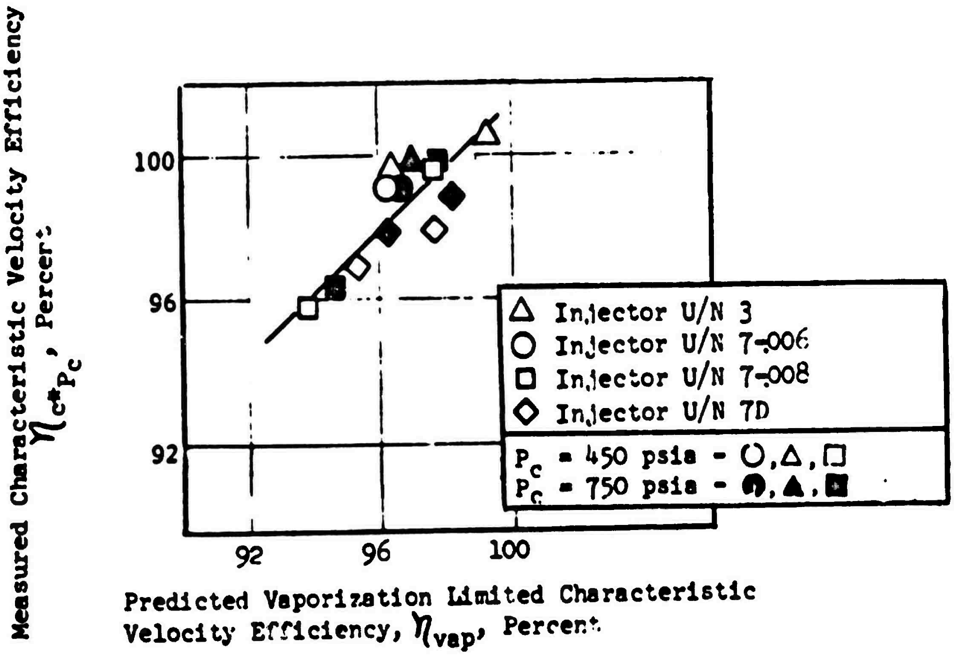

Figure 63. Comparison of Predicted Vaporization Limited Characteristic Velocity Efficiency With Measured Characteristic Velocity Efficiency for Single-Panel Concentric Injectors

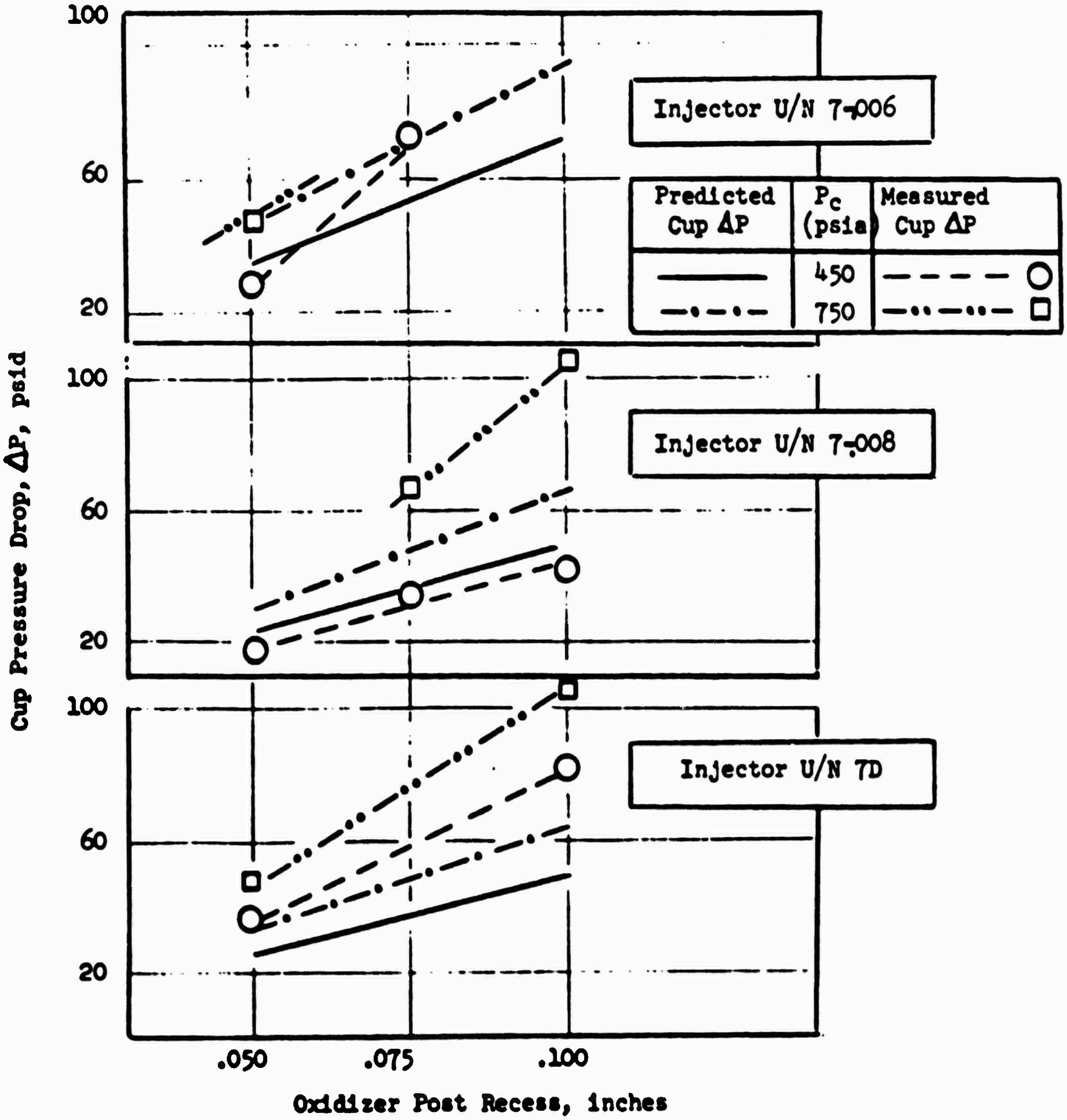

Figure 64.. Comparison of Predicted and Measured Cup Pressure Drop for Single-Panel Concentric Injectors

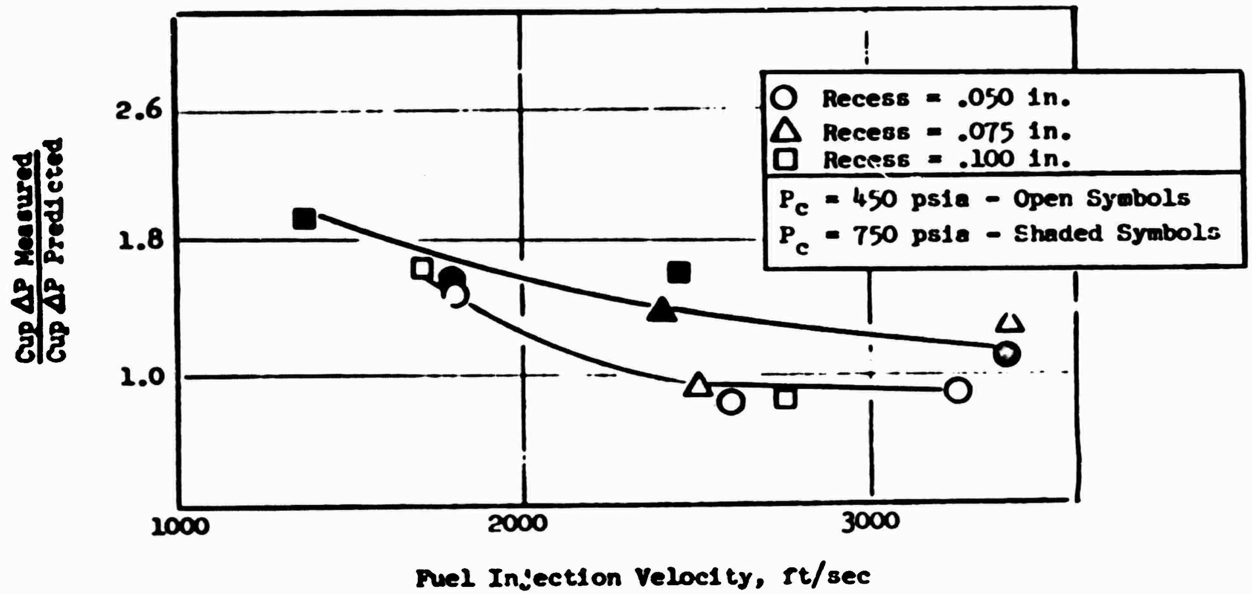

Figure 65. Effect of Fuel Injection Velocity on Cup Combustion for Single-Panel Concentric Injectors

Heat Transfer

Prior to the testing of the single-panel water-cooled chamber, a design gas-side heat transfer coefficient distribution was determined for the design chamber pressure of 750 psia and the 5:1 throttled condition (150 psia), as shown in Fig. 66 and 67. Curves were obtained using analytical predictions and with safety factors applied. These curves with safety factors applied were called conservative curves. The safety factor was 1.16 from X=-1.3 inches to the throat and 1.5 from X=-1.3 inches to the injector. Using these design curves, the coolant channel sizes were initially determined for the regeneratively cooled, single-panel NARloy cast combustor.

After a number of water-cooled chamber tests, the results showed that none of the injector configurations evaluated completely met the design curves. As shown in Fig. 68 through 70, the injector region heat flux was significantly higher than the design value. Below a chamber pressure of 450 psia, the general heat flux axial variation (Fig. 70) was a high injector region heat flux decreasing to a minimum, then increasing to the value at the sonic point. The high injector region heat flux was theorized to be the result of an extremely violent recirculation near the injector face. The high injector region heat flux resulted in a higher-than-design combustion chamber input ($Q_{cc}/\dot{W}_{prop}$) as presented in Fig. 71. To ensure satisfactory thrust chamber cooling, lower values of these parameters would be required.

Of all the injectors evaluated, concentric injector units 7 and 7A demonstrated the highest potential of reducing the heat flux level through variations in hydrogen injection velocity, oxidizer post recess, and number of elements. As shown in Fig. 72 and 73 , reducing the hydrogen injection velocity significantly reduced the first coolant passage (adjacent to the injector) heat flux and the combustion chamber input. The hydrogen injection velocity influence was investigated by independently varying the fuel temperature and the fuel gap (Fig. 73). The resulting injector region heat flux and chamber heat input varied directly with injection velocity, indicating no dependence on fuel injection temperature. This trend with injection velocity supported the recirculation driven heat flux

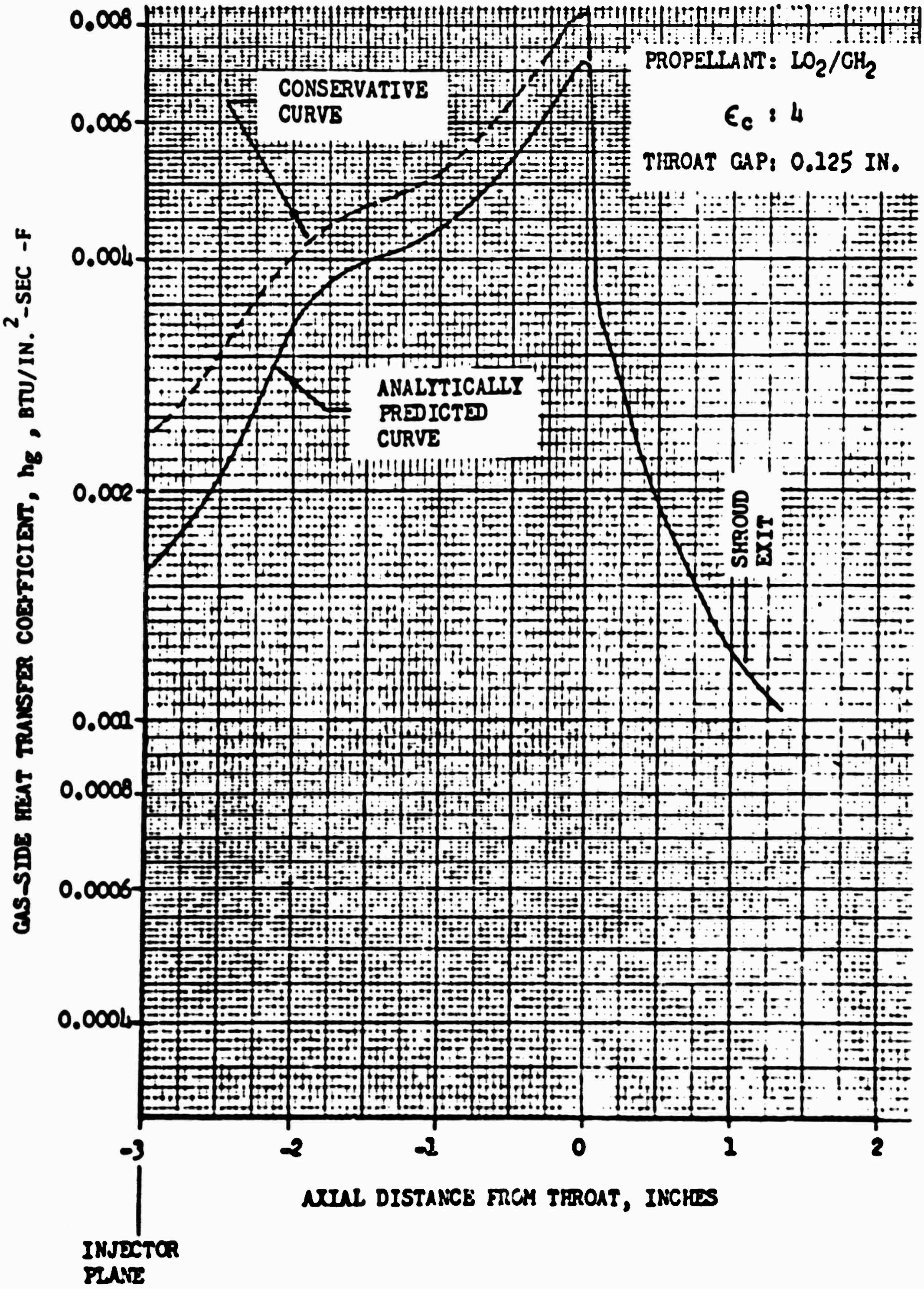

Figure 66. Single-Panel Combustor Gas-Side Heat Transfer Coefficient Distribution (P_c = 750 psia, MR = 5.5)

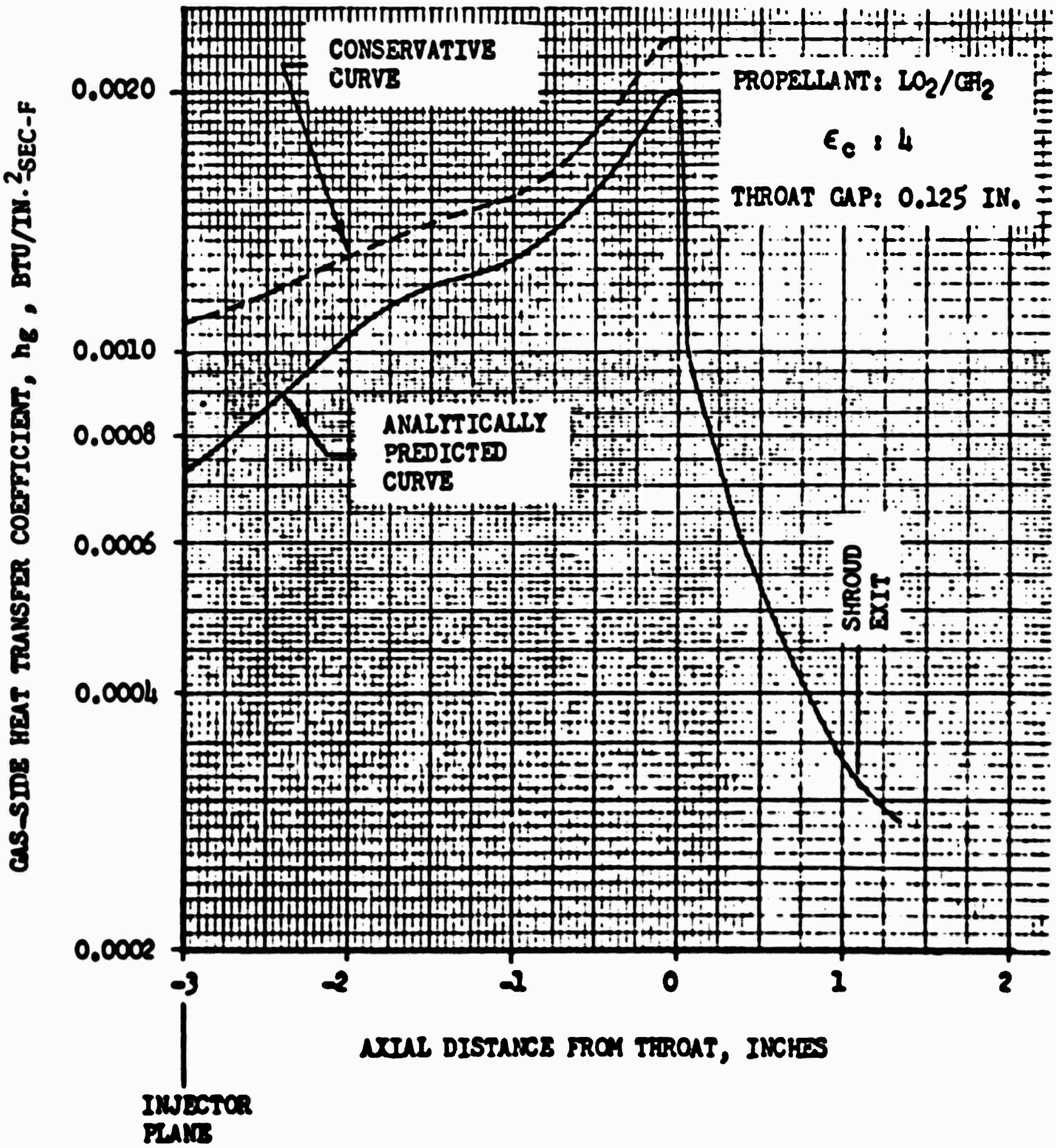

Figure 67. Single-Panel Combustor Gas-Side Heat Transfer Coefficient Distribution (P_c = 150 psia, MR = 5.5)

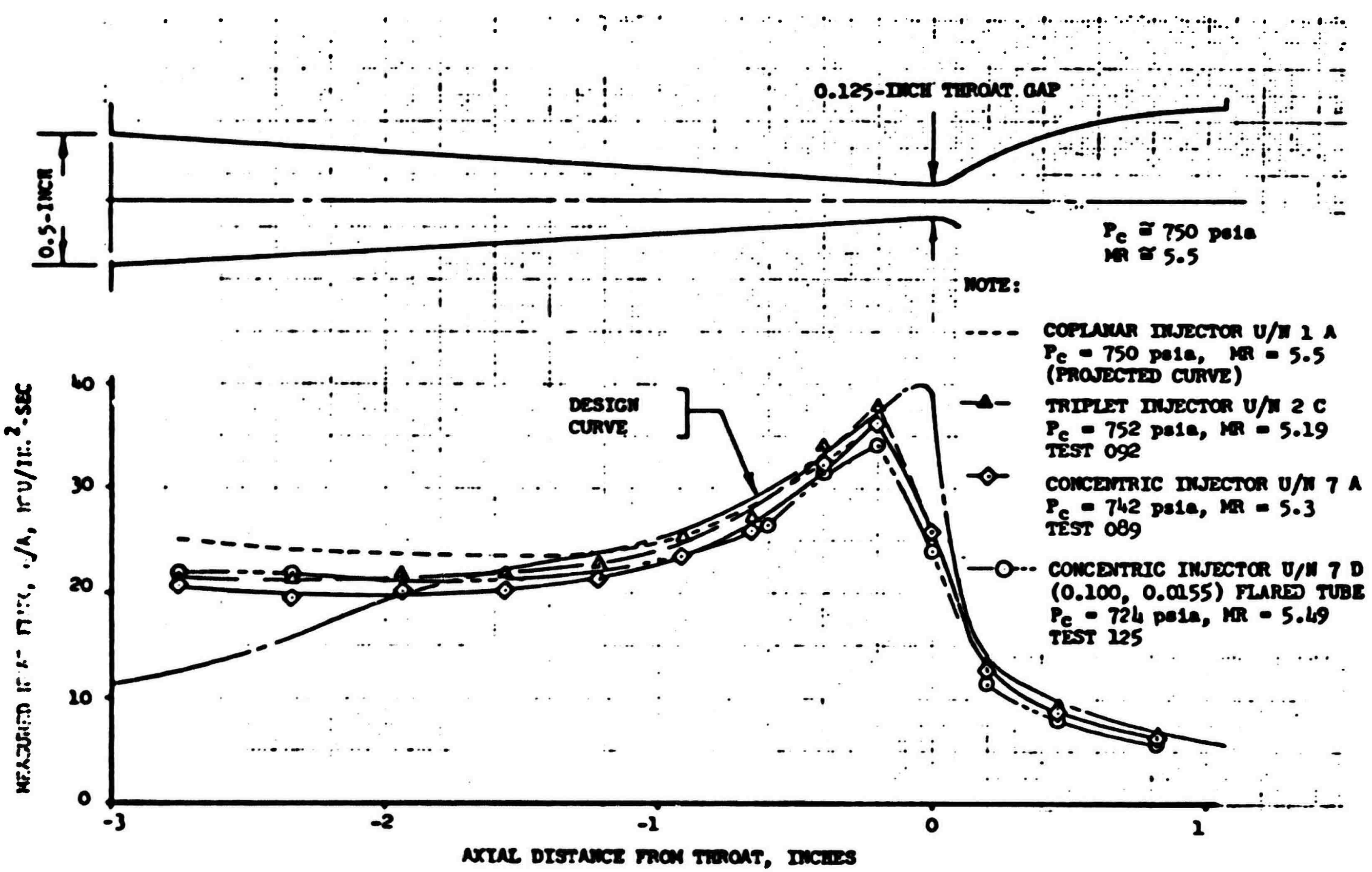

Figure 68. Single-Panel Combustor Heat Flux Distribution, Injector Influence (P_c = 750 psia)

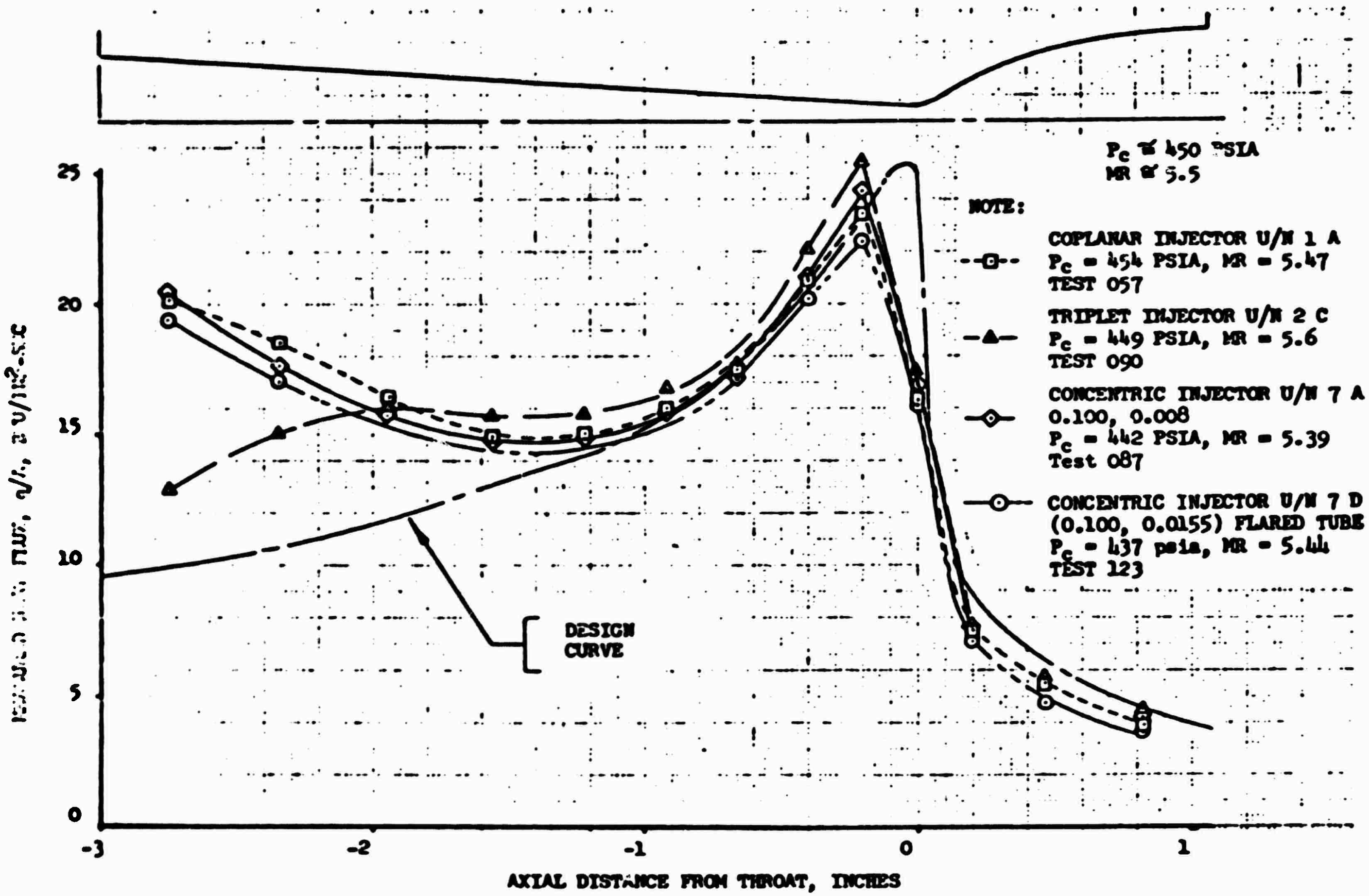

Figure 69. Single-Panel Combustor Heat Flux Distribution, Injector Influence (P_c = 450 psia)

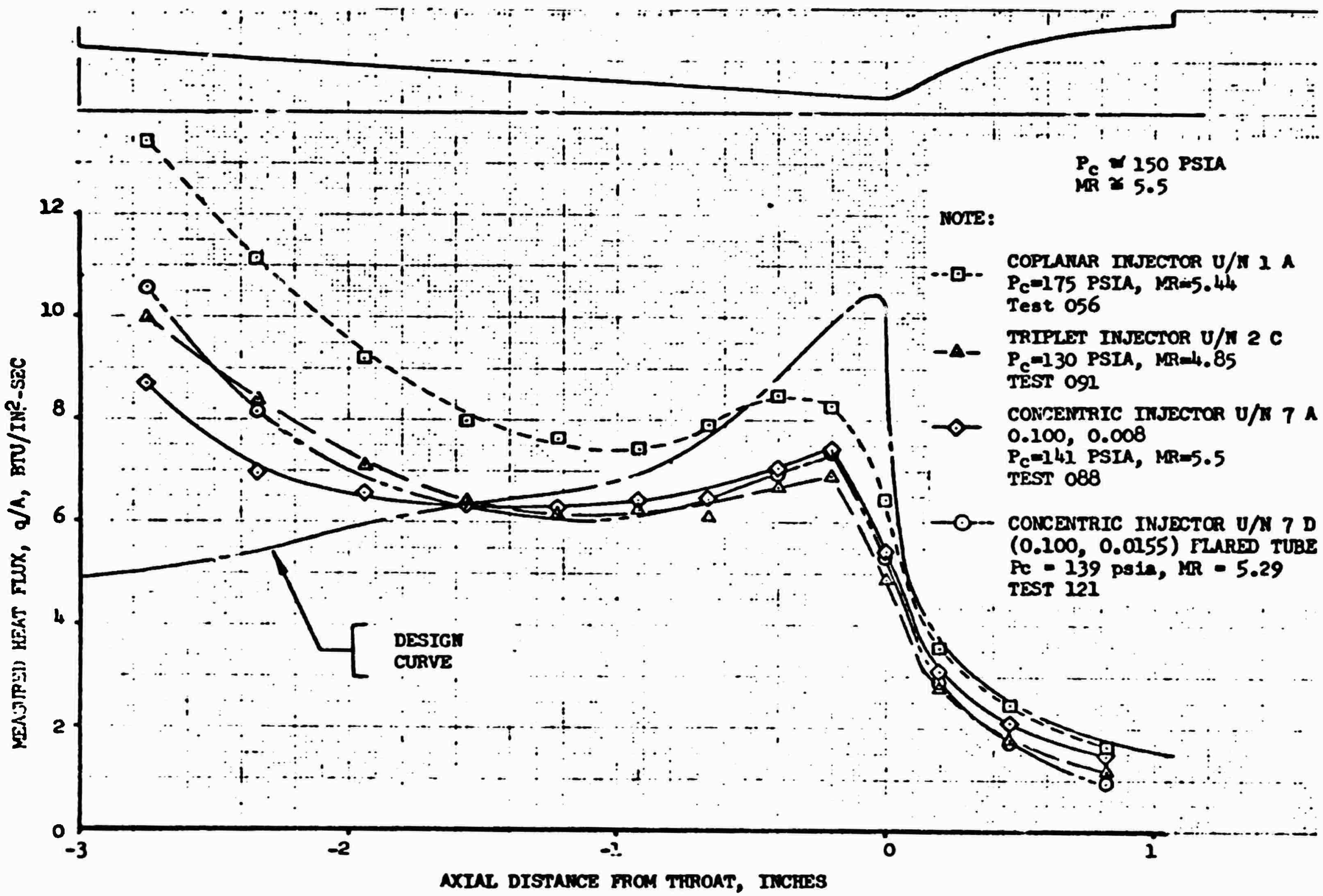

Figure 70. Single-Panel Combustor Heat Flux Distribution, Injector Influence (P_c = 150 psia)

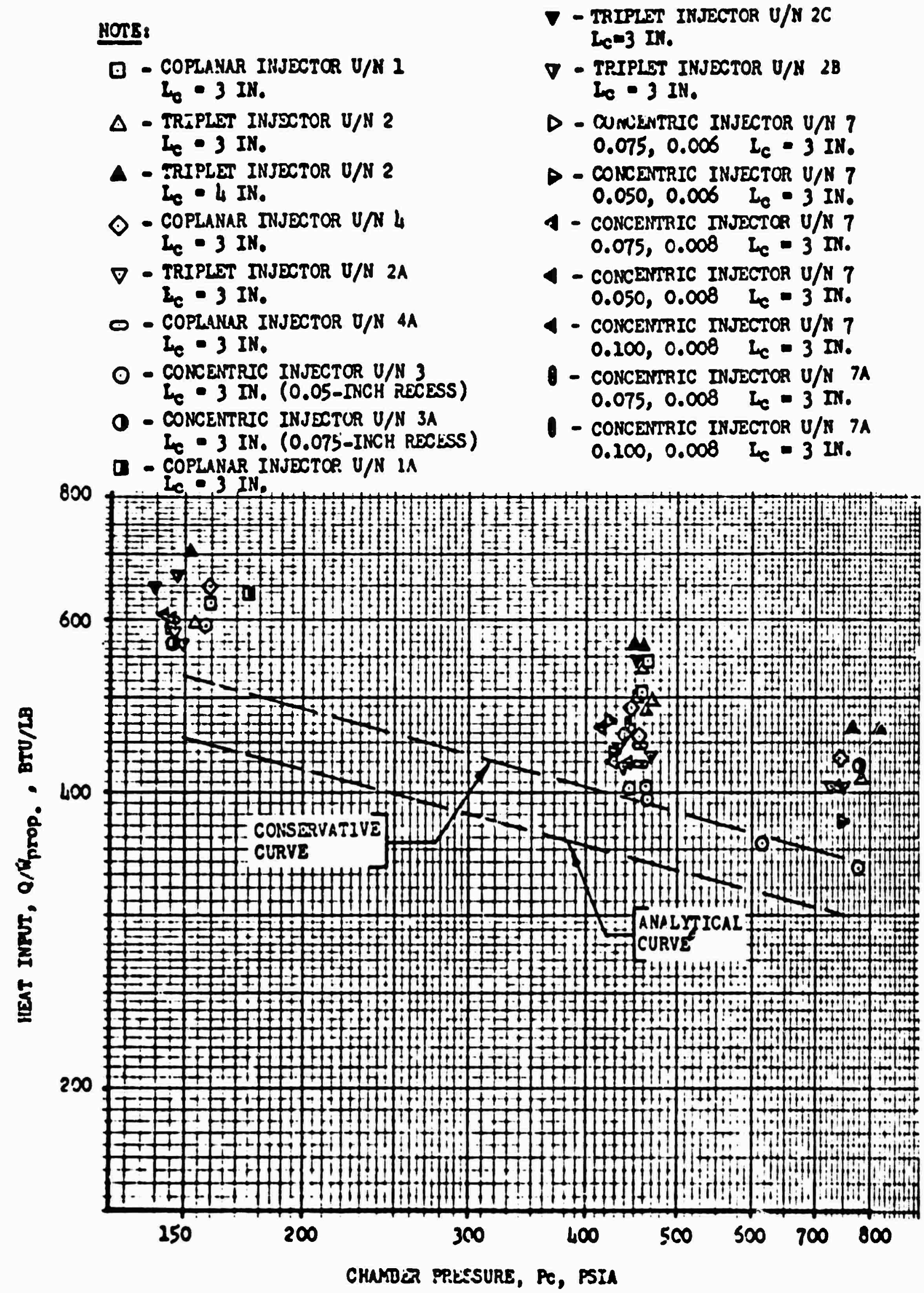

Figure 71. Single-Panel Combustion Chamber Heat Input

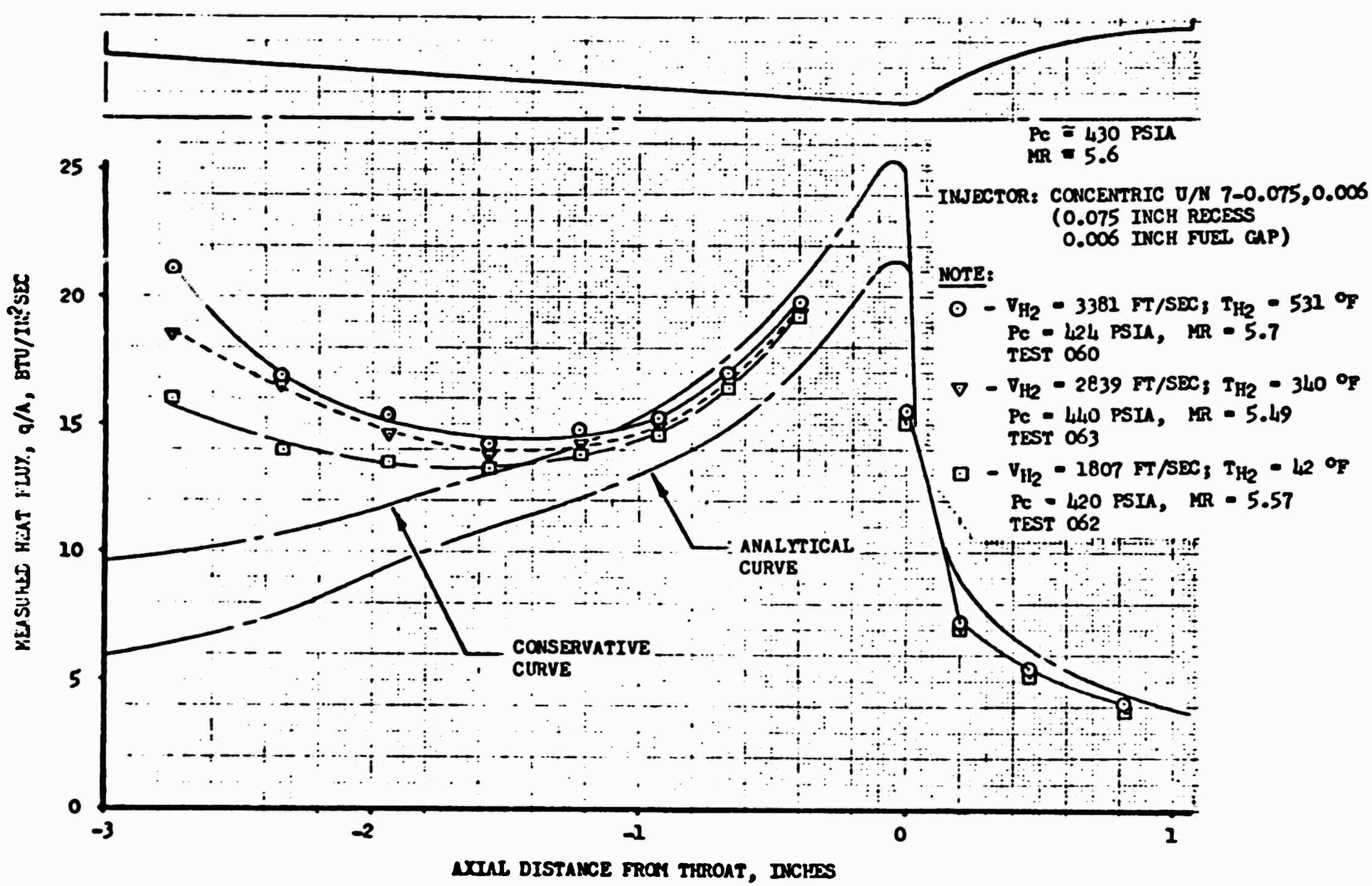

Figure 72. Single-Panel Combustor Heat Flux Distribution, Hydrogen Velocity Influence ($P_c \cong 430$ psia)

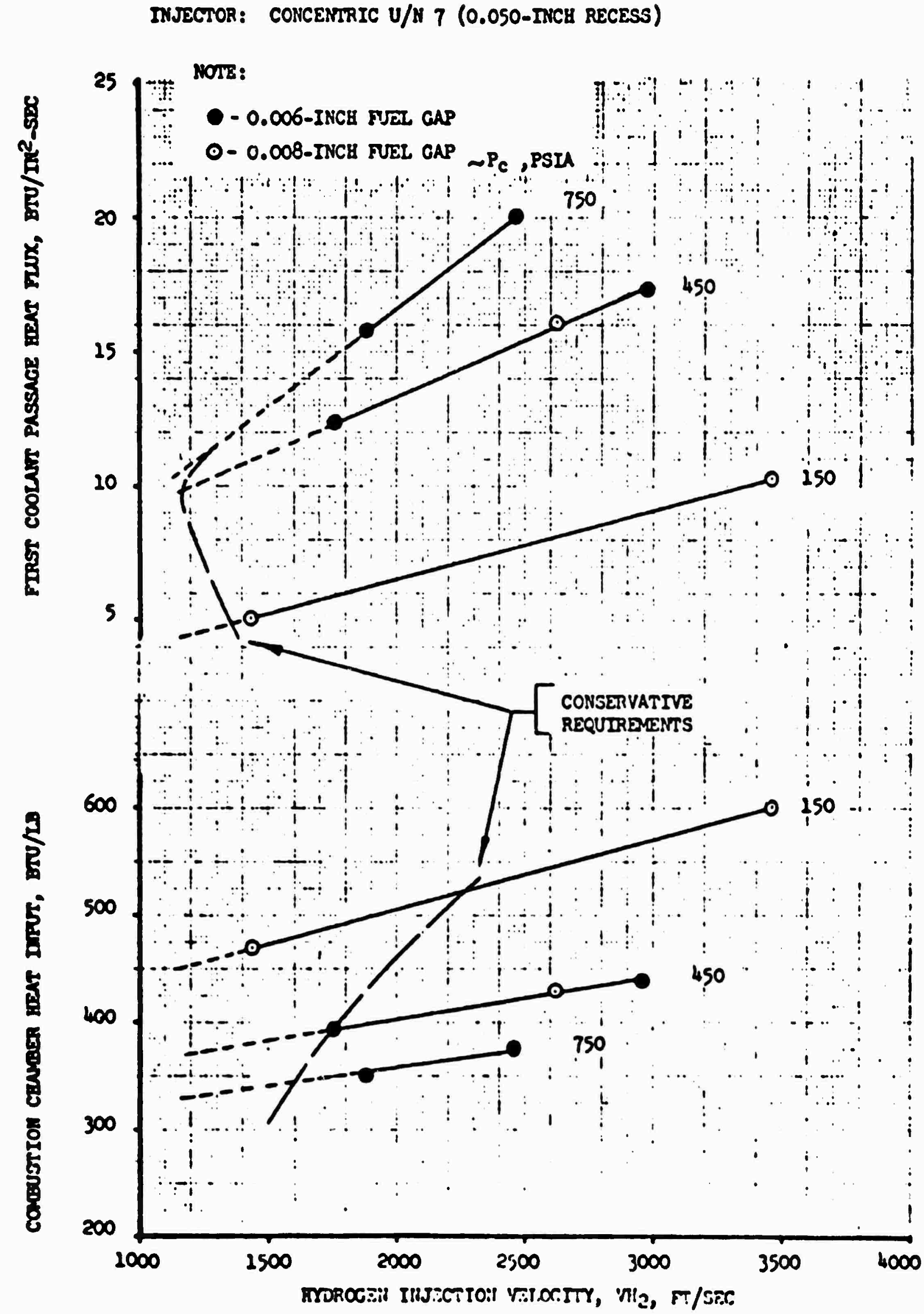

Figure 73. Hydrogen Velocity Influence (0.050-Inch Recess) on Single-Panel Heat Transfer

theory. Lowering the injection velocity apparently decreased the recirculation near the injector and resulted in a decrease in heat flux. For the 0.05-inch oxidizer post recess, a 5-percent decrease in hydrogen injection velocity decreased the injector region heat flux by 20 percent and the heat input by 5 percent.

Decreasing the number of injector elements from 95 to 79 resulted in a decrease in the pertinent heat transfer parameters for the lower injection velocities (Fig. 74 and 75). As shown in Fig. 75 , an increased sensitivity to injection velocity was obtained for the decreased number of elements.

The influence of oxidizer post recess is presented in Fig. 76 and 77 at representative hydrogen injection velocities. At the design chamber pressure of 750 psia, decreasing the recess from 0.100 to 0.050 inch decreased the injector region heat flux by approximately 30 percent, and the combustion chamber heat input by 12 percent (Fig. 77).

At the 5:1 throttled condition (150 psia), the injector region heat flux and the heat input were relatively independent of number of elements and the oxidizer post recess, as shown in Fig. 78 .

Therefore, from a heat transfer standpoint, a concentric injector having the following pertinent heat transfer parameters was recommended:

Number of elements:	Approximately 80
Hydrogen Injector Velocity at 750-psia Chamber Pressure:	Less than 1300 ft/sec
Oxidizer Post Recess:	0.050 inch

The gas-side heat transfer coefficient distributions for the single-panel combustor from the injector plane (X=-3.0 inches) to the sonic point (X=-0.2 inch) were determined through cross plotting, extrapolating, and interpreting the obtained water-cooled test data. The analytically predicted distribution was used

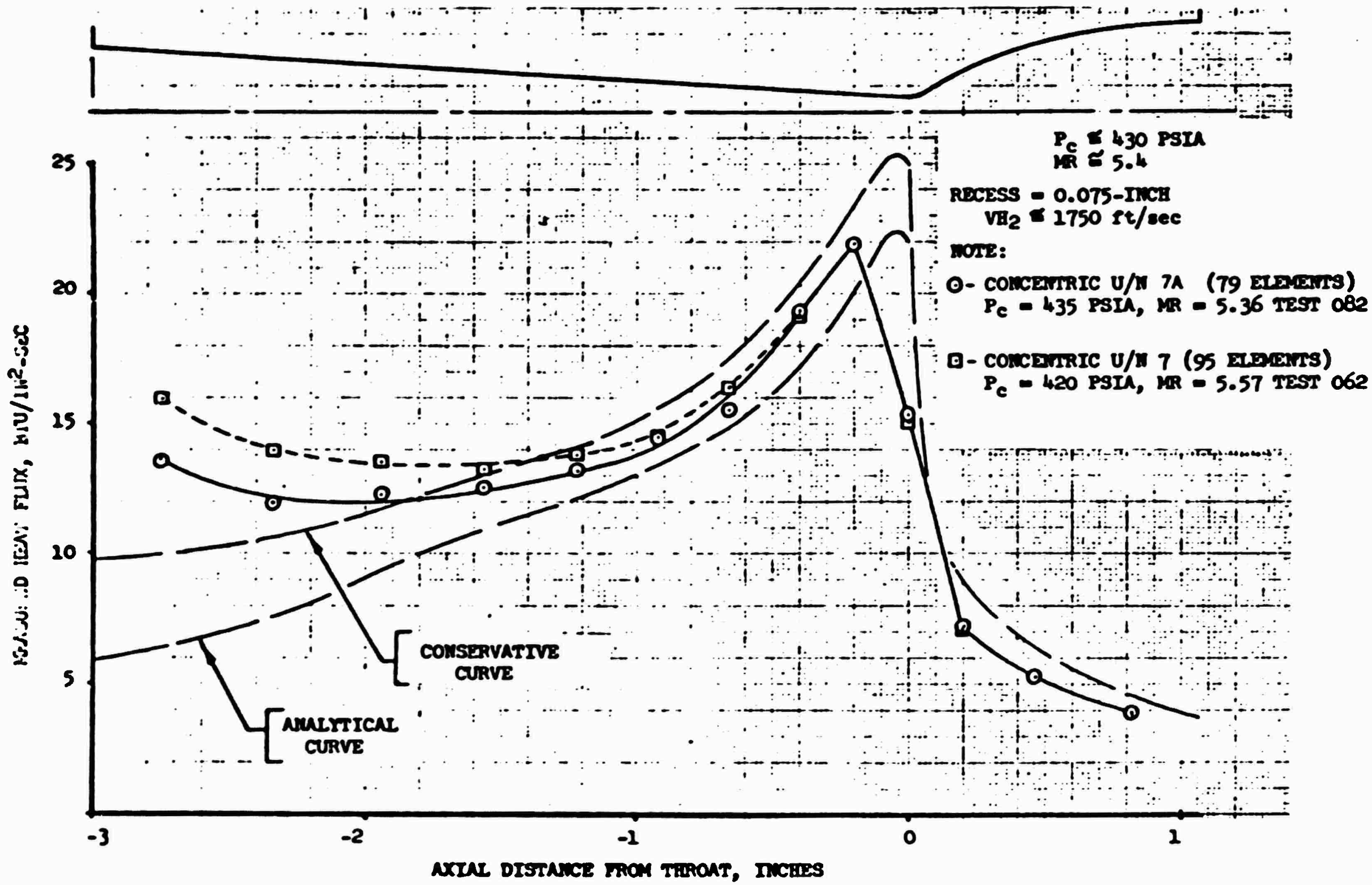

Figure 74. Single-Panel Combustor Heat Flux Distribution--Number of Elements Influence (P_c = 430 psia)

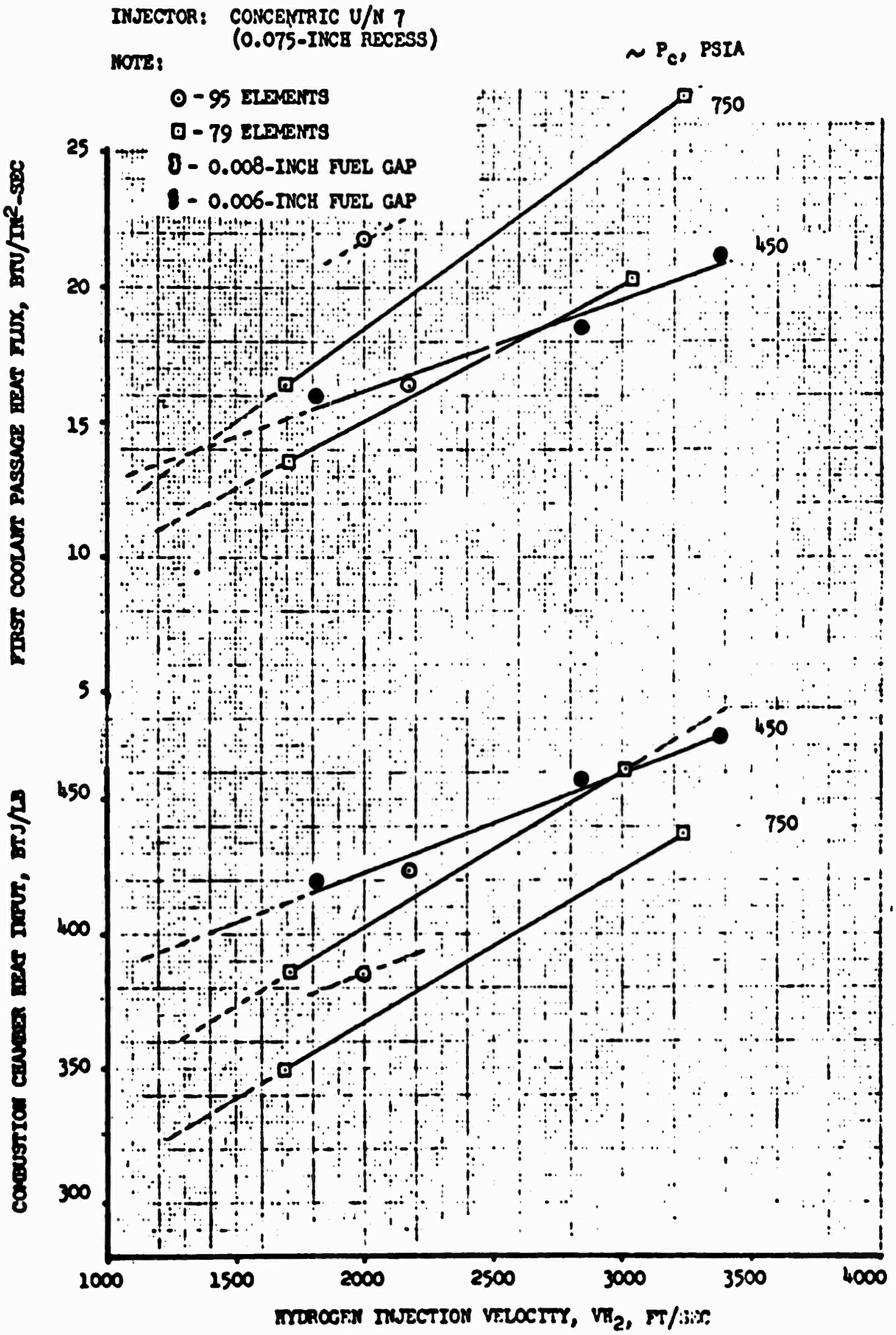

Figure 75. Hydrogen Velocity and Element Number Influences (0.075-inch Recess) on Single-Panel Heat Transfer

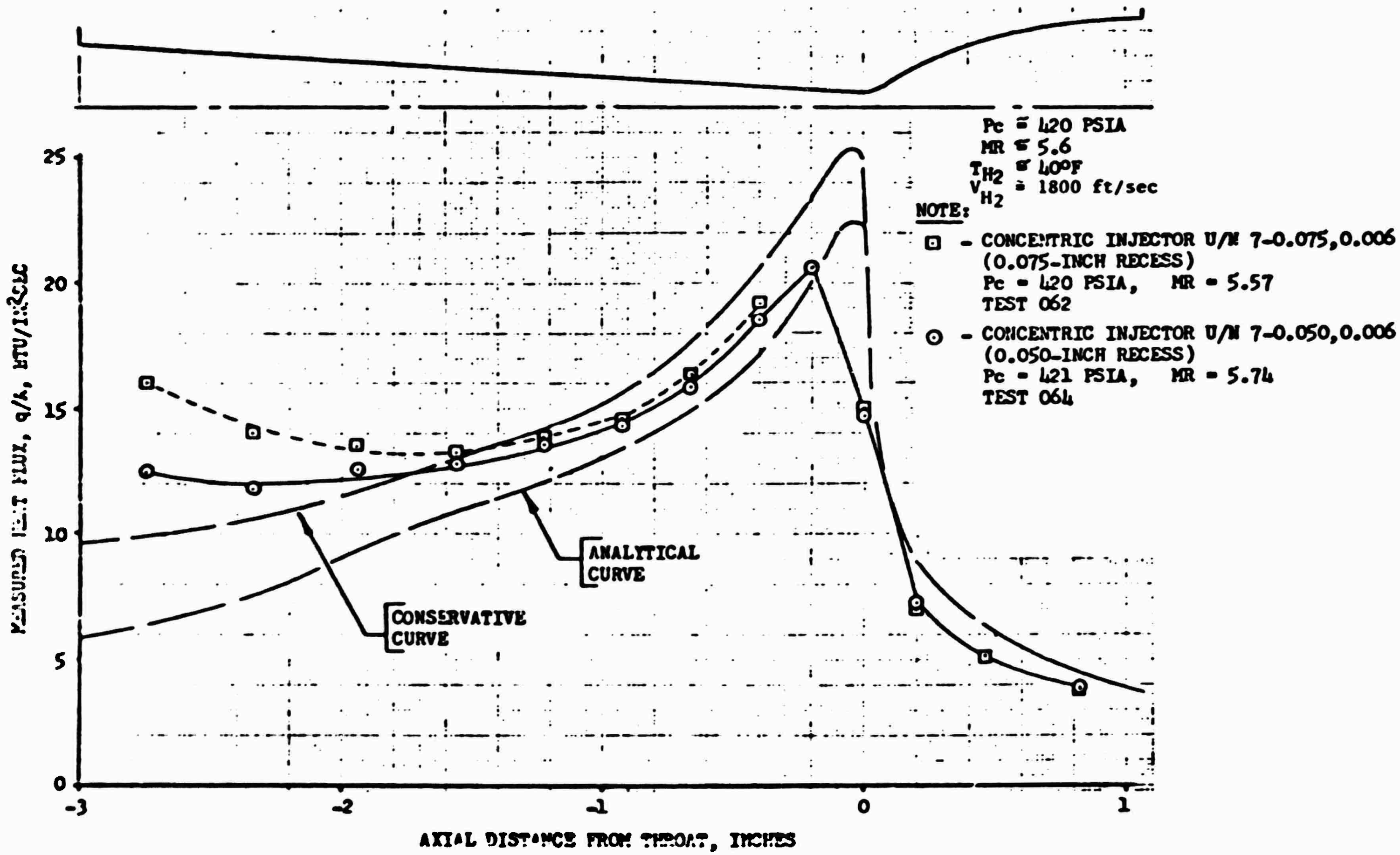

Figure 76. Single-Panel Combustor Heat Flux Distribution, Recess Influence ($P_c \cong 420$ psia)

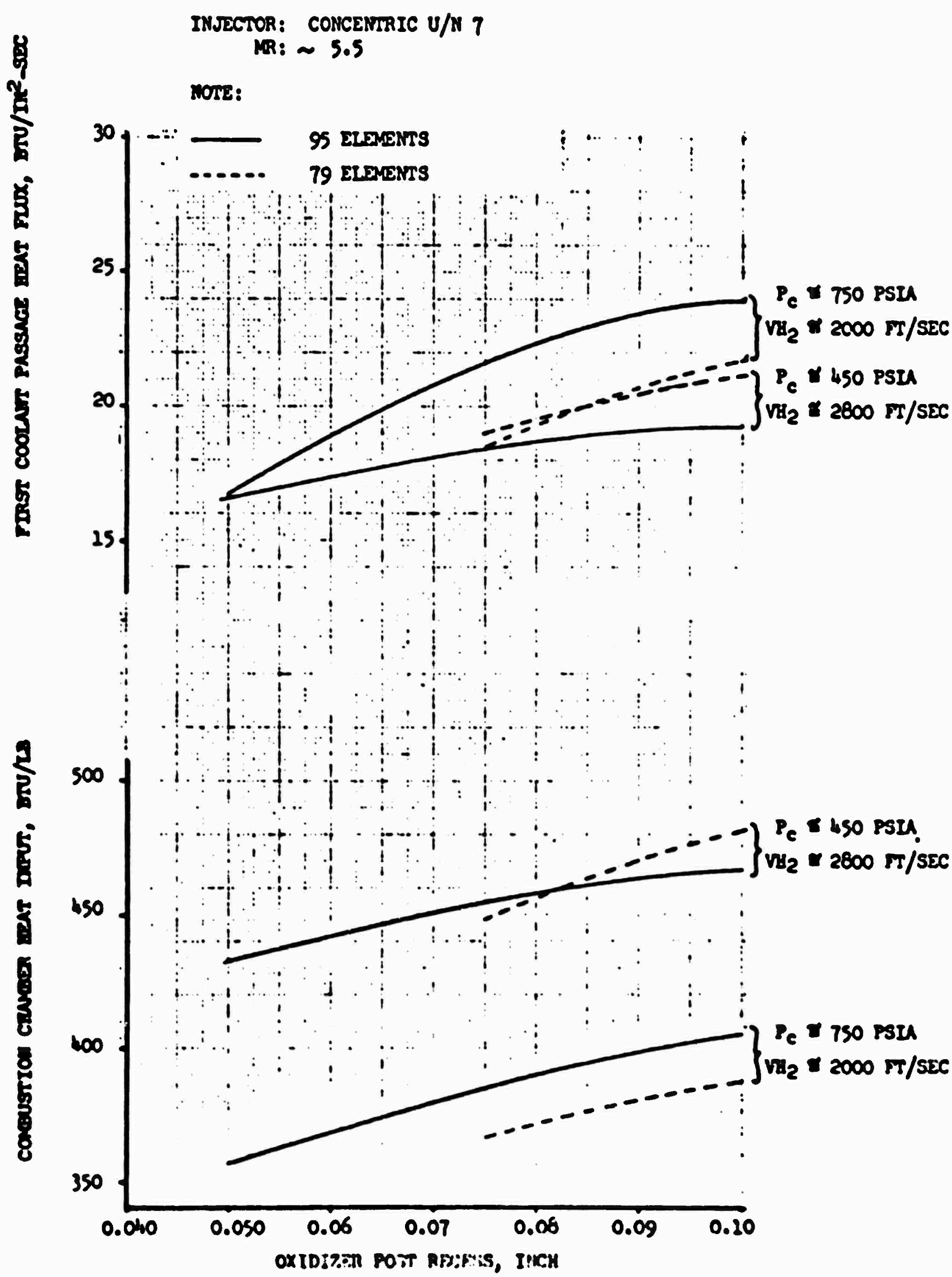

Figure 77. Oxidizer Post Recess and Element Number Inlfuences on Single-Panel Heat Transfer

INJECTOR: CONCENTRIC
P_c = 150 PSIA
MR = 5.5

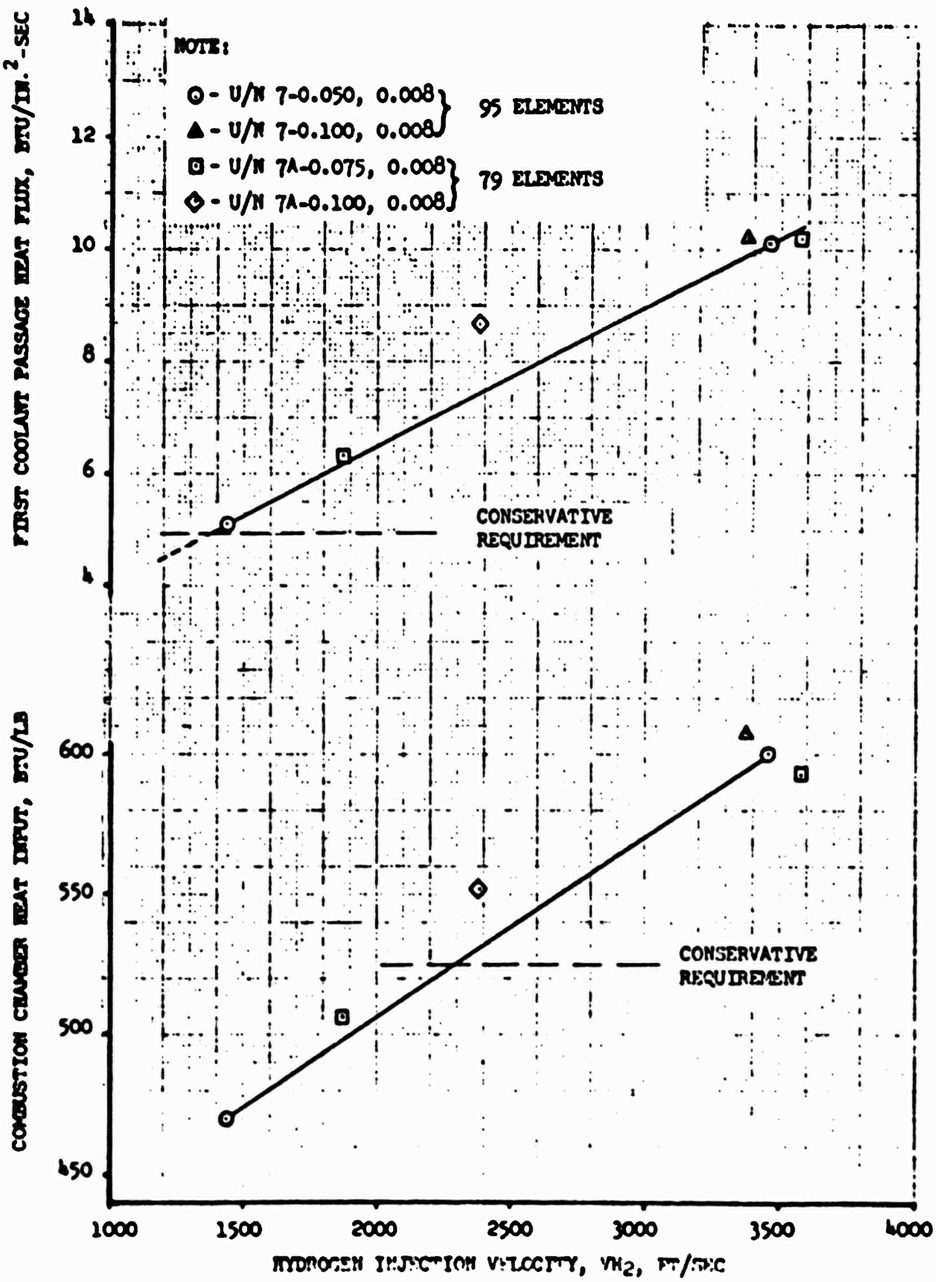

Figure 78. 150-psia Single-Panel Chamber Pressure Operation

downstream of the sonic location because the distribution for this region may have been influenced by local hot-gas flow separation resulting from testing in a non-vacuum environment. The resulting gas-side heat transfer coefficient distributions for three chamber pressures are presented in Fig. 79 . Curves for both 0.050- and 0.100-inch oxidizer post recess are presented for the final concentric injector configuration:

Number of Elements:	80
Hydrogen Injection Velocity at the Design Chamber Pressure:	1250 ft/sec

The resulting peak heat flux at the design pressure of 750 psia was approximately 40 Btu/in.^{2}-sec for a 1000 F gas-side wall temperature.

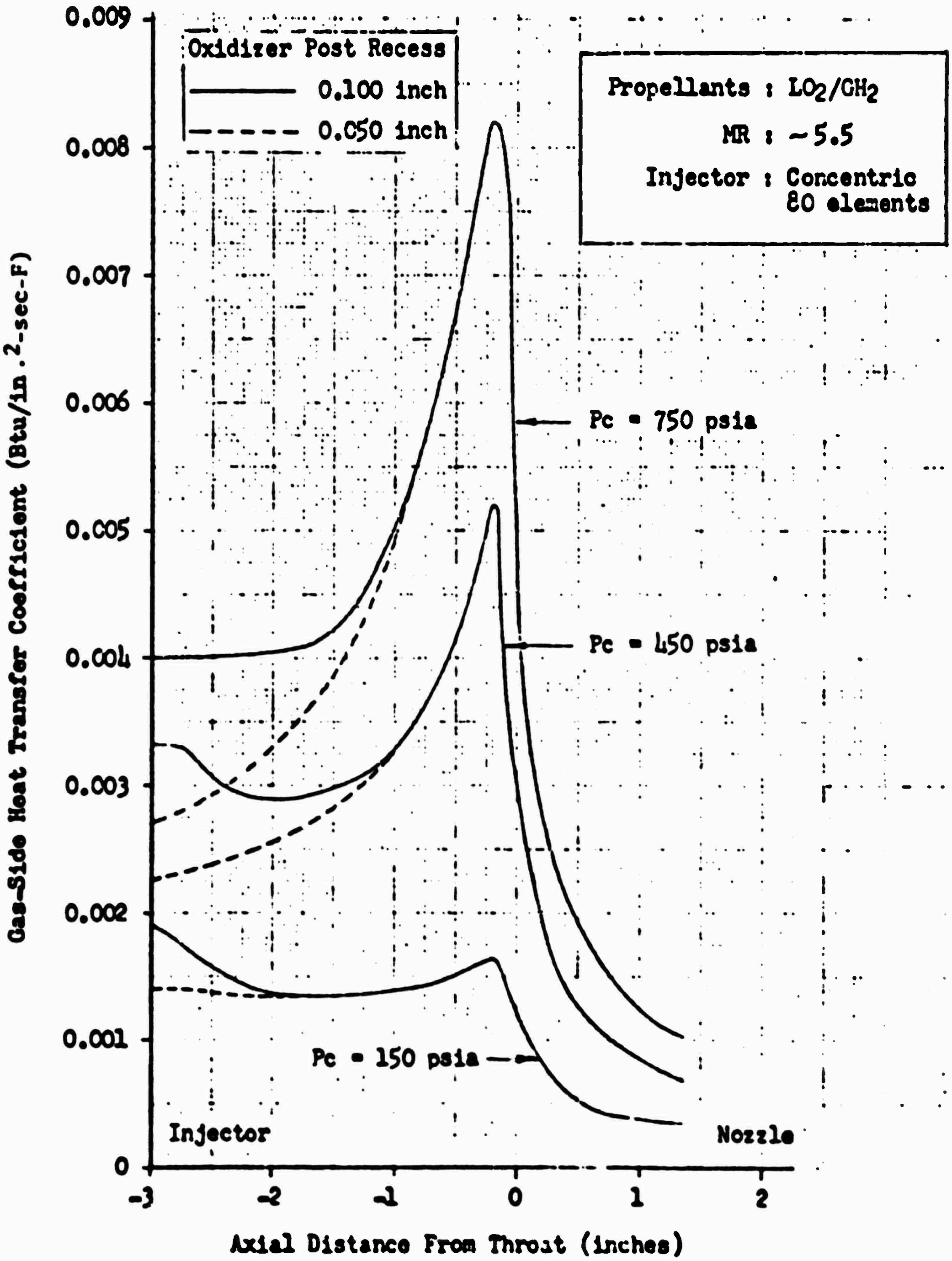

Figure 79. Single-Panel Gas-Side Heat Transfer Coefficient Distribution

Single-Panel Combustion Stability Evaluation

A series of tests was conducted to evaluate the combustion stability characteristics of the concentric orifice injector. The unit 7D injector was used in conjunction with the unit 4 water-cooled segment chamber. The unit 4 chamber had provisions for a directed pulse gun. The pulse-gun assembly, shown in Fig. 15 , consisted of a barrel, burst diaphragm holder, and squib firing pin assembly.

A 38-caliber cartridge case loaded with 10 grains of Bullseye pistol powder was used to provide the pulse. A 7500-psi burst disk was used to produce a steep-fronted chamber disturbance.

A Type 614A4, high-frequency, Kistler helium bleed transducer was used to monitor the disturbance in the combustion zone. The transducer sensing port was located in the end plate, 0.455-inch downstream of the injector face.

The stability evaluation tests were conducted for an average duration of 6 seconds each, with the pulse squib initiated after 5 seconds of mainstage duration, to ensure stabilized mainstage conditions at the time of the pulse. A steep-fronted pressure disturbance in excess of 50 percent of operating chamber pressure was desired on all tests. Recovery from the disturbance was required within 40 milliseconds to meet program objectives.

The test data are summarized in Table 10. Dynamic combustion stability was demonstrated on each of the tests with recovery times of 8 milliseconds or less.

On tests above the mid-chamber pressure range, however, the pulse overpressure values were less than the required 50-percent overpressure. Analysis showed that the charges were insufficient to provide the required pulse.

There was water leakage from the coolant passages into the combustion chamber during the stability evaluation test series. The η_{c*} was degraded slightly, as mentioned on page 110, with the greatest degradation occurring on the final test (127-71) of the series. Because of the minimum degradation for all tests except 127-71, the water leakage was considered to have a negligible effect on the stability evaluation results, except test 127-71.

Table 10

SINGLE-PANEL WATER-COOLED SEGMENT

STABILITY EVALUATION TESTING

Test No.	Chamber Pressure, psia	Mixture Ratio O/F	Pulse (1) Overpressure psia	Pulse Overpressure percentage	Maximum (2) Overpressure psia	Maximum Overpressure percentage	Recovery (3) Time Msec
121	139	5.29	75	54	167	120	7
122	287	5.23	150	52	410	143	3
123	437	5.44	75	17	335	77	6
124	584	5.42	93	16	130	22	8
125	724	5.49	187	26	187	26	4

NOTE

(1), (2), and (3) defined as shown below

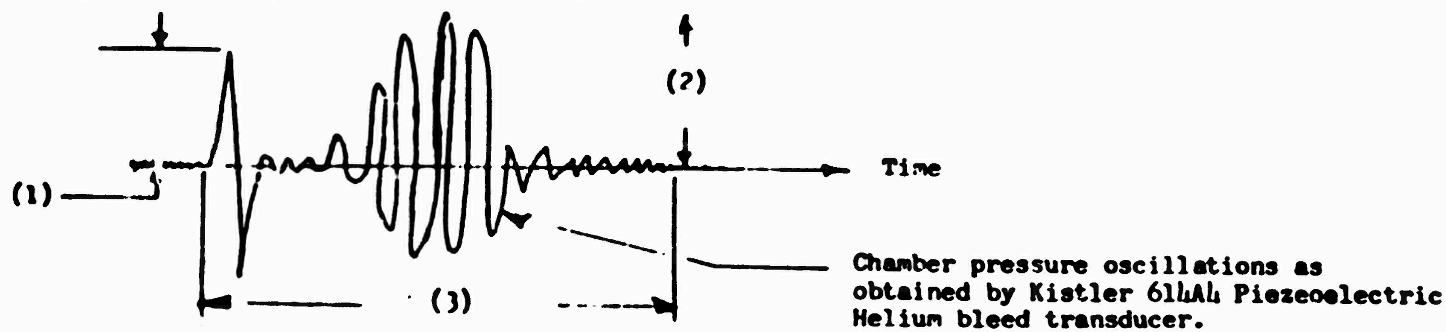

The single-panel segment test program objective was to provide data that would:

1. Permit selection of the segment chamber and injector configuration to be used for the regeneratively cooled segment design.

2. Establish the heat transfer characteristics of the selected segment chamber and injector configuration so that the coolant circuit and coolant passage design for the regeneratively cooled segment chamber could be verified and modified if required.

3. Permit definition of performance and heat transfer characteristics of the selected configuration over the throttle range, 750- to 150-psia chamber pressure.

4. Permit evaluation of the combustion stability characteristics of the selected combustor and injection element configuration.

Figure 80 presents the injector-combustor development flow chart which depicts the various injector-chamber configurations evaluated and the generalized significant results. The results presented in Fig. 80 were applied directly to the final configuration selection. A large amount of supplementary information was obtained, and was discussed previously (pages 95 through 137). The following sections will present the selection criteria for the single-panel injector-combustor configuration and summarize the data obtained from the test program.

Injector-Combustor Selection

The program requirements for the single-panel injector-combustor assembly were as follows. The design shall have high combustion efficiency over the complete throttling range, 97 percent minimum η_{c*} based on full shifting c*, smooth ignition and chamber pressure transient characteristics, no excessive injector streaking, and uniform heat transfer into the chamber wall with no sharp peaks in predicted local wall temperatures that would jeopardize the chamber durability requirements. In addition, cost and ease of fabrication were considered important criteria, although not specifically stated.

Two primary criteria existed for injector configuration selection: (1) combustion efficiency, and (2) heat transfer, with the assumption that the chamber configuration had been established. The chamber configuration selection occurred early in

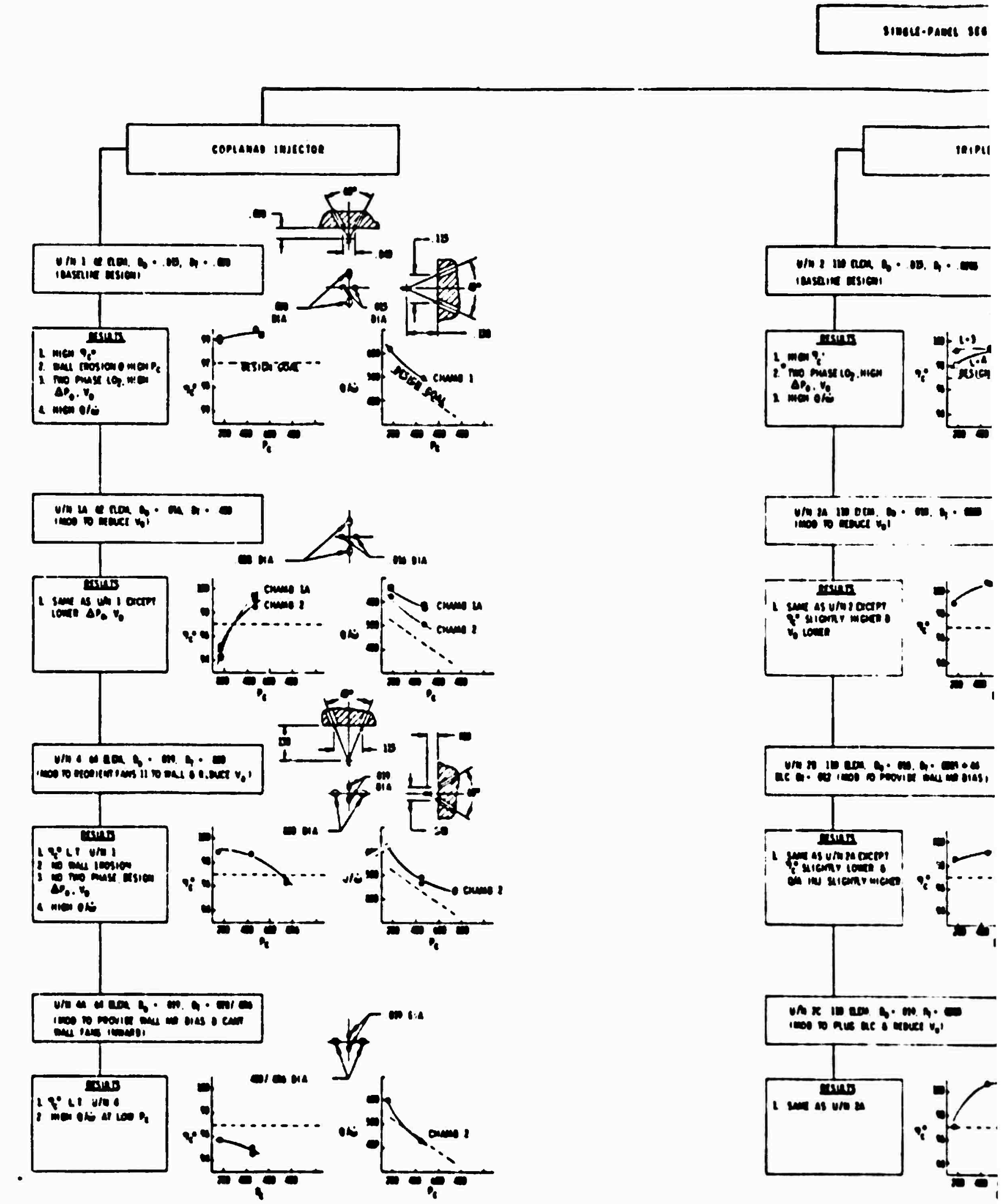
COPLANAR INJECTOR
(BASELINE DESIGN)
RESULTS
DESIGN GOAL
RESULTS
1. SAME AS U/N 1 EXCEPT LOWER ΔP_0, V_0
RESULTS
RESULTS
RESULTS
1. SAME AS U/N 2A

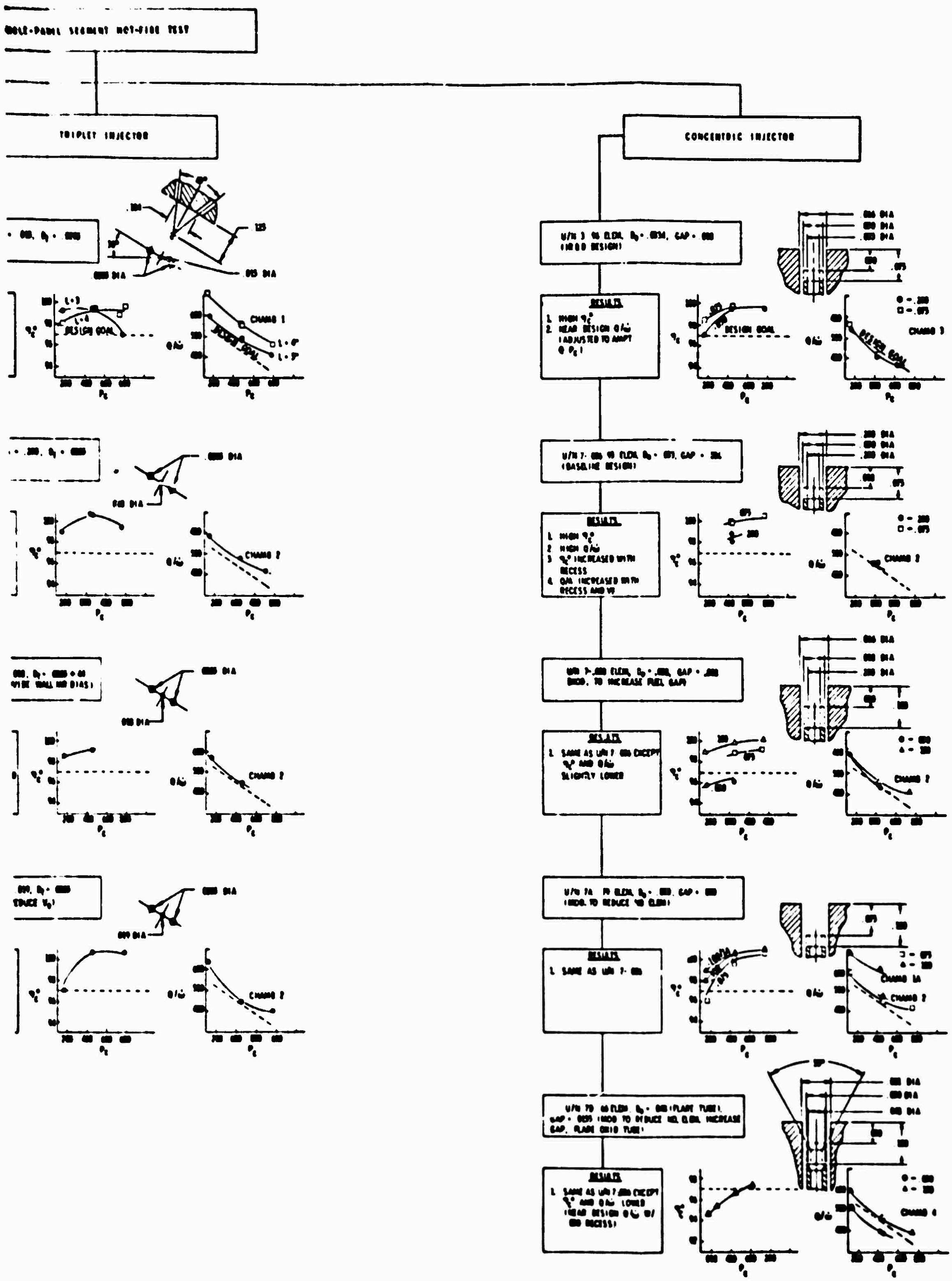

Figure 80. Single-Panel Segment Hot-Fire Test, Development Flow Chart

the development effort, by necessity. The chamber had to be as small as possible to permit realization of the lightweight requirements. Therefore, when the results showed that no significant performance increase would be realized with an increase in L_c over 3.0 inches, and that an L_c greater than 3.0 inches would severely restrict cooling capability based on total integrated heat rejection rate considerations, the chamber configuration was fixed.

The selection criteria applicable to the injector (items 1 and 2) are discussed below.

Performance. Three basic injectors were evaluated with respect to performance in the same thrust chamber segment. The basic types were then modified to establish criteria for increasing performance or decreasing local heat transfer rates. The three basic injectors were:

1. Coplanar, units 1 and 4
2. Triplet, unit 2
3. Concentric, unit 7 (Another concentric injector, unit 3, also was evaluated, but in a different chamber configuration.)

The performance characteristics of these injectors were presented previously on pages 95 through 120. As shown, all of the injectors met the performance requirements over the throttle range tested; however, at this point they did not meet all the heat transfer requirements.

Modifications were made to the injectors for performance and for heat transfer improvement (Fig. 52, 55, and 57). As shown, the required performance was demonstrated by two modified injectors, the unit 7A, 79-element concentric, and the unit 2A triplet. As was the case previously, the unit 1A coplanar indicated very high heat transfer rates, while the concentric and triplet had more moderate rates. Further development effort was limited to the triplet and concentric element injectors only, because these had demonstrated moderate heat transfer rates and satisfactory performance.

The test results obtained showed that both the triplet and concentric injectors could meet the performance requirements. However, from a cost and fabrication standpoint, the concentric was considered superior. Therefore, the remaining injector development effort was concentrated on evaluating and optimizing the concentric element injector in the following areas:

1. Number of elements
2. Wall gap (element centerline to wall distance)
3. Oxidizer post recess
4. Fuel injection velocity

The performance characteristics of the various modifications of concentric orifice injectors tested are compared in Fig. . These data, showed that either a 79- or 95-element injector, with an oxidizer post recess of 0.075 to 0.100 inch, would provide the required c* performance. Using these data and the heat transfer data presented in the following section, the final selection of injector configuration was made as discussed below.

Heat Transfer. From examination of Fig. 69 and 70, which present local heat transfer rates, and Fig. 71, which presents the total combustion zone heat rejection rate, the coplanar injector appeared to be an unsatisfactory injector configuration from a heat transfer standpoint. Therefore, this element was dropped from further consideration.

Reviewing the modified concentric and triplet heat transfer characteristics, (Fig. 71), a comparable level of moderate operation was indicated. The concentric element design was, however, considered superior from a fabrication standpoint. Additional effort was expended on the concentric element to evaluate the effect of propellant injection velocity on upper combustion zone local heat transfer rates. From Fig. 73, a significant decrease in local heat transfer rate was commensurate with decreased propellant injection velocities. This effect established the design point of 1250 ft/sec for the single-panel, regeneratively cooled segment concentric injector.

The performance data had indicated that either a 0.075- or 0.100-inch recess oxidizer post would satisfactorily meet the performance requirements. Figure 81 presents a comparison of unit 7A injector heat transfer data for 0.075- and 0.100-inch recess for several fuel injection velocity conditions. Based on these data, and Fig. 81, the 0.075-inch oxidizer post recess was selected for the single-panel, regeneratively cooled segment assembly.

The injector configuration selected for the single-panel, regeneratively cooled segment chamber was similar to the unit 7A configuration but consisted of an 80-element concentric orifice type, with an oxidizer post recess of 0.075 inch and a fuel injection velocity of 1250 ft/sec at the design point.

The predicted performance and heat transfer characteristics of the injector-combustor configuration selected for the single-panel, regeneratively cooled chamber segment are presented in Fig. 82 through 84 .

Predicted Single-Panel Injector Pressure Loss Characteristics

A detailed analysis of the pressure drop data obtained with the concentric orifice injector was conducted to establish an analytical model to predict the pressure drop characteristics of the fuel and oxidizer portions of the selected 80-element single-panel injector.

The oxidizer model included:

1. The entrance loss to the oxidizer post, including cross-flow loss
2. The nonrecovered pressure loss due to the orifice located at the post inlet
3. The friction loss in the oxidizer post
4. Variable oxidizer injection density, as a function of chamber pressure and fuel injection temperature
5. Combustion or noncombustion in the recessed cup
6. Mixing losses in the cup
7. Dynamic pressure loss at oxidizer post exit

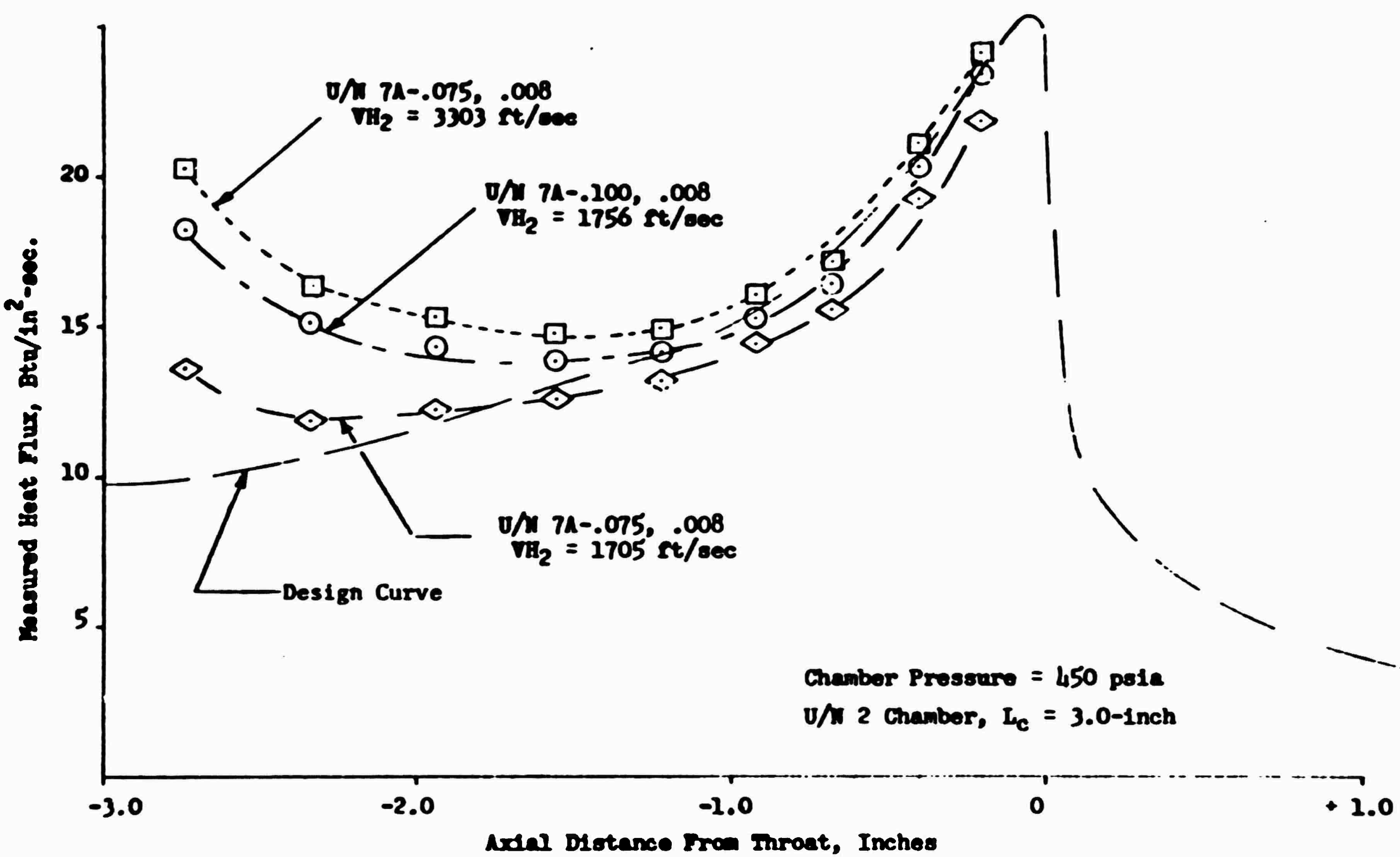

Figure 81. Comparison of Local Heat Transfer Conditions for Concentric Injectors (Single-Panel)

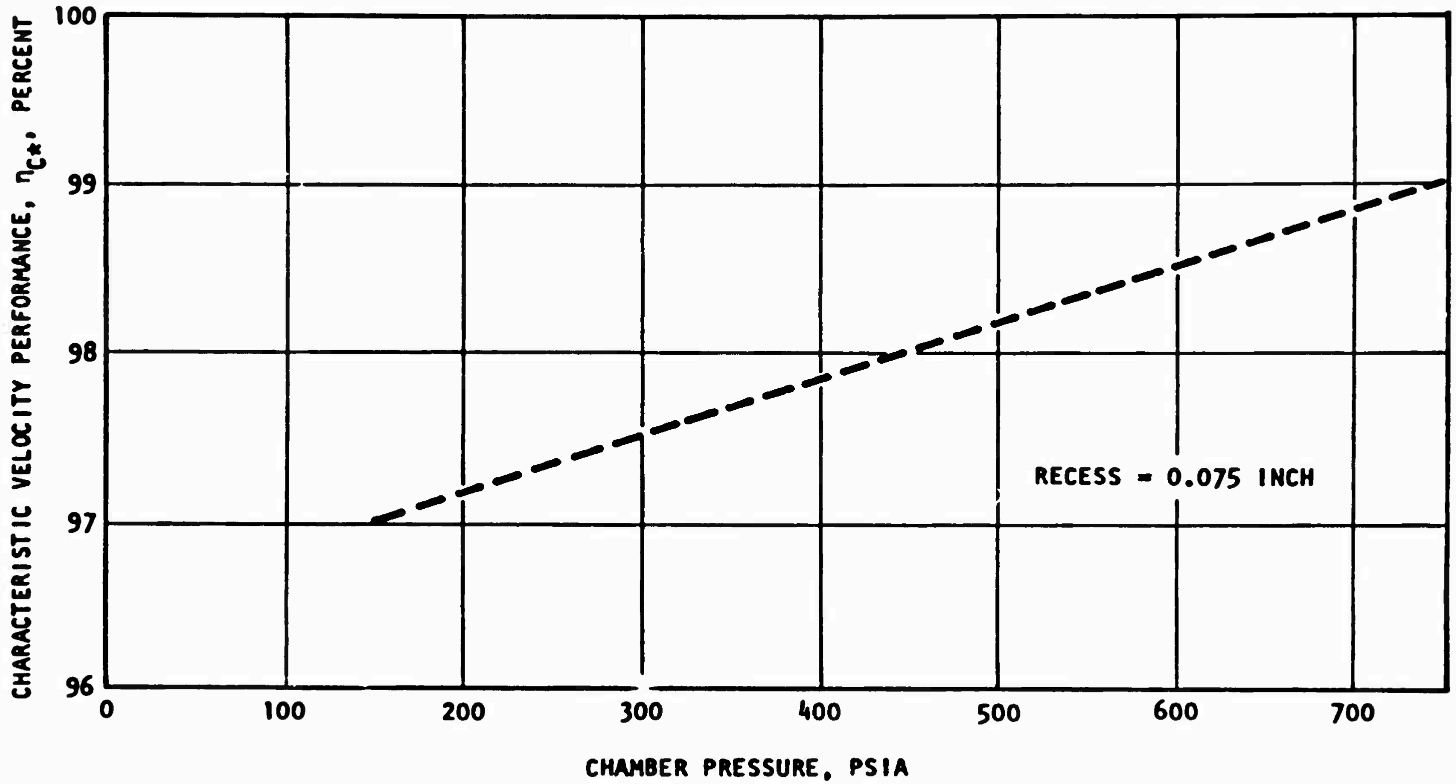

Figure 82. Predicted c* Performance vs Chamber Pressure for the Single-Panel Regeneratively Cooled Segment, 80-Element Concentric Injector

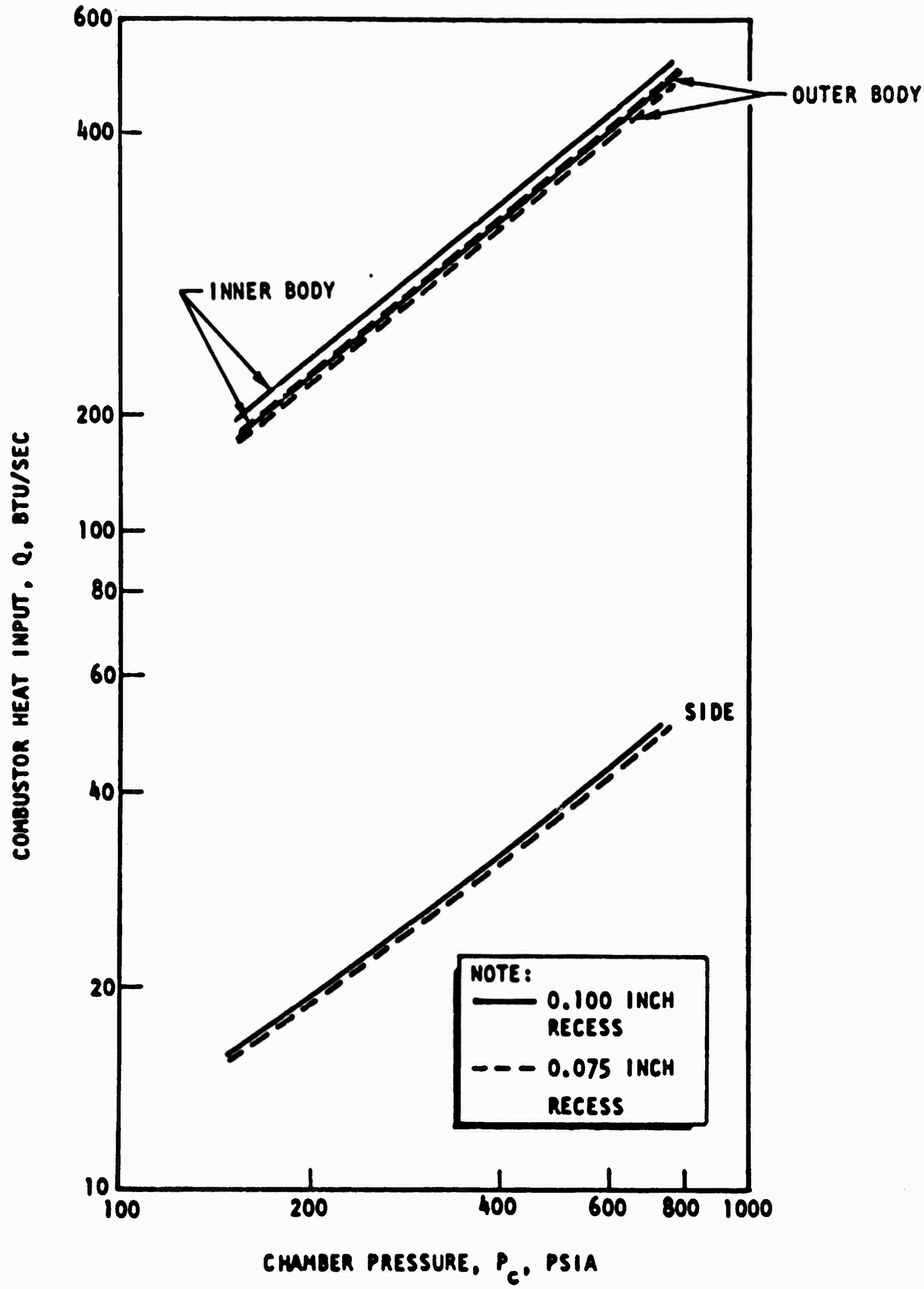

Figure 83. Single-Panel Combustor Heat Input (Q)

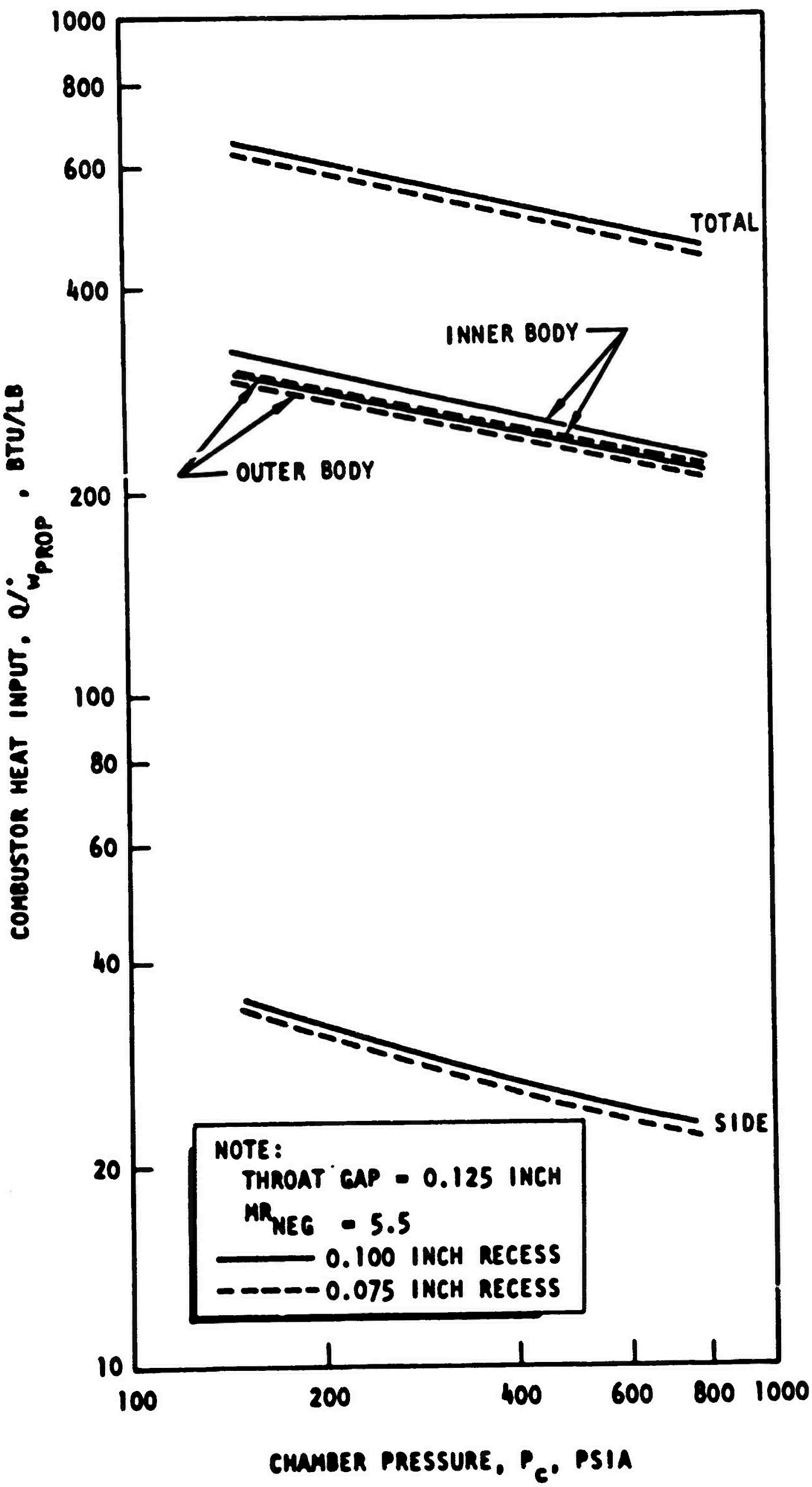

Figure 84. Single-Panel Combustor Heat Input ($Q/\dot{w}_{prop}$)

The unit 7A data were used to establish values for the various parameters that influence the propellant pressure loss in the injector. The parameters which had the largest uncertainty are items 4, 5, and 6 (above).

The oxidizer injection density is a function of the chamber pressure and the fuel injection temperature, with chamber pressure being defined. The fuel injection temperature for the regeneratively cooled chamber at each chamber pressure was predicted by use of heat transfer data obtained during water-cooled segment test. Refined values will not be available until regeneratively cooled chamber heat transfer data are available.

Combustion or noncombustion in the cup region of a recessed oxidizer post concentric orifice injection element was found to be a function of operating chamber pressure, post recess, and fuel injection temperature. The uncertainty associated with fuel injection temperature was evident in this parameter also.

Mixing losses in the cup were a function of several parameters, for which an adequate analytical expression does not exist. The absolute value of these losses were considered to be small (<10 psia) for this particular injector.

The predicted pressure loss characteristics for the single-panel, regeneratively cooled injector are shown in Fig. 85 and 86 .

General Test Program Summary

A total of 117 hot-fire tests was conducted during the single-panel test program. No significant problems were encountered with injector or water-cooled segment chamber durability or structural integrity. When local heat flux conditions in the combustors greatly exceeded the values used for design, local overheating and erosion occurred. This erosion occurred only in unit 1 combustor when used with unit 1 coplanar injector which had abnormally high upper combustion zone heat fluxes. The high heat flux combined with oxidizer-rich fans impinging on the wall resulted in surface melting and erosion.

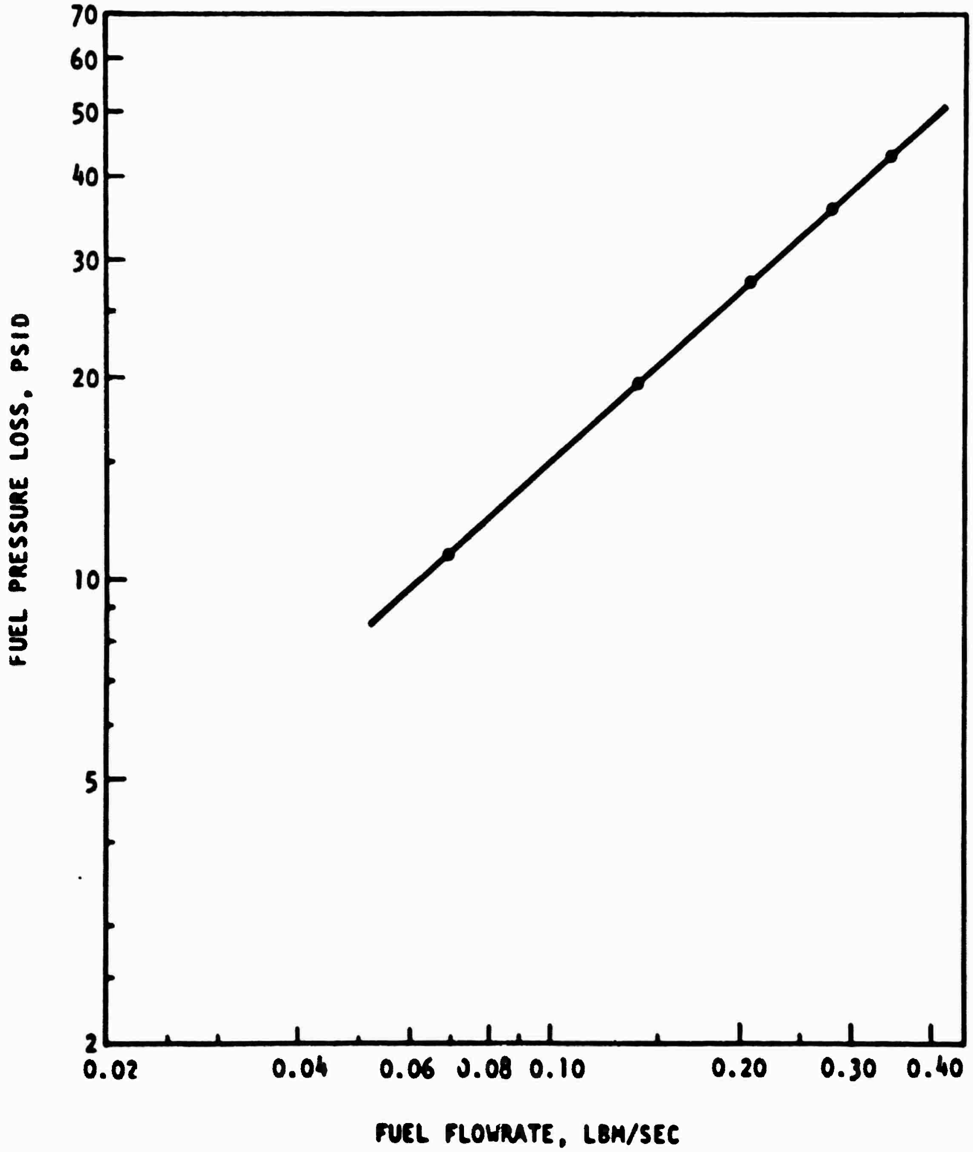

Figure 85. Predicted Fuel Pressure Loss Characteristics for the Single-Panel Regeneratively Cooled Segment Concentric Injector

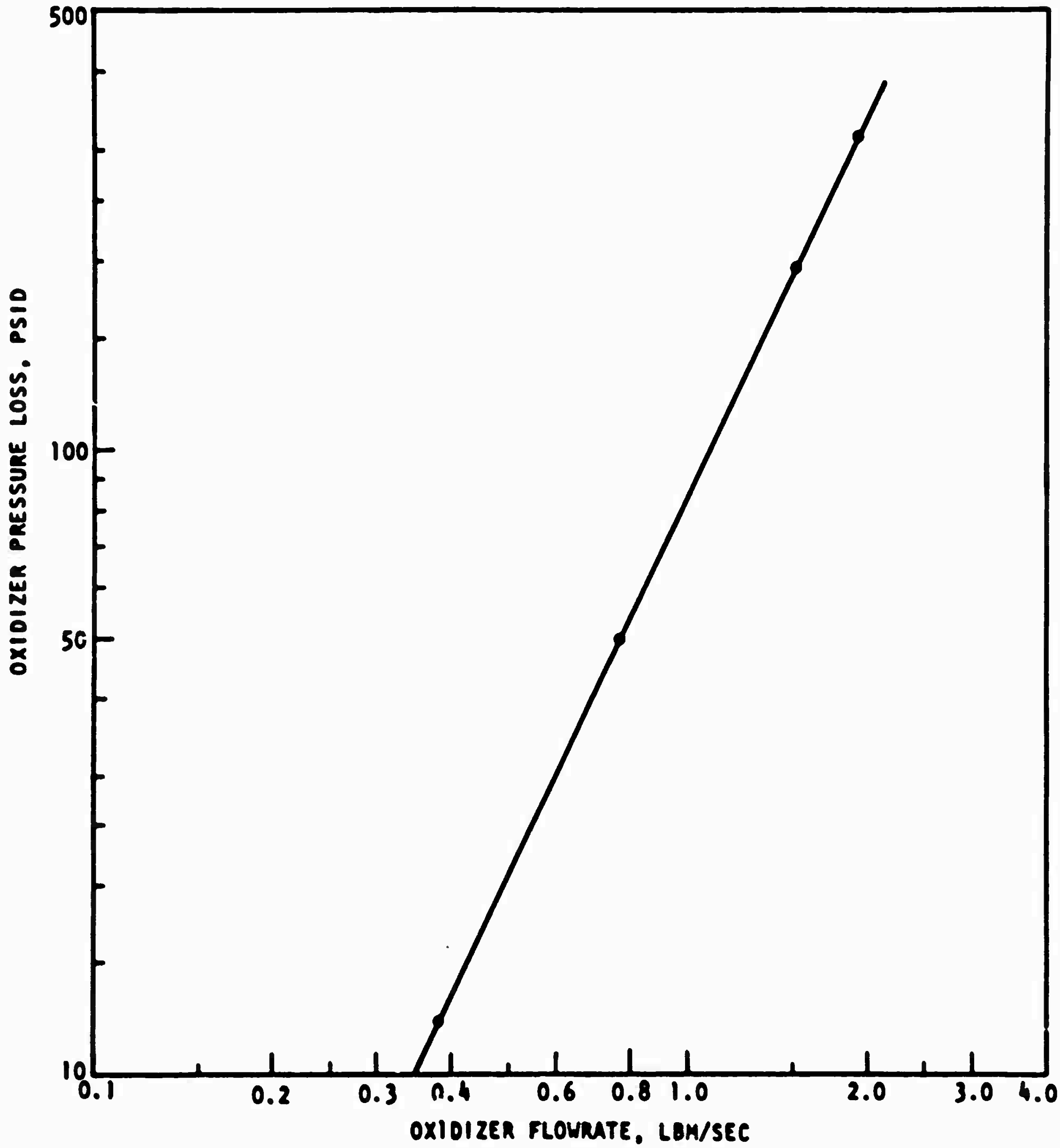

Figure 86. Predicted Oxidizer Pressure Loss Characteristics for the Single-Panel Regeneratively Cooled Segment Concentric Injector

All injectors exhibited excellent durability and structural integrity. No problems were encountered with face overheating, orifice deformation, or orifice plugging. The technical aspects are summarized below.

Combustion Chamber Configuration. Several variations of combustion chamber configuration were evaluated:

1. 0.50- and 0.60-inch width with constant, 6.260-inch injector end length
2. 3.0-, 3.5-, and 4.0-inch combustion zone length (injector face-to-throat plane)

The increase in width from 0.50 to 0.60 inch had a negligible effect on heat transfer and performance, but would result in an increase in weight of the thrust chamber assembly.

The results showed that increased length of 3.0 to 4.0 inches would increase c* performance slightly, but would also result in a significant increase in weight of the thrust chamber assembly. The increased heat rejected to the coolant for the L_c=4.0-inch condition, due to the increase in hot-gas wetted area (not higher local heat fluxes), would result in a large increase in coolant pressure loss and much higher resulting wall temperatures.

A combustor which had a constant convergence combustion zone, an L_c=3.0 inches, a 0.5-inch injector end width, and a 0.0125-inch throat gap was established as the configuration for the single-panel, regeneratively cooled segment chamber.

Injector Configuration. The coplanar injector, although demonstrating excellent performance, had very poor heat transfer characteristics with respect to the combustor.

Both triplet and concentric orifice injectors had satisfactory performance and heat transfer characteristics. An injector similar to the unit 7A concentric orifice injector with 80 elements was selected for the single-panel, regeneratively cooled segment.

Test Facility. Facility operation was satisfactory throughout the test program and no problems were encountered. Slight modifications in operating procedure were made to ensure proper chilldown of the liquid oxygen system.

SECTION V

DOUBLE-PANEL SEGMENT EVALUATION

The double-panel water-cooled segment development program was conducted along the same general lines as the previously described single-panel program. The objective of the program was to develop an injector-chamber configuration that had high c* performance and moderate heat transfer characteristics (both local heat flux and total integrated heat rejection rate). The primary development parameters were injection element configuration and chamber combustion zone length. Two water-cooled, calorimetry-type, segment thrust chambers and three, nonlightweight, bolt-on-type injectors were designed, fabricated, and tested.

The injector-chamber assemblies were designed to operate with gaseous propellants, oxygen and hydrogen. Because vaporization of propellant prior to combustion was not required with the gaseous propellants, as with the liquid-oxygen for the single panel, the thought was that a shorter combustor length could be used for the double-panel segment chamber. The initial basic chamber length, therefore, was 2.5 inches. Injector single-element cold-flow tests were conducted to establish the initial element configuration of the injectors.

The following sections provide a description of the double-panel, water-cooled segment hardware design and fabrication techniques, testing, data analysis, and results.

HARDWARE DESIGN AND FABRICATION

Segment Chambers, Double-Panel

Two new segment chambers, units 5 and 6, were fabricated for this program. The general configuration of the chambers is shown in Fig. 87 .

The double-panel chambers, units 5 and 6, incorporated a 2.5-inch combustion zone length with constant convergence when initially fabricated. As noted previously, the thought was that 2.5-inch L_c would be sufficient to obtain the required c*

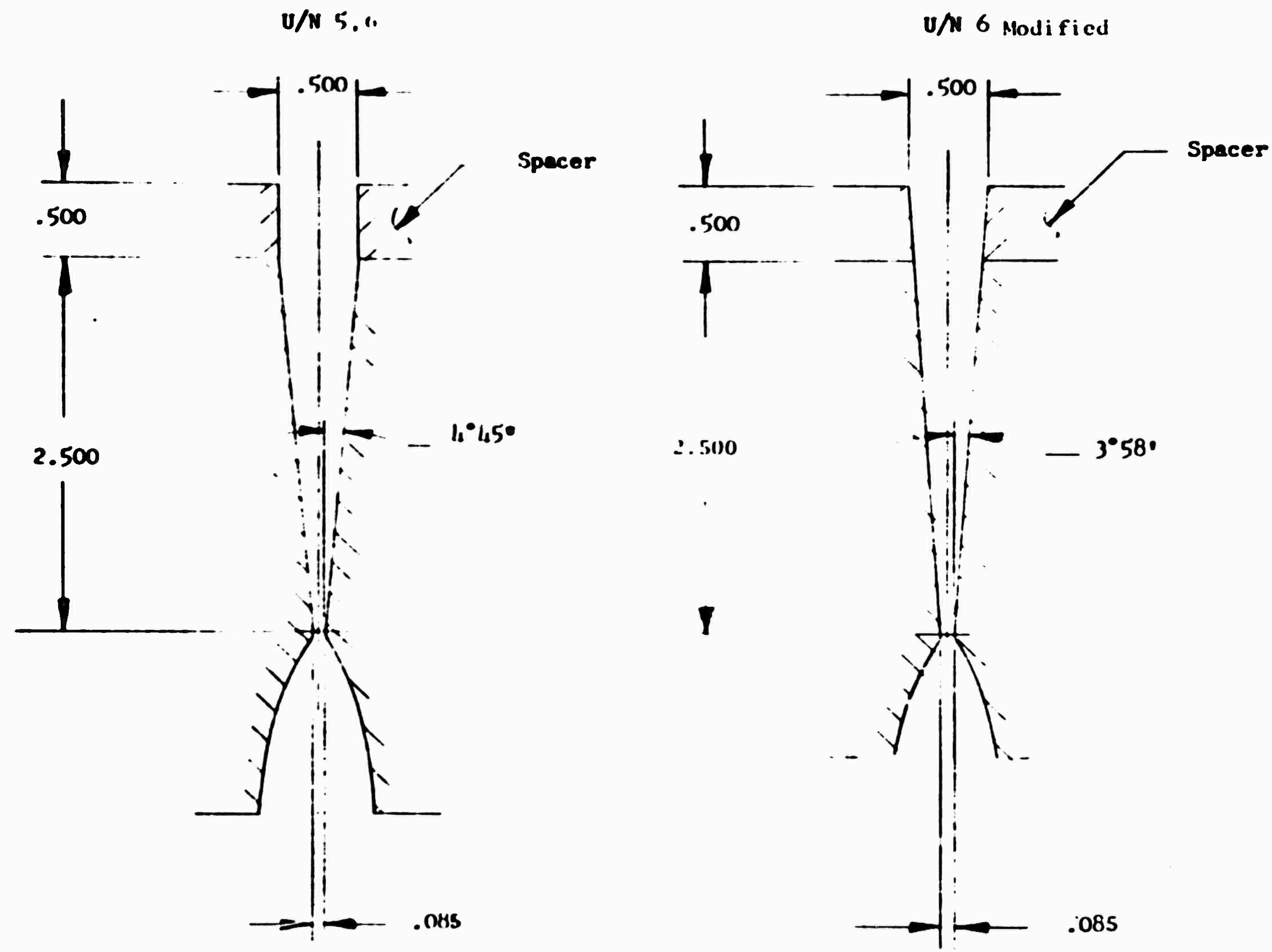

Figure 87. Double-Panel Water-Cooled Segment Chamber Combustor Internal Configurations (units 5, 6, and 6 modified)

performance (>97 percent over the 5:1 throttle range). Initial testing of the triplet injector with unit 5 segment chamber indicated that an L_c of at least 3.0 inches was necessary to obtain the required c* performance. The L_c=3.0 was obtained with the unit 5 chamber by installing a 0.5-inch-length, water-cooled, straight-wall spacer as shown in Fig. 87.

Comparison of the unit 2E triplet injector c* performance obtained in the unit 2 single-panel segment chamber and the unit 5 double-panel segment chamber showed a loss in c* performance due to combustion chamber wall contour for the unit 5 chamber with spacer (Fig. 87). The unit 6 segment chamber was modified prior to use to provide a constant convergence wall combustion zone, L_c = 3.0 inch, when provided with a modified 0.500-inch spacer (convergent type). The detailed design criteria for units 5 and 6 chambers are presented in Table 11, with the same design guidelines as were applicable to the single-panel combustors.

The calorimetry-type segment chambers were fabricated of copper and incorporated coolant passages for water cooling. The chamber design and fabrication techniques were similar to those used for the single-panel except for an additional braze joint on the inner and outer bodies to simplify the coolant passage drilling operation. The inner and outer bodies were machined and drilled separately as 1/2-detail parts and then brazed together (Fig. 88) to form inner and outer body details. The body details were checked for nonplugging of the coolant passages and then brazed together (Fig. 88) to form a complete combustion chamber.

Unit 6 combustor was modified, as mentioned previously, to provide a constant convergence (L_c=3.0 inch) combustor when used with a modified 0.500-inch spacer. The modification, detailed in Fig. 89, consisted of removing structure in the sideplate region and mechanically deforming the chamber to the desired contour. Additional structural support consisting of a CRES plate, pinned in each side plate end, was installed in the unit 6 segment chamber (Fig. 90).

An additional modification, consisting of decreasing the length of the expansion nozzle (decreased expansion ratio) was made to avoid nozzle flow separation at lower chamber pressures and to make the c*, by thrust calculation, accurate over a

TABLE 11. DESIGN CRITERIA FOR DOUBLE-PANEL WATER-COOLED SEGMENT CHAMBER

Design Parameters	Units 5 and 6		Unit 6 (Modified)	
Chamber length (side plate-to-side plate at injector end), inch	6.684		6.684	
Chamber length (side plate-to-side plate at throat), inch	6.684		6.684	
Width at injector end, inch	0.500		0.430	
Throat gap, inch	0.086		0.086	
Throat radius	0.158		0.158	
Contraction ratio, A_{inj}/A_t	5.81		5.0	
Expansion ratio, Ae/A_t	7.8		4.6	
Divergence nozzle shape	Curved to match regenerative-cooled segment		Curved to match regenerative-cooled segment	
Combustion zone wall configuration				
Side plates	straight, convergent		straight, convergent	
Chamber walls	straight, convergent		straight, convergent	
Combustion zone wall Convergence Half angle, degrees	4 Deg 45 min		3 Deg 56 min	
Combustion zone length, L_c, Injector face-to-throat, inch	2.5	3.0	2.5	3.0
Characteristic chamber length, L*, inch	8.5	11.5	7.5	10.2
Chamber Pressure, psia	950	950	950	950

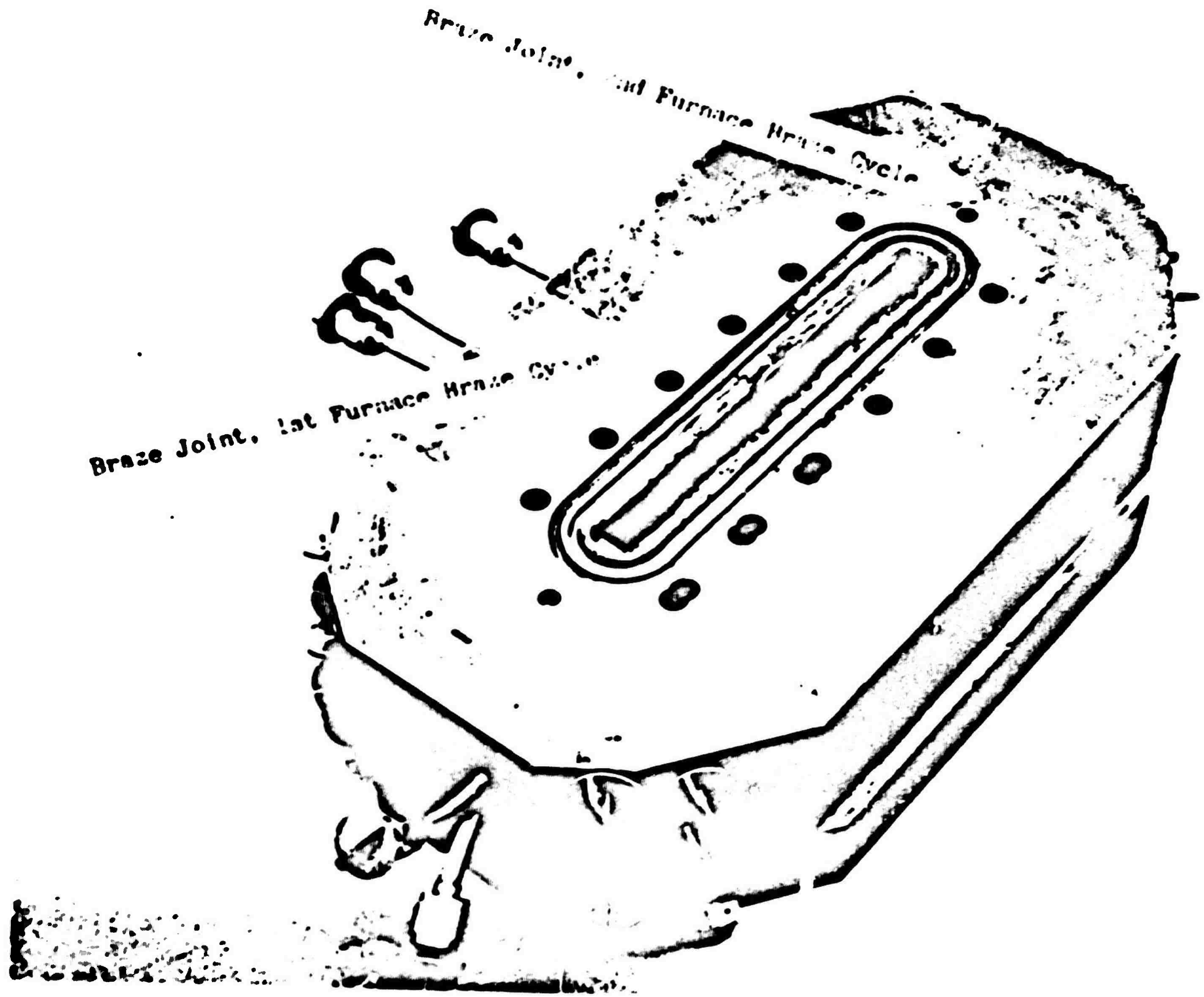

1EH25-12/9/71-1-C2B

Figure 88. Unit 5 Double-Panel Water-Cooled Segment Chamber, Braze Joint Locations

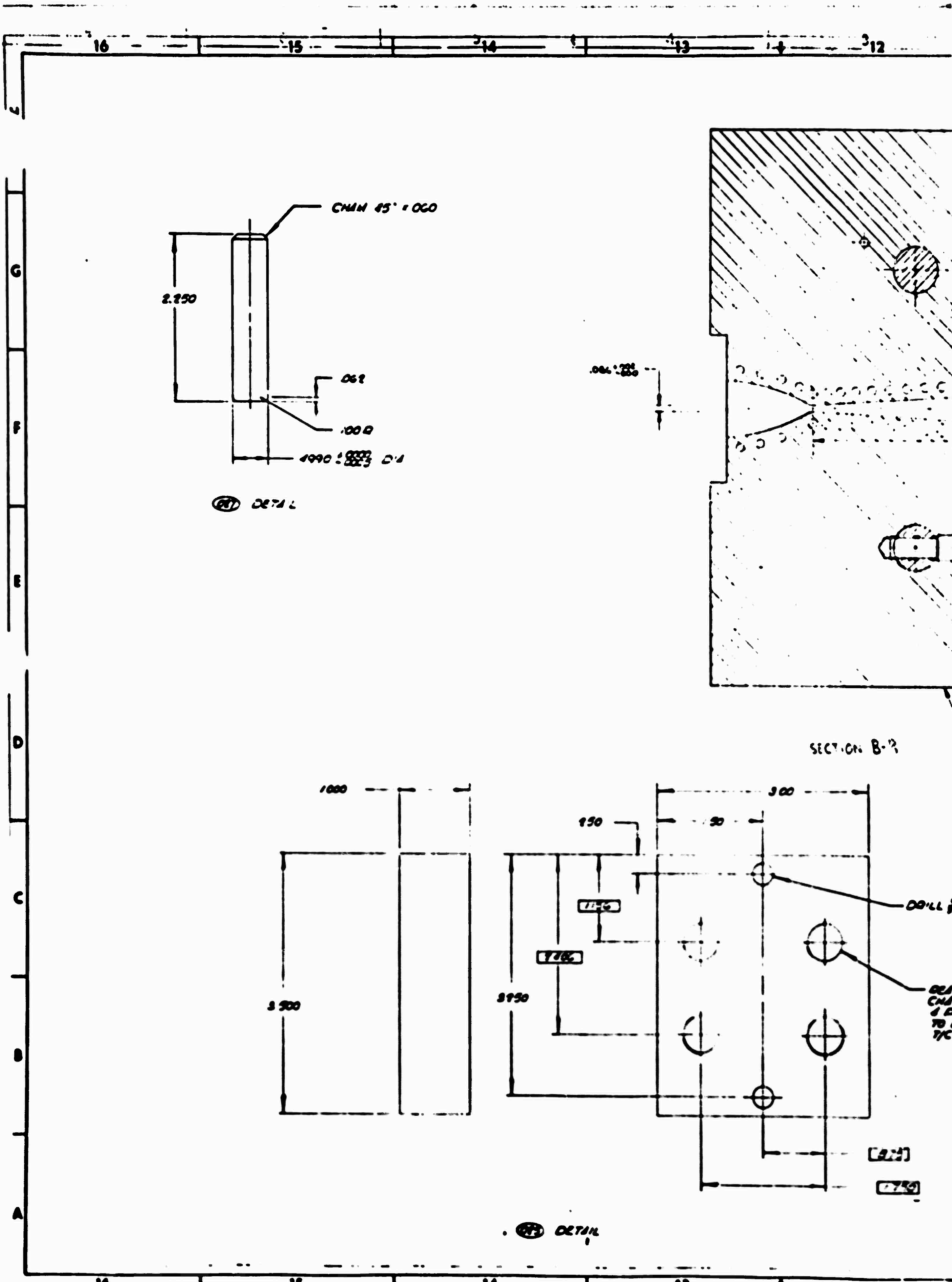

CHAM 45° x .060
2.250
.062
.100 R
DETAIL
SECTION B-B
1.000
3.00
.250
.50
3.500
3.950
DRILL
DETAIL

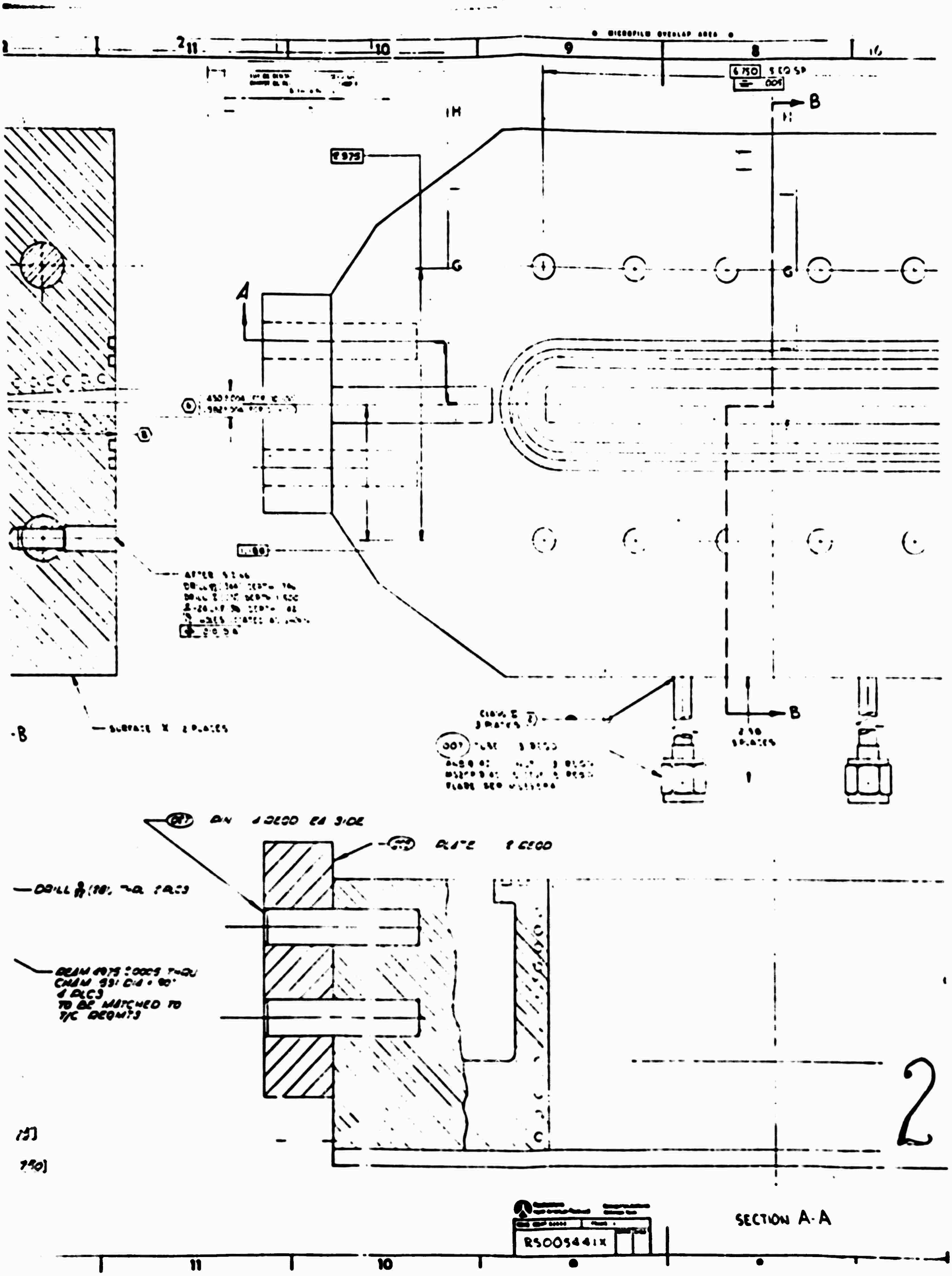
9
8
10
11
B
A
G
SECTION A-A
RS005441X
2

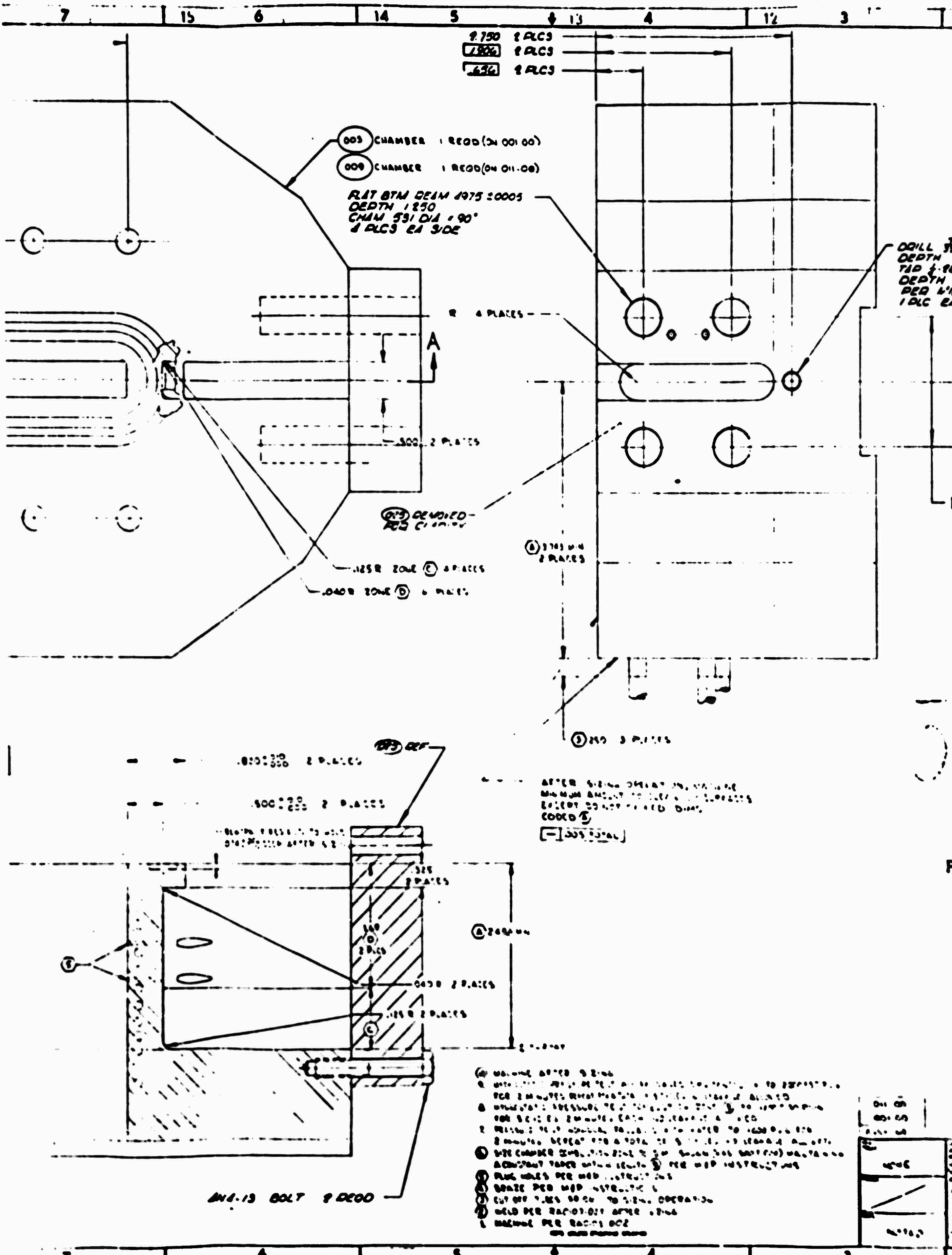
2.750 2 PLCS
1.906 2 PLCS
.656 2 PLCS
003 CHAMBER 1 REQD (24 001 00)
009 CHAMBER 1 REQD (24 011-00)
FLAT BTM DEAM .4975 ±.0005
DEPTH 1.250
CHAM .531 DIA × 90°
4 PLCS EA SIDE
DRILL
DEPTH
TAP
DEPTH
PER
1 PLC EA
R 4 PLACES
A
.500 2 PLACES
.125 R ZONE C 4 PLACES
.040 R ZONE D 4 PLACES
003 DEVOID PER CLARITY
2 PLACES
.250 3 PLACES
003 REF
2 PLACES
2 PLACES
AFTER SIZING OPERATION, MACHINE MINIMUM AMOUNT TO CLEAN UP SURFACES
CODED
.325 2 PLACES
2 PLCS
.040 R 2 PLACES
.125 R 2 PLACES
AN4-13 BOLT 2 REQD
MACHINE PER RACING DC2
001 00
001 00
011 00

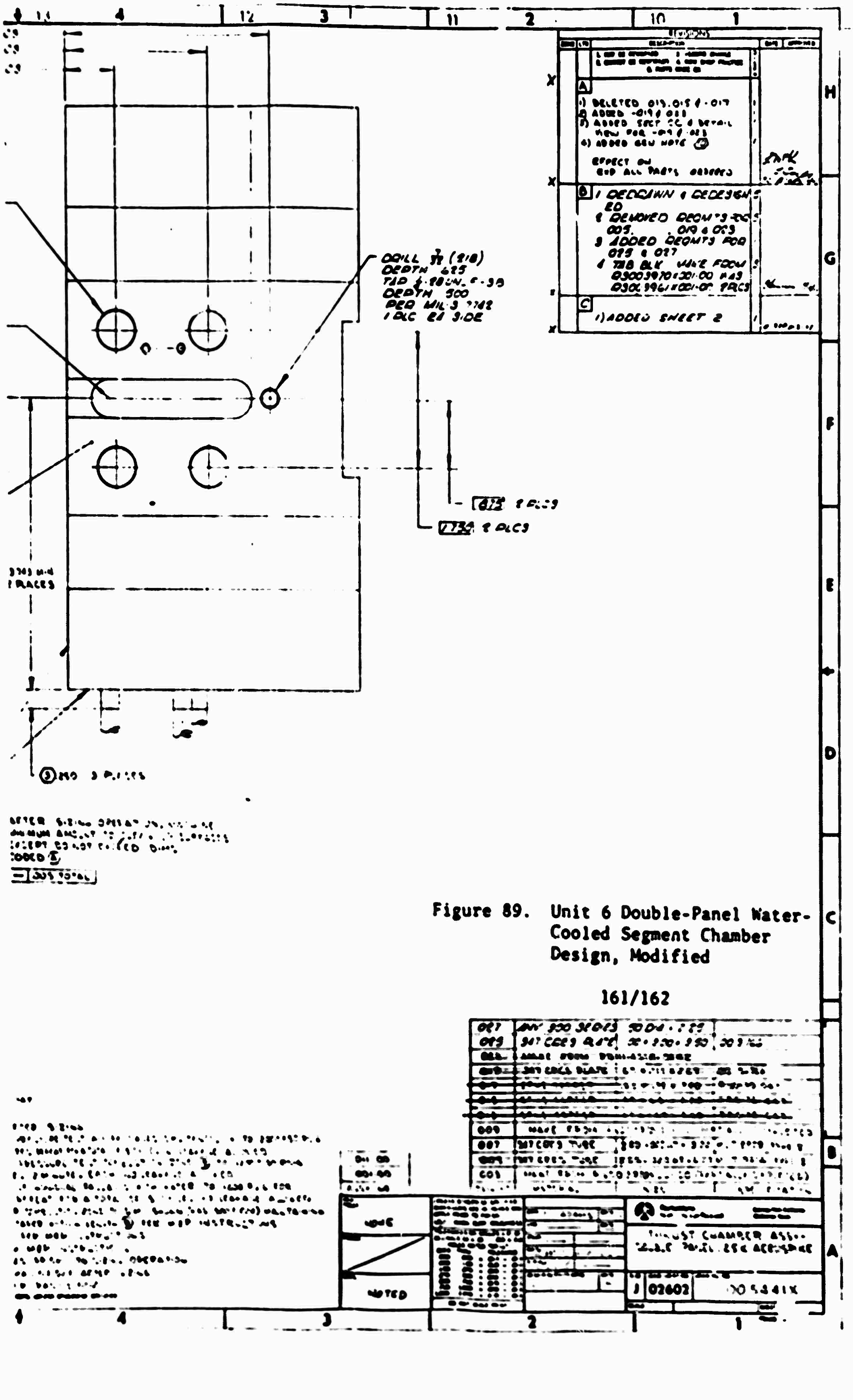

Figure 89. Unit 6 Double-Panel Water-Cooled Segment Chamber Design, Modified

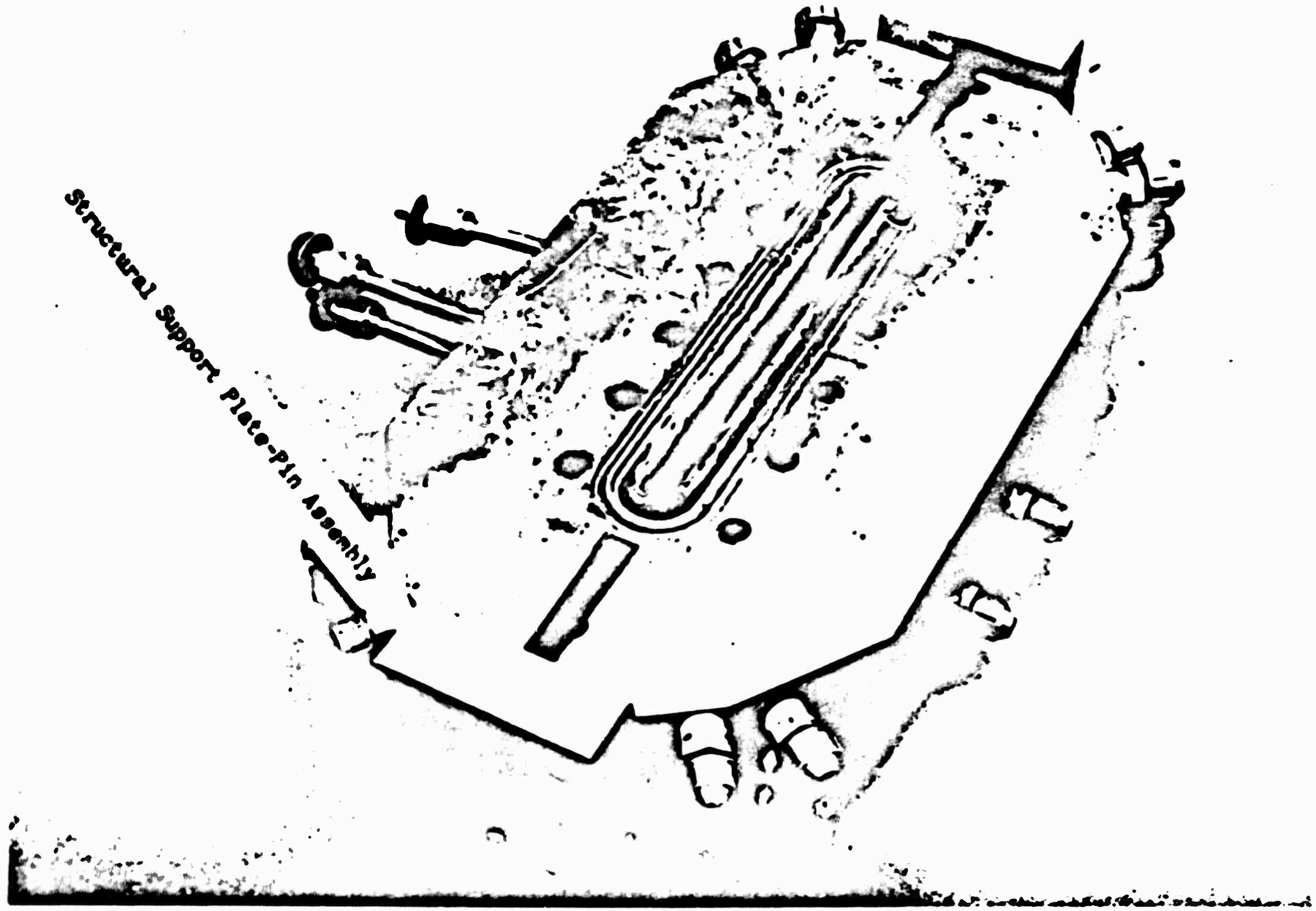

Figure 90. Unit 6 Double-Panel Water-Cooled Segment Chamber, Modified

wider range of chamber pressures. The expansion area ratio was reduced from 7.8 (unit 5) to 4.6 for unit 6 (modified).

The double-panel segment chambers were designed for a maximum chamber pressure of 950 psia, as compared to 750 psia for the single-panel chambers. The chambers incorporated a 0.085-inch throat gap.

Fifteen coolant passages were used which were 0.125 inch in diameter. The design was to provide the capability for 53 Btu/in.^{2}-sec local heat flux at the throat. A two-dimensional heat transfer analysis was conducted for unit 5 chamber with a wall thickness of 0.095-inch and hot-gas-side wall temperatures of approximately 1560 F predicted for the throat region. Figure 91 presents the predicted isothermal temperature distribution in the throat region of the segment chamber.

Additional analyses were conducted to evaluate the effect of wall thickness on the hot-gas wall temperature in the throat region. The results of the analyses are shown in Fig. 92 and resulted in the decision to design the unit 6, water-cooled, double-panel segment chamber with a hot-gas wall thickness of 0.075 inch at the peak heat flux point (0.200 inch upstream of throat).

A structural analysis was made and confirmed that rippling of the chamber hot-gas-side wall surface, in the throat, would not occur. This mode of failure had been noted in calorimetry-type chambers used for other injector development programs, and the cause was due to local yielding of the copper wall due to coolant pressure and heat during a test. The problem was attributed to a very thin wall caused by improper location of the drilled water coolant passage.

All water coolant passages for the single-panel and double-panel calorimetry chambers were gun-drilled with excellent results. The coolant passage positions are established on a jig bore prior to gun-drilling. The chamber half details (for the double-panel segments), corresponding to inner and outer walls, also were separated at the transverse midpoint to reduce the gun-drill length by one-half and maintain better dimensional control of the wall thickness. This design required one additional furnace braze cycle as described earlier.

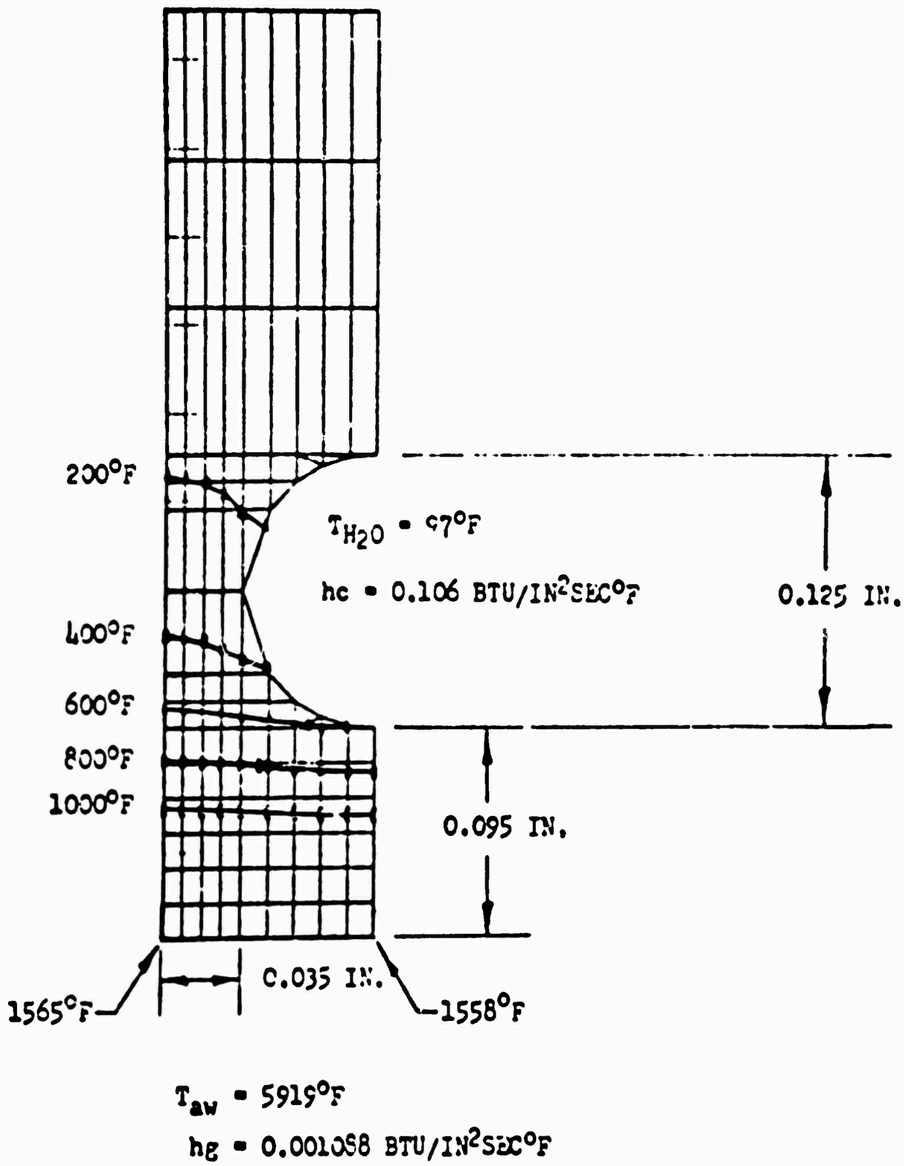

Figure 91. Unit 5 Double-Panel Water-Cooled Chamber Wall Temperature Distribution at X = -0.2 Inch (P_c = 950 psia, MR_{eng} = 5.5

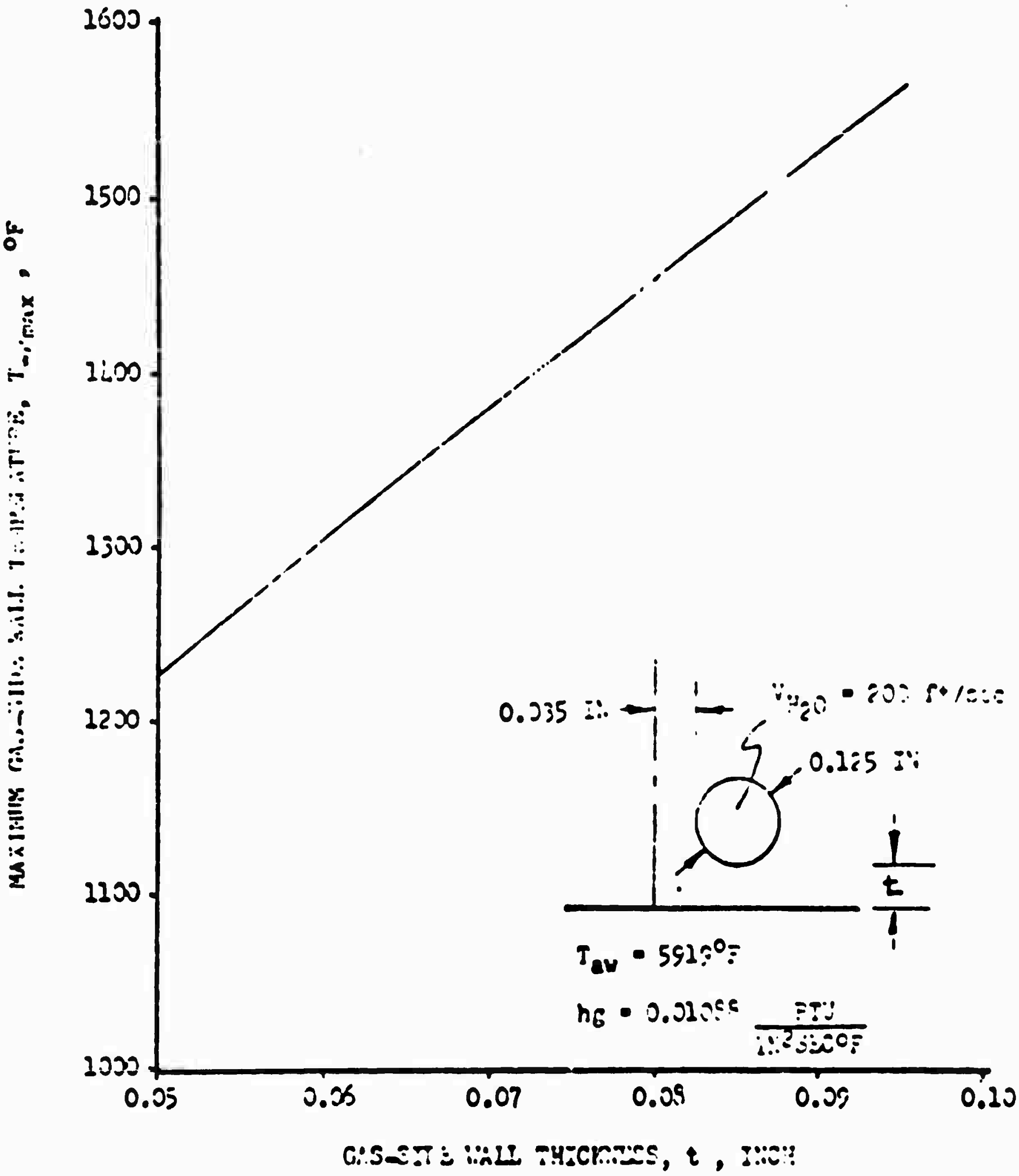

Figure 92. Wall Temperature Variation With Wall Thickness (P_c = 950 psia, MR_{eng} = 5.5) in Double-Panel, Water-Cooled Segment

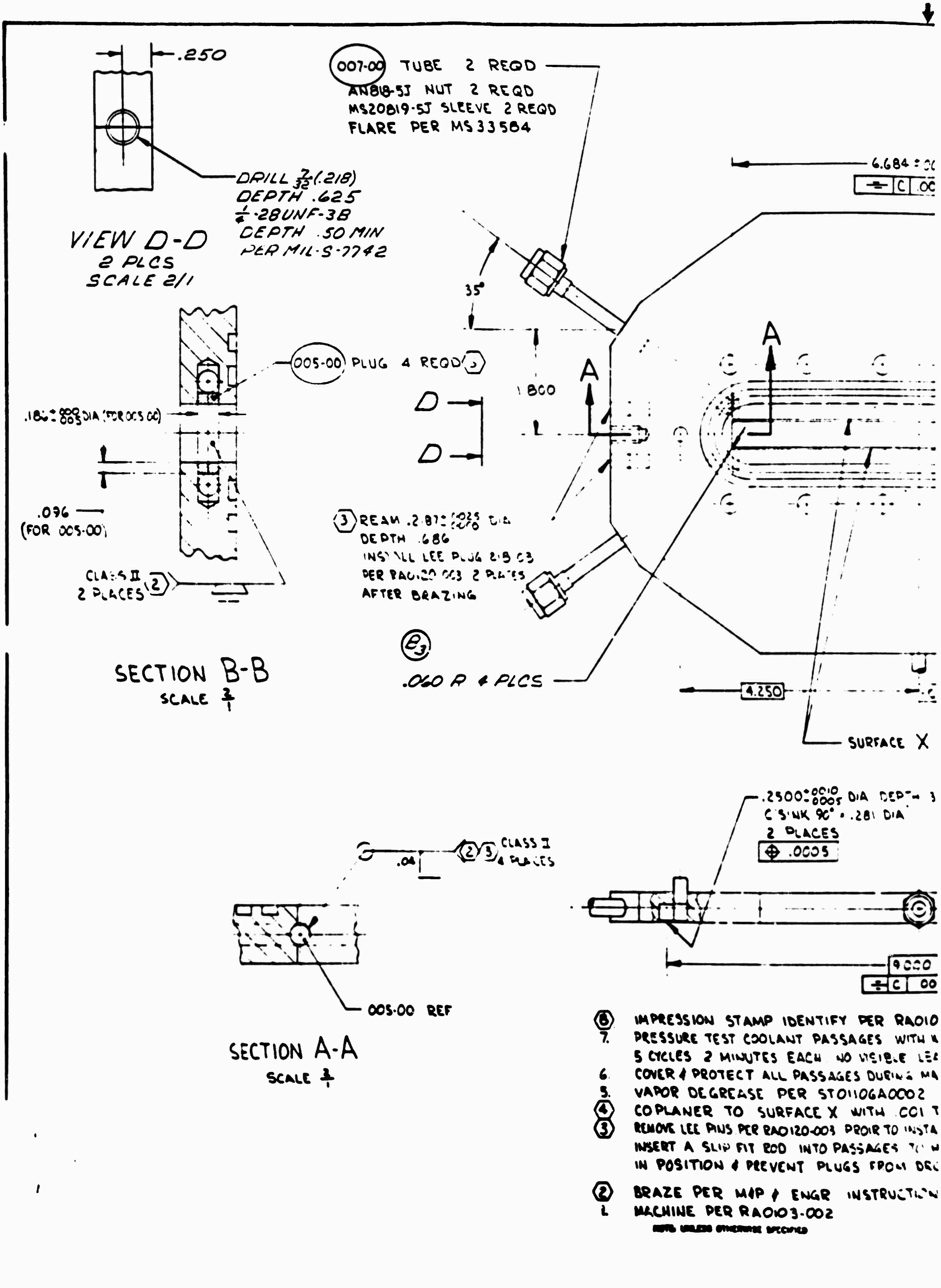

.250
VIEW D-D
2 PLCS
SCALE 2/1
007-00 TUBE 2 REQD
AN818-5J NUT 2 REQD
MS20819-5J SLEEVE 2 REQD
FLARE PER MS33584
DRILL 7/32 (.218)
DEPTH .625
1/4-28UNF-3B
DEPTH .50 MIN
PER MIL-S-7742
35°
005-00 PLUG 4 REQD
.800
A
A
D
D
.096
(FOR 005-00)
CLASS II
2 PLACES
3 REAM .2 87
DEPTH .686
AFTER BRAZING
SECTION B-B
SCALE 2/1
.060 R 4 PLCS
4.250
SURFACE X
CLASS I
4 PLACES
.04
005-00 REF
SECTION A-A
SCALE 2/1
2 PLACES
.0005
8 IMPRESSION STAMP IDENTIFY PER RA010
7. PRESSURE TEST COOLANT PASSAGES WITH
5 CYCLES 2 MINUTES EACH NO VISIBLE LEA
6. COVER & PROTECT ALL PASSAGES DURING MA
5. VAPOR DEGREASE PER ST0110GA0002
4 COPLANER TO SURFACE X WITH .001 T
3 REMOVE LEE PINS PER RA0120-003 PROIR TO INSTA
INSERT A SLIP FIT ROD INTO PASSAGES TO H
IN POSITION & PREVENT PLUGS FROM DRO
2 BRAZE PER M&P & ENGR INSTRUCTION
1 MACHINE PER RA0103-002
NOTE: UNLESS OTHERWISE SPECIFIED

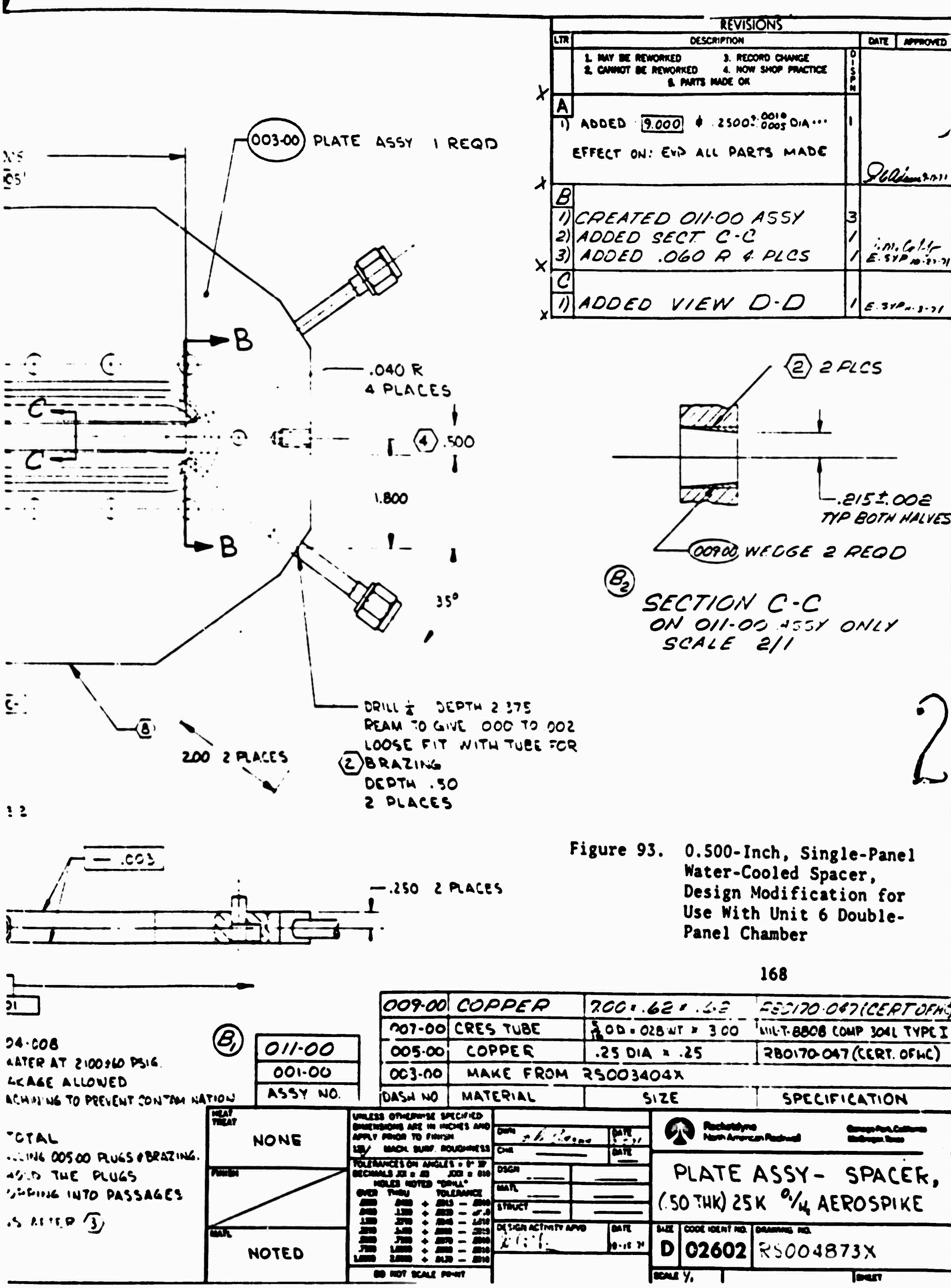

Figure 93. 0.500-Inch, Single-Panel Water-Cooled Spacer, Design Modification for Use With Unit 6 Double-Panel Chamber

The chamber spacers used for the double-panel evaluation were the same hardware items as used for the previous single-panel effort. The 0.500-inch-thick spacer was modified, during the testing as shown in Fig. 93 , to provide a spacer with convergent walls to match the modified unit No. 6, double-panel, water-cooled chamber. The spacer modification consisted of furnace-braze attaching a filler block of OFHC copper that was then machined to match the chamber contour. The modified spacer is shown in Fig. 94.

Double-Panel Segment Injectors

The double-panel injector design is required to operate with gaseous propellants, oxygen and hydrogen, as compared to the single-panel injector which operates with liquid oxygen and gaseous hydrogen. The selection of the propellant configuration to use for the gas-gas injector required considerably more cold-flow evaluation testing because of a general lack of definitive criteria available for design. The state of the art with respect to gas-gas injection elements was not as advanced as for gas-liquid elements.

Two element configurations, triplet and concentric, were initially selected for evaluation based on limited experience with these element configurations on another program (Ref. 5). Initially, the gas-liquid triplet injector (unit 2C) was modified to a gas-gas configuration, unit 2D and subsequently unit 2E, for a rapid preliminary evaluation of gas-gas injector characteristics in low-volume combustors.

The initial gas-gas injector testing with units 2D and 2E injectors was conducted with the unit 2 single-panel water-cooled segment chamber and indicated satisfactory performance and heat transfer characteristics in low-volume combustors. Additional development work was necessary, however, particularly for the reduction of the heat transfer rates to the combustor walls.

A triplet injector, unit 8, was designed, fabricated, and tested in unit 5 double-panel water-cooled segment chamber with a combustion chamber length of 2.5 inches. An improvement in heat transfer was noted, but satisfactory c* performance was not

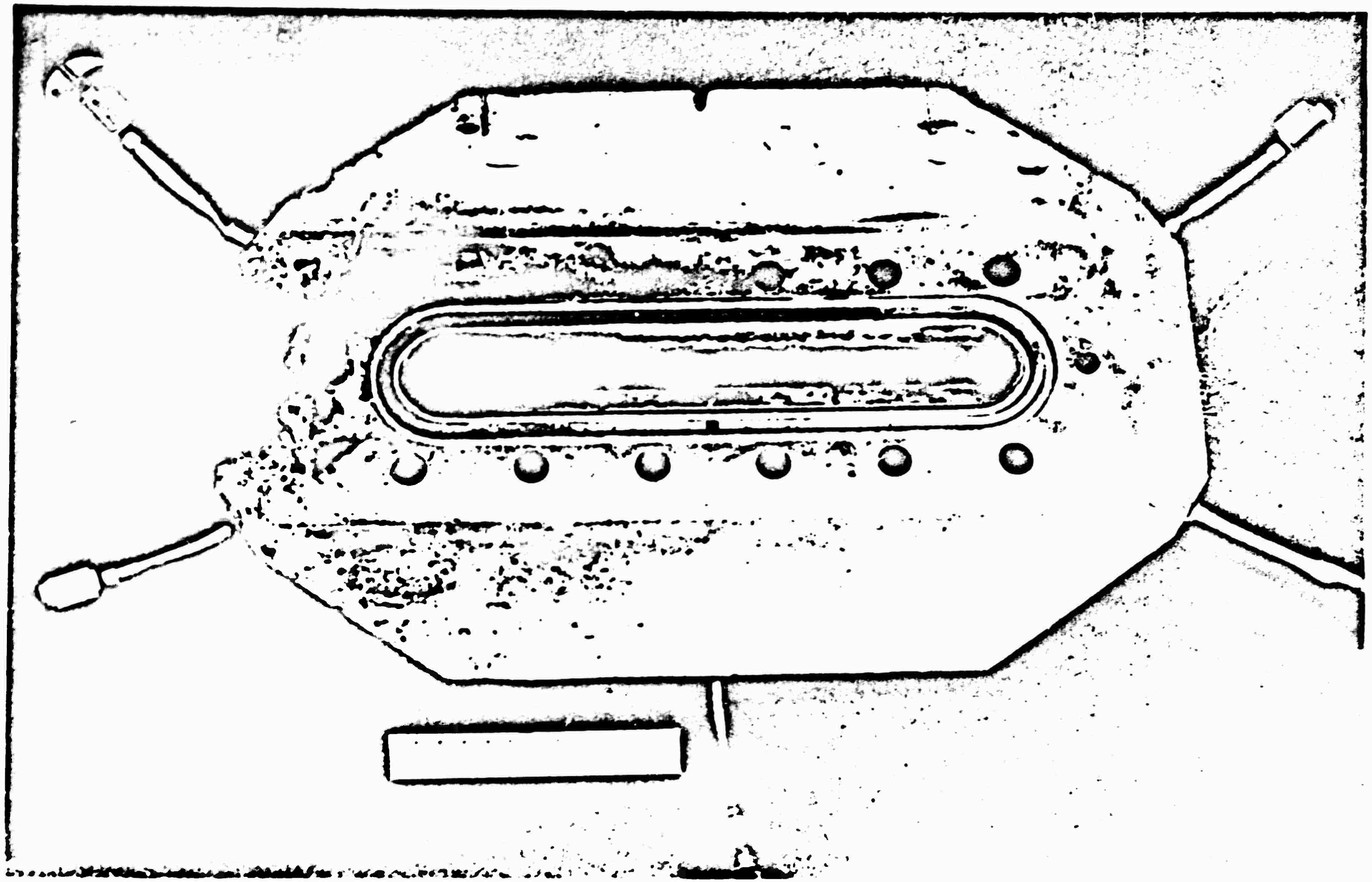

1EH25-12/9/71-1-C3K

Figure 94. 0.500-Inch Water-Cooled Spacer, Modified for Use With Unit 6 Chamber

obtained. The injector was modified to the unit 8A configuration and tested in L_c=3.0- and 3.5-inch chambers. Tests with the L_c=3.0-inch chamber indicated satisfactory performance.

A trislot element injector was the third injector type considered for the double-panel segment. The injector, unit 9, was designed, fabricated, and tested with good results.

Several modifications were made to each injector during the development program. These modifications and the baseline mechanical design parameters are noted in Table 12 and discussed in the following paragraphs.

Cold-flow testing of triplet, concentric, and trislot single elements was conducted and is discussed in a separate, subsequent section (pages 205 to 232).

Triplet Injectors. Three triplet-type injectors were evaluated. Injector units 2D and 2E were modifications of the single-panel gas-liquid triplet unit 2C. The units 8, 8A, and 8B injectors were specifically fabricated and modified for the double-panel program. The unit 7G was a modification of the unit 7F concentric injector used for the double-panel program.

Unit 2D Injector. The injector was fabricated during the single-panel program. The design, fabrication, etc., is discussed in Section IV. The injector was modified to a gas-gas configuration, unit 2D, for the initial gas-gas injector evaluation. The modification, shown in Table 12 and Fig. 95, consisted of increasing all oxidizer (showerhead) orifice diameters from 0.019 to 0.028 inch. Examination of data obtained during another program (Ref. 5) indicated that an oxidizer injection velocity of 850 to 950 ft/sec with a fuel injection velocity of 3000 to 4000 ft/sec would provide satisfactory performance. Ambient temperature, 530 R, gaseous oxygen was used for all double-panel segment tests because of availability and a reasonable simulation of regeneratively cooled chamber conditions was obtained. The predicted range of oxidizer injection temperatures is 392 to 352 R in the regeneratively cooled segment.

The orifice area increase was made to provide the desired oxidizer injection velocity, when using ambient gaseous oxygen. Control of fuel injection velocity was

TABLE 12. MECHANICAL DESIGN CHARACTERISTICS OF DOUBLE-PANEL INJECTORS

PARAMETER	U/N 2-D TRIPLET	U/N 2-E TRIPLET	U/N 7-E CONCENTRIC	U/N 7-F CONCENTRIC	U/N 7-G TRIPLET	U/N 8 TRIPLET	U/N 8-A TRIPLET	U/N 6-B TRIPLET	U/N 9 TRISLOT
Total Orifice Area (Square Inch)									
Fuel	.07897	.07897	.1045	.1114	.0603	.15115	.15115	.14522	.1656
Oxidizer	.04771	.04847	.04438	.04438	.04438	.1042	.1324	.1272	.0973
Number of Rows	5	5	1	1	1	2	2	2	2
Number of Elements	110	110	101	101	101	51	51	49	30
Injection Density (Lb/Sec-In^2)	.776/.155	.776/.155	.776/.155	.776/.155	.776/.155	.776/.155	.776/.155	.776/.155	.776/.155
Orifice Diameter (Inch)									Rectangular
Fuel	.021	.021	.029 Annulus	.029 Annulus	.0225	.044	.044	.044	.017 x .157
Oxidizer	.028	.032	.033	.033	.033	.051	.0575	.0575	.020 x .157
Diameter Ratio, D_o/D_f	1.33	1.52	—	—	1.47	1.16	1.31	1.31	-
Number of Orifices									
Fuel	220	220	101	101	202	102	102	98	60
Oxidizer	110	110	101	101	101	51	51	49	30
Impingement Length-Diameter Ratio									
Fuel	6.59	6.59	0	0	4.66	2.62	2.62	2.62	-
Oxidizer	4.46	3.91	0	0	2.72	1.76	1.56	1.56	-
Included Impingement Angle (Degrees)									
Fuel	45	45	0	0	75	75	75	75	75
Oxidizer	0	0	0	0	0	0	0	0	-
Impingement Distance (Inch)									
Fuel	.125	.125	0	0	.090	.090	.090	.090	.090
Oxidizer	.125	.125	0	0	.090	.090	.093	.090	.090
Fan-To-Wall Angle (Degrees)	30	30	0	0	0	0	0	0	0
Element Density (Elements/Square In.)	35.1	35.1	30.4	30.4	30.4	15.3	15.3	14.7	9.0
Injection Density (Lb/Sec Per Element)	.0207/.0041	.0207/.0041	.0226/.0045	.0226/.0045	.0226/.0045	.0488/.0097	.0488/.0097	.0508/.0101	.762/.0152
Element-to-Wall Spacing (Inch)	.120	.120	.090	.090	.090	.165	.165	.165	.190
Thrust Per Element	9.09/1.82	9.09/1.82	9.9/1.98	9.9/1.98	9.9/1.98	19.6/3.92	19.6/3.92	21/4.08	36.6/7.33
Combustion Chamber Volume, 3-Inch Length (Inch^3)	4.898	4.898	4.898	4.898	4.898	4.898	4.898	4.898	4.898

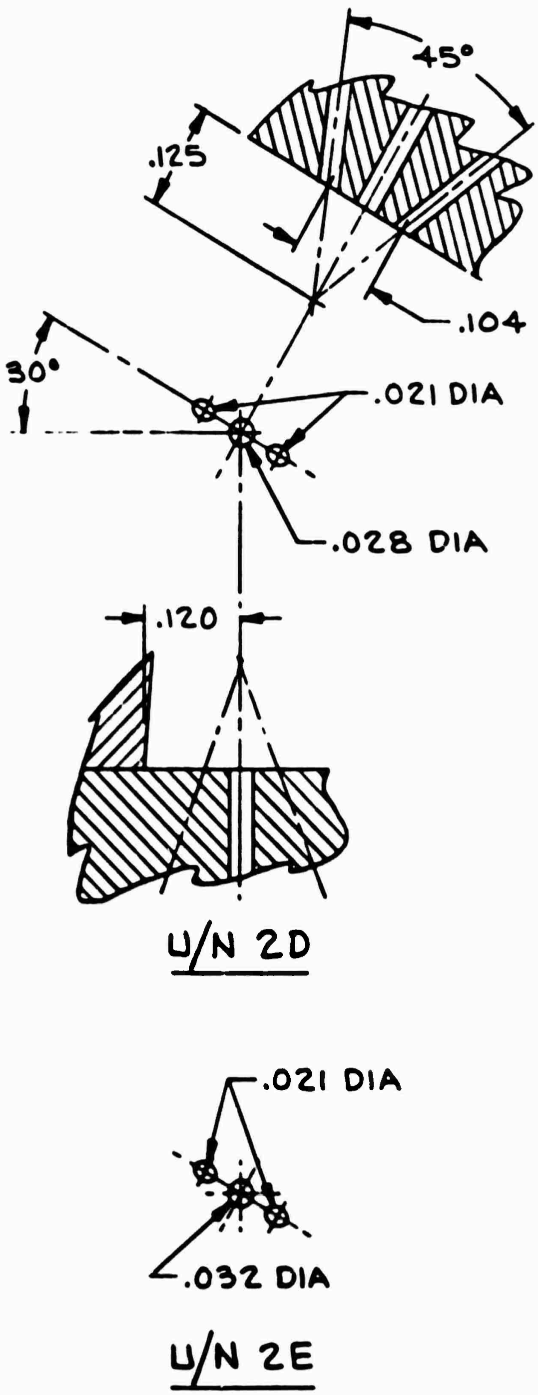

Figure 95. Unit 2D and 2E Triplet, Double-Panel Injector, Injection Element Configurations

accomplished by control of the fuel injection temperature in the same manner as used for the single-panel water-cooled segment testing. Therefore, an increase or change in fuel orifice size was not necessary.

Unit 2E Injector. This modification consisted of an additional increase, to 0.032 from 0.028 inch, for all oxidizer orifice diameters. The modification was made to evaluate the effect of a further decrease in oxidizer injection velocity, ~ 700 ft/sec, on heat transfer and c* performance. There was no change in fuel orifice size.

The final configuration of the unit 2E injector, after completion of testing, is shown in Fig. 96, and the injector flow calibration data are as shown in Fig. 97.

Unit 8 Injector. Triplet injector unit 8 was specifically designed and fabricated for the double-panel program. The injection element configuration is shown in Fig. 98, with mechanical design characteristics presented in Table 12 and in Fig. 99 and 100.

The following design criteria were incorporated:

1. The fuel injection and oxidizer injection velocities were minimized to prevent high upper combustion zone heat transfer rates; $V_{f_{axial}} = 1700$ ft/sec, $V_{o_{axial}} = 700$ ft/sec.
2. The element was F-O-F consistent with previously successful gaseous propellant triplets (Ref. 6).
3. The resultant fans, after primary impingement, were aligned parallel to the hot wall to prevent direct impingement of oxidizer on the wall.
4. The primary impingement angle was 75 degrees for maximum mixing efficiency.
5. Cold-flow testing of impinging triplet elements for other programs (Ref. 6) had indicated a dependence of η_{c^*} performance on "Mr_t" which is defined

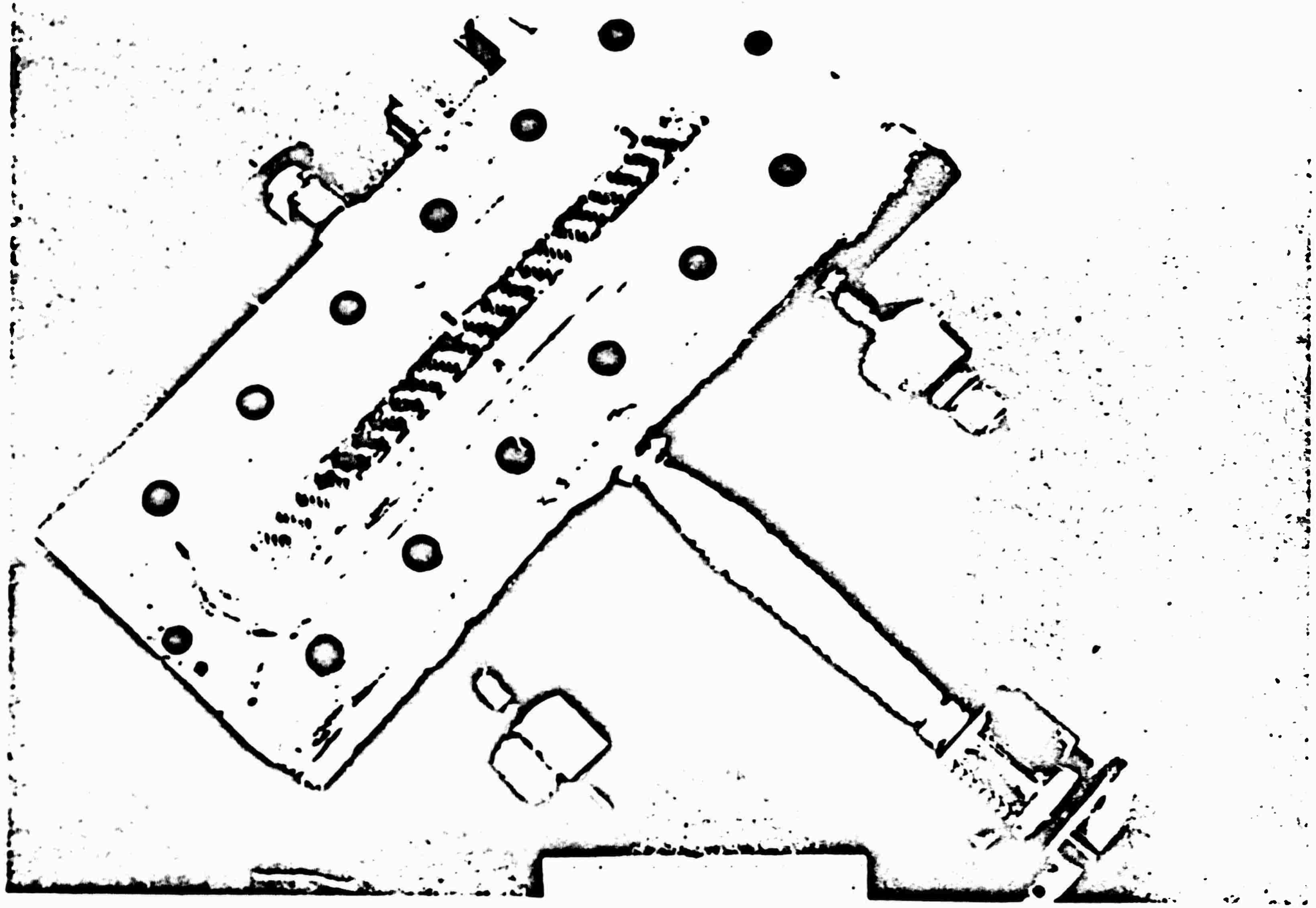

1EH25-12/9/71-C10

Figure 96. Unit 2E Triplet, Double-Panel Injector, Posttest

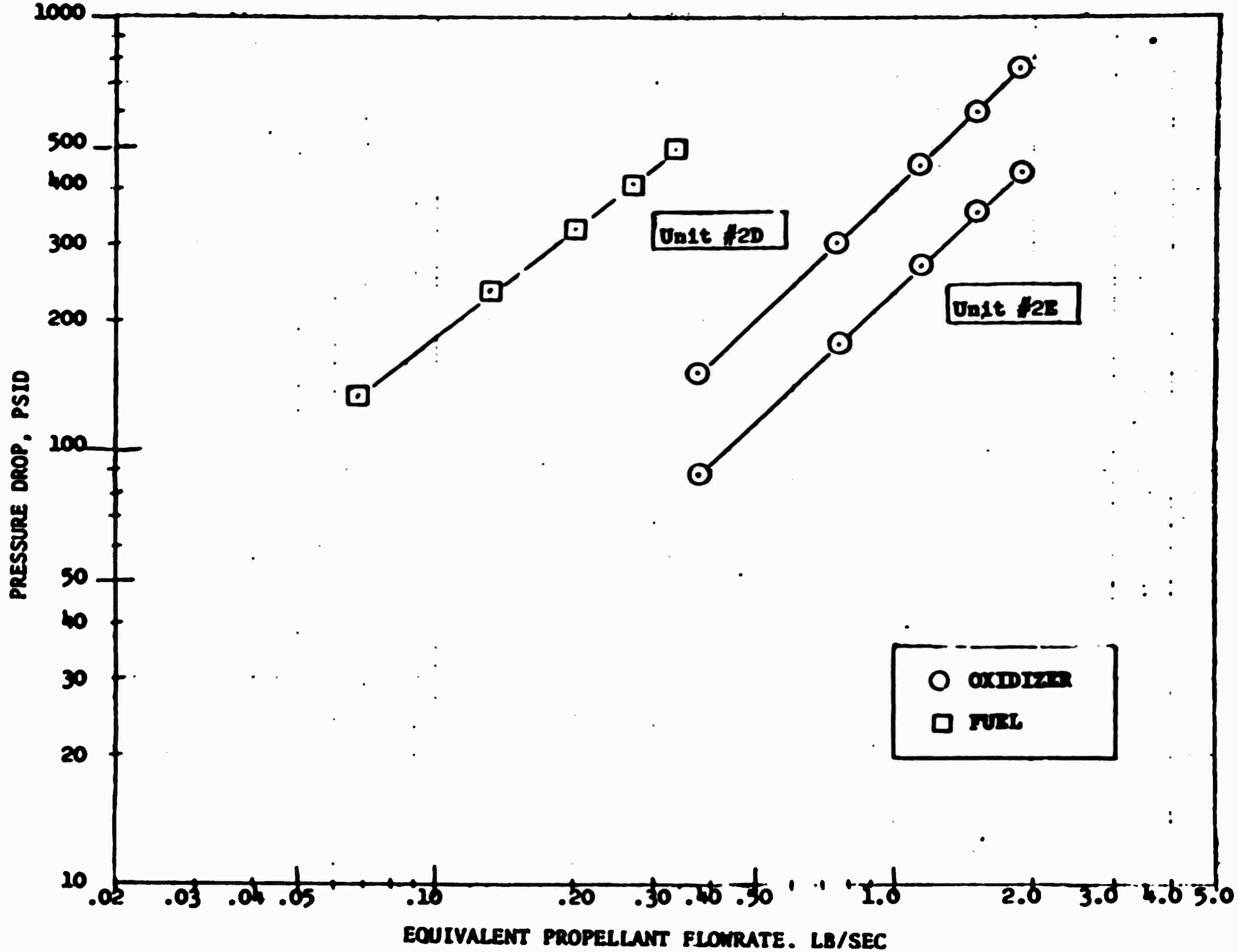

Figure 97. Unit 2D and 2E Triplet Injector Predicted Flow Characteristics (Double-Panel Gas-Gas)

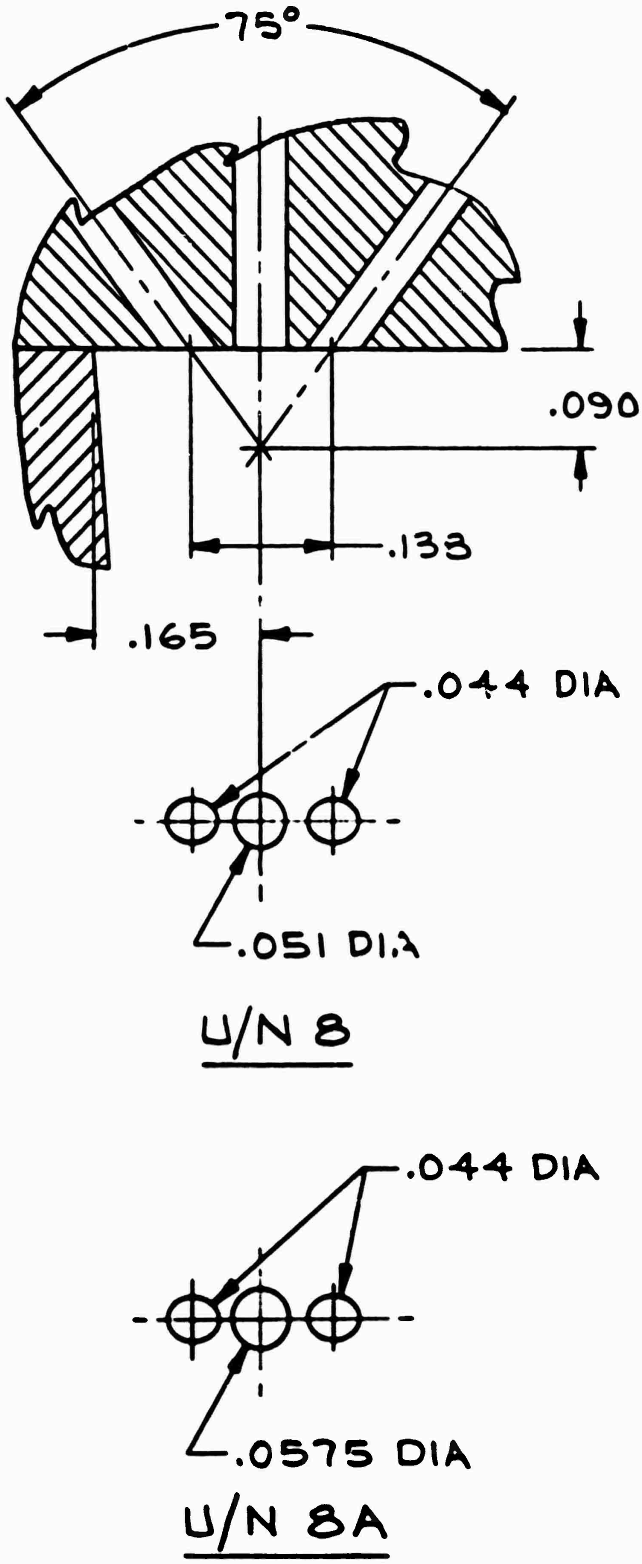

Figure 98. Unit 8 Triplet, Double-Panel Injector, Injection Element Configuration

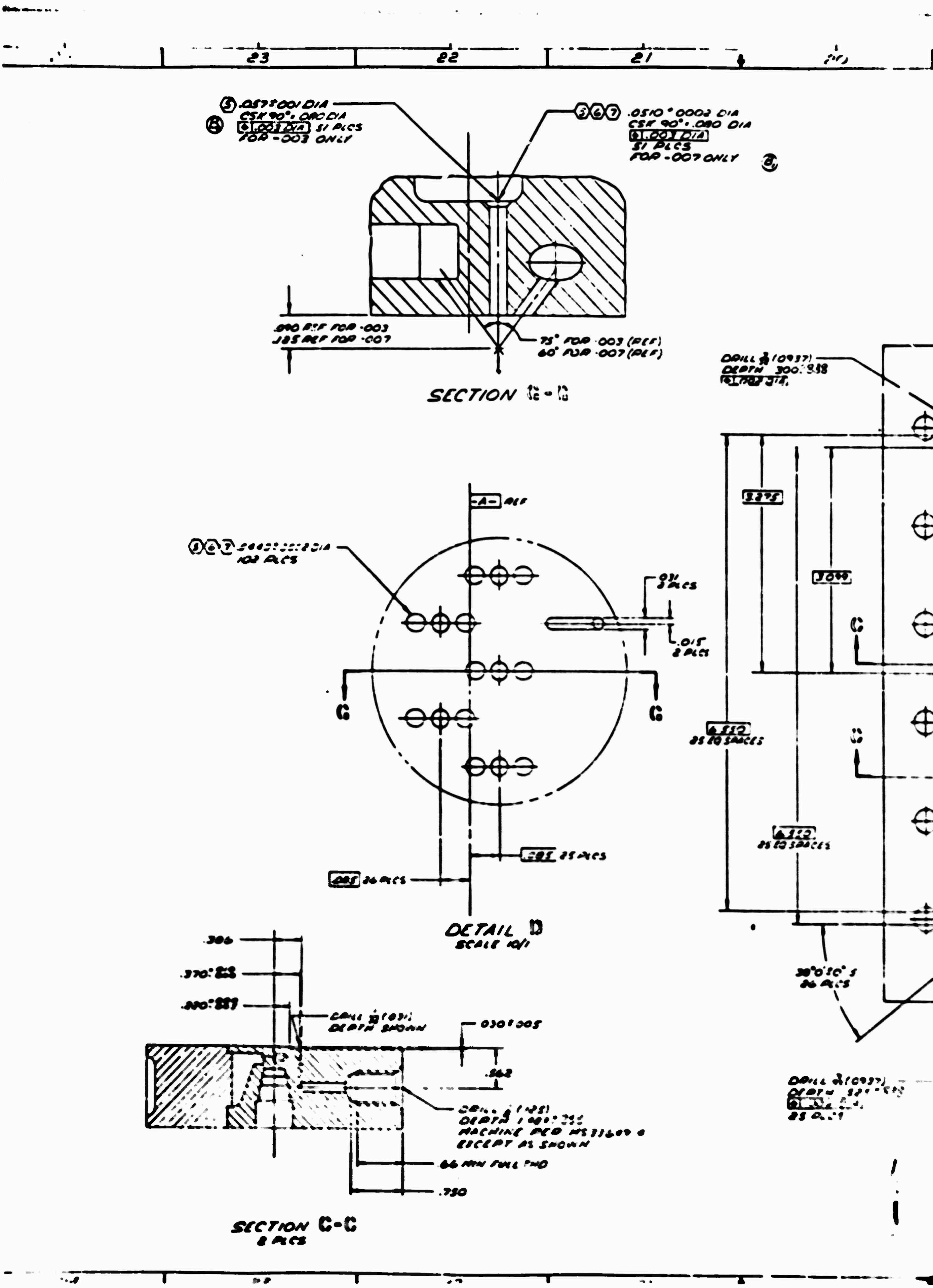

23
22
21
SECTION
60° FOR -007 (REF)
DETAIL
SCALE 10/1
SECTION C-C
8 PLCS

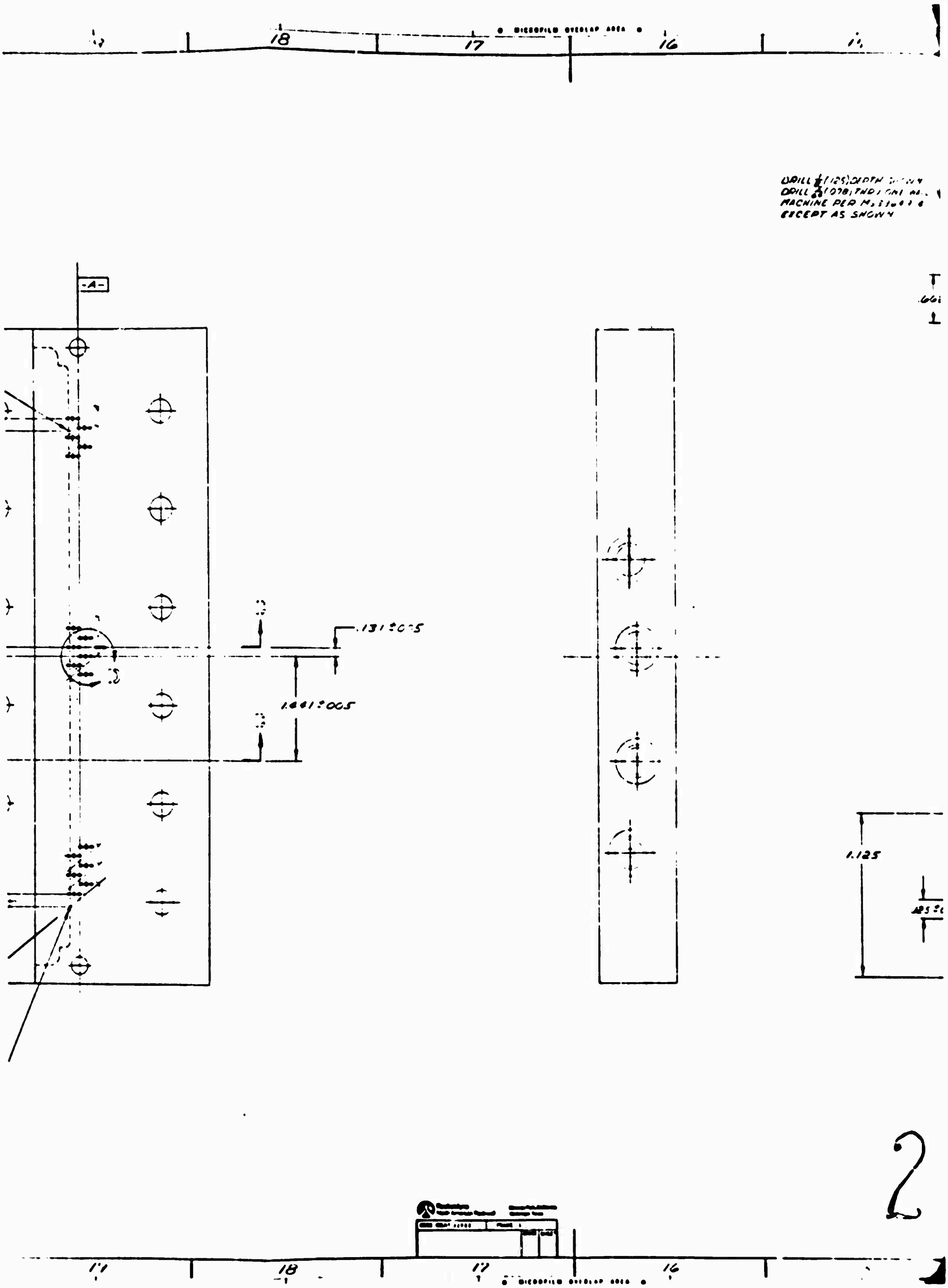

2

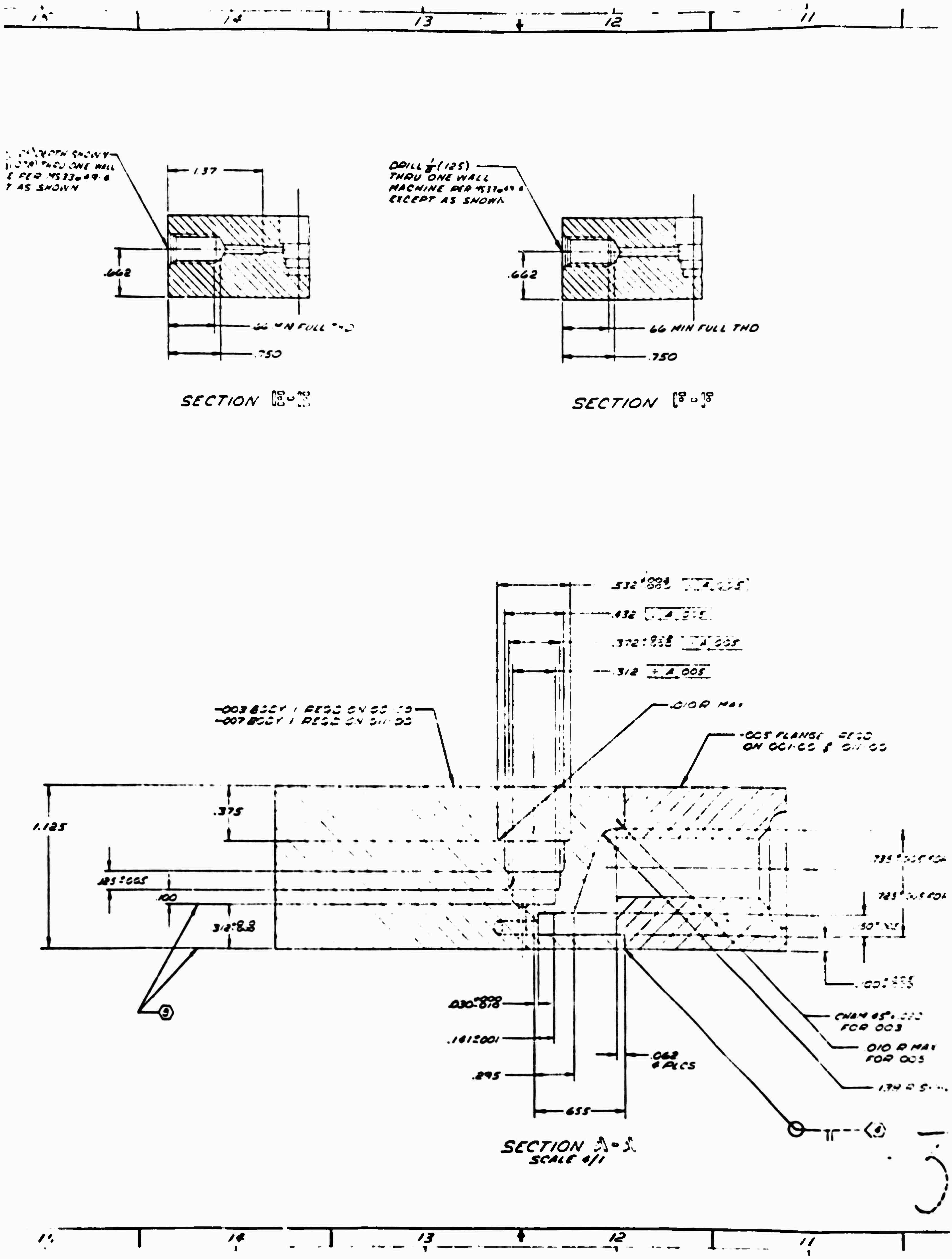

DRILL 1/8 (125)
THRU ONE WALL
MACHINE PER MS33649-6
EXCEPT AS SHOWN
1.37
.662
66 MIN FULL THD
.750
SECTION
SECTION
.432
.312
.010 R MAX
.375
1.125
.100
.655
.295
.062
4 PLCS
CHAM 45°
FOR 003
010 R MAX
FOR 005
SECTION A-A
SCALE 4/1

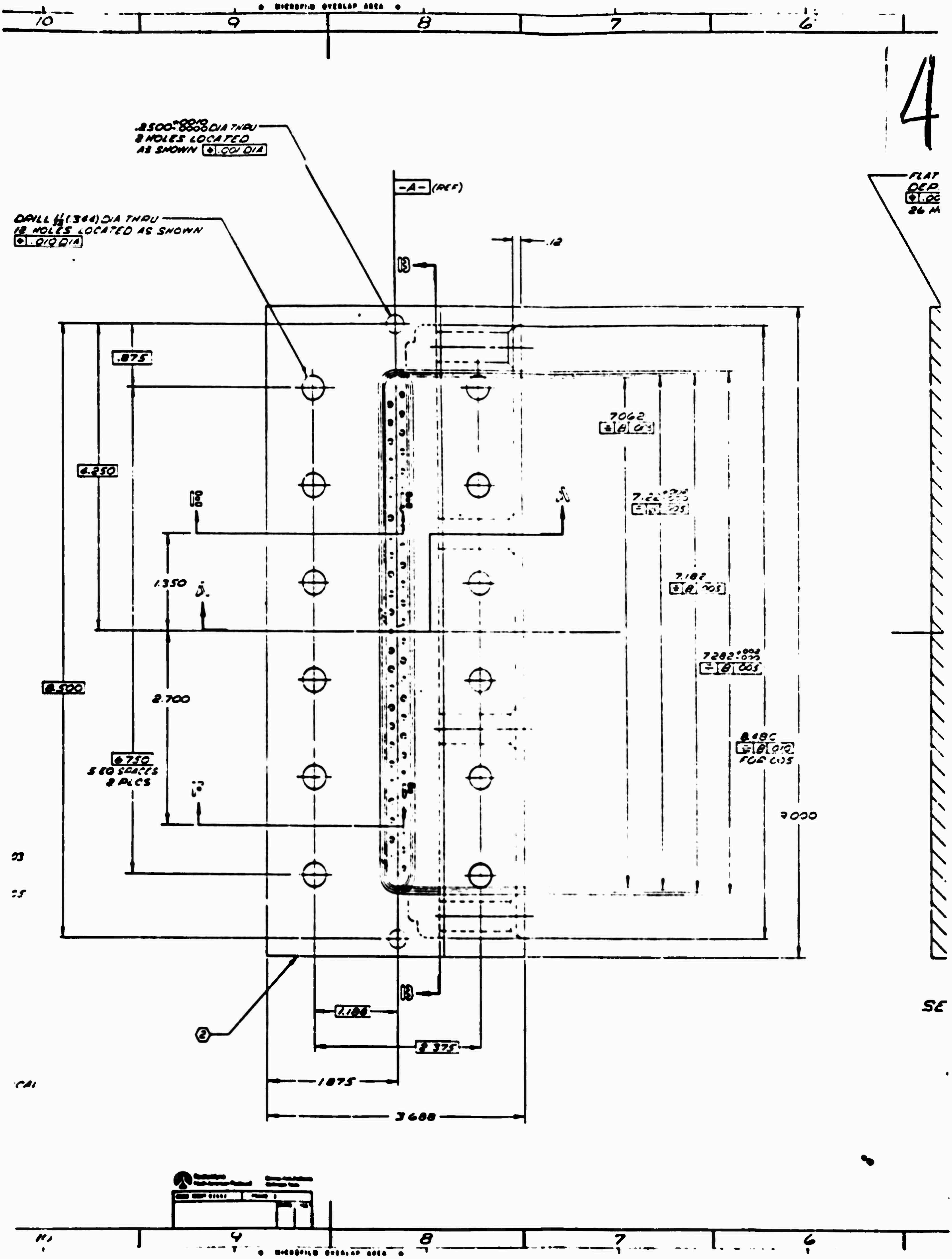

MICROFILM OVERLAP AREA
10
9
8
7
6
4
.2500 DIA THRU
8 HOLES LOCATED
AS SHOWN .001 DIA
-A- (REF)
DRILL (.344) DIA THRU
12 HOLES LOCATED AS SHOWN
.010 DIA
.12
.875
4.250
1.350
8.700
8.500
6.750
5 EQ SPACES
2 PLCS
7.062
7.182
7.282
8.180
FOR COS
7.000
1.188
2.375
1.875
3.688
2
SE

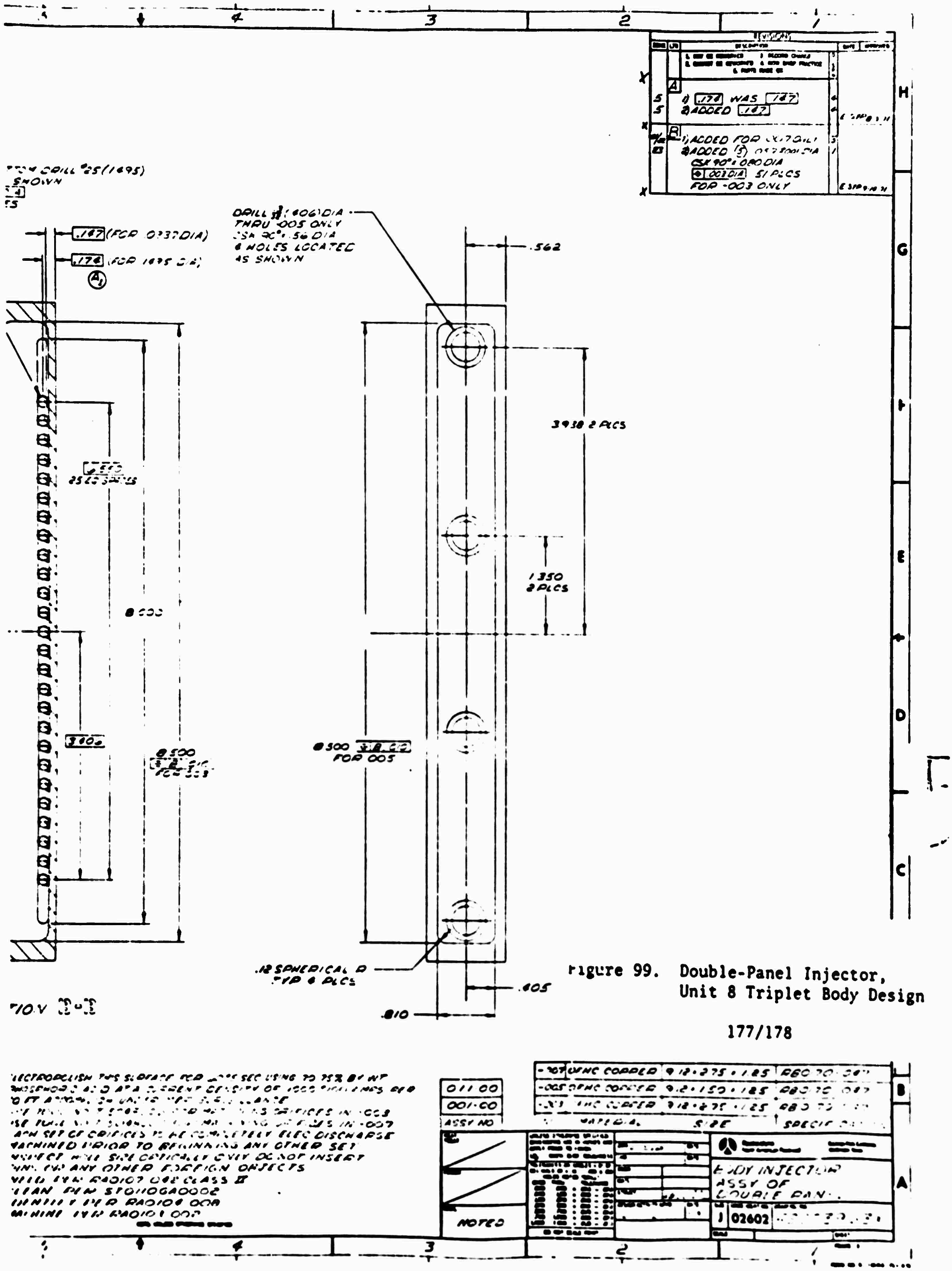

Figure 99. Double-Panel Injector,
Unit 8 Triplet Body Design

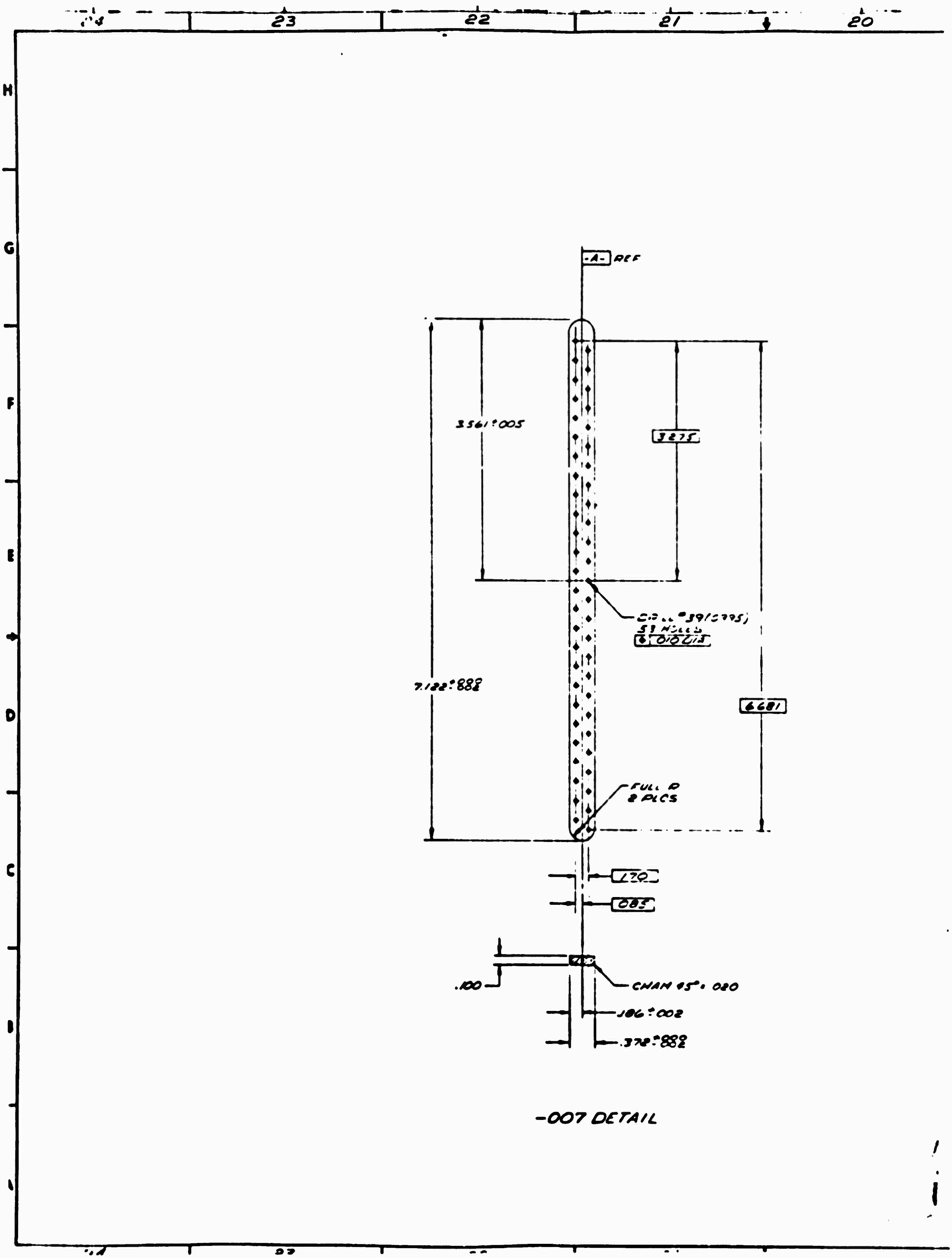

23
22
21
20
H
G
F
E
D
C
B
-A- REF
3561 ±.005
3275
7.122
6681
51 HOLES
FULL R
2 PLCS
.170
.085
.100
CHAM 45° × .020
.186 ±.002

-007 DETAIL

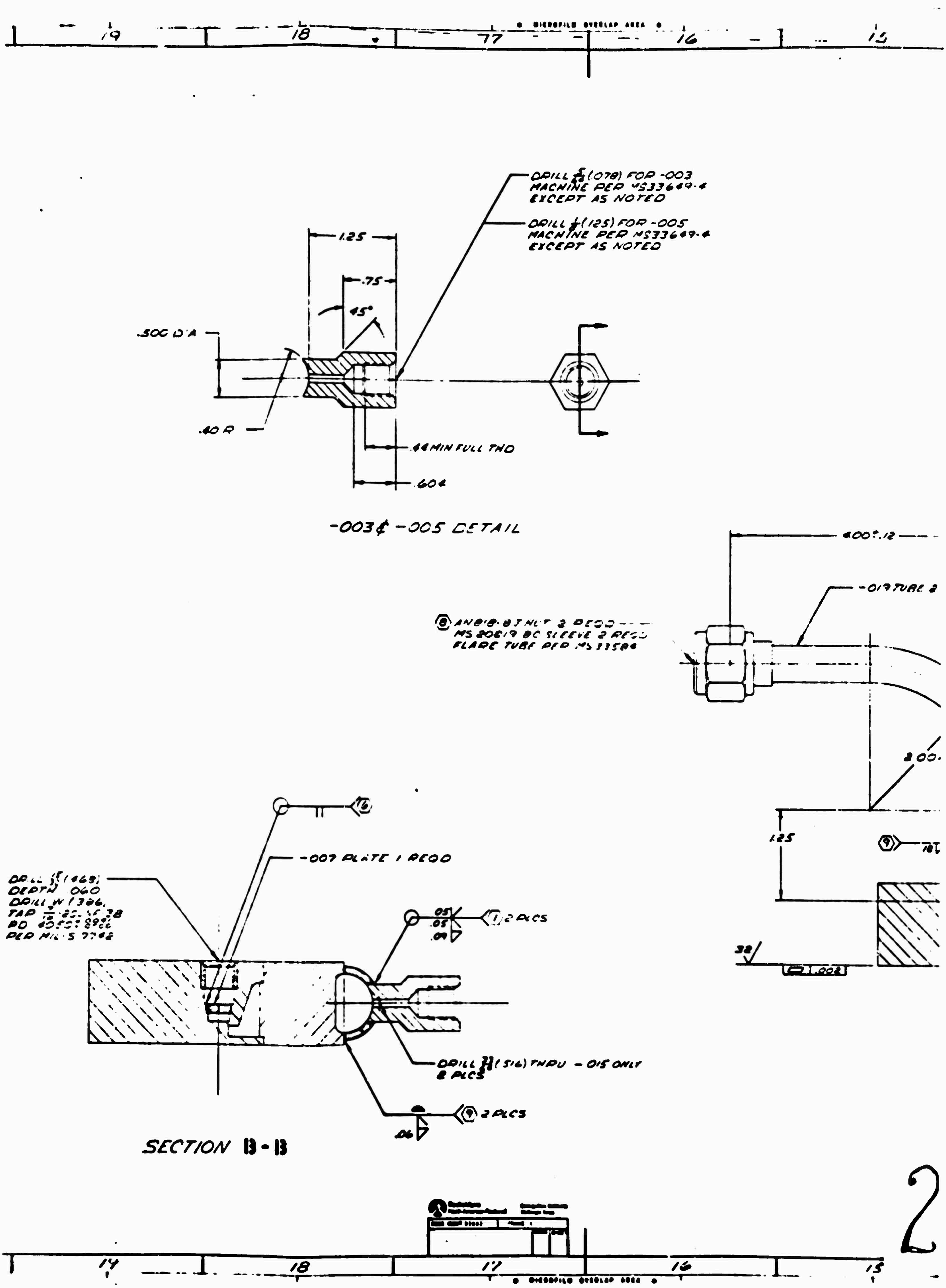
DRILL 5/64 (.078) FOR -003
MACHINE PER MS33649-4
EXCEPT AS NOTED
DRILL 1/8 (.125) FOR -005
MACHINE PER MS33649-4
EXCEPT AS NOTED
1.25
.75
45°
.500 DIA
.40 R
.44 MIN FULL THD
.604
-003 & -005 DETAIL
-017 TUBE 2
1.25
-007 PLATE 1 REQD
.05
.05
2 PLCS
DRILL 21/64 (.316) THRU - 015 ONLY
8 PLCS
2 PLCS
.06
SECTION B-B
2

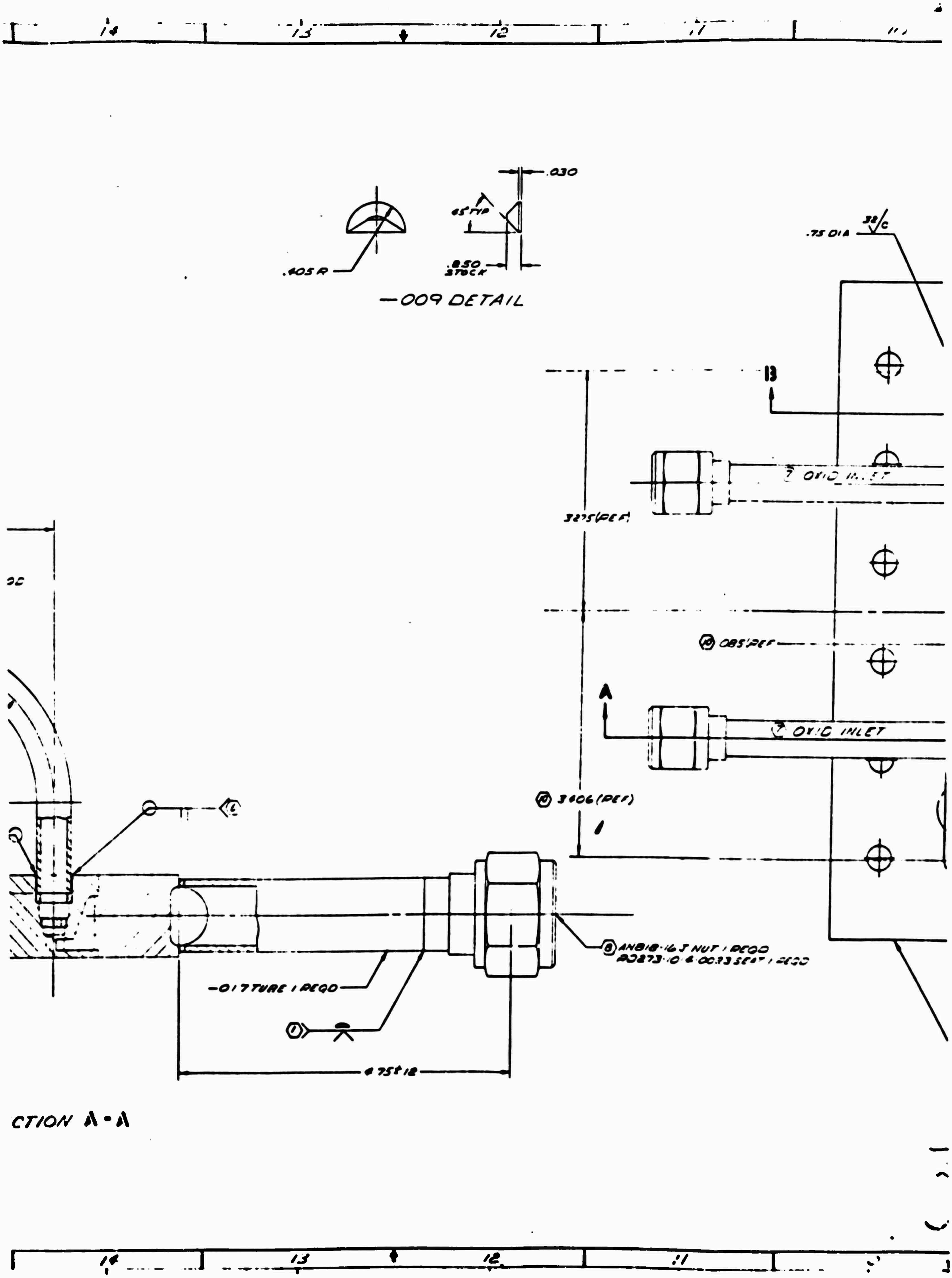
.030
45° TYP
.405 R
.850 STOCK
—009 DETAIL
.75 DIA
3.275(REF)
OBS'REF
OXID INLET
3.406(REF)
ANB18-16J NUT 1 REQD
—017 TUBE 1 REQD
4.75±.12
CTION A-A

14

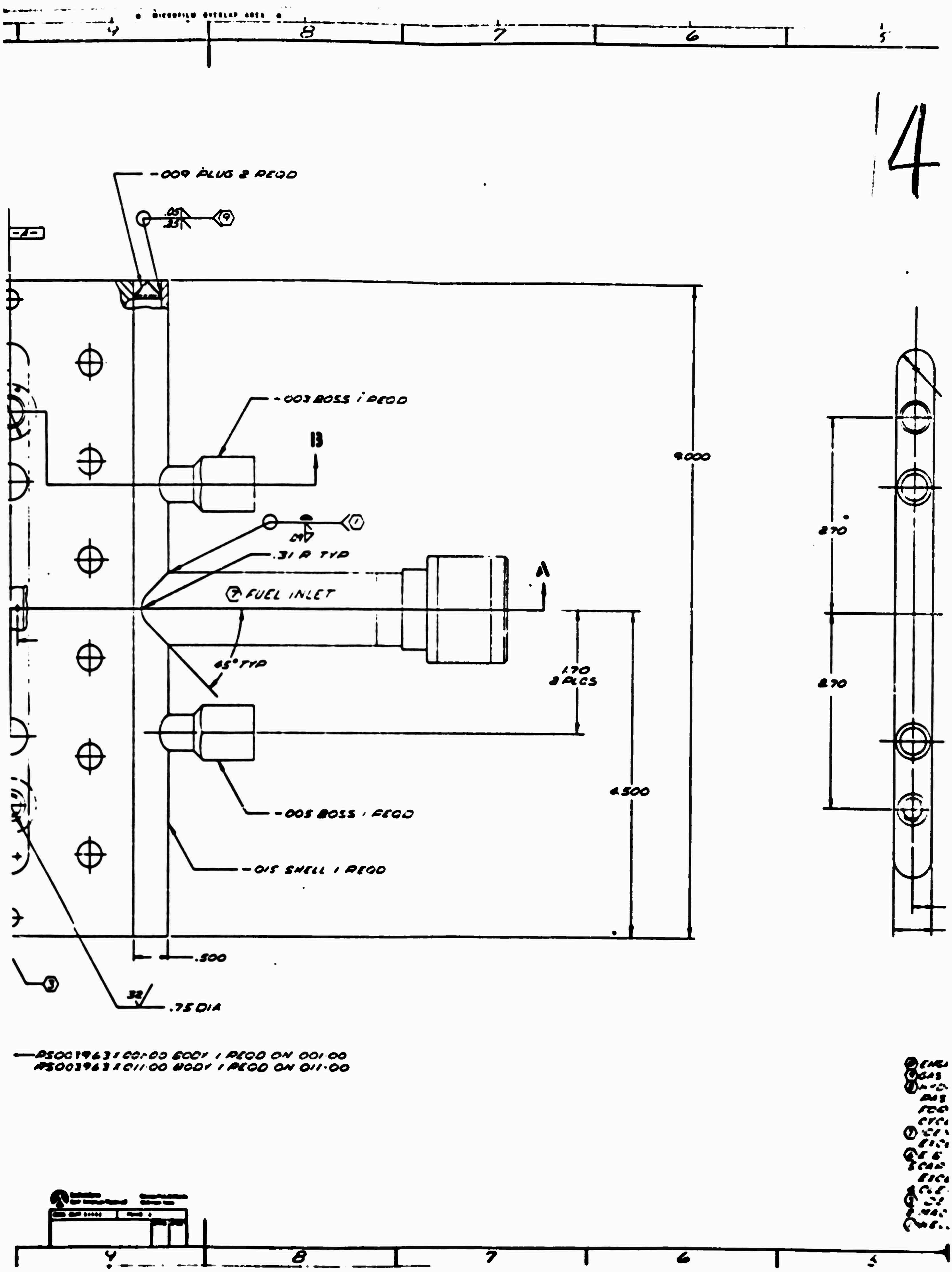

-009 PLUG 2 REQD
-003 BOSS 1 REQD
B
.31 R TYP
FUEL INLET
A
45° TYP
1.70
2 PLCS
9.000
4.500
-005 BOSS 1 REQD
-015 SHELL 1 REQD
.500
.75 DIA
2.70
2.70

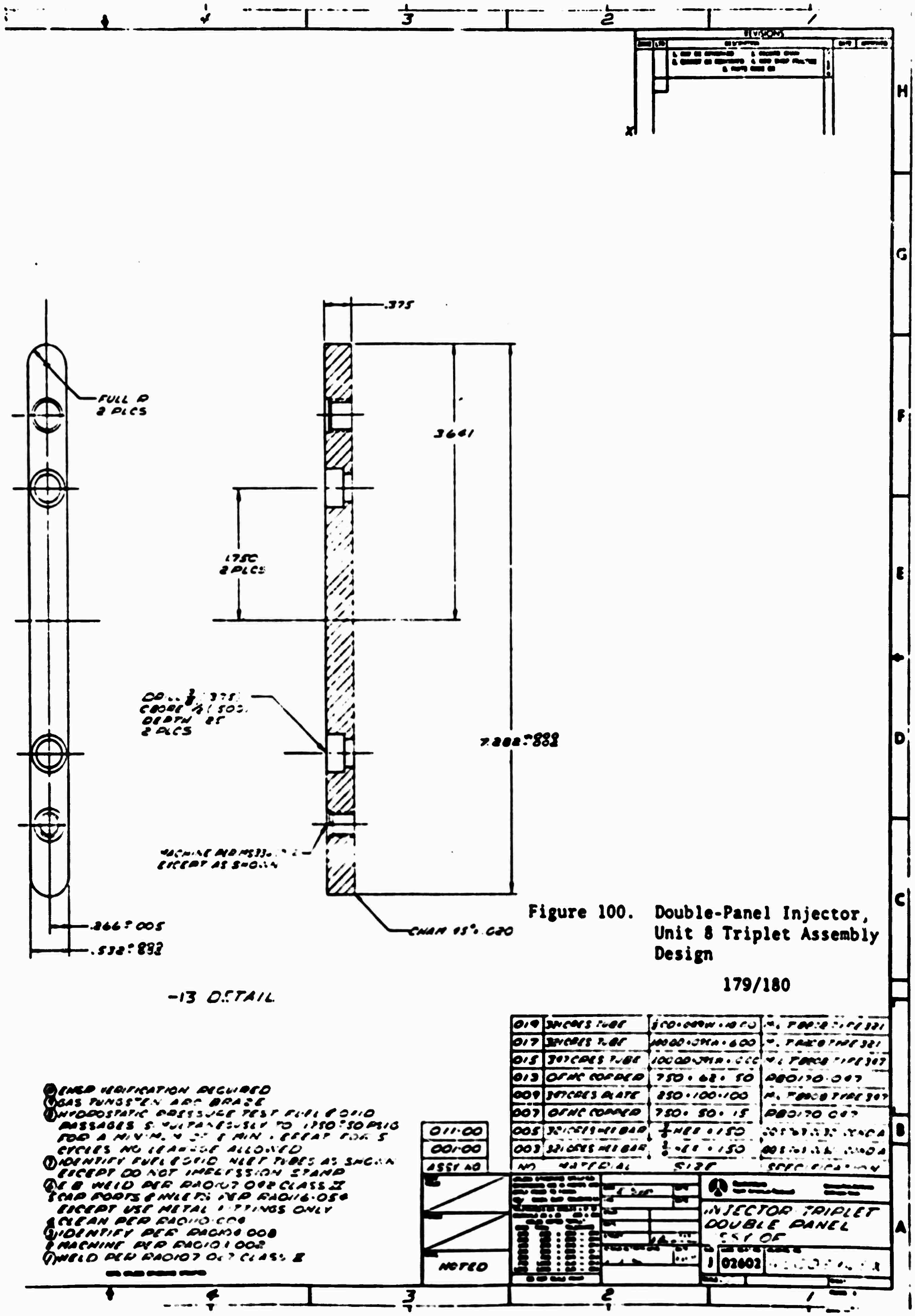

Figure 100. Double-Panel Injector, Unit 8 Triplet Assembly Design

as the transverse momentum ratio, $\frac{\text{Momentum Fuel, Transverse}}{\text{Momentum Oxidizer, Axial}}$, and an axial ΔV which is defined as Fuel Velocity Axial less oxidizer Velocity Axial. The fuel transverse momentum results from resolution of the total fuel momentum into axial and transverse components. A value of $\Delta V_{axail}=1500$ ft/sec and an $Mr_t=0.50$ was selected for the design.

6. The number of elements used in the design was 51 elements and is dependent upon the manifolding available in the regeneratively-cooled segment injector.

There was no preliminary cold-flow evaluation of the above-defined triplet injector element because sufficient knowledge was considered to exist to provide a viable design. Cold-flow evaluation of the element was performed at a later date to provide correlation data and is discussed on pages 203 to 232.

The injector was fabricated from a single piece of OFHC copper and the completed injector after hot-firing is shown in Fig. 101.

After fabrication, the injector was flow tested for pressure drop calibration and visual evaluation of element flow characteristics. The predicted pressure loss characteristics, for hot-fire test, are shown in Fig. 102 . No orifice plugging or stream distortion was noted.

The injector was modified during the test program (Table 12) to:

1. Evaluate the effect of decreased oxidizer injection velocity on heat transfer and c* performance.
2. Decrease the number of elements so that the injector could be used for combustion stability evaluation in the unit 4 water-cooled segment chamber which had directed pulse capability.

The initial modification, unit 8 to 8A, increased all oxidizer orifice diameters from 0.051 to 0.0575 inch. No change was made to the fuel orifices. The final modification, units 8A to 8B configuration, consisted of weld plugging one element

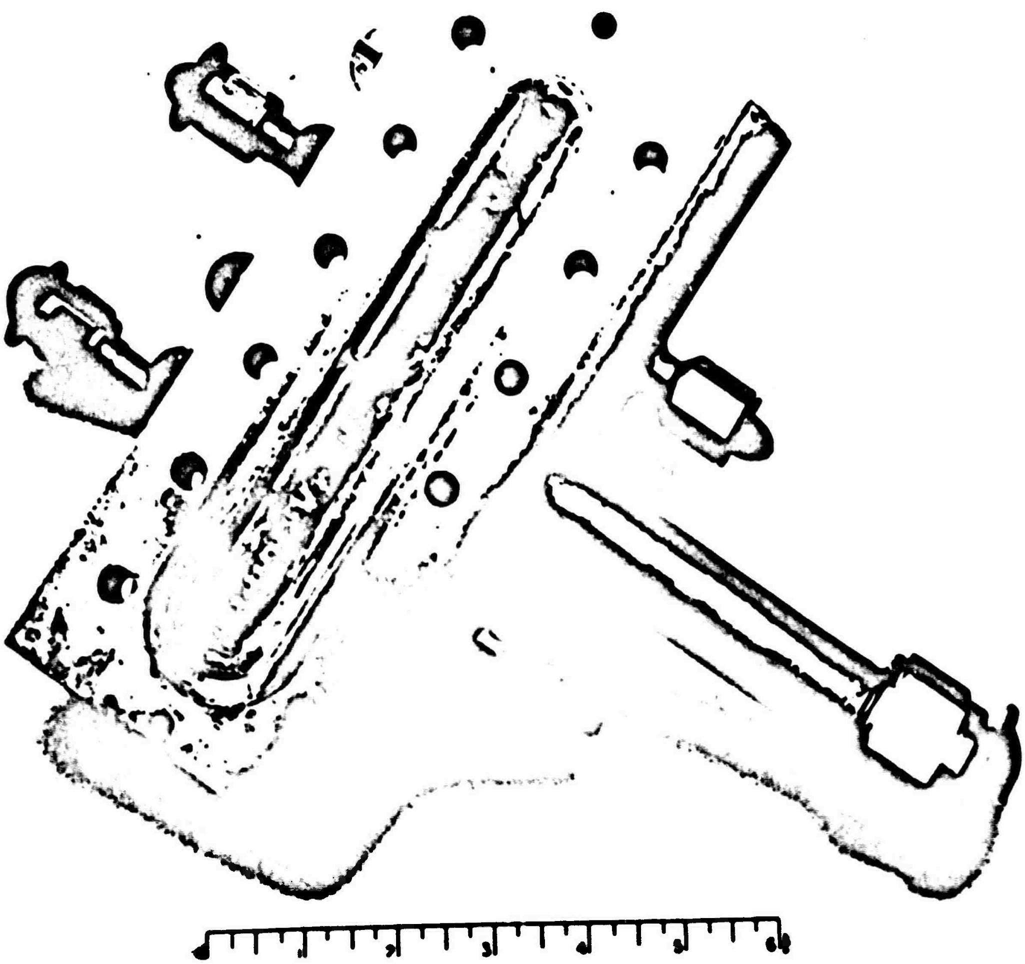

1EJ41-12/2/71-C1C

Figure 101. Unit 8 Triplet Double-Panel Injector, Posttest

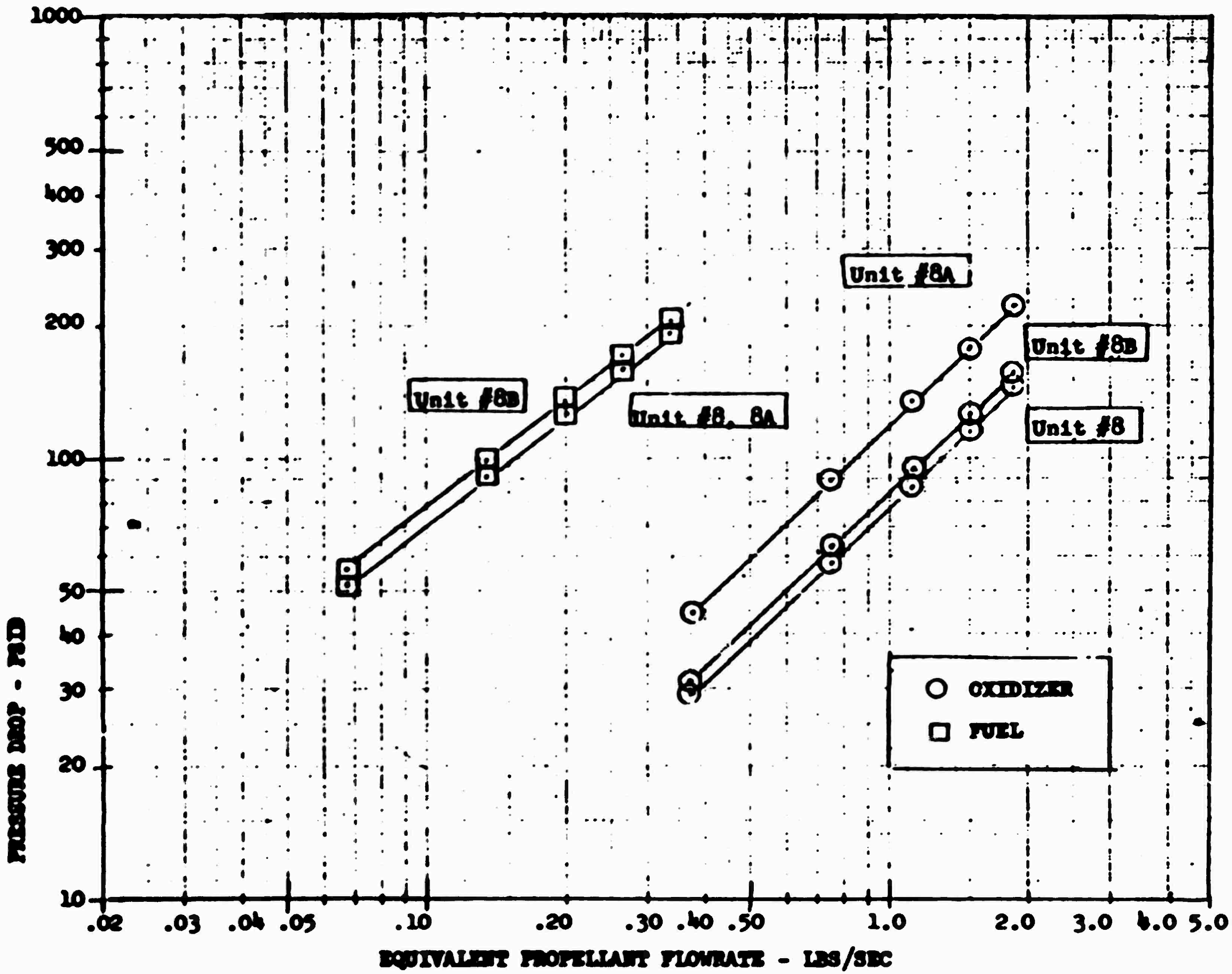

Figure 102. Unit 8 Triplet Injector Predicted Flow Characteristics (Double-Panel)

(2 fuel orifices and 1 oxidizer orifice) at opposite ends (2 total) to decrease the number of elements from 51 to 49. This modification was accomplished to permit testing in the unit 4 chamber which was 6.260 inches long (side plate to side plate) compared to units 5 and 6 which were 6.684 inches long.

The final configuration, unit 8B, is shown in Fig. 104 after completion of testing.

Unit 7G Injector. This injector resulted from a modification to the unit 7F injector. The modification was confined to the faceplate and consisted of providing a new faceplate (Fig. 104) that had the impinging fuel orifices and a close tolerance, referenced to the oxidizer OD, showerhead orifice into which the oxidizer tube was located. (The injector body design is shown in Fig. 105.) The assembled injector is shown in Fig. 106 .

The mechanical design parameters are noted in Table 12, and an injection element is shown in Fig. 107. The new faceplate design features were:

1. The faceplate would be removable, as were the previous faceplates for the concentric injectors.
2. The faceplate incorporated EDM fuel impinging orifices which were referenced to the oxidizer tube locations.
3. The oxidizer tubes, as shown in Fig. 108, were required to fit snugly into orifices in the faceplate to prevent or minimize the concentric mode of fuel injection. The oxidizer tube OD's were measured and found to be in the range of 0.0504 to 0.0508 inch. The faceplate was jig bored and reamed to provide 101 orifices, 0.051-inch diameter, to receive the oxidizer tubes during assembly.
4. No mechanical, braze, weld, or other technique was used to seal the oxidizer tube-to-faceplate joint (Fig. 109) because a minimal annulus flow was considered to be nondetrimental to operation or performance.

The injector was flow-calibrated, and the results are shown in Fig. 110 .

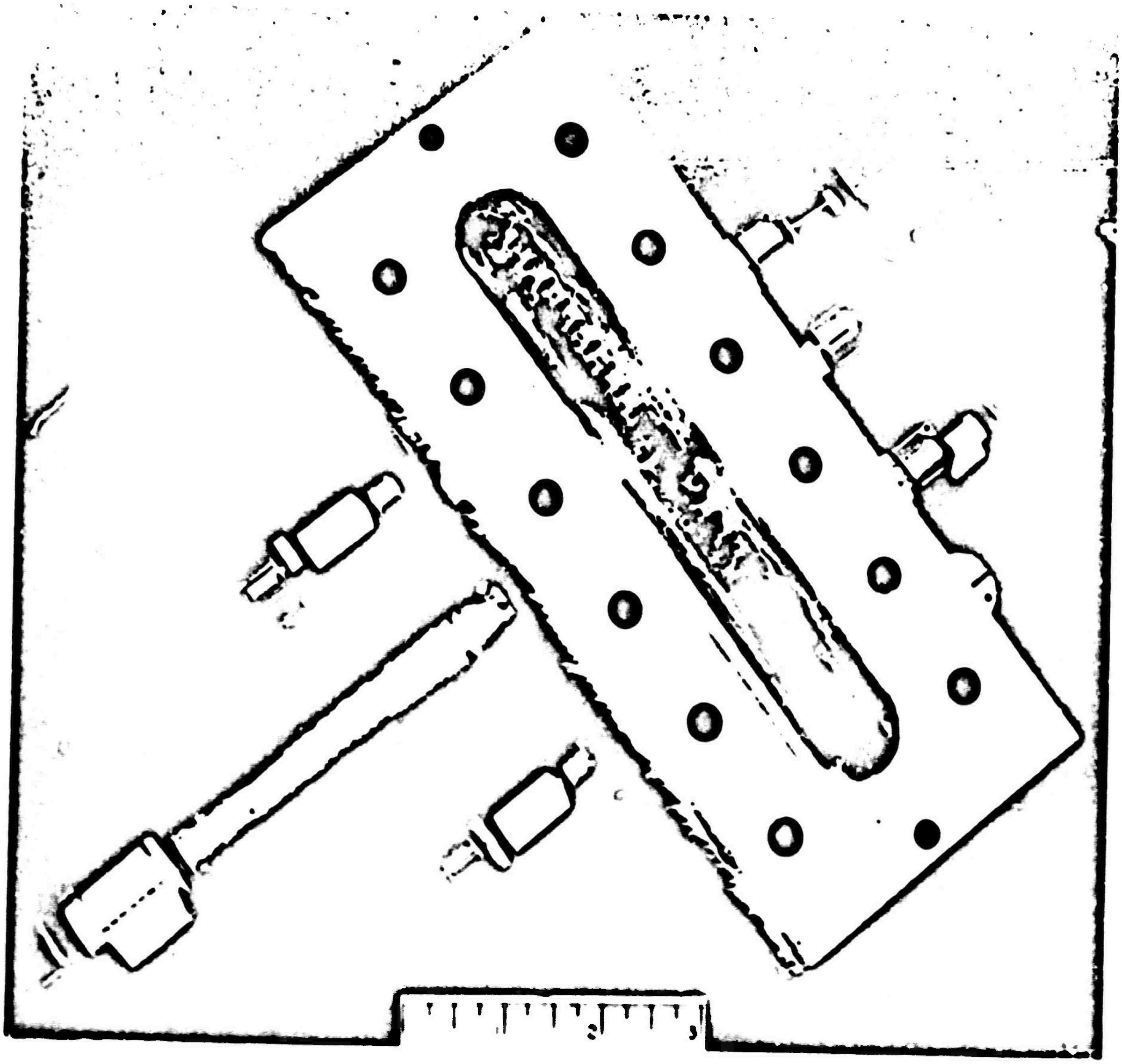

1EH25-12/9/71-1-C2N

Figure 103. Unit 8B Triplet, Double-Panel Injector, Posttest

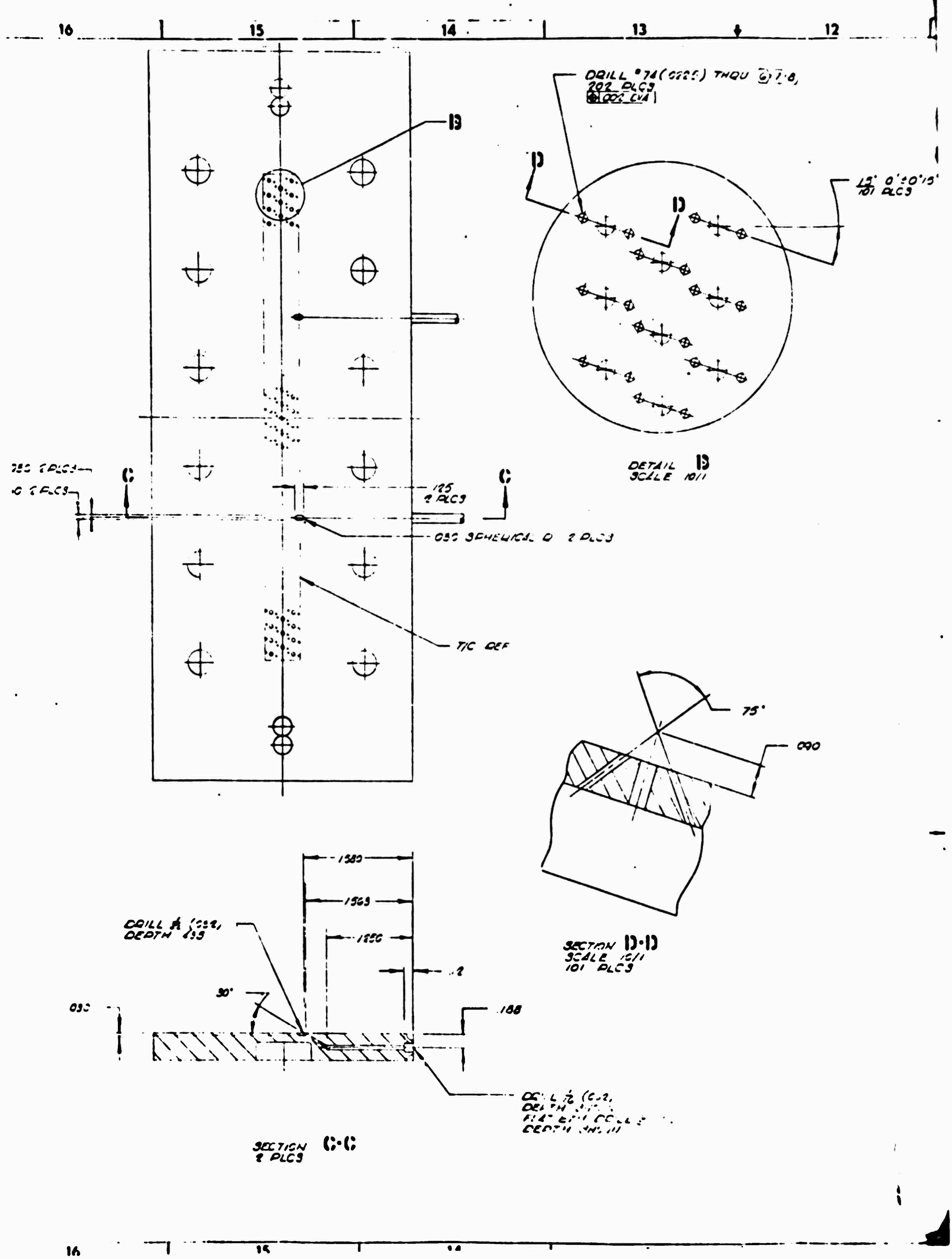
16
15
14
13
12
B
C
C
.125
2 PLCS
T/C REF
D
D
DETAIL B
SCALE 10/1
75°
.090
SECTION D-D
SCALE 10/1
101 PLCS
.1580
.1563
.1250
30°
.188
SECTION C-C
2 PLCS

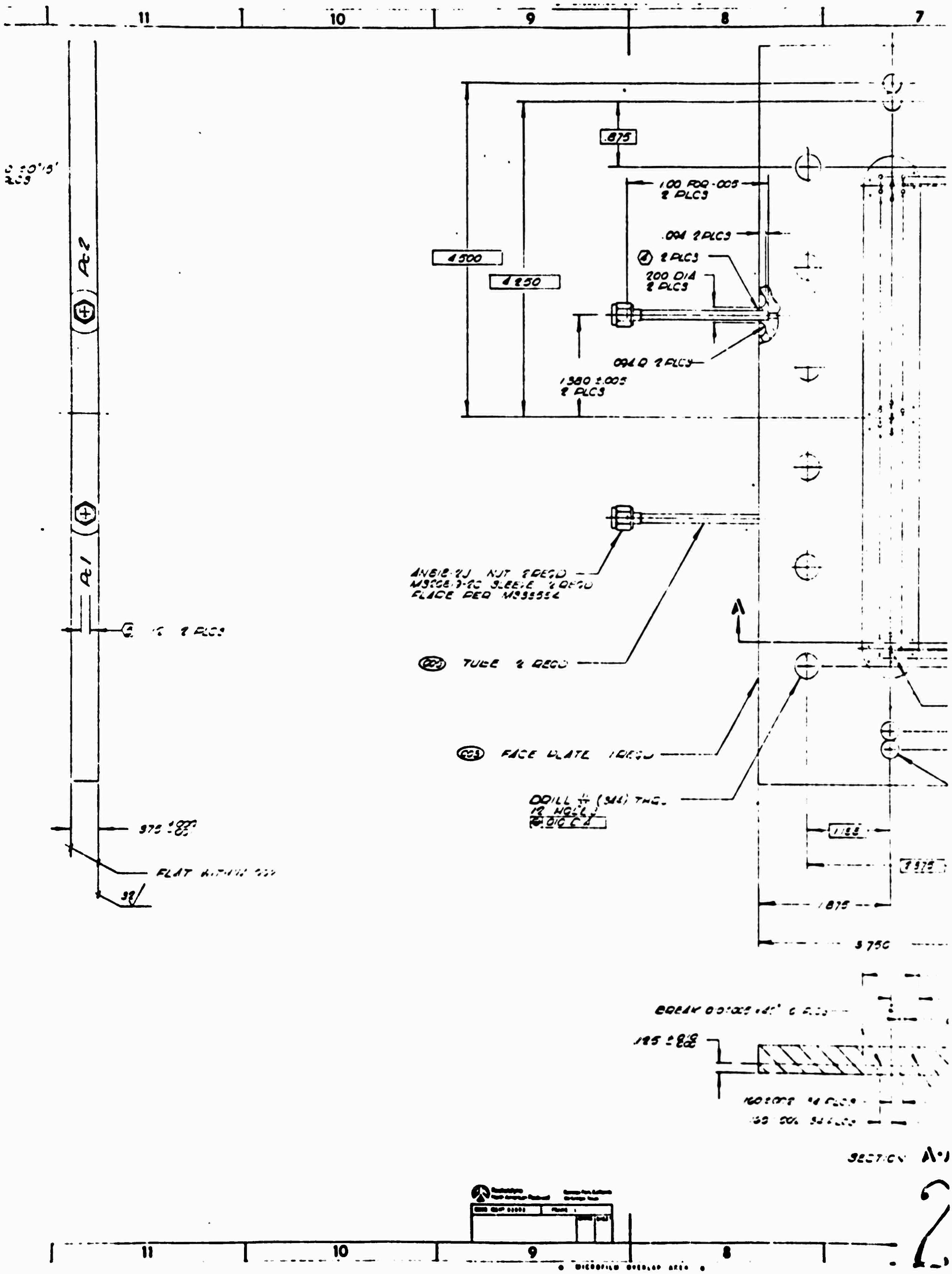

11
10
9
8
7
.875
1.00 REF .005
2 PLCS
.094 2 PLCS
2 PLCS
.200 DIA
2 PLCS
4.500
4.250
.094 R 2 PLCS
1.380 ±.005
2 PLCS
TUBE 2 REQD
FACE PLATE 1 REQD
DRILL
12 HOLES
1.875
3.750
SECTION A-

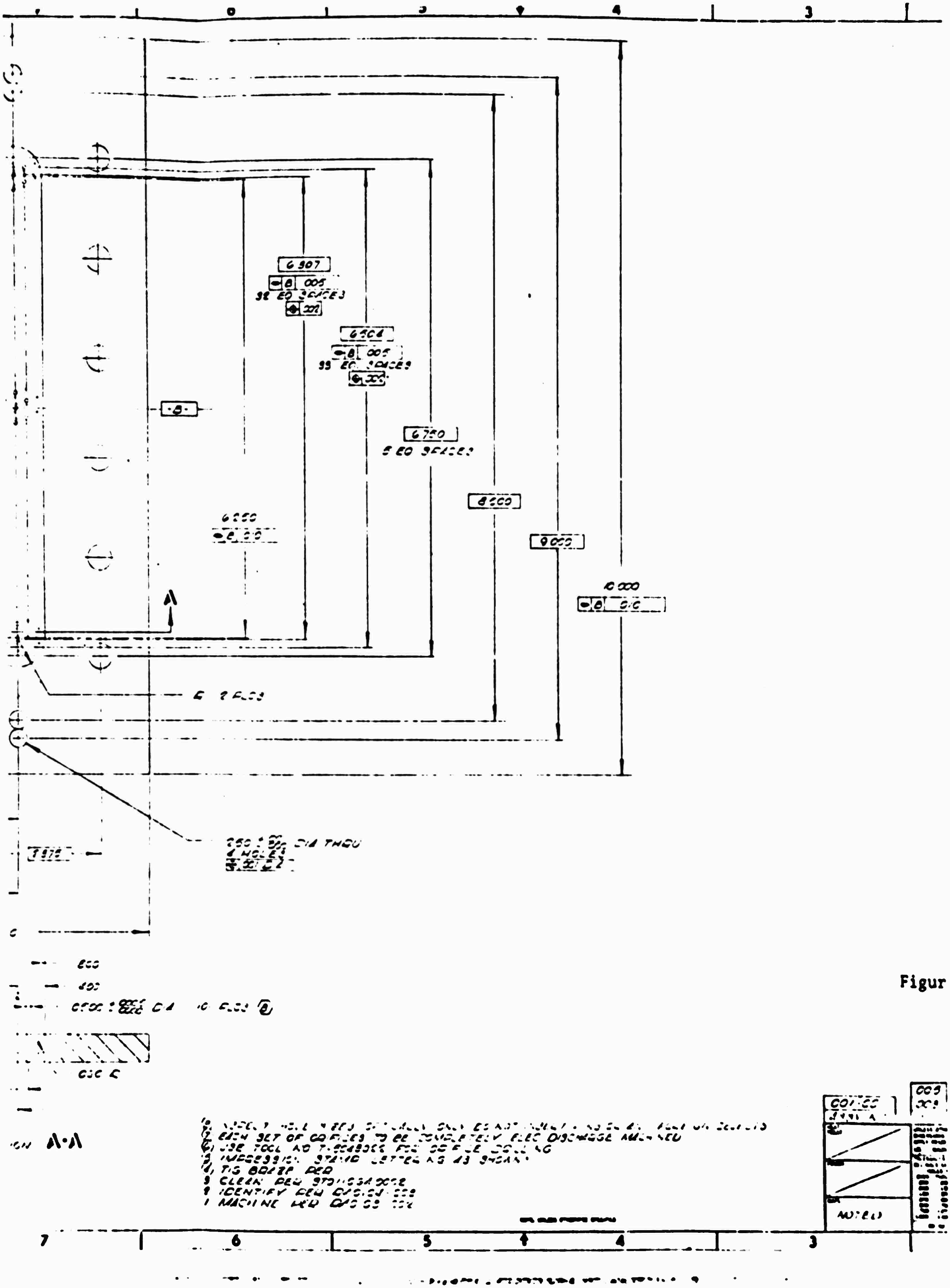

Figur

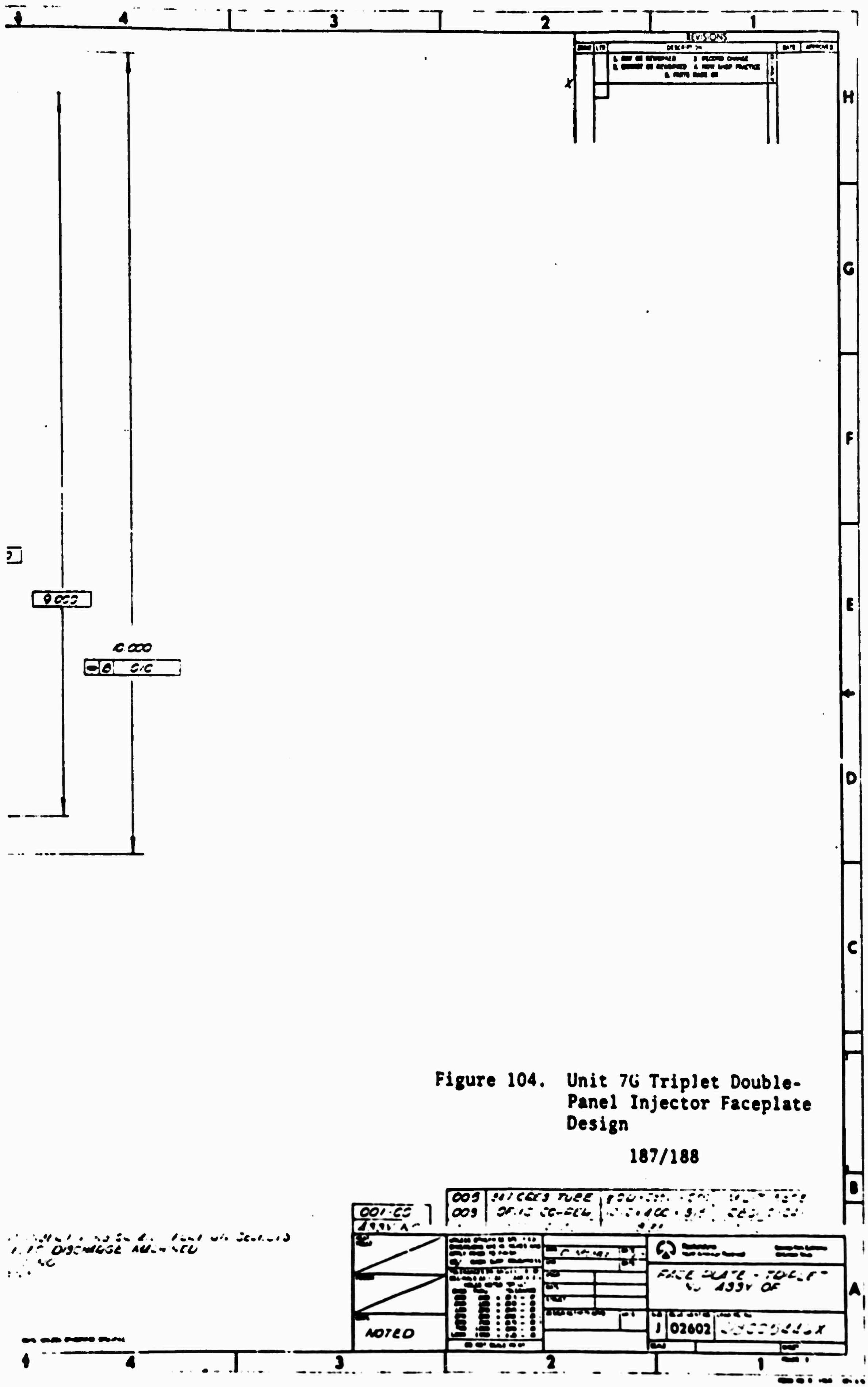

Figure 104. Unit 7G Triplet Double-Panel Injector Faceplate Design

14

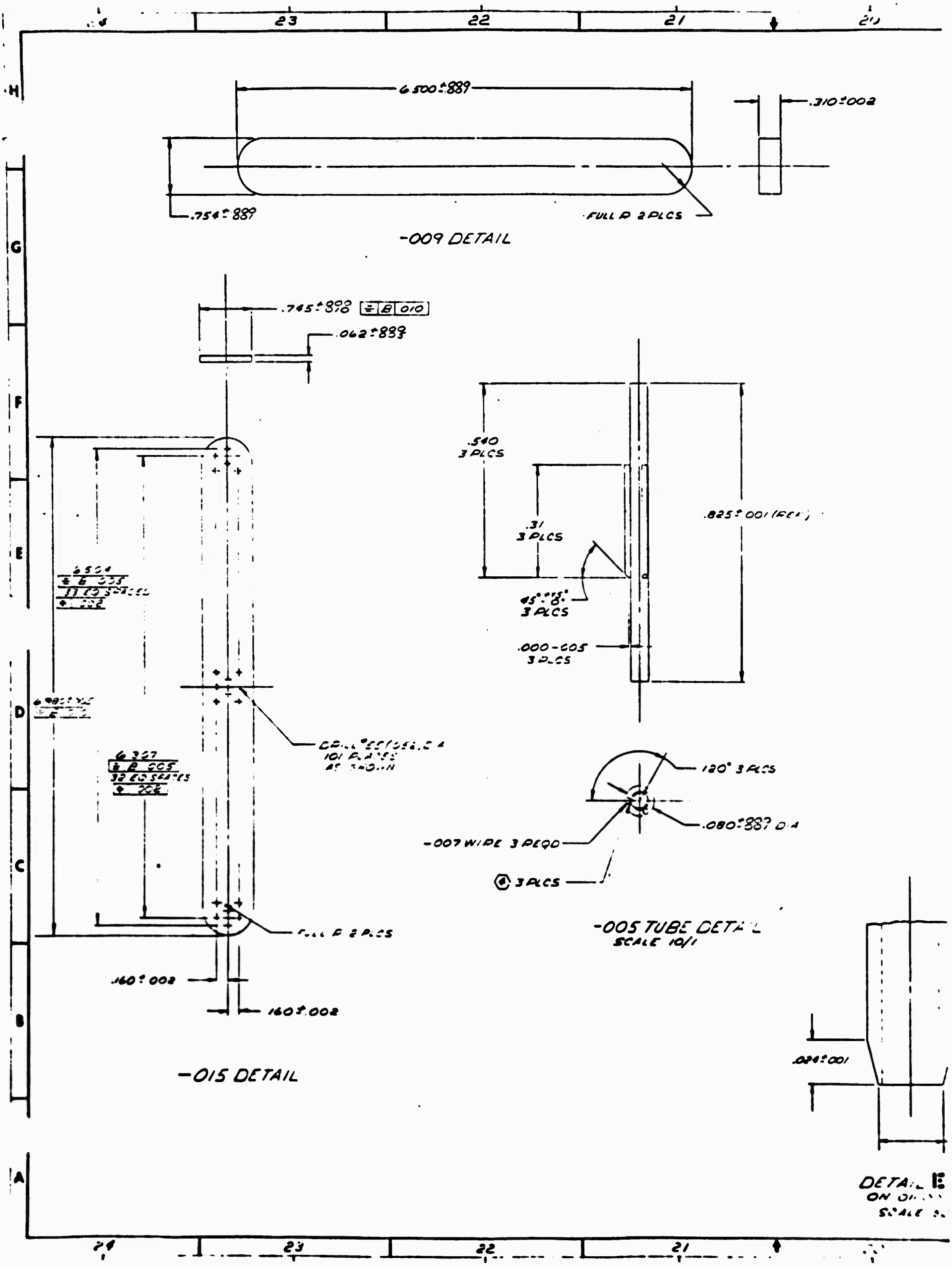

-009 DETAIL
.310±.002
FULL R 2 PLCS
-015 DETAIL
.062±
.160±.002
FULL R 2 PLCS
-005 TUBE DETAIL
SCALE 10/1
.540
3 PLCS
.31
3 PLCS
3 PLCS
.000-.005
3 PLCS
120° 3 PLCS
-007 WIRE 3 REQD
3 PLCS

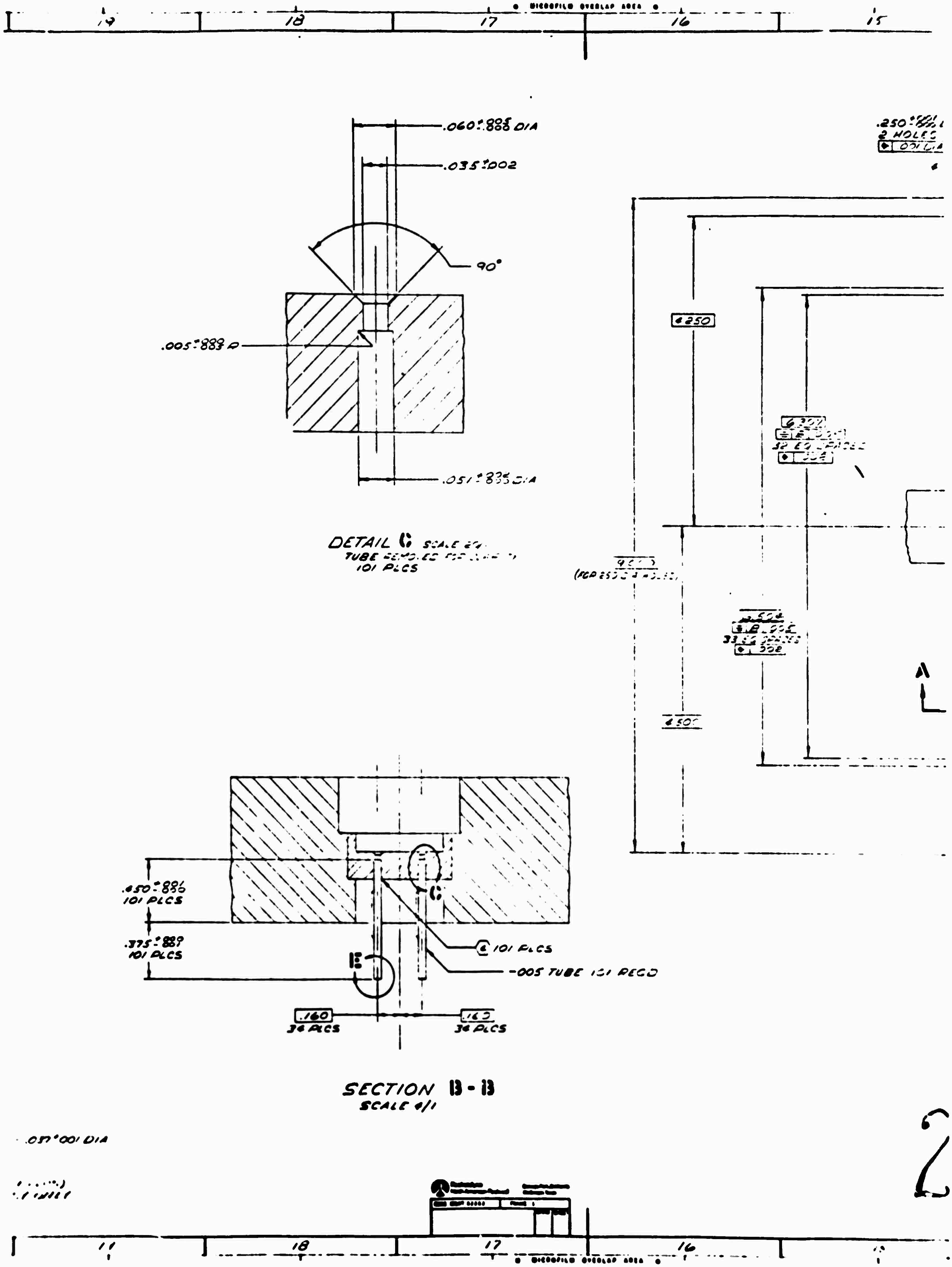

MICROFILM OVERLAP AREA
19
18
17
16
15
90°
.035±.002
DETAIL C
101 PLCS
.250
.450
101 PLCS
.375
101 PLCS
C 101 PLCS
-005 TUBE 101 REQD
.160
34 PLCS
34 PLCS
SECTION B-B
SCALE 4/1
.037±.001 DIA

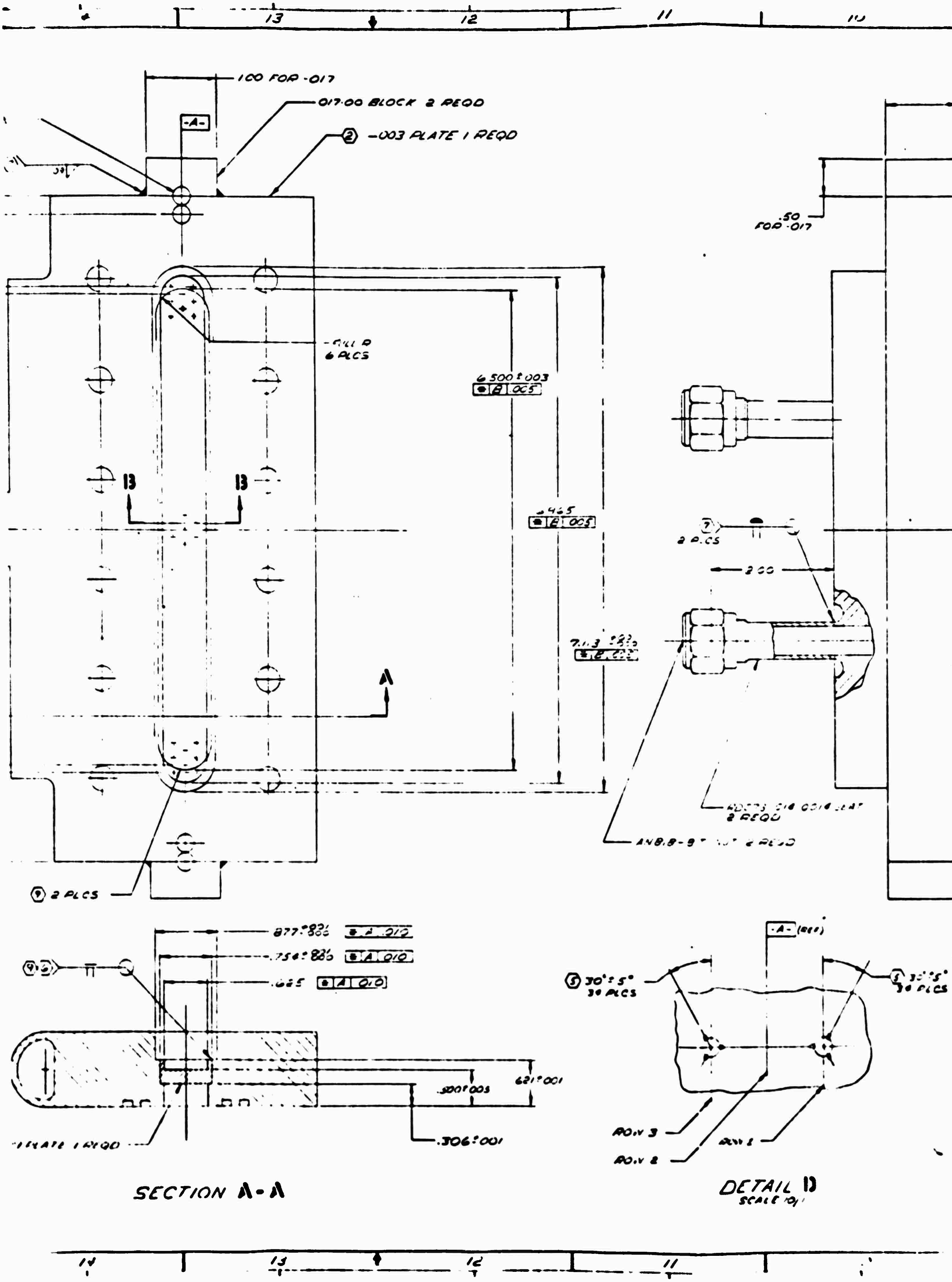

13
12
11
100 FOR -017
017-00 BLOCK 2 REQD
-A-
2 -003 PLATE 1 REQD
.50
FOR -017
6 PLCS
6.500 ± .003
B
B
.005
2 PLCS
2.00
AN8.8-9
2 REQD
2 PLCS
.877
A .010
.754
A .010
.625
A .010
.500 ± .005
.621 ± .001
.306 ± .001
PLATE 1 REQD
-A- (REF)
5 30° ± 5°
30 PLCS
ROW 3
ROW 2
ROW 1
SECTION A-A
DETAIL D
14
13
12
11

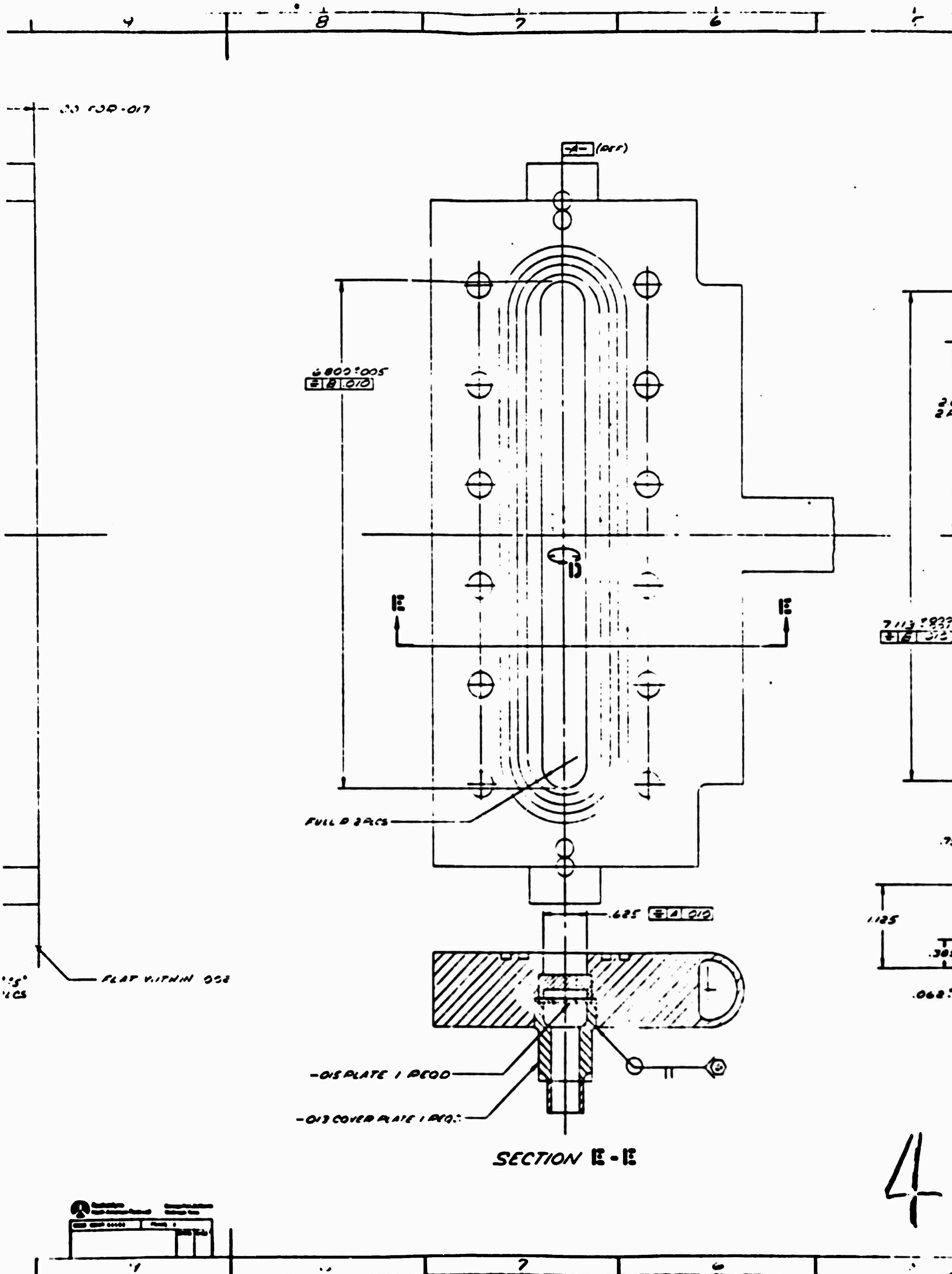

A (REF)
6.800 ±.005
B .010
E
E
D
FULL R 2 PLCS
.625
.010
FLAT WITHIN .002
-015 PLATE 1 REQD
-013 COVER PLATE 1 REQD
SECTION E-E
1.125

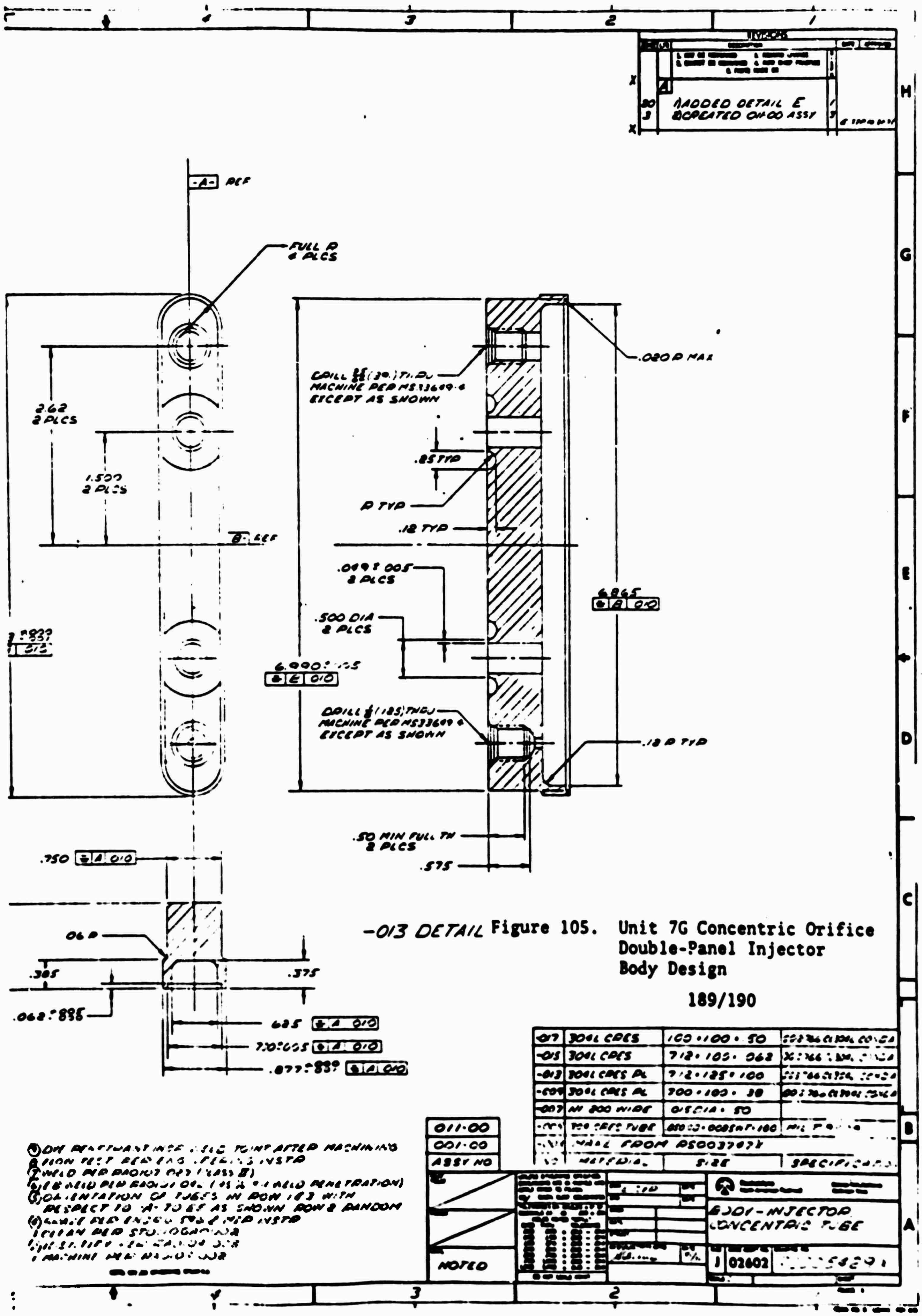

Figure 105. Unit 7G Concentric Orifice Double-Panel Injector Body Design

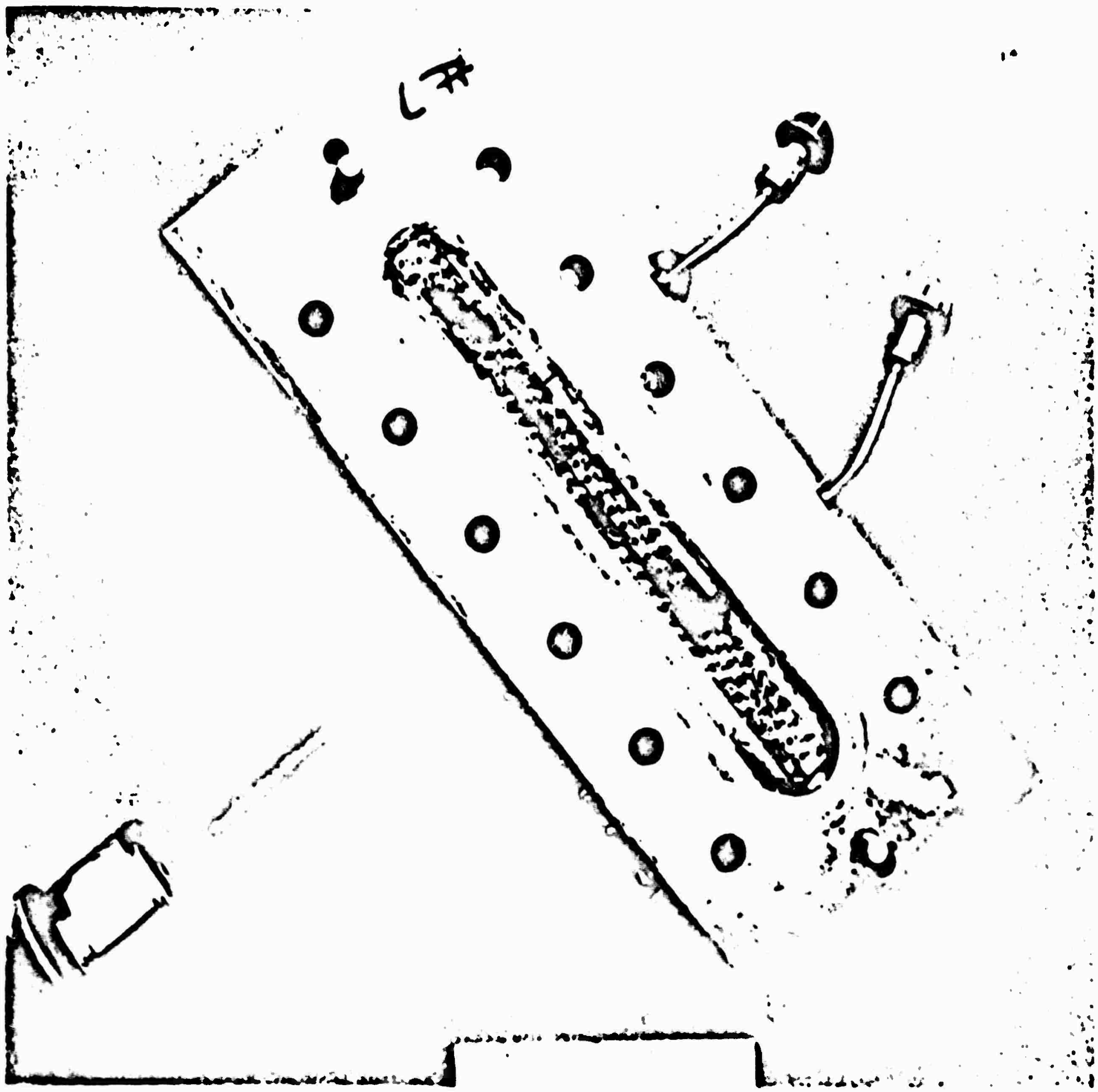

1EH25-12/9/71-1-C2J

Figure 106. Unit 7G Triplet Double-Panel Injector, Postfiring

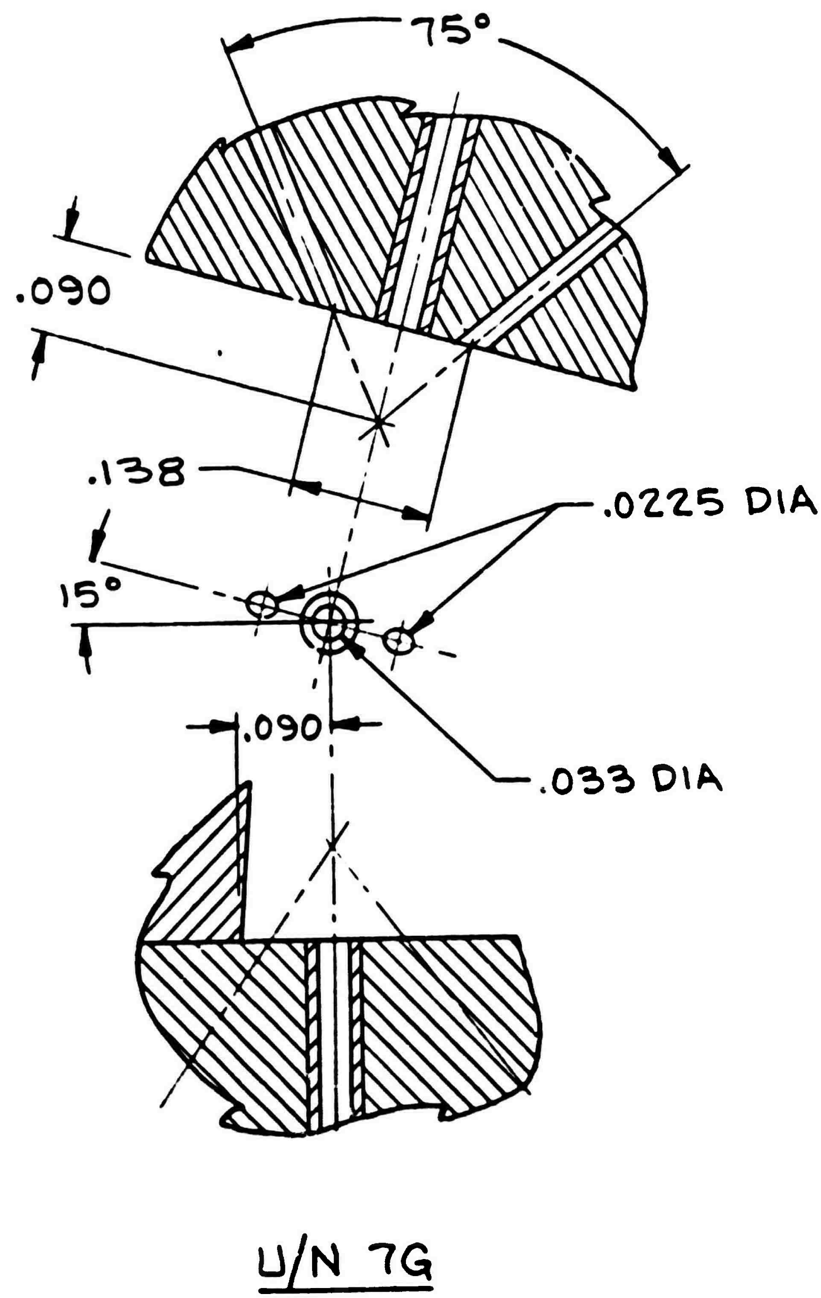

Figure 107. Unit 7G Triplet Double-Panel Injector, Injection Element Configuration

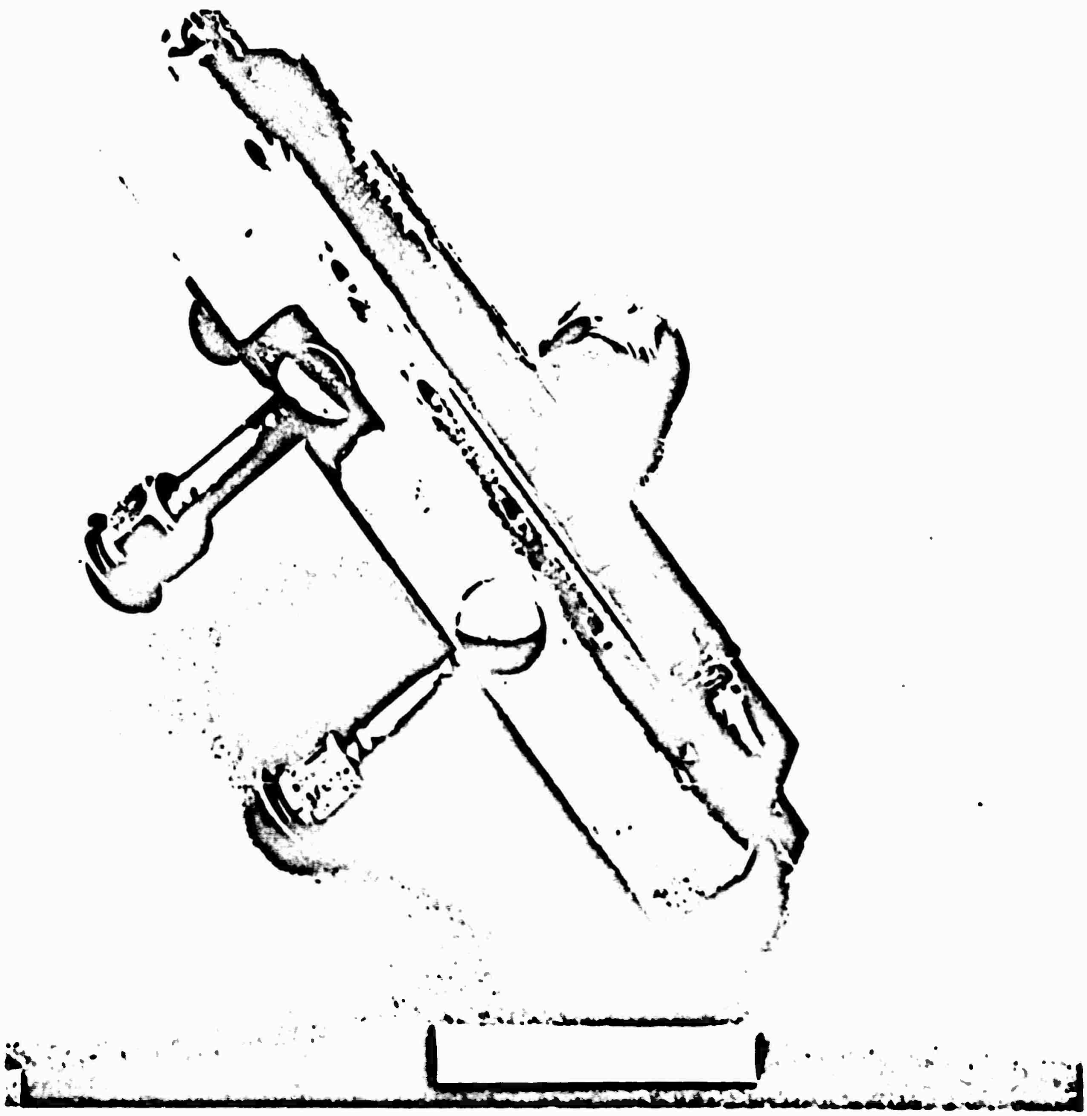

1EH25-12/9/71-1-C2L

Figure 108. Unit 7G Triplet Double-Panel Injector Body (Faceplate Removed)

1EH25-12/9/71-1-C2K

Figure 109. Unit 7G Triplet Double-Panel Injector, Face-to-Oxidizer Post Joint

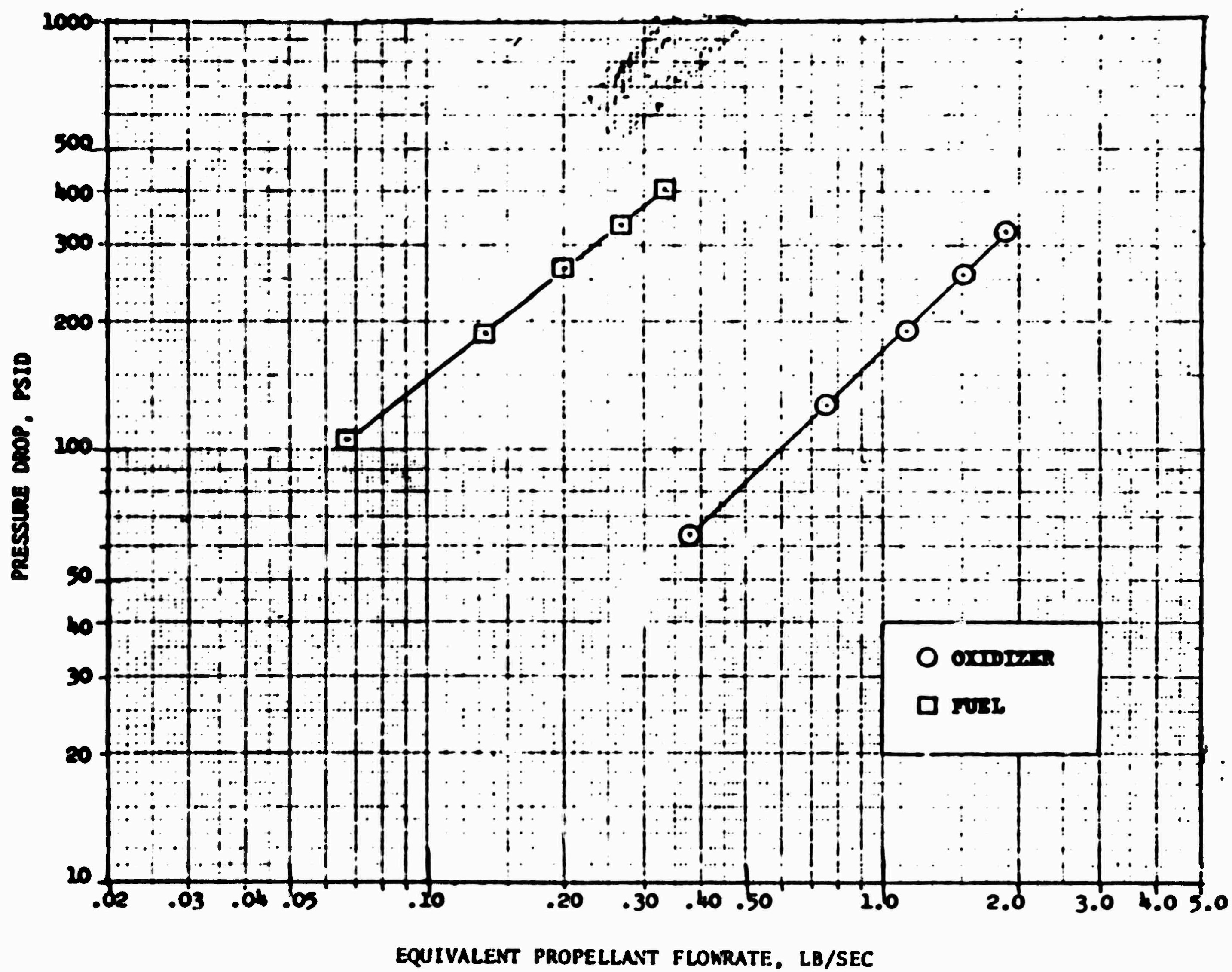

Figure 110. Unit 9G Triplet Injector (Conc. Body) Predicted Flow Characteristics (Double-Panel Gas-Gas)

The primary purpose of this injector was to evaluate the effect of reduced thrust per element, as compared to the unit 8 triplet, on heat transfer and c* performance.

No modifications were made to the unit 7G injector. Cold-flow evaluation of this element configuration was not conducted.

Concentric Orifice Injector. The concentric orifice injector, designated unit 7L, was a modification of the single-panel gas-liquid injector unit 7D. The element design was based on parameters established from previous programs (Ref. 8) and cold-flow test program results reported on pages 205 to 232.

The injection element configuration is shown in Fig. 111, with mechanical design characteristics shown in Table 12.

Basic design criteria consisted of the following:

1. 101 elements arranged in three rows
2. Equal element-to-element spacing with a wall-to-element spacing of 0.090 inch
3. Fuel velocity at the annulus exit of 2000 ft/sec and oxidizer post tip discharge velocity of 500 ft/sec
4. Oxidizer post OD=0.050 inch and ID=0.033 inch; fuel annulus gap of 0.009 inch, and oxidizer post wall thickness of 0.0085 inch

The injector body design, shown in Fig. 105, contained the propellant supply manifolds and the oxidizer posts.

Figure 112 shows the injector faceplate. The two-piece injector assembly provided development versatility by permitting changes in oxidizer post recess, annulus gap, and annulus configuration to be made in the removable and easily modified faceplate.

Program cold-flow test results, combined with previous work accomplished (Ref. 8), indicated that the primary mixing efficiency of a single concentric orifice injection element for gaseous oxygen-hydrogen propellants depended primarily on axial

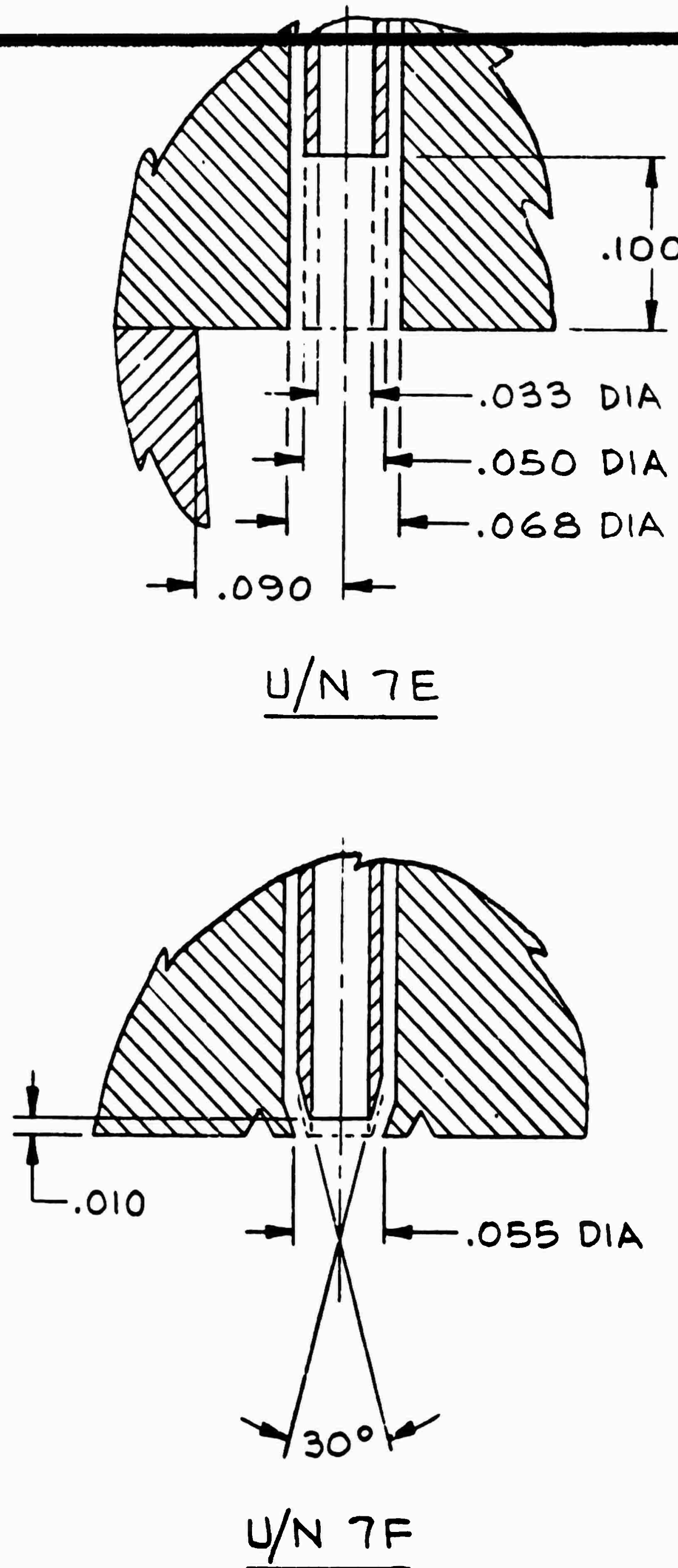

Figure 111. Units 7E and 7F Concentric Orifice Double-Panel Injector, Injection Element Configurations

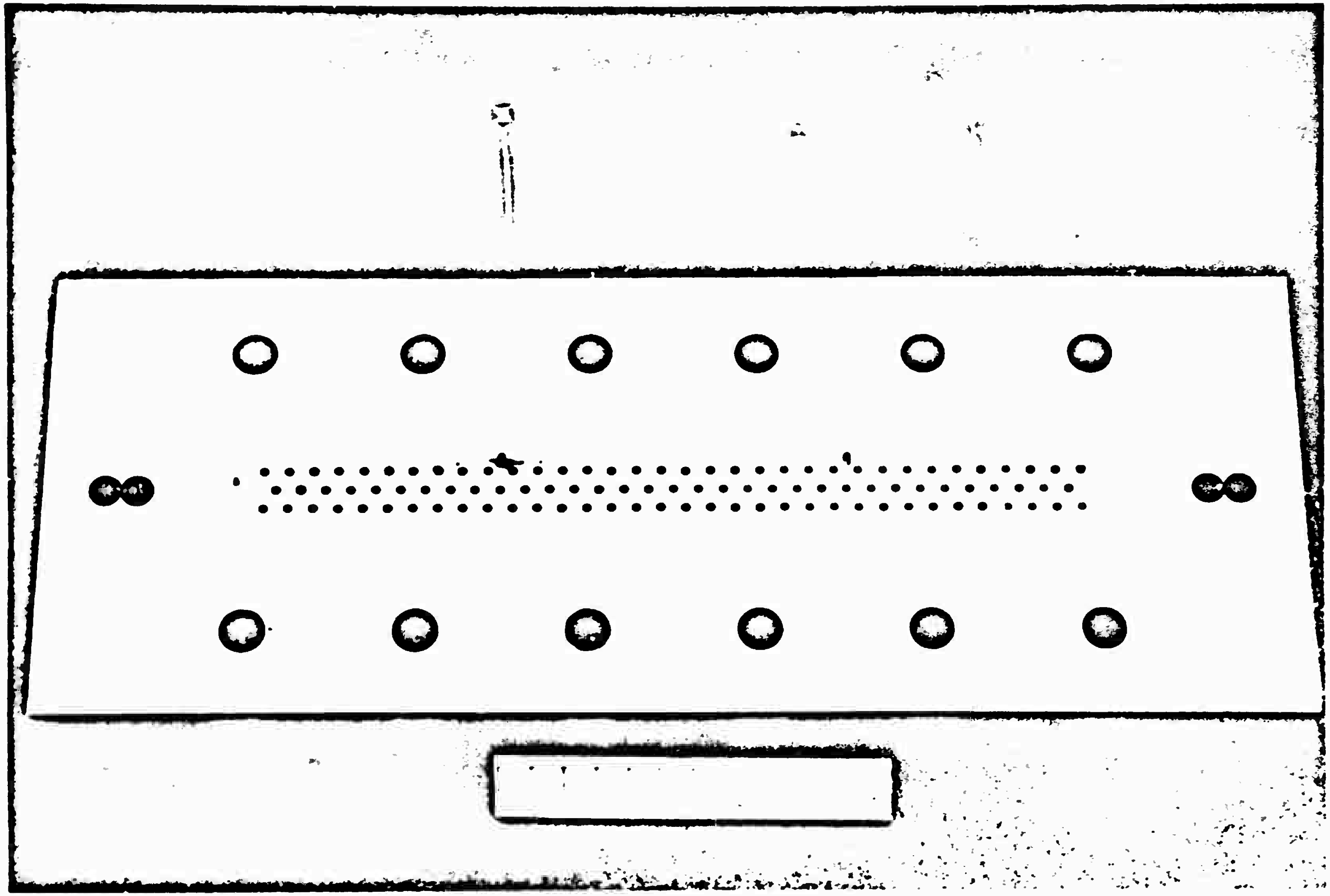

1EH25-12/9/71-1-C2E

Figure 112. Unit 71. Concentric Orifice Double-Panel Injector Faceplate (Hot-Gas Side)

fuel annulus velocity, oxidizer post axial discharge velocity, oxidizer post tip configuration (blunt or flared), and axial velocity difference (fuel velocity less oxidizer velocity). The influence of each parameter was determined while maintaining the other parameters constant during cold-flow testing. In addition, an internally flared (divergent) oxidizer post also was investigated during the Ref. 9 testing.

The unit 7E injection element configuration was based on the cold-flow test results (reported on pages 205 to 232) that indicated the range of ΔV_{axial}/flowrate required for high E_M.

Additional cold-flow evaluation of a modified configuration, unit 7F, indicated the possibility of increased c* performance with this element type (Fig. 111). The modification, made during the test program, was accomplished by machining the end of each oxidizer post to obtain an external chamfer and by mechanically deforming an existent faceplate (Fig. 112 and 113) to obtain the unit 7F configuration.

Cold-flow calibration tests were completed for each injector and are discussed on pages 205 to 232. The predicted pressure loss characteristics are presented in Fig. 114.

Trislot Injector. The third injector type evaluated during the double-panel program was the trislot injector, unit 9. The injection element type is shown in Fig. 115 and is a noncircular impinging stream injector in a hydrogen-oxygen-hydrogen configuration. The injector type was previously evaluated in another program (Ref. 7), and, based on those results, good performance could be expected on the AMPT program.

Part of a cold-flow program, described on pages 205 to 232, was conducted to characterize the element prior to design, and very high mixing efficiency values (>95 percent) were obtained.

The trislot injector, unit 9, which was designed, fabricated, and tested, is shown in Fig. 116, with the mechanical design parameters noted in Table 12. The injector has 30 elements that are located in 2 rows to prevent end impingement of

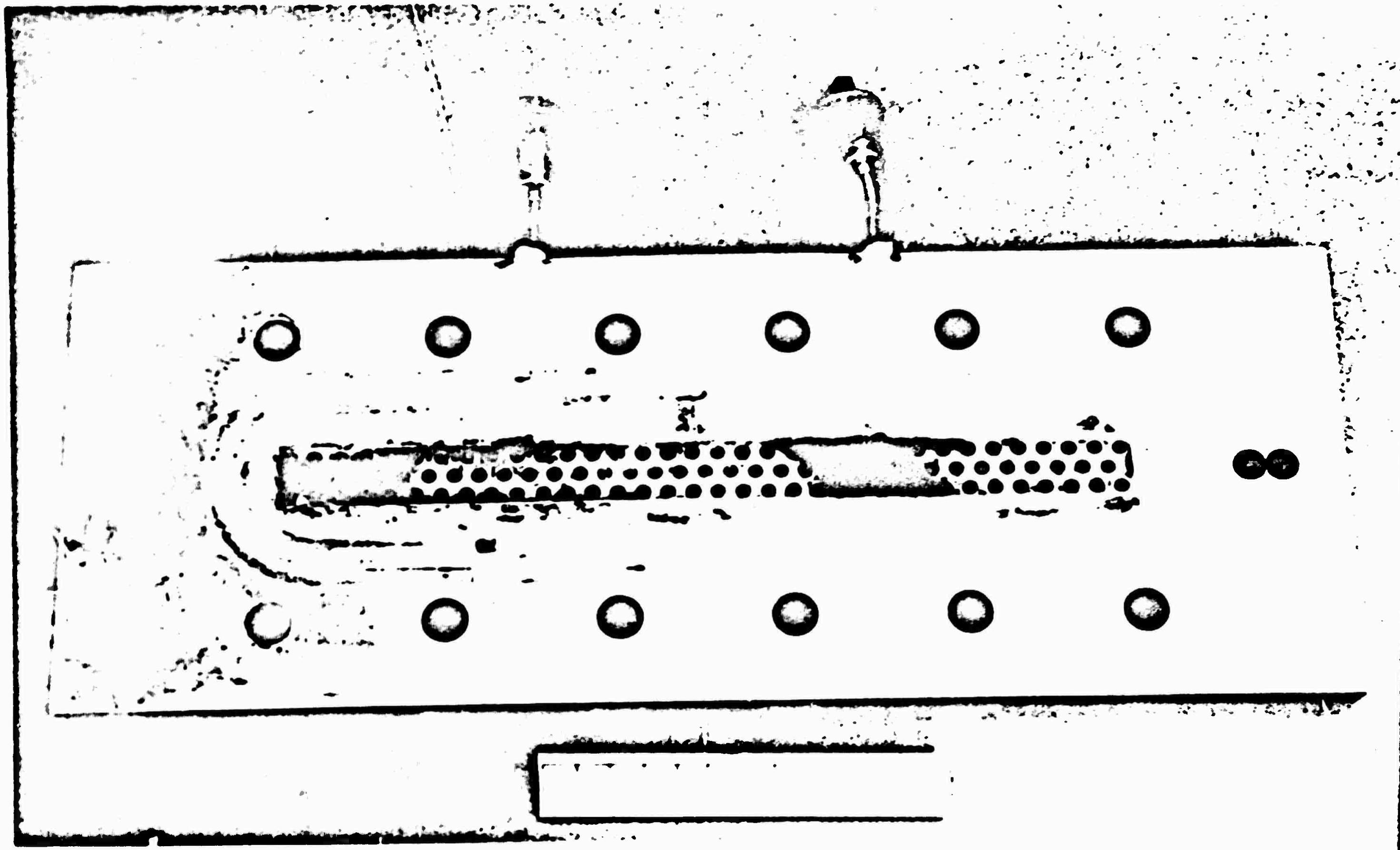

1EH25-12/9/71-1-C2H

Figure 113. Unit 7F Concentric Orifice Double-Panel Injector Faceplate (Hot-Gas Side)

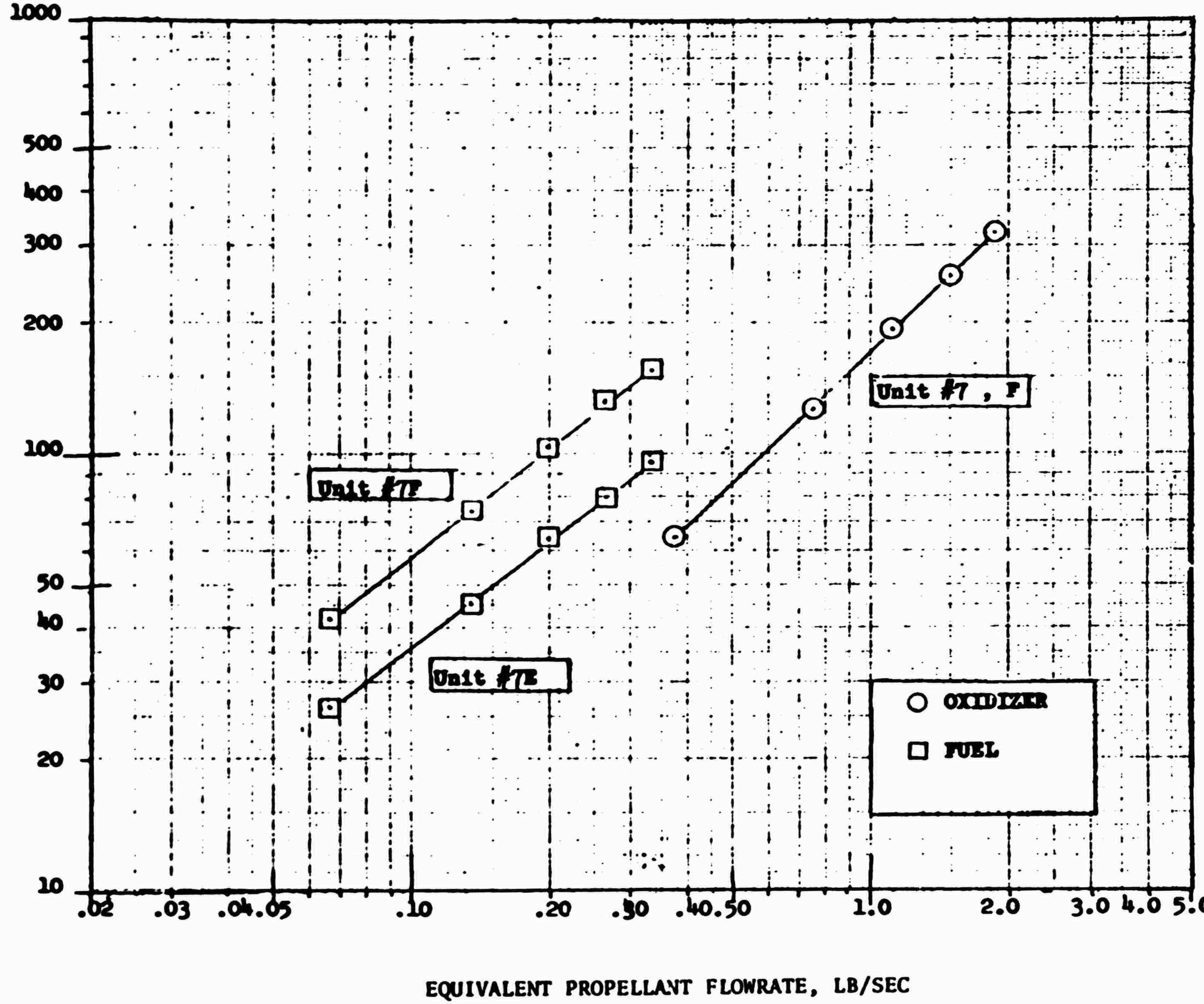

Figure 114. Unit 7E and 7F Concentric Injector Predicted Flow Characteristics (Double-Panel Gas-Gas)

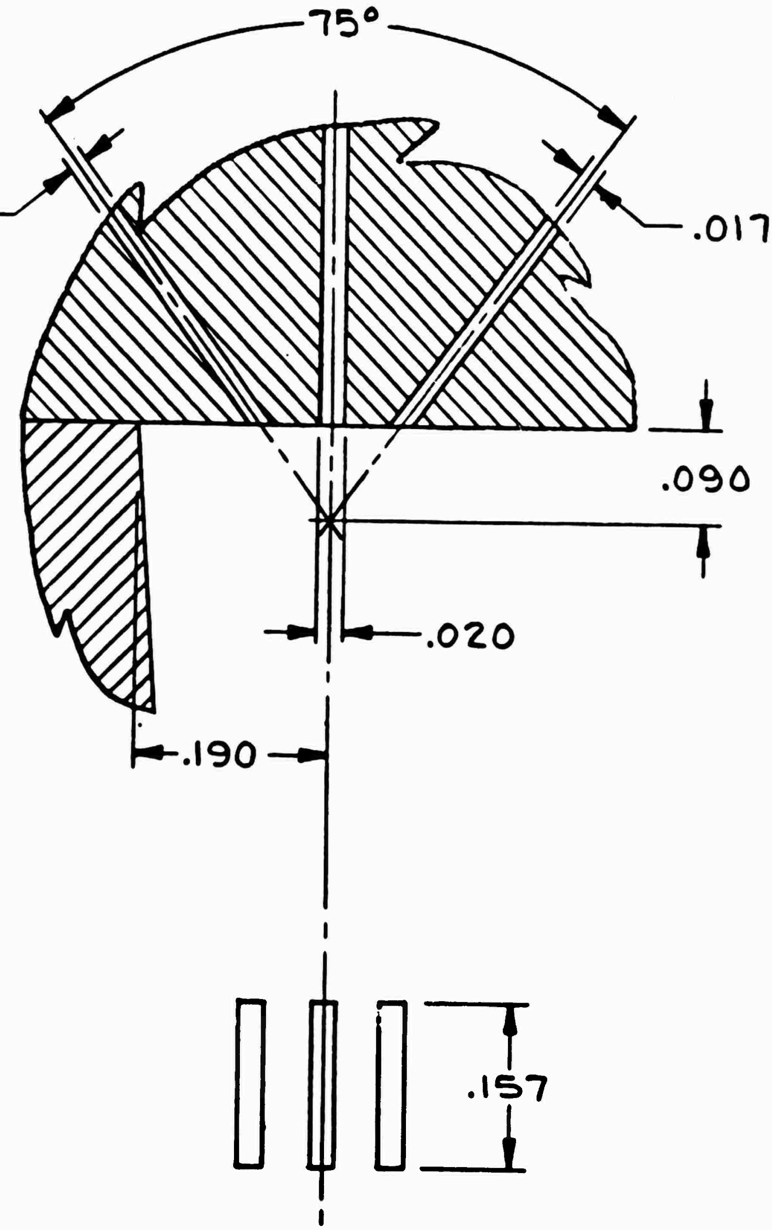

U/N 9

Figure 115. Unit 9 Trislot Double-Panel Injector, Injection Element Configuration

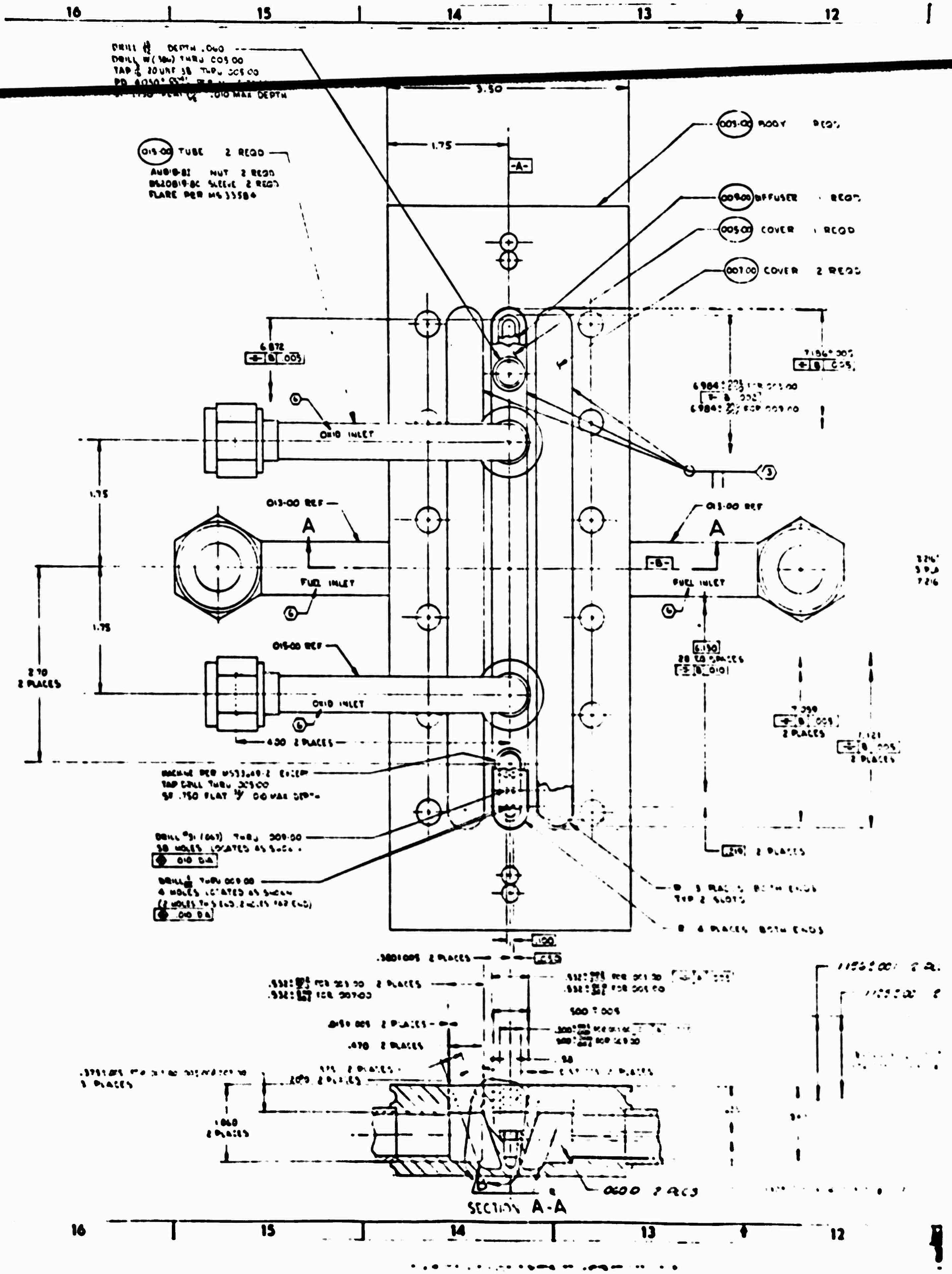

16
15
14
13
12
3.50
1.75
-A-
TUBE 2 REQD
BODY
DIFFUSER
COVER 1 REQD
COVER 2 REQD
OXID INLET
FUEL INLET
013-00 REF
A
A
-B-
1.75
1.75
2.70
2 PLACES
4.00 2 PLACES
.380±.005 2 PLACES
.500±.005
.470 2 PLACES
1.060
2 PLACES
.0600 2 PLCS
SECTION A-A

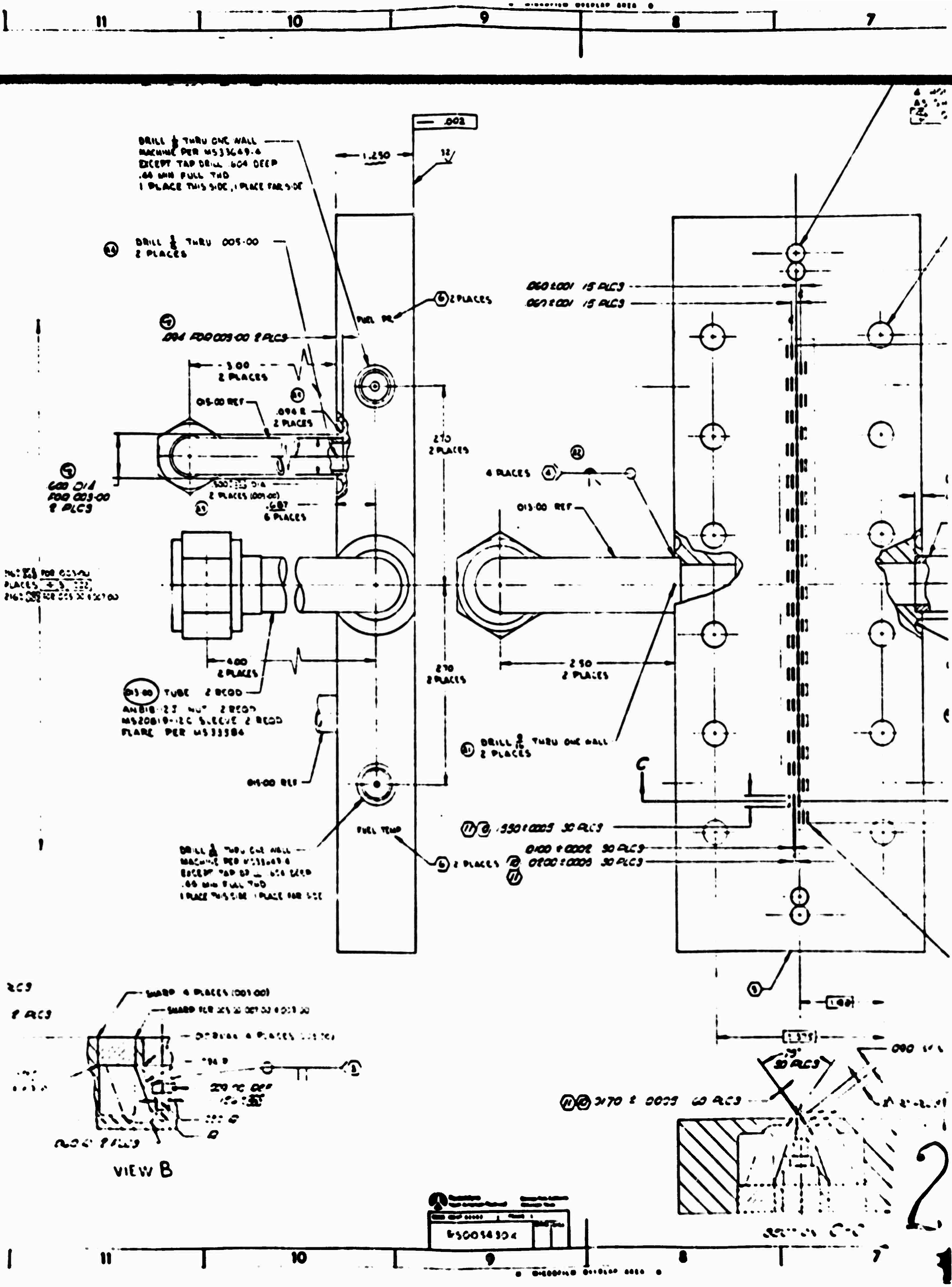

DRILL 1/8 THRU ONE WALL
MACHINE PER MS33649-4
EXCEPT TAP DRILL .604 DEEP
.44 MIN FULL THD
1 PLACE THIS SIDE, 1 PLACE FAR SIDE
DRILL 1/8 THRU 005-00
2 PLACES
FUEL PR
2 PLACES
.094 FOR 003-00 2 PLCS
3.00
2 PLACES
015-00 REF
.094 R
2 PLACES
.600 DIA
FOR 003-00
2 PLCS
2 PLACES (001-00)
.687
6 PLACES
2.70
2 PLACES
4 PLACES
015-00 REF
4.00
2 PLACES
2.50
2 PLACES
TUBE 2 REQD
MS20819-2C SLEEVE 2 REQD
FLARE PER MS33584
DRILL 1/8 THRU ONE WALL
2 PLACES
015-00 REF
FUEL TEMP
2 PLACES
C
.550±.0005 30 PLCS
.0100±.0002 30 PLCS
.0200±.0005 30 PLCS
.060±.001 15 PLCS
.062±.001 15 PLCS
.002
1.250
VIEW B
30 PLCS
.0170±.0005 60 PLCS
2
11
10
9
8
7

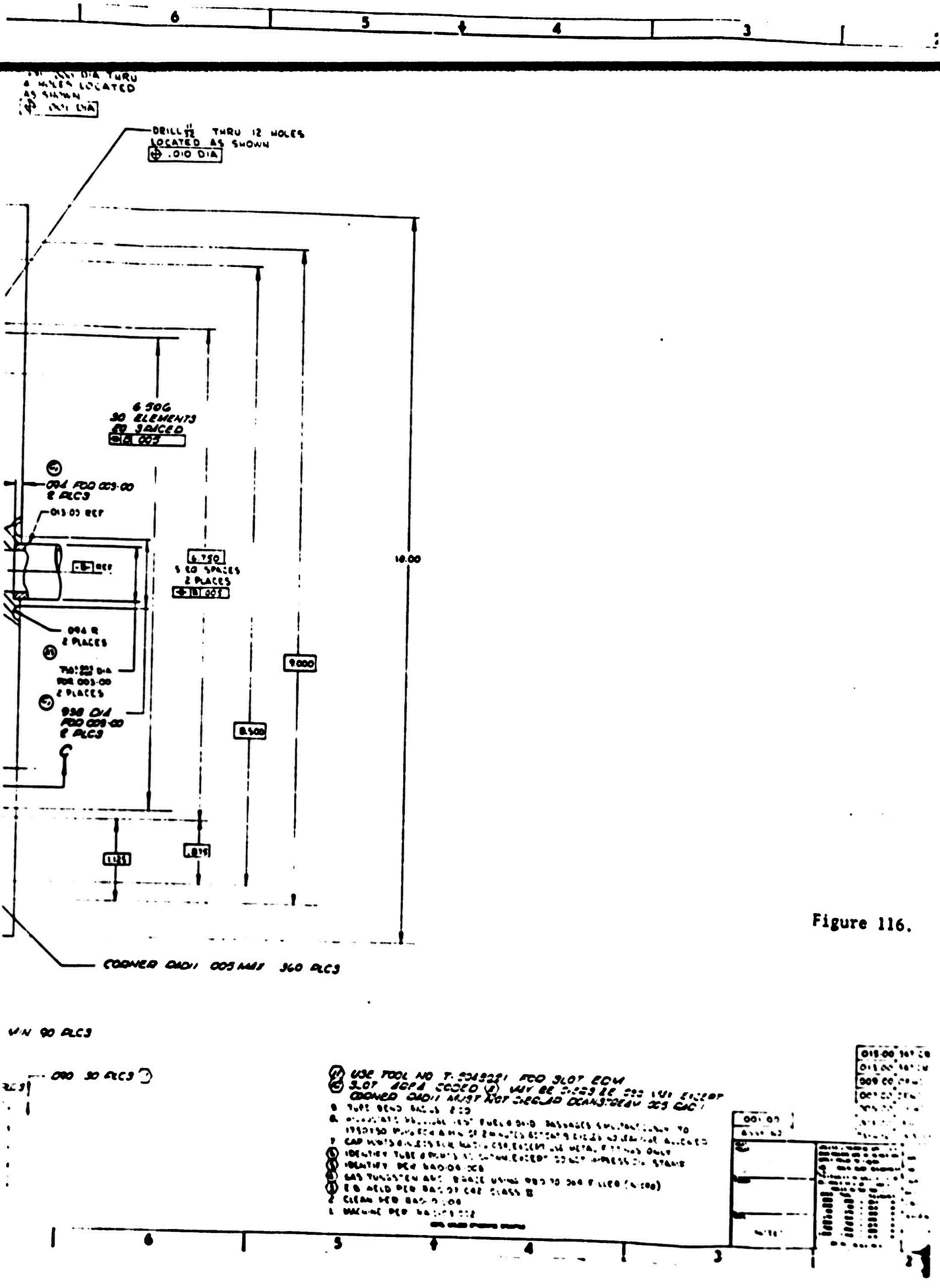

Figure 116.

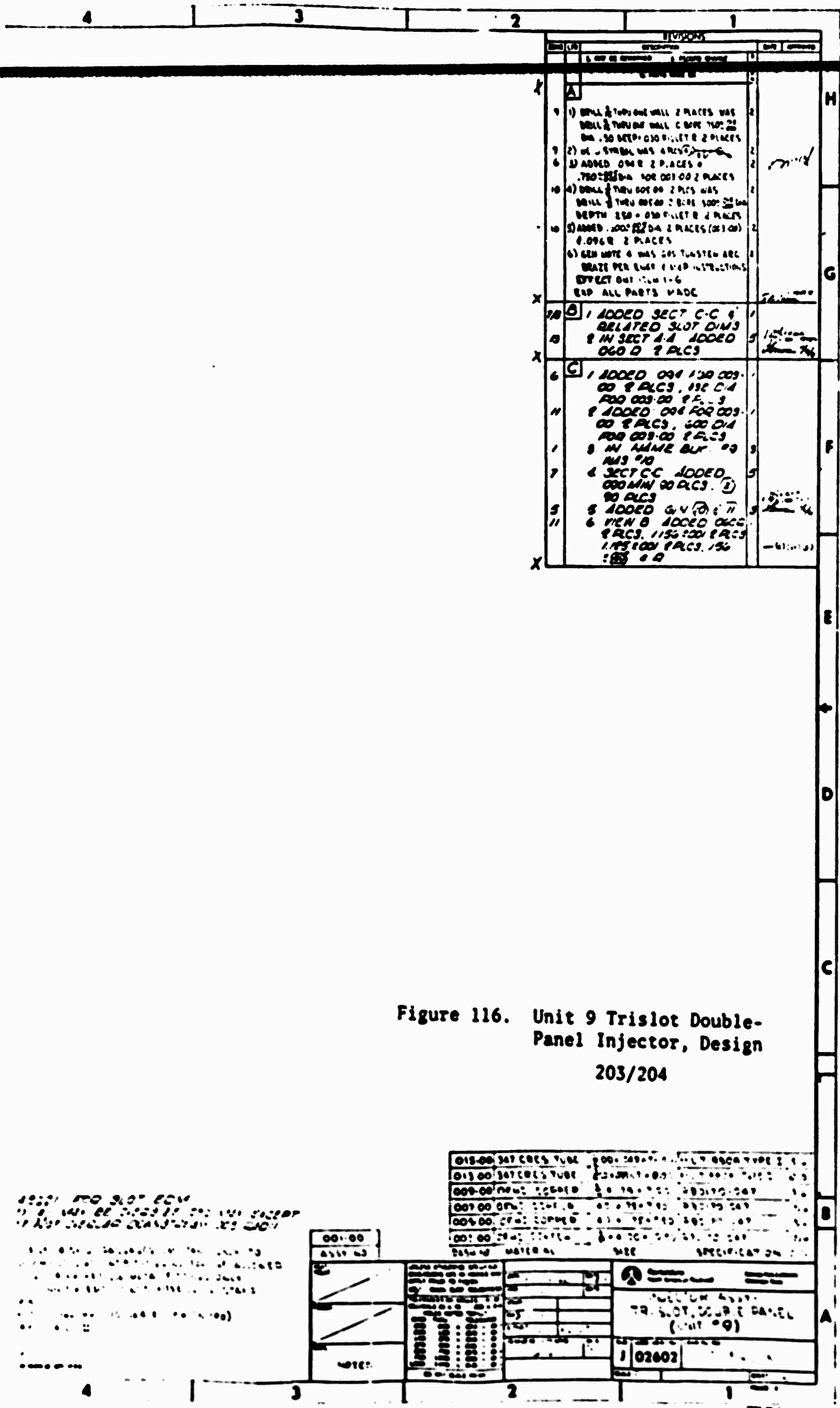

Figure 116. Unit 9 Trislot Double-Panel Injector, Design 203/204

adjacent propellant fans. The injector was fabricated from a single piece of OFHC copper. The orifices were electrodischarge machined using the same bushing-tool location technique developed for the other impinging element-type injectors. The finished injector is shown in Fig. 117 and 118.

The injector was flow calibrated to establish pressure loss characteristics. The calibration results are presented in Fig. 119.

No modifications were made to the injector during the course of the test program.

INJECTOR SINGLE-ELEMENT COLD-FLOW TESTING

The double-panel cold-flow testing was directed at defining the mixing characteristics of various candidate injector element types being evaluated in hot-fire test. The cold-flow testing was used to select optimum element designs prior to hot-fire test and provide modification criteria for the hot-fire test program. The cold-flow test program flow chart and general results are presented in Fig. 120.

The objectives of the cold-flow effort were to: (1) characterize cold-flow mixing efficiency for comparison with measured hot-fire mixing efficiency, (2) characterize the effect of operating variables on cold-flow mixing efficiency for comparison with similar effects on measured hot-fire mixing efficiency, (3) optimize the element configuration prior to the hot-fire testing, and (4) define the test component modification criteria for performance and heat transfer.

For double-panel injectors, the hot-fire characteristic velocity efficiency is equivalent to the hot-fire mixing efficiency because use of gaseous oxygen dictates complete vaporization.

The cold-flow test and data reduction procedures, cold-flow hardware, cold-flow modeling criteria, cold-flow test results, and predicted injector mixing efficiency are discussed sequentially in the following paragraphs. A comparison of the cold-flow and hot-fire mixing efficiency results concludes the cold-flow discussion.

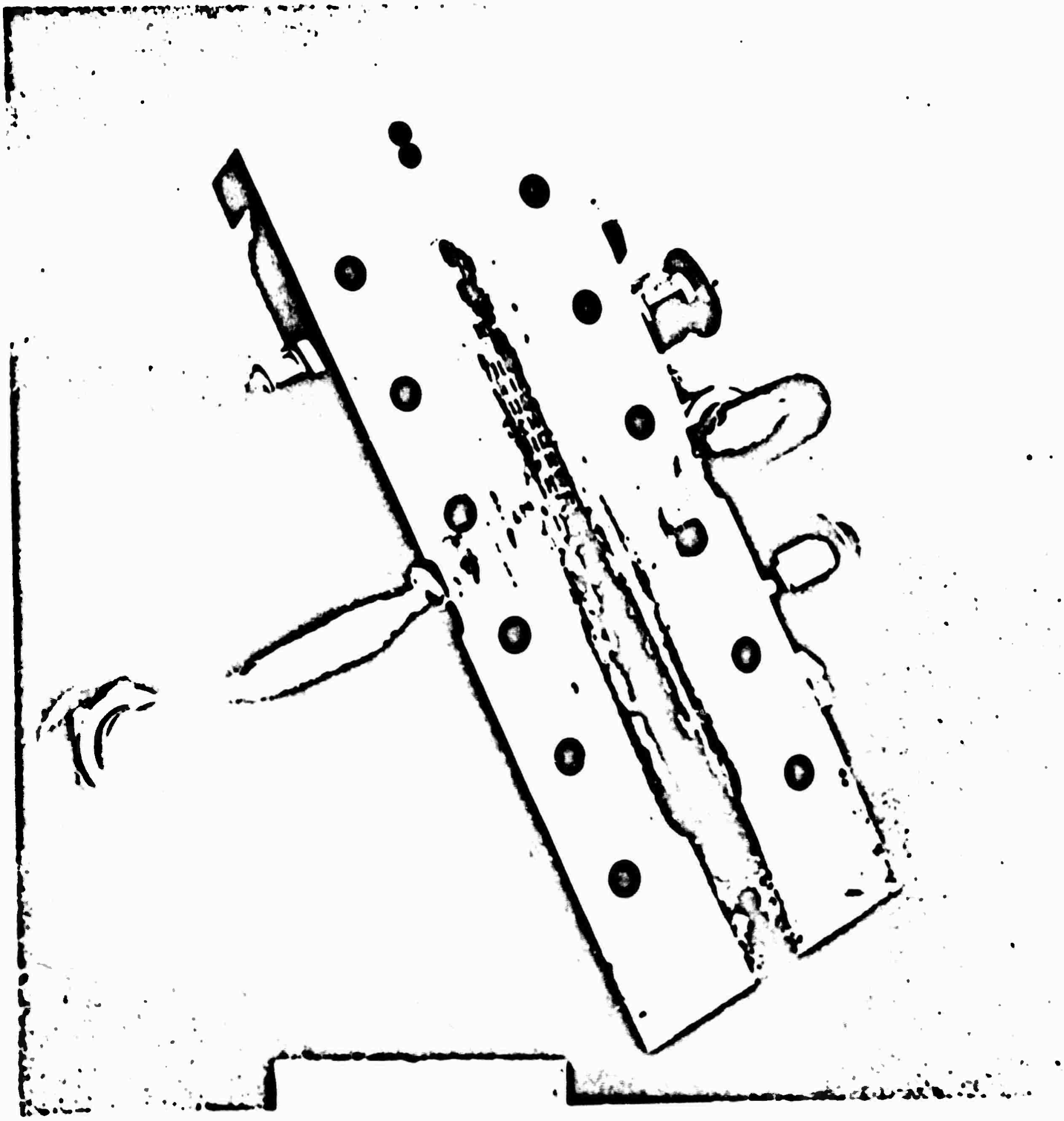

1EH25-12/9/71-1-C2R

Figure 117. Unit 9 Trislot Double-Panel Injector, Posttest

1EH25-12/9/71-1-C2P

Figure 118. Unit 9 Trislot Double-Panel Injector, Posttest, Face and Orifice Detail

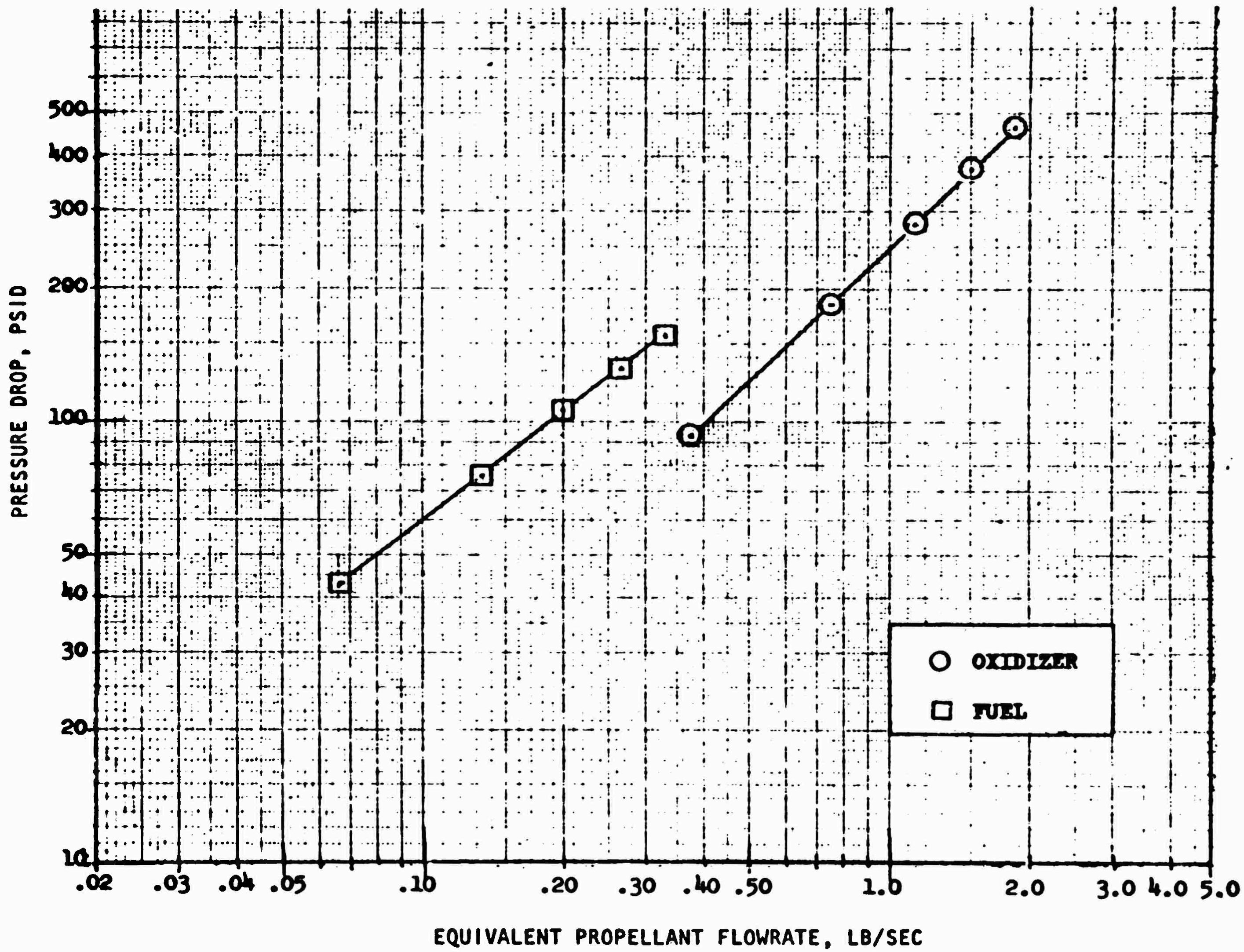

Figure 119. Unit 9 Trislot Injector Predicted Flow Characteristics
(Double-Panel Gas-Gas)

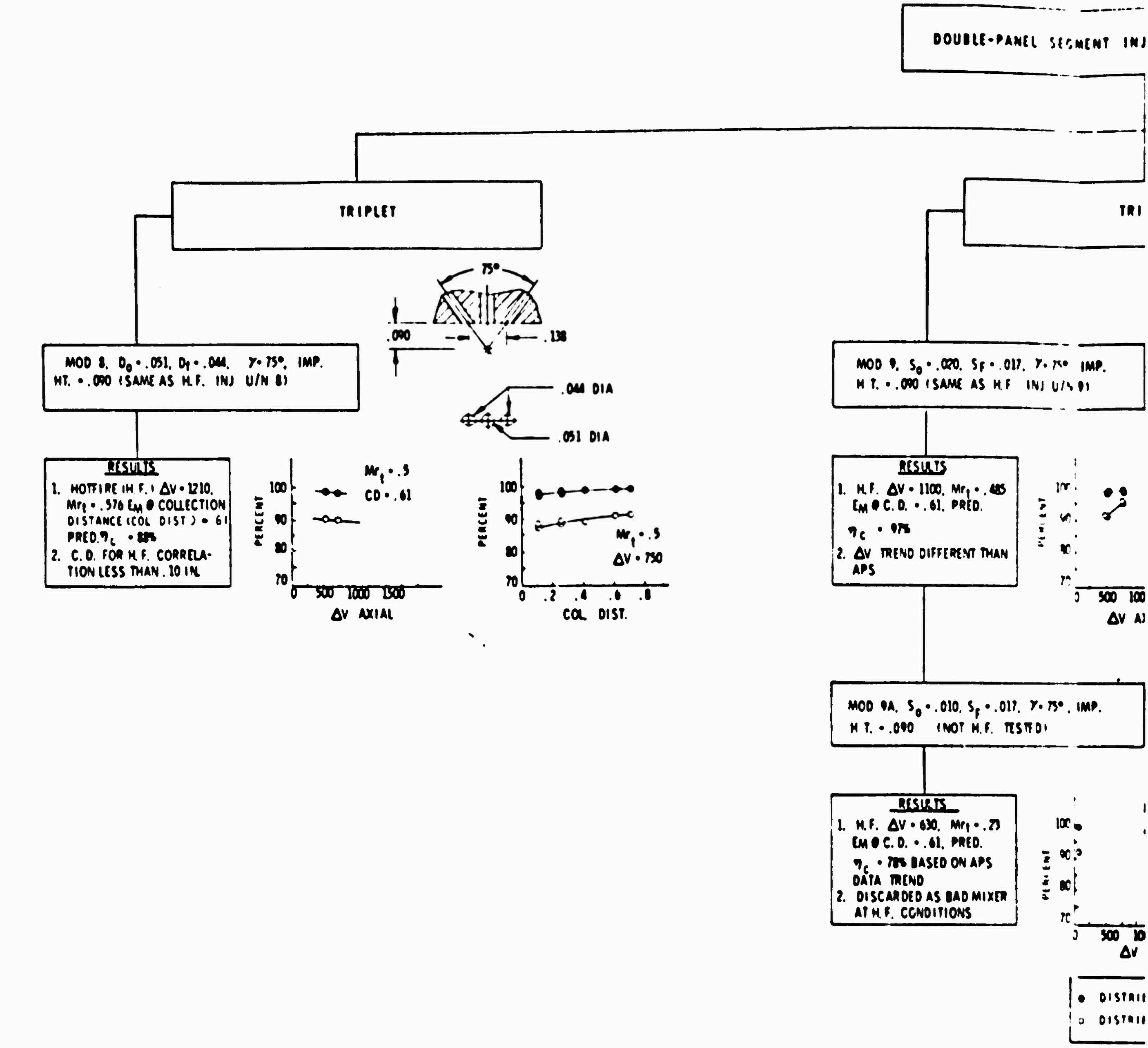
DOUBLE-PANEL SEGMENT INJ
TRIPLET
75°
.090
.138
.044 DIA
.051 DIA
MOD 8, Do = .051, Df = .044, γ = 75°, IMP. HT. = .090 (SAME AS H.F. INJ U/N 8)
RESULTS
1. HOTFIRE (H.F.) ΔV = 1210, Mrf = .576 EM @ COLLECTION DISTANCE (COL DIST) = .61 PRED. ηc = 88%
2. C.D. FOR H.F. CORRELATION LESS THAN .10 IN.
PERCENT
100
90
80
70
0 500 1000 1500
ΔV AXIAL
Mrf = .5
CD = .61
0 .2 .4 .6 .8
COL DIST.
Mrf = .5
ΔV = 750
TRI
MOD 9, So = .020, Sf = .017, γ = 75° IMP. H.T. = .090 (SAME AS H.F. INJ U/N 9)
RESULTS
1. H.F. ΔV = 1100, Mrf = .485 EM @ C.D. = .61, PRED. ηc = 97%
2. ΔV TREND DIFFERENT THAN APS
500 100
ΔV A
MOD 9A, So = .010, Sf = .017, γ = 75°, IMP. H.T. = .090 (NOT H.F. TESTED)
RESULTS
1. H.F. ΔV = 630, Mrf = .23 EM @ C.D. = .61, PRED. ηc = 78% BASED ON APS DATA TREND
2. DISCARDED AS BAD MIXER AT H.F. CONDITIONS
100
90
80
70
500 10
ΔV
● DISTRI
○ DISTRI

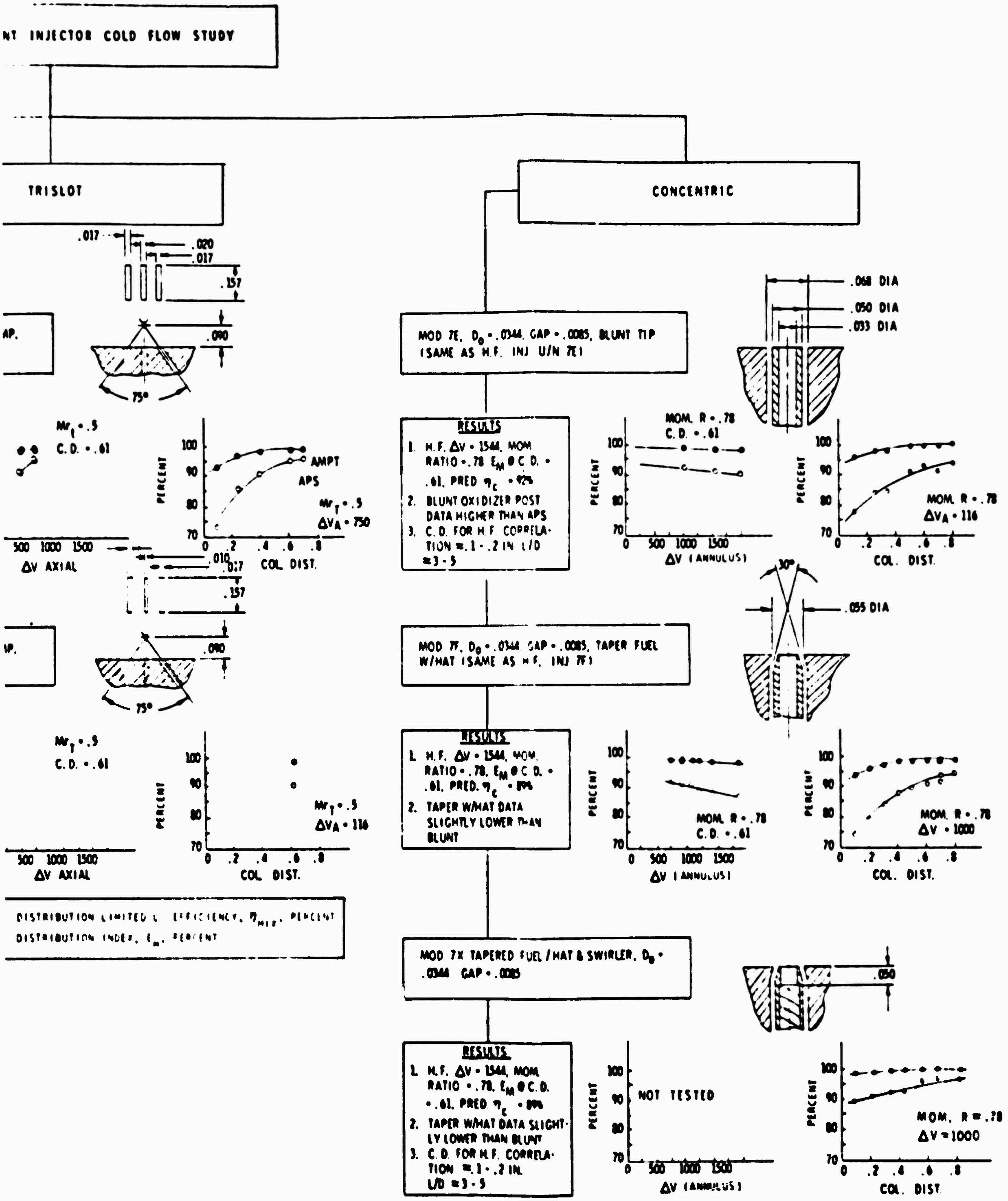

Figure 120. Double-Panel Segment Injector Cold-Flow Study

Comparison of variable effects on cold-flow and hot-fire mixing efficiency are discussed later in the concentric element hot-fire results section (page 243).

Cold-Flow Test and Data Reduction Procedures

Single-element cold-flow experimentation with nonreactive propellant simulant gases has been proved to be a reliable, expedient, and inexpensive means of obtaining an estimate of the performance level of a full-scale injector design (Ref. 6).

Cold-flow experimentation was performed at a specially prepared facility (Ref. 6) that had capability for cold-flow injector modeling experiments that covered a wide range of simulated chamber pressures and flowrates. Conventional gas sampling techniques were used for the measurement of gas flow distribution.

Cold-flow gas distribution results were used for analytical prediction of an injector mixing uniformity index, termed E_m, and combustion efficiency limited by injector mixing, $\eta_{c^* \, mix}$. Definitions of E_m and $\eta_{c^* \, mix}$ were presented previously in the Single-Panel Cold-Flow section (pages 87 and 88).

Cold-Flow Hardware

The results reported in Ref. 7 and 8 indicate that injector element size has a significant effect on predicted performance. Because the characteristic dimensions of candidate AMPT elements are about a factor of 4 less than the characteristic dimensions of elements that had been cold-flow tested in another program (Ref. 6), fabrication and cold-flow testing hardware representative of the AMPT injector-element sizes was considered necessary. Accordingly, emphasis was placed on cold-flow tests utilizing single-element configurations identical to individual element designs to be hot-fire tested (or considered for hot-fire testing) in full-scale candidate injectors. It was possible to use identical size elements because of available accurate gaseous sonic venturi meters.

The various single-element configurations which were cold-flow tested are shown in Fig. 121, along with their characteristic dimensions. These were: (1) the (F-O-F) triplet, (2) the trislot, (3) the blunt tip coaxial, (4) the coaxial with a flared

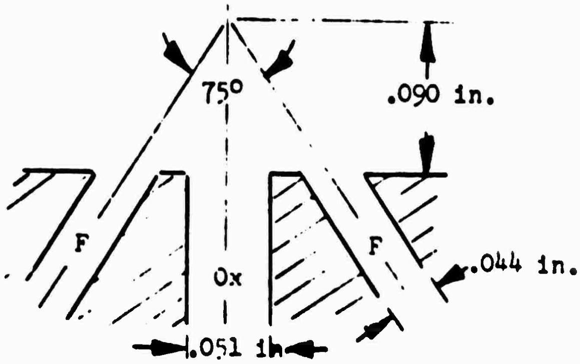

Modeling Criteria:

$$Mr_t = \frac{\dot{W}_f (V_f \sin 37.5^\circ)}{\dot{W}_o V_o}$$

$$\Delta V_{ax} = (V_f \cos 37.5^\circ) - V_o$$

Triplet, Unit 8

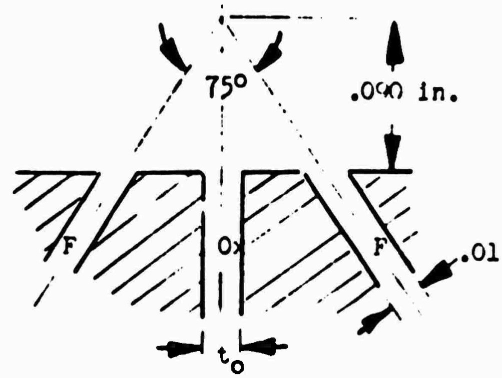

Modeling Criteria:

$$Mr_t = \dot{W}_f (V_f \sin 37.5^\circ)/\dot{W}_o V_o$$

$$\Delta V_{ax} = (V_f \cos 37.5^\circ) - V_o$$

Trislot, Unit 9

Mod 1 t_o = .010 in.
Mod 2 t_o = .020 in.

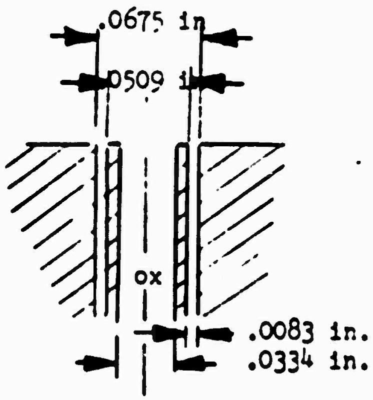

Modeling Criteria:

$$Mr_{tot} = \frac{\dot{W}_f V_f}{\dot{W}_o V_o}$$

$$\Delta V_{annul} = V_f - V_o$$

Blunt-Tip Concentric, Unit 7E

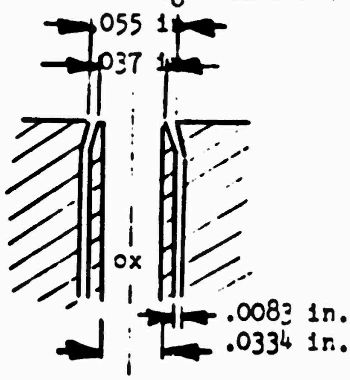

Modeling Criteria:

$$Mr_{tot} = \frac{\dot{W}_f V_f}{\dot{W}_o V_o}$$

$$\Delta V_{annul} = V_f - V_o$$

Concentric With Hat, Unit 7F

Figure 121. Single-Element Cold-Flow Elements and Modeling Criteria for Double-Panel Injectors

inner fuel annulus and a "hat" on the outer fuel annulus, and (5) the flared coaxial with hat plus a swirler vane in the oxidizer post (not shown in Fig. 121). The flared coaxial with "hat" configuration was designed to provide directed transverse momentum while maintaining high axial ΔV at the injector face at injection rates identical to those in the blunt-tip coaxial. The fifth configuration was fabricated by adding an oxidizer tube swirler to the "coaxial with hat" design. The coaxial with hat configuration shown in Fig. 121 was modified to include a 180-degree, two-vane swirler in the oxidizer tube. The objective of this modification was to determine if any increase in performance level over that obtained with both the blunt-tip coaxial and hat coaxial modification could be achieved. The actual test hardware is shown in Fig. 122 (triplet), Fig. 123 and 124 (concentric), and Fig. 125 (trislot).

Cold-Flow Modeling Criteria

For direct comparison, elements were cold-flow tested at the same flow conditions experienced during hot-fire test. However, cold-flow tests employed ambient temperature helium as the fuel (GH_2) simulant (the oxidizer, GO_2, in cold-flow and hot-fire testing being the same) and, therefore, exact flow condition simulation was not possible for most cases. Thus, appropriate modeling criteria, described in the following paragraphs, were selected to best relate cold-flow testing to hot-fire conditions.

Cold-flow mixing correlations, developed in a previous program for the trislot element (Ref. 7), showed a correspondence between mixing efficiency and cold-flow test conditions defined as: (1) transverse momentum ratio, Mr_t, and (2) axial velocity difference, ΔV_{ax} between the fuel and oxidizer gases. These test conditions are further defined in Fig. 121. Because the triplet element bears some similarity in geometry to the trislot element, these modeling criteria (i.e., Mr_t and ΔV_{ax}) were employed for both triplet and trislot cold-flow tests.

For concentric elements with internally flared oxidizer tubes, similar cold-flow mixing correlations (developed in Ref. 8) showed a relationship between mixing efficiency, E_m, and the flow conditions, Mr_t and ΔV_{ax}. However, because the blunt tip concentric element exhibited no transverse momentum, comparison between the

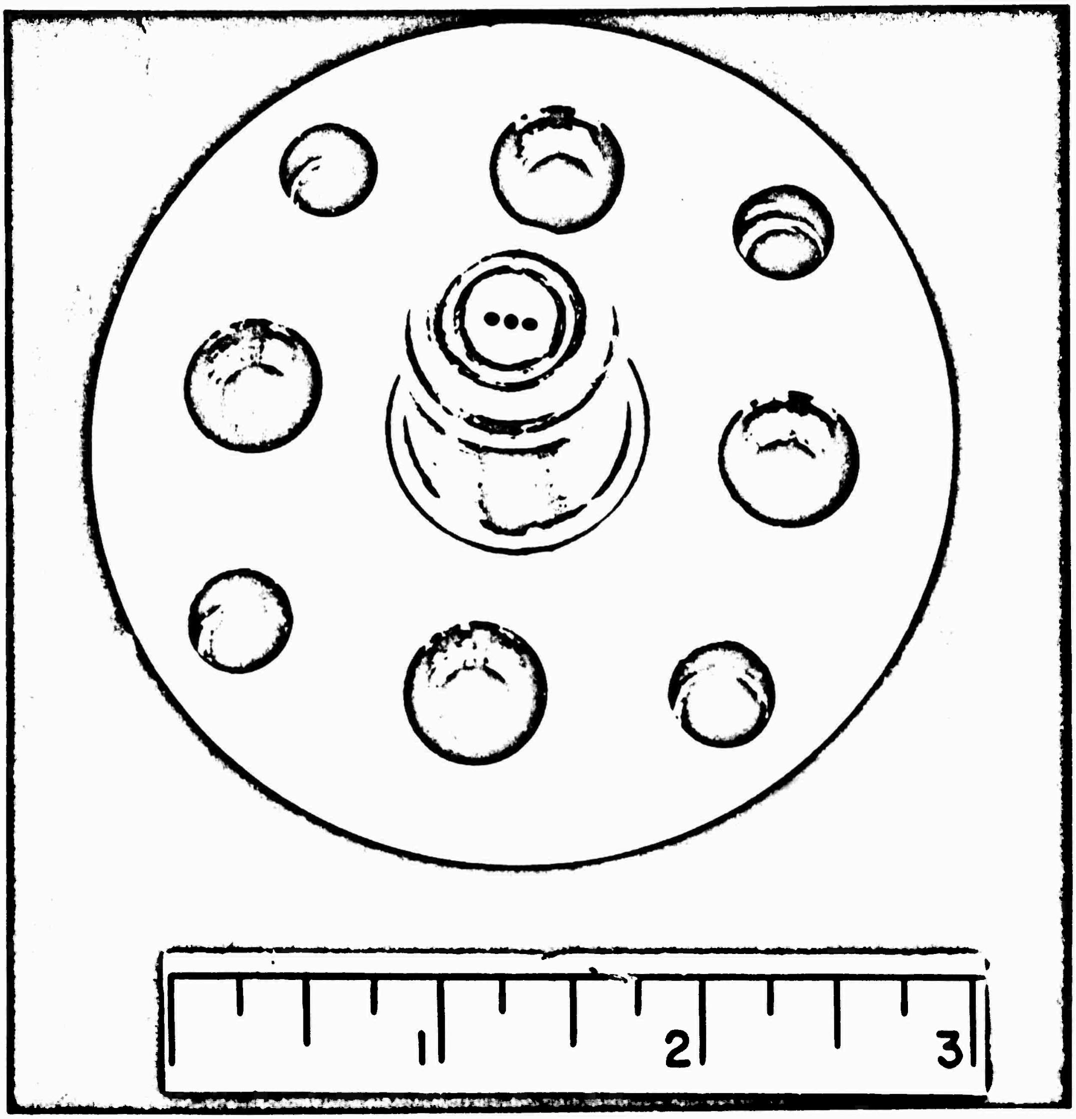

1EH25-12/9/71-1-C3E

Figure 122. Triplet Cold-Flow Element, Double-Panel

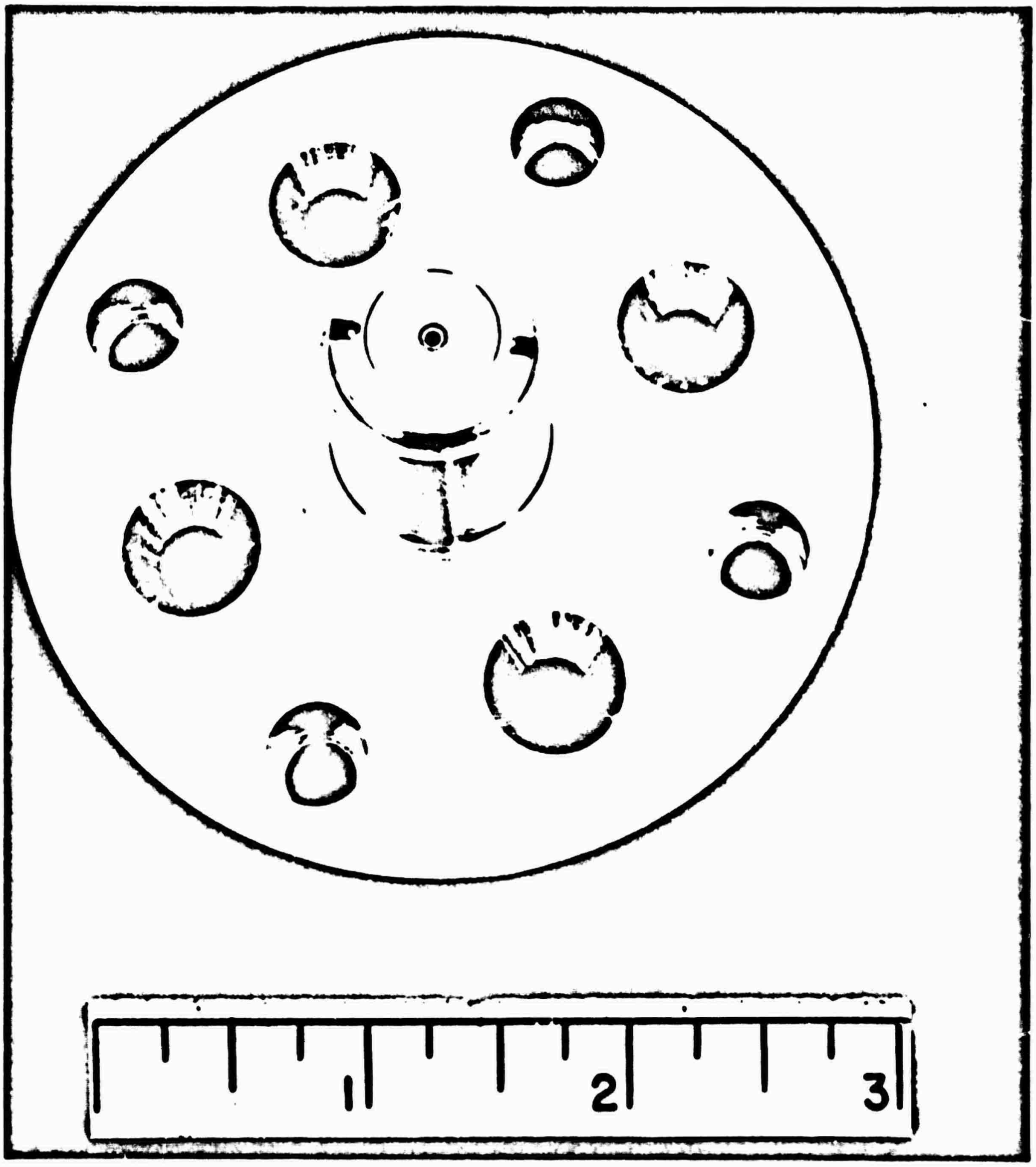

1EH25-12/9/71-1-C3H

Figure 123. Concentric Cold-Flow Element, Double-Panel (Assembled)

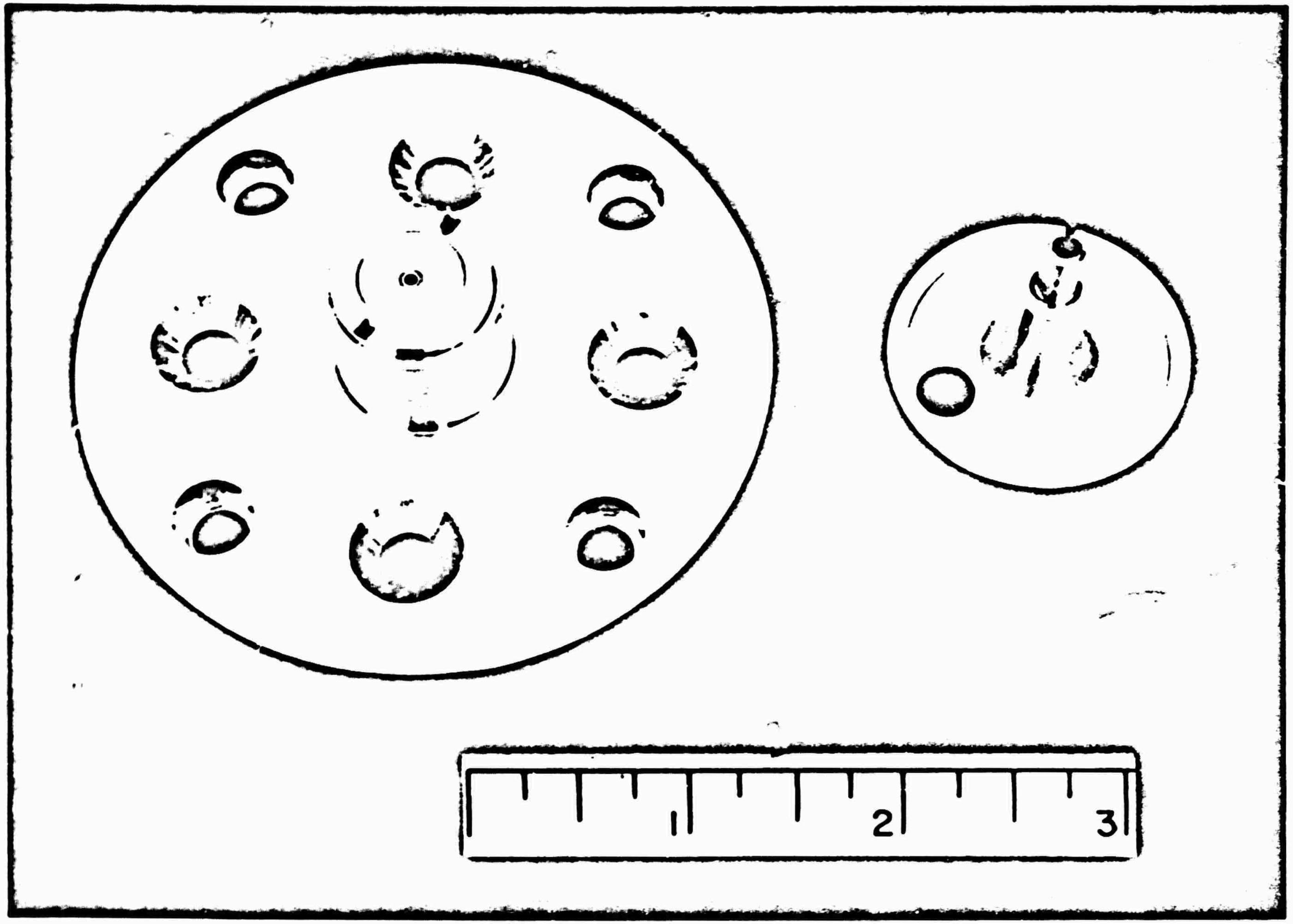

1EH25-12/9/71-1-C3G

Figure 124. Concentric Cold-Flow Element, Double-Panel (Disassembled)

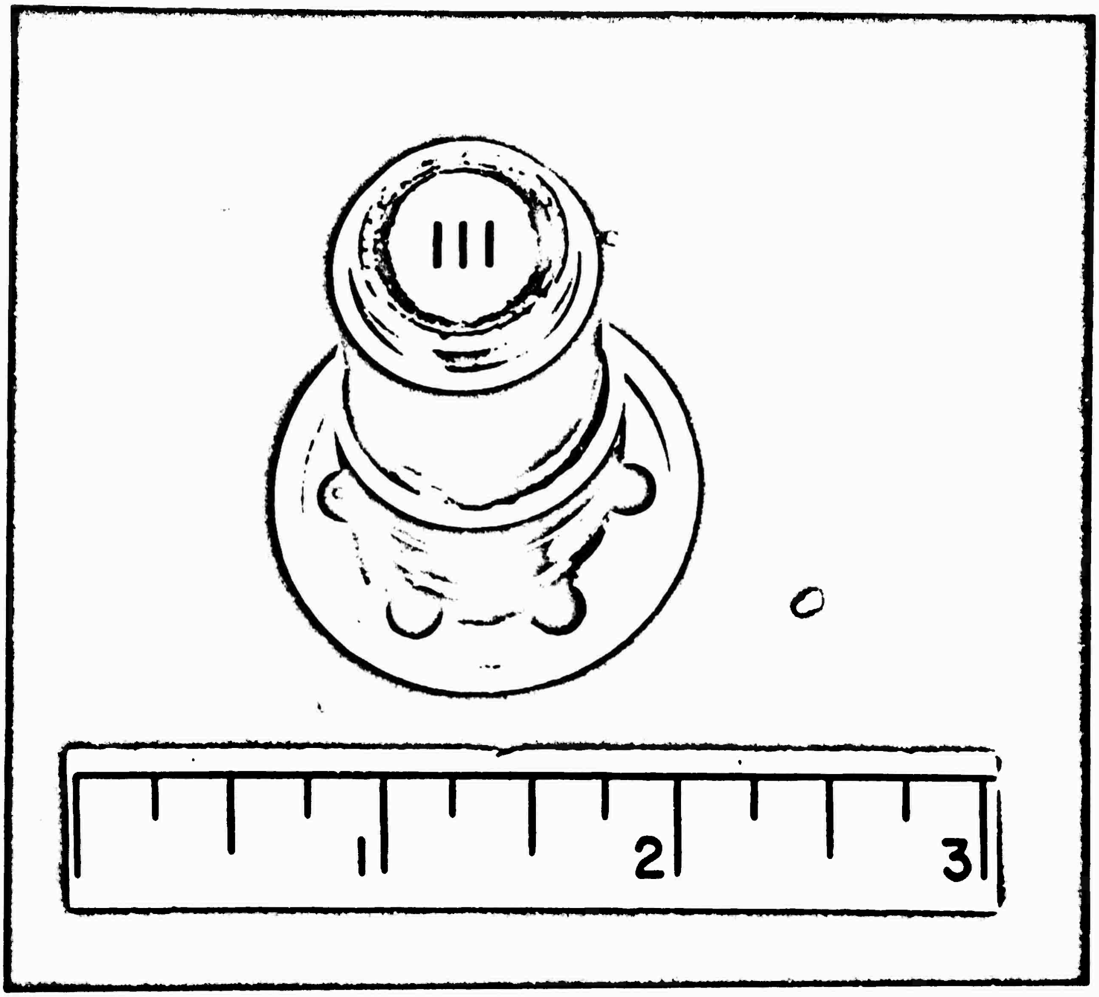

1EH25-12/9/71-1-C3B

Figure 125. Trislot Cold-Flow Element, Double-Panel

concentric elements was based on the modeling criteria of total momentum ratio, Mr_{tot}, and annulus velocity difference, $\Delta V_{annulus}$. These test conditions are defined further in Fig. 121.

Cold-Flow Test Results

For all element types, tests were made to define mixing efficiency at varying collection distances. Additionally, cold-flow tests for the triplet and trislot elements were made to determine the effect of ΔV_{ax} on mixing at fixed collection distance and Mr_t. Likewise, similar tests for the concentric elements were made to determine the effect of $\Delta V_{annulus}$ on mixing at fixed collection distance and Mr_{tot}.

An effort was made to simulate hot-fire conditions, defined by the previously described modeling criteria, as much as possible in cold-flow testing*. For modeling of ΔV effects, the experimental setup did not permit independent evaluation of ΔV because both ΔV and flowrate were varied simultaneously. A summary of the gas/gas cold-flow test data obtained with candidate element types is presented in Table 13.

Effect of Collection Distance. The effect of collection on mixing for each of the different elements is presented in Fig. 126 through 130. η_{E_m} and $\eta_{c^* \, mix}$ are shown and cold-flow test conditions are noted in the figures. With two exceptions, all elements showed a sharp decrease in mixing efficiency as collection distance decreased toward zero. The notable exceptions were the triplet element and concentric with swirler element, which showed only a very small decrease in combustion efficiency as collection distance approached zero. The $\Delta V_{annulus}$ and flowrate/element on the modified tip concentric and concentric with swirler was less than that of the blunt tip concentric for the collection distance tests. Therefore, the modified tip concentric data had an E_m comparable to that of the blunt tip.

*Hot-fire values of ΔV and transverse (or total) momentum ratio were calculated for the following conditions:

P_c, psia	950	Oxidizer Flowrate, lb/sec	1.931
Fuel Injector Temperature, R	1100	Fuel Flowrate, lb/sec	0.349
Oxidizer Temperature, R	420		

TABLE 13. DATA SUMMARY FOR DOUBLE-PANEL INJECTOR ELEMENT

Injector	Spacer	Collection Distance	mr_t	mr_{tot}	ΔV_{ax} fps	ΔV_{anul} fps	E_m	η_{c*}	$W_{o_{sim}}$ lb/sec	$W_{f_{sim}}$ lb/sec
Triplet, Unit 8	0.7	0.61"	0.50		757		90.1	98.8	.001713	.00066
	0.2	0.11	0.5		757		88.1	98.3	"	"
	0.35	0.26	"		"		88.9	98.6	"	"
	0.5	0.41	"		"		89.4	98.9	"	"
	0.7	0.61	"		574		90.3	98.9	.001298	.0005
	0.8	0.71	"		757		90.9	99.0	.001713	.00066
	0.2	0.11	"		"		88.7	98.5	.001713	.00066
	0.35	0.26	"		"		88.7	98.5	.001713	.00066
	0.14	0.05	"		"		86.4	97.6	"	"
Trislot #1	0.7	0.61	0.50		116		91.8	99.1	.00166	.001
Trislot #2, Unit 9	0.7	0.61	0.50		765		95.2	99.5	.00321	.00135
	0.7	0.61	"		566		91.4	98.8	.00238	.0010
	"	"	"		765		95.8	99.5	.00321	.00135
	"	"	"		566		91.3	98.9	.00238	.0010
	0.2	0.11	"		765		73.5	92.4	.00321	.00135
	0.35	0.26	"		"		86.6	97.6	"	"
	0.50	0.41	"		"		91.1	99.1	"	"
	0.80	0.71	"		"		95.1	99.6	"	"
Blunt Tip Coax Unit 7E	0.7	0.7	0	0.777	1554	1554	91.2	98.6	.00115	.000476
	0.7	0.7		"	1000	1000	92.8	99.2	.000741	.000306
	"	0.7		"	2000	2000	90.3	98.5	.001483	.000613
	0.25	0.25		"	1554	1554	83.7	9[illegible].9	.00115	.000476
	0.50	0.5		"	"	"	91.4	98.9	"	"
	0.60	0.6		"	"	"	93.0	99.1	"	"
	0.80	0.8		"	"	"	93.4	99.2	"	"
	0.35	0.35		"	"	"	83.7	96.6	"	"
	0.10	0.10		"	"	"	76.9	93.1	"	"
Coax With Mat, Unit 7F	0.70	0.70	0.2394	0.777	2050	1554	87.6	98.5	.00115	.000476
	"			"	1322	1000	89.7	98.9	.000741	.000306
	"			"	2640	2000	86.7	98.1	.001483	.000613
	"			"	1317	1000	92.4	99.4	.001473	.00061
	"			"	1075	816	92.0	99.1	.00121	.0005
	"			"	1512	1144	90.6	99.1	.001694	.0007
	"			"	1728	1312	88.7	98.5	.001933	.0008
	0.10	0.10	0.2394	0.777	1317	1000	74.1	93.0	.001473	.00061
	0.25	0.25		"	"	"	83.4	96.6	"	"
	0.35	0.35		"	"	"	87.9	98.1	"	"
	0.50	0.50		"	"	"	89.9	98.8	"	"
	0.60	0.60		"	"	"	90.8	99.1	"	"
	0.80	0.80		"	"	"	95.0	99.9	"	"
	0.20	0.20		"	"	"	79.6	94.8	"	"
	0.70	0.70		"	"	"	94.9	99.7	"	"
Coax With Mat and Swirler	0.70	0.70		0.777		1000	96.7	99.9	.001473	.00061
	0.70	0.70		"		"	96.1	99.8	.001473	.00061
	0.60	0.60		"		"	97.0	99.9	"	"
	0.50	0.50		"		"	96.8	99.9	"	"
	0.350	0.35		"		"	93.5	99.5	"	"
	0.250	0.25		"		"	92.4	99.3	"	"
	0.200	0.20		"		"	99.3	98.9	"	"
	0.100	0.10		"		"	89.3	98.9	"	"

$W_{o_{sim}}$ lb/sec	$W_{f_{sim}}$ lb/sec	Test No.	Date	
.001713	.00066	2	10-19	
"	"	2	10-27	
"	"	3	"	
"	"	4	"	
.001298	.0005	1	10-29	
.001713	.00066	5	10-29	
.001713	.00066	2R	11-1	
.001713	.00066	3R	11-1	
"	"	2R	11-15	
.00166	.001	1	10-7	
.00321	.00135	1	10-14	
.00238	.0010	2	10-14	
.00321	.00135	1	10-19	
.00238	.0010	1	10-27	
.00321	.00135	2	"	
"	"	3	"	
"	"	4	"	
"	"	5	"	
.00115	.000476	1	10-22	Above Sonic
.000741	.000306	2	"	"
.001483	.000613	3	"	"
.00115	.000476	1	10-26	"
"	"	1A	"	"
"	"	1B	"	"
"	"	1C	"	"
"	"	1D	"	"
"	"	1E	"	"
.00115	.000476	1	11-1	"
.000741	.000306	2	"	"
.001483	.000613	3	"	"
.001473	.00061	4	"	Sub-Sonic
.00121	.0005	2	11-2	"
.001694	.0007	3	"	"
.001933	.0008	4	"	Just = to Sonic
.001473	.00061	1	11-3	
"	"	2	"	
"	"	3	"	
"	"	4	"	
"	"	5	"	
"	"	6	"	
"	"	7	"	
"	"	8	"	
.001473	.00061	1A	11-17	
.001473	.00061	1B	"	
"	"	2	"	
"	"	3	"	
"	"	4	"	
"	"	5	"	
"	"	6	"	
"	"	7	"	

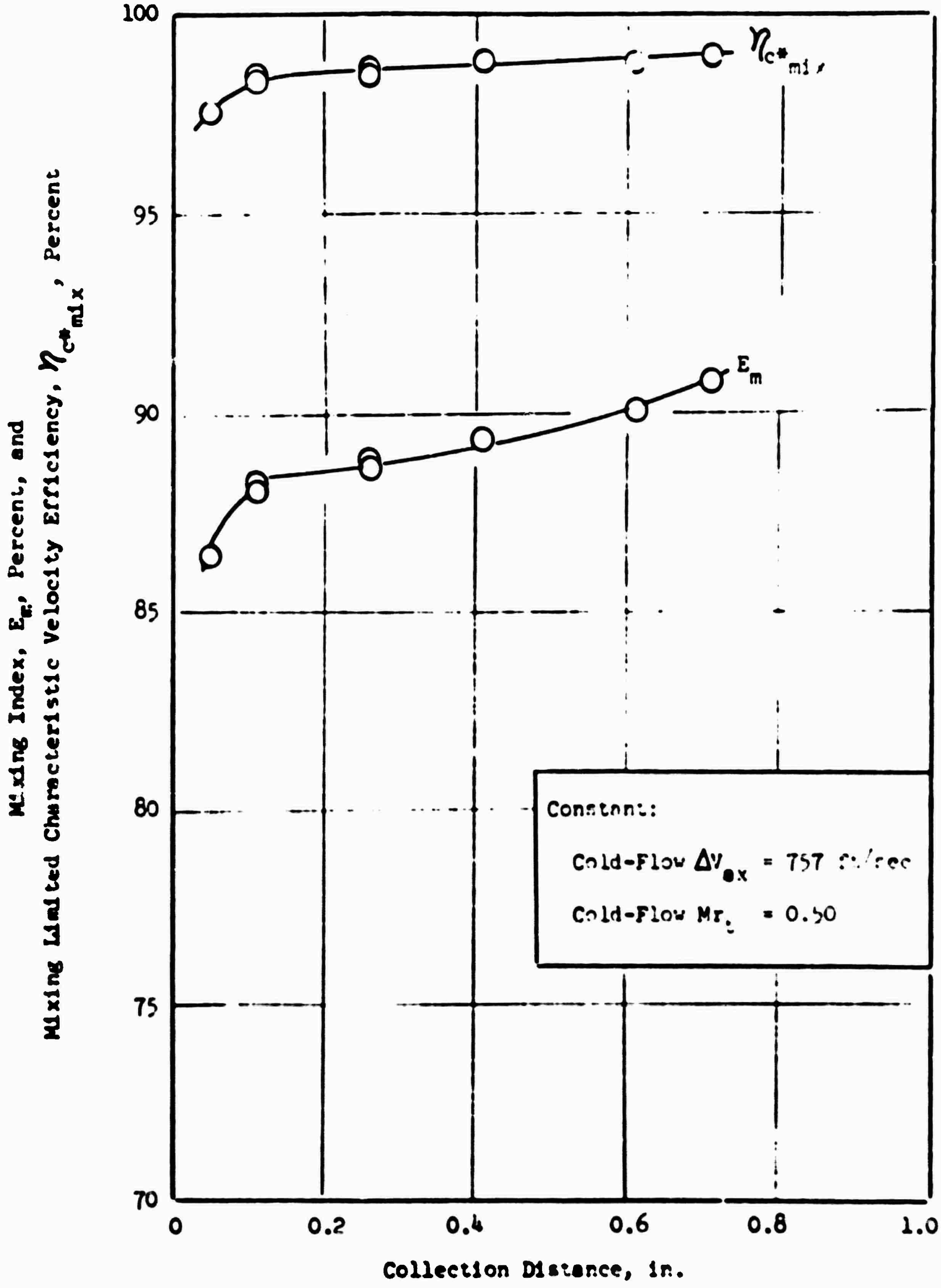

Figure 12b. Triplet Element Cold Flow, Effect of Collection Distance on Mixing

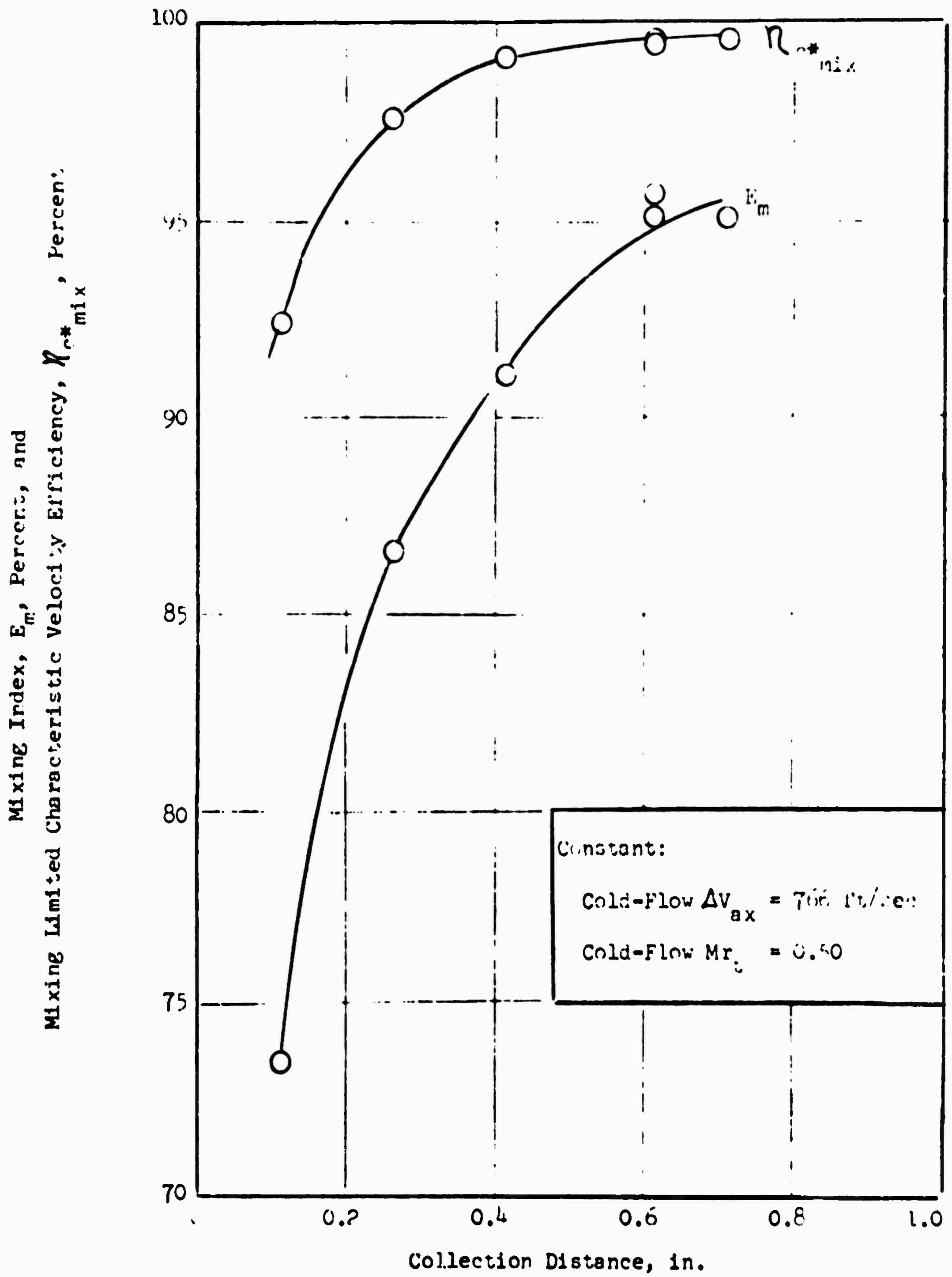

Figure 127. Trislot Element Cold Flow, Effect of Collection Distance on Mixing

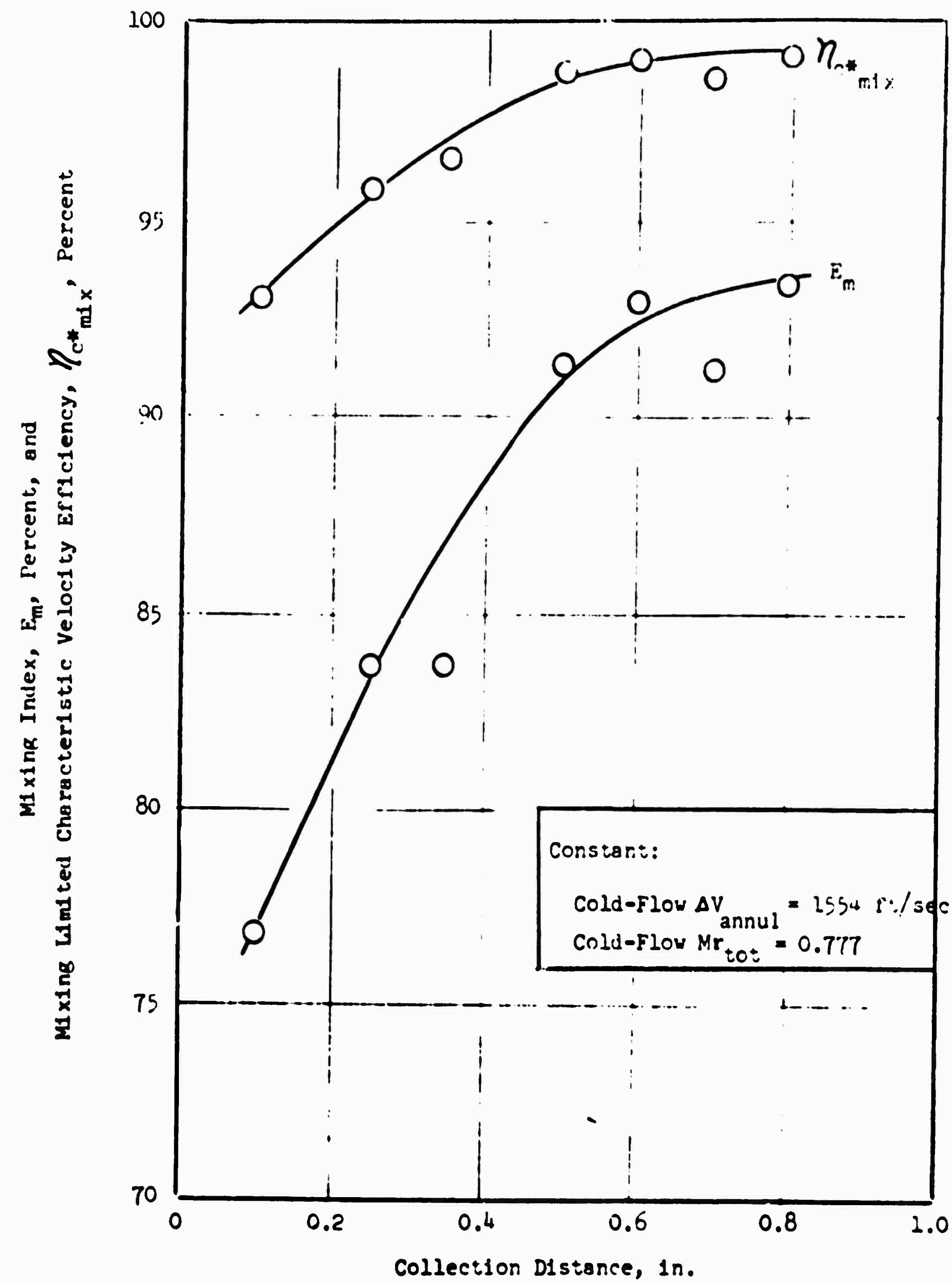

Figure 128. Concentric Element Cold Flow, Effect of Collection Distance on Mixing

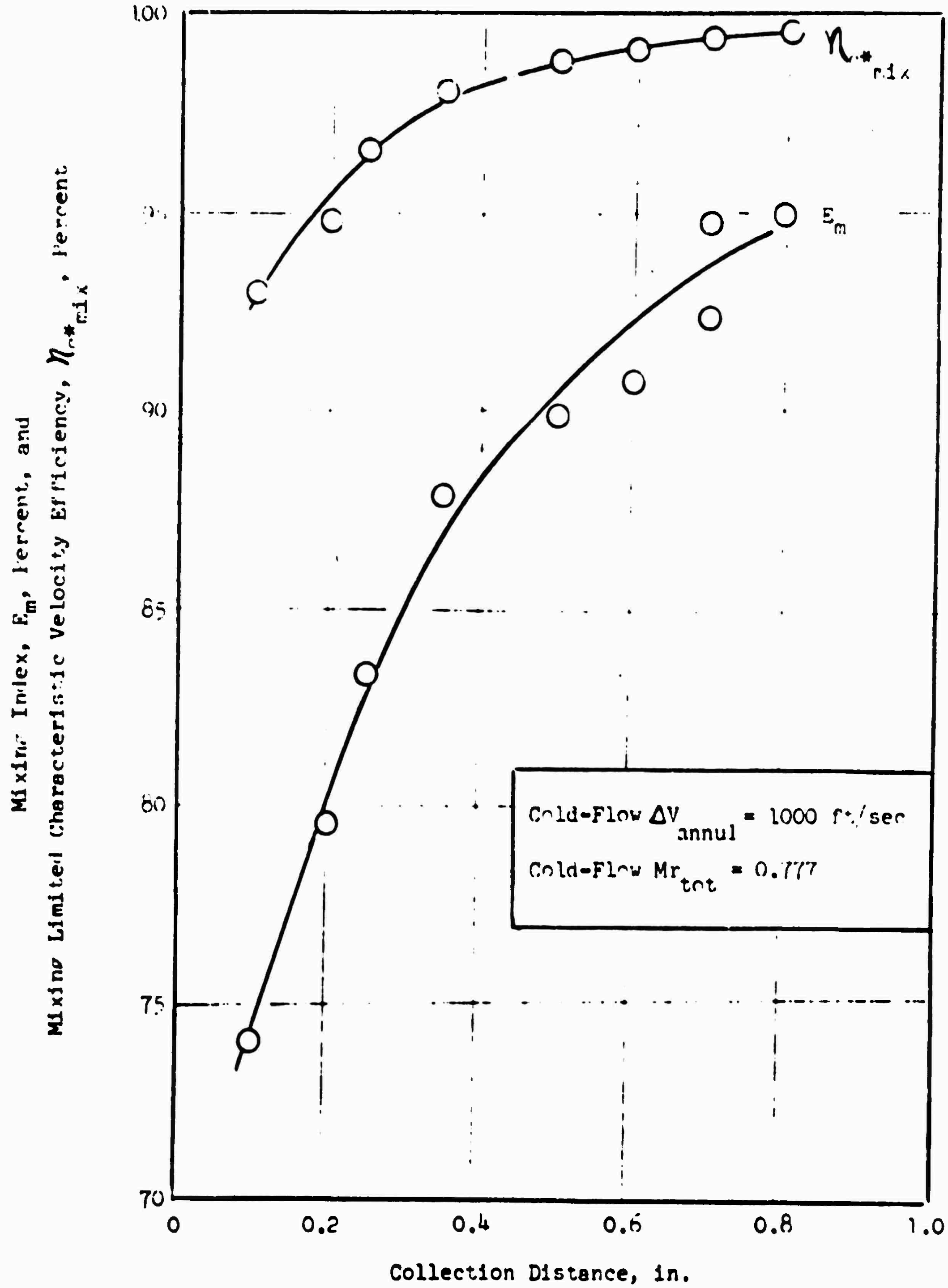

Figure 129. Concentric Element With Hat Cold Flow, Effect of Collection Distance on Mixing

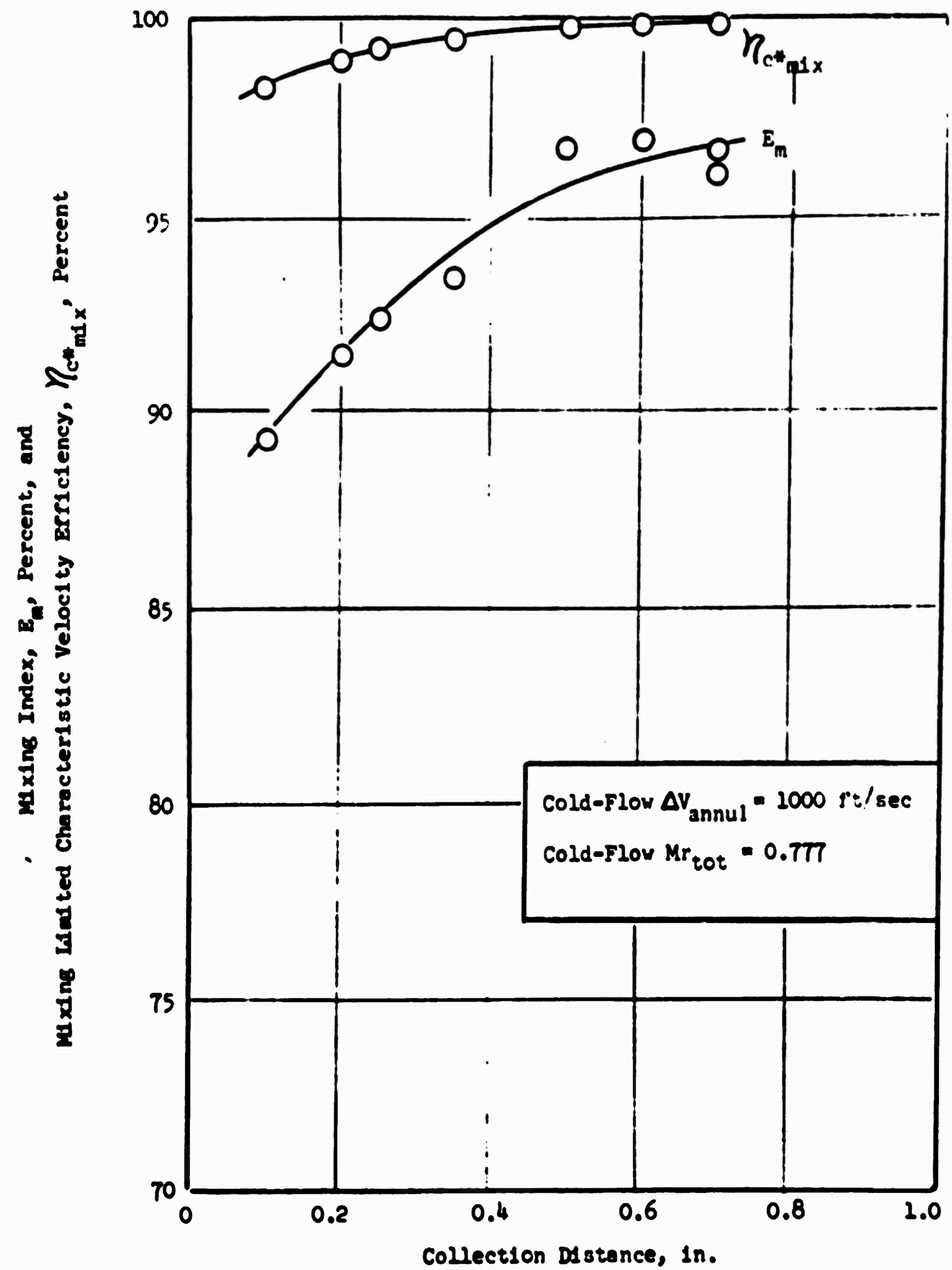

Figure 130. Concentric Element With Hat and Swirler Cold Flow, Effect of Collection Distance on Mixing

element because lower $\Delta V_{annulus}$ and flowrate/element tended to increase E_m. The concentric with swirler results, as shown in Fig. 130, indicated that the coaxial element with hat and swirler was a high performer over a wide range of collection distances. This configuration appeared to offer a significant advantage over either the blunt-tip coaxial or the coaxial with the hat configurations.

Combined Effect of ΔV and Flowrate. The effect of ΔV and flowrate on mixing at a fixed collection distance* is shown for the various elements in Fig. 131 through 134. Flowrate decreased as ΔV decreased for all cold-flow tests on an approximate 1 to 1 relationship (i.e., halving the ΔV halved the flowrate/element). Both actual cold-flow and design hot-fire test conditions for 950-psia chamber pressure operation are noted on the plots. The level of mixing obtained was characterized by both E_m and $\eta_{c^*\ mix}$ (defined previously).

Results obtained using the triplet and the trislot are shown in Fig. 131 and 132, respectively. Mixing efficiency was found to decrease with increased ΔV_{ax}/flowrate for the triplet, whereas the trend was reversed for the trislot. The increase in E_m with increasing ΔV_{ax}/flowrate for the trislot (see Fig. 132) was in contrast with the results of Ref. 7. These data were reproduced successfully, however.

For the blunt-tip coaxial element, the effect of $\Delta V_{annulus}$/flowrate on E_m is shown in Fig. 133. The effect of $\Delta V_{annulus}$/flowrate on E_m for the coaxial with the flared inside fuel annulus and the hat is shown in Fig. 134. Both concentric elements showed the same data trends of decreasing E_m with increasing $\Delta V_{annulus}$/flowrate at constant Mr_{tot}. The level of mixing obtained with the blunt-tip was slightly higher than that for the modified tip. For equivalent GH_2 annulus velocities (as tested in cold flow), the exit GH_2 velocity for the blunt tip was lower than that for the modified tip due to the larger exit area (Fig. 121). Because lower exit GH_2 velocities lower the velocity difference referenced to the exit, the increased performance of the blunt tip may be associated with lower exit GH_2 velocity conditions.

*Collection distance is defined as distance from the impingement point.

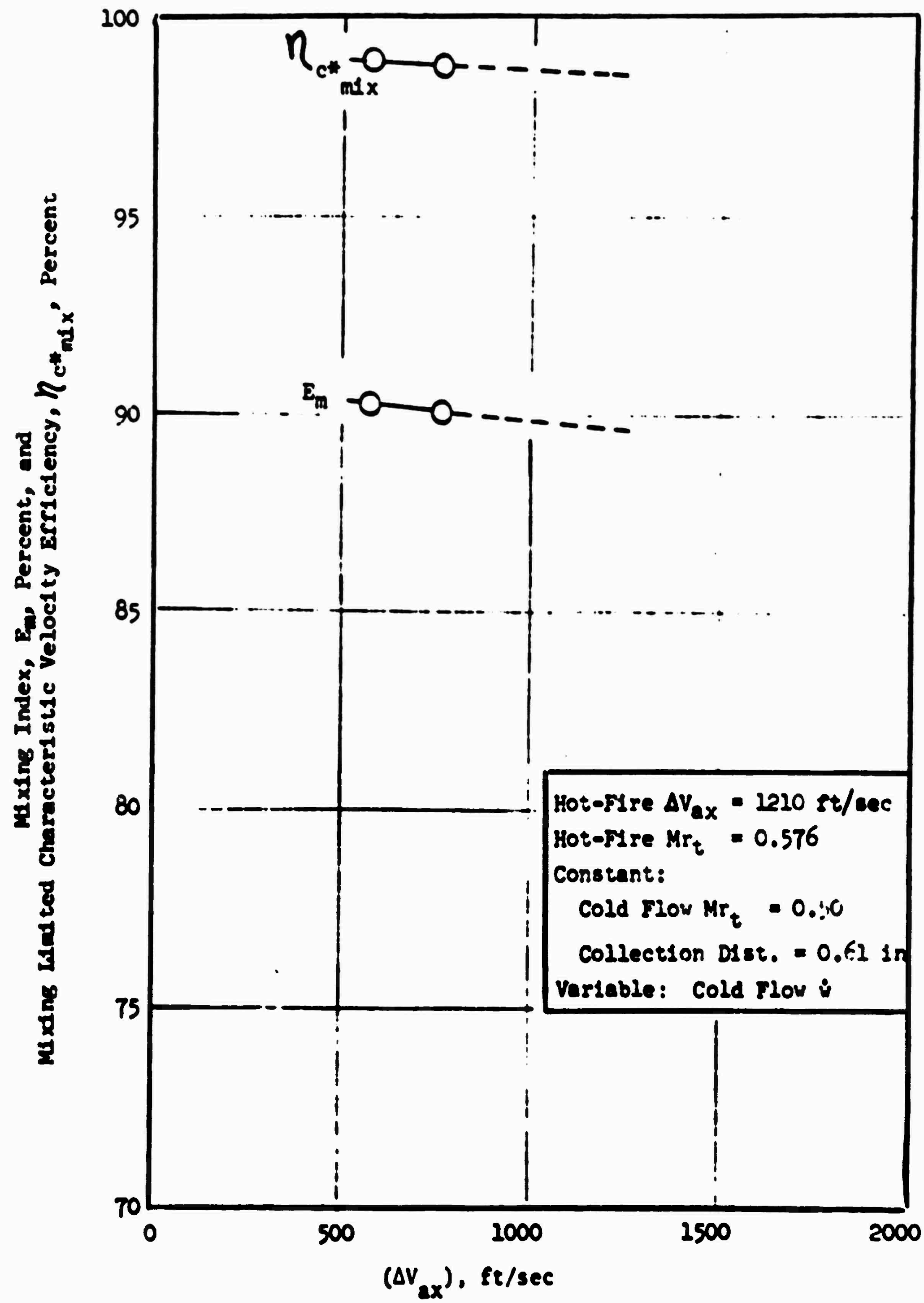

Figure 131. Triplet Element Cold Flow, Effect of ΔV_{ax} on Mixing

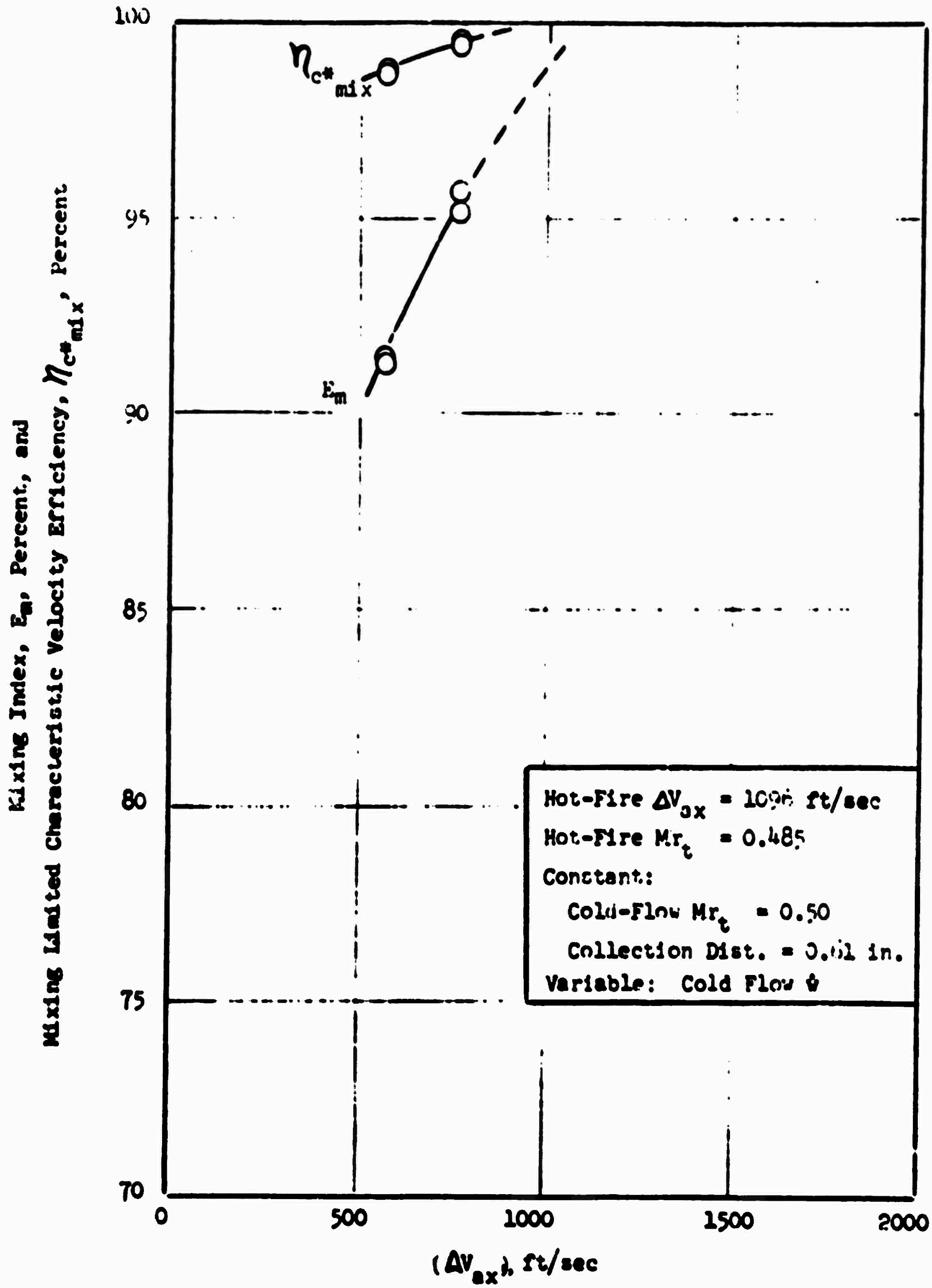

Figure 132. Trislot (Mod II) Element Cold Flow, Effect of ΔV_{ax} on Mixing

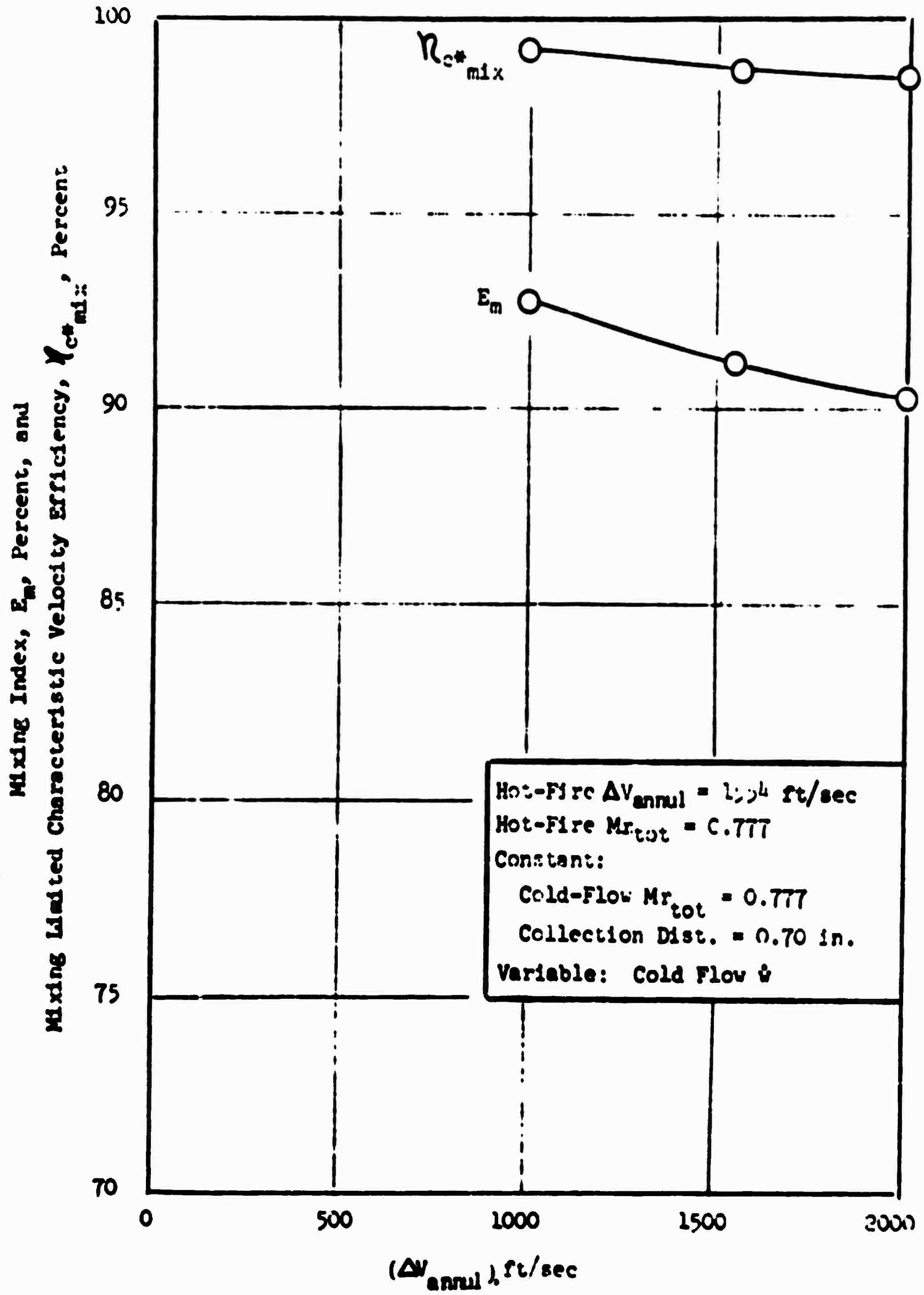

Figure 133. Concentric Element Cold Flow, Effect of ΔV_{annul} on Mixing

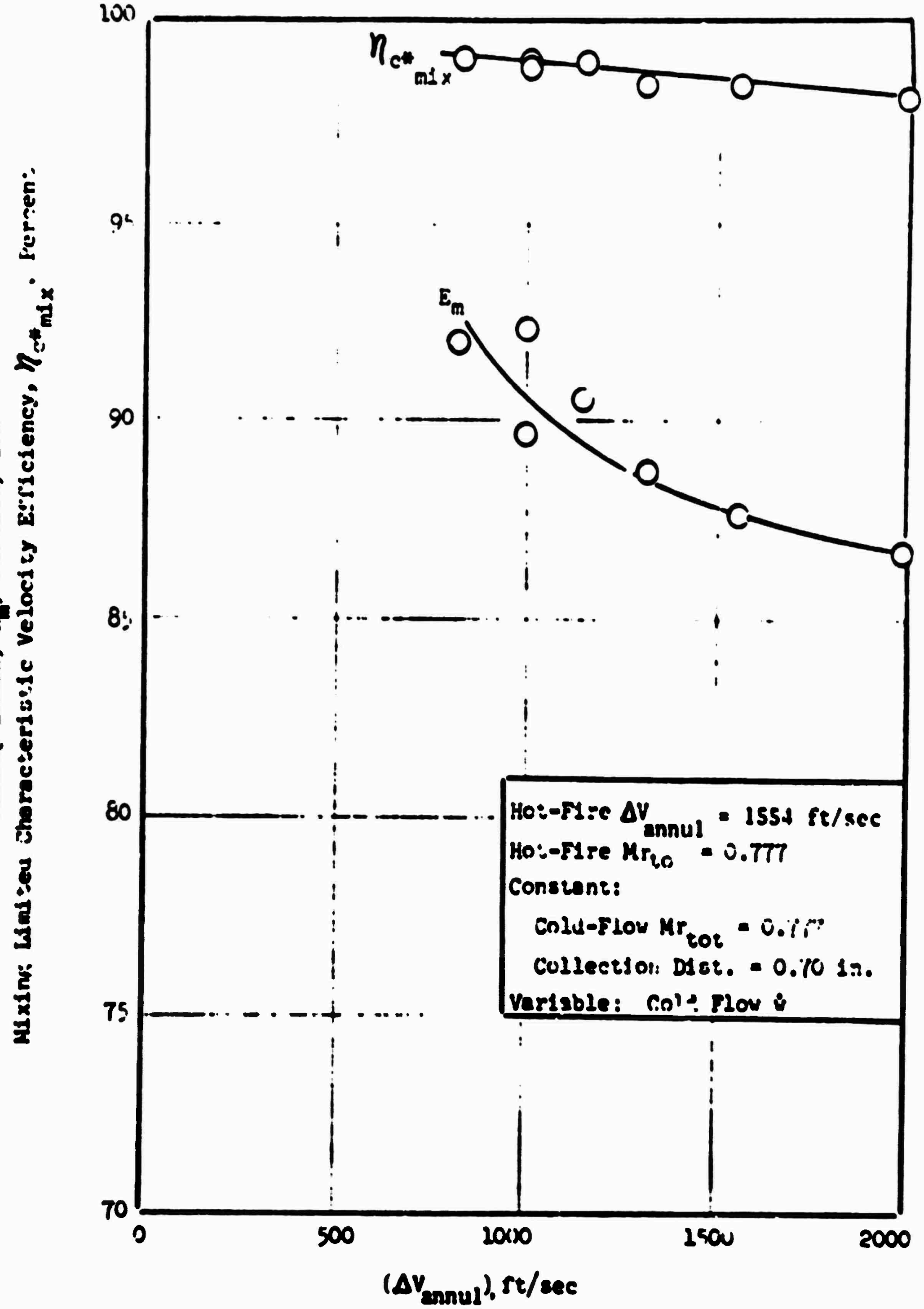

Figure 134. Concentric Element With Hat Cold Flow, Effect of ΔV_{annul} on Mixing

A $\Delta W_{annulus}$ survey was not conducted for the concentric with hat and swirler element.

Prediction of Hot-Fire Injector Performance

The results of the AMPT cold-flow tests keynote the significance of selecting a proper collection distance in predicting mixing efficiency for correlating hot-fire results, and in defining an optimum performing injector element design. Studies on previous contracts (Ref. 9) have indicated that the presence of combustion retards the mixing process. Therefore, cold-flow measurements must be made at a distance which compensates for: (1) mixing retardation due to combustion and (2) further turbulent mixing in the chamber, if the cold-flow results are to be related to hot-fire data. Such a collection distance does not imply that mixing stops at this station but, rather, provides a characteristic collection length which correlates with hot-fire performance (i.e., the combined combustion and turbulent mixing effects not modeled in cold flow are accounted for by a correlating cold-flow collection distance).

To obtain an approximation of the proper collection distance to be employed in predicting AMPT injector performance, the results of Ref. 6 were used. Reference 6 reported that selection of a sampling distance of 0.7 inch (injector face to collection probe) was successful in correlating cold-flow and hot-fire data for the trislot and coaxial element designs.

Furthermore, an IR&D study (Ref. 10) investigated the feasibility of visual techniques for studying coaxial element gas/gas mixing and suggested a mixing core of 3.5 oxidizer orifice diameters in length, prior to the start of vigorous, chamber-filling combustion.

Using the data from Ref. 6, a cold-flow collection factor (Z) was calculated for the concentric and trislot element types in the following manner:

LCD = limited-collection distance

Z = limiting-collection distance/equivalent element diameter

$Z = LCD/D_{eq}$

where

$$D_{eq} = \sqrt{\frac{4}{\pi}(A_{eq})} \tag{3}$$

and

$$A_{eq} = \left(\Sigma A_{ox} + \Sigma A_f\right)/\text{No. of elements}$$

The collection distance was defined as zero at the impingement point. Thus, for Ref. 6 data, the following nondimensional collection factor (Z) were calculated for the coaxial and trislot elements shown in Fig. 135.

	Coaxial	Trislot
LCD	0.70	0.450
A_{eq}	0.0277	0.0547
D_{eq}	0.188	0.264
Z	3.72	1.71

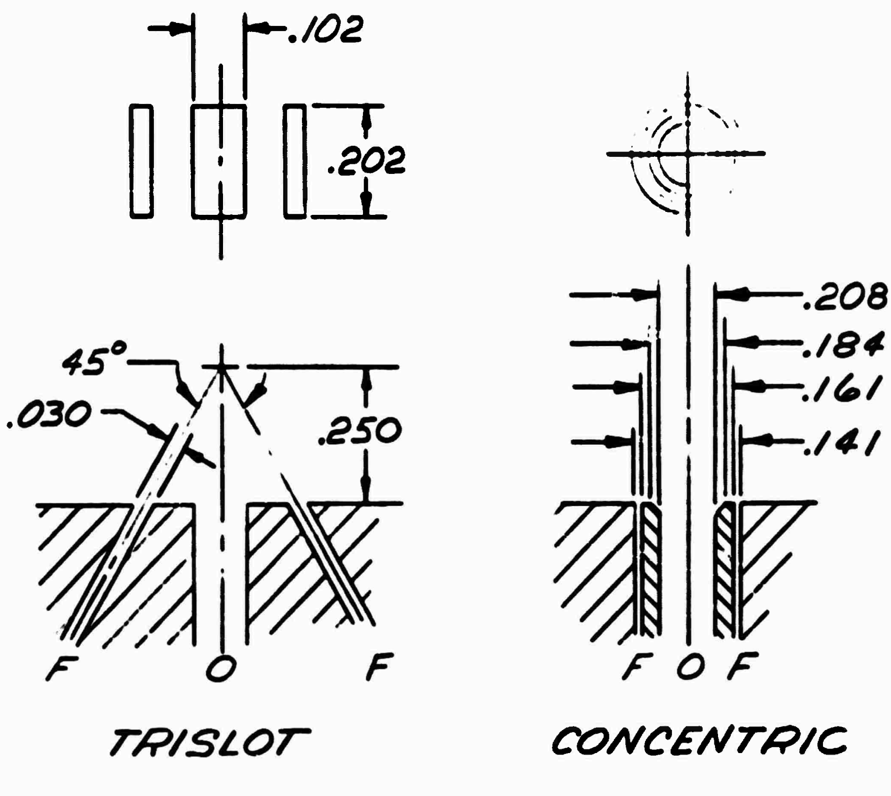

Figure 135. Trislot and Coaxial Element Designs for NASA APS

The nondimensional collection factors (Z) computed above were used to estimate the correlating collection distance (LCD) and, in turn, the predicted performance of the candidate AMPT injector elements. The collection factor for the concentric was used for all concentric element types and the collection factor for the trislot was used for both the trislot and triplet element types. Performance predictions were made using the computed values of LCD and the applicable η_{c^*} versus collection distance cold-flow data (Fig.126 to 130). Results of the computations and predicted AMPT injector performance are tabulated below in Table 14.

TABLE 14. AMPT INJECTOR PERFORMANCE

	Triplet	Blunt Tip Concentric	Concentric With Hat	Concentric With Hat and Swirler	Trislot
A_{eq}, in.^{2}	0.00509	0.00242	0.00218	0.00218	0.00840
D_{eq}, in.	0.0805	0.0555	0.0527	0.0527	0.104
Z	1.71	3.72	3.72	3.72	1.71
LCD = Z x D_{eq}, in.	0.14	0.2	0.2	0.2	0.18
$\eta_{c^*\,mix}$ (predicted)	98.5	95	95.4	98.6	95.5

Based on the above calculations, the candidate elements were ranked according to predicted performance in the following order: (1) triplet, (2) concentric with hat and swirler, (3) trislot, and (4) concentric or coaxial concentric with hat.

COMPARISON BETWEEN PREDICTED AND MEASURED MIXING EFFICIENCY

The predicted mixing efficiency for AMPT injectors, described previously, agreed well (±1 percent) with the hot-fire measured mixing efficiency for corresponding injector types (discussed on page 237). Recall that for gas/gas injectors, the mixing efficiency is equivalent to the characteristic velocity efficiency. Therefore, the method of employing a collection factor (Z) for injector scale (as discussed on page 229) to determine the appropriate collection distance for prediction of mixing efficiency appears to be a useful approach.

DOUBLE-PANEL SEGMENT HOT-FIRE TESTING

A total of 154 water-cooled segment tests was made during the double-panel component evaluation. The total firing time of single-panel segment components was 2214 seconds. Eleven combustion stability evaluation tests were included. All tests were accomplished at site altitude conditions (2000 feet) with GO_2/GH_2 propellants.

Table 15 presents a summary of the tests. All tests were conducted on Peter Test Stand which was used for the single-panel tests, and described in Section VI. In addition to the use of preheated GH_2, use was made of preheated GO_2 for several tests. Table 16 presents the test component configurations that were evaluated, the number of tests, and total test duration applicable to each configuration.

The test conditions for the double-panel, water-cooled segments were:

1. Maximum chamber pressure = 950 psia with intermediate levels of 760, 570, and 380 psia
2. Minimum chamber pressure = 190 psia
3. Injector mixture ratio = 5.0 to 6.0 (5.5 nominal)
4. Propellant injection temperature (nominal) = GO_2 (~520 R), GH_2 (~900 R)
5. Test durations

   10 seconds maximum chamber pressure
   20 seconds minimum chamber pressure
6. Ignition source: gaseous fluorine

TABLE 15. DOUBLE-PANEL WATER-COOLED SEGMENT, TEST DATA AND RESULTS

																Remarks
[illegible]	[illegible]	[illegible]	[illegible]	[illegible]	[illegible]	[illegible]	[illegible]	[illegible]	[illegible]	[illegible]	[illegible]	[illegible]	[illegible]	[illegible]	[illegible]	Satisfactory test
[illegible]	[illegible]	[illegible]	[illegible]	[illegible]	[illegible]	[illegible]	[illegible]	[illegible]	[illegible]	[illegible]	[illegible]	[illegible]	[illegible]	[illegible]	[illegible]	Test terminated [illegible] exhaust [illegible]
[illegible]	[illegible]	[illegible]	[illegible]	[illegible]	[illegible]	[illegible]	[illegible]	[illegible]	[illegible]	[illegible]	[illegible]	[illegible]	[illegible]	[illegible]	[illegible]	Satisfactory test
[illegible]	[illegible]	[illegible]	[illegible]	[illegible]	[illegible]	[illegible]	[illegible]	[illegible]	[illegible]	[illegible]	[illegible]	[illegible]	[illegible]	[illegible]	Thrust not measured	
[illegible]	[illegible]	[illegible]	[illegible]	[illegible]	[illegible]	[illegible]	[illegible]	[illegible]	[illegible]	[illegible]	[illegible]	[illegible]	[illegible]	[illegible]	[illegible]	Satisfactory test (reversed inlets)
[illegible]	[illegible]	[illegible]	[illegible]	[illegible]	[illegible]	[illegible]	[illegible]	[illegible]	[illegible]	[illegible]	[illegible]	[illegible]	[illegible]	[illegible]	[illegible]	Satisfactory test [illegible]
[illegible]	[illegible]	[illegible]	[illegible]	[illegible]	[illegible]	[illegible]	[illegible]	[illegible]	[illegible]	[illegible]	[illegible]	[illegible]	[illegible]	[illegible]	[illegible]	Satisfactory test

Test No.			Chamber Pressure, psia	Mixture Ratio	Duration (Actual), seconds	Fuel Injection Temperature, F	Thrust (Test Site), pounds	Vacuum Thrust, pounds	$\dot{w}_o$, lb/sec	$\dot{w}_f$, lb/sec	Throat Heat Flux, Btu/in.²-sec	Injector End Heat Flux, Btu/in.²-sec	c*(Pc), ft/sec	c*(F), ft/sec	ηc*(Pc), percent	ηc*(F), percent	Nozzle Flow Separated	Remarks
[illegible]	[illegible]	[illegible]	667.8	5.32	20.0	696	--	585.0	1.1707	0.2235	22.0	20.4	7670	7500	98.5	99.5	No	Satisfactory test
[illegible]		[illegible]	661.2	5.00	30.0	800	--	720.5	1.5006	0.3079	27.0	22.5	7705	7521	98.9	[illegible]	No	
[illegible]		[illegible]	197.1	5.51	20.0	305	--	--	0.4003	0.0806	7.0	5.0	7510	--	98.7	--	Yes	
[illegible]			180.0	5.30	20.0	305	--	--	0.8232	0.1572	15.0	5.0	7610	--	98.5	--	Thrust not measured	
[illegible]			522.2	5.30	30.5	64	--	--	1.2306	0.2305	30.0	3.7	7655	--	95.0	--		
[illegible]			500.2	5.36	30.5	670	--	--	1.2164	0.2317	22.0	30.3	7600	--	97.0	--		
[illegible]			601.9	6.30	30.4	115	--	--	1.0120	0.1602	24.0	5.0	7700	--	95.3	--		
[illegible]			605.0	4.00	30.0	507	--	--	1.0276	0.3000	27.5	31.0	7862	--	96.3	--		
[illegible]			762.2	4.73	30.0	111	--	--	1.7030	0.3605	30.9	6.2	7700	--	95.7	--		
[illegible]			770.9	4.72	30.0	907	--	--	1.6000	0.3500	38.6	30.1	7968	--	96.7	--		
[illegible]			180.0	5.03	20.0	180	--	--	0.0502	0.0790	7.2	4.1	7205	--	98.5	--		
[illegible]			180.0	5.00	20.0	736	--	--	0.0536	0.0802	8.0	6.3	7300	--	98.1	--		
[illegible]			180.7	5.33	20.0	843	--	--	0.4225	0.0792	8.1	7.0	7510	--	99.3	--		
[illegible]			170.0	5.13	20.4	84	--	--	0.4105	0.3023	7.1	3.5	7367	--	98.2	--		
[illegible]			360.0	5.22	20.2	70	--	--	0.8096	0.1571	14.0	5.0	7541	--	98.6	--		
[illegible]			360.2	5.10	20.2	806	--	--	0.8257	0.1500	17.0	11.0	7719	--	98.4	--		
[illegible]			580.5	6.00	30.0	706	--	--	1.3530	0.2203	25.3	13.0	7902	--	98.0	--		
[illegible]			560.1	6.00	30.0	216	--	--	1.1900	0.2203	23.0	7.5	7705	--	97.0	--		
[illegible]			636.0	6.07	30.2	136	--	--	1.0002	0.3061	36.0	7.5	7765	--	98.9	--		
[illegible]	9.5	10.5	822.2	4.73	30.0	420	--	--	1.8500	0.3814	38.7	16.2	7722	--	95.0	--		
[illegible]			305.0	5.55	20.0	836	--	--	0.4038	0.0790	8.1	6.0	7622	--	98.9	--		
[illegible]			300.1	5.23	20.0	730	--	--	0.7967	0.1530	14.0	9.0	7682	--	98.0	--		
[illegible]			516.0	5.06	30.0	677	--	--	1.2151	0.2234	25.2	9.6	7777	--	98.8	--		
[illegible]			901.1	5.70	30.0	604	--	--	2.3101	0.4020	60.0	11.5	7610	--	95.6	--		
[illegible]			176.2	5.50	20.3	71	130.0	--	0.4301	0.0787	6.7	4.0	7205	--	97.0	--	Yes	
[illegible]			170.5	5.30	20.0	838	136.9	--	0.4303	0.0700	7.3	0.5	7020	--	98.3	--	Yes	
[illegible]			630.5	5.00	20.3	606	600.3	680.2	0.9975	0.1050	30.5	13.7	7730	7075	98.5	98.2	No	
[illegible]			600.5	5.30	30.0	65	605.5	706.7	1.0720	0.3606	32.1	13.2	7556	7300	[illegible]	95.0	No	
[illegible]			700.1	5.30	30.0	580	720.1	790.0	1.6000	0.3191	32.0	15.2	7705	7371	97.3	96.7	No	
[illegible]			930.0	5.50	7.1	90	961.2	1025.0	2.3077	0.4005	61.1	15.6	7725	7361	96.0	95.5	No	Test terminated by observer because of exhaust flame discoloration
[illegible]			175.0	5.30	20.0	60	130.5	--	0.8157	0.0805	6.0	0.7	7206	--	99.5	--	Yes	Satisfactory test
[illegible]			190.5	5.42	20.0	922	136.9	--	[illegible]	0.0809	0.5	10.2	7087	--	100.7	--	Yes	
[illegible]			462.0	5.06	20.5	712	487.7	600.7	1.0622	0.1961	28.0	14.2	7070	7314	98.7	98.7	No	
[illegible]			634.7	5.10	20.0	66	500.5	670.5	1.0150	0.1960	19.7	7.1	7647	7237	98.3	96.7	No	
[illegible]			667.0	5.11	30.0	60	667.7	730.0	1.6167	0.3465	30.0	13.2	7612	7135	94.2	90.0	No	
[illegible]			721.0	5.07	30.0	560	706.5	775.0	2.0162	0.3191	36.0	16.3	8047	7068	99.5	07.1	No	
[illegible]			182.5	5.32	20.0	670	170.9	--	0.0379	0.0045	2.9	--	7410	--	90.7	--	Yes	
[illegible]			658.5	6.01	20.0	603	600.0	661.7	0.9951	0.2461	30.0	12.2	7082	7587	99.1	90.7	No	
[illegible]			600.0	6.76	30.0	705	671.0	702.7	1.5000	0.3850	15.1	11.2	8071	7629	98.6	97.0	No	
[illegible]			921.0	5.11	2.0	805	850.0	1000.0	2.3515	0.4269	07.0	15.6	7828	7261	95.7	91.0	No	Test terminated by observer because of exhaust flame discoloration
[illegible]	9.5	10.2	207.1	5.36	0.0	817	150.0	--	0.4321	0.0770	9.2	11.2	7635	--	99.0	--	Yes	Test terminated by observer because of water leakage
[illegible]			220.0	5.00	20.0	871	150.5	--	0.4365	0.0707	9.3	12.0	7756	--	101.0	--	No	Satisfactory test
[illegible]			467.6	5.20	20.0	820	385.7	301.1	0.8005	0.1506	10.2	10.5	7964	7100	99.9	99.8	No	
[illegible]			[illegible]	5.31	20.0	806	505.5	302.7	0.8457	0.1503	16.1	10.5	7964	7167	100.0	99.0	No	
[illegible]			667.0	5.00	30.0	600	513.2	500.0	1.2596	0.2205	20.0	22.1	8033	7276	[illegible]	[illegible]	No	
[illegible]			655.3	[illegible]	30.0	917	515.0	551.7	1.2250	0.2207	30.3	20.7	8055	[illegible]	[illegible]	90.2	No	
[illegible]			221.2	5.30	20.0	830	150.0	167.9	0.4290	0.0796	10.0	6.9	[illegible]	7365	90.3	99.2	No	
[illegible]			630.5	5.40	20.0	914	150.0	171.0	0.8297	0.1577	20.0	[illegible]	7022	7302	90.0	[illegible]	No	
[illegible]			695.2	5.07	30.0	660	600.1	558.0	1.1795	0.2327	20.0	11.0	8023	7321	90.0	97.5	No	
[illegible]			220.0	5.00	20.2	850	181.1	181.1	0.4275	0.0770	9.1	10.0	7600	[illegible]	[illegible]	--	No	
[illegible]			[illegible]	5.70	20.0	865	362.0	300.5	0.8367	0.1505	17.0	15.0	8056	7303	100.0	101.0	No	
[illegible]			[illegible]	5.20	30.0	762	665.2	525.0	1.1659	0.2247	27.0	[illegible]	8200	7482	100.3	[illegible]	No	
[illegible]			[illegible]	5.00	20.0	75	100.0	105.0	0.4205	0.0791	6.7	7.0	[illegible]	7113	100.3	100.0	No	

TABLE 15. (Concluded)

Test Number	Injector Type	Chamber Type	L_c	ε	Chamber Pressure, psia	Mixture Ratio	[illegible]	Fuel Injection Temperature, F	Thrust, pounds	[illegible] Thrust, pounds	$\dot{w}_o$, lb/sec	$\dot{w}_f$, lb/sec	Throat Heat Flux, Btu/in²-sec	Injector End Heat Flux, Btu/in²-sec	c*(P_c), ft/sec	c*(F), ft/sec	η c*(P_c), percent	η c*(F), percent	Nozzle Film Separated	Remarks
[illegible]	Triplet, [illegible]	[illegible]	[illegible]	[illegible]	[illegible]	[illegible]	[illegible]	[illegible]	[illegible]	[illegible]	[illegible]	[illegible]	[illegible]	[illegible]	[illegible]	[illegible]	[illegible]	[illegible]	No	Satisfactory test
[illegible]	Triplet, [illegible]	[illegible]			[illegible]	[illegible]	[illegible]	[illegible]	[illegible]	[illegible]	[illegible]	[illegible]	[illegible]	[illegible]	[illegible]	[illegible]	[illegible]	[illegible]		
[illegible]	Triplet, [illegible]	[illegible]			[illegible]	[illegible]	[illegible]	[illegible]	[illegible]	[illegible]	[illegible]	[illegible]	[illegible]	[illegible]	[illegible]	[illegible]	[illegible]	[illegible]		
[illegible]	Triplet, [illegible]	[illegible]			[illegible]	[illegible]	[illegible]	[illegible]	[illegible]	[illegible]	[illegible]	[illegible]	[illegible]	[illegible]	[illegible]	[illegible]	[illegible]	[illegible]		
[illegible]	Triplet, [illegible]	[illegible]			[illegible]	[illegible]	[illegible]	[illegible]	[illegible]	[illegible]	[illegible]	[illegible]	[illegible]	[illegible]	[illegible]	[illegible]	[illegible]	[illegible]		
[illegible]	Triplet, [illegible]	[illegible]			[illegible]	[illegible]	[illegible]	[illegible]	[illegible]	[illegible]	[illegible]	[illegible]	[illegible]	[illegible]	[illegible]	[illegible]	[illegible]	[illegible]		
[illegible]	Triplet, [illegible]	[illegible]			[illegible]	[illegible]	[illegible]	[illegible]	[illegible]	[illegible]	[illegible]	[illegible]	[illegible]	[illegible]	[illegible]	[illegible]	[illegible]	[illegible]		
[illegible]	Triplet, [illegible]	[illegible]			[illegible]	[illegible]	[illegible]	[illegible]	[illegible]	[illegible]	[illegible]	[illegible]	[illegible]	[illegible]	[illegible]	[illegible]	[illegible]	[illegible]		
[illegible]	Triplet, [illegible]	[illegible]			[illegible]	[illegible]	[illegible]	[illegible]	[illegible]	[illegible]	[illegible]	[illegible]	[illegible]	[illegible]	[illegible]	[illegible]	[illegible]	[illegible]		
[illegible]	Triplet, [illegible]	[illegible]			[illegible]	[illegible]	[illegible]	[illegible]	[illegible]	[illegible]	[illegible]	[illegible]	[illegible]	[illegible]	[illegible]	[illegible]	[illegible]	[illegible]		
[illegible]	Triplet, [illegible]	[illegible]			[illegible]	[illegible]	[illegible]	[illegible]	[illegible]	[illegible]	[illegible]	[illegible]	[illegible]	[illegible]	[illegible]	[illegible]	[illegible]	[illegible]		
[illegible]	Triplet, [illegible]	[illegible]			[illegible]	[illegible]	[illegible]	[illegible]	[illegible]	[illegible]	[illegible]	[illegible]	[illegible]	[illegible]	[illegible]	[illegible]	[illegible]	[illegible]		
[illegible]	Triplet, [illegible]	[illegible]			[illegible]	[illegible]	[illegible]	[illegible]	[illegible]	[illegible]	[illegible]	[illegible]	[illegible]	[illegible]	[illegible]	[illegible]	[illegible]	[illegible]		
[illegible]	Triplet, [illegible]	[illegible]			[illegible]	[illegible]	[illegible]	[illegible]	[illegible]	[illegible]	[illegible]	[illegible]	[illegible]	[illegible]	[illegible]	[illegible]	[illegible]	[illegible]		
[illegible]	Triplet, [illegible]	[illegible]			[illegible]	[illegible]	[illegible]	[illegible]	[illegible]		[illegible]	[illegible]	[illegible]		[illegible]		[illegible]		Yes	
[illegible]	Triplet, [illegible]	[illegible]																		Ignition delay, improper purge level
[illegible]	Triplet, [illegible]	[illegible]			[illegible]	[illegible]	[illegible]	[illegible]	[illegible]	[illegible]	[illegible]	[illegible]	[illegible]	[illegible]	[illegible]	[illegible]	[illegible]	[illegible]	No	Satisfactory test
[illegible]	Triplet, [illegible]	[illegible]			[illegible]	[illegible]	[illegible]	[illegible]	[illegible]	[illegible]	[illegible]	[illegible]	[illegible]	[illegible]	[illegible]	[illegible]	[illegible]	[illegible]		
[illegible]	Triplet, [illegible]	[illegible]			[illegible]	[illegible]	[illegible]	[illegible]	[illegible]	[illegible]	[illegible]	[illegible]	[illegible]	[illegible]	[illegible]	[illegible]	[illegible]	[illegible]		
[illegible]	Triplet, [illegible]	[illegible]			[illegible]	[illegible]	[illegible]	[illegible]	[illegible]	[illegible]	[illegible]	[illegible]	[illegible]	[illegible]	[illegible]	[illegible]	[illegible]	[illegible]		
[illegible]	Triplet, [illegible]	[illegible]			[illegible]	[illegible]	[illegible]	[illegible]	[illegible]	[illegible]	[illegible]	[illegible]	[illegible]	[illegible]	[illegible]	[illegible]	[illegible]	[illegible]		
[illegible]	Triplet, [illegible]	[illegible]			[illegible]	[illegible]	[illegible]	[illegible]	[illegible]	[illegible]	[illegible]	[illegible]	[illegible]	[illegible]	[illegible]	[illegible]	[illegible]	[illegible]		
[illegible]	Triplet, [illegible]	[illegible]			[illegible]	[illegible]	[illegible]	[illegible]	[illegible]	[illegible]	[illegible]	[illegible]	[illegible]	[illegible]	[illegible]	[illegible]	[illegible]	[illegible]		
[illegible]	Triplet, [illegible]	[illegible]			[illegible]	[illegible]	[illegible]	[illegible]	[illegible]	[illegible]	[illegible]	[illegible]	[illegible]	[illegible]	[illegible]	[illegible]	[illegible]	[illegible]		
[illegible]	Triplet, [illegible]	[illegible]			[illegible]	[illegible]	[illegible]	[illegible]	[illegible]	[illegible]	[illegible]	[illegible]	[illegible]	[illegible]	[illegible]	[illegible]	[illegible]	[illegible]		
[illegible]	Triplet, [illegible]	[illegible]			[illegible]	[illegible]	[illegible]	[illegible]	[illegible]	[illegible]	[illegible]	[illegible]	[illegible]	[illegible]	[illegible]	[illegible]	[illegible]	[illegible]		Test termination by observer because of exhaust flame discoloration
[illegible]	Triplet, [illegible]	[illegible]			[illegible]	[illegible]	[illegible]	[illegible]	[illegible]	[illegible]	[illegible]	[illegible]	[illegible]	[illegible]	[illegible]	[illegible]	[illegible]	[illegible]		Satisfactory test
[illegible]	Triplet, [illegible]	[illegible]			[illegible]	[illegible]	[illegible]	[illegible]	[illegible]	[illegible]	[illegible]	[illegible]	[illegible]	[illegible]	[illegible]	[illegible]	[illegible]	[illegible]		
[illegible]	Triplet, [illegible]	[illegible]			[illegible]	[illegible]	[illegible]	[illegible]	[illegible]	[illegible]	[illegible]	[illegible]	[illegible]	[illegible]	[illegible]	[illegible]	[illegible]	[illegible]		
[illegible]	Triplet, [illegible]	[illegible]			[illegible]	[illegible]	[illegible]	[illegible]	[illegible]	[illegible]	[illegible]	[illegible]	[illegible]	[illegible]	[illegible]	[illegible]	[illegible]	[illegible]		
[illegible]	Triplet, [illegible]	[illegible]			[illegible]	[illegible]	[illegible]	[illegible]	[illegible]	[illegible]	[illegible]	[illegible]	[illegible]	[illegible]	[illegible]	[illegible]	[illegible]	[illegible]		
[illegible]	Triplet, [illegible]	[illegible]			[illegible]	[illegible]	[illegible]	[illegible]	[illegible]	[illegible]	[illegible]	[illegible]	[illegible]	[illegible]	[illegible]	[illegible]	[illegible]	[illegible]		
[illegible]	Triplet, [illegible]	[illegible]			[illegible]	[illegible]	[illegible]	[illegible]	[illegible]	[illegible]	[illegible]	[illegible]	[illegible]	[illegible]	[illegible]	[illegible]	[illegible]	[illegible]		
[illegible]	Triplet, [illegible]	[illegible]			[illegible]	[illegible]	[illegible]	[illegible]	[illegible]	[illegible]	[illegible]	[illegible]	[illegible]	[illegible]	[illegible]	[illegible]	[illegible]	[illegible]		
[illegible]	Triplet, [illegible]	[illegible]			[illegible]	[illegible]	[illegible]	[illegible]	[illegible]	[illegible]	[illegible]	[illegible]	[illegible]	[illegible]	[illegible]	[illegible]	[illegible]	[illegible]		
[illegible]	Triplet, [illegible]	[illegible]			[illegible]	[illegible]	[illegible]	[illegible]	[illegible]	[illegible]	[illegible]	[illegible]	[illegible]	[illegible]	[illegible]	[illegible]	[illegible]	[illegible]		
[illegible]	Triplet, [illegible]	[illegible]			[illegible]	[illegible]	[illegible]	[illegible]	[illegible]	[illegible]	[illegible]	[illegible]	[illegible]	[illegible]	[illegible]	[illegible]	[illegible]	[illegible]		
[illegible]	Triplet, [illegible]	[illegible]			[illegible]	[illegible]	[illegible]	[illegible]	[illegible]	[illegible]	[illegible]	[illegible]	[illegible]	[illegible]	[illegible]	[illegible]	[illegible]	[illegible]		
[illegible]	Triplet, [illegible]	[illegible]		[illegible]	[illegible]	[illegible]	[illegible]	[illegible]	[illegible]		[illegible]	[illegible]	[illegible]	[illegible]	[illegible]	[illegible]	[illegible]	[illegible]	Yes	Combustion stability evaluation
[illegible]	Triplet, [illegible]	[illegible]			[illegible]	[illegible]	[illegible]	[illegible]	[illegible]		[illegible]	[illegible]	[illegible]	[illegible]	[illegible]		[illegible]		Yes	
[illegible]	Triplet, [illegible]	[illegible]			[illegible]	[illegible]	[illegible]	[illegible]	[illegible]	[illegible]	[illegible]	[illegible]	[illegible]	[illegible]	[illegible]	[illegible]	[illegible]	[illegible]	No	
[illegible]	Triplet, [illegible]	[illegible]			[illegible]	[illegible]	[illegible]	[illegible]	[illegible]	[illegible]	[illegible]	[illegible]	[illegible]	[illegible]	[illegible]	[illegible]	[illegible]	[illegible]		
[illegible]	Triplet, [illegible]	[illegible]			[illegible]	[illegible]	[illegible]	[illegible]	[illegible]	[illegible]	[illegible]	[illegible]	[illegible]	[illegible]	[illegible]	[illegible]	[illegible]	[illegible]		
[illegible]	Triplet, [illegible]	[illegible]			[illegible]	[illegible]	[illegible]	[illegible]	[illegible]	[illegible]	[illegible]	[illegible]	[illegible]	[illegible]	[illegible]	[illegible]	[illegible]	[illegible]		
[illegible]	Triplet, [illegible]	[illegible]			[illegible]	[illegible]	[illegible]	[illegible]	[illegible]	[illegible]	[illegible]	[illegible]	[illegible]	[illegible]	[illegible]	[illegible]	[illegible]	[illegible]		
[illegible]	Triplet, [illegible]	[illegible]			--					--			--	--	--	--	--	--	--	Improperly set automatic redline cutoff device
[illegible]	Triplet, [illegible]	[illegible]			[illegible]	[illegible]	[illegible]	[illegible]	[illegible]	[illegible]	[illegible]	[illegible]	[illegible]	[illegible]	[illegible]	[illegible]	[illegible]	[illegible]	No	Satisfactory test
[illegible]	Triplet, [illegible]	[illegible]			[illegible]	[illegible]	[illegible]	[illegible]	[illegible]	[illegible]	[illegible]	[illegible]	[illegible]	[illegible]	[illegible]	[illegible]	[illegible]	[illegible]	No	
[illegible]	Triplet, [illegible]	[illegible]			[illegible]	[illegible]	[illegible]	[illegible]	[illegible]	[illegible]	[illegible]	[illegible]	[illegible]	[illegible]	[illegible]	[illegible]	[illegible]	[illegible]	No	

TABLE 16. DOUBLE-PANEL WATER-COOLED SEGMENT TEST COMPONENT CONFIGURATIONS

Number of Tests	Total Duration	Injector	Chamber, L_c (Combustion Chamber Length)
5	67.5	Triplet, U/N 2-D	U/N 2, 3.0 inch
4	84.5	Triplet, U/N 2-E	" "
17	226.8	Triplet, U/N 8	U/N 5, 2.5 inch
3	51.1	Triplet, U/N 2-E	" "
4	62.0	Triplet, U/N 8-A	" "
4	62.5	Triplet, U/N 2-E	U/N 5, 3.5 inch
4	62.3	Triplet, U/N 8-A	" "
4	62.0	Triplet, U/N 8-A (Reversed, O-F-O)	" "
3	49.4	Triplet, U/N 8-A (Heated oxidizer)	" "
3	51.4	Triplet, U/N 8-A	U/N 5, 3.5 inch
3	51.2	Triplet, U/N 2-E	U/N 2, 3.0 inch
10	144.9	Concentric, U/N 7-E, 0.000 Recess, 0.009 gap	U/N 5, 3.0 inch
8	123.1	Concentric, U/N 7-E, 0.100 Recess, 0.009 gap	U/N 5, 3.0 inch
4	62.4	Concentric, U/N 7-E, 0.000 Recess, 0.009 gap	U/N 5, 3.5 inch
12	192.7	Concentric, U/N 7-F, tapered oxidizer post O.D. 0.009 gap	" "
4	53.3	Concentric, U/N 7-F, 0.010 Recess, tapered oxid. post, 0.009 gap	" "
6	82.3	Triplet, U/N 2-E	U/N 6, 3.0 inch
3	51.6	Concentric, U/N 7-F	" "
13	175.3	Triplet, U/N 8-A	" "
19	299.5	Triplet, U/N 7-O	" "
10	143.7	Trislot, U/N 9	" "
11	54.0	Triplet, U/N 8-A (Stability Tests)	U/N 4, 3.0 inch
154	2213.5		

Table 15 presents the measured and derived data for each test. The equations and computational techniques used to determine the performance and heat transfer parameters are presented in Appendixes II and III.

Triplet Injector c* Performance

Characteristic velocity (c*) efficiency was evaluated for different injector configurations as a function of chamber pressure, chamber wall contour, chamber length, mixture ratio, fuel injection velocity/density, oxidizer injection velocity/density, and element orifice pattern.

Effect of Chamber Pressure. c* efficiency as a function of chamber pressure for the six triplet injector types tested is shown in Fig. 136. Some variation in performance level (referenced to the 3-inch chamber length) between injector types was noted. Performance for injector units 8A and 8B was approximately the same and represented the highest performance level obtained (η_{c^*} = 100 percent over the chamber pressure range 150 to 800 psia). Injector unit 8B was tested in chamber unit 4 which had a larger throat area. Additionally, injector unit 8B had a lesser number of elements than injector unit 8A. Therefore, for equivalent chamber pressure, the thrust/element for injector unit 8B was greater than that for injector unit 8A. Injector unit 8 was tested in the 2.5-inch chamber length only. However, comparison of injector units 8 and 8A in the 2.5-inch length chamber indicated that the unit 8 injector performance was equivalent to that obtained with the unit 8A and 8B injectors. Performance for injector unit 7G was approximately 1 percent below that of the injector unit 8 configurations. Performance for injector units 2D and 2E was equivalent and slightly below that obtained with injector unit 7G.

The test series with injector unit 8B included pulse tests. Stability results from these tests are presented in a subsequent section (page 265).

Trends of combustion performance with chamber pressure varied for some injector types. Injector units 2D and 2E performance optimized at the mid-range chamber

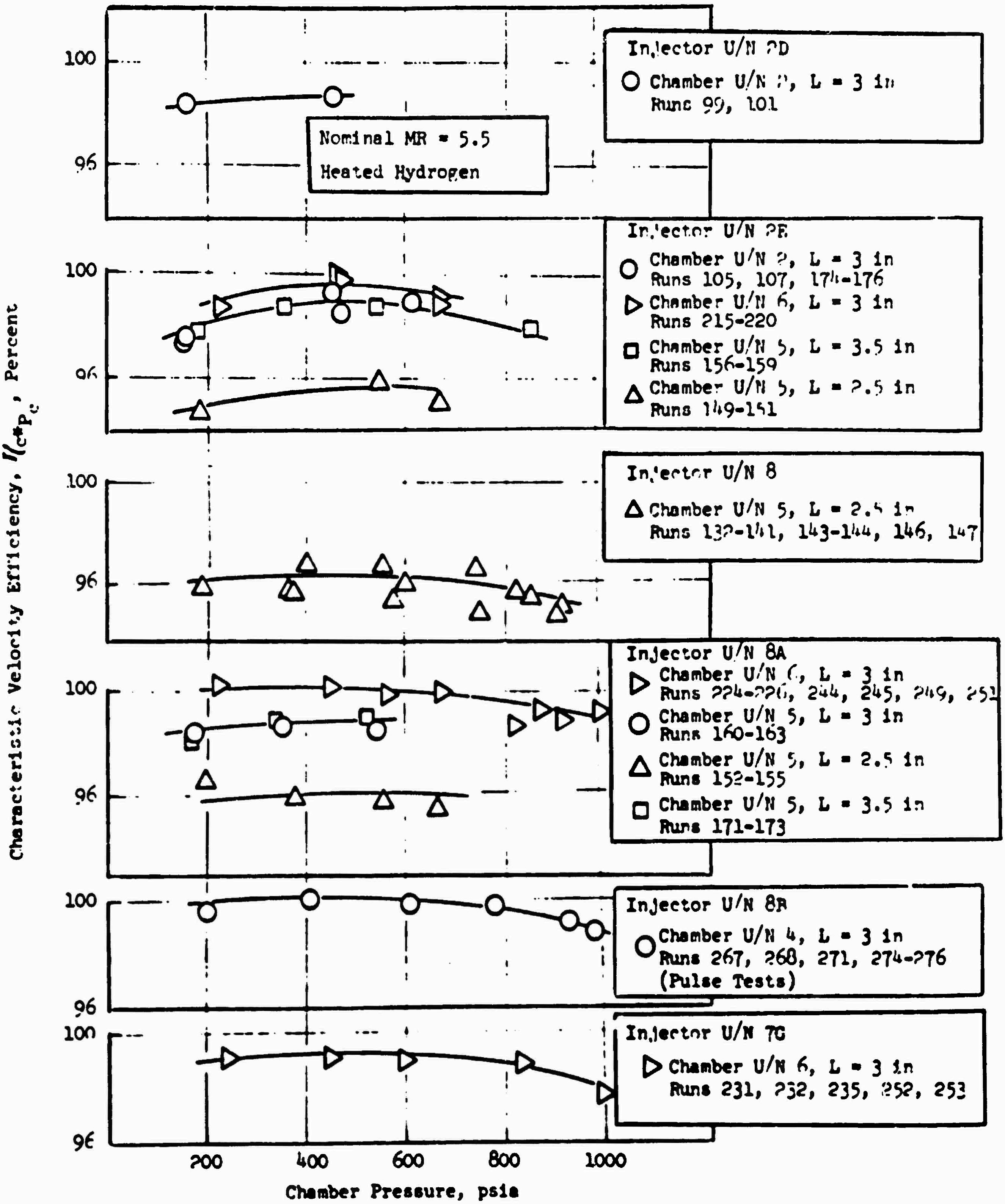

Figure 136. Effect of Chamber Pressure on Characteristic Velocity Efficiency for Double-Panel Triplet Injectors

pressure (P_c = 450 psia) and decreased 1 to 2 percent at the low (P_c = 150 psia) and high (P_c = 950 psia) chamber pressures. Injector units 8, 8A, 8B, and 7G performance was relatively constant over the chamber pressure range (150 to 800 psia) and decreased 1 percent at the high (P_c = 950 psia) chamber pressure.

Effect of Wall Contour

An effect of chamber wall contour on triplet injector performance was noted. The wall contour for chamber units 4 and 6 (L_c= 3 inches) converged continuously from the injector face to the throat. For chamber unit 5 (L_c= 3 inches), a constant contraction ratio section extended from the injector face to a station 0.5 inch downstream, after which the chamber converged to the throat. Comparison of injector units 8A and 8B performance data (Fig.136) in these chambers indicates that the full contour wall chamber exhibited higher performance by approximately 1 percent than the partial contour wall chamber.

Effect of Chamber Length. c* efficiency as a function of chamber length for injector units 2E, 8, and 8A is shown in Fig. 137. Data for chamber units 2 and 6 was reduced 1 percent for comparison with the chamber unit 5 data (refer to previously discussed chamber wall contour effect). Combination of injector units 8 and 8A data was considered valid because both of these injectors exhibited equivalent performance (refer to previously discussed chamber pressure effect). The data shown in Fig. 137 indicated that, essentially, all the mixing that will occur with a given injector and given operating conditions is completed within a 3-inch chamber length and that further lengthening of the chamber leads to negligible additional increase in performance.

Effect of Mixture Ratio. c* efficiency as a function of mixture ratio, at constant chamber pressure, for injector unit 7G is shown in Fig. 138. Performance increased approximately 1 percent as mixture ratio increased from 5 to 6.

Effect of Fuel Injection Velocity/Density. c* efficiency as a function of fuel injection velocity, at constant chamber pressure and chamber length, is shown in Fig. 139. The fuel injection velocity was varied by changing the fuel injection

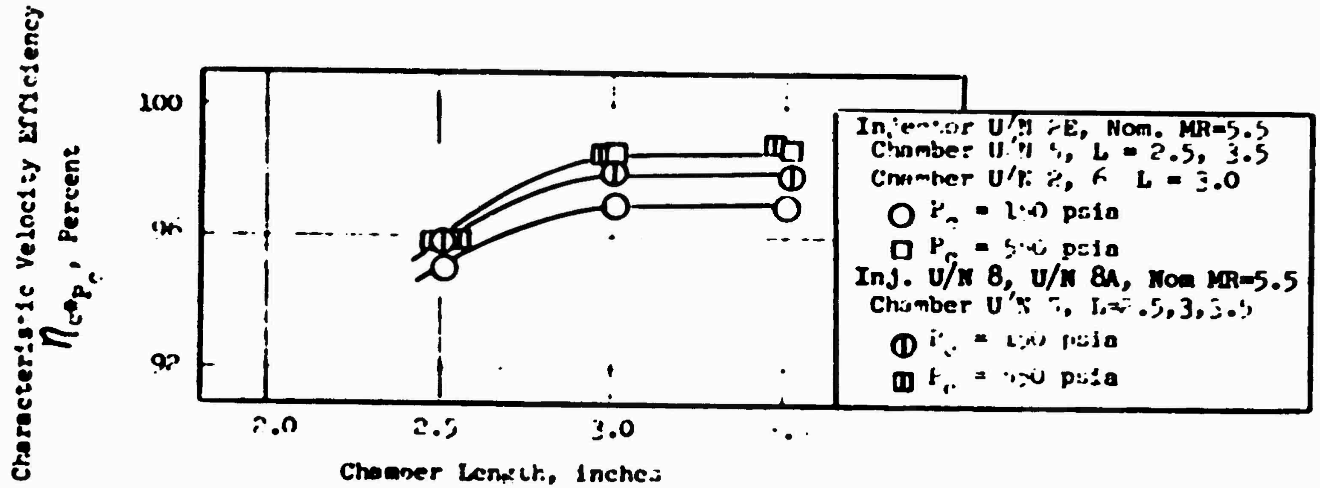

Figure 137. Effect of Chamber Length on Characteristic Velocity Efficiency for Double-Panel Triplet Injectors

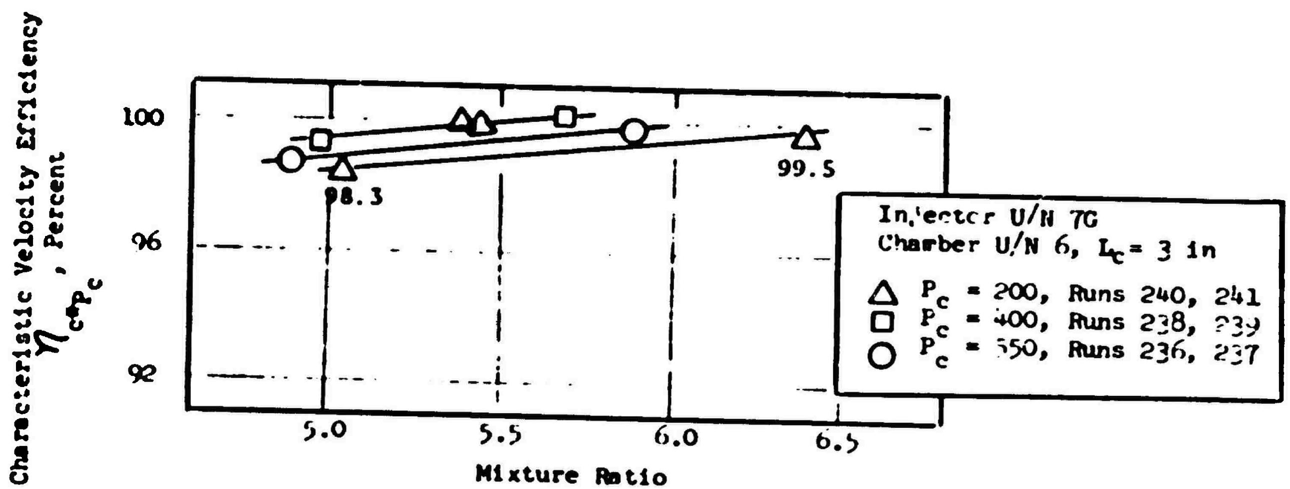

Figure 138.. Effect of Mixture Ratio on Characteristic Velocity Efficiency for Double-Panel Triplet Injector

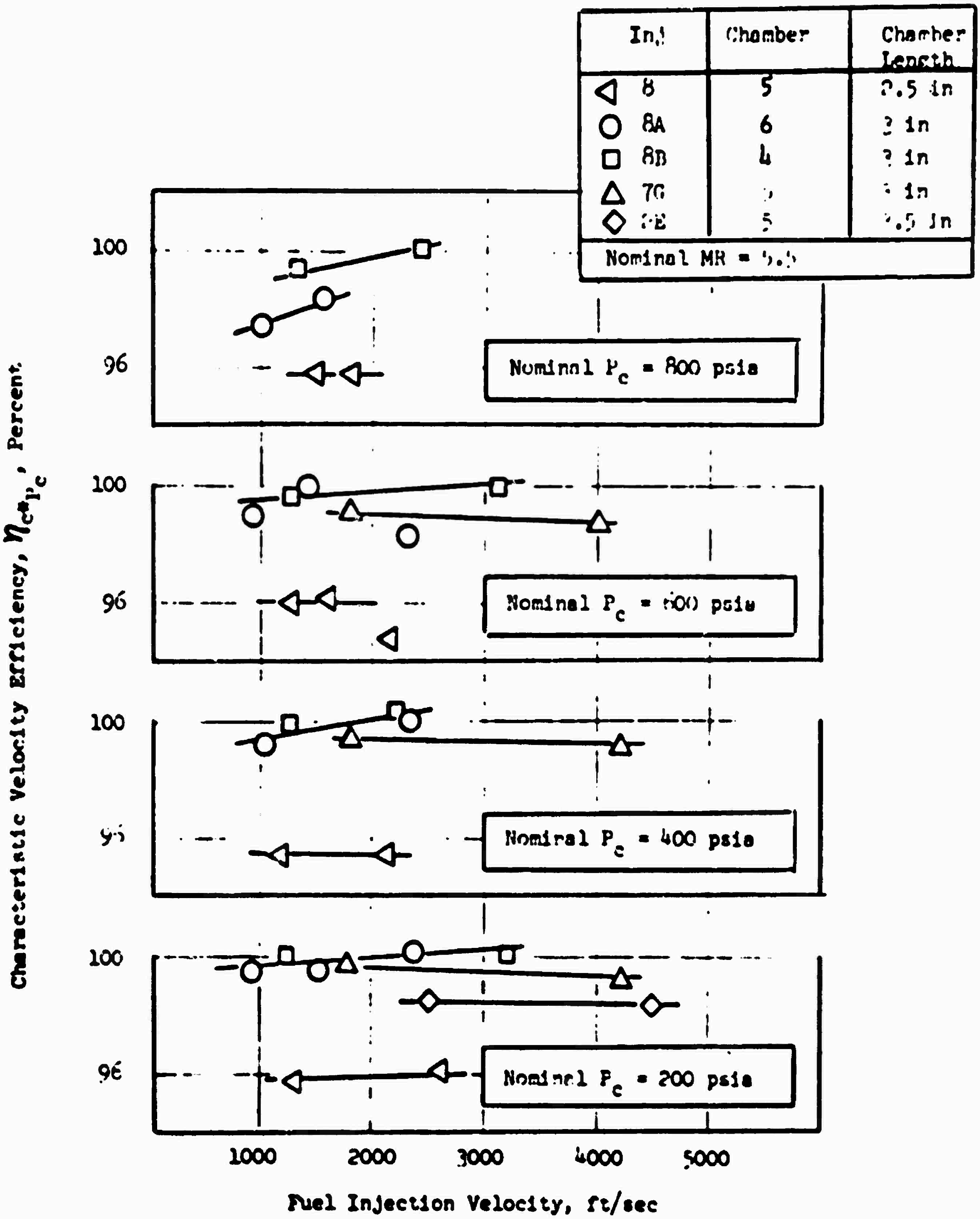

Figure 139. Effect of Fuel Injection Velocity on Characteristic Velocity Efficiency for Double-Panel Triplet Injectors

temperature. In this manner, fuel velocity decreased as fuel density increased, and the $(\rho V)_f$ parameter remained essentially constant. Reduction of fuel injection velocity at constant $(\rho V)_f$, as shown in Fig.139, did not significantly affect performance for most injectors. An exception was a slight decrease in performance with decreased velocity for the units 8A and 8B injectors.

Effect of Oxidizer Injection Velocity/Density. Heated GO_2 was employed in a test series to evaluate the effect of increased oxidizer injection velocity on performance. In this manner, the oxidizer injection density decreased as oxidizer velocity increased and the $(\rho V)_o$ parameter remained essentially constant. The heated GO_2 tests were conducted with hydrogen heated to design temperatures. Combustion performance versus chamber pressure for the heated GO_2 tests is shown in Fig. 140. Test values at chamber pressures greater than 600 psia have been increased to compensate for the low mixture ratios at which these tests were conducted. The previously described mixture ratio effect on performance was used for this correction. Included in the figure are previously presented ambient GO_2 tests. Performance for the heated and ambient GO_2 tests was essentially equivalent.

Effect of Element Orifice Pattern. The basic triplet design employed consisted of two fuel streams impinging on a center oxidizer stream (F-O-F). The propellant feed lines were reversed to the injector manifold for a test series with injector unit 8A. The element orifice pattern consisted of two oxidizer streams impinging on a center fuel stream (O-F-O). Combustion performance versus chamber pressure for the reversed flow tests is shown in Fig. 141. Included in the figure are previously presented triplet (F-O-F) element data. No significant difference in performance between the element flow configurations was noted.

Concentric Injector c* Performance

c* efficiency was evaluated for different injector configurations as a function of chamber pressure, chamber contour, chamber length, oxidizer post recess, and fuel injection velocity/density.

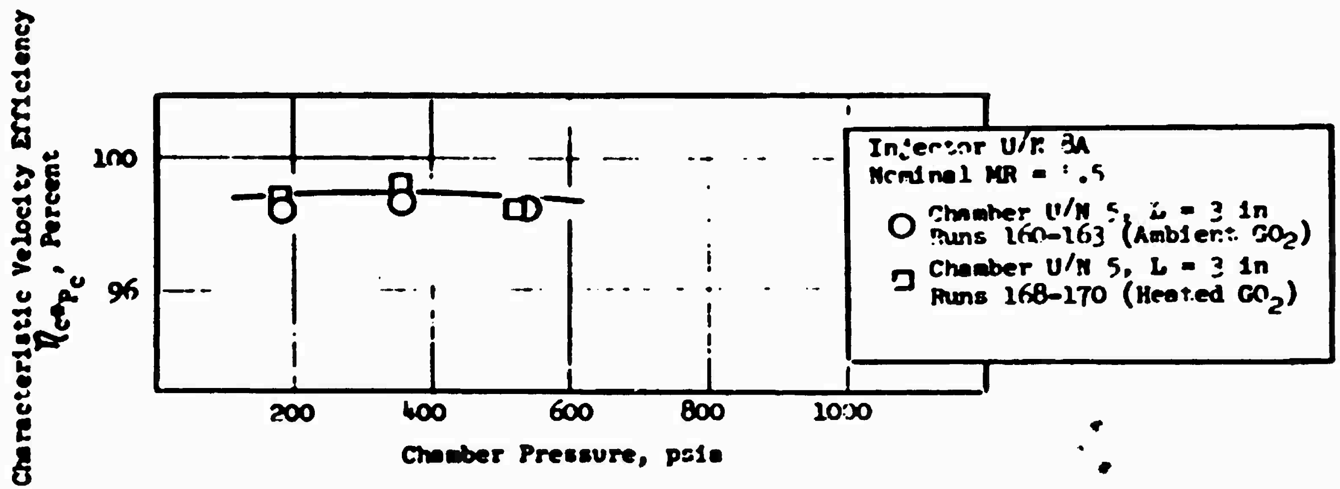

Figure 140. Comparison of Chamber Pressure vs Characteristic Velocity Efficiency for Ambient and Heated GO_2 Tests With Double-Panel Triplet Injector

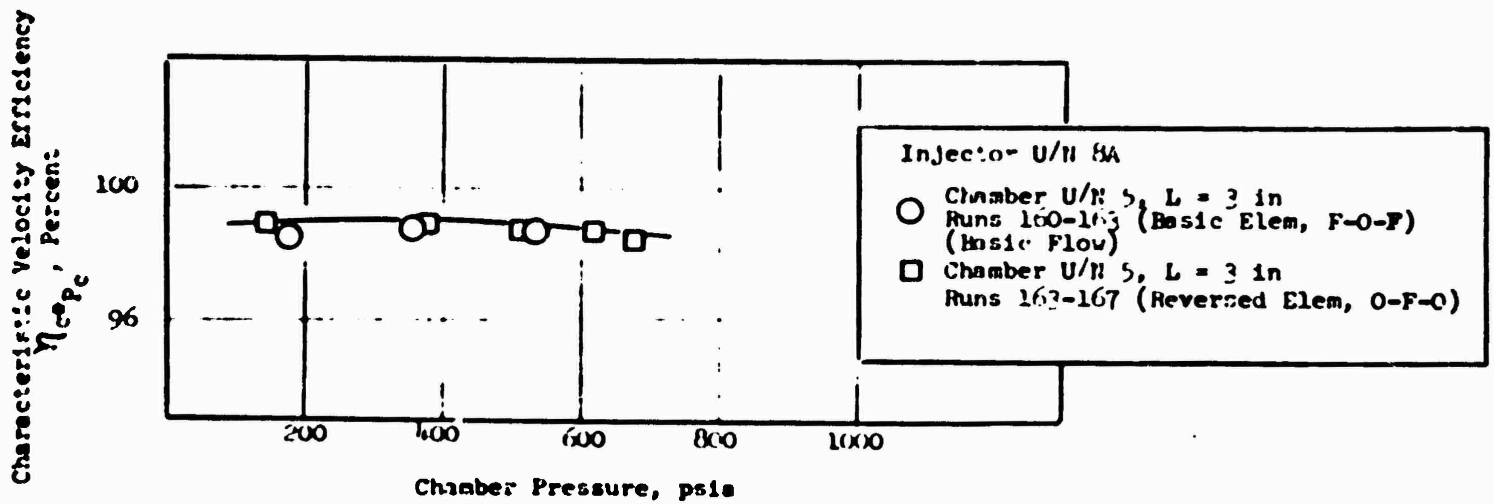

Figure 141. Comparison of Chamber Pressure vs Characteristic Velocity Efficiency for Basic (F-O-F) and Reversed (O-F-O) Elements With Double-Panel Triplet Injector

Effect of Chamber Pressure. c* efficiency as a function of chamber pressure for the concentric injector designs is shown in Fig. 142. The performance of injector units 7E and 7F was approximately equivalent. Both injector units 7E and 7F showed the same trend of decreasing performance with increasing chamber pressure. Tests with injector unit 7F showed the same trend of decreasing performance with increasing chamber pressure. Tests with injector unit 7F conducted with ambient temperature hydrogen at chamber pressures exceeding 600 psia showed high-frequency instabilities, as described later in the stability discussion (page 270). These unstable tests are not included in the data plots for the concentric injectors.

Effect of Chamber Contour. Concentric injector unit 7F was tested in chambers having wall convergences over the full chamber length (chamber unit 6) and over a partial chamber length (chamber unit 5). No significant difference between the performance in chamber units 5 and 6 (L_c = 3 inches) was noted. This result differs from the previously discussed results with the triplet which showed a slight effect of wall contour on performance.

Effect of Chamber Length. Concentric injectors were tested in chamber lengths of 3 and 3.5 inches. Results shown in Fig. 143 indicated no significant difference in performance between the two chamber lengths. This result also was the case for triplet injectors, discussed previously, which showed no performance improvement with chamber lengths exceeding 3 inches.

Effect of Oxidizer Post Recess. Concentric injector units 7E and 7F were modified to provide oxidizer post recesses of 0.100 and 0.010 inch, respectively. Results shown in Fig. 143 indicate performance with the oxidizer-post recess elements was essentially the same as that obtained with the blunt-tip element for both concentric injectors.

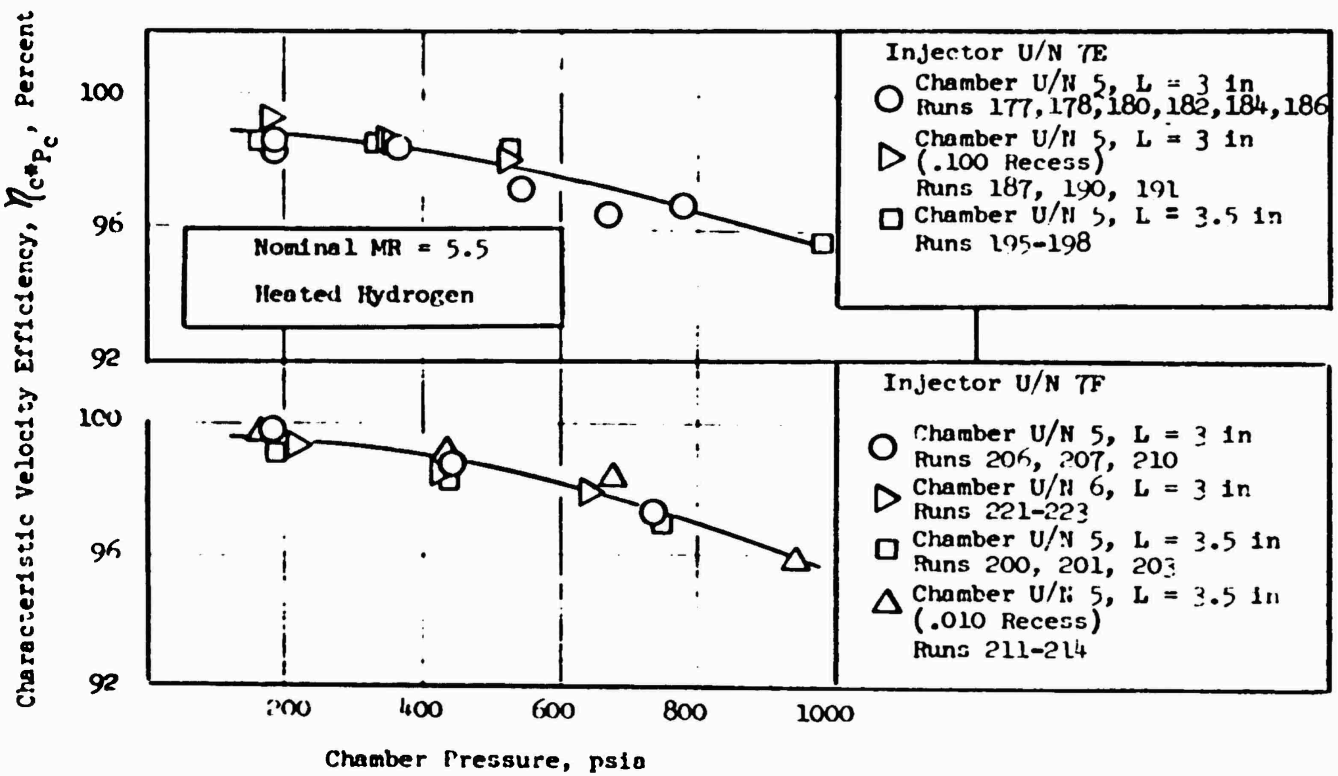

Figure 142. Effect of Chamber Pressure on Characteristic Velocity Efficiency for Double-Panel Concentric Injectors

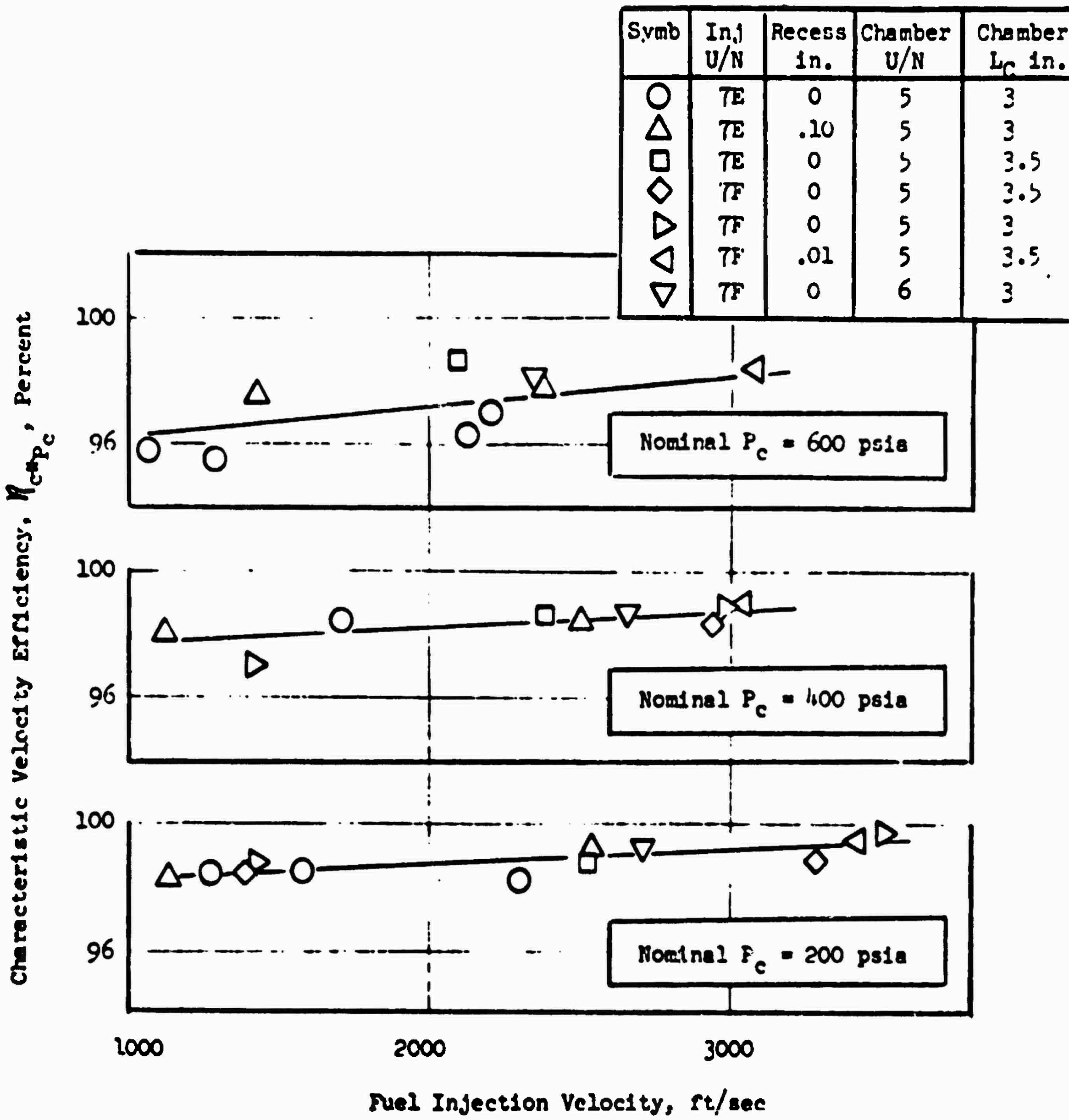

Symb	Inj U/N	Recess in.	Chamber U/N	Chamber L_c in.
○	7E	0	5	3
△	7E	.10	5	3
□	7E	0	5	3.5
◇	7F	0	5	3.5
▷	7F	0	5	3
◁	7F	.01	5	3.5
▽	7F	0	6	3

Figure 143. Effect of Fuel Injection Velocity on Characteristic Velocity Efficiency for Double-Panel Concentric Injectors

Effect of Fuel Injection Velocity/Density. The fuel injection velocity was varied by reducing the fuel injection temperature. Again, the fuel density changed and the $(\rho V)_f$ parameter remained essentially constant. Combustion efficiency as a function of fuel velocity for constant chamber pressure is shown in Fig. 143. The results indicated a slight decrease in performance with decreasing injection velocity.

The decrease in fuel injection velocity reduced the (V_f-V_o) parameter because V_o remained essentially constant. Other investigators (Ref. 9) have noted in cold-flow mixing tests that mixing degrades as (V_f-V_o) is reduced.

To compare the concentric injector hot-fire results with the cold-flow results (Fig. 129 and 130), the individual effect of hot-fire ΔV and hot-fire thrust per element was plotted as shown in Fig. 144 and 145, respectively. Figure 144 shows that as ΔV is halved, the performance decreases ~0.75 percent. Figure 145 shows that as thrust per element is halved, the performance increases ~1.75 percent. Thus, if both ΔV and thrust per element are halved simultaneously, a net increase in performance of ~1 percent is indicated. As previously described in the cold-flow section, Fig. 145 includes the combined effect of both ΔV and thrust per element on performance, where both ΔV and flowrate were approximately halved simultaneously. Comparison of the net increase from hot-fire testing (i.e., ~1 percent) compared closely with the increase of ~0.75 percent noted in cold-flow testing. Therefore, the cold-flow modeling appeared to correctly predict the effects of ΔV and throttling as observed in hot-fire testing.

Trislot Injector c* Performance

c* efficiency was evaluated for one trislot injector configuration as a function of chamber pressure and fuel injection velocity/density.

Effect of Chamber Pressure. c* efficiency as a function of chamber pressure for trislot injector unit 9 is shown in Fig. 145. Performance decreased with increasing chamber pressure dropping from 100 percent at low chamber pressure (P_c=200 psia) to 96 percent at high chamber pressure (P_c=900 psia).

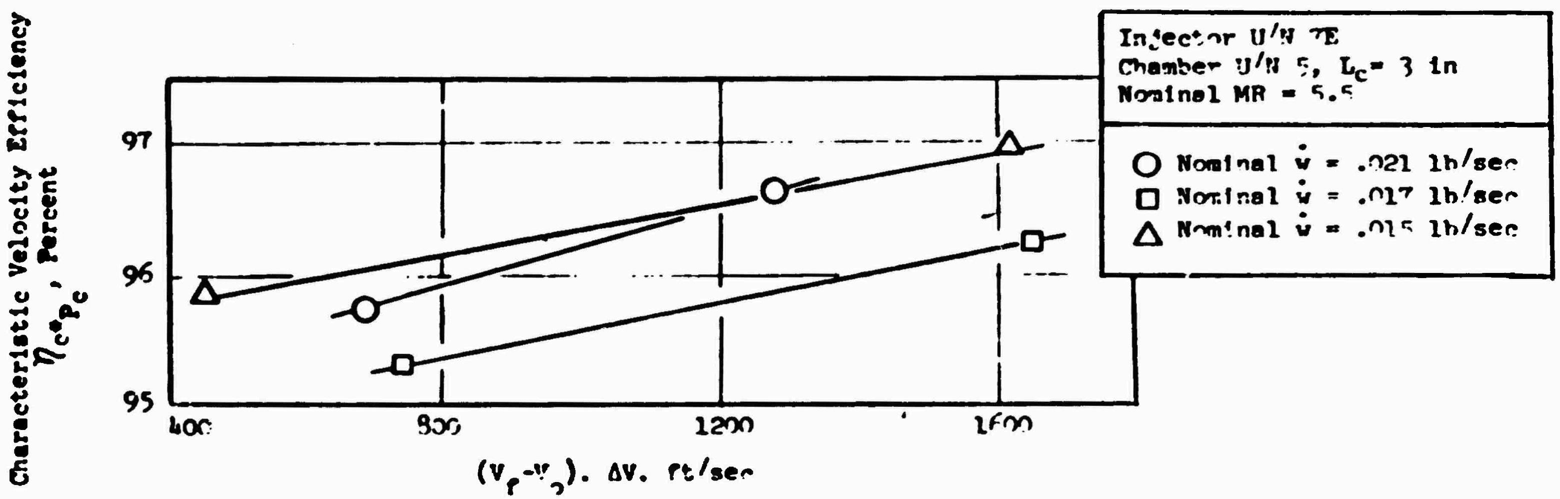

Figure 144. Effect of ΔV on Characteristic Velocity Efficiency for Double-Panel Concentric Injector

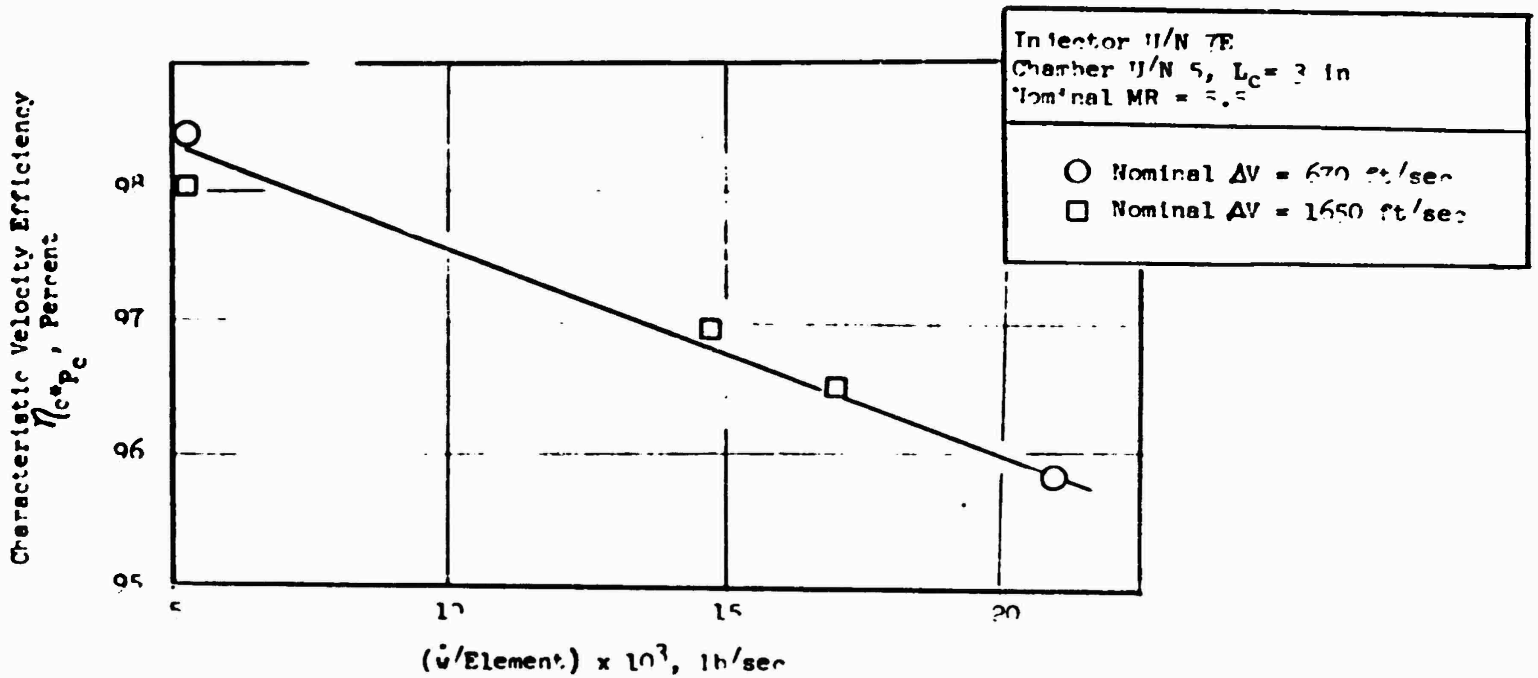

Figure 145. Effect of ẇ/Element on Characteristic Velocity Efficiency for Double-Panel Concentric Injector

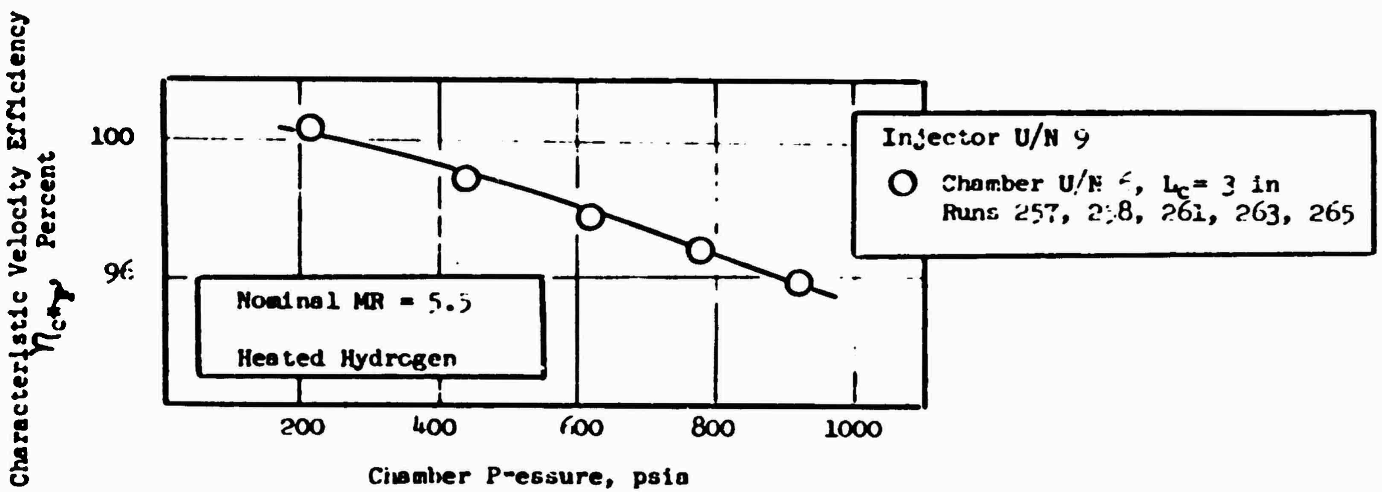

Figure 146. Effect of Chamber Pressure on Characteristic Velocity Efficiency for Double-Panel Trislot Injector

Effect of Fuel Injection Velocity/Density. Fuel injection velocity was varied by varying the fuel injection temperature. Again, fuel density changed and $(\rho V)_f$ remained essentially constant. Combustion efficiency decreased as fuel injection velocity was reduced as shown in Fig. 147.

The decrease in performance with lower fuel injection velocity, at constant flowrate/element, was approximately 1 percent per 1000 ft/sec. Using the same method of cold-flow and hot-fire data comparison previously discussed for the concentric injector (i.e., combining the hot-fire trends for ΔV and flowrate/element to compare with cold-flow results), a correlation between predicted and measured results could not be obtained. The lack of correlation between cold-flow and hot-fire data trends with combined ΔV and flowrate/element perturbations is not presently understood.

Double-Panel Segment Heat Transfer

The basic coolant-channel design philosophy utilized in the single-panel segment was adopted for design of the double-panel segment thrust chamber. Using gaseous oxygen/gaseous hydrogen heat transfer data obtained during the single-panel water-cooled chamber testing, the gas-side heat transfer coefficient distribution shown in Fig. 148 was established and used in the initial coolant channel design for the cast NARloy combustor of the double-panel regeneratively cooled segment thrust chamber.

As mentioned in the performance section, the high c* efficiency objective required a 3-inch injector-to-throat chamber length; therefore, the following discussions are based on this chamber length. As typically shown in Fig. 149, the heat flux distribution obtained from testing was found to be lower than the design curve, particularly in the throat. The measured combustion chamber heat input (Fig. 150) indicated that three of the five injector configurations tested achieved heat inputs lower than the design curve which was desirable from a thrust chamber cooling standpoint. These injectors included: (1) triplet unit 8A, (2) trislot unit 9, and (3) concentric unit 7F (0-inch recess). Comparison of the heat flux distributions of the injectors evaluated (Fig. 151 and 152) indicated that previously mentioned injectors had lower injector region heat fluxes relative to the other injectors.

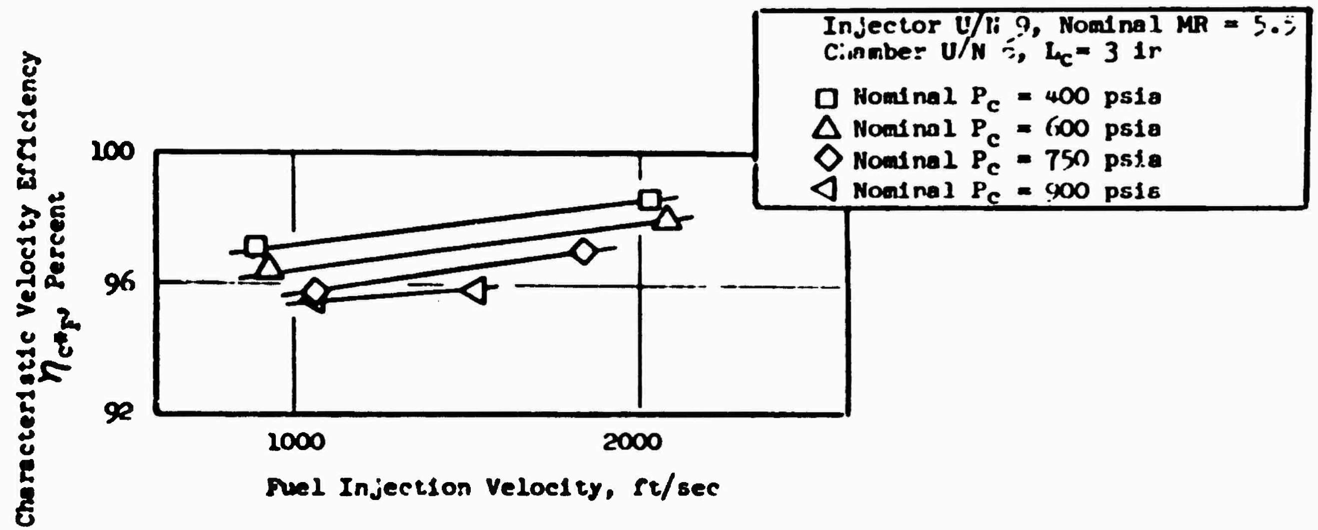

Figure 147. Effect of Fuel Injection Velocity on Characteristic Velocity Efficiency for Double-Panel Trislot Injector

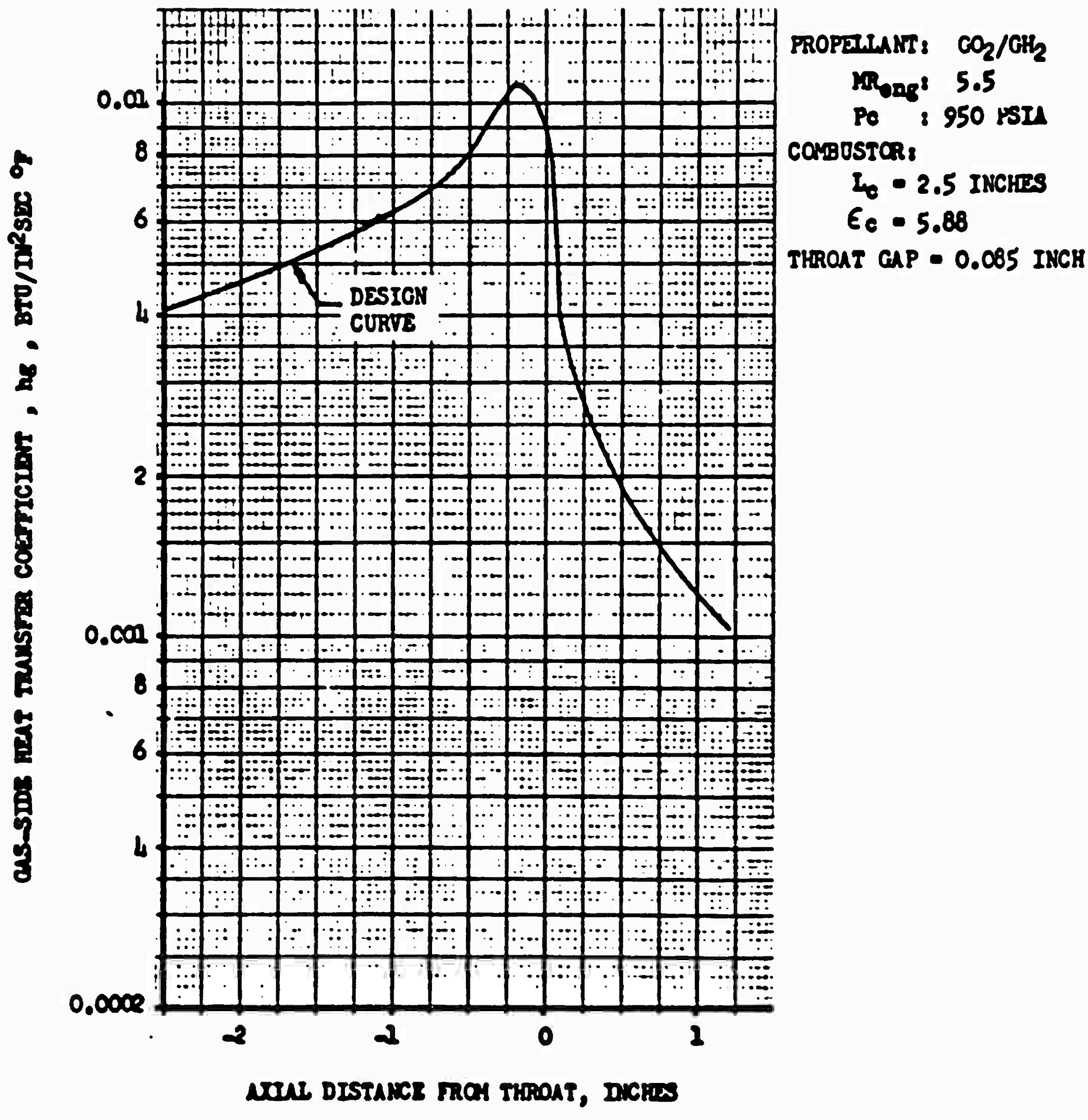

Figure 148. Initial Double-Panel Combustor Design Gas-Side Heat Transfer Coefficient Distribution (Chamber Length = 2.5 inches)

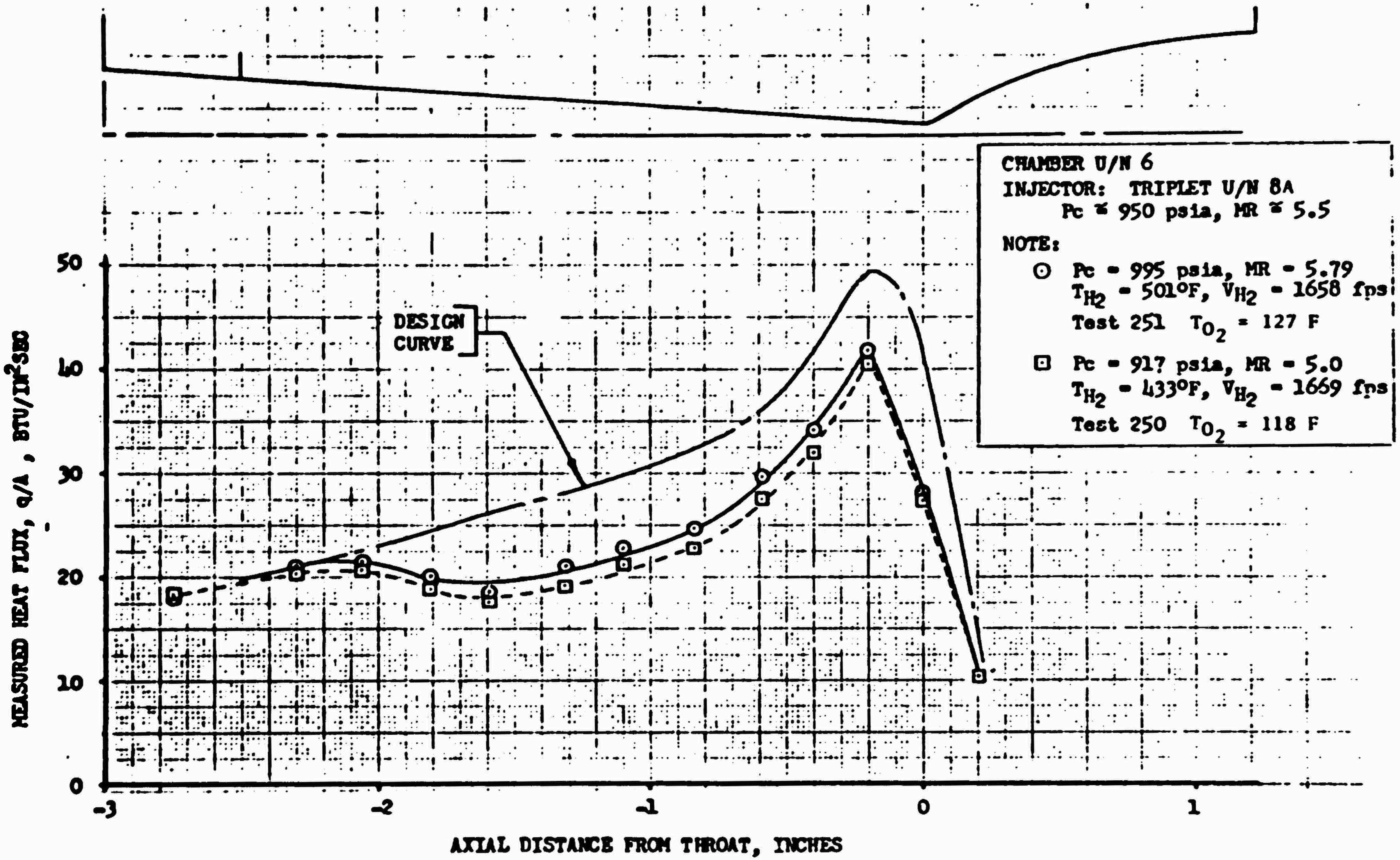

Figure 149. Combustor Heat Flux Distribution, Comparison With Design Curve (P_c = 950 psia, L_c = 3.0 inches)

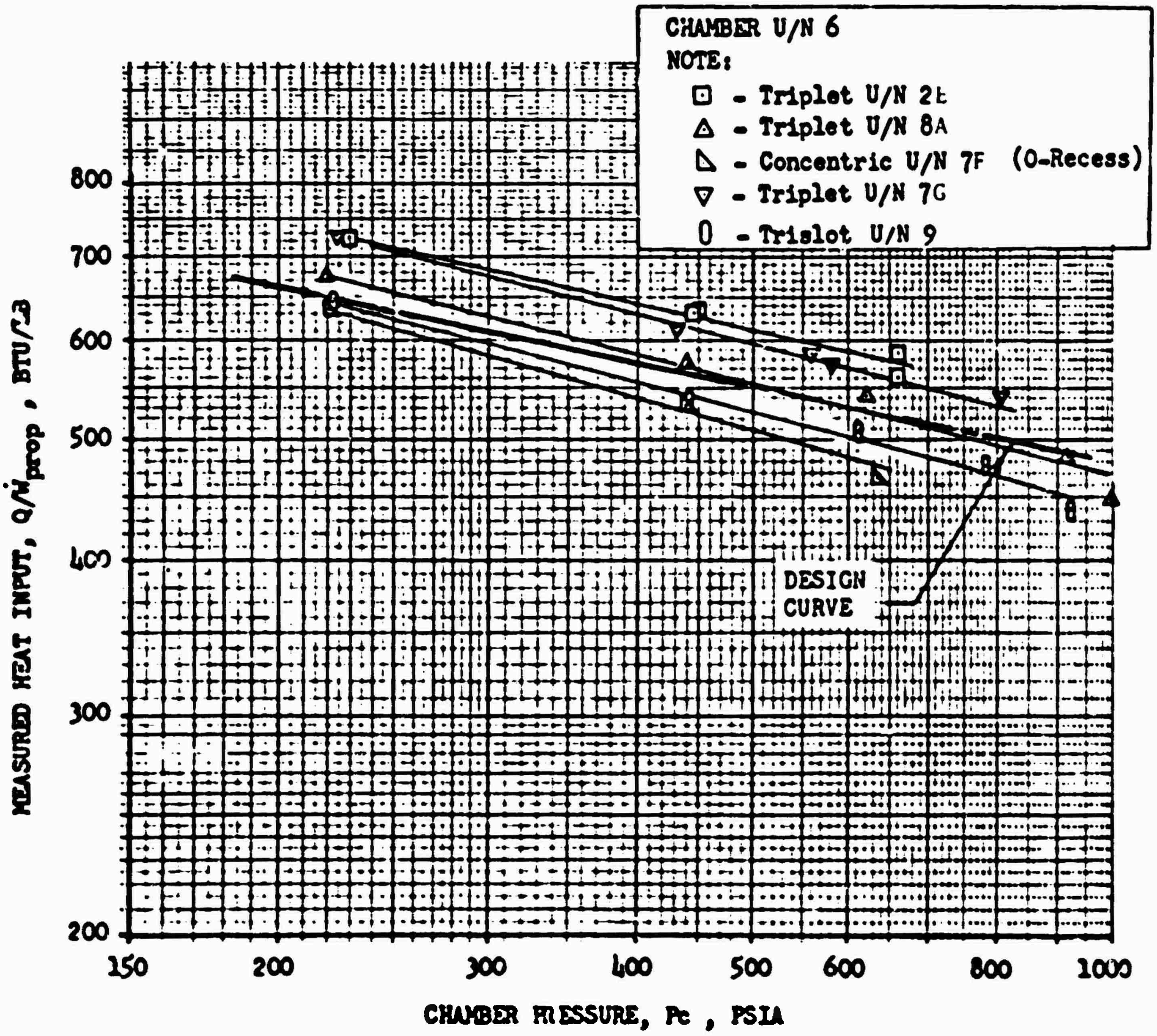

Figure 150. Double-Panel Combustion Chamber Heat Input, Injector Comparison (L_c = 3.0 inches)

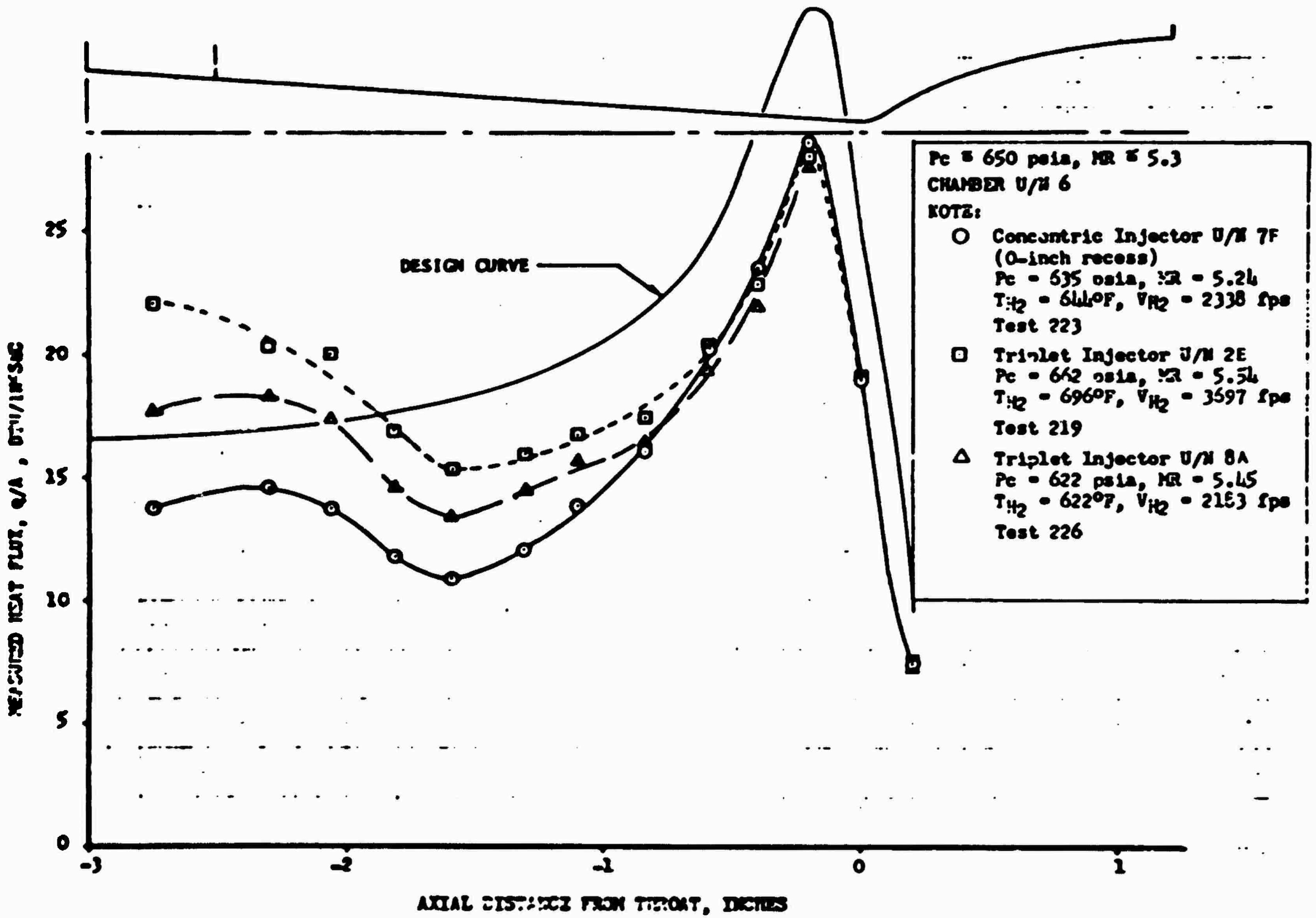

Figure 151. Double-Panel Combustor Heat Flux Distribution--Injector Comparison (Pc ≅ 220 psia, L_c = 3.0 inches)

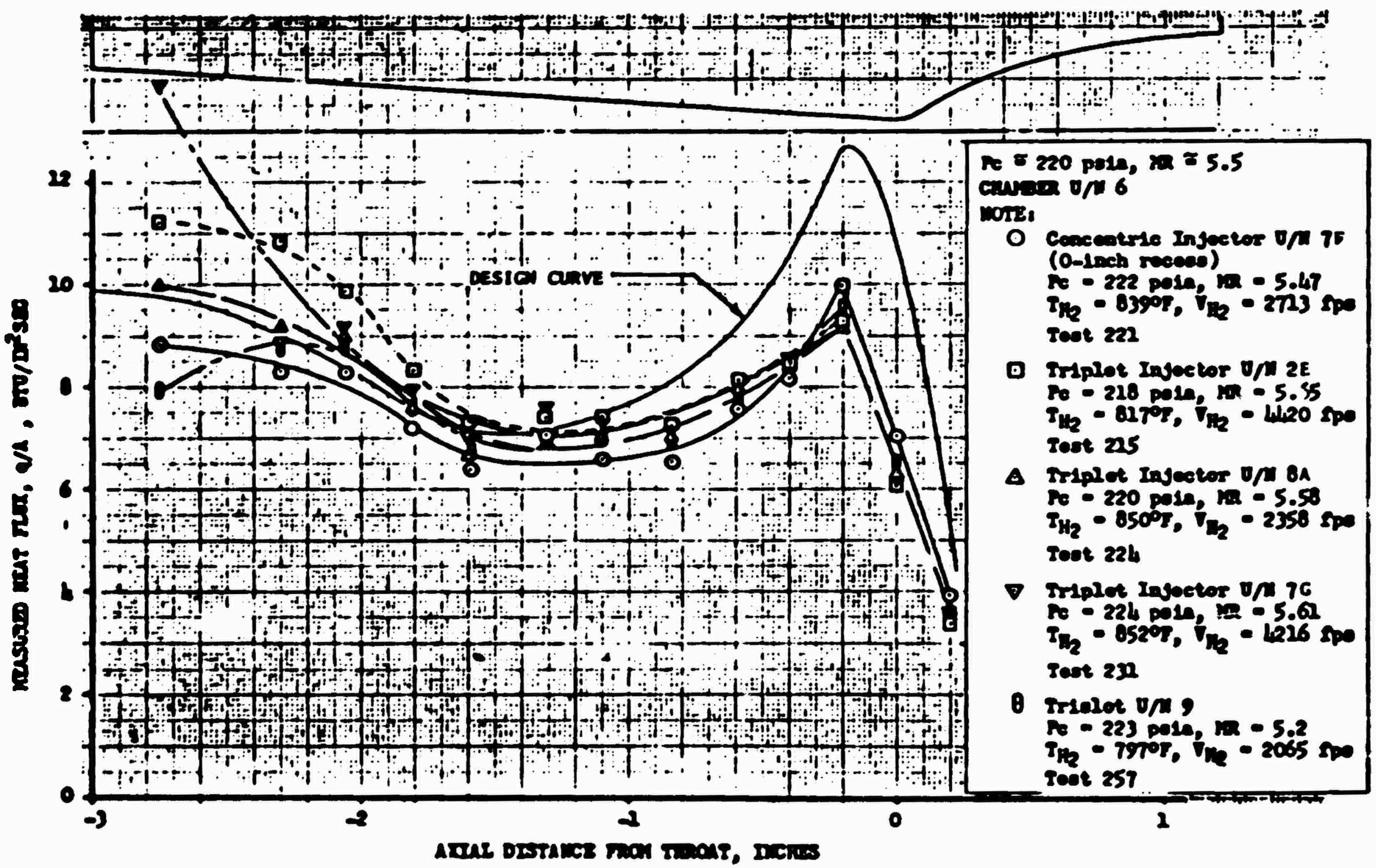

Figure 152. Double-Panel Combustor Heat Flux Distribution--
Injector Comparison (Pc ≅ 650 psia, L_c = 3.0 inches)

As in the single-panel water-cooled chamber testing, an investigation of hydrogen injection velocity revealed that a substantial decrease in injector region heat flux and combustion chamber heat input was achieved with a decrease in injection velocity as illustrated in Fig. 153 through 155. For example, for triplet injector unit 8A at 620-psia chamber pressure, a decrease in velocity from 2000 ft/sec to 1000 ft/sec decreased the injector region heat flux by 50 percent and the heat input by 12 percent, as shown in Fig. 155.

Evaluation of chamber unit 4 (single-panel chamber, $\varepsilon_c = 4.38$) and chamber unit 6 (double-panel chamber, $\varepsilon_c = 5.82$) with triplet injector unit 8A at approximately equal injection velocities (Fig. 154) resulted in essentially the same heat flux from the injector face to approximately 1 inch downstream. This result indicated that the heat flux level in this region of the chamber was primarily dependent on injection velocity and weakly dependent on contraction ratio and fuel temperature. Figure 157 shows that if the injectors were compared at equal injection velocities, triplet injector unit 7G would result in lower injecto egion heat fluxes and lower heat inputs than triplet injector unit 8A for an injection velocity greater than 1500 ft/sec. In general, triplet injector unit 8A and trislot injector unit 9 were more sensitive to variations in hydrogen velocity than triplet injector unit 7G or concentric injector unit 7F.

A comparison of liquid oxygen/gaseous hydrogen test data obtained with the 0.125-inch throat gap chamber and the gaseous oxygen/gaseous hydrogen obtained with the 0.85-inch throat gap chamber is presented in Fig. 156. An interesting result shown in Fig. 156 is that the peak heat flux obtained with the gaseous oxygen/gaseous hydrogen propellant was 3 to 25 percent lower than that obtained with liquid oxygen/gaseous hydrogen propellant. Qualitatively, this phenomenon may be explained by a "softer" combustion fluid with the gaseous propellant creating a longer effective boundary layer development length, resulting in a lower peak heat flux. For the gaseous oxygen/gaseous hydrogen propellant, the peak heat flux varied approximately with the following relationship:

$$q/A \propto P_c^{1.1}$$

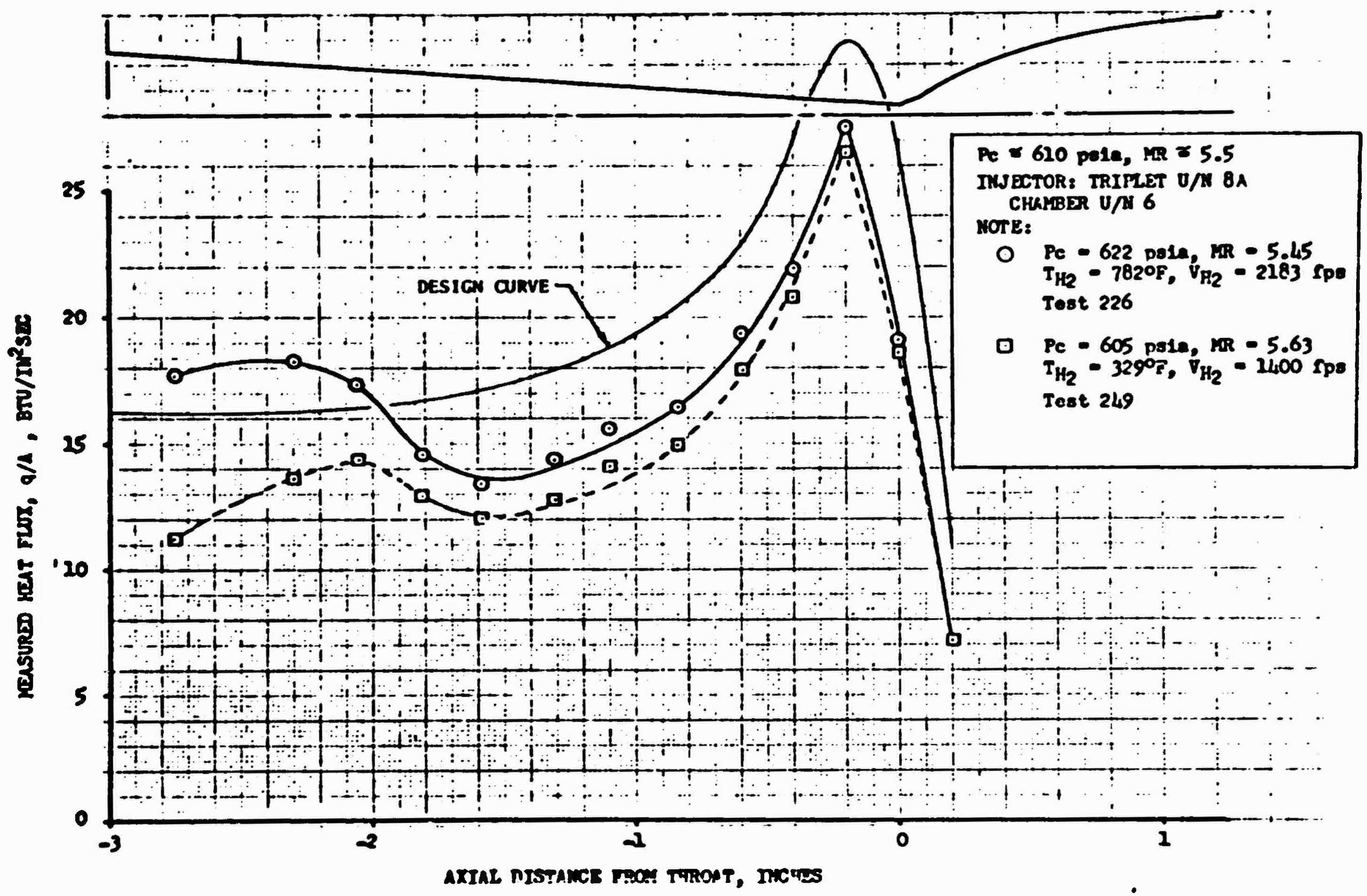

Figure 153. Double-Panel Combustor Heat Flux Distribution--Hydrogen Injection Velocity Influence (Triplet Injector Unit 8A, L_c = 3.0 inches)

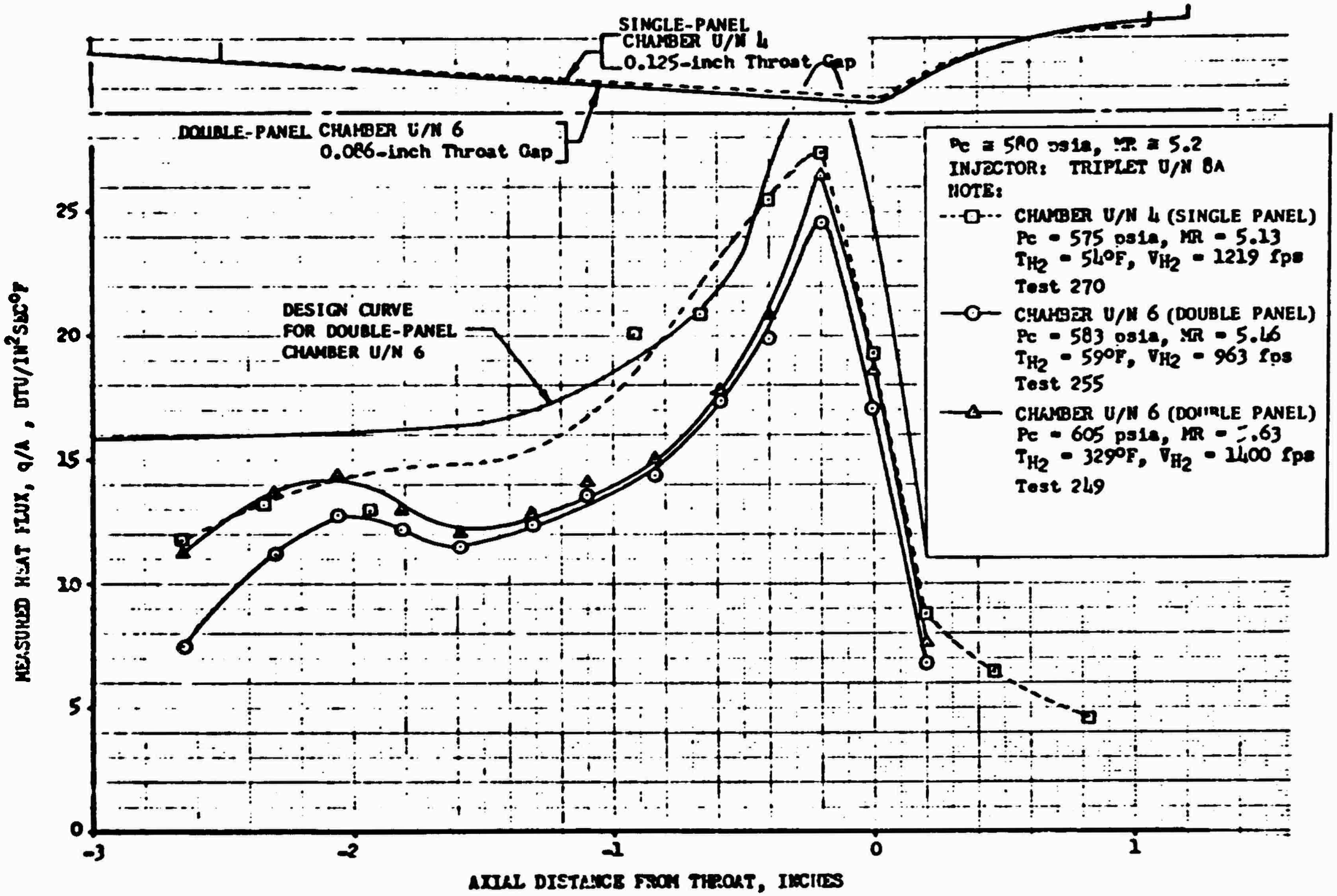

Figure 154. Combustor Heat Flux Distribution--Chamber and Hydrogen Injection Velocity Influences (L_c = 3.0 inches)

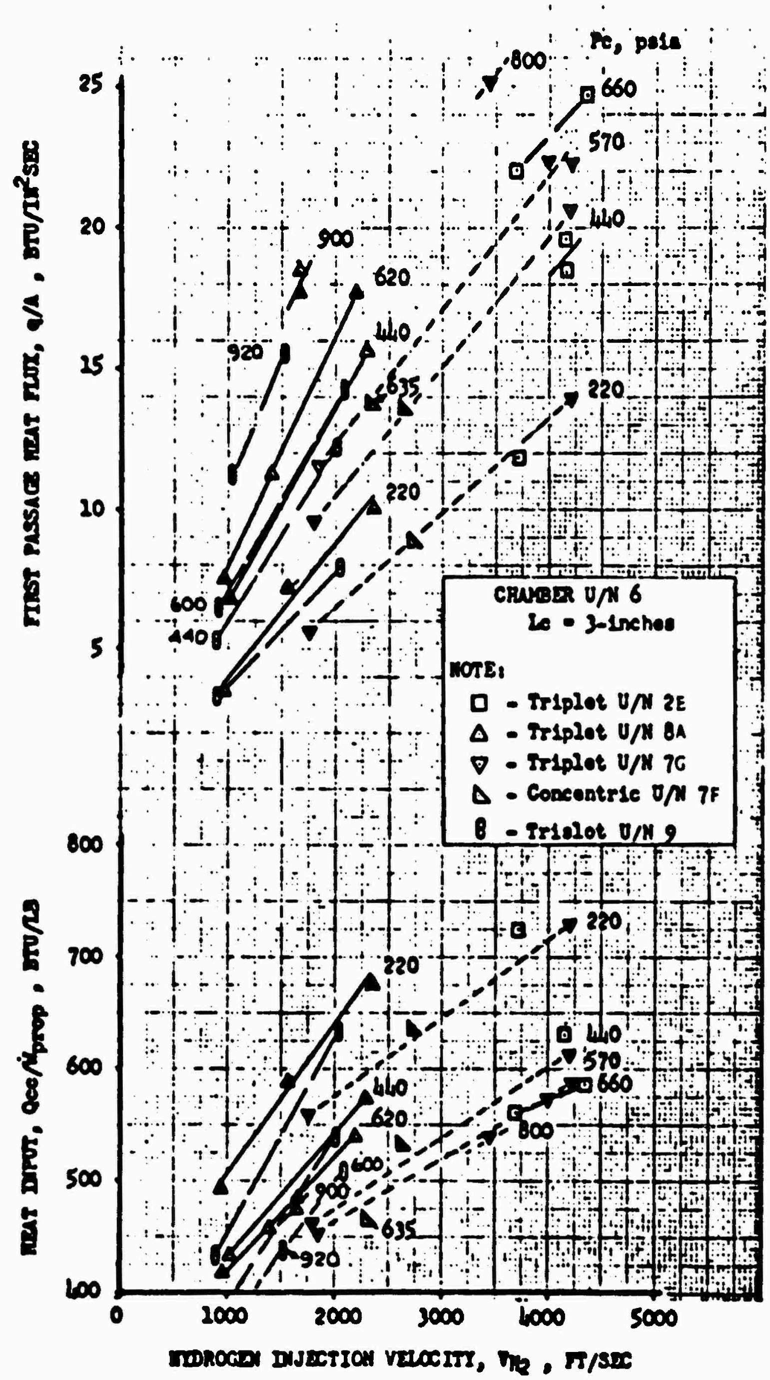

Figure 155. Double-Panel Hydrogen Injection Velocity Influences

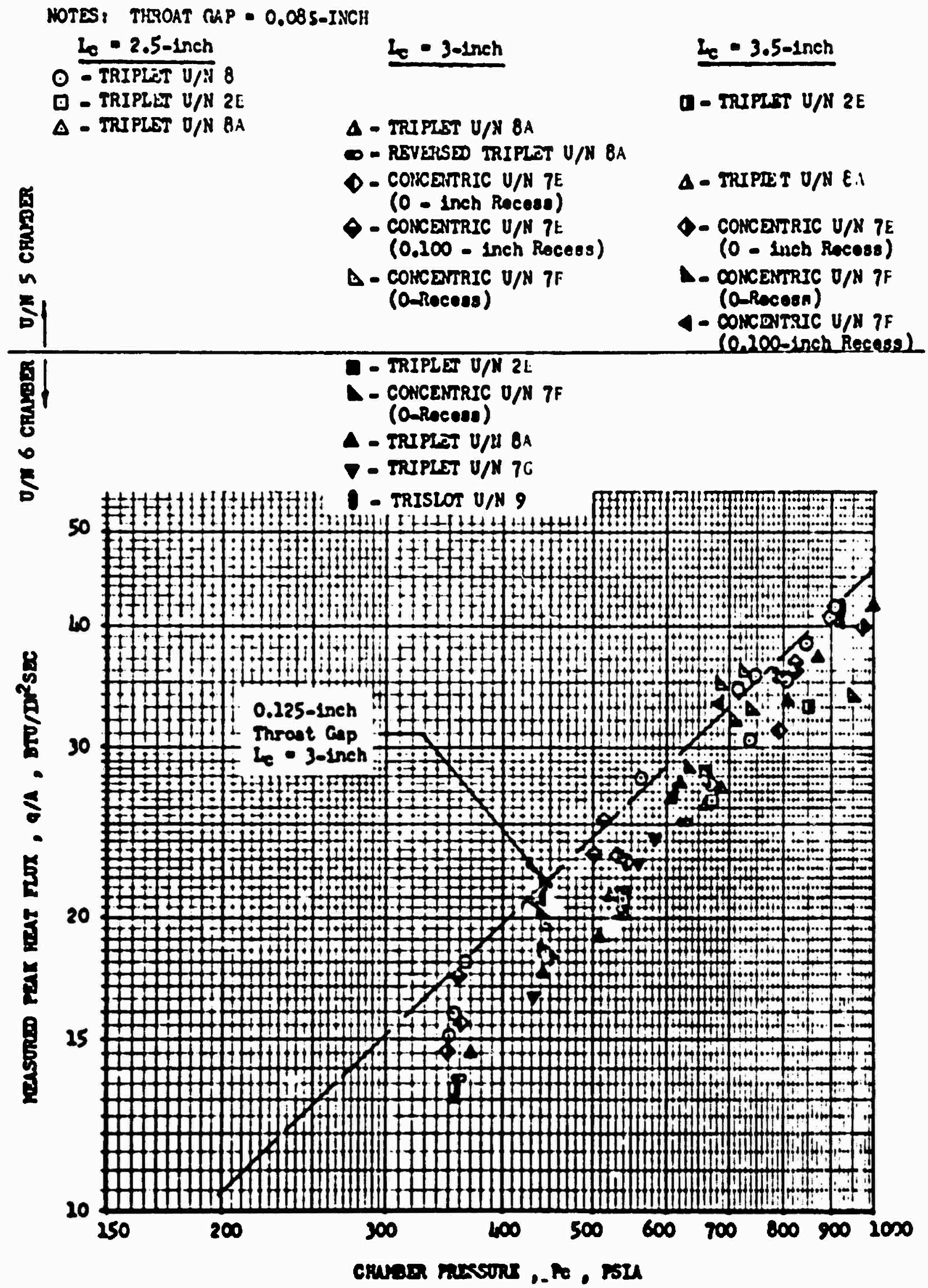

Figure 156. Double-Panel Peak Heat Flux Variation With Chamber Pressure

The final gas-side heat transfer coefficient distributions for triplet injector unit 8A were obtained by cross plotting data for each water passage versus hydrogen injection velocity for different chamber pressures. Based on the design condition injection velocity, velocities at lower chamber pressures were determined. Knowing the injection velocity, the gas-side heat transfer coefficient for each water passage was obtained from the cross plots. This procedure was performed for passages near the injector to the sonic location. Downstream of the sonic location, as for the single-panel combustor, the analytically predicted values were used. The final gas-side heat transfer coefficient distribution for the design chamber pressure, 2 to 1 throttling condition, and the 5 to 1 throttled condition are presented in Fig. 157. For a design gas-side wall temperature of 1000 F, the predicted peak heat flux at 950-psia chamber pressure was 48 Btu/in.^{2}-sec.

Double-Panel Combustion Stability Evaluation

A combustion stability evaluation test series was conducted using the unit 8A triplet injector and unit 4 water-cooled segment chamber. The unit 4 chamber was initially fabricated as a single-panel segment chamber with significant dimensions as noted in Table 12. The unit 8A injector was modified by plugging two injection elements (one adjacent to each side plate) to make the injector compatible with the unit 4 chamber. All other interface items were identical for single-panel and double-panel injectors. The pulse-gun hardware was similar to the assembly used for the single-panel segment combustion stability evaluation, but differed in the size of the pulse charge used.

A 300 H & H magnum cartridge case loaded with 20 or 30 grains of Bullseye pistol powder was used to provide the pulse. A 10,000- or 20,000-psi burst disk was used to produce a steep-fronted chamber disturbance.

A Type 614A4, high-frequency response, Kistler helium-bleed transducer was used to monitor disturbances in the combustion zone. The transducer sensing port was located in the side plate, 0.455 inch downstream of the injector face. A Type 2307, high-frequency response, Photocon transducer located in the oxidizer injection manifold was used to monitor disturbances in the oxidizer injection manifold.

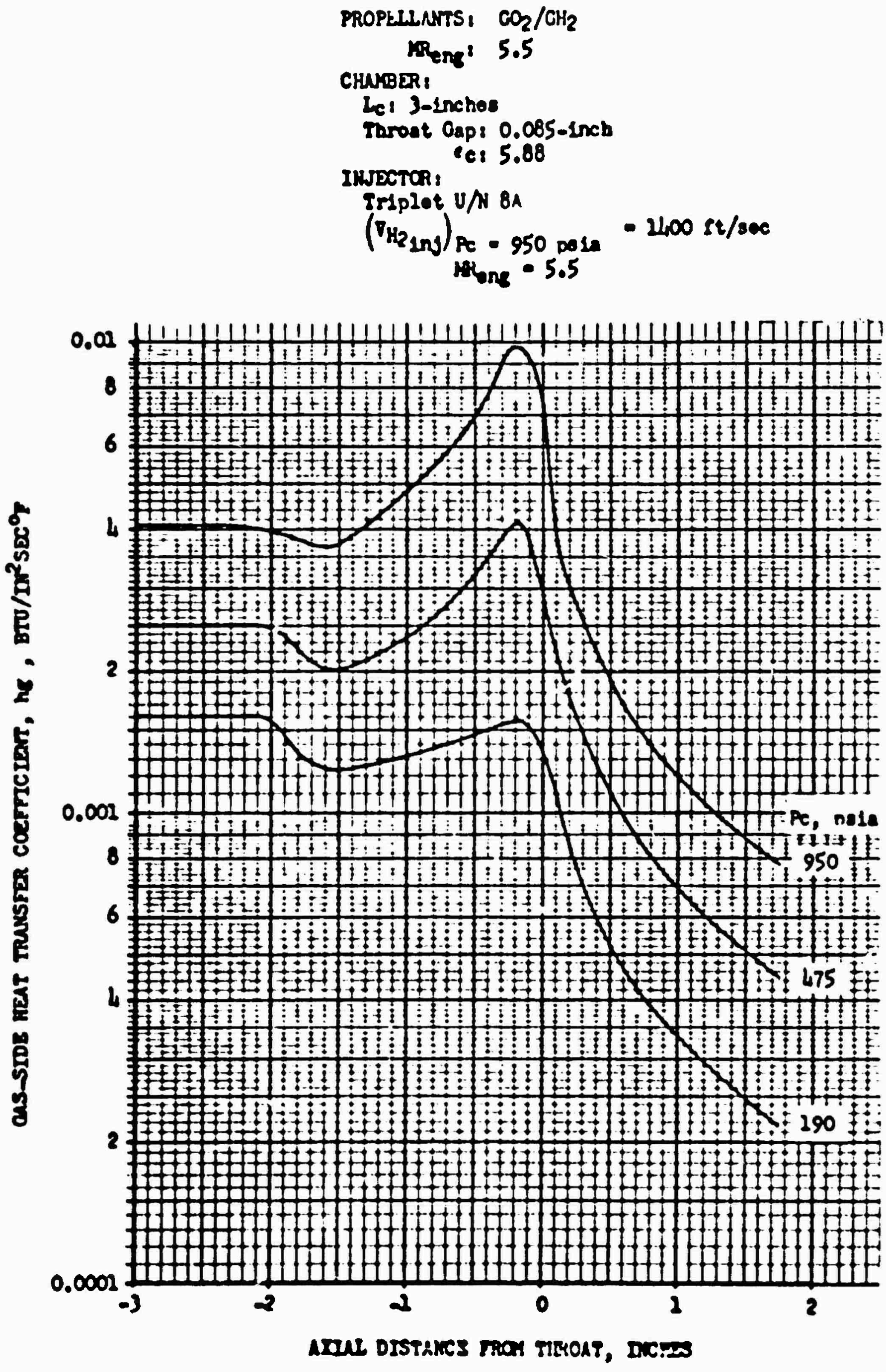

Figure 157. Gas-Side Heat Transfer Coefficient Distribution for Double-Panel Thrust Chamber Combustor

The stability evaluation tests were conducted for an average duration of 6 seconds, with the pulse initiated after 5 seconds of mainstage duration, to ensure stabilized mainstage conditions at the time of the pulse. A steep-fronted pressure disturbance in excess of 50 percent of operating chamber pressure was a program requirement and was obtained on all tests. The pressure disturbance was required to damp within 40 milliseconds per the program requirement.

The test data are summarized in Table 17. In all cases, very high overpressures were obtained and damping occurred within 2 milliseconds. In nearly all cases, the initial pulse overpressure was the maximum pressure noted.

Detail characteristics of a representative pulse (test No. 274) are shown in Fig.158. The amplitude scales differ by a factor of 23, yielding an overpressure of 280 psi in the oxidizer injection manifold for a 3700-psi overpressure in the chamber. This degree of attentuation was caused by the high-resistance oxidizer orifices. The squib detonation was observed as a small vibration appearing in the pressure, and a subsequent rupture of the pulse-gun burst diaphragm could, in most cases, be detected. The chamber overpressure immediately followed the rupture of the burst disk with a rapid rise rate to the maximum level followed by immediate decay. The damp time of this pulse was on the order of 2 milliseconds.

In tests 266 through 269, the Kistler data were somewhat obscured by vibration. In these cases, the chamber overpressure was estimated from the LOX injection manifold Photocon transducer measurement by use of the attentuation factor noted previously, and these estimates appeared reasonable when compared with the Kistler transducer data.

Most of the frequency content was in excess of 10,000 Hz. There were, however, slight indications of the first transverse mode at about 6000 Hz which damped in one or two cycles.

The results of the tests were considered satisfactory evaluation of the combustion stability characteristics of the triplet-type injector for use with the double-panel, regeneratively cooled segment.

TABLE 17. STABILITY EVALUATION TEST RESULTS

(Triplet Injector 8A, Chamber Unit 4)

Test No.	Chamber Pressure, psia	Mixture Ratio, o/f	Chamber Pulse Over-pressure, psia	Chamber Pulse Over-pressure, percent	Charge Size, grain	Burst Disk Rating, psia	Recovery Time, milliseconds
266	197.9	5.61	875*	442	20	10,000	1
267	202.3	5.55	620*	306	20	10,000	1
268	404.7	5.27	860*	212	20	20,000	1
269	400.3	5.30	975*	244	20	20,000	1.5
270	575.2	4.93	2200	382	30	20,000	2
271	593.0	4.89	3575	603	30	20,000	1.5
272	786.7	4.99	3465	440	30	20,000	2
274	761.7	5.55	3700	486	30	20,000	2
275	934.5	5.16	1850	198	30	20,000	2
276	968.5	5.42	1600	165	30	20,000	2

*estimated from oxygen manifold pressure

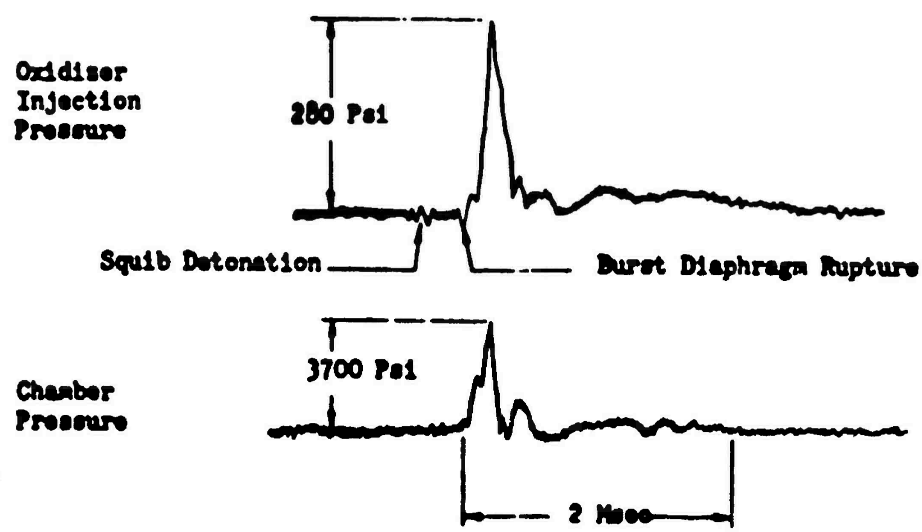

Figure 158. Pulse Test No. 274

Double-Panel Injector Combustion Stability Characteristics

All water-cooled segment chambers were designed and fabricated with the capability for use of a Kistler helium-bleed transducer to monitor chamber pressure during a test. A Kistler transducer was installed in the combustor and monitored during every single-panel and double-panel test.

With the exception of the combustion stability evaluation tests, there were three instances of self-induced, nondamping, high-frequency, acoustic instability noted during the entire single-panel and double-panel hot-fire test programs. These occurred during the double-panel program and were confined to the unit 7F injectors.

The tests of unit 7F injector (12 tests, no oxidizer post recess) with ambient hydrogen injection temperatures resulted in three instances of ignition-chamber pressure surge-induced, high-frequency, ~5700-Hz acoustic instability. The instability occurred on tests 202-71, 204-71, and 205-71 and was confined to tests at chamber pressures of 600 psia and higher.

In the three instances which occurred, there was no recovery during the entire duration of the test; however, no hardware or facility damage occurred. The only significant effect of the instabilities was a very slight increase in upper combustion zone local heat transfer rates and a 2- to 3-percent decrease in η_{c*}.

DOUBLE-PANEL SEGMENT TEST EVALUATION SUMMARY

The double-panel segment test program objectives were the same as those applicable to the single-panel segment program, i.e., injector-combustor performance, heat transfer compatibility in the regeneratively cooled mode, and evaluation of combustion stability characteristics.

Figure 159 presents the injector-combustor development flow chart which depicts the various injector-chamber configurations evaluated.

Injector-Combustor Selection

The program requirements for the double-panel injector-combustor assembly were as follows. The design shall have high combustion efficiency over the complete throttling range, 97 percent minimum η_{c*} based on full shifting c*, smooth ignition and chamber pressure transient characteristics, no excessive injector streaking, and uniform heat transfer into the chamber wall with no sharp peaks in predicted local wall temperatures that would jeopardize the chamber durability requirements.

The combustor assembly was required to be as small as possible so that the thrust chamber assembly weight requirements could be met.

The double-panel concept, although unique, was a logical evaluation of the single-panel design. Therefore, the basic single-panel design philosophy was extended to the double-panel concept.

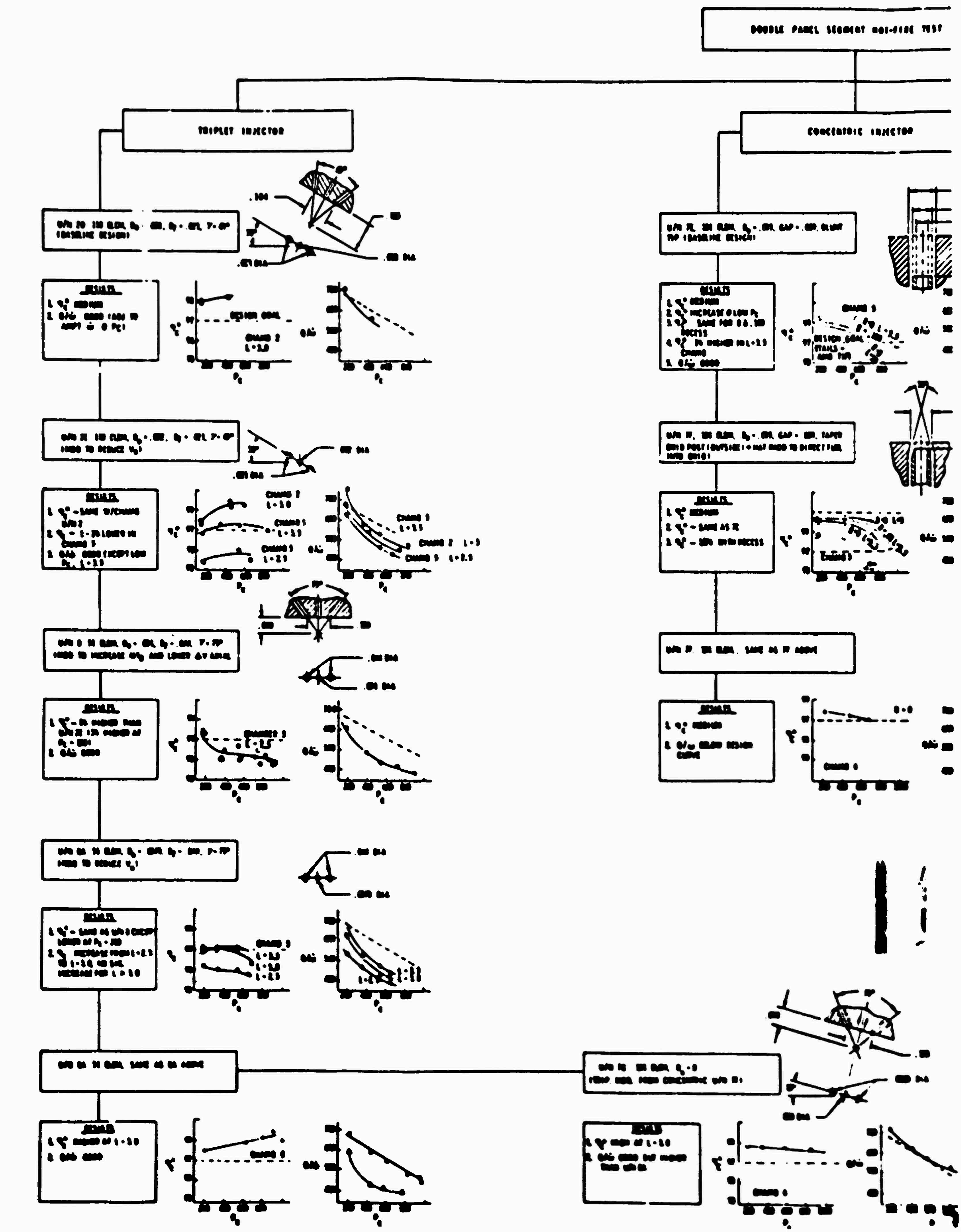
DOUBLE PANEL SEGMENT HOT-FIRE TEST
TRIPLET INJECTOR
CONCENTRIC INJECTOR
RESULTS
RESULTS
RESULTS
RESULTS
RESULTS
RESULTS
RESULTS
RESULTS

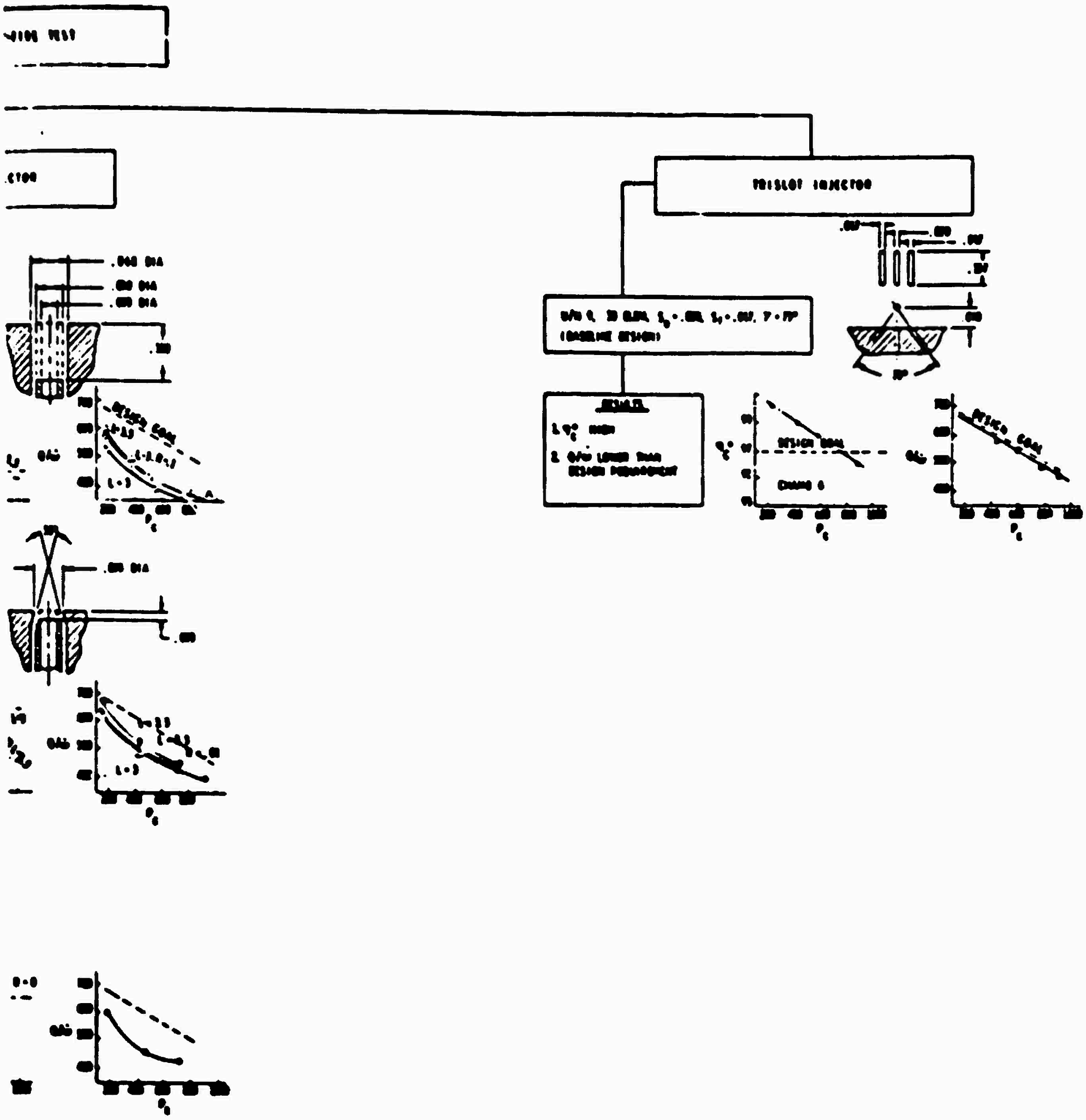

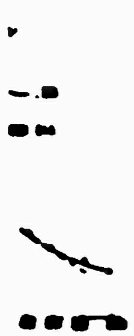

Figure 159. Double-Panel Segment Hot-Fire Test, Development Flow Chart

The minimum L*, L_c, and low-volume combustor approach with a low thrust per element injector was retained for the double-panel segment. Two distinct advantages were realized:

1. Program requirements had been met for the single-panel concept and, therefore, a baseline had been established.
2. Commonality of test components, particularly injectors, provided maximum development versatility, minimum time, and cost.

As noted previously, the initial gas-gas injector investigation was conducted with a modified triplet injector, unit 2D, that had been used for single-panel, gas-liquid injector development.

The initial combustor configuration provided an $L_c = 2.5$ inches, which was 0.5 inch less than the selected single-panel combustor configuration. The decrease in length from that selected for the single-panel design was due to an expectation that gas-gas mixing and combustion could be accomplished in a shorter L_c than gas-liquid due to lack of a vaporization process. Combustion chamber length (L_C) is considered the primary parameter for low-volume combustors and L* is not particularly significant.

The test results showed that an $L_c = 3.0$ inch is required for the double-panel combustor to obtain high performance. The combustor configuration selected for the regeneratively cooled double-panel combustor includes an $L_c = 3.0$ inch and has the characteristics noted in Table 11 (unit 6 modified).

The two primary criteria for selection of the injector were combustion efficiency and injector influenced heat transfer to the combustor. The selection criteria are presented in the following sections.

The injectors which were evaluated all demonstrated acceptable heat transfer, but some were lacking in performance. The triplet-type injectors demonstrated satisfactory performance, 98 to 99.5 percent c* efficiency over the design throttle range. The concentric and trislot types provided good performance (100 percent c* efficiency) at the full chamber pressure design point but marginal performance at the full throttled design point (96 percent c* efficiency).

The injector configuration selected for the double-panel, regeneratively cooled segment assembly was the unit 8 triplet with the following design parameters:

1. Number of elements: 51
2. Oxidizer injection velocity: 500 ft/sec
3. Fuel injection velicity: 1400 ft/sec
4. Two rows of elements equally spaced in the circumferential direction
5. Oxidizer orifice diameter: 0.033
6. Fuel orifice diameter: 0.050
7. Element geometry and wall spacing same as unit 8 triplet

The predicted performance for the double-panel, regeneratively cooled injector is shown in Fig. 160.

Heat Transfer. The heat transfer characteristics of the injectors were presented in Fig. 151 through 154. The triplet injector selected for the double-panel injector adequately met the combustor assembly design requirements. The peak local heat flux in the throat was less than originally predicted (Fig. 149), and the total heat rejection rates were less than originally predicted (Fig. 150).

The final gas-side heat transfer coefficient distribution for the double-panel regeneratively cooled chamber is presented in Fig. 156.

Predicted Double-Panel Injector Pressure Loss Characteristics

The predicted pressure loss characteristics for the double-panel, regeneratively cooled injector during hot-fire test are shown in Fig. 161 and 162.

General Test Program Summary

A total of 154 hot-fire tests was conducted during the double-panel test program. Test component durability was excellent.

Combustion Chamber Configuration. Four variations of combustion chamber configurations, with a constant injector end width of 0.50 inch, were evaluated:

1. Constant convergence, $L_c = 2.5$ inch, unit 5
2. Constant convergence, $L_c = 3.0$ inch, unit 6 modified and unit 2
3. 2.5-inch constant convergence, and 0.50-inch straight section (water-cooled spacer), unit 5
4. 3.0-inch constant convergence, and 1.00-inch straight section (water-cooled spacer), unit 6

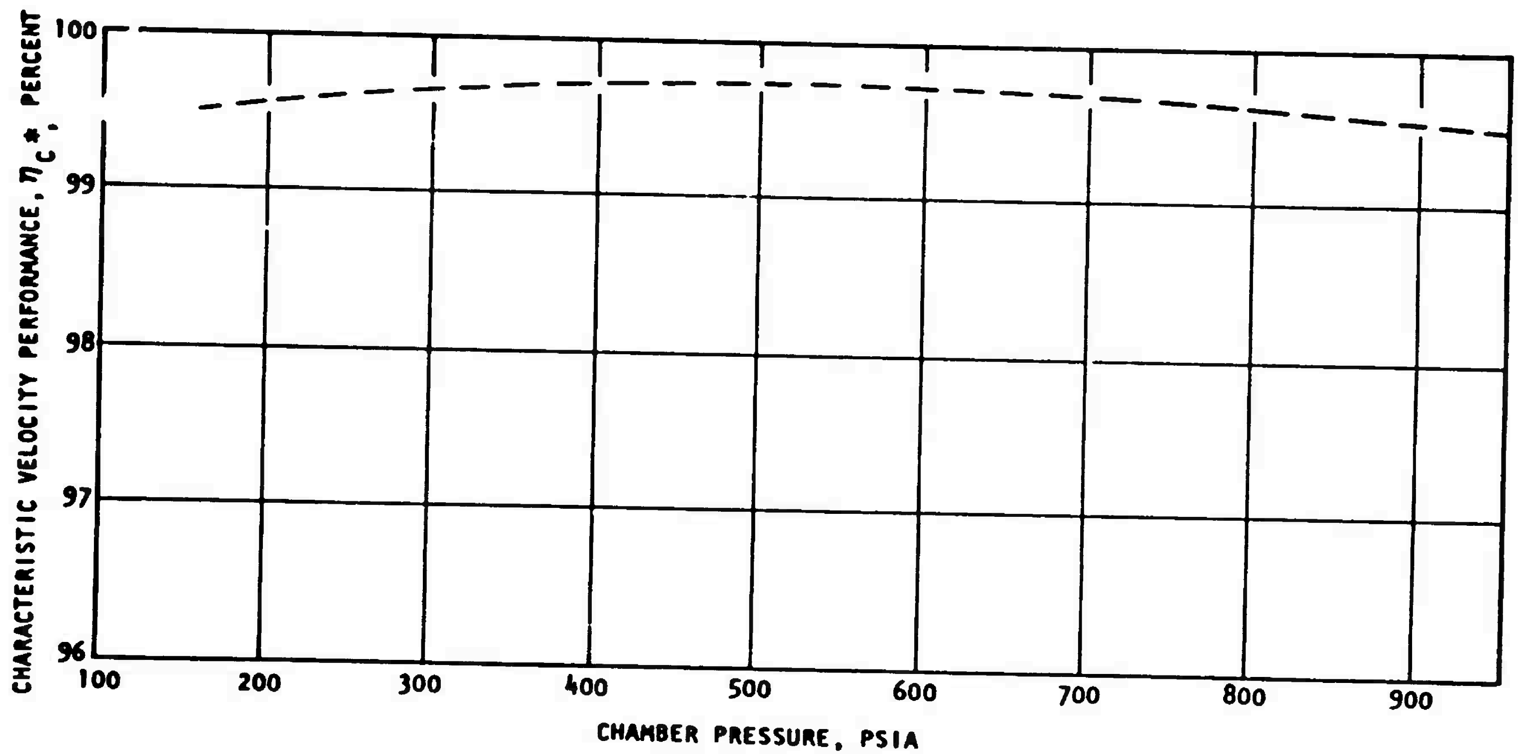

Figure 160. Predicted c* Performance vs Chamber Pressure for the Double-Panel Regeneratively Cooled Segment, 51-Element F-O-F Triplet Injector

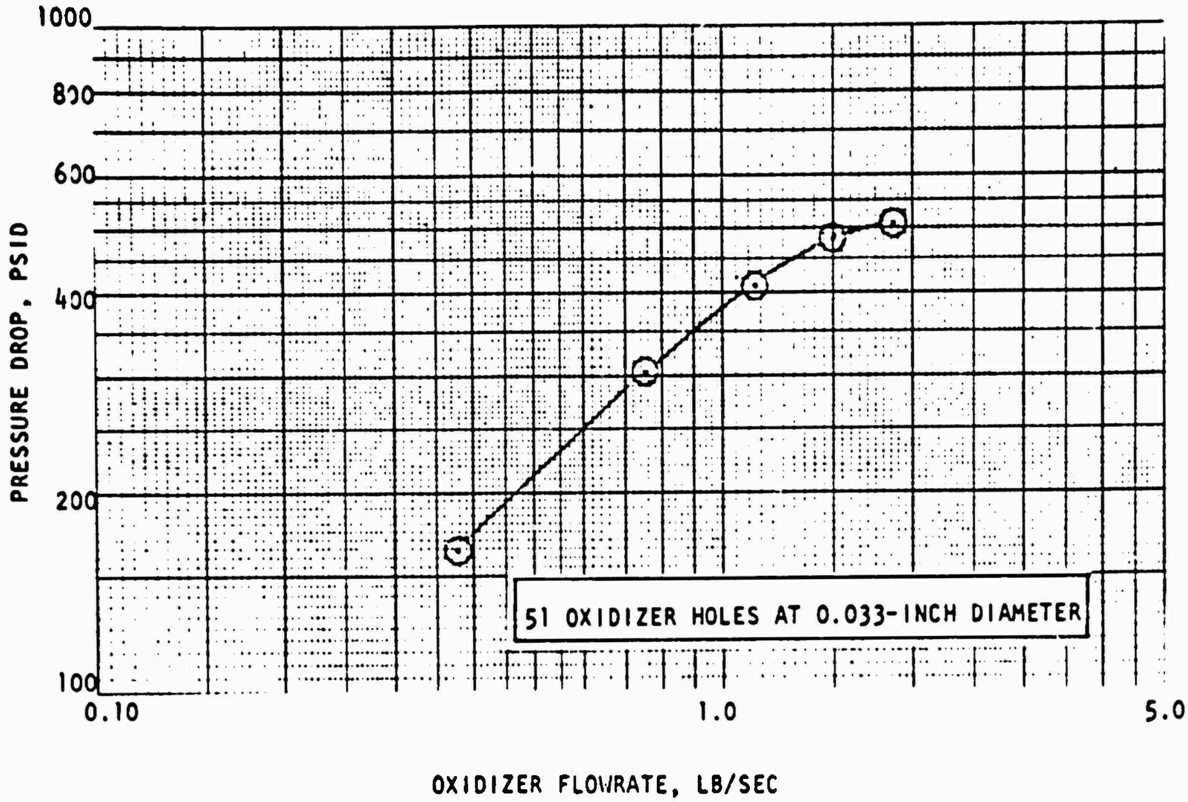

Figure 161. Double-Panel Gas-Gas Triplet Injector, Oxidizer Side, Predicted Pressure Drop

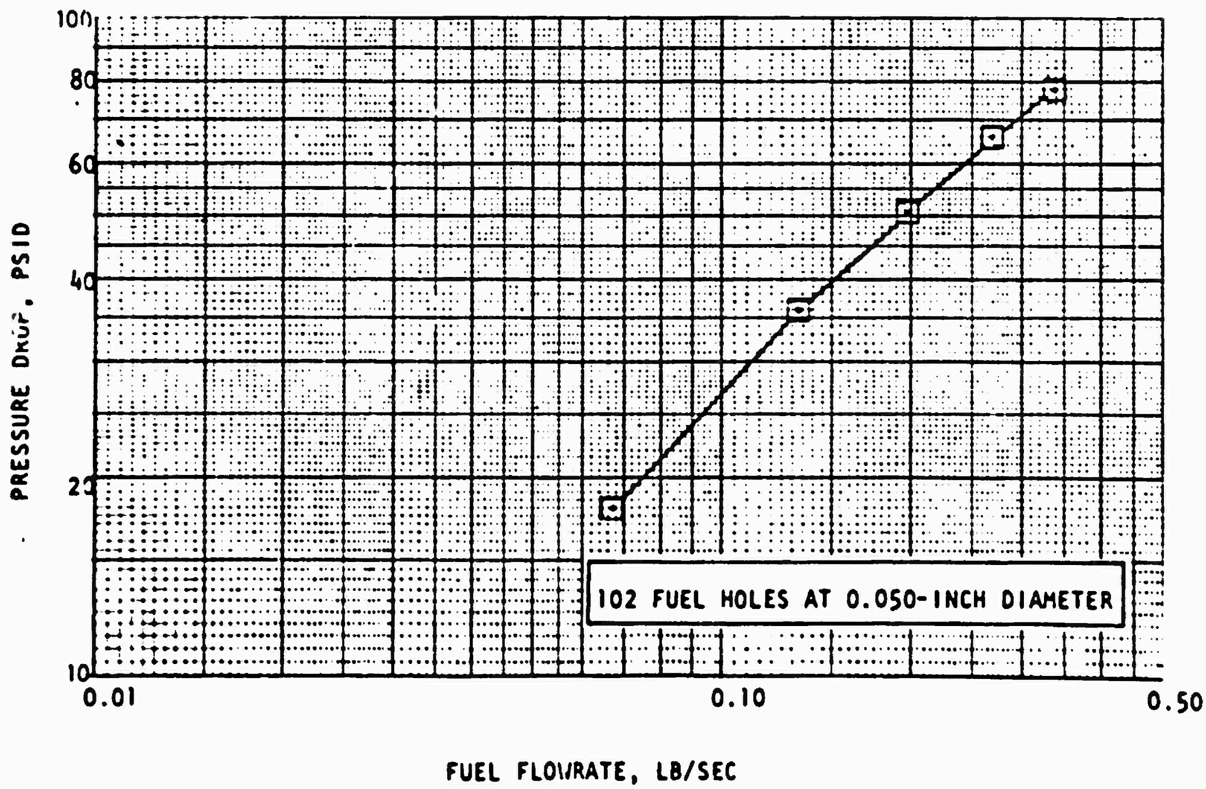

Figure 162. Double-Panel Gas-Gas Triplet Injector, Fuel Side, Predicted Pressure Drop

The increase from 2.5 to 3.0 inch in the constant convergence configuration was necessary to provide the required performance. No distinct advantage was determined for increasing to $L_c = 3.5$ inch.

The straight section adjacent to the injector was found to be detrimental to performance, 0.75- to 1.5-percent decrease, and the degradation was a function of injector type, which was significant with triplet injectors.

A combustor with a constant convergence angle through the combustion zone, an $L_c = 3.0$ inches, a 0.5-inch injector end width, and a 0.085-inch throat gap was established as the configuration for the double-panel, regeneratively cooled segment chamber.

Injector Configuration. The triplet, concentric, and trislot injectors all demonstrated satisfactory heat transfer characteristics.

The triplet injectors and several of the concentric orifice configurations demonstrated satisfactory performance. The trislot injector indicated decreasing performance with increasing chamber pressure. This result appears to be a thrust per element (flowrate per element) effect. The trislot had 30 injection elements compared to 51 for the unit 8 triplet and over 100 for the concentric triplet, unit 2. Sufficient evaluation was not conducted to ascertain the exact cause of the performance decrease, although sufficient data were obtained to detect a dependency on fuel injection velocity.

An injector similar to the unit 8 triplet, with 0.050-inch fuel orifices, 0.033-inch oxidizer orifices, and 51 elements, was selected for the double-panel, regeneratively cooled segment chamber.

Test Facility. Facility operation was satisfactory throughout the test program. No problems were encountered in either facility or data-acquisition systems.

SECTION VI

TEST FACILITY

The test facility used for the single-panel and double-panel water-cooled segment testing is located in the Propulsion Research Area (PRA). The PRA is comprised of five multiposition firing pits with a centrally located blockhouse which permits direct observation of the test firings. Test stand Peter was used for the segment hot-fire tests. Test hardware installation is shown in Fig. 163 and 164.

PROPELLANT SYSTEMS

The propellant system schematic is shown in Fig.165.

Oxidizer

As shown in Fig. 165, a 15-gallon, jacketed, liquid oxygen (LOX) tank was employed as a high-pressure run tank for single-panel segment testing. The LOX was transferred to this tank at the start of each test period from low-pressure LOX storage spheres. The maximum liquid oxygen injector inlet pressure was 1250 psig at the maximum flowrate of 2.0 lb/sec. Two tandem Fischer Porter turbine flowmeters (series 10C1505, 3/4 in.-23) were used for flow measurement complemented by a cavitating venturi meter for flow control and measurement. A filter, 40-micron nominal rating, was located close to the injector inlet to prevent foreign material from entering the injector and plugging the oxidizer orifices.

For the double-panel segment tests employing gaseous oxygen (GOX), the 15-gallon LOX tank GN_2 pressurant supply was disconnected and a 72-bottle gaseous oxygen supply was connected to the system. In this manner, the tank pressurization system was employed to set GOX run pressures, and the rest of the system, excluding LN_2 chill, remained the same. For the heated GOX tests, an open-air heater similar to that used for the fuel (Fig. 165) was employed. The flowmeters and cavitating venturi were replaced with a Flowdyne Company sonic venturi, Type V160-SA, for flow measurements on both heated and ambient GOX tests.

SAA2S-12/3/71-S1B

Figure 163. Water-Cooled Segment Facility Installation

SAA25-12/3/71-S1A

Figure 164 Water-Cooled Segment Facility Installation (Closeup)

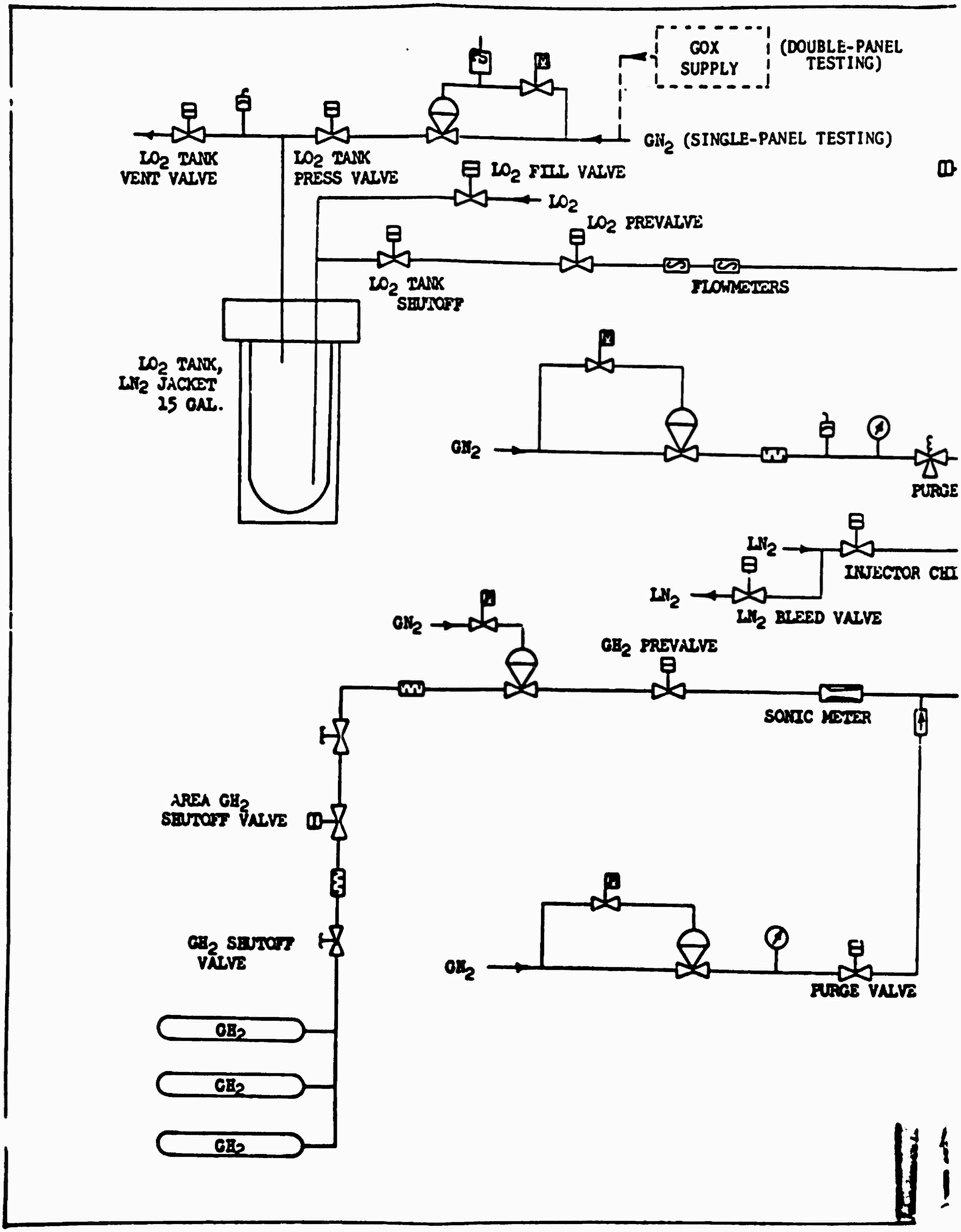
GOX SUPPLY
(DOUBLE-PANEL TESTING)
GN2 (SINGLE-PANEL TESTING)
LO2 TANK VENT VALVE
LO2 TANK PRESS VALVE
LO2 FILL VALVE
LO2
LO2 PREVALVE
LO2 TANK SHUTOFF
FLOWMETERS
LO2 TANK, LN2 JACKET 15 GAL.
GN2
PURGE
LN2
INJECTOR CHI
LN2
LN2 BLEED VALVE
GN2
GH2 PREVALVE
SONIC METER
AREA GH2 SHUTOFF VALVE
GH2 SHUTOFF VALVE
GN2
PURGE VALVE
GH2
GH2
GH2

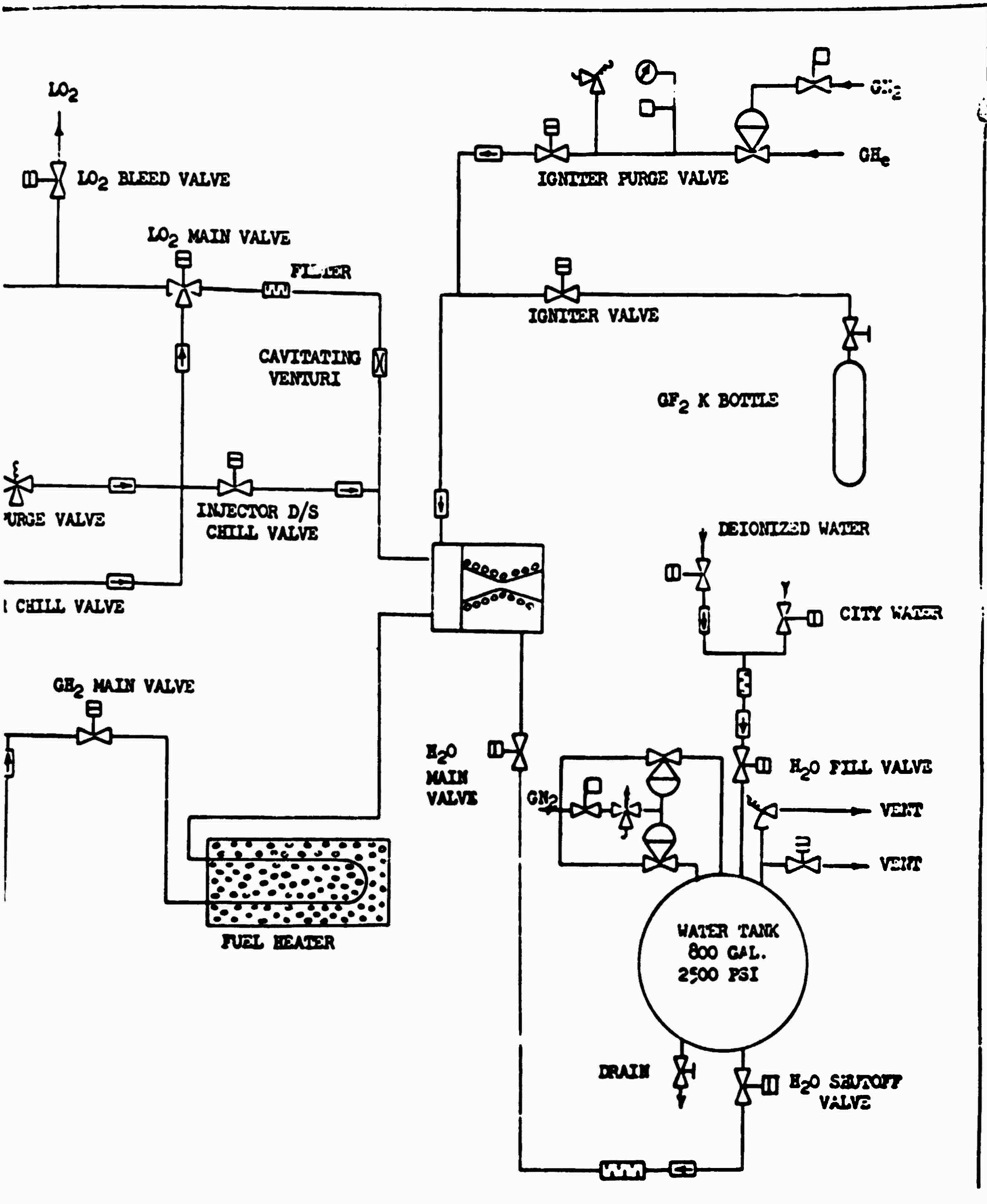

Figure 165. Peter Stand, Propellant and Purge System Schematic

Fuel

The hydrogen was obtained directly from gaseous storage bottles. Maximum gaseous hydrogen injector inlet pressure was 1250 psig with the maximum flowrate of 0.34 lb/sec for the single-panel tests and 1350 psig at 0.33 lb/sec, respectively, for the double-panel testing. A sonic venturi meter fabricated and calibrated by Flow-dyne Company was used for flowrate measurement. The gaseous hydrogen was at ambient temperature at the point of flowrate measurement. A hydrogen-fired soak heater was provided to increase the fuel temperature prior to inlet to the injector. The increased injection temperature was necessary so that an approximate matching of the fuel injection temperature expected with the regeneratively cooled chamber could be obtained for water-cooled segment testing.

SLUG HEATER

The propellant hydrogen for the single-panel and double-panel investigation was heated, where desired, by use of a slug heater. The heater is shown in the fore-ground in Fig. 163. The heater consisted of a heat source and a heat storage device. The heat was provided by burning gaseous hydrogen with air in close proximity to the heat storage device. The storage device consisted of two 6-foot sections of heavy-wall CRES pipe, stacked two high. The pipes were completely filled with 3/8-inch-diameter scrap ball bearings. The ball bearings provided the actual heat storage capability.

The slug heater did not maintain a constant temperature over the complete test duration, but the temperature range of operation during the test was small, as shown in Fig. 166. A slug heater identical to the hydrogen heater was used to heat the gaseous oxygen for tests 168-71 through 170-71.

IGNITION SYSTEM

Ignition was provided by use of ambient temperature, gaseous fluorine from a K-bottle. The GF_2 was introduced into the oxidizer main line upstream of the injector and expelled into the chamber by subsequent oxidizer flow. A supply pressure of 200 to 400 psia was used for ignition. The igniter oxidizer valve was opened for 1.5 seconds, then closed.

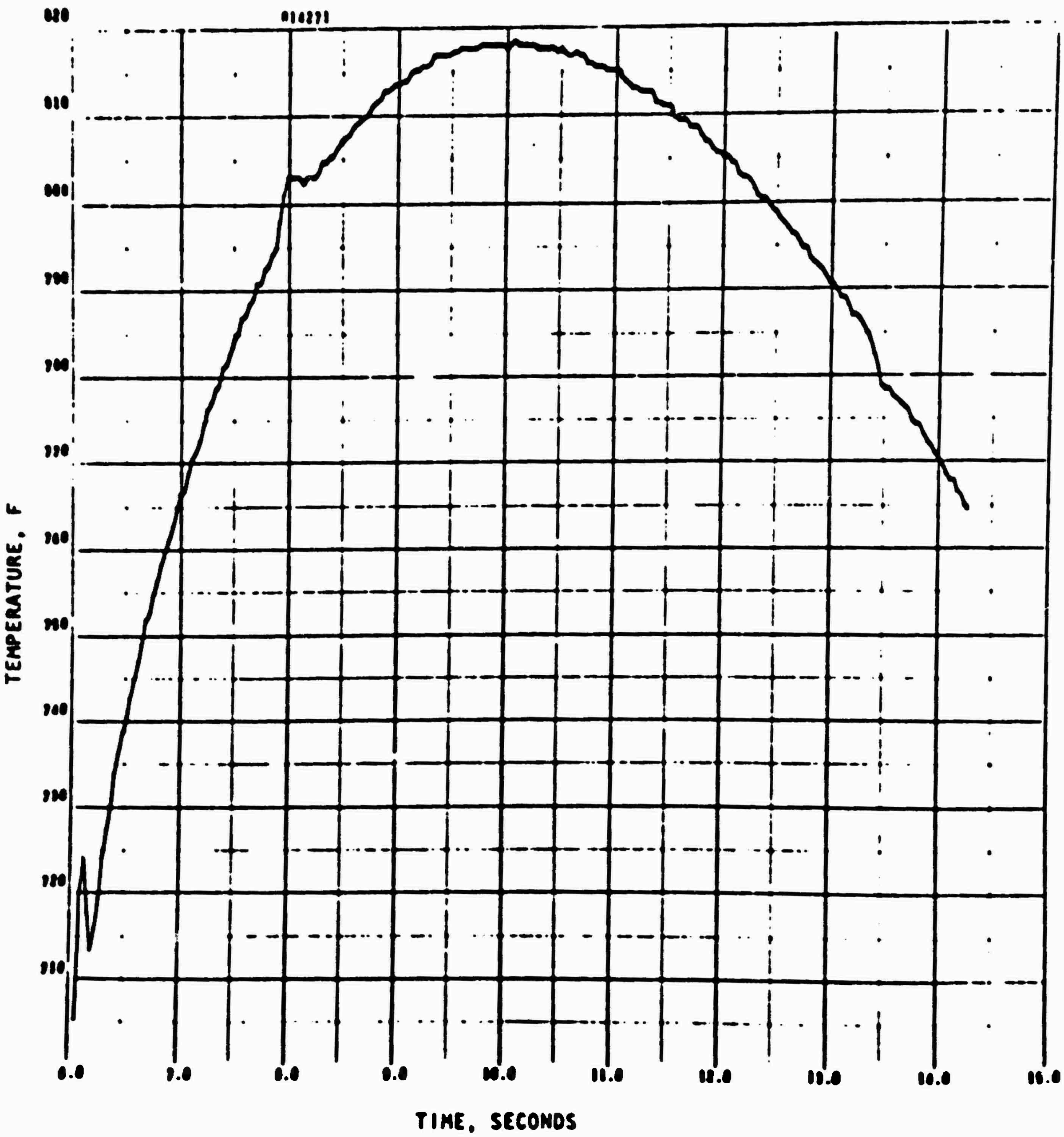

Figure 166. Fuel Injection Temperature vs Time for Test 271-71
Showing Fuel Heater Characteristics

WATER-COOLANT SYSTEM

The water-coolant system was capable of providing 30 lb/sec of water at a water inlet pressure of 2000 psig. The water was filtered through a nominal 100-micron filter prior to entrance into the thrust chamber cooling passages. The coolant flowrate for each circuit was measured by a turbine-type flowmeter. The differential between inlet and exit temperature of the water also was measured with thermocouples.

PRESSURANT AND PURGE SYSTEMS

The purge gas for the fuel system was ambient gaseous nitrogen dried to maintain a water content of 5 ppm or less. No pressurant was required for the fuel system because the hydrogen is taken directly from a high-pressure ambient gas source and regulated to the desired pressure.

The pressurant and purge gas for the oxidizer system was ambient gaseous nitrogen dried to maintain a water content of 5 ppm or less.

The purge gas for the gaseous fluorine ignition system was dried gaseous helium. A water content of 5 ppm or less, at a helium flowrate of 3000 scfm, was maintained.

Ambient gaseous nitrogen was used for the dual O-ring seal purge at the injector-to-thrust chamber joint. The pressure was set at 50 psig greater than operating chamber pressure.

TEST PROCEDURES

Injector Passivation

The injectors were LOX cleaned prior to assembly on the test stand. Prior to initial tests, GF_2 was flowed through the injector to ensure passivation with the igniter propellant.

Test Sequencing

Water-coolant flow was fully established and verified prior to initiating the start sequence. Test sequencing employed for the single- and double-panel testing was the same except for injector chill procedures for the LO_2 side with the single-panel tests. A schematic of the test sequence is shown in Fig. 167. A fuel lead was first established followed by slug injection of GF_2 with oxygen.. System purges were slaved to propellant main valves and the GF_2 was checked off against the oxygen line pressure during ignition. Subsequently, the igniter valve was closed and the mainstage duration of the test conducted. The run duration was controlled by means of an electronic timing device which controlled the opening and closing of the propellant and purge valves. The shutdown sequence consisted of automatic closing of the main oxidizer valve and opening of the oxidizer purge valve followed, after a period of fuel lag, by the main fuel valve closing. The fuel purge valve is opened, at which time both purges are active and, finally, both purge valves are manually activated closed.

System Cutoff Devices

Automatic redline cutoff devices, which were part of the Beckman Data Acquisition system, were used to terminate the test if any of the following parameters exceeded the required limits:

Chamber Pressure	:	automatic cutoff, if greater than 30 psig above desired P_c
Water Coolant Manifold Pressure	:	automatic cutoff, if less than 1500 psig
Oxidizer Flowmeter Temperature	:	automatic cutoff, if higher than -275 F
Fuel Venturi Upstream Pressure	:	automatic cutoff, if lower than 70 psig below desired pressure

Chart observers also were used to monitor the following critical parameters:

1. Water coolant pressure in the three coolant passages in the throat region. Any sudden decrease in established pressure required test cutoff.
2. Water coolant discharge temperature. Any sudden increase in established discharge temperature required test cutoff.
3. Chamber Pressure. Any sudden significant decrease in established chamber pressure required test cutoff.

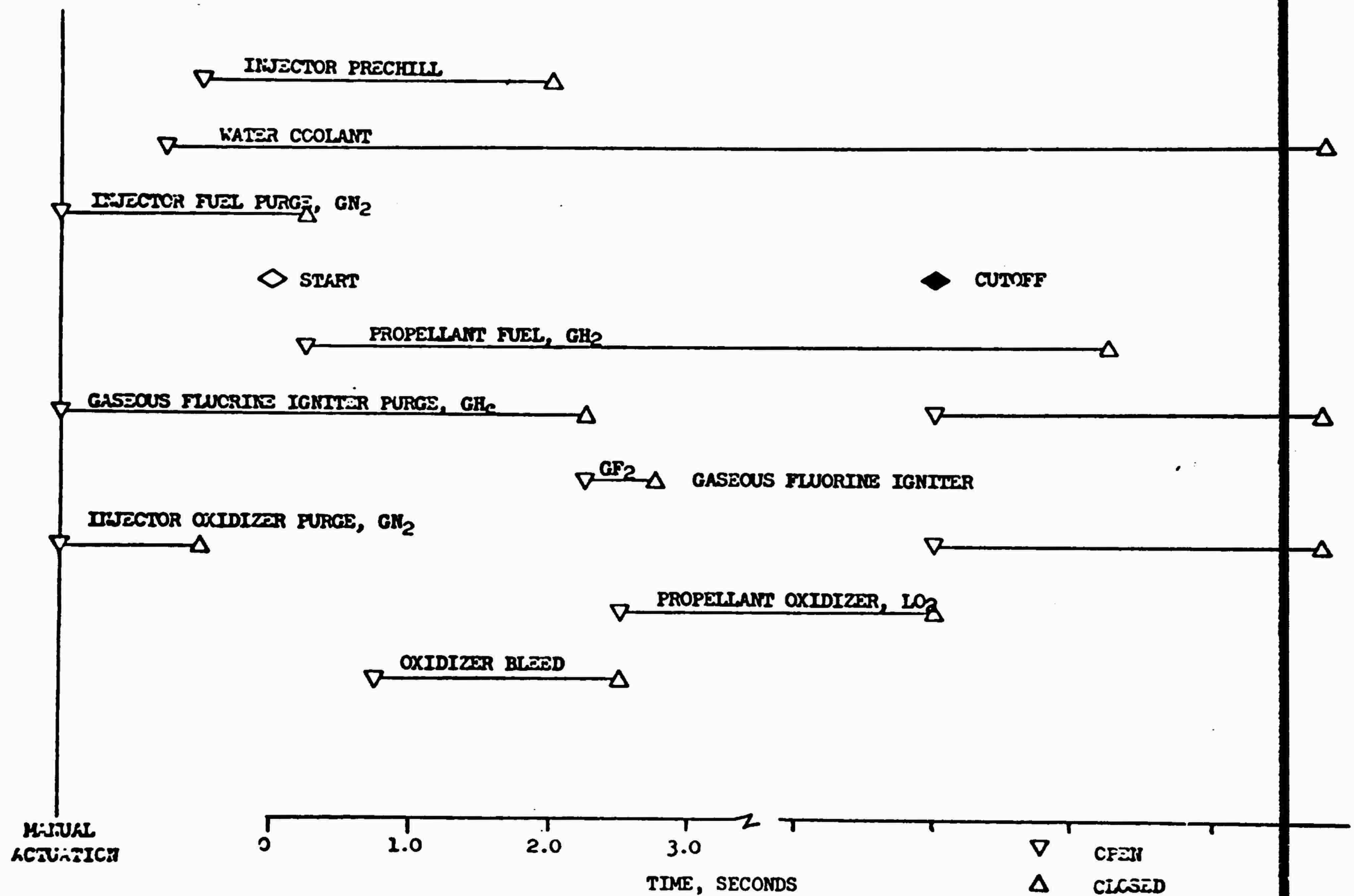

Figure 167. Test Operational Sequence, Water-Cooled Segment Test

4. Analog output from the water turbine flowmeters. Monitored, both pretest and during the test, to ensure that all passages were supplied with water or required test cutoff.

TEST INSTRUMENTATION

Experimental combustion performance was calculated from measurement of propellant flow and both chamber pressure and thrust. Scaled data from the computer print-outs were input into appropriate computer analysis programs to provide corrected c* performance values and heat transfer values (Appendixes II and III).

The hot-fire instrument list for the segment tests is presented in Table 18. Redundant measurements were made on the important experimental parameters to increase data reliability. All instrumentation and control requirements were accommodated by a hard wired J box system located on the test stand. Control switches and data recording amplifiers were "patched" into the system in the blockhouse, while jumper cables were added from Peter stand J boxes to the appropriate valves, loaders, transducers, etc.

The types of measurements and calibration procedures used are described below.

Measurement Types

The particular transducers used for the various types of measurements are described as follows.

Thrust. The thrust chamber mount was supported on flexures which allowed free movement parallel to the engine axis (horizontally) restrained in the thrust direction by a load cell.

Pressure. Low-frequency pressures were measured with bonded strain gage transducers (Taber "Teledyne" Series 206 or equivalent). Chamber pressure was measured at several positions on the injector face and chamber wall. High-frequency pressures were measured with Photocon transducers (injector inlet pressures) and Kistler helium bleed transducers (chamber pressure).

TABLE 18. INSTRUMENTATION LIST

Parameter	Range	Beckman	DIGR	OSC
Low-Frequency Instrumentation				
Chamber Pressure (2-6 Places), psi	0 to 1000	X	X	X
Oxidizer Injection Pressure, psi	0 to 1200	X	X	X
Fuel Injection Pressure, psi	0 to 1200	X	X	X
LOX Cavitating Venturi Inlet Pressure, psi	0 to 2000	X	X	
Fuel Venturi Supply Pressure, psi	0 to 2500	X	X	
Fuel Venturi Throat Pressure, psi	0 to 2500	X	X	
GOX Venturi Supply Pressure, psi	0 to 2500	X	X	
GOX Venturi Supply Temperature	Ambient		X	
Water Log Pressure Manifold, psi	0 to 2500	X	X	
No. 3 Water Passage Pressure, psi	0 to 2500	X	X	
No. 4 Water Passage Pressure, psi	0 to 2500	X	X	
No. 5 Water Passage Pressure, psi	0 to 2500	X	X	
GF_2 Igniter Pressure, psi	0 to 2000	X	X	X
GF_2 Igniter Supply Pressure, psi	0 to 500	X	X	
LOX Flowmeter A Temperature, F	0 to 325	X	X	
LOX Flowmeter B Temperature, F	0 to 325	X		
Oxidizer Injection Temperature, F	0 to 325	X		
Fuel Injection Temperature, F	0 to 1000	X		
Fuel Supply Temperature	Ambient	X		
GOX Supply Temperature	Ambient		X	
Reference Junction Temperature	Ambient	X		
Fuel Heater Discharge Temperature, F	0 to 1000	X		
Injector Fuel Inlet Temperature, F	0 to 1000	X		
Power Supply, volts	0 to 10	X		
Thrust, pounds	0 to 1000	X		X
Water Flowrates (13 or 17 passages), lb/sec	0 to 3	X		
Water Coolant ΔT (13 or 17 passages), millivolts	0 to 5	X		
LOX Flowmeter, lb/sec	0 to 2	X		X
Base Pressure, psi	0 to 14	X		

High-Frequency Instrumentation	Range	Transducer
Chamber Pressure, psi	0 to 2000	Kistler, 614A4
Oxidizer Injection Pressure, psi	0 to 2000	Photocon, 2307

Flowrates. The liquid oxidizer flowrates were measured by means of both a cavitating venturi and Fischer-Porter turbine flowmeter of a type proved suitable for service in oxygen. The oxidizer line had two flowmeters in series to measure the volumetric flowrate. Density of cryogenic propellants is a sensitive function of temperature; therefore, accurate measurements of propellant temperature as close to the flowmeters as practical were required. These measurements were accomplished by use of shielded platinum resistance bulbs (Rosemont Model 176) immersed in the liquid stream immediately downstream of each turbine flowmeter.

The gaseous oxidizer and fuel flowrates were measured using Flowdyne sonic venturis. Both pressure and temperature were measured at the sonic venturi inlet stations.

Calibration Procedures

Transducer calibrations were used to obtain appropriate factors for test data reduction and to develop statistical histories for each transducer so that estimates of short- and long-term deviations could be made and probable error bands calculated. The calibration methods used for the various types of transducers are described below.

Thrust. The thrust-measuring load cell was calibrated in-place. A permanently mounted, manually operated, hydraulic force cell was employed which deflected the load cell exactly as did the thrust chamber, through a yoke-tension rod system. Known loads were applied to the force cell through an electronic Morehouse, compression-type, temperature-compensated, proving ring, Serial No. L-1335, and Serial No. 1292 balance box.

This "end-to-end" calibration technique (i.e., one in which the complete measuring system is included, in addition to the transducer itself) provided reliable determination of the thrust force acting on the load cell. An extensive series of thrust calibrations was made with the feed lines in place, chilled and unchilled, pressurized and unpressurized, to determine possible effects of line temperature and pressure on the thrust readings.

Pressure. Pressure transducers were calibrated end-to-end by mounting them on stand manifolds in which pressures were read with high-precision Heise Bourdon-tube gages. The latter were calibrated periodically on Ruske deadweight testers.

Flowrate. Calibrations of the turbine flowmeters to obtain volume flowrates as functions of rotational speeds were made on a water flow bench. Corrections were made for the hot-firing tests to account for the density changes between the calibration fluid (water) and the propellant. Cavitating venturis were calibrated in the system, during initial tests, using the system flowmeters to define a venturi C_D. The sonic venturi meters were calibrated with GN_2 by the manufacturer to determine the discharge coefficient (C_D). Gaseous oxidizer and fuel flowrates were calculated from the venturi flow equations using the appropriate values for specific heat ratio, as explained in Ref. 11.

Temperature. Resistances of the platinum resistance thermometers used in the liquid oxidizer line were converted to millivolt outputs by a triple-bridge system. Calibration was accomplished by substituting a decade resistance box for the sensor, and setting various resistances corresponding to a temperature-resistance calibration supplied by the manufacturer for each instrument. These precision platinum resistance sensors had no significant calibration drift.

Thermocouple data were reduced on the basis of the standard NBS millivolt/temperature tables. Thermocouple recorders were electrically calibrated.

Data Recording

All pressure, temperature, and flow measurements were recorded on tape during each firing by means of a Beckman Model 210 Data Acquisition and Recording System. This system acquired analog data from the transducers, which converted the data to digital form in binary-coded decimal format. The latter was recorded on tapes which were then used for computer processing.

The Beckman Data Acquisition Unit sequentially sampled the input channels at a rate of 5625 samples per second. Programmed computer output consisted of tables of time versus the average parameter value over an approximate 200-millisecond slice time, printed out at the approximately 200-millisecond intervals during the firings, together with calibration factors, prerun and postrun zero readings, and related data. The instantaneous parameter values were machine-plotted and displayed as CRT outputs on appropriately scaled and labeled grids for simple determination of gradients, establishment of steady-state conditions, etc.

Although primary data recording for these firings was on the Beckman 210 System, the following auxiliary recording systems were employed:

1. An eight-channel, Brush, Mark 200 recorder was employed in conjunction with the Beckman unit, primarily to establish time intervals for computer data reduction and, additionally, for "quick-look" information on the most important parameters. This system was direct-inking, with display high-gloss graduated paper moving at 20 mm/sec.

2. A CEC, No. 5-119P4-36-01, 36-channel direct reading oscillograph was used as backup for the Beckman 210 System and for indication of any oscillatory combustion.

3. Direct-inking graphic recorders (DIGR's), both Dynalog rotary chart and Esterline-Angus strip chart were used to set prerun propellant supply pressures, for recording of propellant manifold pressures, to provide quick-look information, and as secondary backup to the Beckman and oscillograph recorders.

4. An Esterline-Angus, 20-channel event recorder was used for direct-inking recording of main propellant valve signal and travel, as well as for chart drive and camera actuations.

5. High-frequency tapes were used to monitor Photocon and Kistler responses.

REFERENCES

1. Space Storable Propellant Performance, Contract NAS3-12051, NASA-LeRC, Rocketdyne, a division of North American Rockwell Corp., (to be released).
2. Mehegan, P. F., Campbell, D. T., Scheuermann, C. H., Investigation of Gas Augmented Injectors, Final Report, NASA CR-R-8361, Rocketdyne, a division of North American Rockwell Corp., Canoga Park, California, September 1970.
3. Rupe, J. H., "Experimental Correlation of the Nonreactive Properties of Injection Schemes and Combustion Effects in a Liquid Propellant Rocket Engine," Tech. Report No. 32-255, JPL, 15 July 1965.
4. Nurick, W. H., Experimental Investigation of Combustor Effect on Rocket Thrust Chamber Performance, PR9308-12, Rocketdyne, a division of North American Rockwell Corp., Canoga Park, California, 16 November 71.
5. R-7475, Advanced Engine Aerospike Experimental Program, Final Report, Vol. 2 Rocketdyne, a division of North American Rockwell Corp., Canoga Park, Calif., 1969.
6. Nagai, C. K., R. N. Gurnitz, and S. D. Clapp; Cold-Flow Optimization of Gaseous Oxygen/Gaseous Hydrogen Injectors for the Space Shuttle APS Thruster, AIAA Paper No. 71-673 presented at AIAA/SAE 7th Propulsion Joint Specialist Conferences, Salt Lake City, Utah, 14-18 June 1971.
7. Kesselring, R. C., SS/ACPS Trislot Injector Cold Flow/Hot Fire Correlation, Rocketdyne Memo EE71-12-8, 21 April 1971.
8. Kesselring, R. C., SS/ACPS Concentric Element Cold-Flow Investigation, Rocketdyne Memo EE71-12-8, 21 April 1971.
9. Kohs, D. L., and D. V. Calhoon, Gaseous Oxygen/Gaseous Hydrogen Injector Element Modeling, AIAA Paper No. 71-674 presented at AIAA/SAE 7th Propulsion Joint Specialist Conference, Salt Lake City, Utah, 14-18 June 1971.
10. Kusak, L., R. C. Kesselring, and L. W. Carlson; IR&D Task Demonstrating Gas/Gas Injector Element Manifolding, Element Interaction and Single Element Hot Fire Visualization Techniques, Rocketdyne Memo 71-12-17, 7 June 1971.
11. Johnson, R. C., Real-Gas Effects in Critical-Flow-Through Nozzles and Tabulated Thermodynamic Properties, NASA TN D-2565, January 1965.

COMBUSTION MODEL STUDIES

Combustion model studies were conducted to support the single-panel injector development effort. These studies included prediction of: (1) the vaporization limited combustion efficiency, and (2) the chamber stagnation pressure loss.

The objective of combustion model studies, for prediction of vaporization-limited combustion efficiency, was to provide information for performance analysis of hot-fire results. More specifically, the studies afforded: (1) an analytic prediction of vaporization losses for comparision with vaporization losses implied by hot-fire results, and (2) an evaluation of the validity of combustion modeling to correctly predict vaporization losses. Furthermore, the assignment of vaporization losses, enhanced by correlation of both analytic and measured results, can be used as guidance for improvement of hot-fire test performance. The approach toward performance analysis and the contribution of combustion model studies in these analyses are described in the subsequent paragraphs.

The approach used in performance analysis has been developed in other programs (Ref. I-1 and I-2) conducted at Rocketdyne. Overall combustion efficiency is expressed as the product of mixing and vaporization efficiencies:

$$\eta_{c^*} = \eta_{c^*\,mix} \times \eta_{c^*\,vap} \tag{I-1}$$

where

η_{c^*} = overall combustion efficiency

$\eta_{c^*\,mix}$ = mixing limited combustion efficiency (assuming complete vaporization)

$\eta_{c^*\,vap}$ = vaporization-limited combustion efficiency (assuming complete mixing)

Predictions of mixing limited combustion efficiency can be obtained from: (1) cold-flow mixing tests with propellant simulants, or (2) hot-fire performance in large L* chambers where vaporization is essentially complete.

Prediction of vaporization-limited combustion efficiency can be obtained from: (1) combustion model analysis using dropsize data from cold-flow atomization tests with propellant simulants, or (2) hot-fire performance in vaporization-limited chambers, with known mixing losses, through use of Eq. I-1. Although cold-flow mixing and atomization (dropsize) experiments with the LO_2/GH_2 AMPT injectors were not conducted (except for single-element coplanar cold-flow mixing tests), parametric combustion model analysis of vaporization efficiency for impinging-type elements can provide the ranges of predicted propellant dropsizes required to attain desired performance levels. Assuming complete propellant mixing (i.e., no mixing losses), the combustion model analysis defines an upper limit on propellant dropsize concomitant with performance goals. Additionally, relative magnitudes of chamber operating/geometric variable effects on vaporization efficiency are described. For the concentric-type element, a special version of the combustion model is available (discussed later) which internally computes a dropsize distribution. Therefore, for this element type, an estimate of vaporization efficiency can be made even without cold-flow atomization (dropsize) data.

The objective of combustion model analyses for prediction of chamber stagnation pressure loss was to provide information for performance computation. These analyses provide prediction of stagnation pressure loss correction factors to convert measured injector face stagnation chamber pressure to a predicted throat stagnation pressure for computation of combustion efficiency.

The following sections sequentially describe: (1) the combustion model employed, (2) the calculated impinging stream element (coplaner and triplet) vaporization efficiency as a function of propellant dropsize and chamber operating/geometric variables, (3) the calculated concentric element vaporization efficiency and cup pressure drop as a function of element geometry and chamber operating variables, and (4) the stagnation pressure loss associated with the predicted chamber enthalpy release profiles.

COMBUSTION MODEL DESCRIPTION

The droplet heating and burning processes occurring within a rocket have been described (Ref. I-3) and are briefly reviewed herein. Consider the behavior of an oxidizer droplet when suddenly placed into a near-stagnant, subcritical-pressure, hot fuel-rich gas. The processes which occur, as reflected in droplet temperature changes, are shown in Fig. I-1. The droplet temperature initially increases until the droplet approaches an evaporative "wet bulb" temperature. After some time, the mole fraction of droplet vapors around the drop reaches a critical temperature and ignition occurs. The droplet temperature rapidly adjusts to a higher combustion wet bulb condition, and the burning rate is more rapid. Under convective flow conditions present in a rocket combustion chamber, the residnce time of droplet vapor in the gas film boundary is short compared to the induction time required for ignition. Therefore, ignition occurs when droplet vapor enters the droplet wake. As a consequence, droplets see bulk gas temperature, and flame enhancement of vaporization does not occur (i.e., quasi-steady evaporation continues to t_{life}, which is the time to complete vaporization of the droplet).

Combustion models have been developed at Rocketdyne which treat the evaporation process alone (KPRIME model) or the complete preheat/vaporization process (CSS model). In the KPRIME model, droplets are assumed to be injected at the wet bulb (vap) temperature (i.e., quasi-steady evaporation is assumed, $\frac{dT_{drop}}{dt} = 0$, and preheat time is neglected as being small compared to quasi-steady evaporation time). A detailed description of the combustion models is presented in Ref. I-3. Differences between the two combustion models, as they relate to selection of a model for the O_2/H_2 AMPT combustion model analysis, are described in the following paragraphs.

The importance of including preheat time can be assessed by consideration of the propellant combination which strongly influences the relative magnitude of droplet heating time compared to quasi-steady evaporation time. For liquid/liquid propellant combinations with similar vaporization rates, the combustion gas mixture

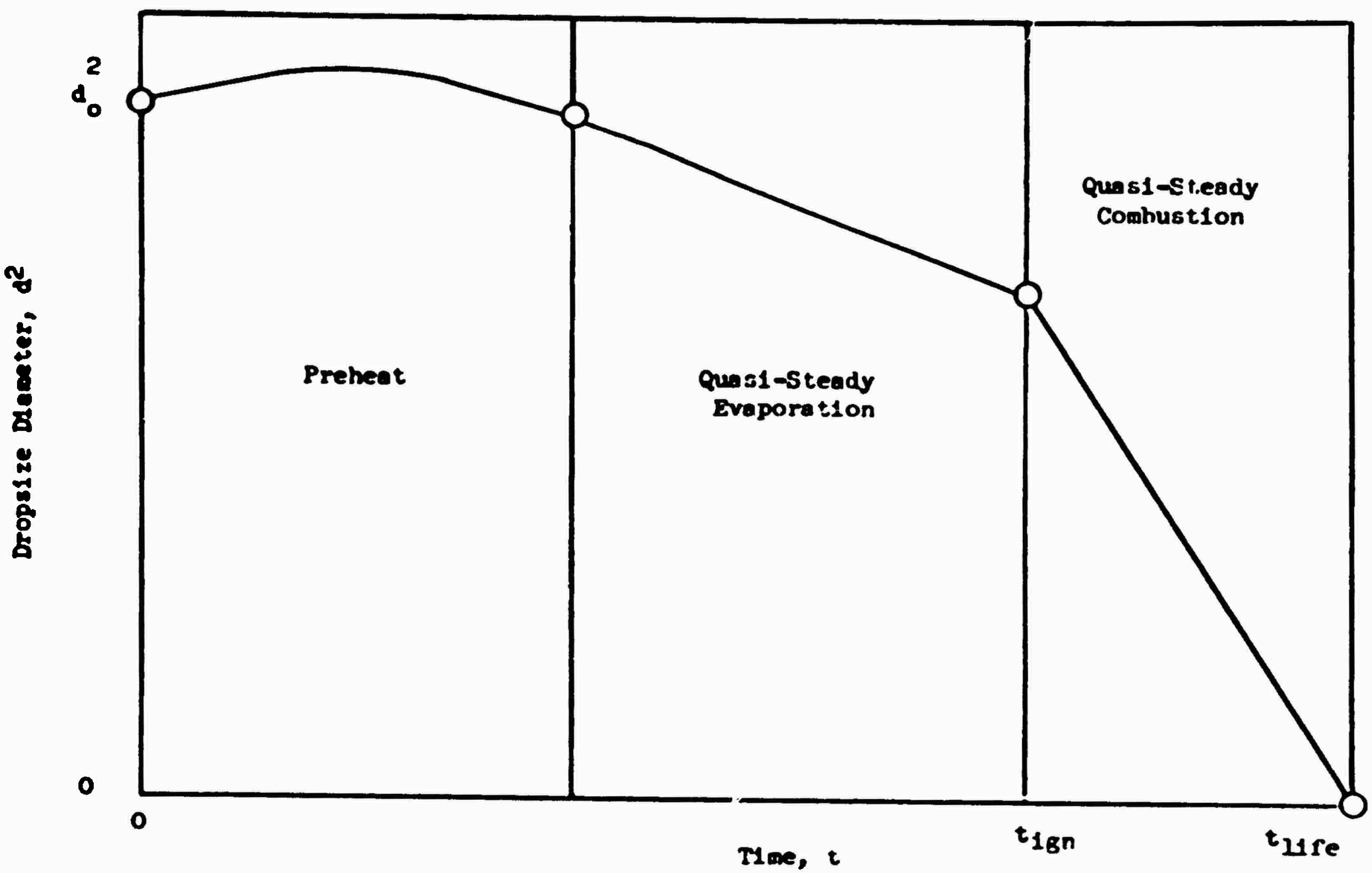

Figure I-1. Drop Diameter Decrease as a Function of Time ratio is near the injected mixture ratio and the gas temperature rapidly increases. Thus, the preheat process (Fig. I-1) can be relatively short. Conversely, for gas/liquid propellant combinations, such as LO_2/GH_2, the combustion gas mixture ratio at injection is essentially zero and the combustion gas temperature increases at a lesser rate. Therefore, the preheat time can be extended and consideration of the preheat time (i.e., use of the CSS model) becomes very important.

Further differences between the two combustion models (KPRIME and CSS) result from the treatment of the properties (specifically, thermal conductivity of combustion gas film surrounding the droplets).

KPRIME is a thin flame droplet burning model which envisions the droplet as being surrounded by an actual flame envelope. The film properties are integrated between the droplet wet bulb temperature and the temperature corresponding to the local bulk gas mixture ratio. Such an integral path for thermal conductivity is shown in Fig. I-2 (point A to point B). For LO_2/GH_2 propellants, this technique biases oxidizer drop film properties toward those of O_2 at low temperatures corresponding to low injection mixture ratios. In actuality, the gas film surrounding a heating oxidizer droplet is primarily fuel and, therefore, influences of H_2 on film properties must be considered. This result is particularly important when the properties of the oxidizer and fuel are considerably different. Such is the case with O_2/H_2 where the thermal conductivity of H_2 is considerably larger than that of O_2.

CSS is a diffusion model which provides for diffusion of combustion gas into the film surrounding the drop. Film properties are based on an assigned mole fraction of H_2 in the gas film. In this manner, the effect of H_2 properties on the gas film are taken into account. The net result is that the thermal conductivity of gas film at low combustion gas temperature is greater for CSS than KPRIME and, concomitantly, the vaporization rate (dependent on thermal conductivity) is increased.

Considering the two combustion models, KPRIME and CSS, the CSS model is considered to best represent the combustion process for the LO_2/GH_2 AMPT chamber. The CSS model provides for droplet heating which can be significant and accounts for the

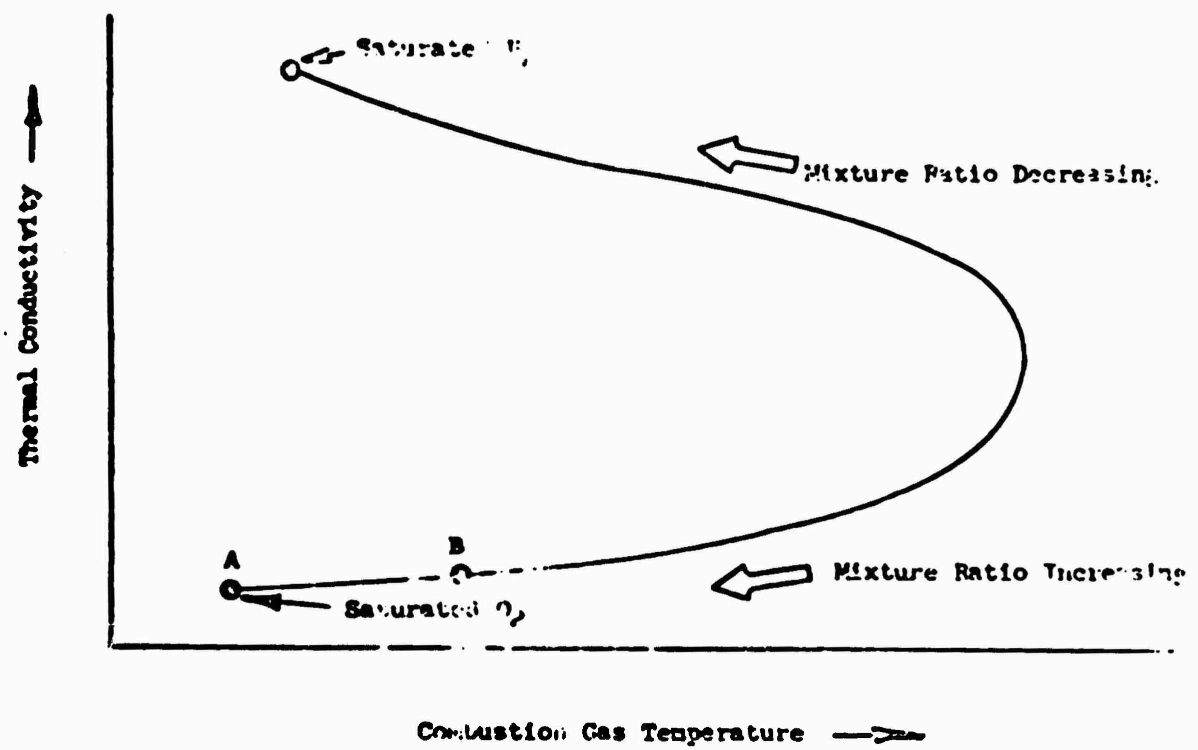

Figure I-2. Thermal Conductivity as a Function of Mixture Ratio/Combustion Gas Temperature influence of H_2 on film properties. The applicability of KPRIME is limited by the specific propellant combination employed and that KPRIME can often satisfactorily model the combustion process for other type propellant combinations, particularly liquid/liquid propellant combinations with nearly equal oxidizer and fuel vaporization rates. The CSS model was used for the parametric combustion model analysis of LO_2/GH_2 AMPT vaporization efficiency. A set of generalized vaporization efficiency charts, generated using the particular droplet combustion droplet combustion model used in CSS, was recommended by the JANNAF Performance Subcommittee to NASA for combustion model analysis of the LO_2/GH_2 SSME engine system (Ref. I-4).

IMPINGING STREAM ELEMENT VAPORIZATION EFFICIENCY

Combustion Model Input

A total of 16 cases were run. Combustion model input consists of injector spray parameters, chamber operating conditions, and chamber geometry. Specific data input for all cases are tabulated in Table I-1.

Injector spray parameter input includes mean oxidizer dropsize, dropsize distribution, oxidizer injection temperature, oxidizer injection velocity, and injected mixture ratio. Four mean propellant dropsizes ($\bar{D}_{30}$=60, 120, 180, and 240 microns) were input at each of three (cases 1-12) injection velocities (173, 110, and 37 ft/sec) corresponding to flowrates for the coplaner injector at three different chamber pressures. A Nukiyama-Tanasawa (NT) dropsize distribution, about the mean dropsize (Ref. I-1), was used for all cases. The NT distribution was used for comparative purposes in the absence of experimental dropsize distribution data for the coplaner injector element. Oxidizer injection temperature and injected mixture ratio were 170 R (-290 F) and 5.87, respectively, for all cases.

Chamber operating pressure inputs were 700, 450, and 150 psia. The design chamber pressure of the O_2/H_2 AMPT single-panel engine is 750 psia at full thrust. However, to avoid possible combustion model computation problems near the critical

TABLE I-1. TABULATION OF COMBUSTION MODEL CASES

Cases	Chamber Pressure, psia	Propellant Dropsize, microns	Oxidizer Injection Temperature, R	Oxidizer Injection Velocity, ft/sec	MR	Chamber Length, inches	η_{vap}, percent
1	700	60	170	173	5.87	3	99.98
2		120					93.21
3		180					75.64
4		240					60.32
5	450	60		110			99.94
6		120					92.80
7		180					77.40
8		240					60.14
9	150	60		37			99.99
10		120					96.76
11		180					87.60
12		240					77.70
13	700	60		173		4	100.00
14		120					97.30
15		180					86.60
16		240					69.90

oxidizer pressure, 738 psia, the high-pressure combustion model case was input at 700 psia. Results for cases run at 700 psia should closely represent performance at 750 psia.

The nominal design, 3-inch length LO_2/GH_2 AMPT chamber geometry was input for cases 1-12. Additionally, a 4-inch-length LO_2/GH_2 AMPT chamber geometry, consisting of the 3-inch-length chamber with 1-inch spacer, was input (cases 13-16) for the aforementioned four dropsizes at a chamber pressure of 700 psia. Respective chamber characteristic lengths, L*, for the 3- and 4-inch chamber are 7.87 and 12.15 inches.

Combustion Model Results

The effect of oxidizer dropsize on vaporization efficiency for each of three chamber pressures is shown in Fig. I-3. All data are for the 3-inch-length chamber. Increased dropsize reduces vaporization efficiency at constant chamber pressure. At 700-psi chamber pressure, the maximum dropsize, D_{30}, yielding complete vaporization, is 60 microns.

The effect of chamber pressure on vaporization efficiency at constant oxidizer dropsize can be seen in Fig. I-4, which is a cross plot of the Fig. I-3 data. For small oxidizer dropsize (D_{30}=60 microns), there is no significant effect of chamber pressure on vaporization efficiency. At larger oxidizer dropsizes (D_{30}=120 microns), the vaporization efficiency increases at lower chamber pressures. This improvement in vaporization efficiency at lower chamber pressures is attributed to the lower oxidizer injection velocity, associated with the lower chamber pressures, which increases the droplet residence time in the chamber and thereby improves performance. In actual rocket engine throttling, with a fixed area injector such as the LO_2/GH_2 AMPT injector, the dropsize increases as injection velocity is decreased due to a lesser degree of hydraulic atomization. Therefore, the improvement in η_{vap} at low chamber pressure can be offset by an increased dropsize, and the performance may drop rather than increase with chamber pressure throttling.

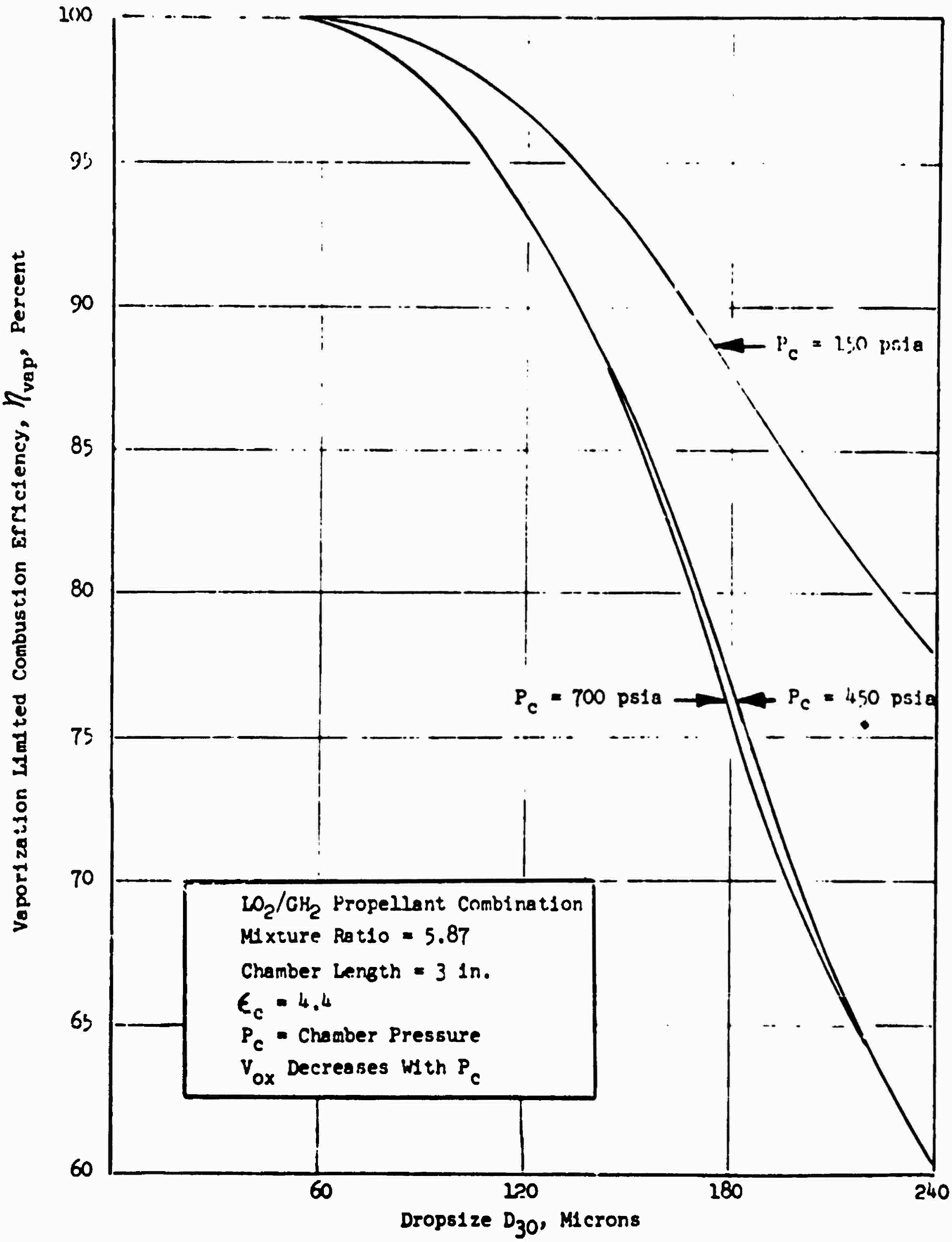

Figure I-3. Vaporization Limited Combustion Efficiency, η_{vap}, Versus Oxidizer Dropsize, D_{30} for Varying Chamber Pressure

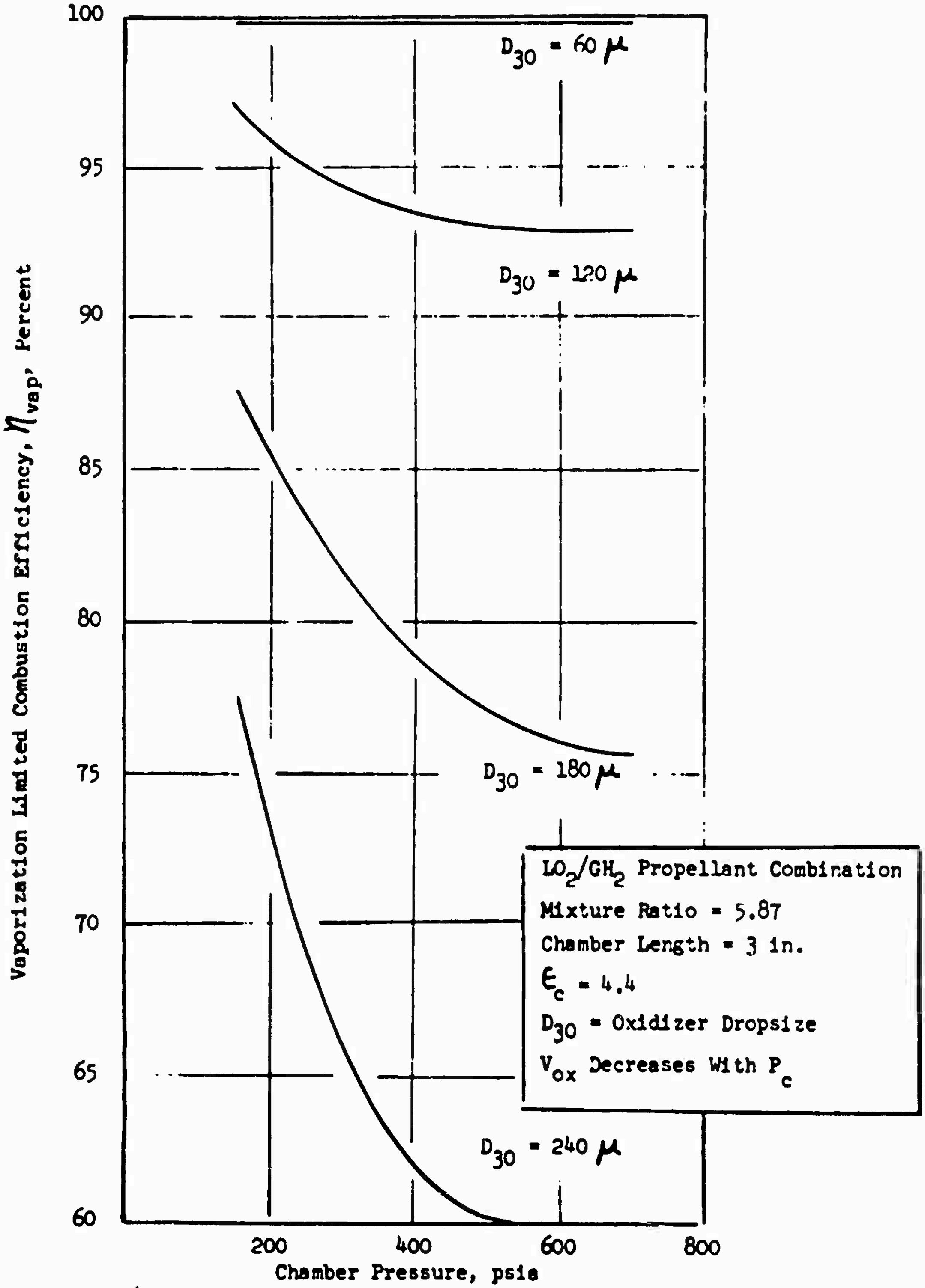

Figure I-4. Vaporization Limited Combustion Efficiency, η_{vap} Versus Chamber Pressure for Varying Oxidizer Dropsize

The effect of chamber length, L_c, on vaporization efficiency, is shown in Fig. I-5 All data are for a chamber pressure of 700 psia. The maximum allowable dropsize, $\bar{D}_{30}$, yielding complete vaporization is increased from 60 microns with the 3-inch chamber to 70 microns with the 4-inch chamber. For larger propellant dropsizes, the improvement in vaporization efficiency with the 4-inch-length chamber becomes more pronounced.

All parameters evaluated affected vaporization efficiency with the strongest dependence being attributed to dropsize. This result emphasizes the need for good atomization to obtain high combustion performance.

CONCENTRIC ELEMENT VAPORIZATION EFFICIENCY

Additional combustion model analyses for concentric element-type injectors were conducted. The objective of the analyses was analytic prediction of: (1) the vaporization efficiency, $\eta_{c^* \, vap}$, and (2) the cup pressure drop. Cases were run for: (1) the concentric injector unit 3, and (2) various designs for the concentric injector unit 7 (7-.006, 7-.008, and 7D).

The combustion model, designated as CSS, was employed for the analysis. A cursory description of the model was presented in a previous section. Basically, the model considers the complete preheat/vaporization process occurring in the combustion chamber. Additionally, for the specific concentric element configuration, the model describes the liquid jet stripping and resulting droplet formation (i.e., the model computes propellant dropsize and dropsize distribution from input element geometry and operating conditions). The CSS combustion model as used here assumes that the flame does not enter the recessed cup of the concentric injection elements and does not account for any increased performance or cup ΔP associated with combustion in the cup.

Combustion model results for the concentric injectors are tabulated in Table I-2 and are described in the following paragraphs.

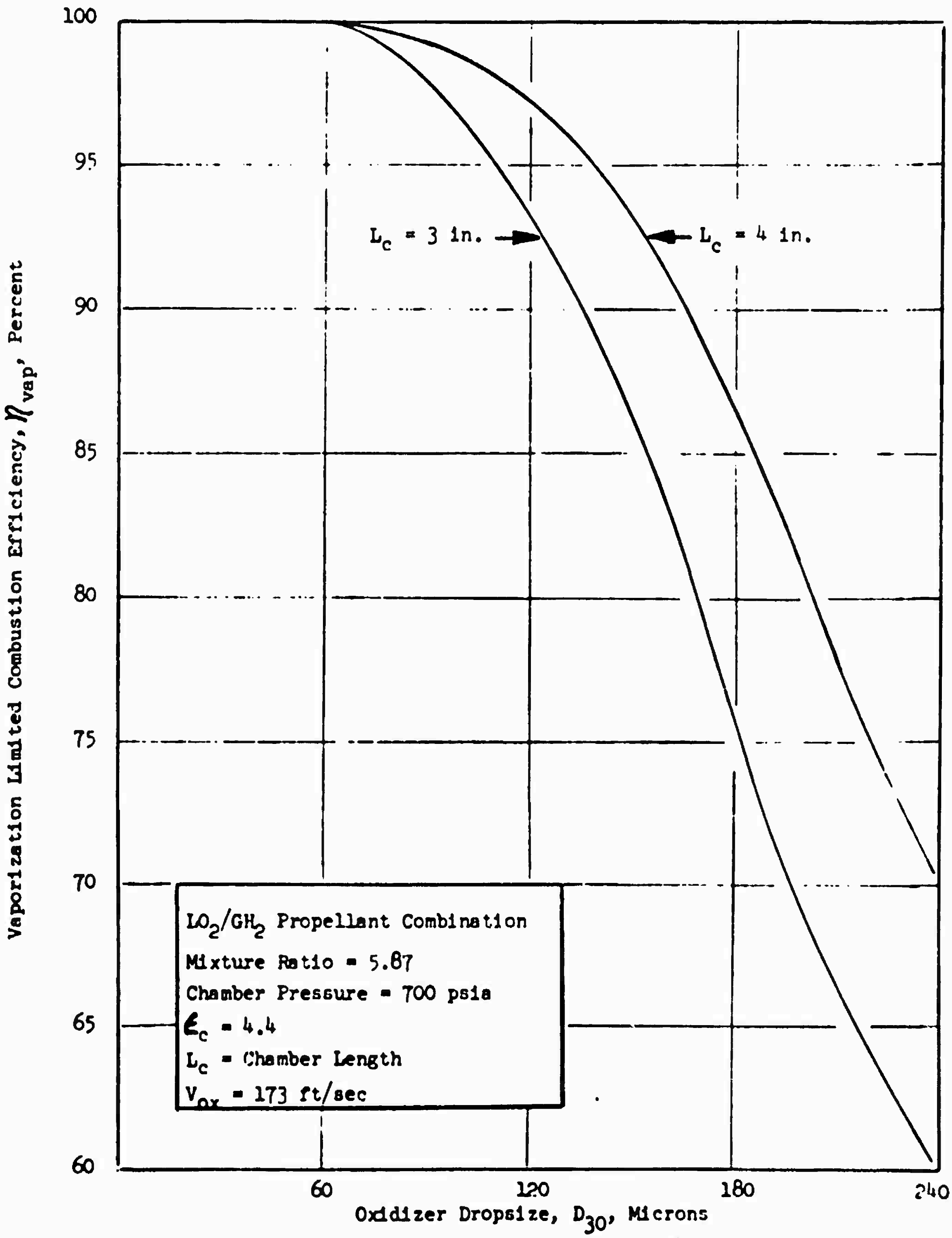

Figure I-5. Vaporization Limited Combustion Efficiency, η_{vap}, Versus Oxidizer Dropsize for Varying Chamber Length

TABLE I-2. COMPUTER COMBUSTION MODEL RESULTS FOR CONCENTRIC INJECTOR

	Injector U/N 7-006(2) 96 Elements (4) .006 Fuel Gap			Injector U/N 7-008(2) 96 Elements (5) .008 Fuel Gap			Injector U/N 3(2) 95 Elements (6) .008 Fuel Gap			Injector U/N 7D(3) 66 Elements .0155 Fuel Gap		
	η_{vap}	Cup ΔP	Cup Vap %	η_{vap}	Cup ΔP	Cup Vap %	η_{vap}	Cup ΔP	Cup Vap %	η_{vap}	Cup ΔP	Cup Vap %
700 psia P_c (1)												
.050 Recess	96.38	46.5	19.2	94.59	31.6	16.3	96.9	66	17.2	96.3	32	15.0
.100 Recess	99.05	94.4	40.3	97.65	66	35.5	99.4	135	36.8	98.3	65	32.2
450 psia P_c (1)												
.050 Recess	95.91	35.4	21.8	93.79	25	18.8	96.3	51	19.6	95.[illegible]	25	19.5
.100 Recess	99.12	74	44.5	97.65	51	39.7	99.3	105	41.0	97.8	50	41.0

(1) AMPT Full Tapered Chamber, L = 3 in.

(2) Blunt tip elements (D_o = .0334 in. and oxidizer post thickness = .0083 in. at exit)

(3) Internal tapered oxidizer post (D_o = .048 in., oxidizer post thickness = .001 in. at exit)

(4) Same as injector U/N 7 candidate (Case I)

(5) Same as injector U/N 7 candidate (Case II)

(6) Same as injector U/N 7 candidate (Case III), 68-element, 0.008 fuel gap which was not fabricated.

Injector Unit 3

Combustion model cases were run for varying post recesses (0.050, 0.075, and 0.100 inch) at chamber pressures of 450 and 700 psia. Combustion model predictions of vaporization efficiency, η_{vap}, and cup pressure drop are listed in Table I-2. Vaporization efficiency increased with: (1) increasing chamber pressure at constant recess, and (2) increasing recess at constant chamber pressure. Cup pressure drop and percent of oxidizer vaporized in the cup increased in a similar manner.

Injector Unit 7

Injector unit 7 was tested in various configurations. The element configurations and corresponding combustion model results are tabulated in Table I-2. All element configurations utilized an oxidizer post geometry identical to injector unit 3.

Injector unit 7-.006 represented an element design that: (1) had a fuel injection velocity and total number of elements the same as injector unit 3, and (2) had a fuel gap and oxidizer injection velocity less than injector unit 3. The latter two constraints result from the lower thrust/element requirements of injector unit 7 compared to injector unit 3.

Injector unit 7-.008 represented an element design which: (1) had a fuel gap and total number of elements the same as injector unit 3, and (2) had a fuel and oxidizer injection velocity less than injector unit 3.

Injector unit 7D represented an element design which has a lesser number of elements, 66, and a larger fuel gap, resulting in a lower fuel injection velocity and higher oxidizer injection velocity.

For all cases, both increased chamber pressure and post recess improved $\eta_{c^* \, vap}$. The vaporization efficiency of injecto.. unit 7-.006 was similar to that of injector unit 3. For injector unit 7-.008, the vaporization efficiency was slightly lower due to the reduced fuel injection velocity resulting from an increased fuel gap. The vaporization efficiency predicted for injector unit 7D, which had the largest fuel gap, was intermediate between injector units 7-006 and 7-008.

The reason for the intermediate performance with injector unit 7D, even though this injector had the largest fuel gap, is related to the element geometry. Figure I-6 schematically shows the gaseous fuel jet expansion in the concentric element cup, as treated by the combustion. The expanded fuel gas area and, in turn, the fuel velocity for injector unit 7D is intermediate between that for injector units 7-.006 and 7-.008 (Fig. I-6). This intermediate expanded fuel velocity, which affects droplet stripping and formation (i.e., atomization), results in the prediction of an intermediate performance level for injector unit 7D.

STAGNATION PRESSURE LOSS

Stagnation chamber pressure loss in a thrust chamber results from irreversible processes occurring in the combustion zone (Ref. I-5). As heat is released, the gas volume increases and the gas must be accelerated to satisfy conditions of constant mass flow. Energy must be expended to accelerate the gases and, because this energy becomes unavailable, the process in nonisentropic. The energy expended on accelerating the gases is manifested as a pressure force which, for dynamic flow equilibrium, must equal the time rate of change of flow momentum. The pressure difference associated with this pressure force describes the stagnation pressure loss.

For conventional, constant cross-sectional area thrust chambers, the Rayleigh criterion (Ref. I-5), describing heat addition in a constant area duct, can be used to approximate the stagnation pressure loss. Assuming complete combustion prior to nozzle convergence, the difference between flow momentum (stream impulse) at the injector and at nozzle convergence describes the pressure force expended in accelerating the combustion gases. Because the area over which this pressure force is expended remains constant, stagnation pressure loss also is defined by the boundary flow conditions at the injector and at nozzle convergence (i.e., stagnation pressure loss is not a function of the enthalpy release/Mach number profile in the constant area chamber section where combustion is completed).

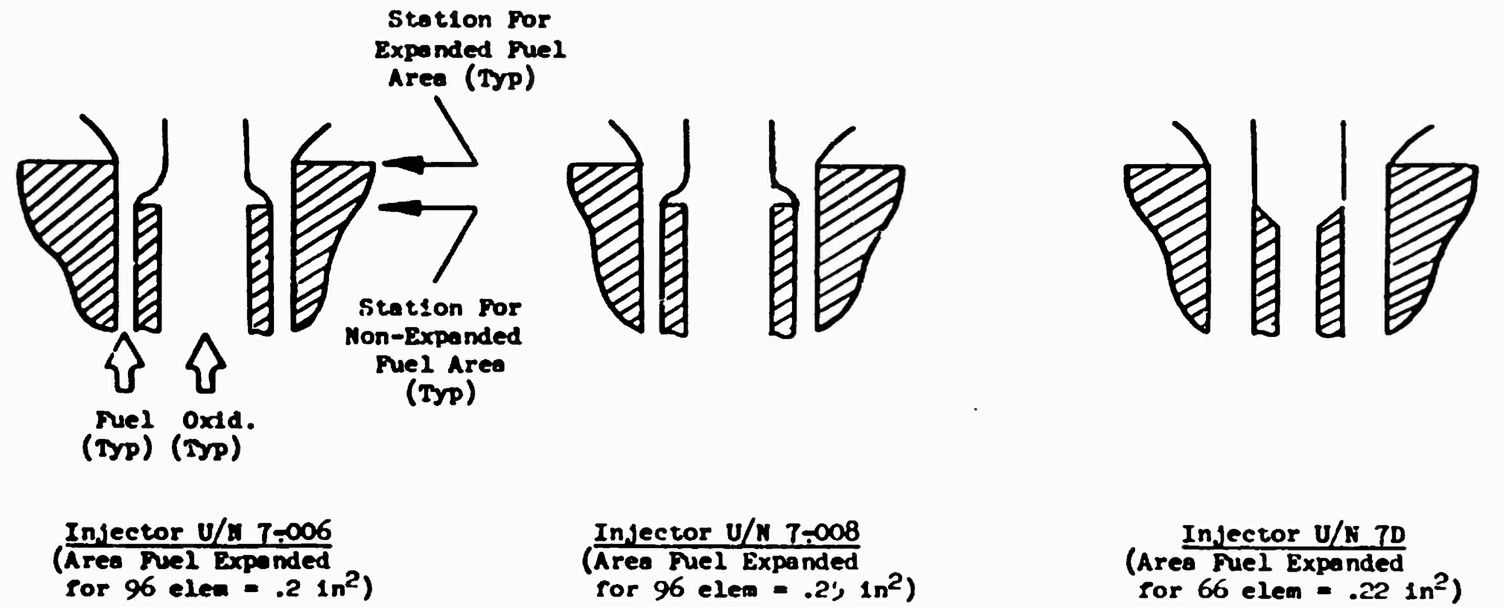

Figure I-6. Propellant Flow in the Concentric Cup as Treated by the Combustion Model

Prediction of stagnation pressure loss for the AMPT thrust chamber requires additional considerations specific to the chamber geometry. The LO_2/GH_2 AMPT segment thrust chamber employs a tapered wall design in which the chamber cross-sectional area decreases continually from the injector face to the throat. Therefore, the area over which the pressure force is expended, to accelerate gases, varies and consideration of the enthalpy release/Mach number profile is needed to predict stagnation pressure loss. The Mach number profile and, in turn, stagnation pressure loss, for heat addition in a variable area duct can be approximated by the method of influence coefficients (Ref. I-5) using an assumed enthalpy release profile. Prediction of the enthalpy release profile can be obtained from combustion model analysis of the injector/thrust chamber. However, combustion model analysis provides, in addition to the enthalpy release profile, definition of the Mach number and stagnation pressure profile. In the combustion model, stagnation pressure is computed as the sum of the static pressure and dynamic pressure (velocity equivalent) at stepwise axial positions from the injector to throat. Therefore, direct use of the combustion model to predict stagnation pressure profile was selected as the best approach for prediction of AMPT thrust chamber stagnation pressure loss.

Combustion model analyses were conducted, as described in a previous section, to predict impinging stream element vaporization efficiency as a function of injected oxidizer dropsize, chamber pressure, and chamber geometry (specifically length). As output from these combustion model analyses, the chamber stagnation pressure loss also was provided. A tabulation of the combustion model cases is listed in Table I-3 with corresponding chamber stagnation pressure losses. (Data for large dropsize, D_{30}=240 microns, runs have been omitted because vaporization efficiency was below that of interest.)

The stagnation pressure loss, expressed as $(P_{throat}/P_{injector})_o$, versus vaporization efficiency is plotted in Fig. I-7. Stagnation pressure loss for all cases correlates with vaporization efficiency. Changes in chamber pressure and chamber length do not significantly alter stagnation pressure loss for a fixed combustion efficiency. As vaporization efficiency decreases from 100 to 75 percent, the stagnation pressure loss increases, reflected by a respective $(P_{throat}/P_{injector})_o$ decrease from 0.99 to 0.93.

TABLE I-3. TABULATION OF STAGNATION PRESSURE LOSS RATIO

Case No.	Chamber Pressure, psia	Injected MR	Propellant Dropsize, microns	Chamber Length, L, inches	η_{vap}, percent	Stagnation Pressure Loss, percent
1	700	5.87	60	3.0	99.98	0.009
2			120		93.21	0.963
3			180		75.64	0.927
5	450		60		99.94	0.988
6			120		92.80	0.962
7			180		77.40	0.935
9	150		60		99.99	0.988
10			120		96.76	0.979
11			180		87.60	0.959
13	700		60	4.0	100.00	0.994
14			120		97.30	0.982
15			180		86.60	0.953

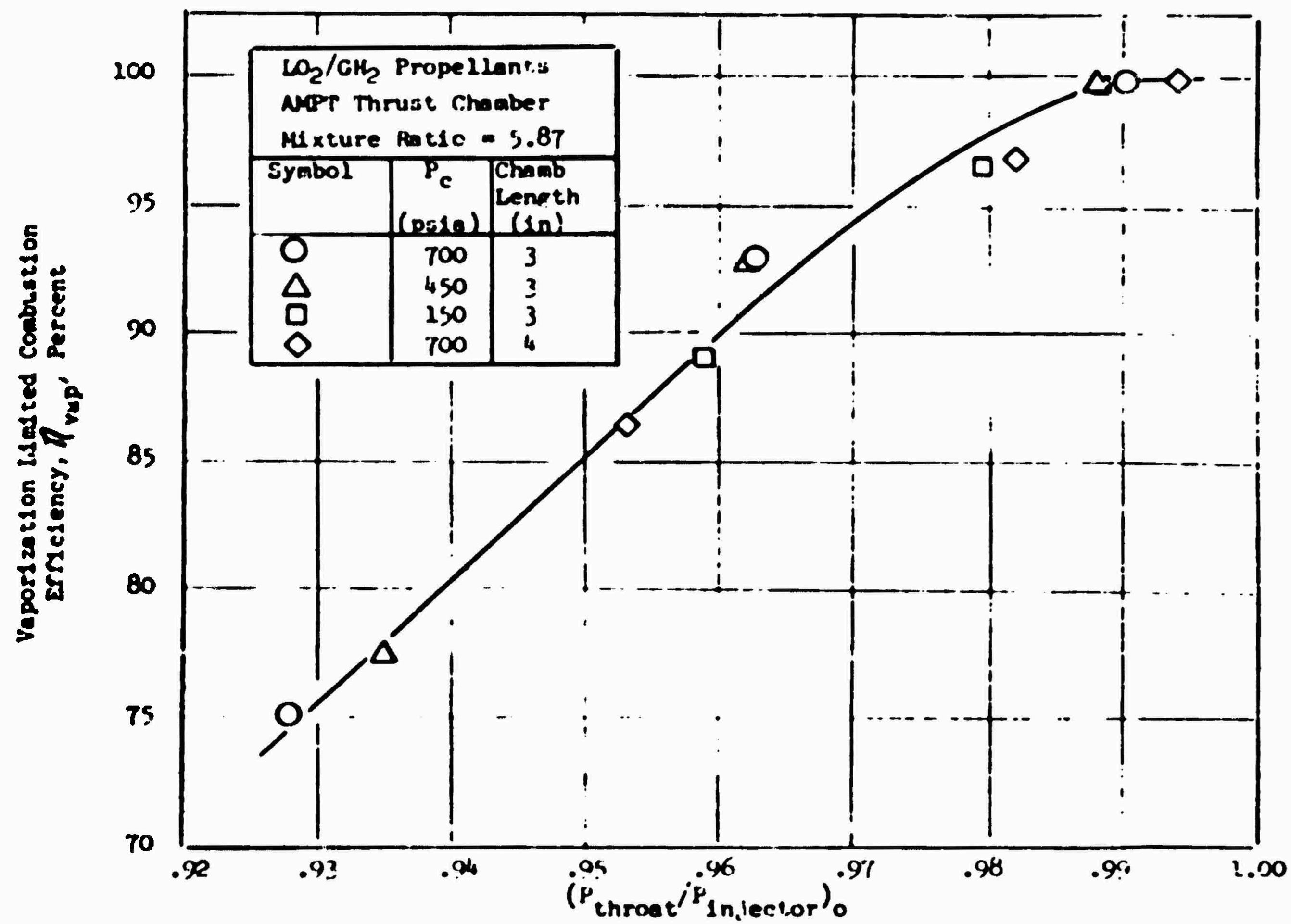

Figure I-7. $(P_{throat}/P_{injector})_o$ vs Vaporization Limited Combustion Efficiency, η_{vap}, for AMPT Segment Thrust Chamber

The stagnation pressure loss variation with vaporization efficiency can be explained by consideration of the combustion process. The differences between vaporization efficiency for the cases tabulated in Table 20 result from variations of input dropsize, chamber pressure, and chamber geometry. However, the net result is that vaporization efficiency is a direct function of the enthalpy release profile. For high vaporization efficiency, a large portion of the enthalpy is released close to the injector where the chamber contraction ratio is largest. For low vaporization efficiency, the enthalpy is: (1) partially released further downstream where the chamber contraction ratio is smaller, and (2) released in the nozzle divergence (i.e., not burned in the chamber). Because the enthalpy release for lower performance cases occurs at smaller contraction ratios, the pressure force required to accelerate the gas is necessarily greater than that required for enthalpy release at larger contraction ratios (i.e., high-performance cases). Therefore, the stagnation pressure loss is greater. This result occurs in lieu of the fact that combustion is not complete in the chamber for low performance cases (i.e., unburned propellants result in a reduction of the required pressure forces).

This stagnation pressure loss relationship with combustion efficiency was used to determine throat stagnation pressure as described in Appendix III, Performance Calculations.

APPENDIX I NOMENCLATURE

AMPT	Advanced Maneuvering Propulsion Technology
c	contraction
CSS	Combs, Sutton, Schuman
d	diameter
$\bar{D}_{30}$	mean dropsize diameter
ε	area ratio
F	degrees Fahrenheit
f	feet
f	fuel
GH_2	gaseous hydrogen
H_2	hydrogen
in.	inch
JANNAF	Joint Army, Navy, NASA, Air Force
L*	characteristic length
LO_2	liquid oxygen
mix	mixing
MR	mixture ratio
NASA	National Aeronautics and Space Administration
NT	Nukiyama-Tanasawa
O_2	oxygen
ox	oxygen
p	pressure, static
P_o	pressure, stagnation
psia	pressure, absolute
P_c	chamber pressure
R	degrees Rankine
t_{ign}	time of ignition
t_{life}	time of complete drop vaporization
vap	vaporization
V	velocity
ΔP	pressure drop

η_{c*}	overall combustion efficiency
$\eta_{c*\ mix}$	mixing-limited combustion efficiency
$\eta_{c*\ vap}$	vaporization-limited combustion efficiency
η_{mix}	mixing efficiency
η_{vap}	vaporization efficiency
dt	time differential
dT	temperature differential

APPENDIX I REFERENCES

I-1. Dickerson, R., and Tate, K.: Correlation of Spray Injector Parameters with Rocket Engine Performance, AFRPL-TR-68-147, Rocketdyne, a Division of North American Rockwell, June 1968.

I-2. Falk, A. Y., Nagai, C. K., Clapp S. D.: Space Storable Propellant Performance Study, Final Report, NASA CR-72-187,24 November 1968.

I-3. Sutton, R. D., Propellant Spray Combustion Processes During Stable and Unstable Liquid Rocket Combustion, AFOSR TR 70-2714, Rocketdyne, a Division of North American Rockwell, October 1970.

I-4. Thirteenth Monthly Contract Status Report, Contract NAS7-746, "Effect of Distributed Energy Release on Rocket Engine Performance," Rocketdyne, a Division of North American Rockwell Corporation, Canoga Park, California, 22 December 1970.

I-5. Shapiro, A. H., The Dynamics and Thermodynamics of Compressible Fluid Flow, the Ronald Press Co., New York, 1953.

APPENDIX II

HEAT TRANSFER ANALYSIS METHOD

Analysis of the test data was directed toward determining the effects of various parameters on the heat transfer rates throughout the thrust chamber, and particularly at the throat of the nozzle. The effects of chamber geometry, injector pattern, and propellant injection velocities were evaluated.

The method of analyzing the heat transfer data is discussed first, followed by presentation of typical results.

METHOD OF ANALYSIS

The heat transfer test data included the coolant water flowrate and overall bulk temperature rise for each transverse water-coolant passage in the chamber and nozzle. The water flowrates were measured with turbine flowmeters, and the bulk temperature rises were determined with chromel-alumel thermopiles installed to measure directly the difference between the inlet and outlet temperatures at each passage. The analysis procedure is illustrated in Fig. II-1.

The heat transfer rate into each water passage is given, in terms of the water flowrate ($\dot{m}$), the water specific heat (C_p), and the water bulk temperature rise (ΔT_b), by:

$$Q = \dot{m} \; C_p \; \Delta T_b \tag{II-1}$$

The average chamber heat flux in the region of each coolant passage is obtained by associating a one-dimensional, gas-side heat transfer area with the passage and dividing the heat transfer rate into the passage by the appropriate area:

$$\dot{q}/A = \frac{\dot{m} \, C_p \, \Delta T_b}{A} \tag{II-2}$$

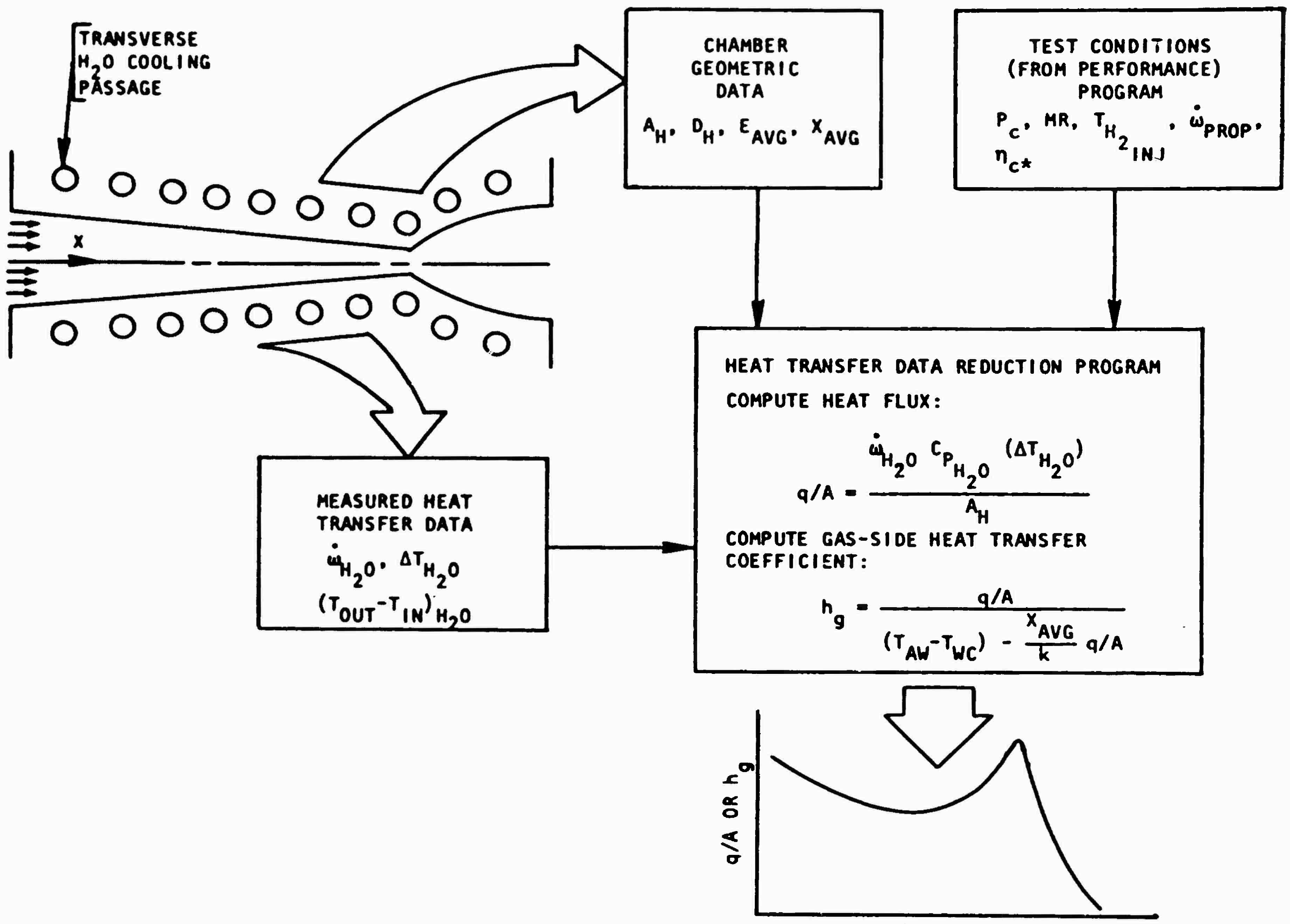

Figure II-1. Heat Transfer Data Reduction

The coolant-side film coefficient is computed by using the relation:

$$h_c = 0.023 \frac{k}{D} \left(\frac{VD\rho}{\mu}\right)^{0.8} \frac{C_p}{k}^{0.4} \tag{II-1}$$

where k, ρ, μ, and V are the thermal conductivity, density, viscosity, and velocity, respectively, of the coolant water.

A coolant-side wall temperature, T_{wc}, assuming forced convection with no nucleate boiling, is then computed from the bulk temperature, T_b, as:

$$T_{wc} = T_b + \frac{q/A}{h_c} \tag{II-2}$$

If this value exceeds the coolant saturation temperature, T_{sat}, the coolant-side is assumed to be in a nucleate boiling regime and the coolant-side wall temperature is found by the relation:

$$T_{wc} = T_{sat} + 50 \tag{II-3}$$

Otherwise, the value for forced convection given by Eq. II-3 is used. An average gas-side film coefficient is then obtained for each passage using the one-dimensional equation:

$$h_g = \frac{q/A}{T_{aw} - t_{wc} - \frac{X}{k_W} q/A} \tag{II-4}$$

X and k_W are the effective thickness and thermal conductivity, respectively, of the wall between the chamber and the cooling passage. The adiabatic wall temperature, T_{aw}, is obtained from the actual combustion temperature by the relation:

$$T_{aw} = T_c \frac{1 + \sqrt[3]{N_{PR}} \frac{\gamma-1}{2} M_\infty^2}{1 + \frac{\gamma-1}{2} M_\infty^2} \tag{II-5}$$

N_{PR} is the Prandtl number, γ is the specific heat ratio, and M_∞ is the free-stream gas Mach number.

The actual combustion temperature, T_c, is given in terms of the ideal combustion temperature corresponding to 100-percent combustion efficiency by:

$$T_c = T_{c_{ideal}} \left(\eta_{c*}\right)^2 \qquad \text{(II-6)}$$

The combustion tempeature, combustion gas specific heat (C_p), and the specific heat ratio (gamma) are in equation form in the computer program and are calculated for the test run conditions of chamber pressure, mixture ratio, and the fuel injection temperature.

Although the coolant passage geometry is highly two dimensional, a one-dimensional relation, such as Eq. II-4, will yield correct heat transfer coefficients if the proper value of the wall thickness is used. Use of the arithmetic average between the maximum and minimum "reaches" for each passage was previously substantiated by the conduction analysis of the segment chamber.

Heat transfer data correlations using either the local heat flux or gas-side flow coefficient have two distinct advantages: (1) these parameters are functions of chamber pressure, propellant combustion, mixture ratio, and characteristic velocity efficiency; and (2) these parameters vary strongly with the local mass velocity (area ratio) and, therefore, increase at a rapid rate in the throat region. A more general correlating parameter can be obtained by nondimensionalizing the heat transfer coefficient by dividing by $\rho V C_p$ to form the Stanton number, and multiplying by $(C_p \mu)^{2/3}/k$, thereby forming the Stanton-Prandtl parameter which is related to Reynolds number based upon the momentum boundary layer thickness through the modified Reynolds analogy:

$$N_{ST} \times N_{PR}^{2/3} \left(\frac{\rho V \theta}{\mu}\right)^{-0.25} \qquad \text{(II-7)}$$

where θ is the momentum boundary layer thickness.

This relation indicates that the Stanton-Prandtl parameter is a weak function of local mass velocity and, hence, chamber pressure, area ratio, and characteristic velocity efficiency, and also a weak function of combustion product properties. The Stanton-Prandtl parameter can be used to provide a direct indication of the local boundary layer development. The distribution of this parameter along a thrust chamber wall surface indicates which regions of the chamber contour are effective in promoting boundary layer growth.

In addition, using turbulent flow analogies between energy and momentum transfer, the Stanton-Prandtl parameter can be closely related to the skin friction coefficient. For flow over a flat plate:

$$N_{ST} \times N_{PR}^{2/3} = \frac{C_F}{2} \qquad \text{(II-8)}$$

This relationship is affected by the presence of free-stream turbulence, pressure gradients, and surface roughness. However, based on this simplified relationship of Eq. II-8 typical experimental values of skin friction coefficient versus length Reynolds number can be used to indicate approximate values of $N_{ST} \times N_{PR}^{2/3}$.

Typical test results are shown in Table II-1 and Fig. II-2.

TABLE II-1

AMPS - WATER COOLED TEST 251 SLICE 61 PC= 995.2 PSIA

PASS	ST*PR↑2/3	HG	EPSILN	MASS VEL
1	0	0	0	0
2	0	0	0	0
3	0	0	0	0
4	1.45804E-3	2.00116E-3	2.98	1.33087
5	1.97246E-3	5.9759E-3	1.35	2.93776
6	3.13681E-3	9.2101E-3	1.393	2.84708
7	3.05813E-3	7.36624E-3	1.698	2.33568
8	3.16112E-3	6.40055E-3	2.02	1.96336
9	2.98789E-3	5.15637E-3	2.37	1.67341
10	3.12915E-3	4.70528E-3	2.72	1.45808
11	3.33413E-3	4.26414E-3	3.198	1.24014
12	3.24746E-3	3.73622E-3	3.555	1.11561
13	3.8883E-3	4.03126E-3	3.945	1.00532
14	4.65557E-3	4.37937E-3	4.348	.912139
15	5.44182E-3	4.33865E-3	5.13	.773096
16	5.7124E-3	4.01443E-3	5.82	.68144
17	5.27868E-3	3.70963E-3	5.82	.68144

PASS	TAW-F	TWG-F	TWC-F	Q/A B/IN2
1	0	0	0	0
2	0	0	0	0
3	0	0	0	0
4	5797.89	518.508	243.41	10.5649
5	5845.91	1135.8	530.815	28.1472
6	5902.49	1358.87	550	41.8472
7	5904.89	126[illegible].17	550	34.1478
8	5906.17	1265.56	550	29.7024
9	5906.94	1111.7	505.323	24.7261
10	5907.4	1023.[illegible]	454.871	22.9805
11	5907.8	95[illegible].093	417.781	21.1233
12	5908.	8[illegible]0.535	404.428	18.7464
13	5908.15	921.601	417.744	20.1021
14	5908.27	961.049	415.656	21.6657
15	5908.4[illegible]	1024.85	422.686	21.1881
16	5908.45	1234.35	550	18.7638
17	5908.45	1188.58	550	17.[illegible]09

PASSAGE	Q(B/SEC)	SUM Q	W(#/SEC)	DELTA T
1	0	0	0	0
2	0	0	0	0
3	0	0	0	0
4	32.6898	32.6898	2.41871	13.5154
5	108.772	141.462	2.32631	46.7572
6	108.732	250.193	2.27017	47.8959
7	102.454	352.647	2.42056	42.3264
8	85.7212	438.368	2.26806	37.7949
9	81.2943	519.662	2.16101	37.6187
10	76.922[illegible]	596.585	2.32277	33.1167
11	74.[illegible]43	670.87	2.38318	31.1702
12	65[illegible]923	736.362	2.15941	30.3288
13	67.[illegible]1	804.116	2.24382	30.1959
14	75.1799	879.296	2.48245	30.2345
15	94.0328	973.328	2.31789	40.5682
16	67.3997	1040.73	2.4321	27.7126
17	62.8922	1103.62	2.53351	24.8241
			32.74 #/SEC	

M*

TABLE II-1 (Concluded)

AMPS - WATER COOLED TEST 251 SLICE 61 PC= 995.2 PSIA

TEST NO	SLICE NO	PC PSIA	MR	W DOT TOT
251	61	995.2	5.79	2.2687

AREA	C SUB P	GAMMA	PR NO	TIF-F
.57204	.90653	1.13815	.82416	500.747

PASSAGE	MACH NO	LOC GAS TEMP	HC	H.T. AREA
1	0	0	0	0
2	0	0	0	0
3	0	0	0	0
4	2.368	4590.67	5.88772E-2	3.0942
5	1.65	5360.68	6.25183E-2	3.8644
6	.483	6267.79	6.14788E-2	2.5983
7	.379	6306.22	6.38303E-2	3.0003
8	.31	6326.79	5.98949E-2	2.886
9	.26	6339.19	5.75961E-2	3.2878
10	.225	6346.59	6.03005E-2	3.3473
11	.19	6352.95	.06123	3.5167
12	.1695	6356.17	5.64564E-2	3.4936
13	.1528	6358.53	5.81939E-2	3.3705
14	.138	6360.42	6.31099E-2	3.47
15	.1168	6362.79	6.13812E-2	4.438
16	.1106	6363.41	3.01452E-2	3.592
17	.1106	6363.41	3.08953E-2	3.592

PASSAGE	WALL THICK	RES NO.	H2O VEL
1	0	0	0
2	0	0	0
3	0	0	0
4	.1203	5.29521E-2	227.416
5	.0993	5.09294E-2	218.729
6	.0893	4.97002E-2	213.45
7	.0973	5.29927E-2	227.59
8	.1113	4.96541E-2	213.252
9	.1133	4.73105E-2	203.187
10	.1143	5.08519E-2	218.396
11	.1173	5.21744E-2	224.076
12	.1198	4.72754E-[illegible]	203.036
13	.1158	4.91233E 2	210.972
14	.1163	5.43477E-2	233.41
15	.1313	.050745	217.937
16	.1685	5.32453E-2	206.559
17	.1685	5.54654E-2	215.172

Q(TOTAL)/W DOT PROP = 486.455
CZ HEAT LOAD, INJ TO HALF OF THROAT IS 1016.54 BTU/SEC

CZ HT. LD. / W DOT PROP. = 448.074

C* EFF	H2O LOG PR	H2O TEMP	CH CODE	SPACER
.993	2086.41	57.036	60	3

UNITS OF HC AND HG ARE: B/(IN2-SEC-F)

WATER F/M FACTORS (1- 17):
.0105 .01035 .0104 .01038 .01038 .01017 .01068 .01017
.01062 .01042 .0103 .01049 .01058 .0107 .01064 .005526
.005377
M?

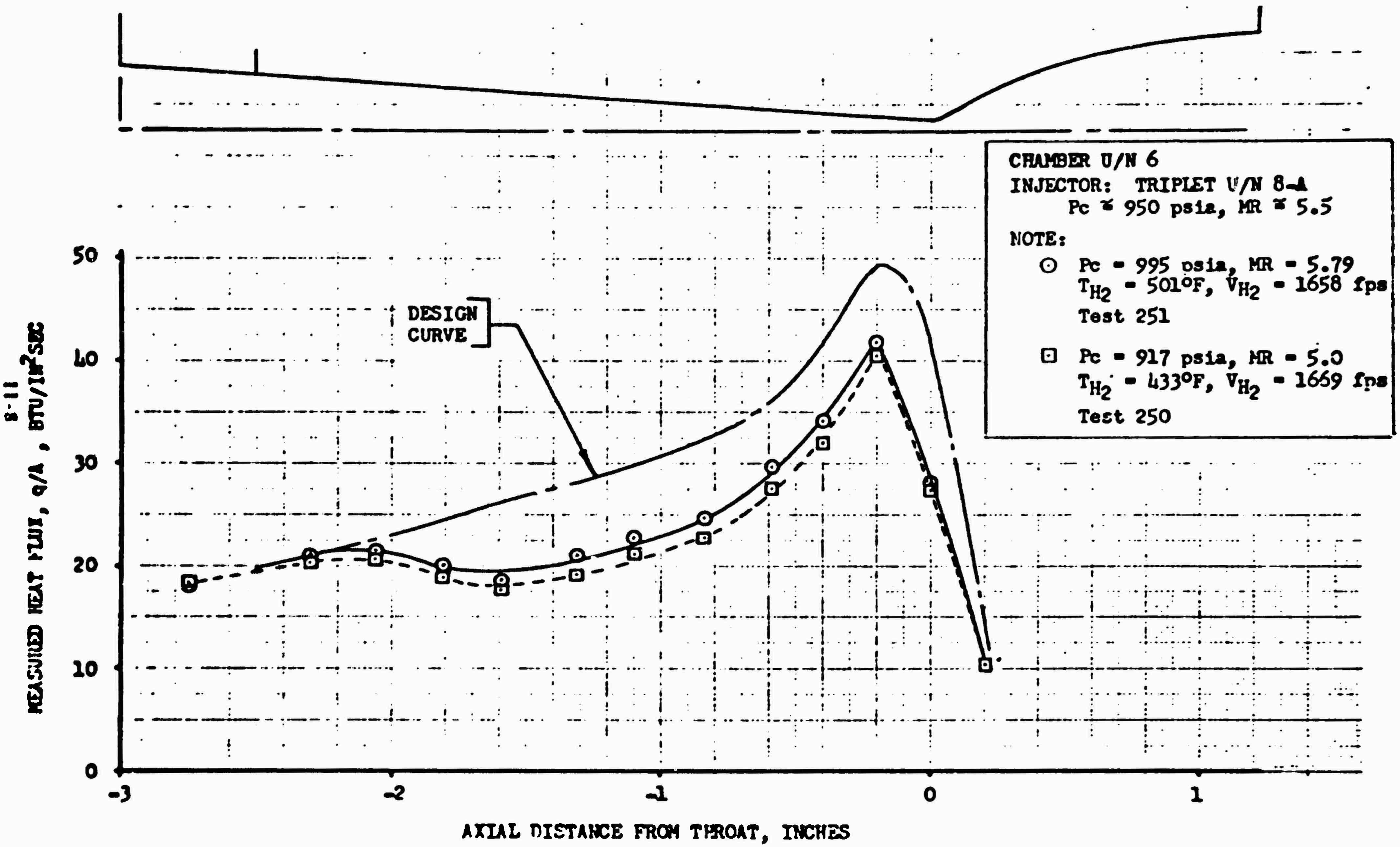

Figure II-2. Combustor Heat Flux Distribution - Comparison with Design Curve (Pc ≅ 950 psia)

APPENDIX II NOMENCLATURE

A	area
BTU	British Thermal Units
b	bulk
C_F	skin friction coefficient
c_p	specific heat
c_z	combustion zone
c*	characteristic velocity
D	diameter
F/M	flowmeter
h_c	coolant-side heat transfer film coefficient
h_g	gas-side heat transfer film coefficient
H_2	hydrogen
in.	inch
k	thermal conductivity
M	mach number
$\dot{M}$	water flowrate
N_{PR}	Prandtl Number = $\mu c_p/k$
N_{ST}	Stanton Number = $hg/V_\rho c_p$
Q	heat, Btu/sec
q/A	heat flux, BTU/in.^{2}-sec
PR	pressure
PROP	propellants, fuel + oxidizer
R	degrees Rankine
sec	second
T	temperature
T_{aw}	temperature, adiabatic wall
T_b	temperature, coolant bulk
T_c	temperature, combustion
T_{SAT}	temperature, water saturation
T_{wc}	temperature, coolant wall
T_{wg}	temperature, gas wall
V	velocity

W	wall
$\dot{W}$	weight flowrate
ΔT_b	water bulk temperature rise
γ	ratio of specific heats
η	efficiency
θ	momentum boundary layer thickness
ρ	density
μ	viscosity
∞	free stream

APPENDIX III

PERFORMANCE DATA REDUCTION WATER-COOLED THRUST CHAMBER TESTS

Data analysis procedures used for the AMPT testing were compatible with the JANNAF Liquid Rocket Engine Performance Calculation Methodology. The data from the AMPT water-cooled thrust chamber test were obtained using a "Beckman" digital data acquisition system coordinated with an IBM Type 360 computer system. The magnetic tape from the Beckman system was read and interpreted by the IBM computer, which provides a tabular printout of digitial data in engineering units. These digital data were provided for a series of preselected sequential time increments through the entire test run. A graphic presentation was also provided of selected data parameters versus time, using the CRT (cathode ray tube) feature of the IBM computation system.

The data (both tabular and graphic) were reviewed to select a representative steady-state test "slice." The data were extracted from the tabular printout and manually input by keyboard to a previously established data file in the Honeywell 440 Time Sharing Computer System. This data file was utilized by the data reduction program stored in this computer system to provide the calculated, corrected performance data.

DATA REDUCTION PROGRAM

The data reduction program was written in FORTRAN computing language for the Honeywell 440 Time Sharing Computer System. The program used the overlay feature available in this system to call numerous subroutines, permitting rigorous computation techniques without making the primary data reduction program ponderous and cumbersome. The program has the capability of reducing data taken for any of the numerous combinations of thrust chambers and injectors for either gas-liquid or gas-gas injector operation. The data file for this program can be set up to hold a single test or several hundred tests with varying configurations.

Many of the performance parameters were computed by redundant methods to provide a cross check on the validity of the input data and to ensure the most accurate results. For example, c* was computed using as many as six different chamber pressure taps, and a thrust method as well. Likewise, liquid oxygen flow was computed by the use of two turbine flowmeters and a cavitating venturi. The printout options with this program were also flexible, providing the full-page format printout either on the teletype console or listing it to a file for subsequent high-speed printer output. A one-line output was also available for quick checkout of data results. A simplified block diagram of the data reduction program is shown in Fig. III-1.

The data reduction program read the input data from a previously prepared input file which could contain either a single test or up to several hundred tests. As the data from each test run were read, the program made a simple test to determine if the proper number of input items have been supplied. The program then called for a subroutine which reads the injector and thrust chamber codes and supplied appropriate physical values and proper instructions for operations influenced by these hardware differences. Liquid oxygen flowmeter information was also included in this subroutine.

The program then selected the appropriate procedures based on gas-gas or gas-liquid coding, and computed propellant flowrates and mixture ratios. Fuel flowrate was computed using a sonic venturi, and oxidizer flow was computed from two turbine flowmeters and a cavitating venturi, for the liquid tests, and a sonic venturi for gaseous tests. The next parameters were vacuum corrected thrust and c* efficiency values based on the various redundant flowrate measurements, and the different chamber pressure measurements. Propellant momentum, and momentum ratios, were also computed at this point.

Propellant enthalpy values were determined using subroutines called "PHENTH" and "OXYHS." These values of propellant enthalpy were used in a subroutine called "THEOSH" to obtain the proper value of theoretical performance for the test mixture ratio and chamber pressure.

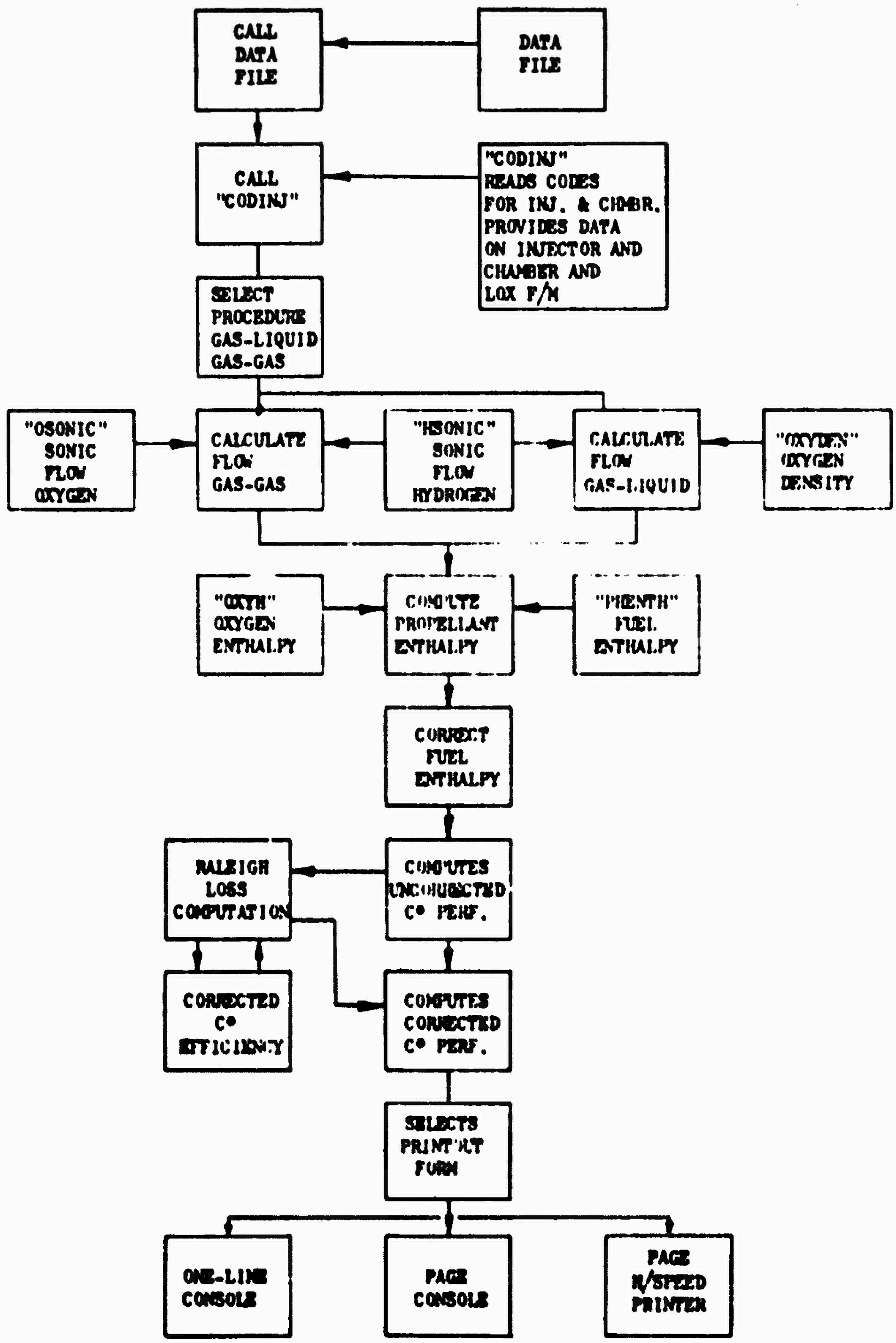

Figure III-1. Data Reduction Program Diagram

Uncorrected c* efficiency based on thrust was calculated at this point using a thrust coefficient dependent upon the test assembly $\epsilon_{expansion}$, obtained from the theoretical data subroutine.

c* efficiency corrections were computed using input values and computed parameters at this point, and were combined with other corrections that were provided. Corrections were made for: combustion zone heat load, throat flow coefficient, throat thermal/pressure area change, propellant kinetic energy, propellant momentum, and Raleigh loss. c* efficiency from thrust was corrected for: kinetic losses, divergence losses, drag, propellant kinetic energy, and combustion zone heat load. Further detail on these corrections is contained in a later section of this appendix.

Figures III-2 through III-4 show samples of the program printout. The short one-line printout (Fig. III-2) is valuable for providing relatively quick performance values for a series of tests. The information provided by this output was the test run number, injector code number, thrust chamber code number, corrected chamber pressure from the injector end measurement, and chamber pressure from the wall taps. Six different values of c* efficiencies were presented, based on injector end pressure, wall pressure, and thrust, first using turbine flowmeter values for flowrates, and then the same parameters using venturi flowrates.

The gas-liquid printout (Fig. III-3) demonstrates the large amount of information presented by this program. Performance data are shown for injector end chamber pressure measurement, thrust, and wall chamber pressure measurement. Flowrate data are shown for both turbine-type flowmeters and the cavitating venturi. A typical gas-gas test printout is shown in Fig. III-4. This printout is largely the same as the gas-liquid printout except that turbine flowmeters were not used, as indicated by the zeros in those columns. An example of the one-line data printout is shown in Fig. III-2. These again are gas-gas tests, and no data are shown for the turbine flowmeters.

```
[illegible]

READY
[illegible]

[illegible]      [illegible]  JAN. 17,197?

WHICH OUTPUT FORMAT DO YOU WANT?  INPUT CODE NUMBER
     CODES ARE:
          1 - PRINT DATA ON CONSOLE
          2 - PRINT [illegible] ON CONSOLE
          3 - WRITE TO A FILE (PRINT ON LINE [illegible])
          4 - [illegible] AND WRITE FILE FOR [illegible]
 ? 2
```

RUN	KINJ	KCH	PC	PCW	ETA	ETW	EFF	ETACV	ETWV	EFFCV
247	51	[illegible]	[illegible]	519.3	0.0	0.0	0.0	99.6	99.1	99.1
248	51	60	[illegible]	[illegible]	0.0	0.0	0.0	99.6	99.3	[illegible]
249	51	60	[illegible]	[illegible]	0.0	0.0	0.0	100.4	100.0	[illegible]
250	51	60	911.0	[illegible]	0.0	0.0	0.0	99.5	99.1	97.7
251	51	60	[illegible]	[illegible]	0.0	0.0	0.0	100.1	99.4	99.0

```
[illegible]

[illegible] TIME:  [illegible]    I/O TIME :   [illegible]
```

KINJ - injector code

KCH - chamber code

PC - injector end chamber pressure

PCW - wall tap chamber pressure

ETA - chamber pressure c* efficiency - average of flowmeters

ETW - wall pressure c* efficiency - average of flowmeters

EFF - thrust c* efficiency - average of flowmeters

ETACV - chamber pressure c* efficiency based on oxidizer cavitating venturi flowrate

ETWV - c* efficiency based on turbine flowmeter flowrate

EFFCV - thrust c* efficiency based on oxidizer cavitating venturi flowrate

Figure III-2.Typical One-Line Printout

```
                              A M P S
OXYGEN/GH2 WATER COOLED CHAMBER TEST AT PRA        TEST NO.   112
CHAMBER CODE   40   INJ CODE  740     PC WALL = 774.549
U/N 4 CH. NO SPACER,  7D COAX,  .050 RECESS,  8-9-71

                         PERFORMANCE DATA
PC INJ END = 765.814 PSIA  SITE THRST= 632.208 LBF  VAC THRUST=887.324
SLICE NUM=   70          M/S DURAT = 10.430 SEC  SLICE TIME=  9.700 SEC
                             #A METER    #B METER    AVG A&B     CAV VENT
TOTAL FLOWRATE (LBM/SEC)      2.2843      2.2941      2.2892      2.2553
MIXTURE RATIO                 5.5371      5.5652      5.5511      5.4541
MEASURED C* FROM PC (FPS)    7878.81     7845.11     7861.93     7980.12
MEASURED C* FROM F (FPS)     7432.84     7401.04     7416.90     7528.41
THEORETICAL C* (FPS)         7860.59     7852.39     7856.49     7884.90
UNCORRECTED C* EFF (PC)     100.2318     99.9072    100.0692    101.2076
UNCORRECTED C* EFF (F)       94.5582     94.2520     94.4048     95.4788
CORRECTED C* EFF (PC)        96.5578     96.2451     96.4011     97.4979
CORRECTED C* EFF (F)         99.2670     98.9455     99.1059    100.2334
CORRECTED C* EFF (WALL)      97.6592     97.3429     97.5007     98.6099
THEOR. I-SUB-S =  412.0706     THEOR. CF = 1.6814     EPSILON = 5.5821

                            INPUT DATA
START TIM=  9.270   CAV VEN CD=    0.975          FUEL VEN P= 2239.435 PSIA
SLICE TIM= 15.970   CAV VENT P= 1946.043 PSIA  FUEL VEN T=   87.255 DEGF
END TIME = 19.700   OX #A CPS =  306.334 CPS   FUEL INJ P=  873.932 PSIA
CMOM     =  1.006   OX #B CPS =  315.350 CPS   FUEL INJ T=  326.343 DEGF
THRT CORR=  0.951   OX #A TEMP= -291.098 DEGF  INJ END PC=  779.111 PSIA
CD  CORR =  0.996   OX #B TEMP= -292.694 DEGF  INJ END PC=  780.141 PSIA
DRAG CORR=  0.993   OX INJ PRS=  970.040 PSIA  SITE THRST=  632.238 LBF
DIV  CORR=  0.999   OX INJ TEM= -276.609 DEGF  AREA THRT =   0.7175 SQIN
KIN CORR =  0.994   % GOX VENT=  100.000       GF2 PRESS =  260.932PSIA
HAL LOSS =  0.976   TOT HT LD=   366.000 B/LB  FRAS COR =    1.0022
FAL COR  =  0.9759  ENERGY COR=    0.999

                          OXIDIZER DATA
CAV VEN D= 0.1060 INCH  CAV VEN P= 1946.04 PSIA  VAP PRES= 17.93 PSIA
DELTA F/M= 0.5000 %     SAT RHOL= 30.43 #/FT**3
                             #A METER    #B METER    AVG A&B     CAV VENT
FLOWRATE (LBM/SEC)            1.9349      1.9447      1.9398      1.9059
CALC AND INPUT CD             0.8883      0.8928      0.8906      0.8750
TEMPERATURE (DEG F)        -291.0980   -292.6940               -295.5120
DENSITY (LBM/FT**3)          71.8799     72.1423                 71.7081
FLOWMETER FACTOR           1507.3206   1551.0076
INJ  VEL =  22.04 FPS   INJ TEMP =-276.609 DEGF  INJ PRES= 970.04 PSIA
INJ AREA =0.11943 SQIN  INJ RHOL = 106.110 #/FT3 OX QUAL =   0.00
INJ MOMT =   1.33 LBF   INJ DEL P= 190.414 PSID  WDOT GF2= 0.0164 #/SEC
OX MACH# =  0.720       RHO*DP   = 20204.782

                            FUEL DATA
FLOWRATE= 0.3494 #/SEC  INJ  VEL = 1285.69 FPS   INJ TEMP =  326.34 DEGF
INJ AREA= 0.2105 SQ IN  INJ MACH#= 0.2487        INJ  RHF = 0.186  #/FT3
INJ PRES= 873.93 PSIA   VENT DIA = 0.1860 INCH   K FACTOR =  0.00000E+00
INJ DELP=  94.31 PSID   VEN SUP P= 2239.43 PSIA  VEN SUP T=   87.25 DEGF
RHOF*DP =  17.542       FMOM     = 13.9571       ADJ TIF  =  326.34 F
                  MISCELLANEOUS OPERATING CONDITIONS
DURATION= 10.4300SEC   CALC TH A =  0.6897 SQIN  VF - VOX = 1263.05 FPS
VHAT F/O=   58.30 MOM RAT= 10.593   DEL PC=  0.132    DEL PCW=  0.000
THRT Q/A=  37.000   WALL PCS =   762.672   778.830     0.000      0.000
(THEOR-INTERP) - REDUCTION DATE    20125      JAN 03, 1972
```

Figure III-3. Typical Printout Gas-Liquid Test

```
                              A M P S
OXYGEN/GH2 WATER COOLED CHAMBER TEST AT PRA       TEST NO.   248
CHAMBER CODE    60     INJ CODE   81       PC WALL = 426.165
U/N 6 CHAMB.,  3-INCH,  8A TRIPLET INJ.,  11-29-71

                          PERFORMANCE DATA
PC INJ END = 430.140 PSIA  SITE THRST= 335.827 LBF  VAC THRUST=373.225
SLICE NUM=  115           M/S DURAT = 10.404 SEC  SLICE TIME= 19.593 SEC
                                  #A METER    #B METER     AVG A&B     CAV VENT
TOTAL FLOWRATE (LBM/SEC)          0.1578      0.1578      0.9901      0.9901
MIXTURE RATIO                     0.0000      0.0000      5.2761      5.2761
MEASURED C* FROM PC (FPS)           0.00        0.00        0.00     7877.27
MEASURED C* FROM F (FPS)            0.00        0.00        0.00     7341.32
THEORETICAL C* (FPS)                0.00        0.00        0.00     7931.29
UNCORRECTED C* EFF (PC)           0.0000      0.0000      0.0000     99.8223
UNCORRECTED C* EFF (F)            0.0000      0.0000      0.0000     93.0505
CORRECTED C* EFF (PC)             0.0000      0.0000      0.0000     99.7773
CORRECTED C* EFF (F)              0.0000      0.0000      0.0000    101.1658
CORRECTED C* EFF (WALL)           0.0000      0.0000      0.0000     99.3192
THEOR. I-SUB-S =  405.2064       THEOR. CF = 1.6521     EPSILON = 4.9841

                             INPUT DATA
START TIME 10.267   CAV VEN CD=     0.965       FUEL VEN P= 1655.333 PSIA
SLICE TIME= 29.920  CAV VENT P= 1643.515 PSIA  FUEL VEN T=   64.446 DEGF
END TIME = 20.671   OX #A CPS = 1111.000 CPS   FUEL INJ P=  464.456 PSIA
CMOM     =  1.010   OX #B CPS =    0.000 CPS   FUEL INJ T=   90.133 DEGF
THRT CORR=  0.968   OX #A TEMP=   64.526 DEGF  INJ END PC=  425.224 PSIA
CD  CORR =  0.996   OX #B TEMP=    0.000 DEGF  INJ END PC=  426.437 PSIA
MAG CORR=   0.955   OX INJ PRS=  497.653 PSIA  SITE THRST=  335.427 LBF
HIN  CORR=  0.970   OX INJ TEMP=  71.686 DEGF  AREA THRT =   0.5592 SQIN
HIN CORR =  0.959   % OX VENT=   100.000       GF2 PRESS =  213.910PSIA
CAL LOSS =  1.000   TOT WT LB=   435.525 #/LB  FLAS COR =    1.0048
FML COR  =  0.9735  ENERGY CORR=   0.979

                           OXIDIZER DATA
CAV VEN D= 0.1585 INCH  CAV VEN P= 1643.51 PSIA  VAP PRES=1V3.30 PSIA
DELTA F/M=05.4844 %     SAT RHO =  0.19 #/FT**3
                                  #A METER    #B METER     AVG A&B     CAV VENT
FLOWRATE (LBM/SEC)                0.0000      0.0000      0.8323      0.8323
CALC AND INPUT CD                 0.0000      0.0000      0.0000      0.9650
TEMPERATURE (DEG F)              64.6260      0.0000                 64.6260
DENSITY (LBM/FT**3)               0.0000      0.0000                  9.9255
FLOWMETER FACTOR                  0.0000      0.0000
INJ  VEL = 301.57 FPS   INJ TEMP =  71.686 DEGF  INJ PRES= 497.65 PSIA
INJ AREA =0.13243 SQIN  INJ RHOL =   2.903 #/FT3 OX QUAL =   1.00
INJ MOMT =    9.35 LBF  INJ DEL P=  71.022 PSID  WT OF GF2= 0.0151 #/SEC
OX MACH# =  0.334       RHOOJP   =   179.775

                              FUEL DATA
FLOWRATE= 0.1578 #/SEC  INJ  VEL = 1029.54 FPS    INJ TEMP =   93.13 DEGF
INJ AREA= 0.1511 SQ IN  INJ MACH= 0.2376          INJ RHO  = 0.144  #/FT3
INJ PRES= 464.46 PSIA   VENT DIA = 0.1430 INCH   K FACTOR =  0.00000E+00
INJ DELP=  34.33 PSID   VEN SUP P= 1655.33 PSIA  VEN SUP T=   64.45 DEGF
RHOF*OF =    5.619      FRCM      =  5.0480        ADJ TIF  =  300.78
                   MISCELLANEOUS OPERATING CONDITIONS
DURATION= 10.4040SEC  CALC TH A =  0.5580 SQIN  VF - VOX =  667.78 FPS
VRAT F/O=     2.05 NOM RATE   0.540   DEL PC=  0.285   DEL PC=  0.306
THRT O/A=  17.191   WALL PCS =      0.000      0.000   430.010   425.714
(THEOR-INTERP) - REDUCTION DATE     21177      JAN. 05, 1972
```

Figure III-4. Typical Printout Gas-Gas Test

CORRECTION FACTORS

Practical considerations prevent the direct measurement of many of the performance parameters of interest. For instance, to measure the total pressure at the throat station during hot fire is impractical, and to mechanically measure throat area during the firing is equally difficult. For this reason, a technique of applying correction factors, to parameters which can be measured, was generally used to compute the desired parameters. The correction factors utilized in this data reduction program are described herein, grouped under the parameters to which they are applied.

FORMULAS

Formulas for computation of various performance parameters using correction factors are described in this section.

η_{c^*} from injector end P_c measurement:

$$\eta_{c^*} = \frac{c^* \text{ measured}}{c^* \text{ perfect injector}}$$

$$\eta_{c^*} = \frac{P_c \left(R_L \times M_c\right) \times A_{throat} \left(C_d \times PR_c \times H_c\right) \times g}{\dot{w}_{total} \times c^*_{ODIE} \times (HL_c \times E_c)} \times 100\%$$

η_{c^*} from wall P_c measurements:

$$\eta_{c^*} = \frac{P_c \left(G_c \times S/T_c \times \frac{R_L + 2}{3}\right) \times A_{throat} \left(C_d \times PR_c \times H_c\right) \times g}{\dot{w}_{total} \times c^*_{ODIE} \times (H_1 \times E_c)} \times 100\%$$

η_{c^*} from thrust:

$$\eta_{c^*} = \frac{I_{s_{measured}}}{I_{s_{perfect\ injector}}}$$

$$\eta_{c^*} = \frac{F\left(B_c \times K_{inc} \times DR_c \times DIV_c\right) \times g}{\dot{W}_{total} \times I_{s_{ODIE}} \times (H_c \times E_c)} \times 100\%$$

Abbreviations used above:

Corrections

R_L = Raleigh loss

M_c = momentum correction

C_d = throat discharge coefficient

PR_c throat pressure deflection correction

H_c throat thermal distortion correction

HL_c = combustion zone heat loss correction

E_c = injected kinetic energy correction

G_c = wall tap geometric correction

S/T_c = static to total pressure correction

B_c = thrust base pressure correction

KIN_c = kinetic correction

DR_c = drag loss correction

DIV_c = divergence correction

Parameters

P_c = chamber pressure

A_{throat} = geometric throat area

$\dot{W}_{total}$ = total propellant weight flowrate

F = thrust

I_s = specific impulse

g = gravitational constant (32.18 ft/sec^2)

ODIE = one-dimensional ideal isentropic equilibrium

Chamber Pressure

Raleigh Loss. A stagnation pressure loss occurs in a thrust chamber combustion zone as a result of irreversible processes. As heat is released, the gas volume increases and the gas must be accelerated to satisfy conditions of constant mass flow. Energy must be expended to accelerate the gases, and because this energy becomes unavailable, the process is nonisentropic. The energy expended on accelerating the gases is manifested as a pressure force which, for dynamic flow equilibrium, must equal the time rate of change of flow momentum. The pressure difference associated with this pressure force describes the stagnation pressure loss. For a conventional, constant, cross-section area combustion zone thrust chamber, the Raleigh criterion is accepted as a reasonable approximation of this pressure loss.

The magnitude of this pressure loss bears an inverse relationship to the contraction ratio of the combustion zone. Since the AMPT thrust chamber is a constant convergence combustion chamber, the precise definition of the contraction ratio at the mean flame front is difficult to determine. For this reason, the combustion process in the AMPT chamber was modeled using a vaporization-limiting combustion model computer program to establish a relationship between combustion efficiency and mean flame front location. These data were used to compute the resulting relationship between combustion efficiency and the pressure loss correction (Fig. III-5). The data reduction program uses a curve-fit technique to compute the pressure loss correction as a function of combustion efficiency, and a small iteration loop is used to converge the interrelationship between the pressure loss correction and computed combustion efficiency. The normal range of this correction is a decrease of 1 to 3 percent. Total Raleigh loss is applied to injector end P_c computations, and one third of this decrement is applied to the wall tap pressure computations. (The combustion reaction is essentially complete upstream of the wall pressure tap.)

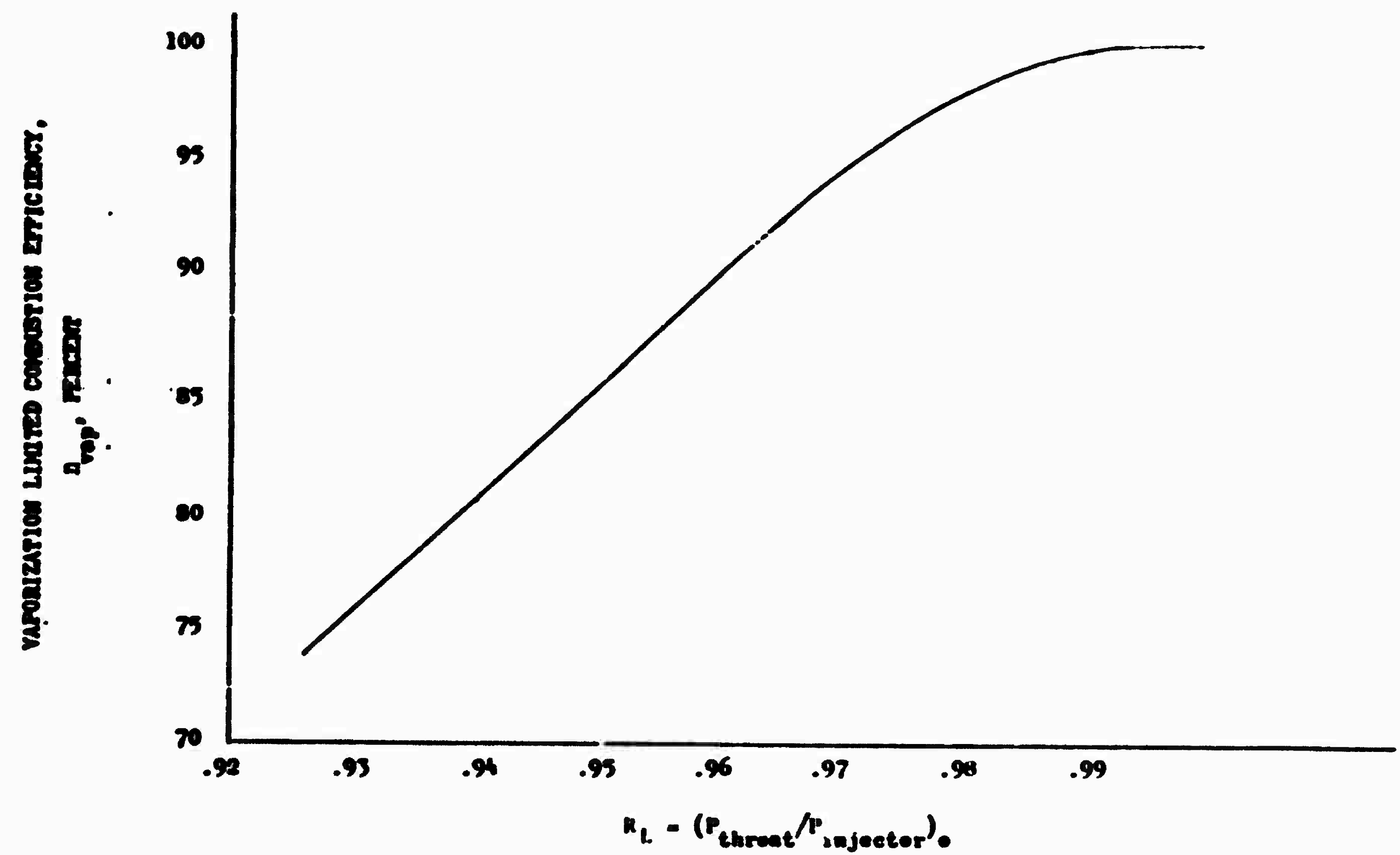

Figure III-5 $(P_{throat}/P_{injector})_o$ vs Vaporization Limited Combustion Efficiency, η_{vap}

Propellant Injection Momentum. The injector end chamber pressure tap is located upstream of the propellant injection plane, and the measured pressure value is depressed by the momentum of the propellant injection velocity. The total propellant injection momentum is divided by the injector face area to provide a momentum pressure. This value is added to the measured pressure at the injector end pressure taps. This correction is not applied to the wall pressures. The normal range for this correction is about 1 to 3 percent.

Injection Energy. The kinetic energy of the injected propellants represents additional energy supplied to the combustion chamber and is converted to heat over and above the available combustion energy. The equivalent value of this energy is computed. This correction is typically less than 0.5 percent, and is applied to all methods of computing c*.

Wall Pressure Tap Correction. The wall chamber pressure taps measure the static pressure component of the flowing gases, requiring a static-to-total pressure correction. An additional correction is required for the geometric configuration of the chamber wall and the pressure tap. A flush static pressure tap of finite diameter will recover a portion of the flow velocity component from the downstream edge of the hole. Also, a static pressure tap on a converging wall will recover a component of the velocity head. The geometric corrections were made to the measured data, and an isentropic static-to-total pressure conversion was computed based on gamma and contraction ratio. These corrections applied only to the wall tap chamber pressure measurements.

Throat Area

Pressure Correction. A small throat area change occurs during hot fire due to the deflection of the thrust chamber walls from chamber pressure. This change is in the direction of increasing throat flow area. The magnitude of this effect was computed for each water-cooled thrust chamber by structural analysis. A typical correction curve for one of the water-cooled thrust chambers is shown in Fig. III-6.

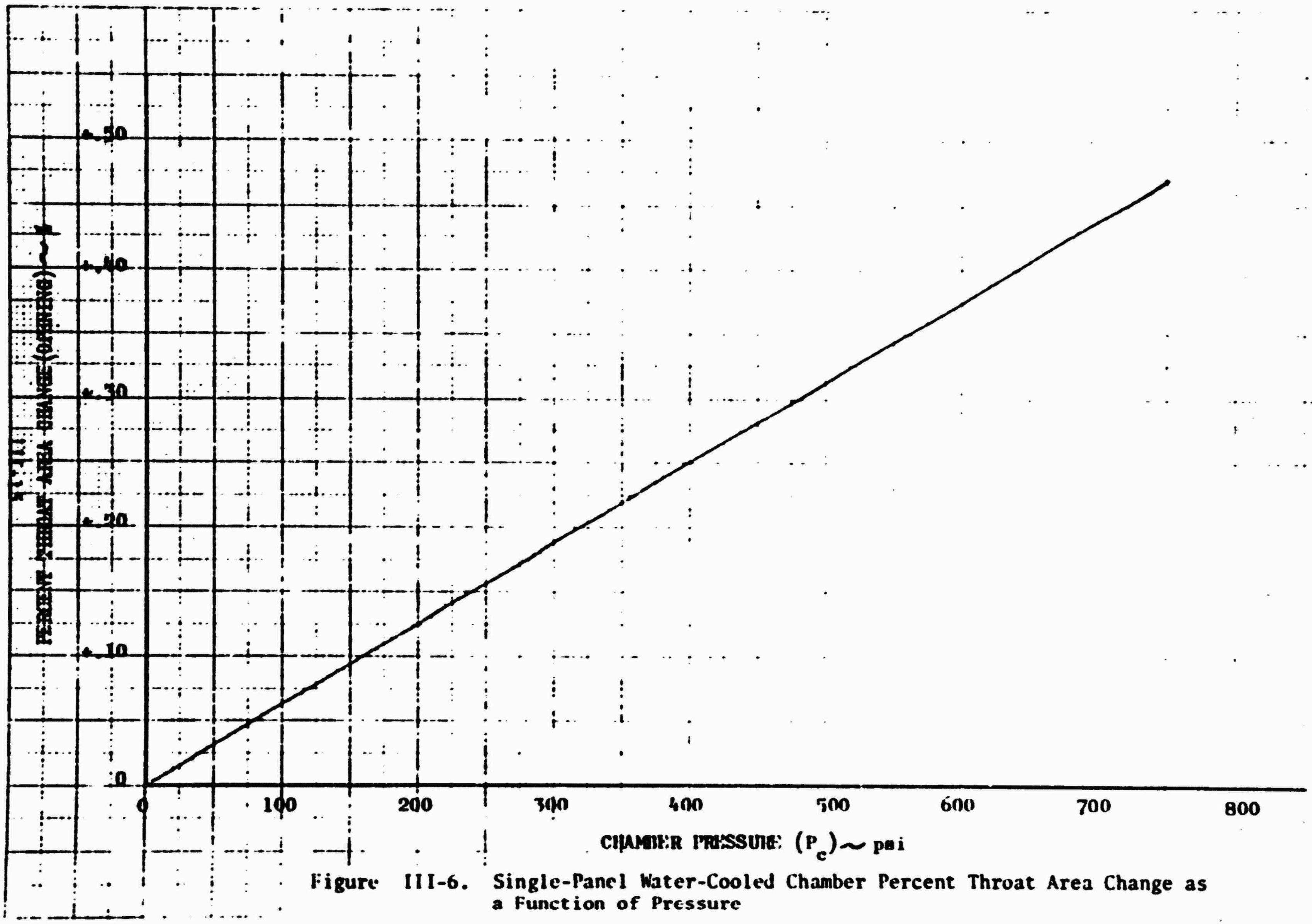

Figure III-6. Single-Panel Water-Cooled Chamber Percent Throat Area Change as a Function of Pressure

Thermal Correction. A significant change in throat area of the water-cooled thrust chambers results from differential expansion under hot-fire thermal loadings. This type of dimensional change is experienced by virtually all types of thrust chambers, but is even more significant in high-aspect-ratio, noncircular throat configurations. The inner wall is heated by the combustion gases while the outer wall is cooled by water flow. The resulting differential expansion bows the walls inward, reducing throat area. The throat area change was computed for various values of throat heat flux using a finite-element stress analysis computer program which has as its primary input: temperature distribution. The isothermal temperature distribution was computed by a two-dimensional heating, thermal analyzer program. Typical values of the area correction for one of the water-cooled thrust chamber is shown in Fig. III-7.

Throat Discharge Coefficient (C_d). The discharge coefficient is defined as the ratio of actual flowrate through the throat, to the theoretical maximum based on geometric throat area and ideal one-dimensional flow. The coefficient accounts for the deviation from predicted one-dimensional flow, and the calculated potential value of 0.996 was determined by use of the Nozzle Transonic Flow Computer Program. The program computes the flow properties in the region extending from a Mach number of 0.8 to 1.2 for a constant gamma with irrotational flow using a series-type solution.

Propellant

Enthalpy. The actual inlet enthalpy of the propellants to the injector is used in the calculation of perfect injector performance.

Combustion Zone Heat Loss (H_L). In a regeneratively cooled, nonadiabatic, wall thrust chamber the heat rejected from the products of combustion to the chamber walls is added to propellant enthalpy, and is thus not lost to the system. With a water-cooled thrust chamber, this heat transfer causes a reduction in measured performance which should be corrected for, to provide proper evaluation of injector performance. With dimensionally small combustion chambers, which have a high ratio of "wetted area" to volume, this heat rejection to the wall becomes

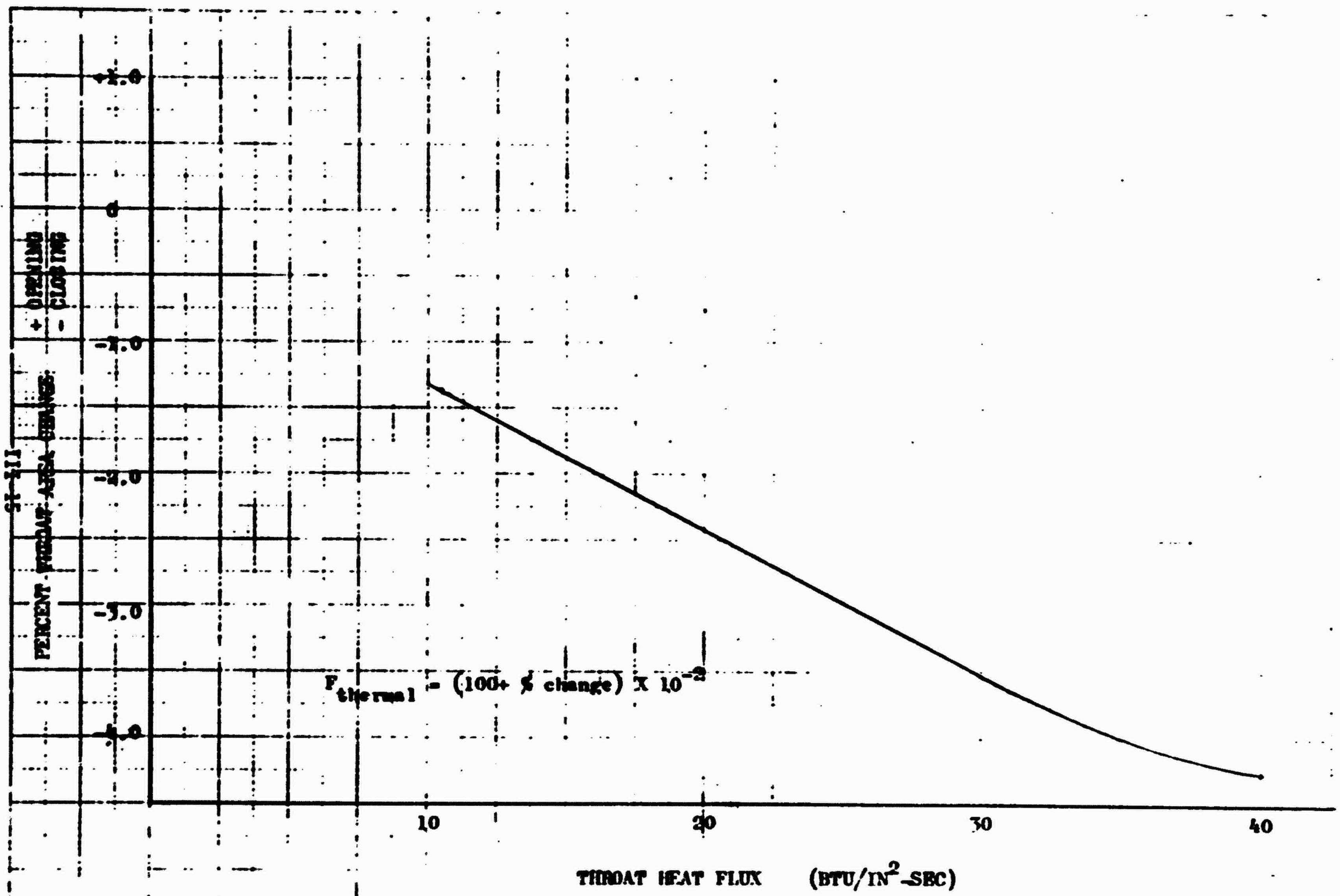

Figure III-7. Single-Panel Water-Cooled Chamber Percent Throat Area Change as a Function of Local Heat Flux a very significant parameter. For example, the total enthalpy from the reaction process is about 10,500 Btu/lb of propellants, and a midpoint operating point with the water-cooled thrust chamber typically will reject about 450 Btu/lb of propellants, equivalent to about 4.3 percent of the total heat available.

The heat loss in the combustion zone is assumed to occur in two ways. In the upper combustion zone the reaction is progressing vigorously and no ordered boundary layer flow has been established. The heat rejected in this zone is assumed to come from the entire reacting flow. Farther downstream, the boundary layer is established, and the reaction is primarily complete. In this zone, the heat loss is corrected for in terms of the boundary layer. The demarcation line between the two zones is established by analysis of the experimental heat transfer data. The performance correction values for various heat loads are shown in Fig. III-8.

Thrust

The basic thrust value is corrected for a base pressure area term which is taken from pressure measurements made in the area around the thrust chamber exit. These pressures are multiplied by the appropriate area values and the result subtracted from the measured thrust.

The normal exit area-ambient pressure correction is also made to compute a vacuum thrust value.

Frictional Drag Correction ($\emptyset_{drg}$). This factor corrects for energy losses due to drag forces resulting from the viscous action of the combustion gases on the nozzle walls. Its magnitude, which is the integral of the local friction forces over nozzle inside wall, is determined by means of a boundary layer analysis utilizing the integral momentum equation for turbulent flow. The values determined by analysis, which are a function of chamber pressure, are presented in Fig. III-9.

Kinetic Correction ($\emptyset_{kin}$). A correction to account for kinetic losses in the nozzle which consist of a deviation from full chemical equilibrium expansion is calculated by the JANNAF one-dimensional exact kinetic performance program. The value, as a function of chamber pressure, is shown in Fig. III-10.

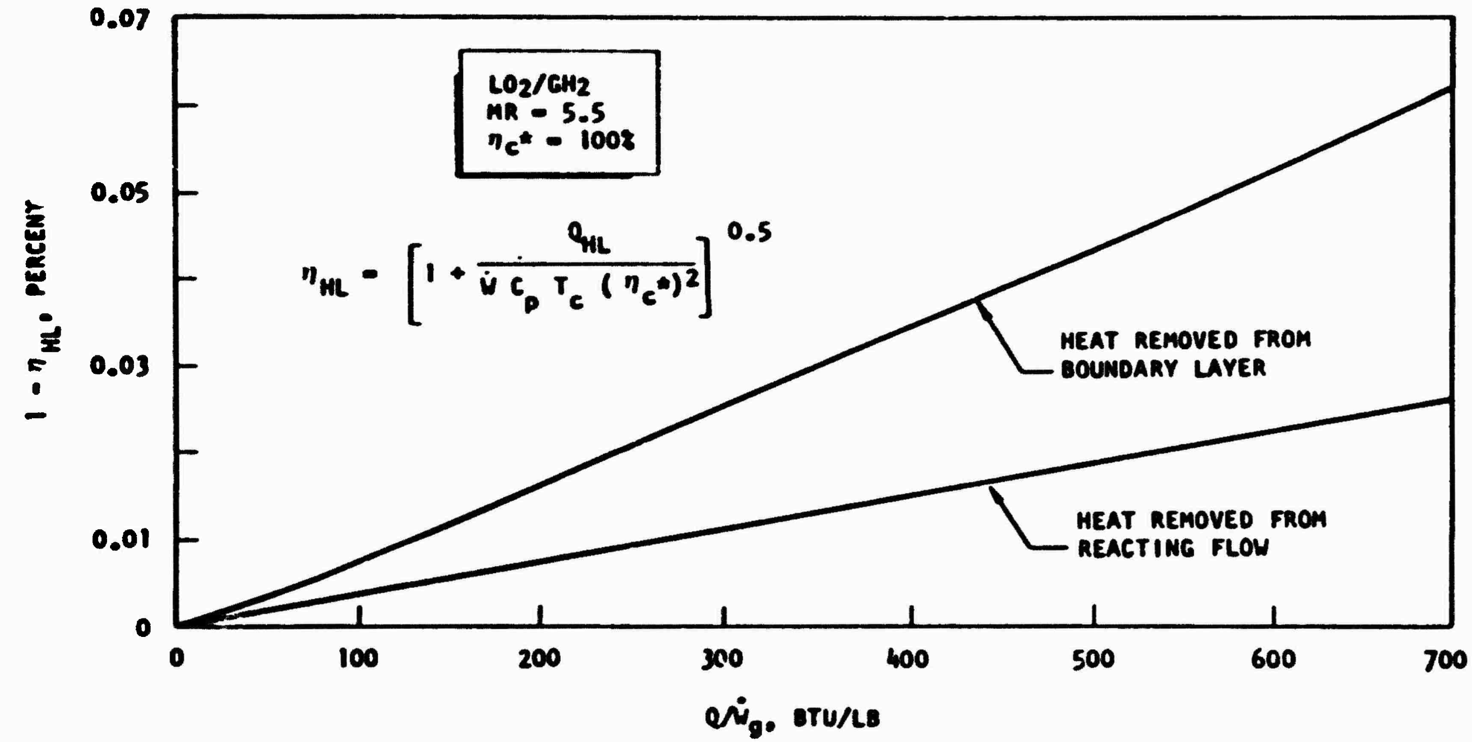

Figure III-8. Bulk Heat Loss Correction

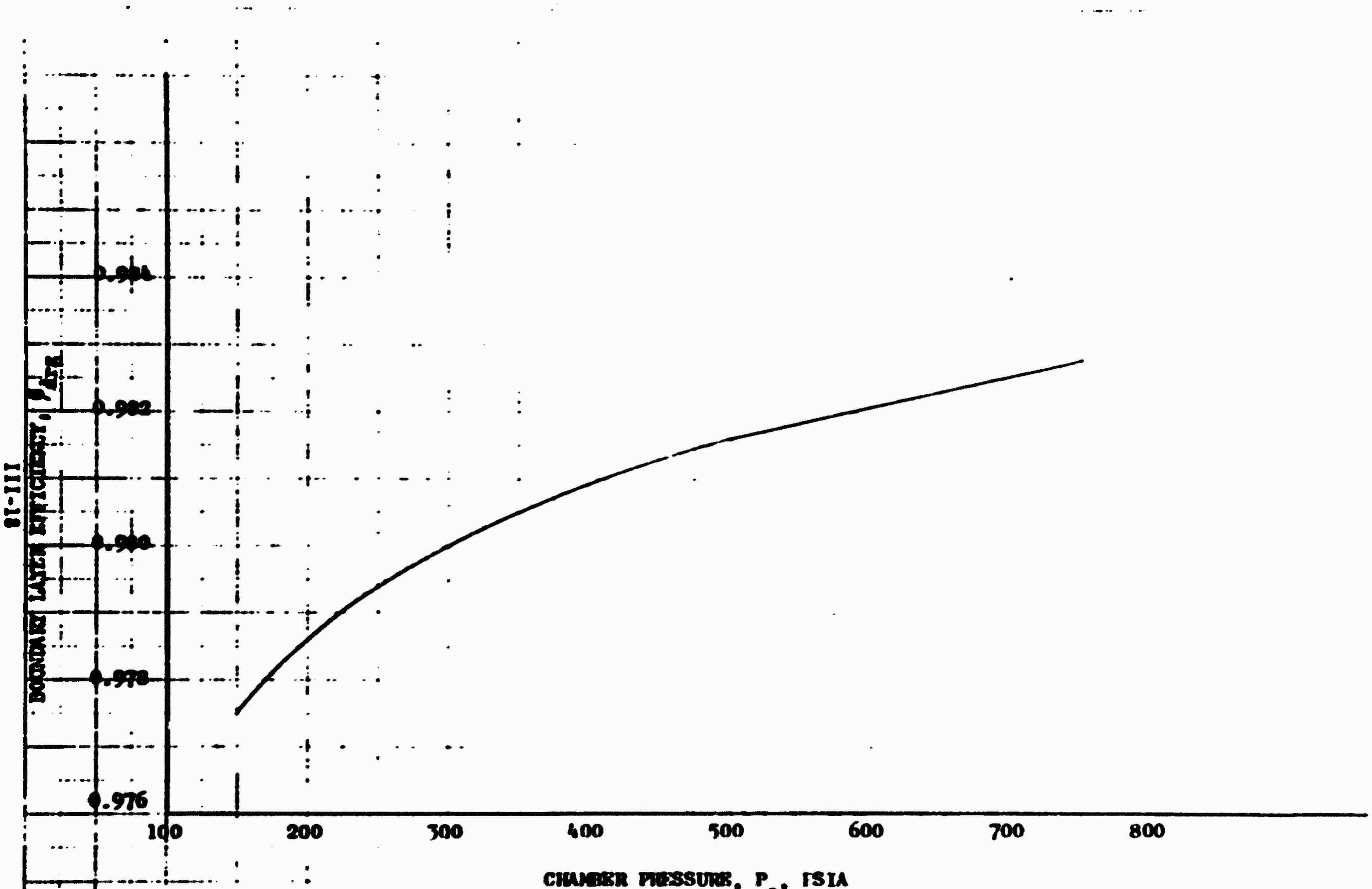

Figure III-9. Frictional Drag Correction ϕ_{drg}

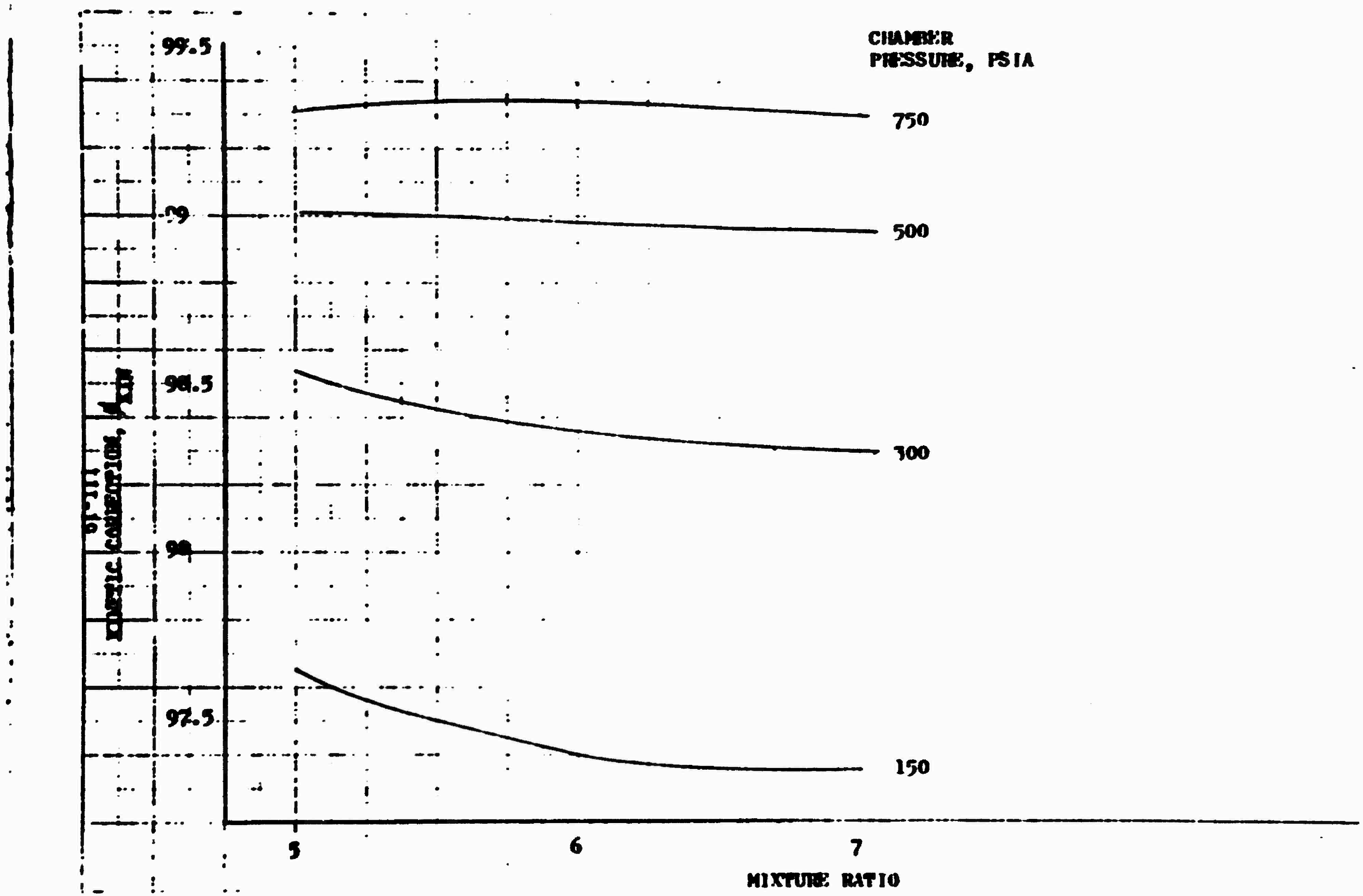

Figure III-10. Kinetic Correction vs Mixture Ratio

III-16

Divergence Correction ($\emptyset_{div}$). The one-dimensional theoretical performance calculations assume that flow at the nozzle exit is uniform and parallel to the nozzle axis. The correction factor, $\emptyset_{div}$, allows for nozzle divergence (i.e., for non-axial flow) and nonuniformity across the nozzle exit plane. The divergence factor is calculated by a computer program (which has been checked against the JANNAF TDK program) which utilizes the axisymmetric method of characteristics for a variable property gas. The factor is almost completely independent of chamber pressure and mixture ratio and is 0.999.

APPENDIX III NOMENCLATURE

A	area
B_c	thrust base pressure correction
C_d	throat discharge coefficient
CODINJ	injector identification code
c*	characteristic velocity
div_c	divergence correction
dr_c	drag loss correction
ε	area ratio
E_c	injected propellant kinetic energy correction
F	thrust
G_c	wall tap geometric correction
g	gravitational constant
H_c	throat thermal correction
HL_c	combustion zone heat loss correction
HSONIC	hydrogen flowrate calculation subroutine
I_s	specific impulse
KIN_c	kinetic correction
Mc	momentum correction
ODIE	one-dimensional ideal isentropic equilibrium
OSONIC	oxygen flowrate calculation subroutine
OXYDEN	oxygen density calculation subroutine
OXYH	oxygen enthalpy calculation subroutine
P_c	chamber pressure
PHENTH	hydrogen enthalpy calculation subroutine
PR_c	throat pressure deflection correction
R_L	Raleigh loss
S/T_c	static-to-total pressure correction
vap	vaporization
$\dot{W}$	weight flowrate
η	efficiency
%	percent

The following are applicable to Fig. III-3 and III-4 only

ADJ	adjusted
CALC	calculated
CAV VEN, CAV VENT	cavitating venturi
CD	throat discharge coefficient (C_D)
CF	thrust coefficient
CMOM	momentum correction (M_C)
COR	correction
CPS	cycles per second
D	diameter
DEG	degree
DEL P	pressure drop
DIV CORR	divergence correction (DIV_C)
DRAG CORR	drag loss correction (DR_C)
DURAT	duration
EFF	efficiency
ENERGY CORR	injector kinetic energy correction (E_C)
F	thrust
f	fuel
F	degrees Fahrenheit
FHL	combustion zone heat loss correction (HL_C)
FT	foot, feet
FPS	feet per second
F/M	flowmeter
GF_2	gaseous fluorine
GH_2	gaseous hydrogen
INJ	injector, injection, injected
ISUBS	specific impulse
KIN CORR	kinetic correction (KIN_C)
LBM	pound (mass)
MACH#	Mach number
MOMT CORR	momentum correction (M_C)

MOM RAT	momentum ratio
M/S	mainstage
NUM	number
OX	oxygen
PC	chamber pressure, injector
PCW	chamber pressure, wall
PRESS	pressure
PSID	pressure difference
QUAL	quality
RAL LOSS	Raleigh loss correction (R_L)
RHO	density
RHOL	liquid density
SAT	saturated
SEC	second (time)
SUP	supply
TEM, TEMP	temperature
THRST CORR	thrust
THRT CORR	throat thermal correction (H_C)
TIM	time
VAC	vacuum
VAP	vapor
VEL	velocity
VRAT	velocity ratio
WDOT	flowrate
WOX VEN	oxidizer flowrate, cavitating venturi meter
%	percent
#	pound
*	multiplied by
**	to the power

UNCLASSIFIED

Security Classification

DOCUMENT CONTROL DATA - R & D

(Security classification of title, body of abstract and indexing annotation must be entered when the overall report is classified)

1. ORIGINATING ACTIVITY (Corporate author) ROCKETDYNE a division of North American Rockwell Corporation 6633 Canoga Avenue, Canoga Park, California 91304	2a. REPORT SECURITY CLASSIFICATION UNCLASSIFIED 2b. GROUP

3. REPORT TITLE

O_2/H_2 Advanced Maneuvering Propulsion Technology Program, Water-Cooled Segment Testing Final Report

4. DESCRIPTIVE NOTES (Type of report and inclusive dates)

Final Report (1 December 1970 to 3 December 1971)

5. AUTHOR(S) (First name, middle initial, last name)

Rocketdyne Engineering

6. REPORT DATE	7a. TOTAL NO. OF PAGES	7b. NO. OF REFS
April 1972	370	11

8a. CONTRACT OR GRANT NO. F04611-67-C-0116 b. PROJECT NO. c. d.	9a. ORIGINATOR'S REPORT NUMBER(S) R-8906 9b. OTHER REPORT NO(S) (Any other numbers that may be assigned this report) AFRPL-TR-72-25

10. DISTRIBUTION STATEMENT Distribution limited to U.S. Government Agencies only; data based on test and evaluation; December 1971. Other requests for this document must be referred to AFRPL (STINFO), Edwards, California 93523

11. SUPPLEMENTARY NOTES	12. SPONSORING MILITARY ACTIVITY
	Air Force Rocket Propulsion Laboratory Air Force Systems Command, USAF, Edwards AFB, California 93523

13. ABSTRACT

This report describes the analysis, design, fabrication, and test of water-cooled segments to define the most suitable injector configurations and combustion chamber geometries for 25,000-pound-thrust, O_2/H_2, lightweight, aerospike thrust chambers. Two-hundred and seventy-one hot-fire tests with numerous injector and chamber configurations were conducted at chamber pressures between 140 and 988 psi. The injector development was supplemented with cold-flow tests of single injection elements. High measured performance (η_{c^*} ~99 percent) was demonstrated in low-volume combustion chambers (3.0-inch length from injector face to the throat). Favorable heat transfer characteristics were established which will enable satisfactory coolant-circuit design for the regeneratively cooled segments which are to be demonstrated in the next phase of the program.

DD FORM 1473

UNCLASSIFIED

Security Classification

UNCLASSIFIED
Security Classification

14. KEY WORDS	LINK A		LINK B		LINK C	
	ROLE	WT	ROLE	WT	ROLE	WT
Single-Panel Segment						
Double-Panel Segment						
Regeneratively Cooled						
Water Cooled						

UNCLASSIFIED